

AD-A171 212

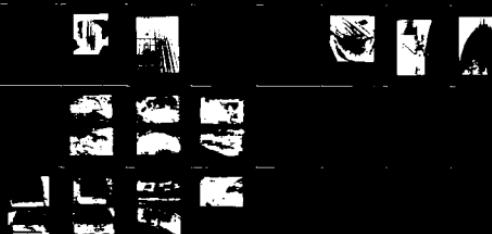
KACHINA TEST SERIES: DYNAMIC ARCH TEST THREE (DAT-3)
ANALYSIS REPORT(U) AIR FORCE WEAPONS LAB KIRTLAND AFB
MM J L SMITH ET AL. MAR 86 AFWL-IR-85-63

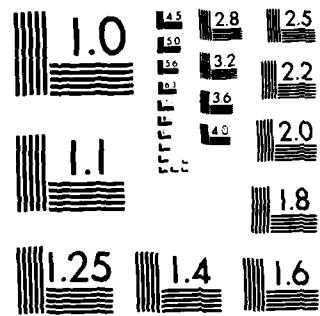
1/6

UNCLASSIFIED

F/G 19/4

ML





MICROCOPY RESOLUTION TEST CHART
NATIONAL BUREAU OF STANDARDS 1961 A

AFWL-TR-85-63

AFWL-TR-
85-63

AD-A171 212



KACHINA TEST SERIES: DYNAMIC ARCH TEST THREE (DAT-3) ANALYSIS REPORT

Joseph L. Smith
John F. Betz
Glenn T. Baird

March 1986

Final Report

2
DTIC
ELECTED
AUG 25 1986
S D
D

Approved for public release; distribution unlimited.

DTIC FILE COPY

AIR FORCE WEAPONS LABORATORY
Air Force Systems Command
Kirtland Air Force Base, NM 87117-6008

UNCLASSIFIED

SECURITY CLASSIFICATION OF THIS PAGE

REPORT DOCUMENTATION PAGE

1a REPORT SECURITY CLASSIFICATION UNCLASSIFIED		1b. RESTRICTIVE MARKINGS										
2a SECURITY CLASSIFICATION AUTHORITY		3. DISTRIBUTION/AVAILABILITY OF REPORT Approved for public release; distribution unlimited.										
2b DECLASSIFICATION/DOWNGRADING SCHEDULE												
4 PERFORMING ORGANIZATION REPORT NUMBER(S) AFWL-TR-85-63		5. MONITORING ORGANIZATION REPORT NUMBER(S)										
6a NAME OF PERFORMING ORGANIZATION Air Force Weapons Laboratory	6b. OFFICE SYMBOL <i>(If applicable)</i> NTES	7a. NAME OF MONITORING ORGANIZATION										
6c ADDRESS (City, State and ZIP Code) Kirtland Air Force Base, NM 87117-6008		7b. ADDRESS (City, State and ZIP Code)										
8a NAME OF FUNDING/SPONSORING ORGANIZATION	8b. OFFICE SYMBOL <i>(If applicable)</i>	9. PROCUREMENT INSTRUMENT IDENTIFICATION NUMBER										
8c ADDRESS (City, State and ZIP Code)		10 SOURCE OF FUNDING NOS										
		PROGRAM ELEMENT NO. 64711F	PROJECT NO. 3763									
		TASK NO. 03	WORK UNIT NO. 21									
11 TITLE <i>(Include Security Classification)</i> KACHINA TEST SERIES: DYNAMIC ARCH TEST THREE (DAT-3) ANALYSIS REPORT												
12 PERSONAL AUTHORISI Smith, Joseph L.; Betz, John F.; and Baird, Glenn T.												
13a TYPE OF REPORT Final	13b. TIME COVERED FROM Sep 82 TO Sep 83	14 DATE OF REPORT (Yr. Mo. Day) 1986 March	15 PAGE COUNT 504									
16 SUPPLEMENTARY NOTATION												
17 COSATI CODES		18 SUBJECT TERMS <i>(Continue on reverse if necessary and identify by block number)</i> <table border="0"> <tr> <td>DAT-3</td> <td>Nuclear weapons effects</td> <td>Ground shock</td> </tr> <tr> <td>Fiber optics</td> <td>KACHINA Test Series</td> <td>Structural response</td> </tr> <tr> <td>HEST</td> <td>Plastic deformation</td> <td>Buried arches (over)</td> </tr> </table>		DAT-3	Nuclear weapons effects	Ground shock	Fiber optics	KACHINA Test Series	Structural response	HEST	Plastic deformation	Buried arches (over)
DAT-3	Nuclear weapons effects	Ground shock										
Fiber optics	KACHINA Test Series	Structural response										
HEST	Plastic deformation	Buried arches (over)										
19 ABSTRACT <i>(Continue on reverse if necessary and identify by block number)</i> <p>This report documents the posttest efforts for the Dynamic Arch Test #3 (DAT-3). Pretest predictions and structural design details are presented in AFWL-TR-83-56. This test was designed to simulate a one-quarter scale 100-kt nuclear surface burst (airblast and ground shock only) at a range corresponding to MPa. This scales to a 1.56 kt detonation at approximately 44.6 m. The actual test environment achieved was a 1.56 kt simulation with a peak pressure of 14 MPa. The structures tested in this event included two short arches, and one long arch composed of four arch segments. Field operations, arch construction, simulation analysis, ground shock analysis, and structural response are all discussed. The results of a fiber optics add-on experiment are also presented.</p>												
20 DISTRIBUTION/AVAILABILITY OF ABSTRACT <input type="checkbox"/> UNCLASSIFIED/UNLIMITED <input type="checkbox"/> SAME AS RPT <input checked="" type="checkbox"/> DTIC USERS		21. ABSTRACT SECURITY CLASSIFICATION UNCLASSIFIED										
22a NAME OF RESPONSIBLE INDIVIDUAL Capt Mary G. Crissey		22b TELEPHONE NUMBER <i>(Include Area Code)</i> (505) 846-6468	22c OFFICE SYMBOL NTES									

UNCLASSIFIED

SECURITY CLASSIFICATION OF THIS PAGE

18. SUBJECT TERMS (Contd)

Nuclear simulation

PREFACE

The authors wish to express their thanks to and acknowledge the efforts of the AFWL personnel who assisted in producing this technical report: Lt Christopher M. Hazen, the test director, for his efforts in coordinating pretest and posttest field activities and supervising the construction of the DAT-3 arches; Mr Ken Havens for his detailed and accurate HEST design; Mr Joseph Edwards for his analysis of the blast pressure and time-of-arrival data; Lt Todd Steiner, the instrumentation project officer, for his design of the instrumentation recording system which produced high-quality, low-noise data and his contributions to Section IV; Mr Josef Schneider for his design and analysis of the fiber optics experiment and his contributions to Section VII; and others involved in the various aspects of this report.

Accesion For	
NTIS	CRA&I
DTIC	TAB
U: announced	
Justification	
By	
Distribution /	
Availability Codes	
Dist	Avail and/or Special
A-1	



CONTENTS

<u>Section</u>		<u>Page</u>
I	INTRODUCTION	1
	BACKGROUND	1
	OBJECTIVES	2
II	MODEL CONSTRUCTION	3
III	TEST SITE OPERATIONS	17
IV	INSTRUMENTATION	40
	TRANSDUCERS, HARDWARE, AND PLACEMENT	40
	INSTRUMENTATION RESULTS	41
V	SIMULATION ANALYSIS	43
	PRETEST DESIGN	43
	POSTTEST ANALYSIS	43
	COMMENTS	46
VI	GROUND SHOCK ANALYSIS	49
	INTRODUCTION	49
	EXPERIMENT DESCRIPTION	50
	DATA RECOVERY	50
	RESULTS	53
	SUMMARY AND CONCLUSIONS	72
VII	FIBER OPTIC CABLE VULNERABILITY EXPERIMENT	74
	OBJECTIVE	74
	APPROACH	74
	ENVIRONMENT	82
	RESULTS	84
	DISCUSSION	90
	CONCLUSIONS AND RECOMMENDATIONS	92
VIII	STRUCTURAL RESPONSE	93
	INTRODUCTION	93
	POSTTEST PICTORIAL REVIEW	94
	GAGE RESULTS	127
	KACHINA SERIES FINDINGS	149
	CONCLUSIONS	150
IX	FINDINGS AND CONCLUSIONS	154

CONTENTS (Concl)

<u>Section</u>	<u>Page</u>
REFERENCES	156
APPENDIXES	
A. STRUCTURAL DETAIL AND CONSTRUCTION DRAWINGS	157
B. MEASUREMENT AND INSTRUMENTATION LIST	169
C. MISCELLANEOUS PHOTOGRAPHS AND STRUCTURAL DAMAGE DRAWINGS	187
D. PHOTOPOLE DATA	205
E. AIRBLAST PRESSURE DATA	237
F. FREE-FIELD SOIL DATA	253
G. NEAR-FIELD AND STRUCTURAL DATA, ARCH A5	315
H. NEAR-FIELD AND STRUCTURAL DATA, ARCH A6	395
I. NEAR-FIELD AND STRUCTURAL DATA, ARCH A7	443

ILLUSTRATIONS

<u>Figure</u>		<u>Page</u>
1	Test-bed layout	4
2	Butt-joint detail	5
3	Key-joint detail	6
4	Arch segment assembly	7
5	Cast-in-place instrumentation hardware	8
6	Typical circumferential section	9
7	Arch segment forms	11
8	Concrete mobile mixer and boom pumper	12
9	Key-joint wooden mold in place	13
10	Fiber optic cable egress holes	14
11	Typical cyclic compression test results	16
12	Generalized stratigraphy and average index soil properties	18
13	Backfill material gradation	19
14	Backfill material compaction test results	19
15	Arch A7 placement	21
16	Arch A5-1 placement	21
17	Backfilling and compaction of cable trenches	22
18	Instrumentation wiring and cable harness	22
19	Bulkhead placement	23
20	Backfill compaction	23
21	Density measurement frequency curve	24
22	Near-surface instrumentation and cable trenches	26
23	Detonation cord placement	27

ILLUSTRATIONS (Contd)

<u>Figure</u>		<u>Page</u>
24	HEST overburden placement	27
25	Overburden gradation curves	28
26	Overburden compaction test results	28
27	Completed DAT-3 test site	29
28	Excavated test-bed and structures	29
29	North side of Arch A6	34
30	South side of Arch A6	34
31	North side of Arch A7	35
32	South side of Arch A7	35
33	South side of Arch A5	36
34	Interior of Arch A5	36
35	Interior of Arch A7	37
36	Typical photopole data	45
37	Typical pressure gage data	47
38	Best estimate of DAT-3 pressure and impulse time history	48
39	Free-field gage layout	51
40	Determination of seismic speed	55
41	Determination of loading wave speed	56
42	Typical free-field vertical motions at depths of 0.75, 2.0, 4.0, and 8.0 m	58
43	Peak vertical acceleration versus depth	61
44	Peak vertical velocity versus depth	62
45	Peak vertical displacement versus depth	64

ILLUSTRATIONS (Contd)

<u>Figure</u>		<u>Page</u>
46	Typical free-field horizontal motions at depths of 0.75, 2.0, 4.0, and 8.0 m	66
47	Peak horizontal accelerations versus depth	68
48	Peak horizontal velocity versus depth	70
49	Peak horizontal displacement versus depth	71
50	Siecor Cable 144 cross section	75
51a	Math associates cable cross section, single fiber	76
51b	Math associates cable cross section, dual fiber	77
52	General cable layout in section	79
53	Cable protection detail	80
54	Cable penetration location, bulkhead view	81
55	Instrumentation	83
56	Siecor Cable black (BB #1)	85
57	Siecor Cable orange (BB #2)	86
58	Math dual cable #1	87
59	Math dual cable #2	88
60	Math single cable	89
61	Posttest bulkhead inspection	91
62	View of test-bed from upstream north side	95
63	View of test-bed from downstream north side	96
64	View of Arch A5 from north end (upstream on right)	97
65	View of Arch A5 from south side (upstream is left)	98
66	View of Arch A5 upstream exterior	100
67	View of Arch A5 downstream exterior	101

ILLUSTRATIONS (Contd)

<u>Figure</u>		<u>Page</u>
68	View of Arch A5 center key joint at crown	102
69	Inside view of north end of Arch A5 (downstream at left)	103
70	View of upstream north end interior of Arch A5	104
71	Downstream interior north end view of Arch A5	105
72	Interior view of south end of Arch A5 (upstream is left)	106
73	Interior upstream south end wall of Arch A5	107
74	Interior downstream south end wall of Arch A5	108
75	View of Arches A6 and A7 (foreground) from downstream north side	110
76	North end of Arch A6 (upstream is right)	111
77	South end view of Arch A6 (upstream is left)	112
78	Upstream exterior of Arch A6	113
79	Downstream exterior of Arch A6	114
80	Upstream interior wall of Arch A6	115
81	Close-up of Arch A6 upstream interior wall	116
82	Downstream interior wall of Arch A6	117
83	Close-up of Arch A6 downstream interior wall	118
84	North end of Arch A7 (upstream is right)	120
85	South end of Arch A7 (upstream is left)	121
86	Upstream exterior wall of Arch A7	122
87	Downstream exterior wall of Arch A7	123
88	Upstream interior wall of Arch A7	124
89	Close-up of Arch A7 upstream interior wall	125

ILLUSTRATIONS (Concl)

<u>Figure</u>		<u>Page</u>
90	Close-up of Arch A7 downstream interior wall	126
91	Normal stresses on Arch A5	128
92	Normal stresses on Arch A6	130
93	Normal stresses on Arch A7	131
94	Longitudinal velocities in Arch A5 segments	133
95	Vertical velocities in Arch A5 end segments	134
96	Vertical and horizontal velocities in Arch A5 middle segments	136
97	Vertical and horizontal velocities in Arch A6	138
98	Arch A7 vertical velocities	139
99	Circumferential strains in south end segment of Arch A5	141
100	Circumferential strains in northern middle segment of Arch A5	142
101	Circumferential strains in Arch A6	142
102	Circumferential strains in Arch A7	144
103	Longitudinal strains in Arch A5 northern segments	145
104	Strains in chamfer shear rebar in Arches A6 and A7	146

TABLES

<u>Table</u>		<u>Page</u>
1	Concrete mix design	15
2	Concrete compressive strength tests	15
3	Reinforcing bar tensile strength tests	16
4	Blast pressure gage locations	31
5	Structure locations	32
6	Passive displacement gages	33
7	Photopole data analysis	38
8	Instrumentation results	42
9	TOA results	44
10	Free-field gage locations	52
11	Time of arrival and time of peak velocity	54
12	Peak vertical free-field motions	60
13	Peak horizontal free-field motions	67
14	Fiber cable parameters	78
15	Fiber optics data summary	84
16	KACHINA Arch relative displacements	151

INTRODUCTION

BACKGROUND

The Air Force Weapons Laboratory (AFWL) has been tasked to provide state of the art in nuclear survivability of existing and future Air Force systems. Many of these systems are, or will be, based on the ground and, as such, will be vulnerable to a variety of nuclear effects. The effects of airblast and ground shock are important in understanding structural hardness and response. The results of field tests verify current methods being developed to:

- (1) improve survivability/vulnerability assessment techniques, (2) define and quantify technological uncertainties, and (3) reduce uncertainties through data acquisition.

The Dynamic Arch Test-3 (DAT-3) was the third in a series of structural tests on generic arch designs. In this test, three different arches were subjected to a High Explosive Simulation Technique (HEST) environment designed to simulate a 1.56 kt nuclear detonation at the 12 MPa (1740 psi) range. The HEST had a design impulse of 0.058 MPa-s and a simulation time of 72 ms. The calibration shot was constructed and fired on 16 Feb 83 to confirm the HEST design for the DAT-3 event which was subsequently fired on 13 May 83.

The arches were tested with different footing and joint designs. Two of the arches were 1.7 m long, one with a footing, the other without. The third arch (6.8 m long) was composed of four 1.7 m arch segments joined together with three different joint designs.

The DAT-3 event was a combined effort of AFWL and the New Mexico Engineering Research Institute (NMERI). AFWL supervised the overall effort, designed the arches and the HEST, performed instrumentation amplification and recording, and conducted posttest analysis. NMERI performed construction, site preparation, instrumentation installation, HEST construction, and all excavation and backfill work on the test. The 1369 AVS, Det 1, provided high-speed and still photography.

OBJECTIVES

The main objectives of DAT-3 were to:

- a. Investigate the effects of reinforcing bar layout on failure patterns.
- b. Investigate the effects of joint load transfer on structural response and failure.
- c. Characterize the response of a KACHINA arch resting on a continuous footing.
- d. Provide data on structural response and failure modes through shallow buried arches loaded to postyield stress levels.
- e. Characterize the free-field and the near-field soil environment from the HEST loading.
- f. Provide data for use in improving computer modeling of soil media and structural modeling.
- g. Validate the simulation design using active measurements and photographic results.

Overall, DAT-3 met or exceeded the expectations of all its objectives.

II. MODEL CONSTRUCTION

Figure 1 shows the test-bed layout and the locations of the three structures, A5, A6 and A7. Structure A5 was composed of four arch segments, A5-1 through A5-4. Structures A6 and A7 were each single-arch segments. Construction drawings and structural details are shown in Appendix A. Because the number of forms was limited, the arch structures were assembled and cast in two phases. In the first phase, arch segments A5-3, A6 and A7 were cast. The last three segments, A5-1, A5-2 and A5-4, were cast 19 days later.

Three types of joints were used between the arch segments making up arch A5. These joints are shown in Figures 2 and 3. Two were butt-type joints with steel face plates on each side. An elastomeric pad was placed between the steel face plates on one of these joints. The third joint was a key joint, located at the center of the structure.

The segments were assembled with the longitudinal axis of the arch in the vertical direction (Fig. 4). The rebar was placed in position around the inner steel form. Care was taken to ensure that all tolerances for cover thickness and rebar location were met.

Strain gages were welded onto the rebar before the rebar was placed in the structure. Weldable-type strain gages proved to be valuable time savers for the project. The unit cost of the weldable gages is greater than that of the conventional bondable gage, but the weldable gage requires less critical surface preparation, can be installed more quickly, and provides a comparable accuracy of results. Consequently, the cost of the installed gages was lower than it would have been had bondable-type gages been used, and three manhours per gage were saved.

During the assembly process, steel plates were placed on the inner arch form to serve as mounts for the structural accelerometers and passive displacement gages. Provisions were made for placing normal stress gages on the outside arch wall with cable egress protection to the interior of the arch (Fig. 5).

The structural reinforcement for a typical arch cross section is shown in Figure 6. This reinforcement layout allows for improvement of the floor-arch joint and provides ease of assembly. The forms used to case the arch

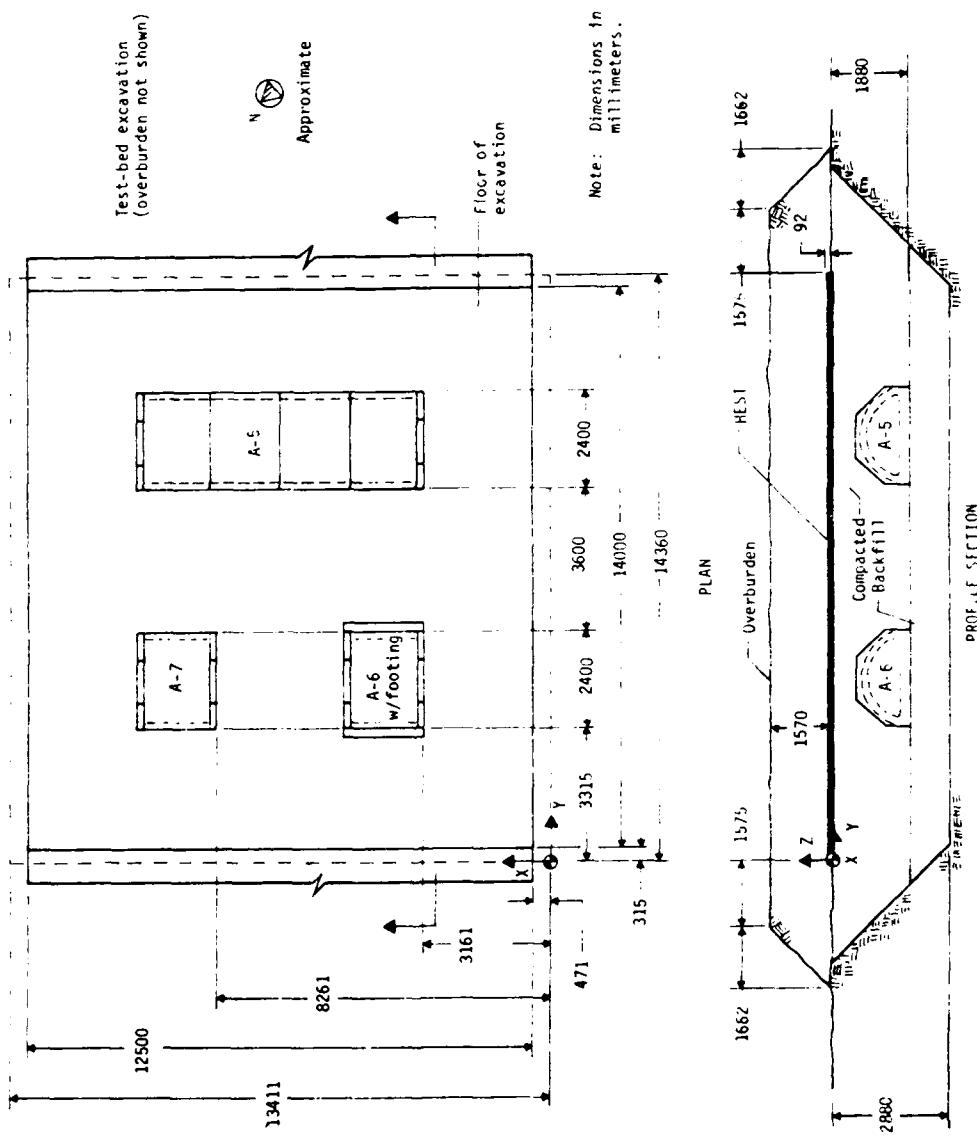


Figure 1. Test-bed layout.

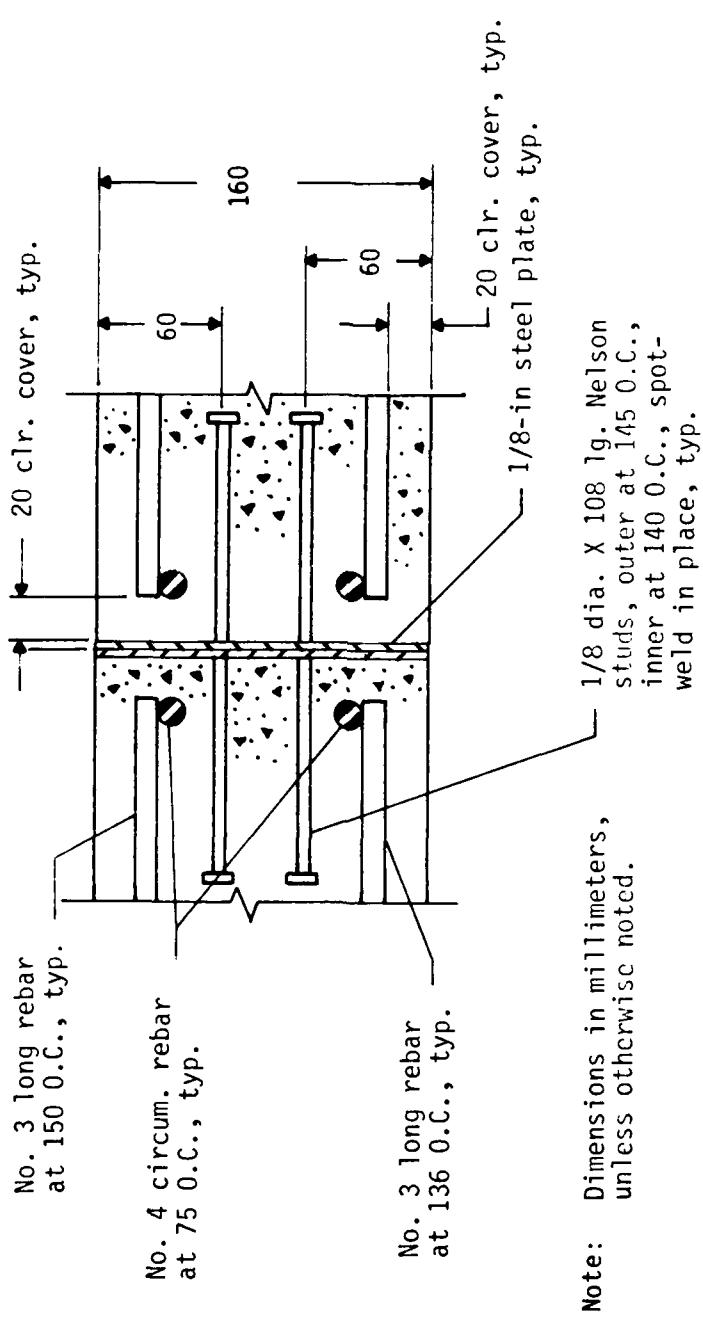


Figure 2. Butt-joint detail.

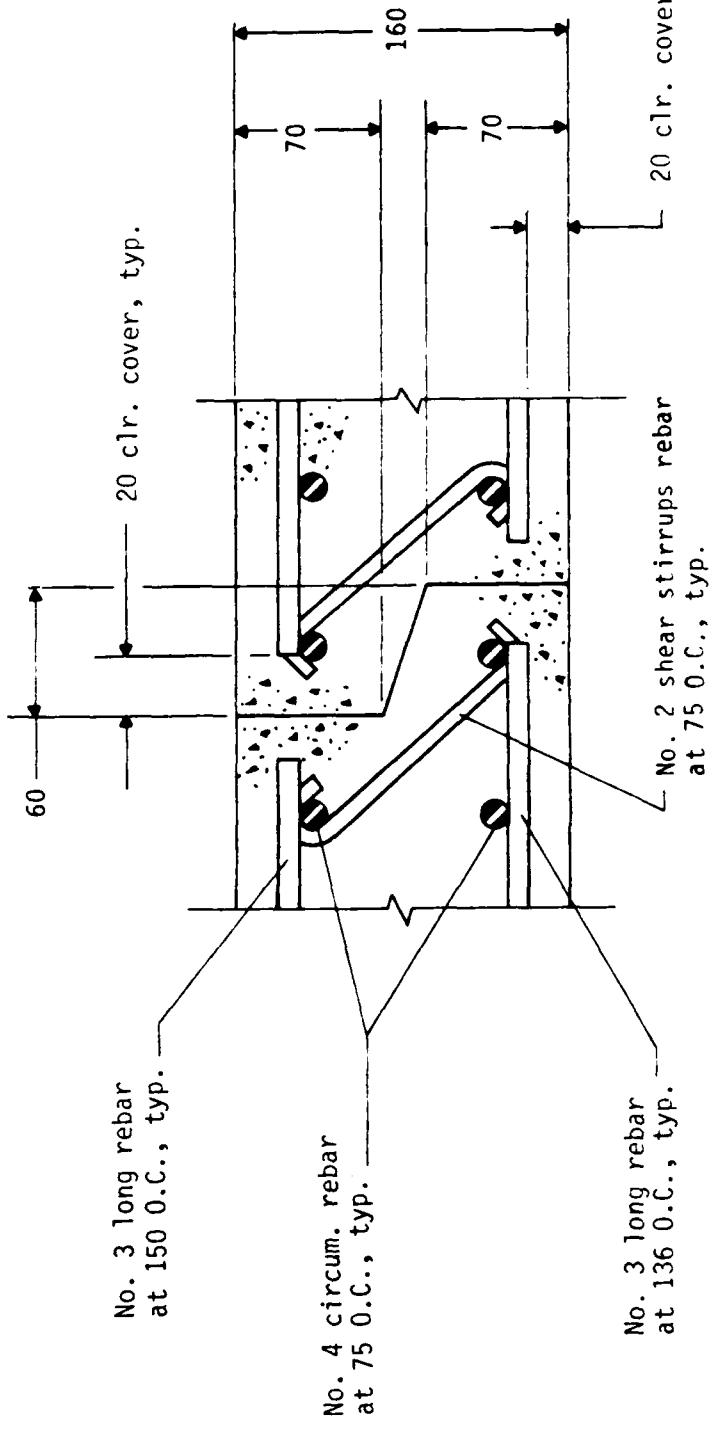


Figure 3. Key-joint detail.

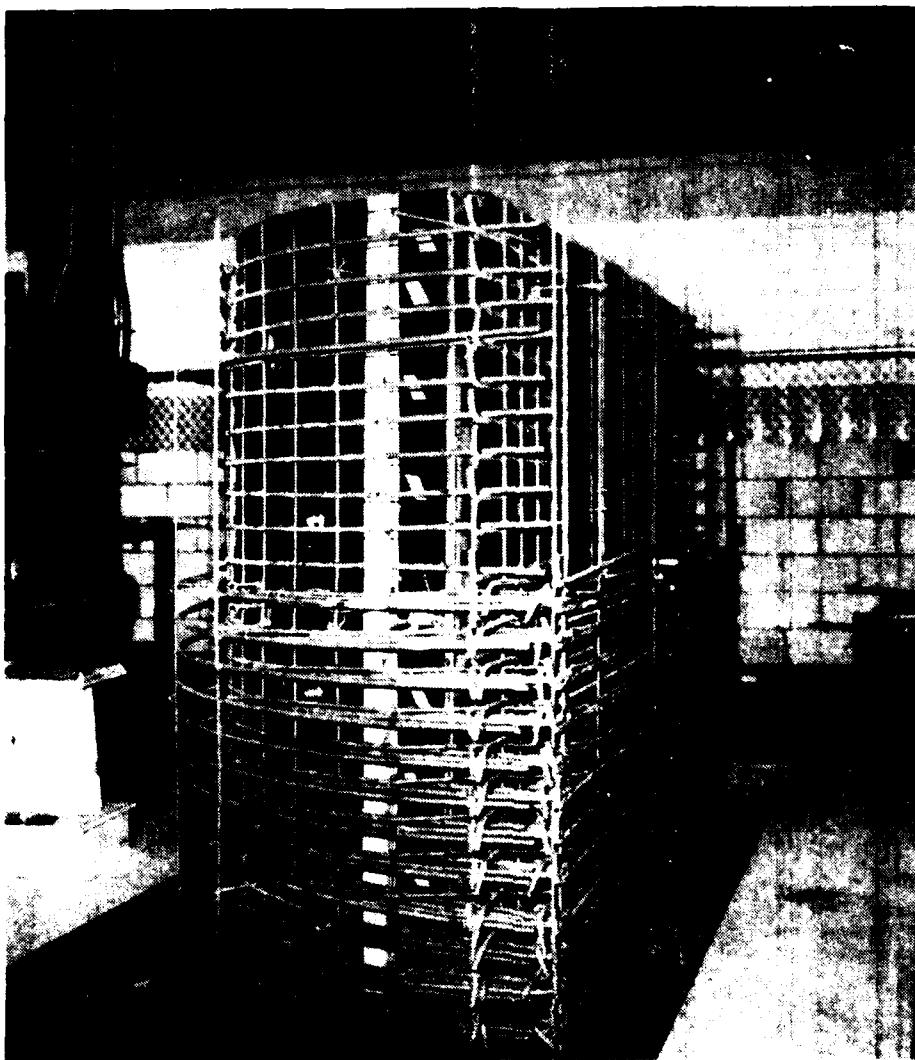


Figure 4. Arch segment assembly.



Figure 5. Cast-in-place instrumentation hardware.

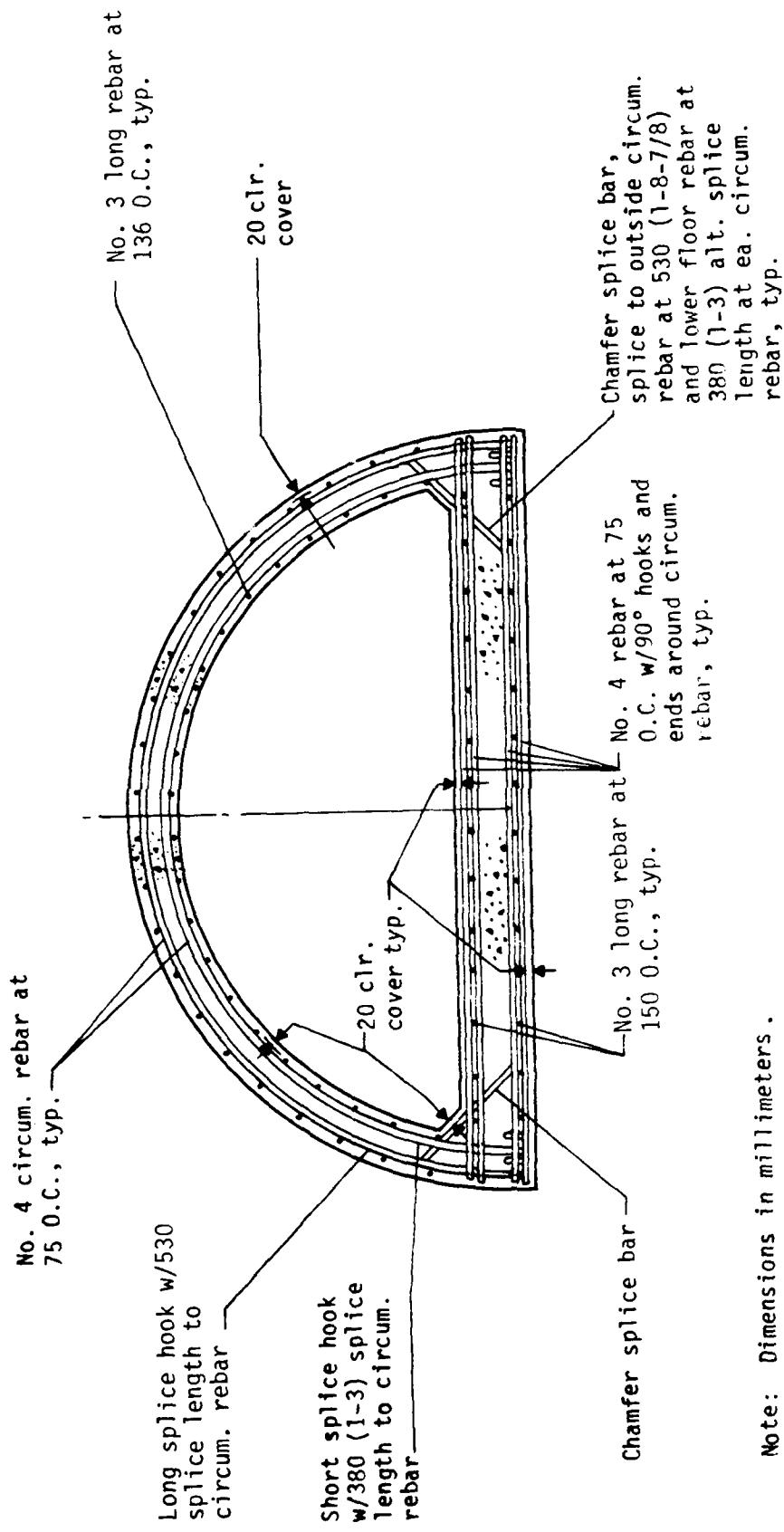


Figure 6. Typical circumferential section.

segments were not perfectly circular, and the inner and outer forms were not concentric (Fig. 7). Therefore, the arch wall was thicker at the crest than at the corner area. Because of these irregularities, allowances for variations in construction were provided. The minimum cover of 20 mm was determined to be the controlling factor, and in some areas the inner and outer circumferential rebars were not evenly spaced.

After the arch segments had been assembled and the outer form placed, the structures were cast. A concrete boom pumping unit and a mobile concrete mixer were used (Fig. 8). The 1.7 m (5.58 ft) height of the open end of the form required a boom pumper, which did a much cleaner job and wasted less concrete than the slurry-type pumper.

The key joint between arch segments A5-2 and A5-3 was formed by inserting a wooden mold into the open end of the arch form at the conclusion of the pour (Fig. 9). After 5 days of curing, the wooden mold was removed and the concrete was ground and patched to create a smooth joint. The joint was oiled, and the mating arch segment was assembled above the previously cast and cured segment. The outer form was then placed and the concrete poured. This procedure provided a well-formed key joint with excellent tolerances. The two arch segments were separated with relative ease.

Another detail included in the A5 structure was fiber optic egress holes. Fiber optic cables and three different types of egress were included in the DAT-3 test to evaluate the survivability of the cables. Steel pipe, hydraulic pressure hose, and no protection were the three egress schemes used (Fig. 10).

The concrete mix design for the DAT-3 structures is shown in Table 1. The design has a water-cement ratio of 0.50. A 9.5 mm (3/8 in) crushed gravel and a standard concrete sand were used as aggregate in the mix. The dry rod-ded weights for the stone and sand were 1518 kg/m^3 (94.8 lb/ft^3) and 1653.1 kg/m^3 (103.2 lb/ft^3), respectively. The results of the concrete compressive tests are shown in Table 2. The values shown are averages for samples taken from each of the two pours. Cyclic compressive tests were also performed on the concrete cylinders. Typical test results are shown in Figure 11. Table 3 gives the average tensile strength test results for the rebars used in the structures.

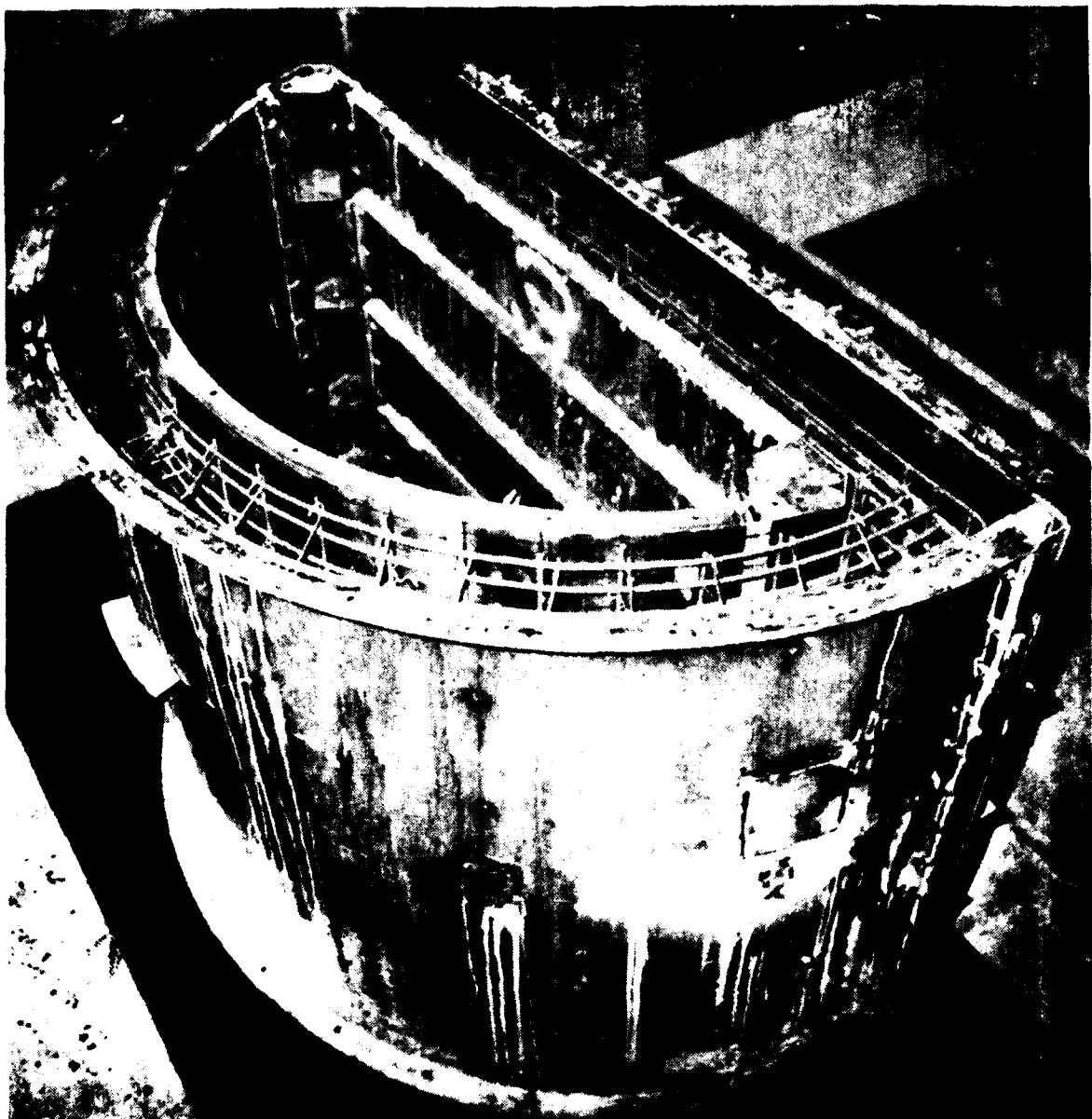


Figure 7. Arch segment forms.

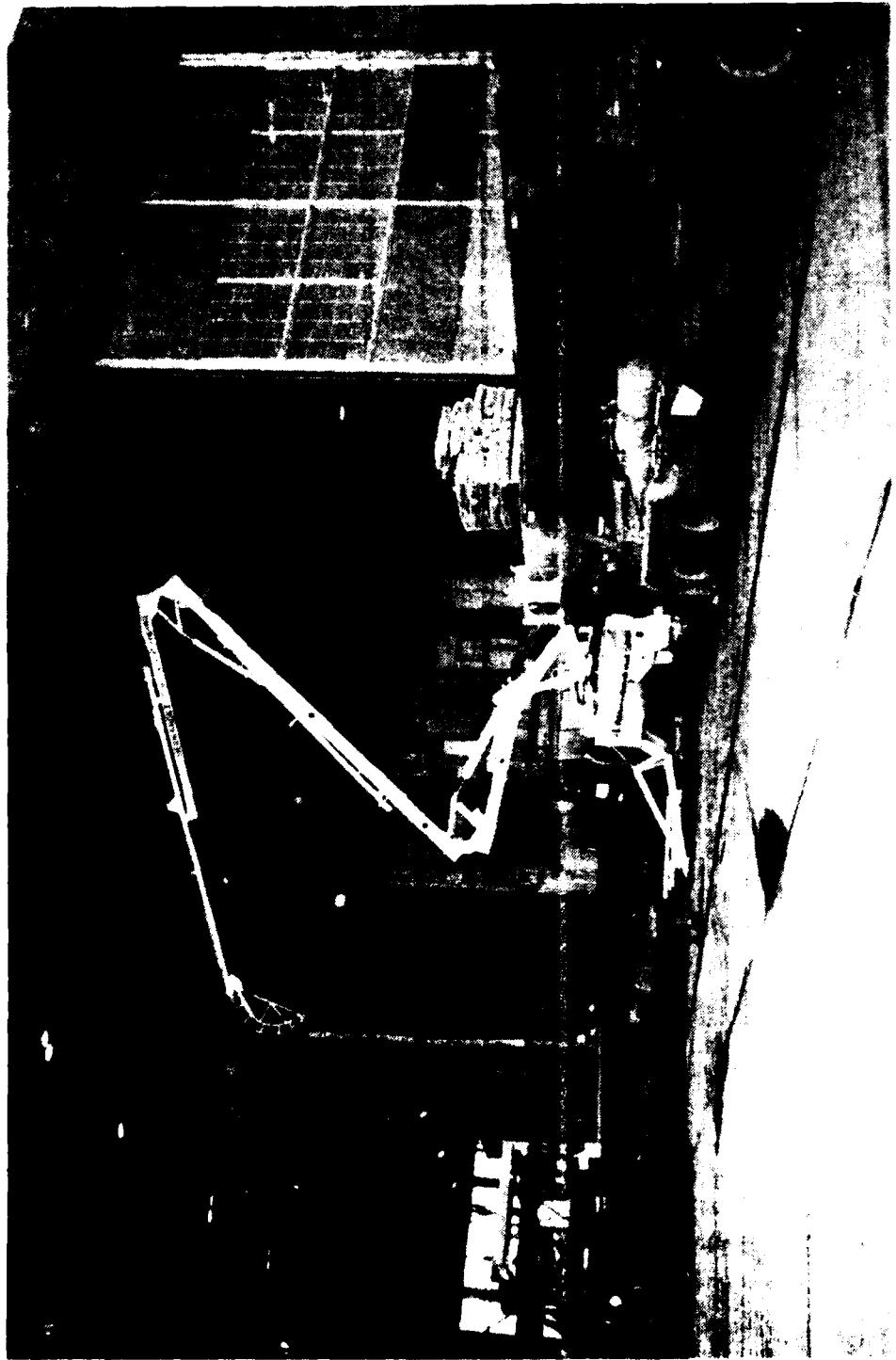
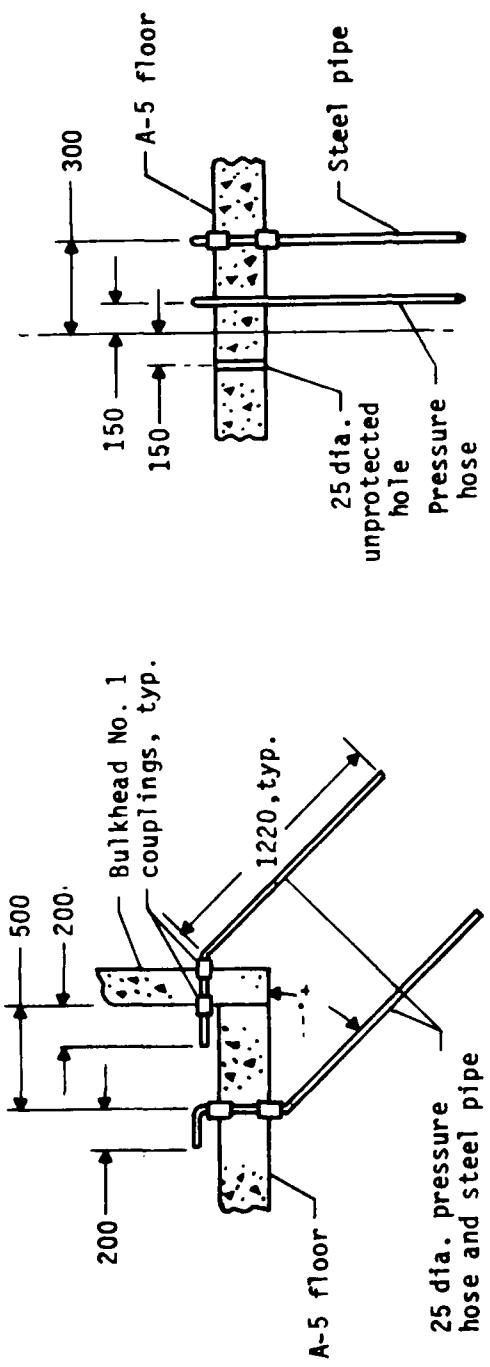


Figure 8. Concrete mobile mixer and boom pumper.



Figure 9. Key-joint wooden mold in place.



Note: Dimensions in millimeters.

Figure 10. Fiber optic cable egress holes.

TABLE 1. CONCRETE MIX DESIGN

Material	Amount	
	per m ³	per yd ³
Sand	680.4 kg	1500 lb
Stone	521.6 kg	1150 lb
Cement	349.3 kg	770 lb
Water	174.6 kg	385 lb
Water	174.6 l	46 gal

Note: Water-cement ratio, by weight, is 0.50. An LA-9 water-reducing admixture was used to increase workability and prevent aggregate segregation. Design concrete strength is 34.5 MPa (5000 lb/in²).

TABLE 2. CONCRETE COMPRESSIVE STRENGTH TESTS

(a) Casting Date 2/21/83.

Arch segment	3-day (2/24/83), MPa (lb/in ²)	7-day (2/28/83), MPa (lb/in ²)	28-day (3/21/83), MPa (lb/in ²)	Test day (5/13/83), MPa (lb/in ²)
A5-3	25.67 (3723)	36.22 (5253)	50.36 (7304)	58.90 (8542)
A6	24.99 (3625)	35.41 (5136)	48.59 (7048)	57.67 (8365)
A7	20.31 (2945)	31.65 (4590)	47.07 (6827)	55.48 (8047)

(b) Casting Date 3/12/83.

Arch segment	3-day ^a	7-day (3/19/83), MPa (lb/in ²)	28-day (4/9/83), MPa (lb/in ²)	Test day (5/13/83), MPa (lb/in ²)
A5-1	---	37.38 (5421)	40.80 (5917)	54.02 (7835)
A5-2	---	36.13 (5240)	43.60 (6323)	53.29 (7729)
A5-4	---	36.22 (5253)	42.80 (6208)	49.26 (7145)

^aNo data.

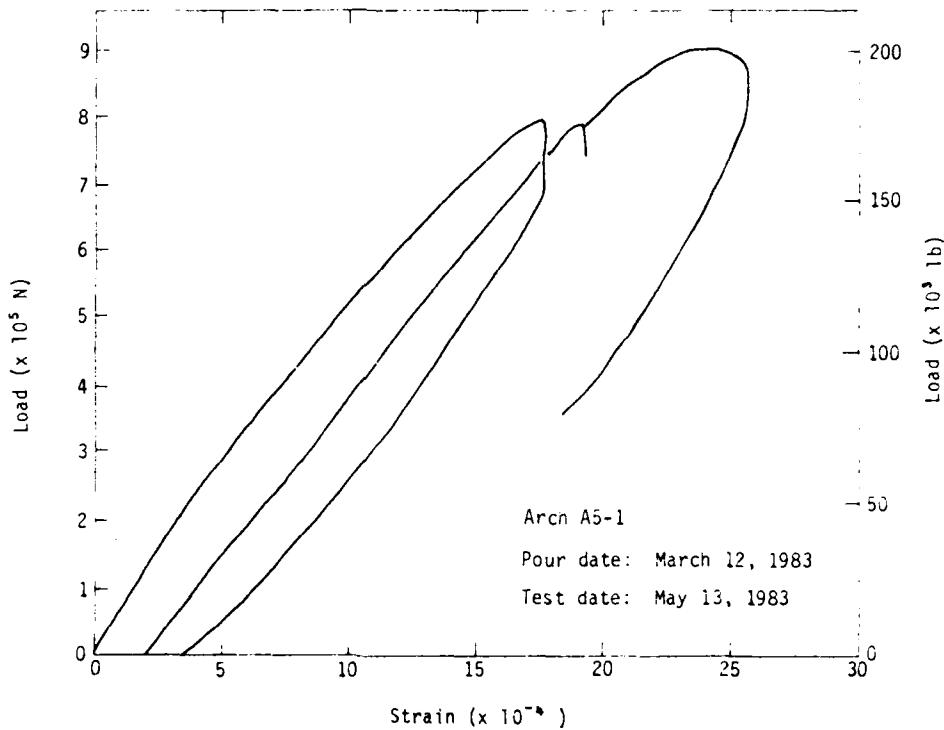


Figure 11. Typical cyclic compression test results.

TABLE 3. REINFORCING BAR TENSILE STRENGTH TESTS

Bar size	Average yield strength, MPa (lb/in ²)	Average ultimate strength, MPa (lb/in ²)
3	521.24 (75,600)	774.28 (112,300)
4	474.36 (68,800)	775.66 (112,500)
6	465.40 (67,500)	771.52 (111,900)

III. TEST SITE OPERATIONS

The Air Force Weapons Laboratory (AFWL) and the New Mexico Engineering Research Institute (NMERI) performed a joint geotechnical investigation at the DAT-3 test site (Ref. 1). A typical geological cross section and soil properties are shown in Figure 12.

Grain size analyses and modified Proctor compaction tests were performed on representative backfill materials for the DAT-3 structures. Results are shown in Figures 13 and 14, respectively. The backfill material was placed at 90 to 95 percent of the in situ density. The geotechnical investigation indicated that the average density for the upper 4 m of material was 1668 kg/m^3 (104.1 lb/ft^3). Therefore, the compacted backfill material was required to be in the range of 1500 kg/m^3 (93.7 lb/ft^3) to 1584 kg/m^3 (98.9 lb/ft^3).

Excavation of the test area required approximately 4 days. The excavated material was stockpiled in the vicinity of the test site. The bottom of the excavation was 2.88 m (9.45 ft) below final grade.

When the excavation was completed, a drill rig was moved onto the test-bed, where it drilled four holes for placement of the free-field gage canisters. Each drill hole was backfilled with a fine sand to the approximate level at which the canister would be located. A small amount of rapid-setting grout was then placed in the bottom of the hole, and the canister was placed at the desired depth. Additional grout was poured into the hole to fix the canister in place. After the grout had been allowed to set for approximately 15 minutes, the placing tool was withdrawn from the canister. The hole was then backfilled to the next canister location and the sequence repeated. The technique is believed to have $\pm 10 \text{ mm}$ ($\pm 0.4 \text{ in}$) tolerance in the vertical direction and $\pm 20 \text{ mm}$ ($\pm 0.8 \text{ in}$) tolerance in the horizontal direction. Seven free-field gage canisters were placed below the 2.88 m (9.45 ft) depth.

Backfill operations began when all of the free-field gages were in place. At the 2.0 m (6.56 ft) depth, additional free-field canisters were placed.

1. Bedsun, David A., and Callahan, John A., "Geotechnical Investigations for the Dynamic Arch Test at McCormick Ranch," Kirtland AFB, NM, December 1982.

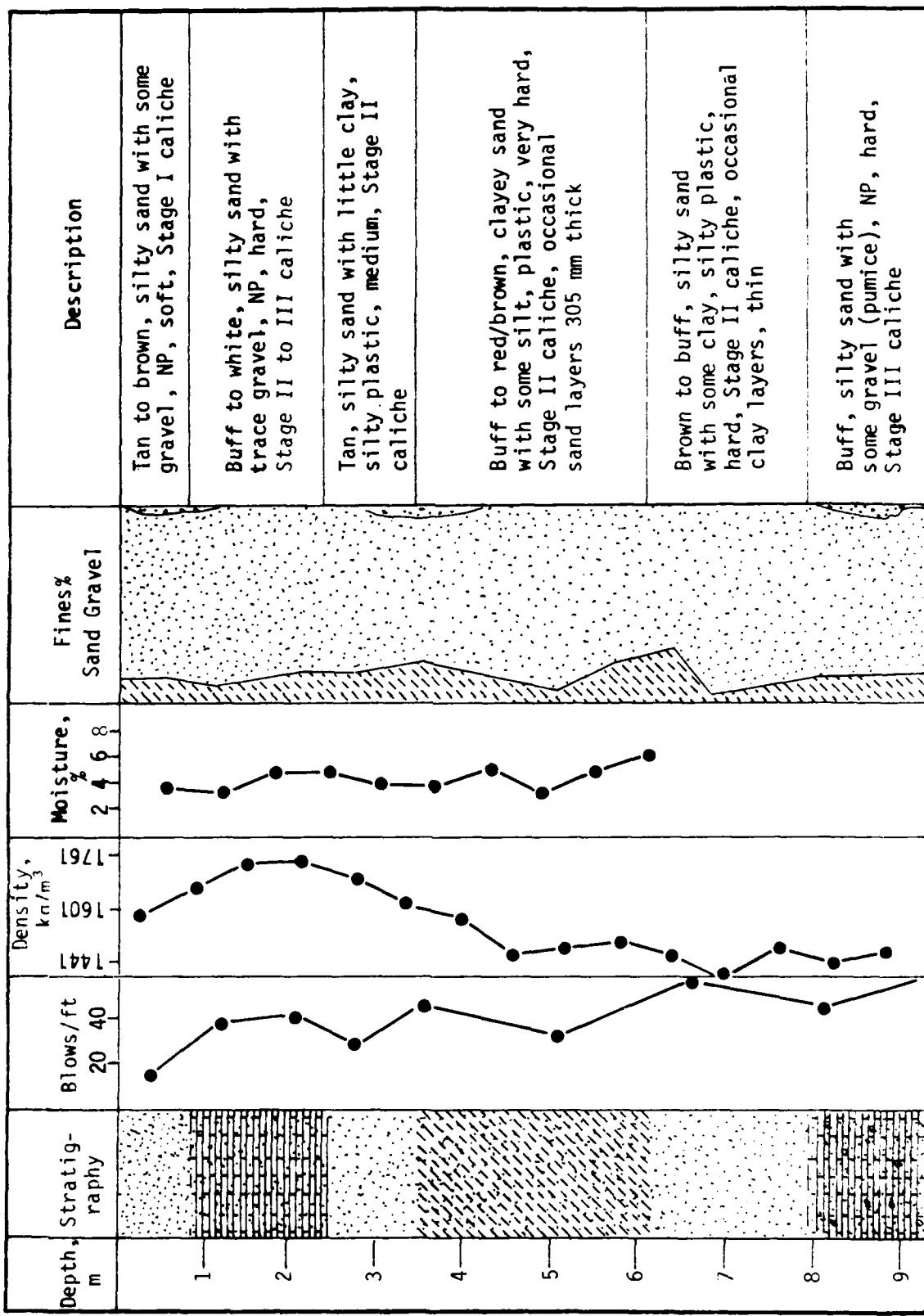


Figure 12. Generalized stratigraphy and average index soil properties (Ref. 1).

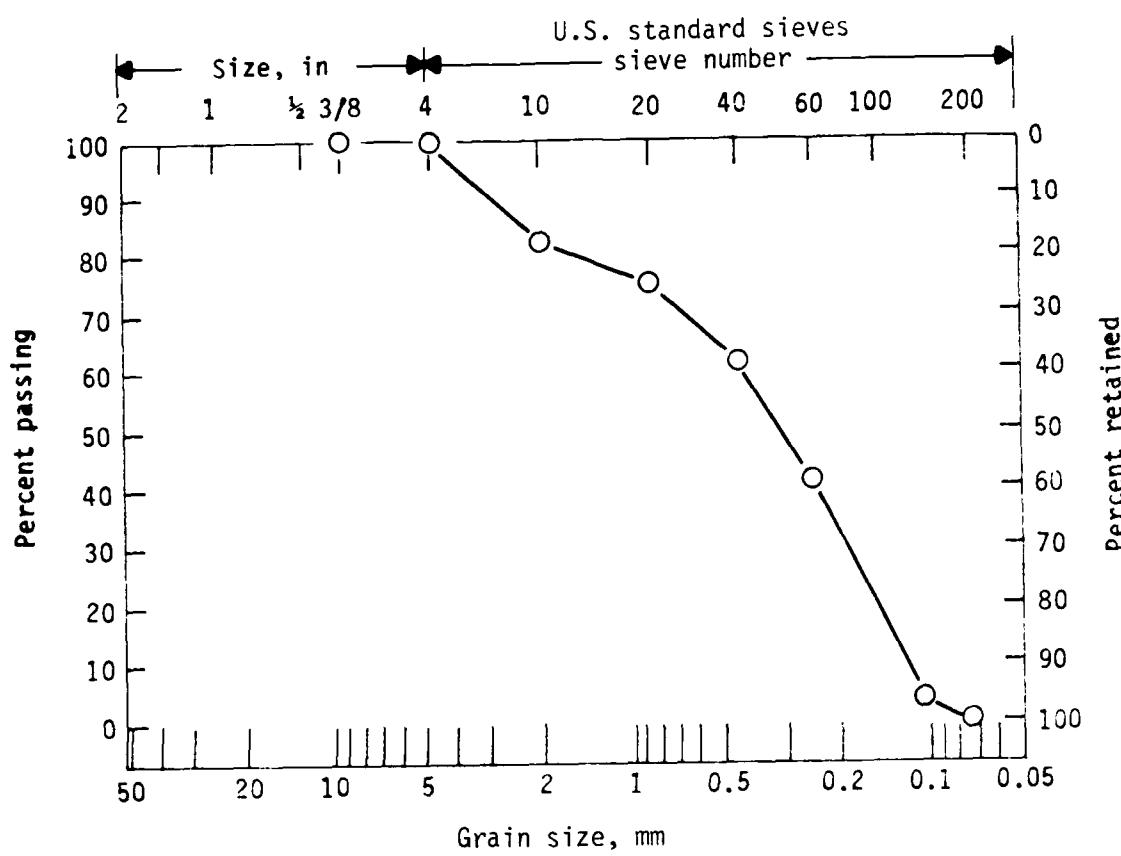


Figure 13. Backfill material graduation.

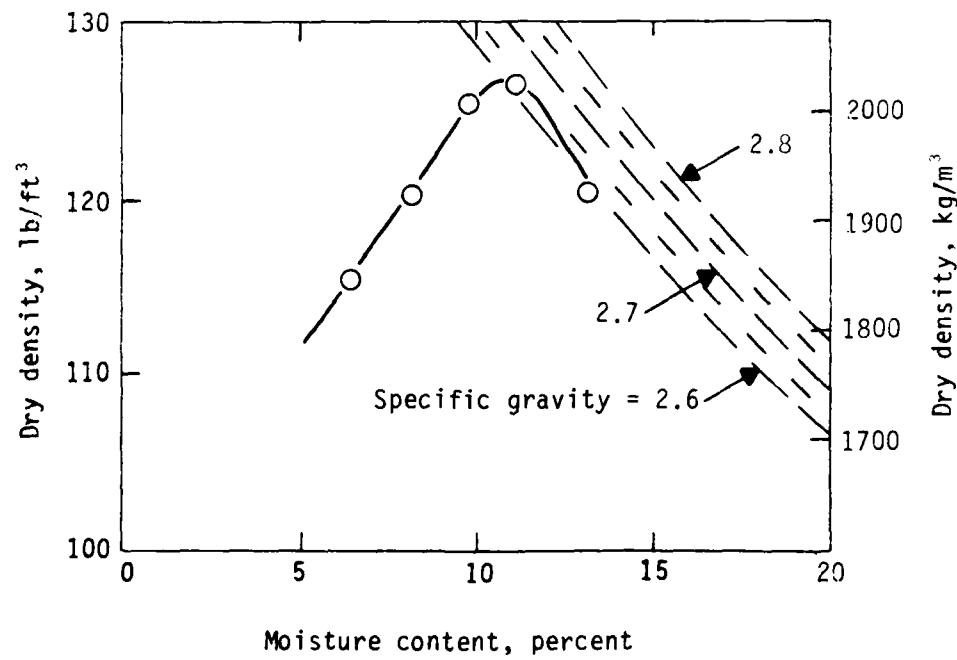


Figure 14. Backfill material compaction test results.

These emplacements were manually backfilled with native material and then hand-compacted. At the 1.88 m (6.17 ft) depth, trenches were excavated for the free-field, near-field, and structure instrumentation. The trenches were approximately 1 m (3.28 ft) deep. The area for the footings of the A6 structure was also excavated and cast with 34.5 MPa (5000 lb/in²) concrete.

The accelerometers and the normal stress gages were installed in the arches before the structures were placed in the field. All gages were checked for continuity and the as-built locations recorded. Design and as-built instrumentation lists are included in Appendix B.

Figures 15 and 16 show the emplacement of the arch segments at a depth of 1.88 m (6.17 ft). Portions of the instrumentation cable trenches are also visible in the photographs. The bottoms of the trenches were lined with a fine sand before the cables were laid. After all of the cables had been placed in the appropriate trenches, they were covered with sand. The trenches were then backfilled with native soil and compacted (Fig. 17). Figure 18 shows a completed instrumentation wiring and cable harness for structure A7. The bulkhead for structure A5, with the square structure instrumentation egress port and the three fiber-optic egress ports, is shown in Figure 19.

After the excavation was backfilled, a double-drum vibratory compactor (Fig. 20) was used to compact it to the final grade elevation. It was observed early in the backfill operation that if uniform compaction were to be obtained, the excavated material would have to be blended extensively by a grader. This allowed the soil moisture content to attain a mean value of approximately 8 percent. Because a density of 90 to 95 percent of in situ density was required, use of the vibrator with the compactor was not necessary. A frequency plot of the density measurements made with the nuclear density device during the backfill operations indicates a normal distribution of measurements (Fig. 21). The specific density measurements are available in a NMERI task report (Ref. 2).

The last operation in the test-bed preparation was the installation of the airblast gage canisters and the shallow near-field and free-field

2. Baird, Glenn T., Backfill and HEST Overburden Material Properties for the DAT-3 Test Event, NMERI Task Report to AFWL, June 1983.

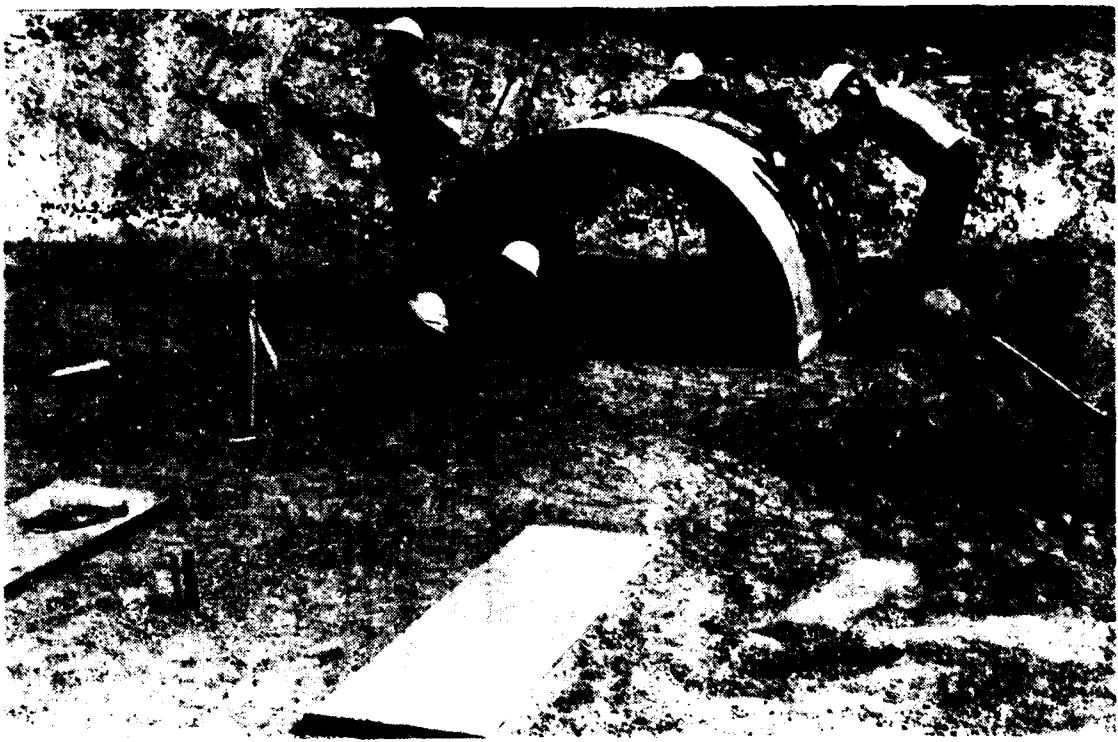


Figure 15. Arch A7 placement.



Figure 16. Arch A5-1 placement.

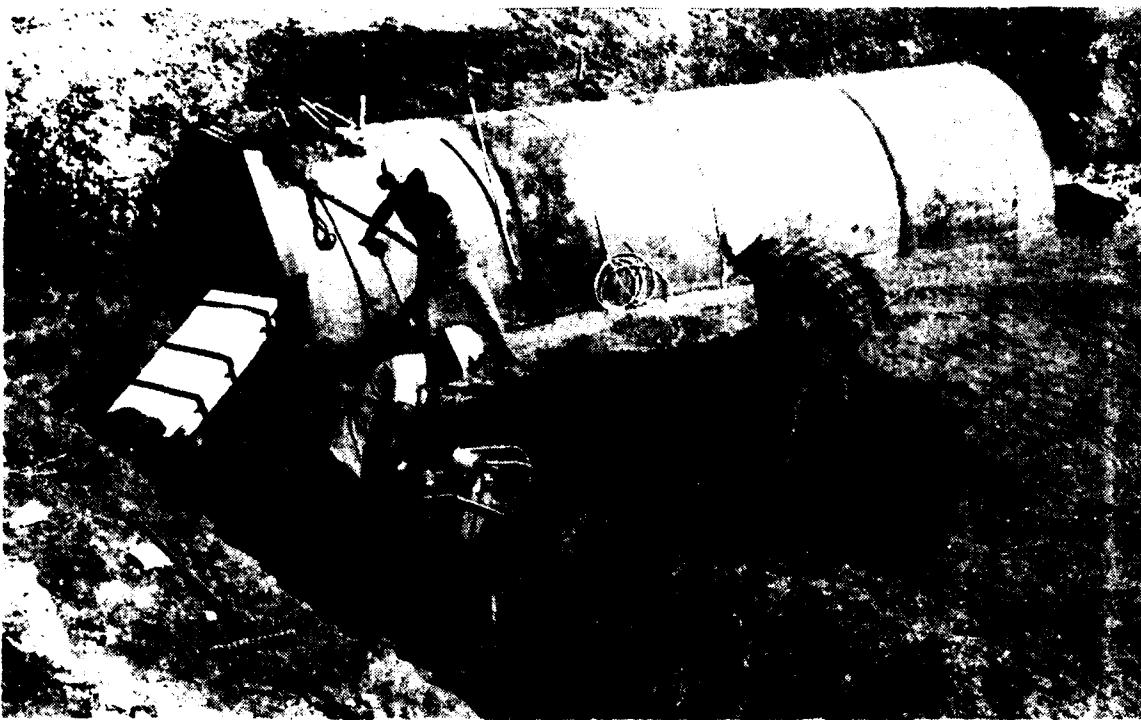


Figure 17. Backfilling and compaction of cable trenches.



Figure 18. Instrumentation wiring and cable harness.

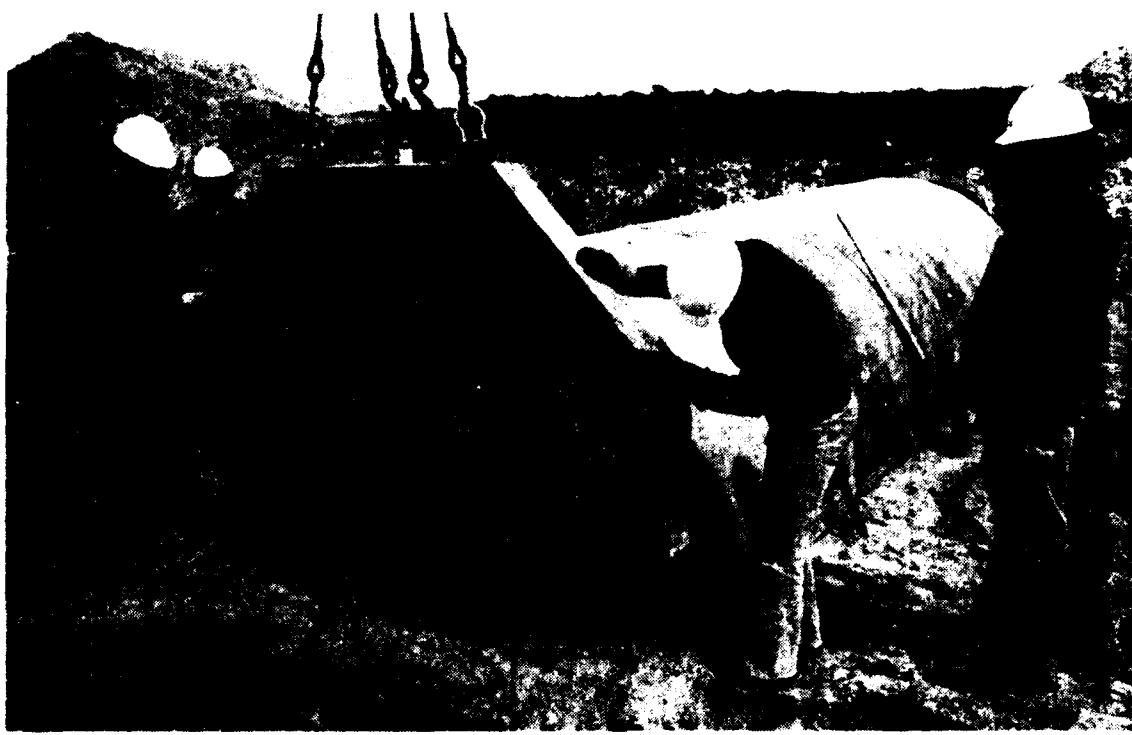


Figure 19. Bulkhead placement.

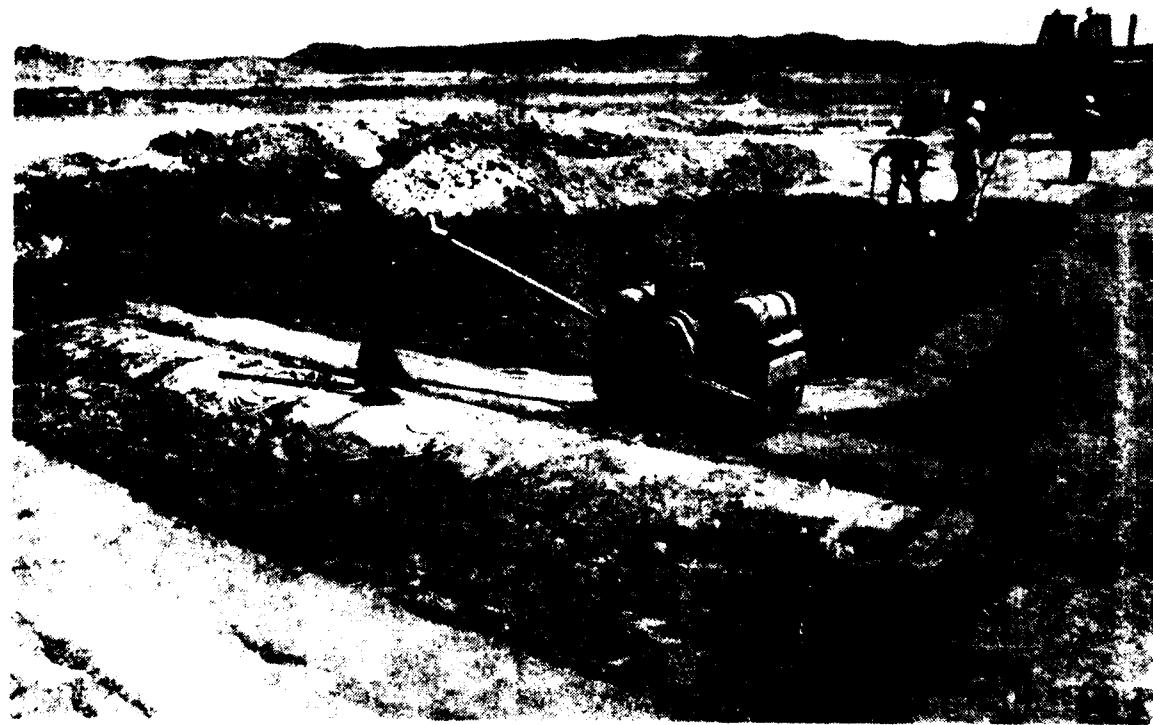


Figure 20. Backfill compaction.

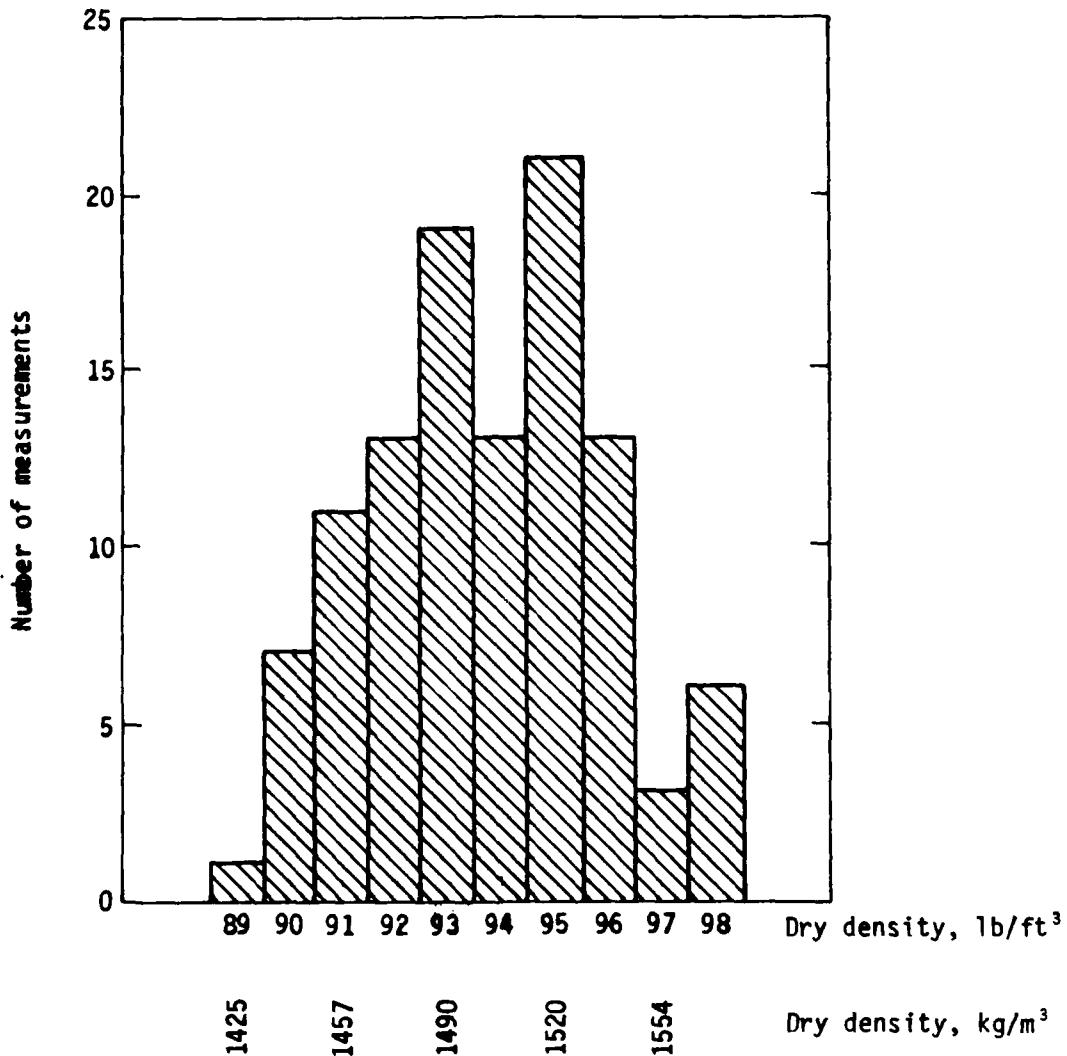


Figure 21. Density measurement frequency curve.

instrumentation canisters. Shown in Figure 22 are the concrete airblast gage canisters, the remaining instrumentation, and the cable trenches at the test-bed surface. The trenches were backfilled and compacted to final grade after cable connections and continuity checks were complete.

The HEST cavity consisted of a 51 mm (2 in) foam bottom layer on which the first layer of explosives was placed. The second foam layer was 25 mm (1 in) thick; on this, a second layer of explosives was placed. Finally, a third layer of foam, 16 mm (5/8 in) thick, was placed on top of the second explosives layer. The explosive was 400 grain/ft detonation cord, placed at an angle of 29.3 deg. The 100 grain/ft reignition cord was run at an angle of 27.40 deg. Figure 23 shows the placement of the second layer of detonation cord on the foam.

After the photopoles were in place, the foam HEST cavity was covered with 1.57 m (5.15 ft) of native material (Fig. 24). As-built measurements of the foam cavity indicated a pretest thickness of 0.101 m (0.331 ft). The charge density was measured at 17.94 kg/m³ (1.12 lb/ft³). The average overburden density ranged from 1395 kg/m³ (87.1 lb/ft³) to 1417 kg/m³ (88.5 lb/ft³). Gradation curves and modified Proctor compaction test results are shown in Figures 25 and 26, respectively. The completed HEST test-bed is shown in Figure 27.

The DAT-3 test was performed on Friday, 13 May 1983. Posttest recovery operations began on Monday, 16 May. The structures were excavated, and all gages encountered during the excavation were recovered. The excavated test-bed and structures are shown in Figure 28.

Posttest density measurements were made on the overburden fallback material at the top of the test-bed and at the approximate depth of the floor of the arch structures.

Six types of measurements were made on the fallback material at the site:

Minimum wet density	1376 kg/m ³ (85.9 lb/ft ³)
Maximum wet density	1480 kg/m ³ (92.4 lb/ft ³)
Average wet density	1425 kg/m ³ (88.95 lb/ft ³)
Standard deviation	33 kg/m ³ (2.07 lb/ft ³)



Figure ?? Near-surface instrumentation and cable trenches.



Figure 23. Detonation cord placement.

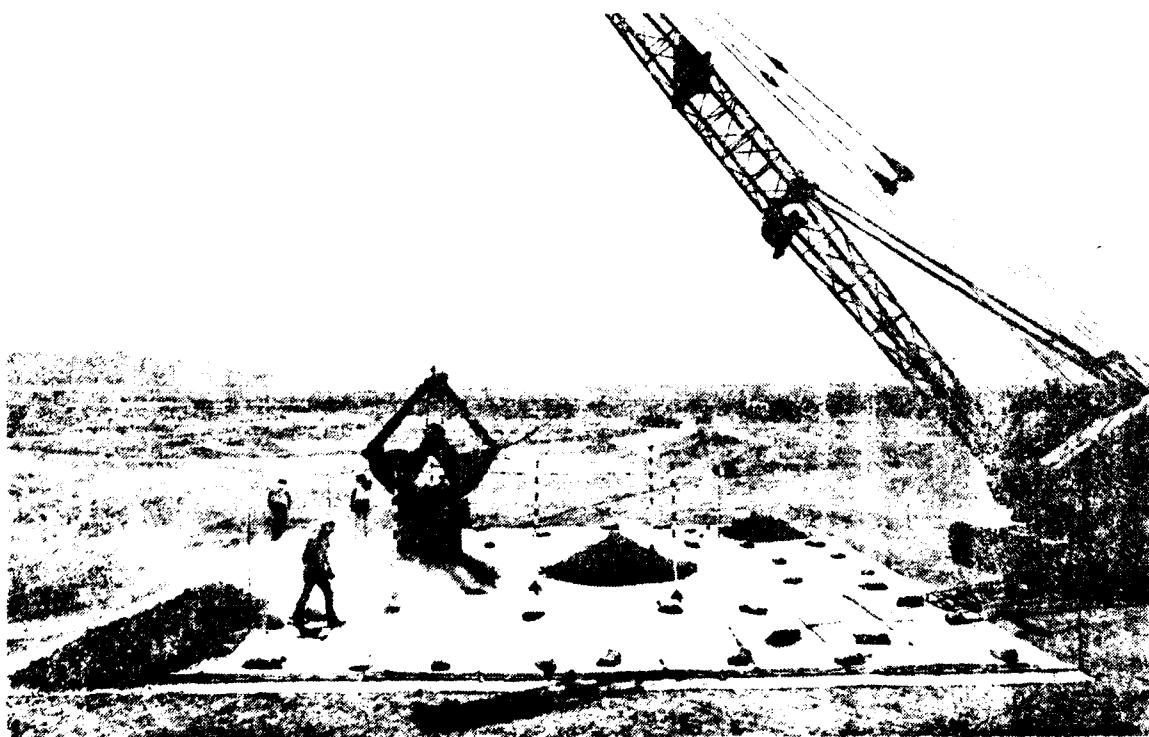


Figure 24. HEST overburden placement.

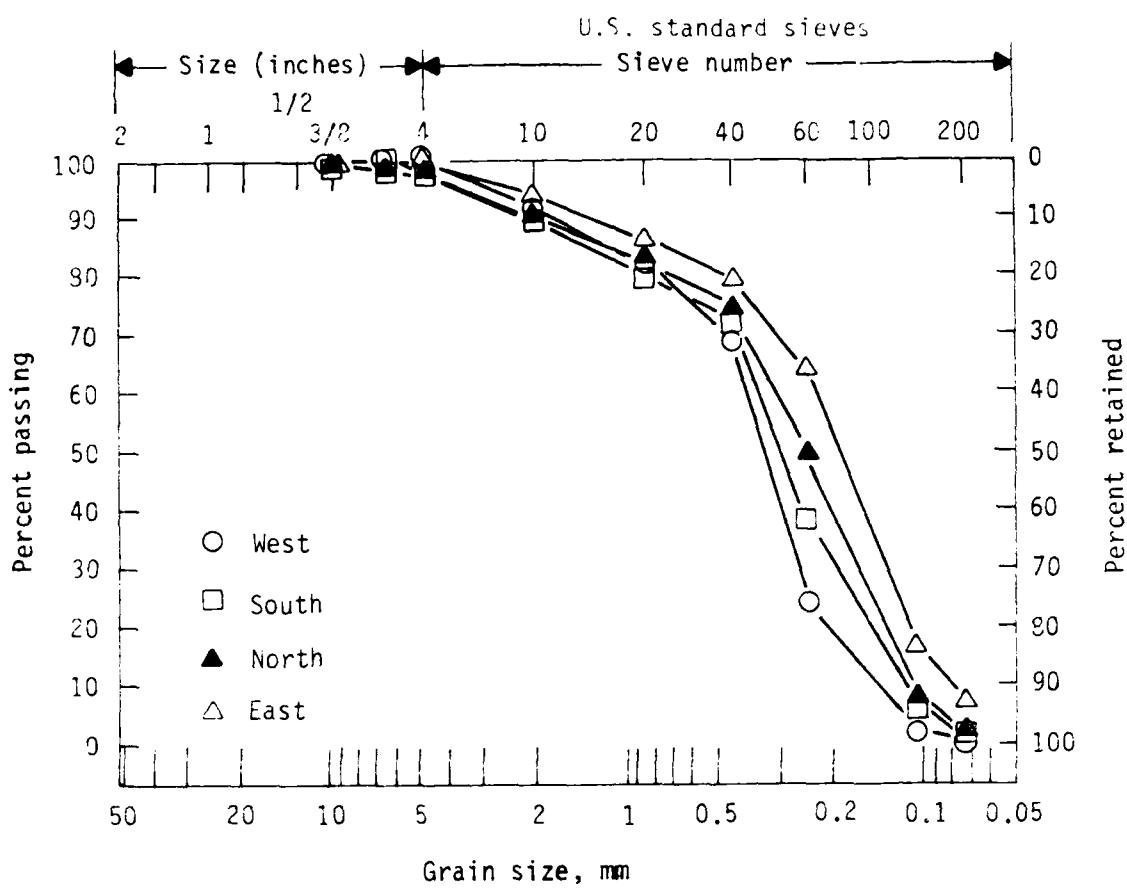


Figure 25. Overburden gradation curves.

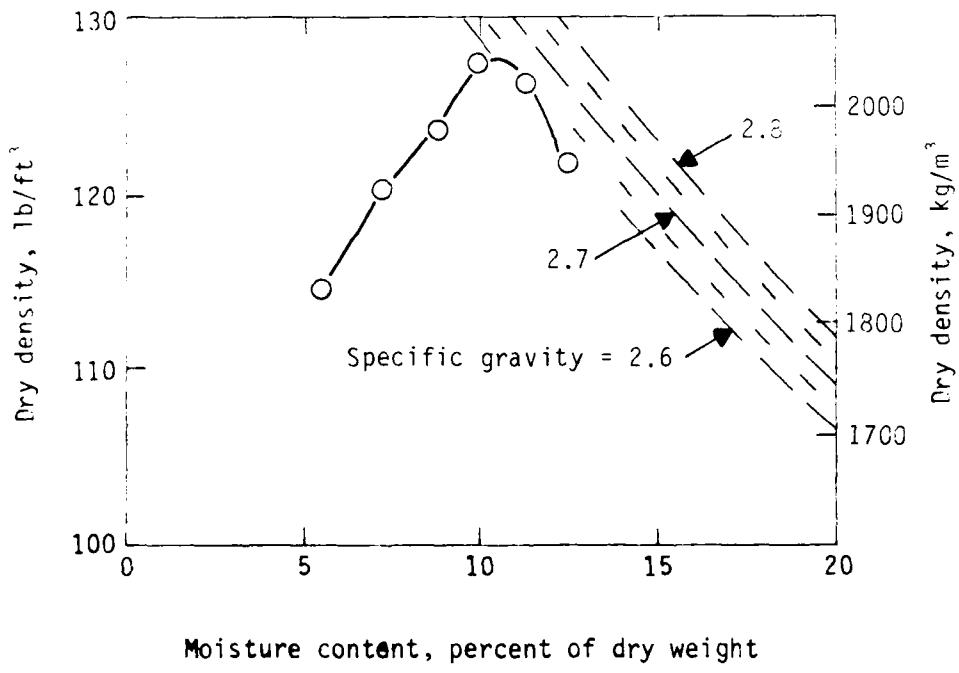


Figure 26. Overburden compaction test results.



Figure 27. Completed DAT-3 test site.



Figure 28. Excavated test-bed and structures.

Four measurements were made on the top of the test-bed. Five measurements were requested, but damage to the driving rod used to create a guide-hole for the density sensor precluded the taking of the fifth measurement.

Minimum dry density	1831 kg/m ³ (114.3 lb/ft ³)
Maximum dry density	1941 kg/m ³ (121.2 lb/ft ³)
Average dry density	1863 kg/m ³ (116.28 lb/ft ³)
Standard deviation	52 kg/m ³ (3.23 lb/ft ³)

During gage recovery, five measurements were made at the depth of the structure floors:

Minimum dry density	1439 kg/m ³ (89.81 lb/ft ³)
Maximum dry density	1629 kg/m ³ (101.68 lb/ft ³)
Average dry density	1515 kg/m ³ (94.56 lb/ft ³)
Standard deviation	71 kg/m ³ (4.42 lb/ft ³)

The pretest and posttest locations of the blast pressure canisters are listed in Table 4. The pretest elevations of gages 0002, 0005, 0007 and 0010 were taken at the top of the concrete pad. After the casting was complete, B-filter gage protection units were used on these gages. In order to have the B-filters flush with the ground surface, the canisters for these gages had to be set deeper than the other canisters. The posttest locations of these gages were measured at the tops of the B-filters. The average downward displacement for the blast pressure canisters was 340 mm (13.4 in.).

Pretest and posttest locations of the structures are presented in Table 5. The survey locations were at the crest of the arch on each end and at the normal stress gage location at the crest, approximately in the center of the arch. When the structure survey had been completed, the positions of arch segments A5-2 and A5-3 were reversed. That is, the arch segments, instead of being in sequential order in the positive X-direction, were in the following order: A5-1, A5-3, A5-2, and A5-4. As a result, the upstream instrumentation (gages designed to be placed on the face of the structure toward the HEST initiation) was actually downstream and reversed. However, the reversal had no adverse effect on the objectives of the instrumentation or on the test. The discrepancies are noted on Table 5 and on the instrumentation list in Appendix B; but the gage locations for arch segments A5-2 and A5-3 shown on the design drawings in Appendix A do not agree with those

TABLE 4. BLAST PRESSURE GAGE LOCATIONS

Blast pressure gage number	Pretest location, mm (ft)			Posttest location, mm (ft)		
	X	Y	Z	X	Y	Z
0001	2450	2840	0 (0.00)	2349	2835	-366 (-1.200)
0002	6535	2332	-21 (-0.07)	6531	2317	-378 (-1.240)
0003	6857	2317	0 (0.00)	6837	2310	-375 (-1.230)
0004	10957	2848	0 (0.00)	10976	2880	-383 (-1.255)
0005	3981	6327	-24 (-0.08)	3915	6365	-349 (-1.145)
0006	4304	6305	-2 (-0.005)	4213	6320	-343 (-1.125)
0007	9066	6292	-15 (-0.05)	9027	6360	-374 (-1.228)
0008	9407	6313	0 (0.00)	9249	6310	-399 (-1.310)
0009	2436	8834	6 (0.02)	2323	8833	-343 (-1.125)
0010	6549	8783	-21 (-0.07)	6475	8830	-302 (-0.990)
0011	6876	8785	-3 (-0.01)	6775	8826	-300 (-0.985)
0012	10961	8835	0 (0.00)	10943	8911	-361 (-1.185)
0013	4005	12328	-3 (-0.01)	3955	12319	-291 (-0.955)
0014	4326	12336	-6 (-0.02)	4217	12355	-297 (-0.975)
0015	9068	12358	3 (0.01)	8977	12419	-297 (-0.975)
0016	9384	12327	6 (0.02)	9220	12367	-306 (-1.005)

TABLE 5. STRUCTURE LOCATIONS

Survey point description	Pretest			Posttest		
	X, mm	Y, mm	Z, mm (ft)	X, mm	Y, mm	Z, mm (ft)
S. Side A6	3243	4560	-588 (-1.930)	3220	4634	-884 (-2.900)
Gage 115 (MN 6010)	4005	4530	-590 (-1.935)	3961	4586	-892 (-2.925)
N. Side A6	4852	4514	-590 (-1.935)	4771	4556	-890 (-2.920)
S. Side A7	8291	4524	-588 (-1.930)	8254	4628	-917 (-3.010)
Gage 110 (MN 6015)	9060	4524	-587 (-1.925)	9002	4629	-911 (-2.990)
N. Side A7	9861	4510	-585 (-1.920)	9806	4621	-902 (-2.960)
S. Side A5-1	3180	10397	-573 (-1.880)	3119	10345	-843 (-2.765)
N. Side A5-1	4810	10426	-582 (-1.910)	4762	10446	-896 (-2.940)
S. Side A5-3	4922	10427	-585 (-1.920)	4898	10504	-1009 (-3.310)
N. Side A5-3	6445	10503	-585 (-1.920)	6358	10564	-1361 (-4.465)
S. Side A5-2	6601	10521	-582 (-1.910)	6553	10586	-1408 (-4.620)
Gage 106 (MN 6001)	7465	10517	-576 (-1.890)	7378	10606	-1527 (-5.010)
N. Side A5-2	8213	10532	-576 (-1.890)	8049	10513	-1018 (-3.340)
S. Side A5-4	8332	10544	-588 (-1.930)	8266	10587	-933 (-3.060)
Gage 107 (MN 6008)	9173	10523	-585 (-1.920)	9000	10554	-887 (-2.910)
N. Side A5-4	9881	10511	-582 (-1.910)	9766	10514	-847 (-2.780)

shown in the instrumentation list in Appendix B. The as-built locations of the gages accurately reflect the actual positions of the gages in the field.

The passive displacement gages located in the structures indicated an average maximum compression of 215 mm (8.5 in). The individual measurements are presented in Table 6.

Arch segments A5-1, A5-4, A6 and A7 displayed similar types of damage. (See Figures 29 through 35 and the photographs and drawings in Appendix C.) The floors of the structures buckled inward because of the downward movement of the arch walls. Extensive cracking in the floor occurred in the central portion, starting at approximately 152 to 228 mm (6 to 9 in) from the interior corner or chamfer. After the arch walls had moved sufficiently to compact the underlying soil, a longitudinal crack developed on both sides of each arch. Each crack began at the end point of the circumferential splice hook cast in the corner of the wall and ran along the outside of the arch, approximately 530 mm (20.9 in) above the base of the structure.

TABLE 6. PASSIVE DISPLACEMENT GAGES

Measurement number	Maximum compression displacement, mm (in)	Final displacement from initial location, mm (in)
7001	234 (9.2)	191 (7.5)
7002	--- ^a	--- ^a
7003	--- ^a	--- ^a
7004	--- ^a	--- ^a
7005	--- ^a	--- ^a
7006	--- ^a	--- ^a
7007	235 (9.25)	206 (8.1)
7008	210 (8.25)	152 (6.0)
7009	196 (7.7)	157 (6.2)
7010	208 (8.2)	175 (6.9)
7011	211 (8.3)	175 (6.9)

^aGage damaged; no data obtained.



Figure 29. North side A6.

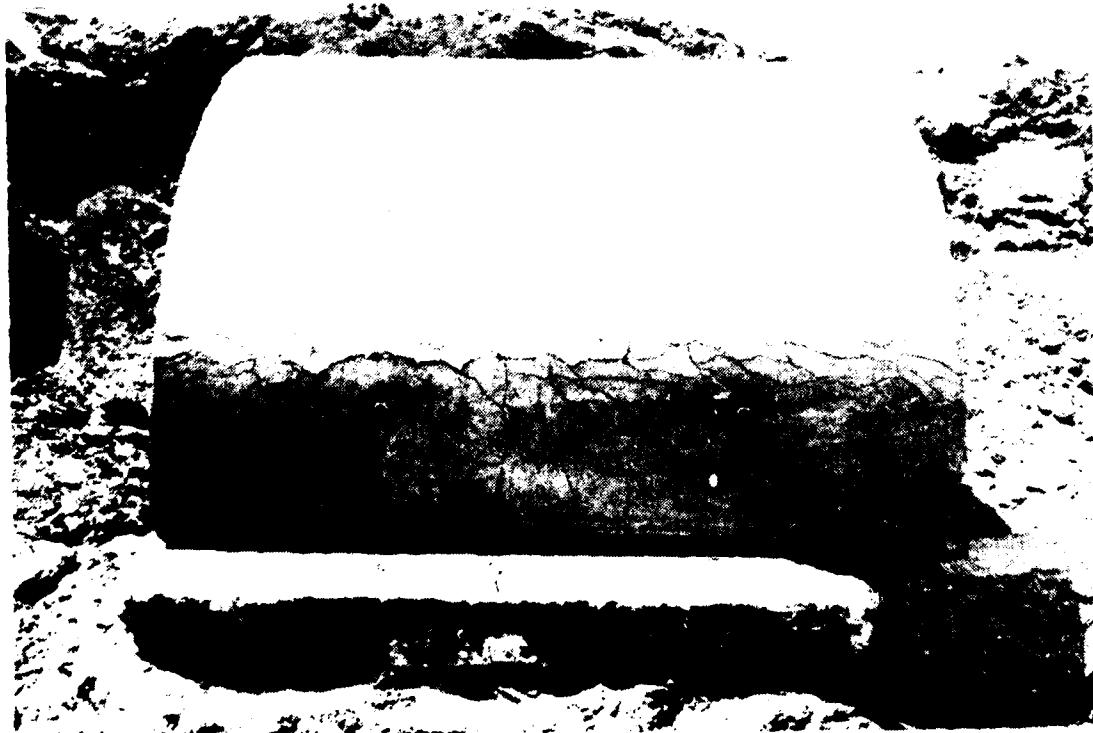


Figure 30. South side A6.



Figure 31. North side A7.

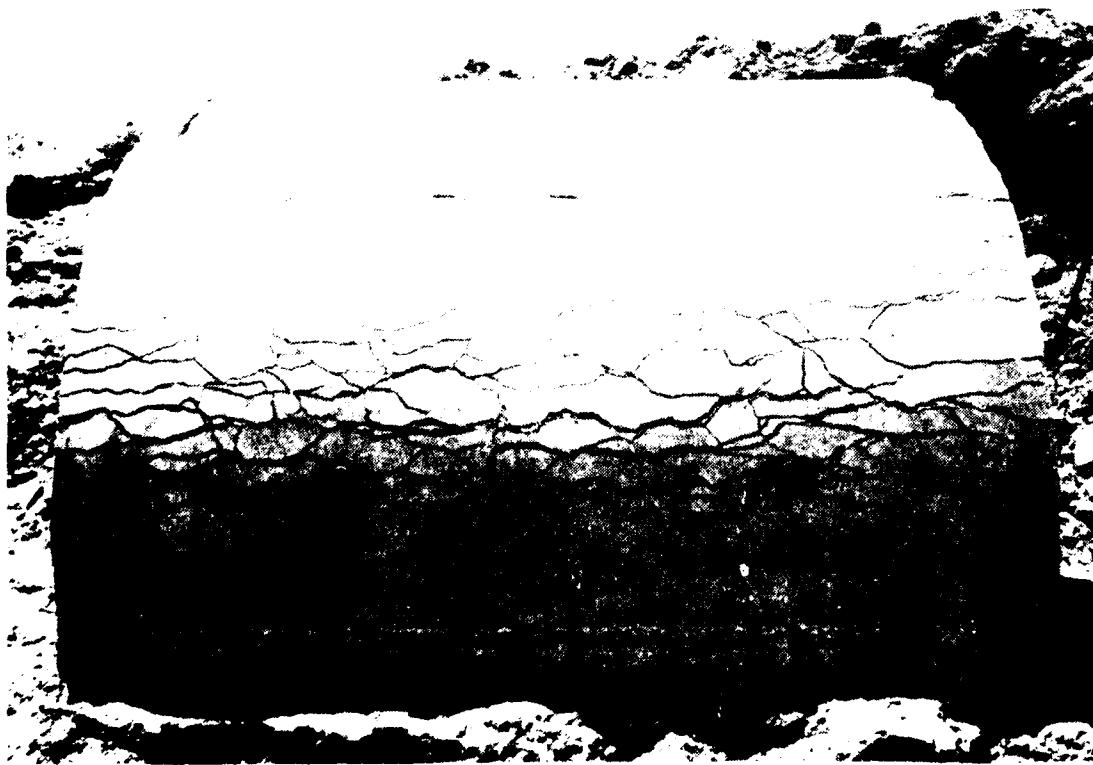


Figure 32. South side A7.



Figure 33. South side A5.

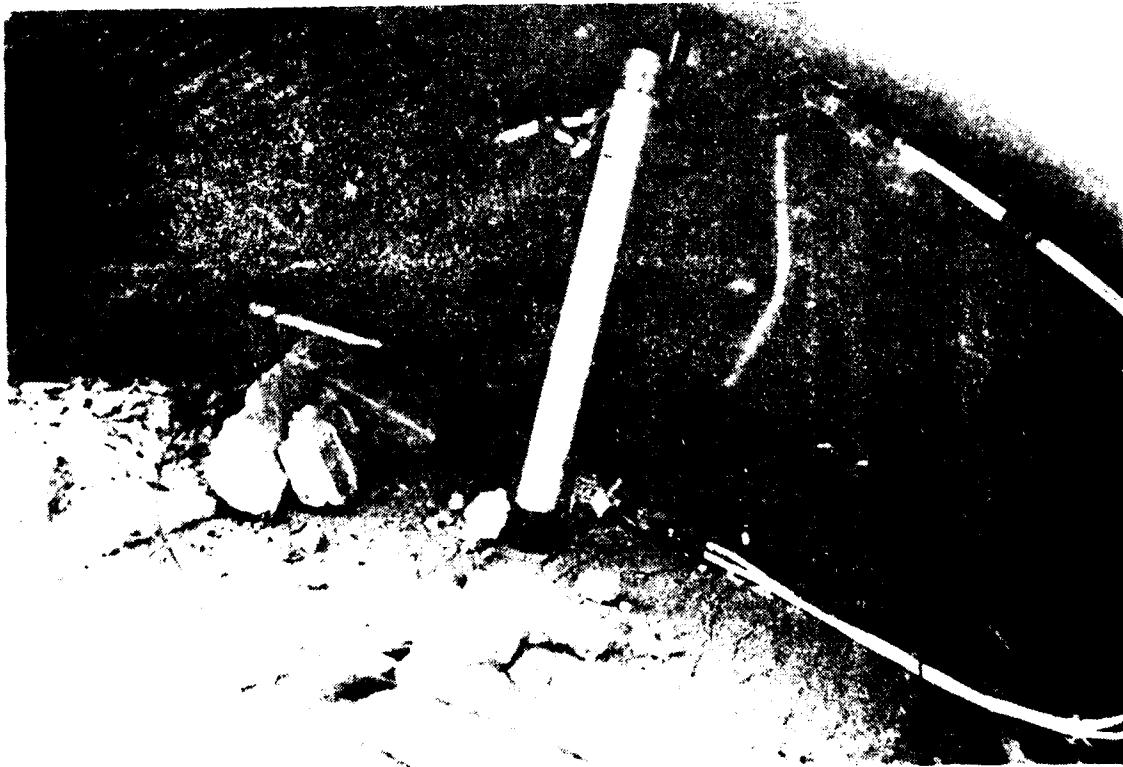


Figure 34. Interior of arch A5.

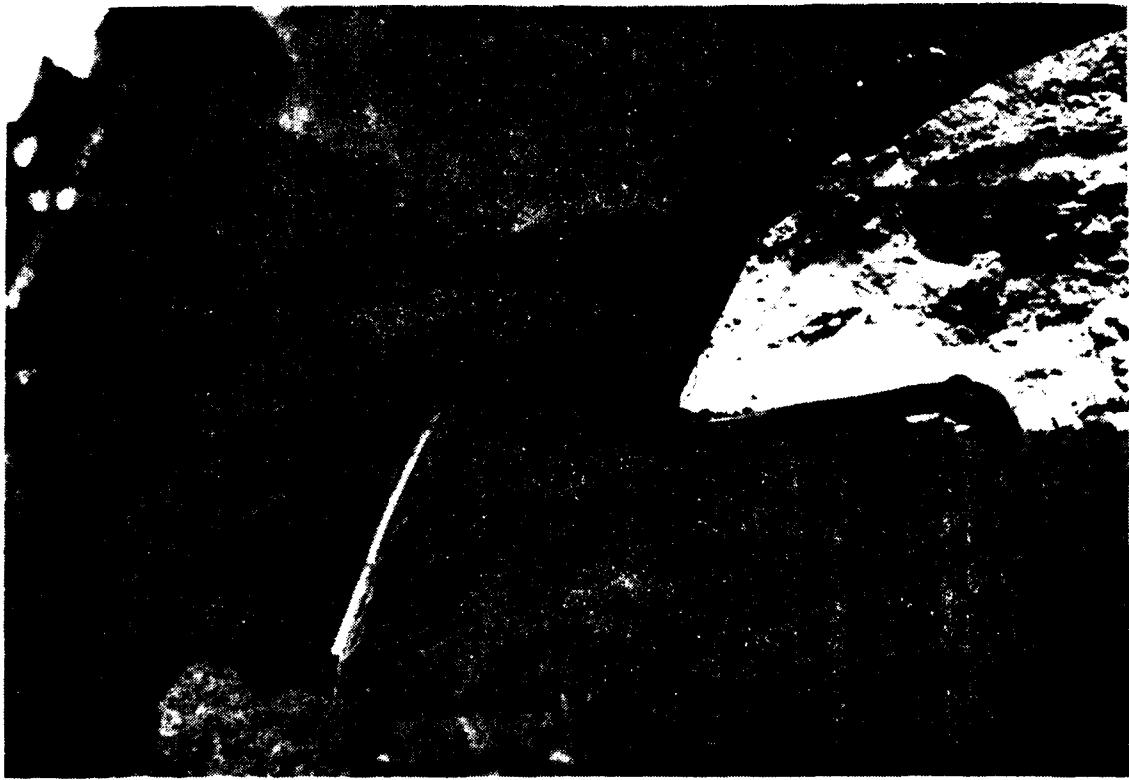


Figure 35. Interior of Arch A7.

Contributing to the development of the crack was the inward bending of the floor section, which compounded the bending stresses in the arch wall caused by the corner rebar splices.

Arch segments A5-2 and A5-3 experienced a catastrophic failure that caused the arch wall to collapse completely onto the floor. All the arch segments were identical in design except for the joint detail between arch segments A5-2 and A5-3; therefore, it appears possible that the key joint for load transfer was the source of the failure.

The impulse developed by the HEST, as indicated by the photopole and time-of-flight (TOF) sphere data, was as calculated. The mean peak impulse was 0.0635 MPa-s. The photopole data are presented in Table 7 and Appendix D. The timing circuit of one of the three TOF spheres did not turn off at impact. The remaining two spheres indicated total flight times of 6.29 and 6.25 s. The average flight time, 6.27 s, corresponds to an impulse value of 0.0673 MPa-s.

TABLE 7. PHOTOPOLE DATA ANALYSIS

Photopole number	Film 1B		Film 2B		Film 2C	
	Average velocity, m/s	Peak impulse, MPa-s	Average velocity, m/s	Peak impulse, MPa-s	Average velocity, m/s	Peak impulse, MPa-s
P001	27.7	0.0625	27.725	0.0625	28.125	0.062
P002	27.7	0.0605	27.725	0.061	28.125	0.060
P003	27.7	0.060	27.725	0.062	--- ^a	--- ^a
P004	26.25	0.0587	26.65	0.0595	--- ^a	--- ^a
P005	26.25	0.0565	26.65	0.0575	26.5	0.0575
P006	27.9	0.0675	29.5	0.0695	28.75	0.068
P007	27.9	0.069	29.5	0.0685	28.75	0.068
P008	27.9	0.069	--- ^a	0.069	28.75	0.068

^aNo data plotted.

CONCLUSIONS

The DAT-3 structures were easily assembled because the rebar splice hooks allowed specified tolerances to be attained. Because the arch forms were not perfectly concentric, the walls of the models were thicker at the crest than at the corners. To eliminate these deviations, improved forms should be constructed.

The wooden mold used to form the key joint performed well, and a very tight joint was constructed.

Weldable-type rather than bondable-type strain gages were installed on the rebar. The weldable-type gage is more expensive than the bondable-type, but requires a less critical surface preparation and saves a great deal of time.

Installation of the structure instrumentation prior to placement of the structures allowed work to progress in the field with minimal down time for connecting instrumentation cables. However, close supervision must be provided to ensure that the structures are placed properly if the models are similar in design and instrumentation.

IV. INSTRUMENTATION

This section describes the transducers, hardware and placement techniques used for the instrumentation of the DAT-3 test and includes a summary of the instrumentation results.

TRANSDUCERS, HARDWARE AND PLACEMENT

Acceleration--Endevco 2262C, 2260A and 2264A accelerometers were used for measuring both structural acceleration and free-field acceleration. The gage mounts for the structural accelerometers were placed in the rebar before the arches were poured. Between the pouring and the field placement, all of the gages were placed on the mounts and the cables were routed in bundles. Bundling the cables provides cable protection and also helps minimize cable motion during the test.

Free-field gages were mounted in epoxy minicanisters and microcanisters. Free-field accelerometer canisters, below the 3-m depth, were placed in the test-bed while it was excavated at 3 m. These canisters were placed in holes using lock-in grout for setup and native soil for backfill. Free-field canisters above 3 m were placed as the test-bed was being backfilled. All of the free-field gages used rubber hose for protection. The cables for all of the gages set at 1 m or above were bundled and routed at 1 m. Cables for all other canisters were bundled and routed at a depth of 3 m.

Pressure--Blast pressure was measured with Kulite KKS-11-375-10K pressure gages mounted in standard AFWL hardware. The L12 debris shields were used in 12 of the 16 modules and B-filter hardware was used in the other 4. The AFWL hardware was then set into a NMERI concrete blast pressure pad. The L12 system was used for its high mechanical filter rate at 7000 Hz. This insures a high data bandwidth. But since the L12 system is vulnerable to failure from high frequency spikes, the more survivable, but less accurate, B-filter system was also fielded to ensure a minimum of data recovery. The blast pressure pads were placed in the test-bed when it was backfilled to a depth of 1 m. Cables were routed at 1 m, and rubber hose was used for protection.

Interface pressure was measured with NMERI NS gages in NMERI normal stress mounts. The interface pressure mounts and gages were constructed

and placed in the field identical to the procedure previously discussed for structural accelerometers.

Strain--Rebar steel strain was measured with Alitech SG 159-11 weldable strain gages in a 2-active-arm bridge configuration which canceled out bending. The gages were attached to the same rebar used in measuring the interface pressure and structural acceleration and thus were placed in the field as previously discussed.

Stress--Soil stress measurements were made with LOK-080-H soil pressure transducers and its coinciding hardware. These gages were placed in the field in the same manner as previously discussed for the free-field accelerometers.

Passive Instrumentation--Passive instrumentation included scratch gages which measured relative displacement in the arches, time-of-arrival crystals used to measure burn rates in the HEST, and photopoles and time-of-flight spheres used to measure impulse.

INSTRUMENTATION RESULTS

Table 8 summarizes the active instrumentation results from DAT-3.

As Table 8 shows, the overall success of the instrumentation was quite high. The only significant failures were in the blast pressure gages. The four B-filter gages survived with six of the eleven L12 gages surviving.

The data for DAT-3 were virtually noiseless, due to the care taken in cable routing and cable protection. All free-field gages used rubber hose for protection until their cables were 3 m outside the test-bed. Structural instrumentation cables were bundled together and routed in a foam trench until they exited the test-bed. All cables left the test-bed in the minimum distance to avoid noise from cable motion. Of the 11 scratch gages, 6 gave data. The results are given in Table 6.

TABLE 8. INSTRUMENTATION RESULTS
(OVERALL SUCCESS 92%)

	No. of gages	Number successful	Scrapped pretest	Recorded data	Noise	No signal
Structural Acceleration	31	30	1	30	0	0
Free-field Acceleration	30	29	0	30	0	0
Near-field Acceleration	20	16	0	20	3	1
Airblast Pressure	16	10	1	15	0	0
Interface Pressure	18	17	1	17	0	0
Steel Strain	53	53	0	53	0	0
Near-field Stress	3	3	0	3	0	0
TOTALS	171	158	3	168	3	1

V. SIMULATION ANALYSIS

PRETEST DESIGN

The DAT-3 HEST was designed to match the environment experienced in a 1.56-kt nuclear surface burst at a range where the peak pressure was 12 MPa. The shock velocity at this range was calculated to be 3317 m/s.

The DAT-3 main event consisted of a HEST 14.63 m long and 13.41 m wide. The 364 kg of 400 grain/ft detonating cord was spread evenly in two layers in the 9.21-cm HEST cavity. The cavity was covered by 1.57 m of native soil. More detail on the HEST design can be obtained from the pretest report (Ref. 3).

POSTTEST ANALYSIS

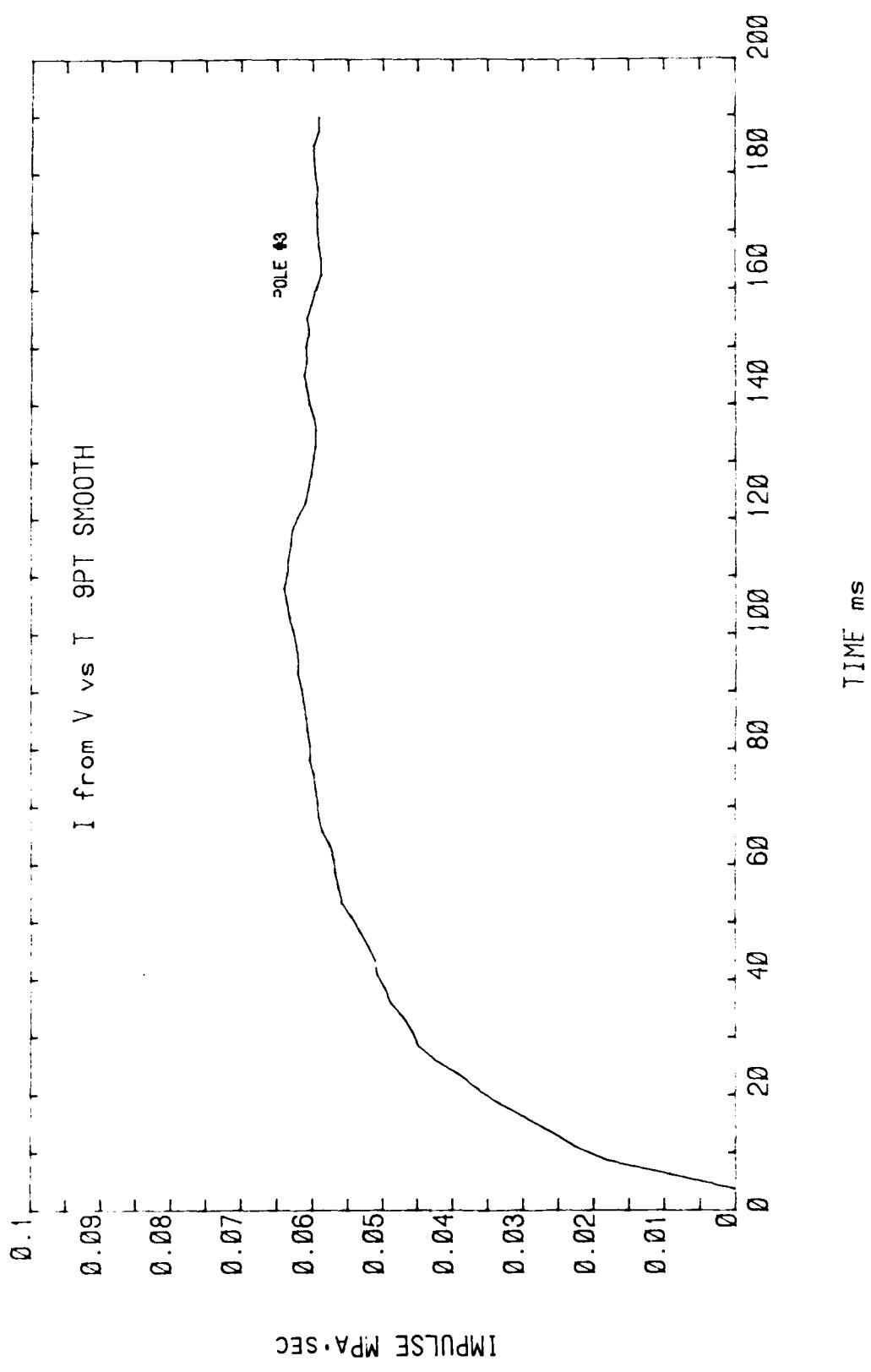
The as-built dimensions for the DAT-3 test were close to the predicted dimensions for the HEST. The HEST cavity was 14.63 m long and 13.41 m wide. Cavity thickness was slightly larger at 10.08 cm high. The total charge for the main event was 355 kg of 400 grain/ft detonating cord which was 2.3 percent low compared to the predicted value. The as-built charge density for the main event was 17.94 kg/m³.

The shock velocity measured in the HEST was 3348 m/s (1.1 percent higher than expected). Table 9 lists the time of arrival data. Two of the three Time of Flight (TOF) spheres recorded good data. The TCF spheres recorded a maximum impulse of 0.067 MPa-s in late time. The third TOF sphere failed to turn off its timing mechanism.

Photopole and photoball data were in agreement. The photopole and photoball data suggested a peak pressure of 14.5 MPa with an impulse at 70 ms of 0.061 MPa-s. A typical photopole plot is shown in Figure 36. The pressure gage data received by matching the actual gage data with the LOCKUP code suggest a peak pressure of 12.7 MPa with an impulse at 70 ms of 0.56 MPa-s.

TABLE 9. TIME OF ARRIVAL (TOA) RESULTS

<u>Measurement No.</u>	<u>Time (μs)</u>
8000	7.5
8001	1488.5
8002	1499.9
8003	1497.9
8004	1515.1
8005	1960.9
8006	1979.9
8007	1982.7
8008	1991.9
8009	2469.9
8010	2456.9
8011	2484.7
8012	2479.7
8013	2972.7
8014	2953.1
8015	2946.1
8016	2962.5
8017	3435.7
8018	3446.1
8019	3438.9
8020	3436.1
8021	3935.5
8022	3928.7
8023	3939.7
8024	3928.9
8025	4424.5
8026	4424.7
8027	4426.3
8028	4413.5
8029	Failed
8030	4891.9
8031	4894.1
8032	4888.3
8033	5404.1
8034	5390.1
8035	5389.7
8036	5378.3



*DATA-3 (FILE 1B) POLES1,2,3,7,8,4,6,5/3PTSMTH-ZERO

Figure 36. Typical photopole data.

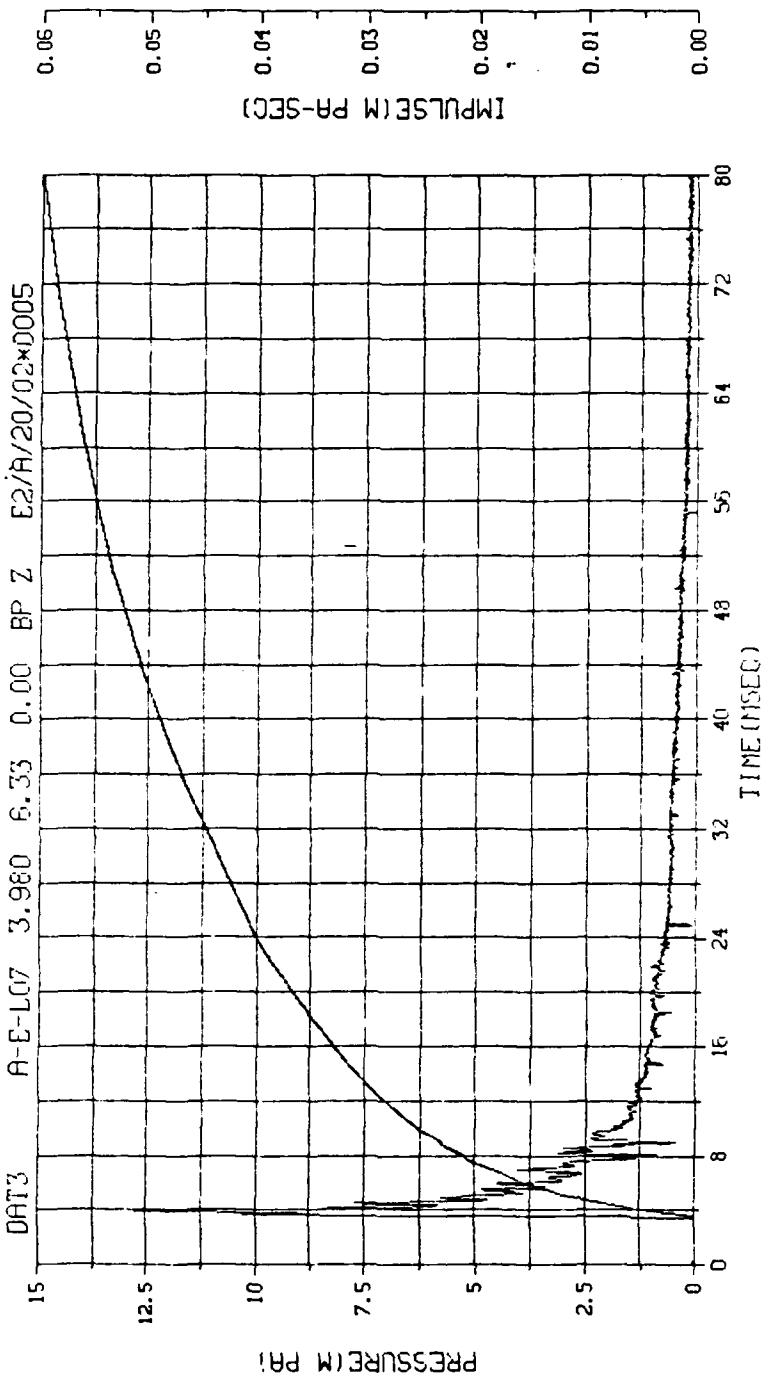
A typical pressure gage plot is shown in Figure 37. The LOCKUP code is a code that simulates a given HEST and calculates the pressure in the cavity as a function of time. The TOF sphere data correlate with the photopole data in late time peak impulse. This shows that the photopole data read a higher peak pressure than the pressure gage data. Since the mass of the photopoles is greater than the mass of the overburden which causes the photopoles to lag, the photopoles must always read a lower peak pressure than the pressure gages. This test, however, had just the opposite occurrence, possibly due to the filtering mechanism used on the pressure gages. Therefore, the peak pressures from the pressure gages may be incorrect. The photopole data were read from three different cameras, and all three correlated well with each other.

Several density measurements were taken in the overburden and the test-bed. The measured densities varied only 5 percent through the measurements, indicating that the densities were uniform. The overburden and test-bed densities used in LOCKUP were 3 percent higher than those measured at the site. Therefore, the best estimate of the peak pressure in the DAT-3 is 14 MPa. The impulse at 70 ms was 0.06 MPa-s, showing that the test was 16.7 percent high on the peak pressure and 7.1 percent high on late time impulse.

The nuclear match to the test data shows a yield of 1.56 kt. The peak pressure was 14 MPa. The waveform in Figure 38 shows that the test did produce the correct yield, but the peak pressure was 16.7 percent high.

COMMENTS

The HEST in general performed well on test day. The error obtained may have been because the calibration HEST was too small. The LOCKUP code does not have the ability to handle a small HEST; so the calibration shot may have been too small for the code to calculate the edge effects accurately.



M.N. = 0AC5	E.U. = 0.000, 12.000	VSN=GG142
NSKIP=7.000	BITS=0.000, 8825, HIGH	TAPE#2
S.R. = 25.00 KHZ	7.33 AM, THR, 10 MAY 83.	FILE=258 1

Figure 37. Typical pressure gage data.

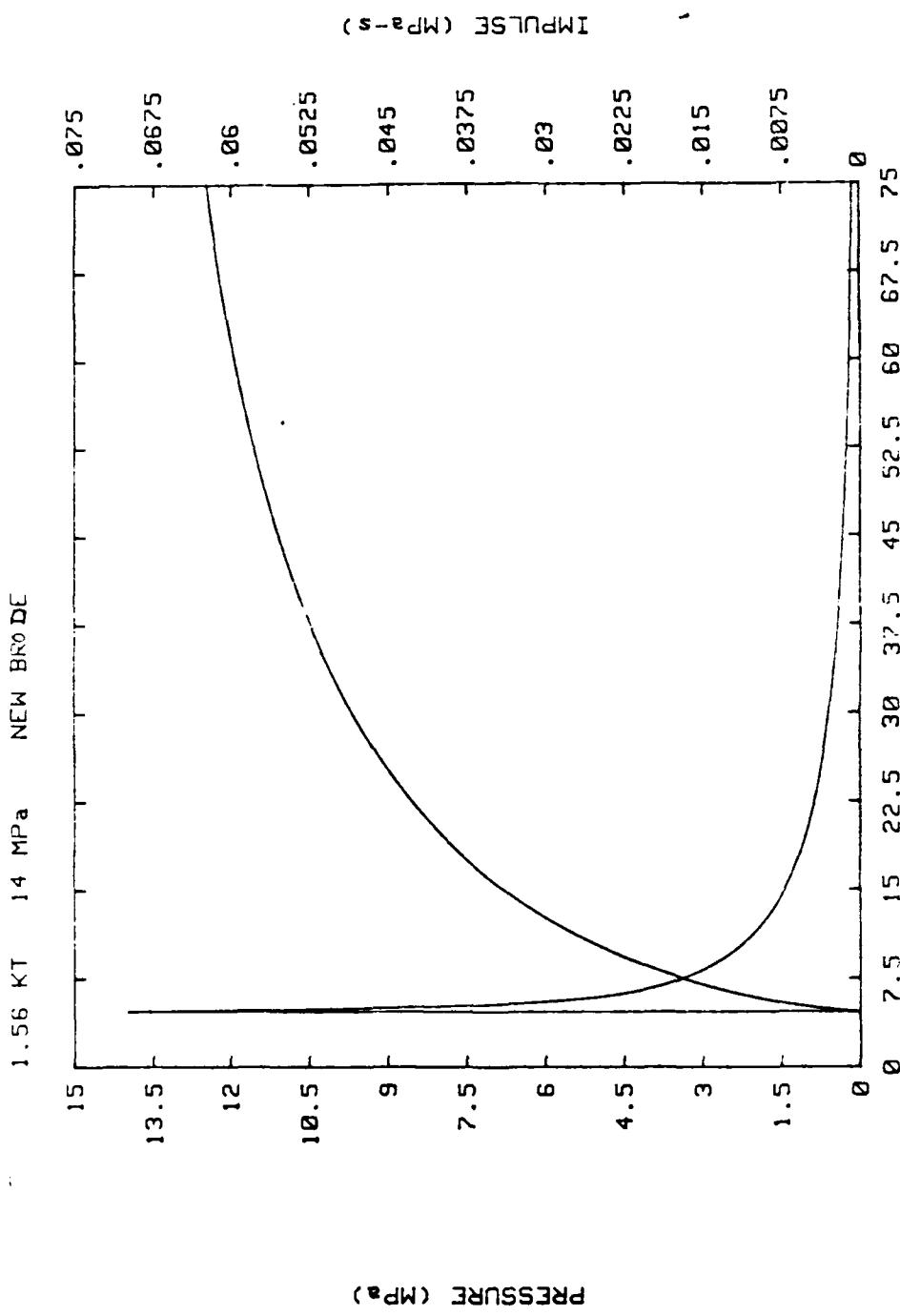


Figure 38. Best estimate of DAT-3 pressure and impulse time history.

VI. GROUND SHOCK ANALYSIS

INTRODUCTION

DAT-3 is the fourth event in the KACHINA test series. The first test, Acid, was primarily designed as a simulator development effort and used a simultaneously detonated HEST-DIHEST. The following three tests, Butterfly Maiden (KBM), Eagle Dancer (KED), and DAT-3, tested the response of buried arches and other generic structures to a variety of simulated nuclear environments. Butterfly Maiden used a HEST with a 1-week delayed DIHEST, while KED and DAT-3 were solely HEST simulations. From a ground shock perspective, DAT-3 is an airblast simulation of a 1.56 kt nuclear surface burst at a range of 44.64 m (146.44 ft). In order to simulate the local airblast effects for this environment, a 13.41 by 14.63 m HEST was used with a design peak overpressure of 12 MPa and an airblast shock front velocity of 3317 m/s. Posttest analysis indicates that the overpressure achieved was approximately 13.78 MPa and the airblast shock front velocity was 3348 m/s. This corresponds to a 1.56 kt nuclear surface burst at 42.53 m.

This section is a discussion and analysis of a variety of recorded and observed phenomena associated with the DAT-3 ground shock environment. First, general geologic parameters and site investigation results are discussed. Data recovery is presented next, followed by an analysis of the seismic and loading wave speeds. Both vertical and horizontal soil motions are analyzed, and discussion of general phenomenology, peak accelerations, peak velocities, peak displacements and permanent displacements are presented. Since the DAT-3 was designed and located to reproduce approximately the same ground shock conditions as experienced in KED, comparisons are made wherever applicable. In addition, spall and relief effects are discussed. Finally, the data is compared to the pretest calculations. The primary emphasis of this section is an analysis of the free-field data; however, the near-field data is briefly discussed and compared to the free-field results. The near-field results are discussed further in the structural response analysis.

EXPERIMENT DESCRIPTION

The following is a brief discussion of the test site location, geology and backfill properties. Section III contains more details.

Location--The DAT-3 event was fielded on the southwest quadrant of the McCormick Ranch test area approximately 11 km south of Albuquerque, New Mexico on Kirtland Air Force Base. The test bed was located approximately 75 m from the KBM and KED sites. This area was selected in order to field DAT-3 in approximately the same geology as the previous KACHINA tests.

Geology--Surficially, the DAT-3 area is generally flat with a gentle slope to the southwest. The test area is located near the center of a shallow basin bounded on the west by an eastward dipping cuesta and on the east by alluvial fan deposits from the Manzano Mountains. Surficial soil deposits are primarily brown to reddish brown, nonplastic, fine to medium silty sands.

The average in situ soil density is 1668 kg/m^3 and moisture content is relatively constant with depth averaging 4.7 percent. These values are typical of most McCormick Ranch soil. The test-bed backfill pit was 2.88 m deep. This pit was backfilled with native McCormick Ranch soil to 90 to 95 percent of the in situ density. The average backfill density was 1510 kg/m^3 . Posttest analysis of density indicates that considerable near surface compaction occurred. Measurements taken at the top of the test-bed indicate an average density of 1863 kg/m^3 , while measurements taken at approximately the 1.9 m depth indicate an average density of 1515 kg/m^3 .

DATA RECOVERY

The DAT-3 free-field was instrumented with 30 accelerometers arranged in four gage holes at depths of 0.75, 2, 4 and 8 m. Of these 30 gages, there were 15 accelerometers oriented in the vertical (+Z) direction and 15 accelerometers oriented in the horizontal (+Y) direction. Figure 39 and Table 10 show the location of these gages and the global coordinate system used to locate the free-field instrumentation. Since the DAT-3 test was designed to approximate the environment experienced in the KED event, all of the free-field gages were ranged, based on the KED data. Reference the pretest prediction report for further information (Ref. 3).

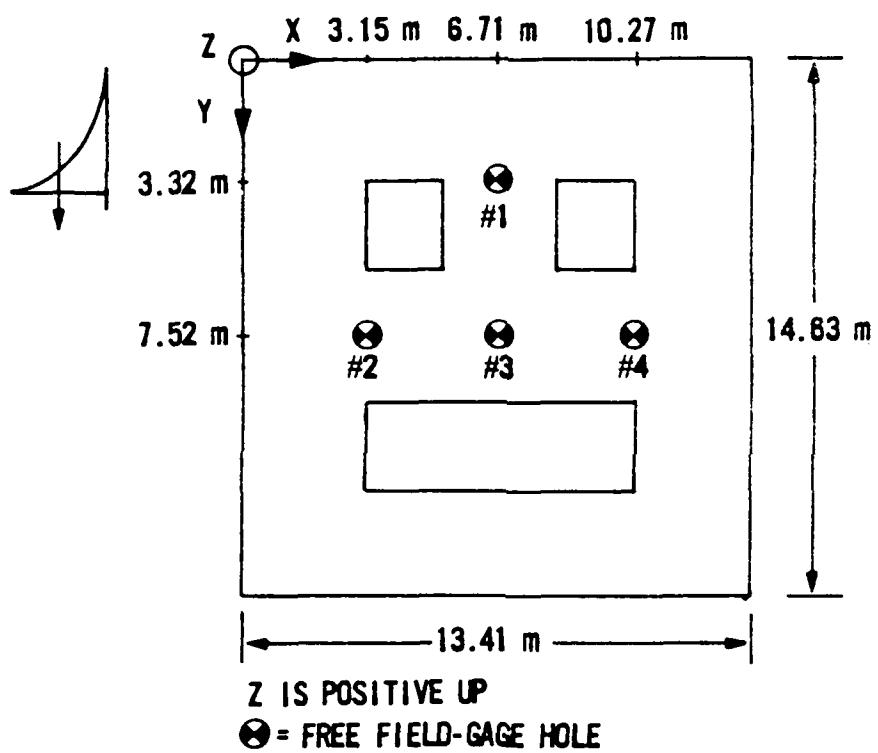


Figure 39. Free-field gage layout.

TABLE 10. FREE-FIELD GAGE LOCATIONS

HOLE No.	GAGE DEPTH (m)			
	0.75	2.0	4.0	8.0
1	*	*	*	
2	*	*	*	*
3	*	*	*	*
4	*	*	*	*

* - INDICATES VERTICAL AND HORIZONTAL
ACCELEROMETER

Overall, data recovery for the free-field instrumentation was excellent. Of the 30 gages fielded, all yielded some information. Ninety-three percent of these gages provided complete data traces with noise well below the maximum acceptable 10 percent of the signal. Two gages, measurement numbers 1311 and 1328, yielded only partial data. Measurement 1311 displays what appears to be cable slap or grout seating problems at approximately 50 ms. The late time motions recorded by this gage, however, seem reasonable when compared to the other measurements taken at this depth. The peak acceleration recorded by measurement 1328 was truncated at approximately 32 G while similar measurements at this depth indicated peak values of 85 to 95 G. This gage did, however, provide good time of arrival and late time data. Most of the vertical and horizontal velocity and displacement records exhibit considerable base line shifts. These were corrected in order to facilitate the analysis of late time motions.

RESULTS

Wave Speed Determination--The seismic and loading wave speeds are determined by plotting the time of first arrival and time to peak velocity respectively with depth. In order to properly time vertical gages with different horizontal locations, corrections must be applied to account for the finite burn velocity of the HEST. Using the average HEST burn speed of 3348 m/s, the time of arrival and time to peak velocity were corrected to eliminate the HEST burn travel time. Table 11 gives the corrected times of arrival and times to peak velocity for the vertically oriented free-field gages. Seismic wave speeds are plotted in Figure 40 and loading wave speeds are plotted in Figure 41. The seismic velocity is 197 m/s above 0.75 m, 637 m/s between 0.75 and 4 m, and 784 m/s below 4 m. The loading velocity determined in Figure 41 is 106 m/s near surface and 286 m/s below approximately 4 m. These wave speeds are reasonable and are very close to the speeds observed in KED and KBM. For KED the loading velocity was 128 m/s, while the seismic velocity was 192 m/s above 1 m and 662 m/s below 1 m. Similarly, the KBM data indicated a loading velocity of 125 m/s, a near surface seismic velocity of

3. J.L. Smith, et al, KACHINA Test Series: Dynamic Arch Test - 3 Pretest Report, AFWL-TR-83-56, Air Force Weapons Laboratory, Kirtland AFB, NM, Sep 83.

TABLE 11. TIME OF ARRIVAL AND TIME TO PEAK VELOCITY

Measurement Number	Depth (m)	Corrected Time of Arrival (ms)	Corrected Time of Peak Velocity (ms)
1301	0.75	4.00	6.50
1307	0.75	3.75	7.75
1315	0.75	2.25	7.55
1323	0.75	4.55	7.35
1303	2.0	7.00	20.50
1309	2.0	5.75	21.25
1325	2.0	5.75	20.75
1327	2.0	4.75	20.75
1305	4.0	8.80	39.0
1310	4.0	8.75	35.25
1319	4.0	9.0	37.0
1328	4.0	9.75	No data
1313	8.0	13.25	51.25
1321	8.0	14.75	53.75
1329	8.0	13.75	52.65

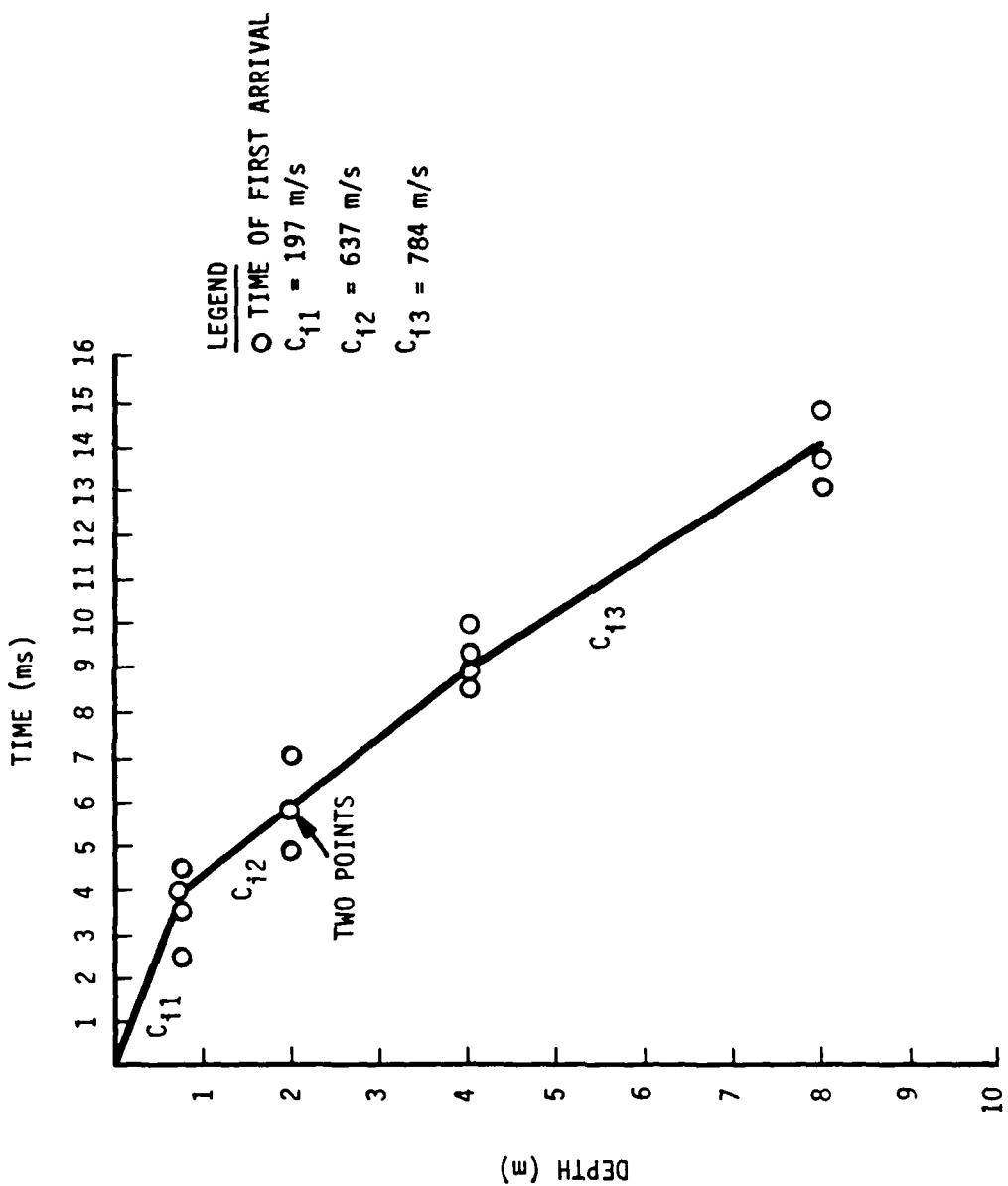


Figure 40. Determination of seismic speed.

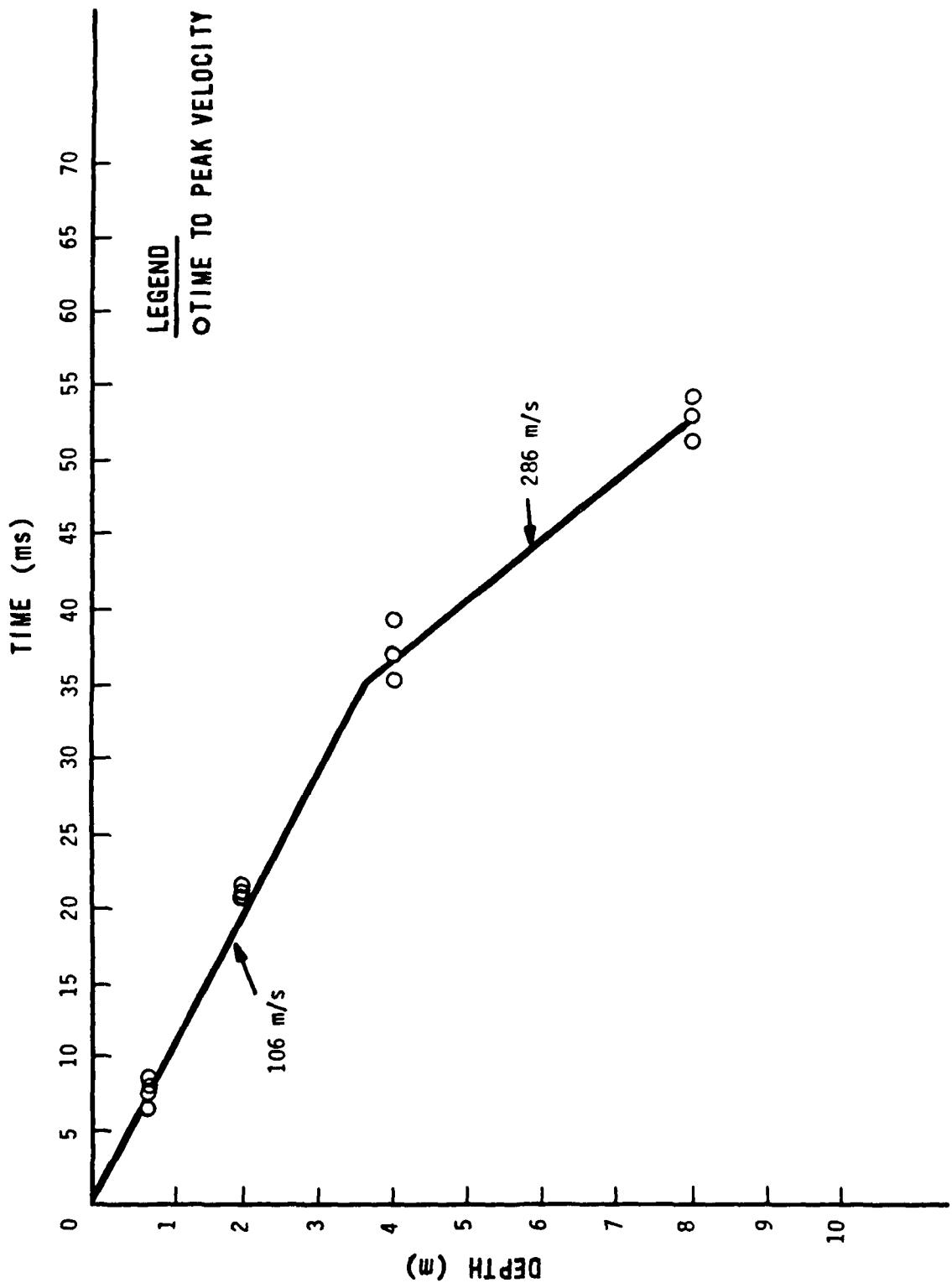


Figure 41. Determination of loading wave speed.

227 m/s, and a seismic velocity of 720 m/s at greater depth. A comparison of these wave speeds indicate that the DAT-3 soil is, in general, a slightly faster material than the KED and KBM soil. However, the wave speeds determined agree very well, within the bounds of the experimental data.

Using this analysis coupled with the best estimates of soil density for the backfill and in situ material allows calculation of the acoustic impedances of the two media. Acoustic impedance is defined as the product of the media density and loading velocity. Such calculation indicates that the ratio of backfill to in situ acoustic impedances for DAT-3 is 0.35. Based on this ratio, one-dimensional analytic theory (Ref. 4) suggests that there is a 48 percent increase in stress across the backfill/in situ interface. In reality non-one-dimensional stress tensors would cause this increase to be lower than that predicted above. This test was not well instrumented for stress measurements; however, one would expect as a first order approximation a similar increase in velocity across the boundary. A slight increase in vertical velocity was observed between the 2- and 4-m depths. This is shown in Figure 44.

Vertical Motions--In order to provide general insight into the vertical motions, a composite graph of typical vertical acceleration, velocity and displacement time histories for depths of 0.75, 2, 4 and 8 m is shown in Figure 42. One thousand millisecond plots are shown in order to present the entire waveforms. As one would expect, the motions in the vertical direction are an initial downward pulse followed by recovery of the soil with an upward motion of longer duration. Evidence of spall is also clearly present in measurements taken at or below the 2-m depth. Spall is identified as an upward motion followed by an approximate 1-G free-fall and positive rejoin signal as the lofted soil hits the test-bed. The general motions of the near-field were the same as the free-field except for those gages located directly beneath the test arches. These gages indicated an initial upward motion which is felt to be the result of the initial upward bending of the arch floors.

4. Crawford, Robert E., et al, The Air Force Manual for Design and Analysis of Hardened Structures, AFWL-TR-74-102, AFWL, Kirtland AFB, NM, Oct 74, p. 236.

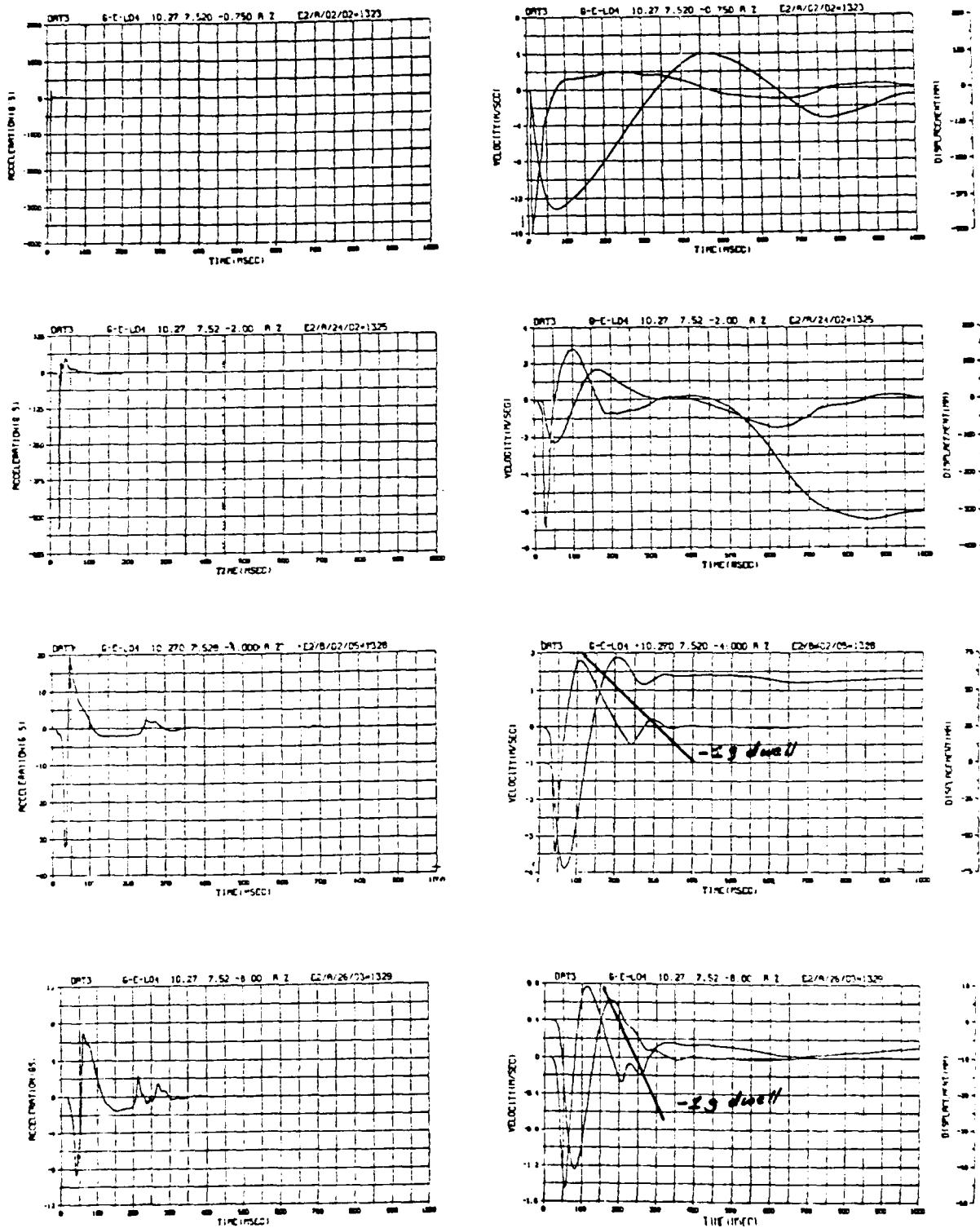


Figure 42. Typical free-field vertical motions at depths 0.75, 2.0, 4.0 and 8.0 m. (See Appendix F for enlargements)

Table 12 presents the peak vertical accelerations, velocities and displacements recorded in the free-field. Peak vertical acceleration is plotted versus depth in Figure 43. Near surface accelerations tend to follow the rule of thumb that peak acceleration can be estimated as "one G per psi" of overpressure. A least squares fit to this data indicates that peak accelerations for DAT-3 attenuate as Equation 1.

$$A = 2091 (D/1m)^{-2.17} \quad (1)$$

where

A = Peak vertical acceleration in G's

D = Depth in meters

The data displays relatively low experimental scatter and a high regression coefficient of 0.9. In comparison, the KED accelerations attenuate slightly faster as shown in Figure 43 and Equation (2). The DAT-3 vertical accelerations are greater than the KED accelerations by a factor of 1.74 at the 1 m depth to a factor of 2.76 at the 10 m depth. This difference can be attributed to the slightly higher peak pressures experienced in DAT-3 as well as the soil wave speed differences between the two tests.

$$A = 1200 (d/1m)^{-2.37} \quad (2)$$

where

A = KED peak vertical acceleration in G's

D = Depth in meters

Figure 44 shows peak vertical velocity versus depth for the DAT-3 data, for the KBM and KED data, and for the one-dimensional finite difference pre-test prediction (Ref. 3). As for the vertical accelerations, the peak vertical velocities attenuate slower for DAT-3 as compared to KBM and KED. However, the DAT-3 peak velocities are approximately equal to the KBM and KED velocities at the 1-m depth and are higher than these velocities by a factor of 1.7 at a depth of 10 m.

TABLE 12. PEAK VERTICAL FREE-FIELD MOTIONS

MN	Location			Peak Acceleration (G)	Peak Velocity (m/s)	Peak Displacement (mm)
	X (m)	Y (m)	Z (m)			
1301	6.71	3.32	-0.75	2625	18.3	438
1307	3.15	7.52	-0.75	4560	15.9	444
1315	6.71	7.52	-0.75	4450	18.0	450
13.23	10.27	7.52	-0.75	3500	16.4	412
1303	6.71	3.32	-2.00	531.3	6.8	172
1309	3.15	7.52	-2.00	539.9	9.2	179
1325	10.27	7.52	-2.00	546.9	6.5	125
1327	6.71	7.52	-2.00	389	5.1	175
1305	6.71	3.32	-4.00	83.8	5.1	129
1310	3.15	7.52	-4.00	87.0	4.5	97.6
1319	6.71	7.52	-4.00	81.0	4.4	116
1328	10.27	7.52	-4.00	No	Peak	Data
1313	3.15	7.52	-8.00	16.0	1.9	51.9
1321	6.71	7.52	-8.00	10.6	1.9	52.8
1329	10.27	7.52	-8.00	8.7	1.5	41.0

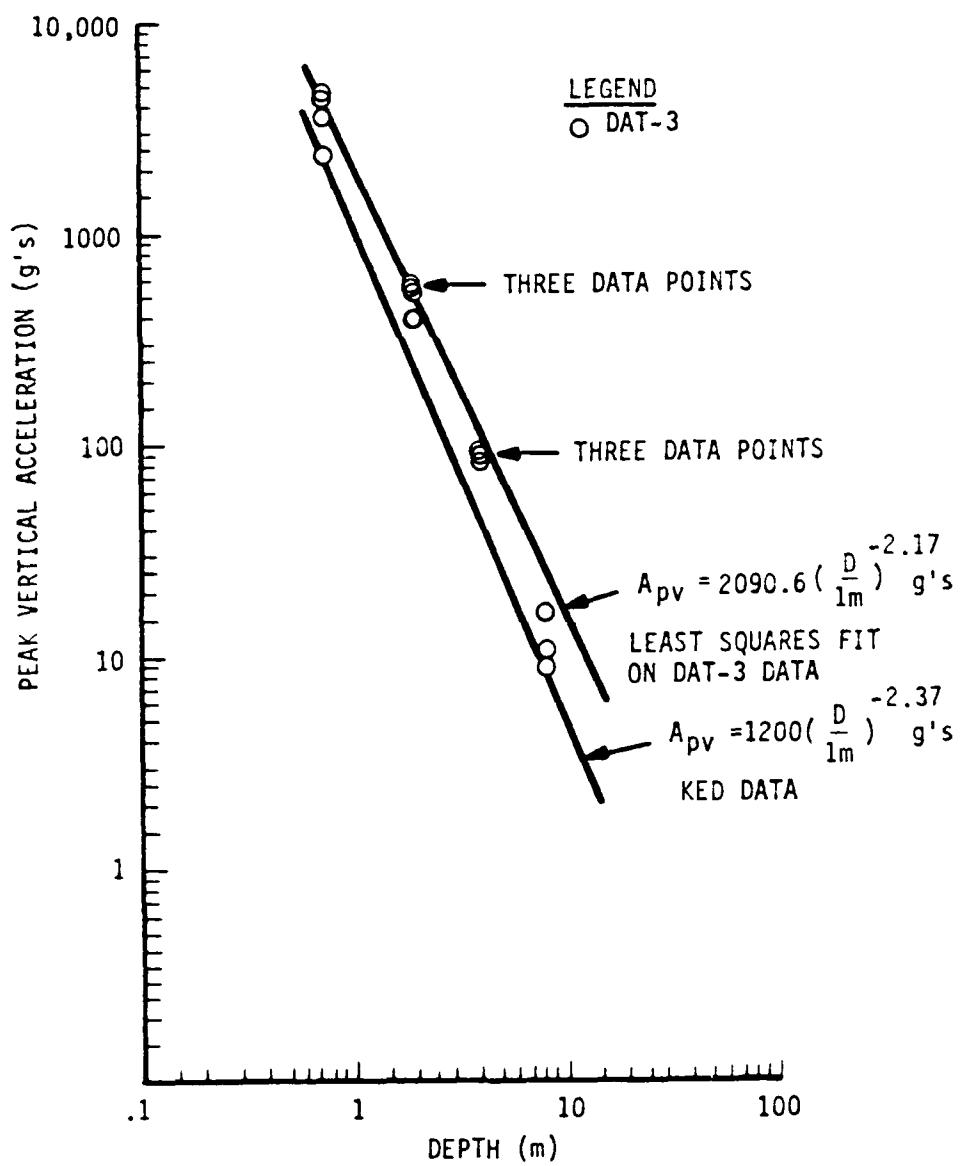


Figure 43. Peak vertical acceleration versus depth.

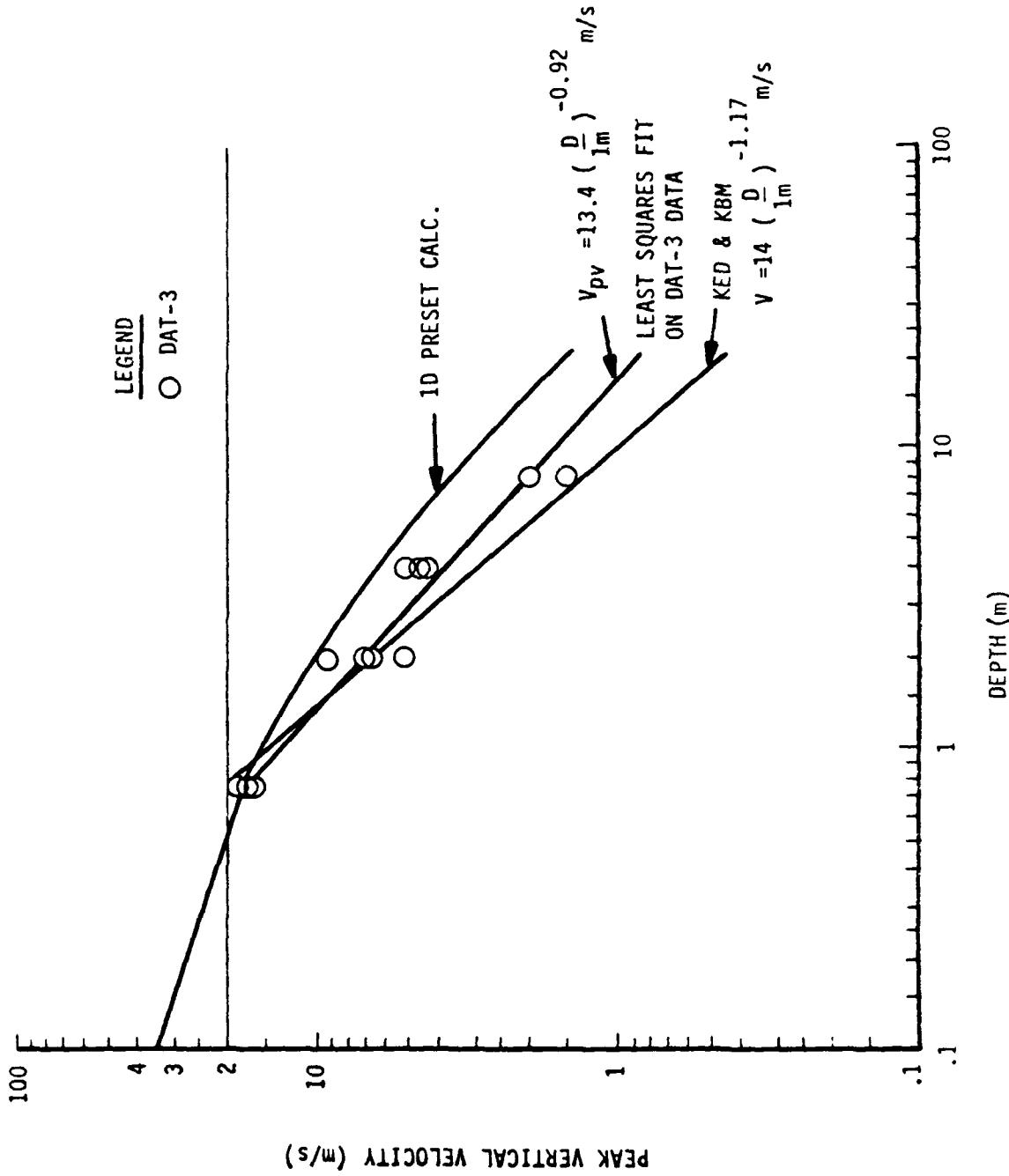


Figure 44. Peak vertical velocity servus depth.

The DAT-3 data show little experimental scatter and a regression coefficient of 0.95. This high data correlation coupled with the measurement redundancy achieved in DAT-3 provides confidence in the precision of these measurements. Note that the DAT-3 data are almost equally bounded by the pretest calculation on the high side and the previous KACHINA data on the low side. Equation 3 is the least squares fit to the DAT-3 results and Equation 4 is the fit to the KBM and KED data.

$$V = 13.4 (D/1m)^{-0.92} \quad (3)$$

$$V = 14.0 (D/1m)^{-1.17} \quad (4)$$

where

V = Peak vertical velocity in m/s

D = Depth in meters

Peak vertical displacements are plotted versus depth in Figure 45. The least squares fit to the DAT-3 data which has a regression coefficient of 0.96 is shown in Equation 5.

$$Dv = 0.35 (D/1m)^{-0.92} \quad (5)$$

where

Dv = Peak vertical displacement in meters

D = Depth in meters

Note that both the vertical velocity and displacement attenuate as $D^{-0.9}$. For comparison, the KED data and the pretest prediction results are also shown in Figure 45. The KED data display considerably more scatter, but in general seem to have similar magnitudes and attenuation rate. Accurate estimates of permanent displacements are not possible since no posttest free-field gage surveys were conducted; and, without this information, baseline corrections to determine permanent displacements have little meaning. Posttest surveys of the blast pressure gages were performed and provide some information. These surveys indicate permanent displacements of approximately 0.3 to 0.4 m at the test-bed surface.

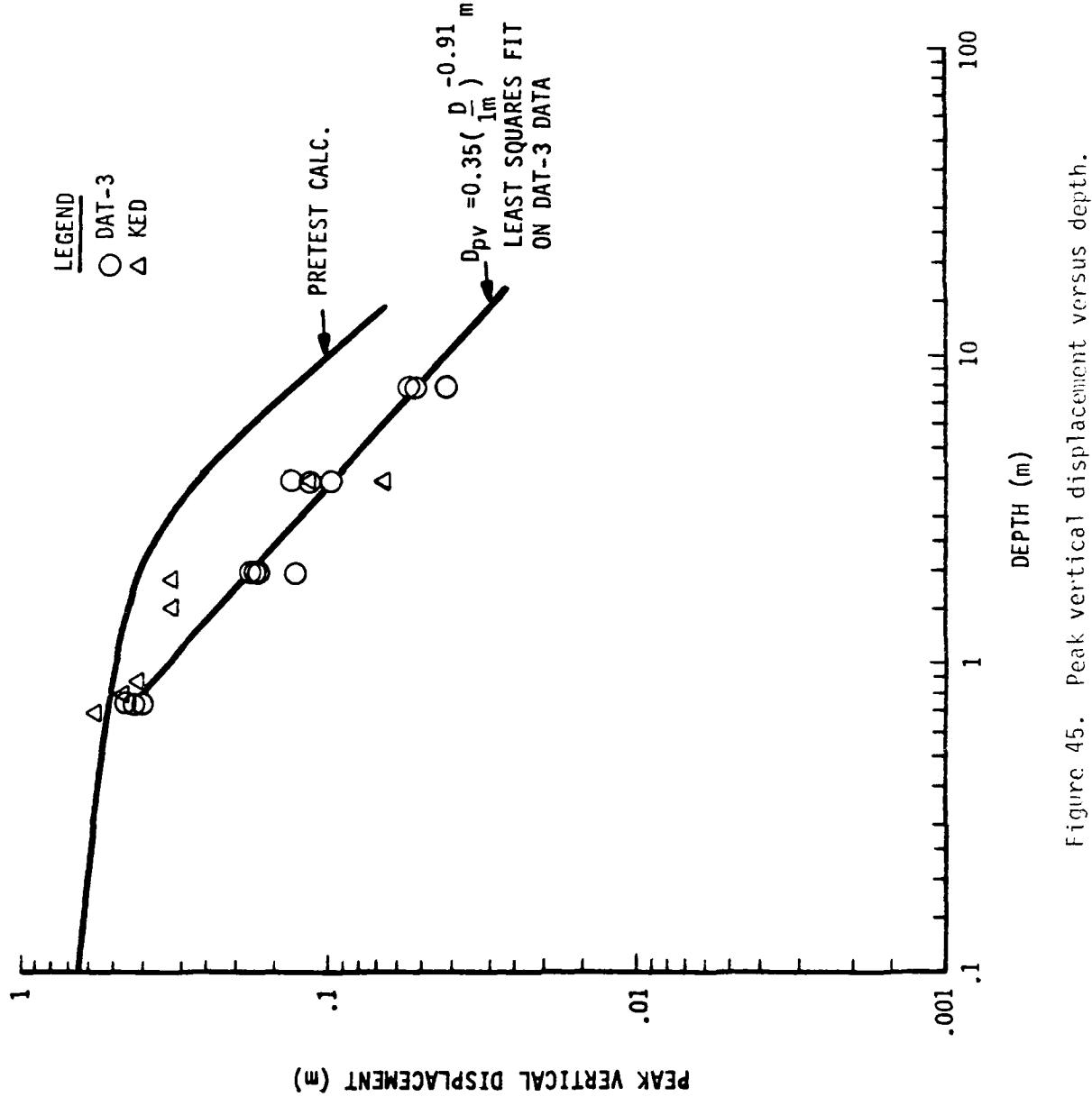


Figure 45. Peak vertical displacement versus depth.

When compared to the free-field data, the near-field peak accelerations, velocities, and displacements show no appreciable difference in magnitudes. Due to the limited depth of the near-field measurements, no meaningful comparison can be made between the attenuation rates of these parameters.

Horizontal motions--In order to provide general insight into the horizontal motions, a composite graph of typical horizontal acceleration, velocity and displacement time histories for depths of 0.75, 2, 4 and 8 m is shown in Figure 46. These horizontal records correspond to the vertical records depicted in Figure 42. As expected, initial motion is in the horizontal direction of the airblast propagation. This pulse is followed by an inward movement of slightly longer duration. Late time motions are characterized by a low magnitude, lower frequency oscillatory component and signals associated with spall.

Table 13 presents the peak horizontal free-field motions. Peak horizontal acceleration is plotted versus depth in Figure 47. The horizontal accelerations exhibit slightly more scatter and attenuate somewhat faster than the vertical accelerations. A least squares fit indicates that the peak horizontal accelerations attenuate as Equation 6.

$$A = 379 (D/1m)^{-2.42} \quad (6)$$

where

A = Peak horizontal acceleration in G's

D = Depth in meters

The ratio of peak horizontal to peak vertical acceleration ranges from 18 percent at the 1-m depth to 10 percent at 10 m. Assuming that the near-surface motions are one-dimensional, Equation 7 may be used to predict this ratio analytically.

$$AH/AV = \tan (\arcsin (Ci/U)) \quad (7)$$

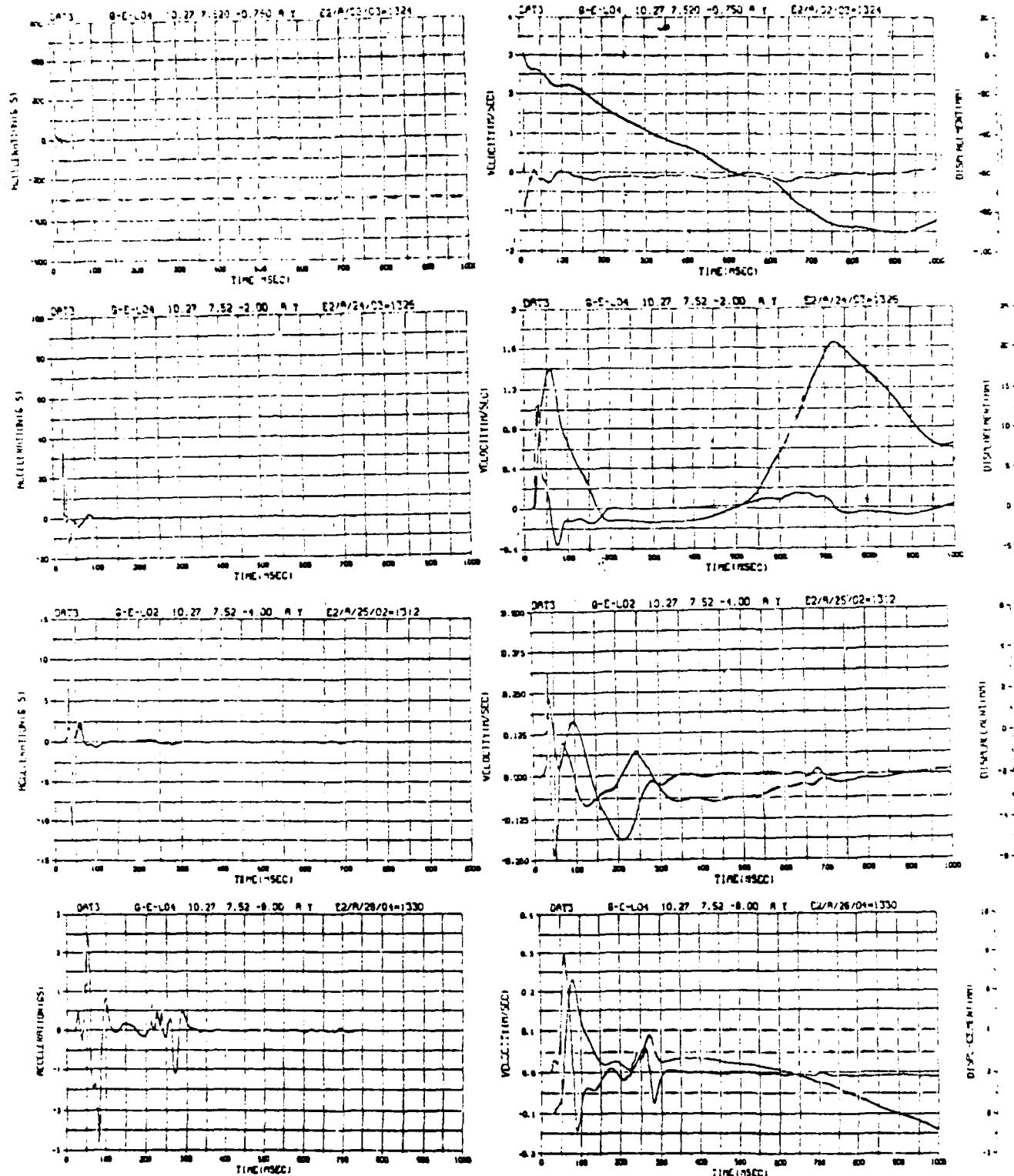


Figure 46. Typical free-field horizontal motions at depths of 0.75, 2.0, 4.0, and 8.0 m. (See Appendix F for enlargements)

TABLE 13. PEAK HORIZONTAL FREE-FIELD MOTIONS

MN	Location			Peak Acceleration (G)	Peak Velocity (m/s)	Peak Displacement (mm)
	X (m)	Y (m)	Z (m)			
1302	6.71	3.32	-0.75	887.5	3.84	67.5
1308	3.15	7.52	-0.75	950	4.0	*
1316	6.71	7.52	-0.75	885	5.63	144
1324	10.27	7.52	-0.75	490	1.7	*
1304	6.71	3.32	-2.0	62.5	0.33	*
1317	3.15	7.52	-2.0	115	1.36	16
1318	6.71	7.52	-2.0	84	0.84	13.8
1326	10.27	7.52	-2.0	72.8	1.13	17.6
1306	6.71	3.32	-4.0	3.82	0.25	3.3
1311	3.15	7.52	-4.0	4.2	0.44	9.9
1312	10.27	7.52	-4.0	13.0	0.31	1.75
1320	6.71	7.52	-4.0	10.8	0.61	13.75
1314	3.15	7.52	-8.0	3.75	0.39	9.75
1322	6.71	7.52	-8.0	2.00	0.068	*
1330	10.27	7.52	-8.0	2.83	0.295	6.7

* - No data

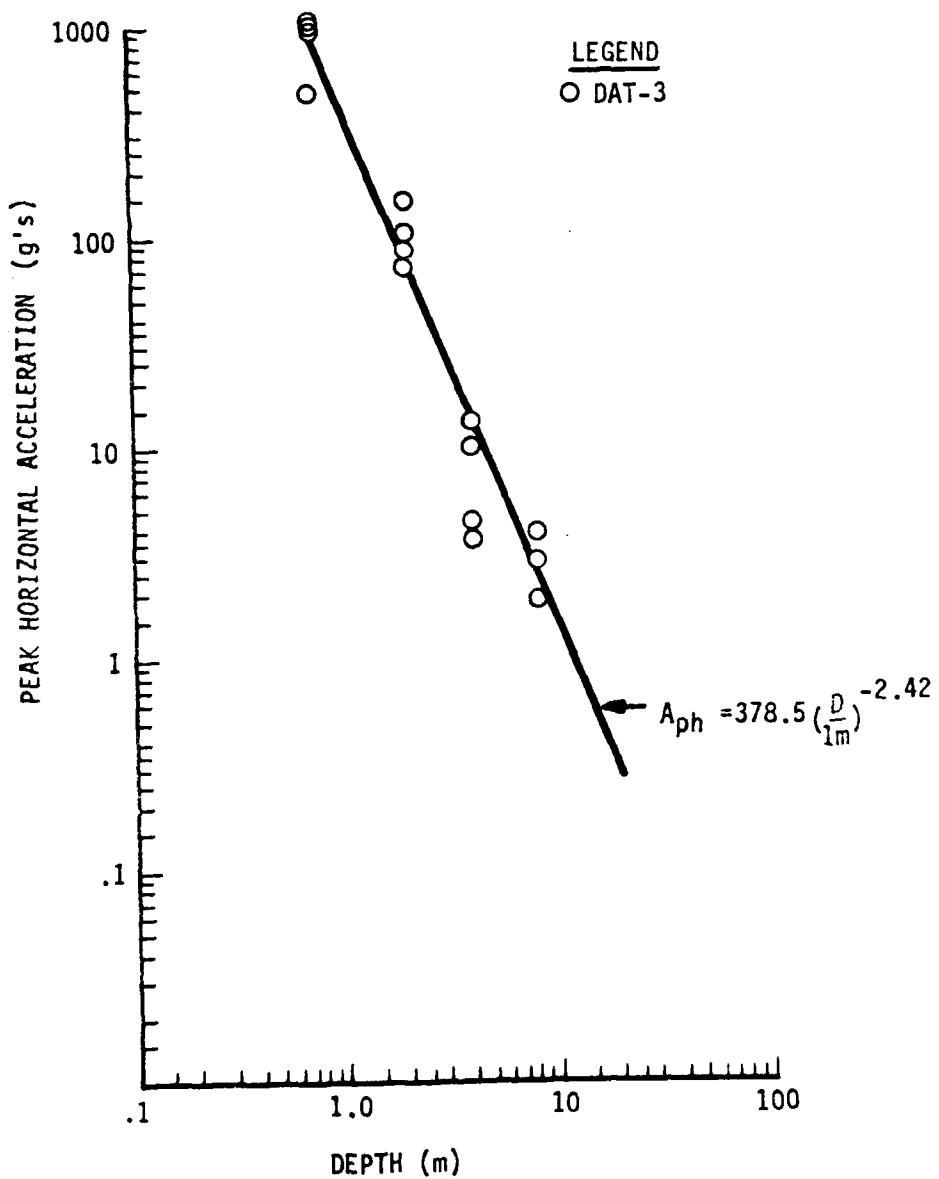


Figure 47. Peak horizontal acceleration versus depth.

where

AH/AV = Ratio of peak horizontal to peak vertical acceleration

C_i = Seismic speed of soil

U = Airblast shock front velocity

Using the best estimates of 637 m/s for C_i and 3348 m/s for U, this equation indicates a near-surface ratio of 19.4 percent.

Similarly, peak horizontal velocities attenuate faster and exhibit more scatter than the peak vertical velocities. The horizontal velocities attenuate as:

$$V = 2.2 (D/1m)^{-1.22} \quad (8)$$

where

V = Peak horizontal in m/s

D = Depth in meters

In general, the horizontal velocities range from 16.4 to 8.3 percent of the vertical velocities at depths of 1 m and 10 m, respectively. Similar values were also observed in the KED event. Peak horizontal velocities are plotted versus depth in Figure 48.

Figure 49 shows the peak horizontal displacements versus depth. A least squares fit to this data indicates that the displacements attenuate as Equation 9.

$$DH = 0.05 (D/1m)^{-1.4} \quad (9)$$

where

DH = Peak horizontal displacement in meters

D = Depth in meters

As was the case for accelerations and velocities, the horizontal displacements attenuate faster than the vertical displacements. Due to the difficulty of accurately correcting base line shifts, four of the horizontal records could not be used to provide reasonable estimates of peak displacements.

Relief Effects--Relief or boundary effects are a complex set of stresses and motions (generated at the edge of a finite simulator) which tend to

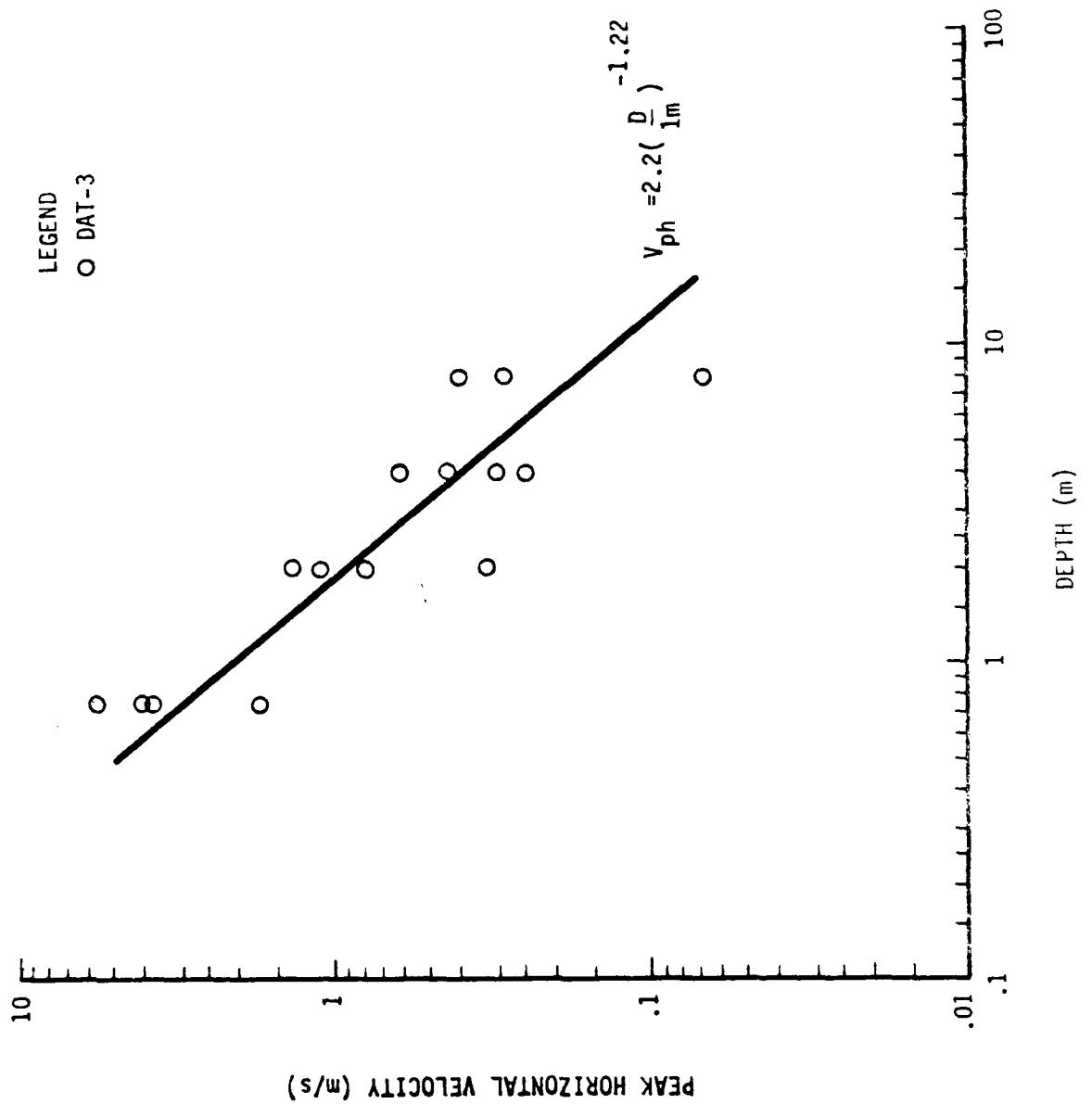


Figure 48. Peak horizontal velocity versus depth.

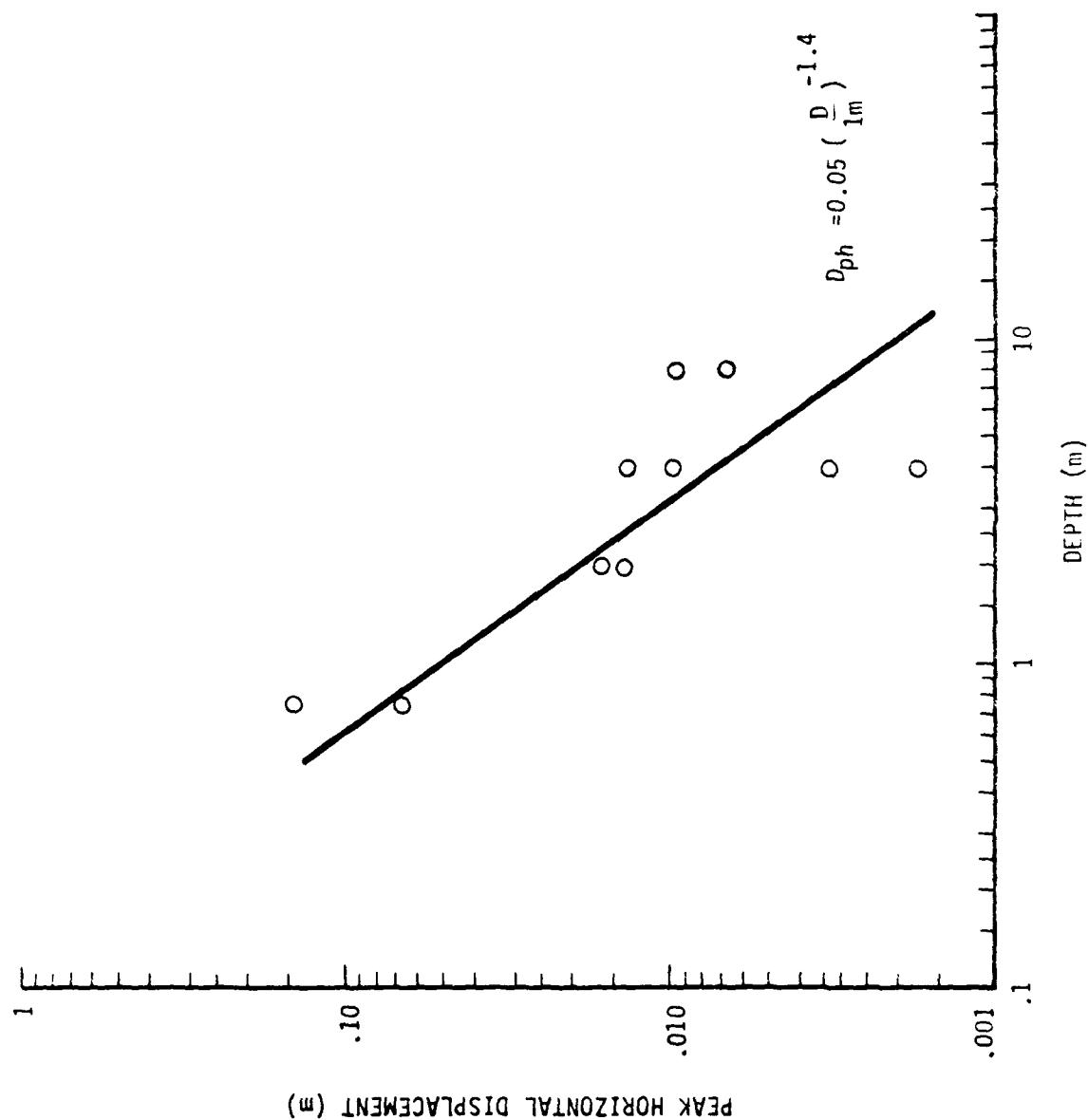


Figure 49. Peak horizontal displacement versus depth.

degrade the fidelity of a nuclear simulation. The relief effects are earlier and more significant at locations close to the boundary of the simulator. Since relief effects are inherent to finite size simulators, it is the job of the designer to size the simulator large enough to prevent deleterious relief effects from significantly degrading the simulation for at least the desired simulation time. Similarly, it is the job of the analyst to verify that the designer accomplished this objective.

A spatial analysis of the peak vertical accelerations and velocities in both the x- and y- directions show no significant or consistent trends which would suggest that these values are significantly degraded by relief. In addition, no clearly identifiable relief wave characteristics can be traced in the data. These observations show that the simulator and the relief effects were not significant during the simulation time.

Peak vertical displacements, however, do show a consistent trend which indicates that relief effects did degrade the one-dimensional simulation objective in the late time. On the average, peak vertical displacements were approximately 13 percent higher at the center of the test-bed, compared to displacements at approximately 3.15 m from either edge of the test-bed along the x- test-bed coordinate.

SUMMARY AND CONCLUSIONS

Overall, DAT-3 was fully successful in meeting its ground shock objectives. Of the 30 ground shock gages fielded, all yielded some information and 93 percent provided complete data traces with noise well below the maximum acceptable 10 percent of the signal. From these data, the following observations and conclusions can be drawn.

a. Soil seismic and loading wave speeds determined from the DAT-3 data are in excellent agreement with the speeds determined for the KED and KBM tests.

b. Peak vertical acceleration, velocity and displacement attenuate as $D^{-2.17}$, $D^{-0.92}$, and $D^{-0.91}$, with depth respectively.

c. Peak horizontal motions attenuated slightly faster than the vertical motions. Peak horizontal acceleration, velocity and displacement attenuate with depth as $D^{-2.42}$, $D^{-1.22}$, and $D^{-1.4}$ respectively.

d. As in the KED and KBM test, evidence of spall is clearly present in vertical measurements taken at or below the 2-m depth.

e. The DAT-3 vertical accelerations are greater than the KED accelerations by a factor of 1.74 at the 1-m depth to a factor of 2.76 at the 10-m depth.

f. As for the vertical accelerations, the peak vertical velocities attenuate slower in DAT-3 than in KBM and KED. DAT-3 velocities are approximately equal to the KBM and KED velocities at the 1-m depth and then increase by a factor of 1.7 by the time they reach the 10-m depth.

g. The ratio of peak horizontal to peak vertical acceleration ranges from 18 percent at the 1-m depth to 10 percent at 10 m. Similarly, the horizontal velocities range from 16.4 to 8.3 percent of the vertical velocities at depths of 1 m and 10 m, respectively.

h. Relief effects apparently did not significantly affect accelerations and velocities during the simulation time. However, peak vertical displacements which average 13 percent higher along the centerline of the test-bed, compared to those displacements approximately 3 m from the edge of the test-bed, indicate that relief effects did degrade the one-dimensional simulation in late time.

VII. FIBER OPTIC CABLE VULNERABILITY EXPERIMENT

OBJECTIVE

This experiment was designed to return data on the vulnerability of certain optical fibers in an explosive environment. In connection with the DAT-3 test, cable penetration through structure boundaries was investigated. Data was sought on the amount of protection necessary to ensure cable integrity during an event, in relation to the event environment of soil stress, acceleration and displacement near the cable penetrations.

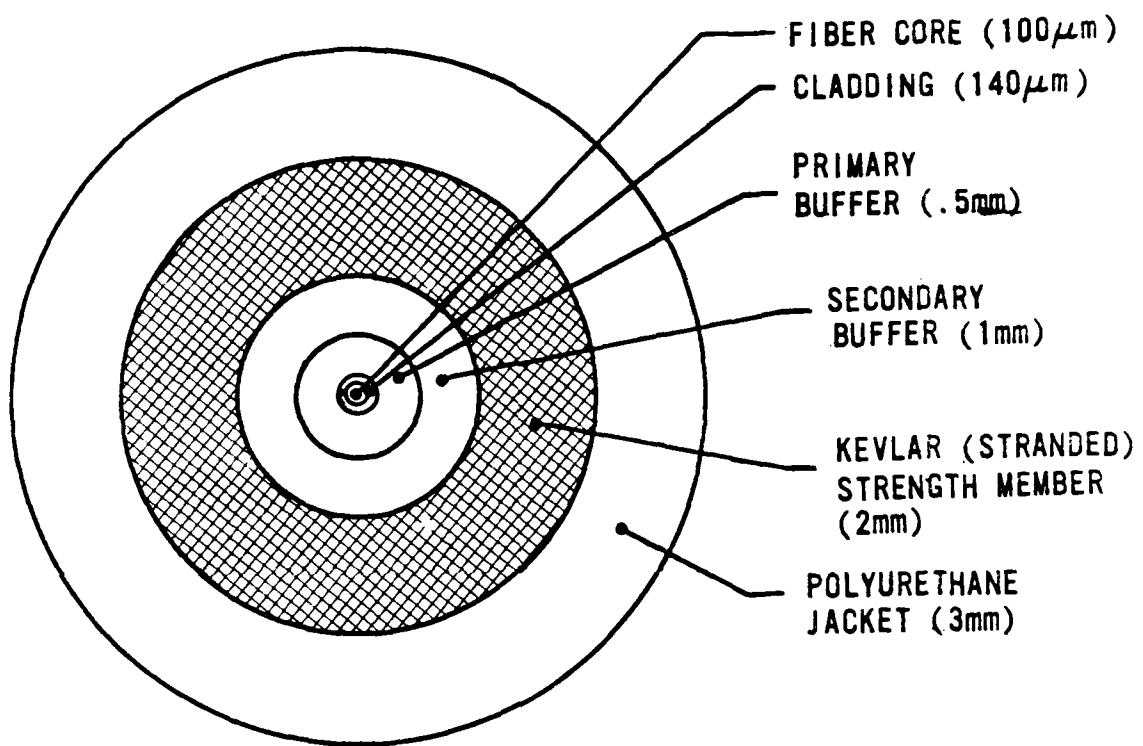
APPROACH

Cable Selection--Fiber cables available from other projects were used. Figure 50 shows the cross section of a Siecor 144 cable, while Figures 51a and b show the cross sections of a single Math Associates Cable and a dual fiber version, respectively. Table 14 is a collection of cable parameters available from published data. No measurements were made to confirm these data. All together, five fibers were used in four cables.

Cable Layout--The general layout is shown in Figure 52, and Figure 53 shows the cable protection details. Figure 54 is a dimensional diagram of the penetration locations.

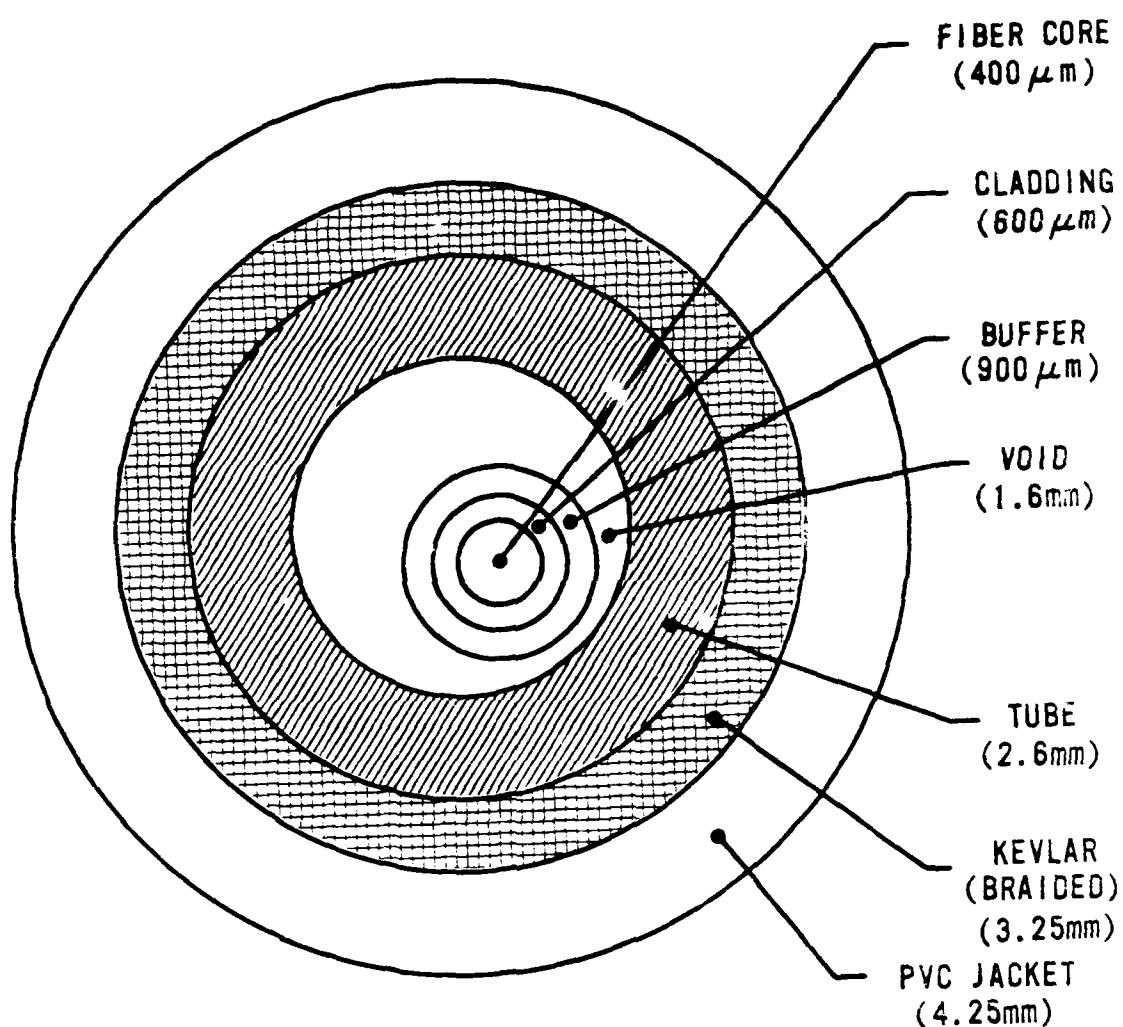
Since the two Math Associates Cables have fairly good jacket protection (and a loose tube construction), no protection was provided for these other than filling the penetration hole with RTV to prevent sharp bending of the cable around the edge of the hole. One Siecor cable (orange jacket) was protected by a $\frac{1}{4}$ -inch steel pipe, and the black-jacketed Siecor cable was protected by a hydraulic rubber hose. Both protections extended 4 ft away from the structure and extended 6 in from the surface into the structure, except for the steel pipe in the bulkhead which was flush with the inside surface. RTV was also used to seal off the pipe and hose ends and to prevent cable contact with the sharp rim of the ends. The cable in the steel pipe was further cushioned by a foam wrap throughout the pipe length.

Instrumentation--Each cable was started at the IS5 shelter, run through the structure, and back to the instrumentation van for recording the data. Of the five optical link systems available, one was a true analog link and



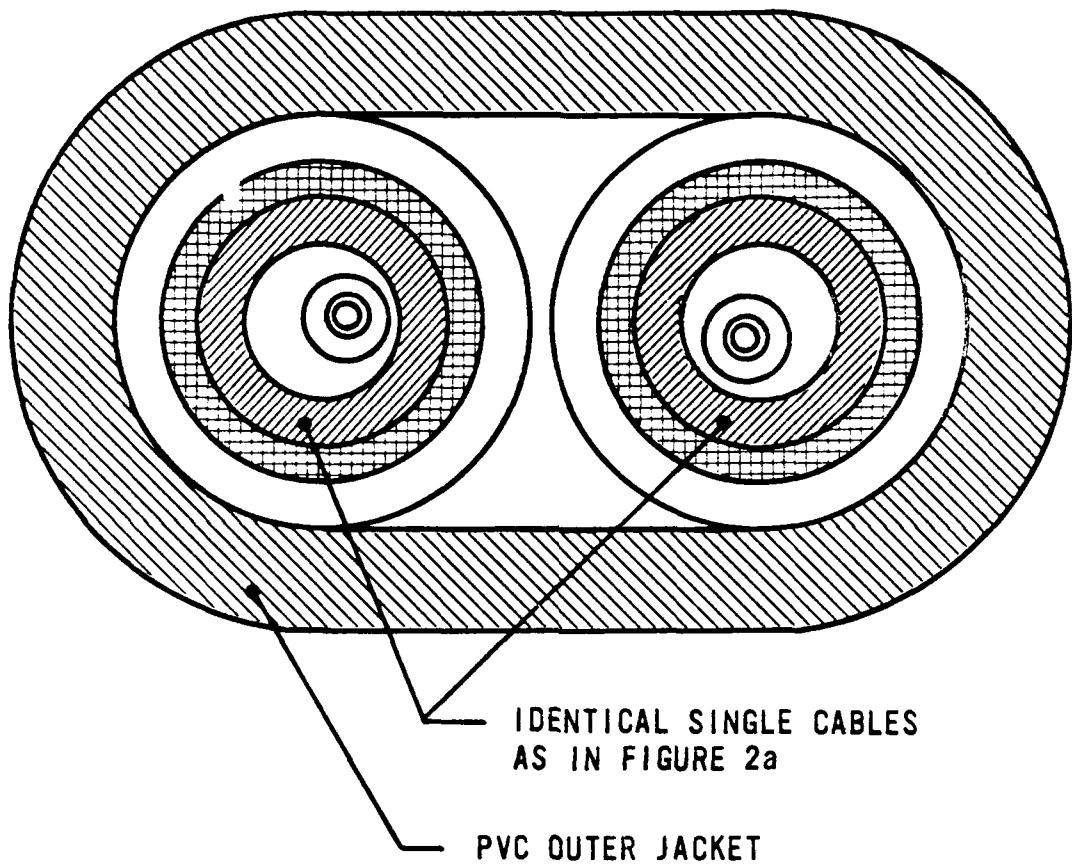
SCALE = 33:1

Figure 50. Siecor cable 144 cross section.



SCALE 30:1

Figure 51a. Math associates cable cross section single fiber.



SCALE 15:1

Figure 51b. Math associates cable cross section dual fiber.

TABLE 14. FIBER CABLE PARAMETERS

	Siecor 144	Math Assoc. 1050s	Math Assoc. 1040s2
Core	100	400	300
Cladding	glass	plastic	plastic
Index	partially graded	step	step
Number of Fibers	1	1	2
Numerical Aperture	0.3	0.27	-
Attenuation at 850/890 nm	10	10	10
Bandwidth	20	10	20
Maximum Tensile Load	300	N	N
Minimum Pulling Strength	50	63	63

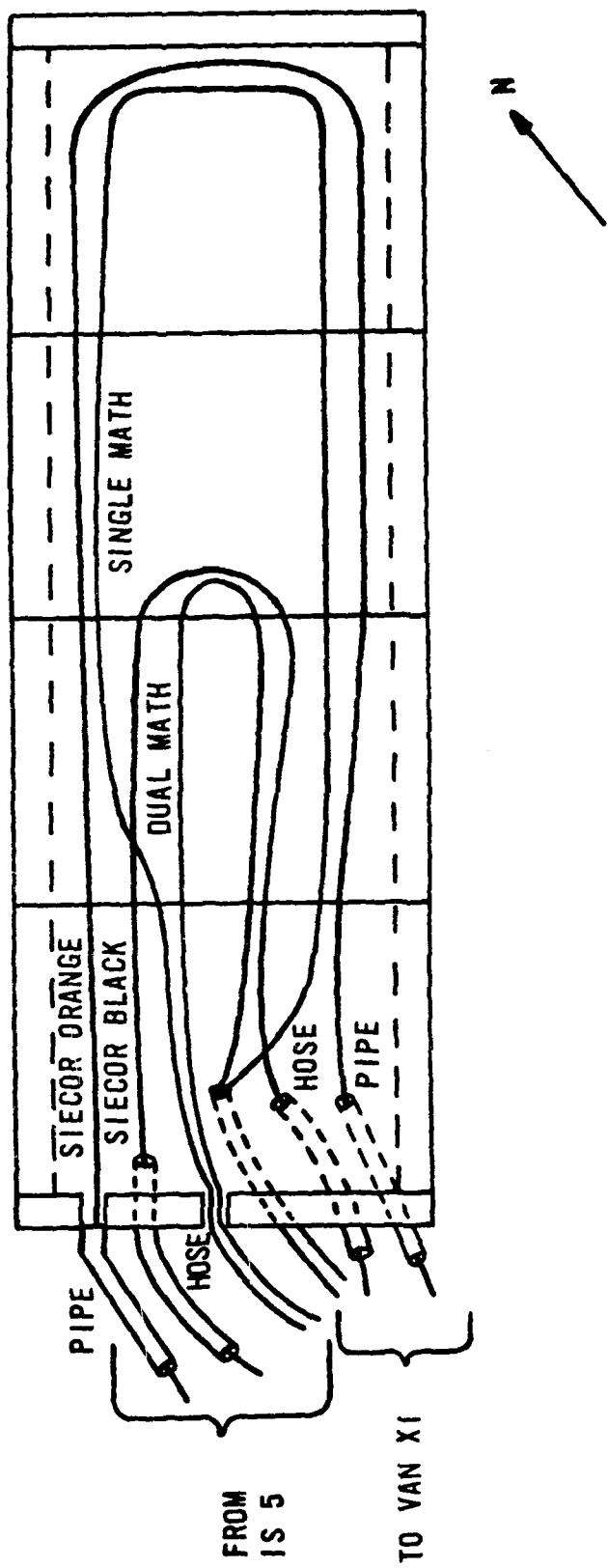


Figure 52. General cable payout in section.

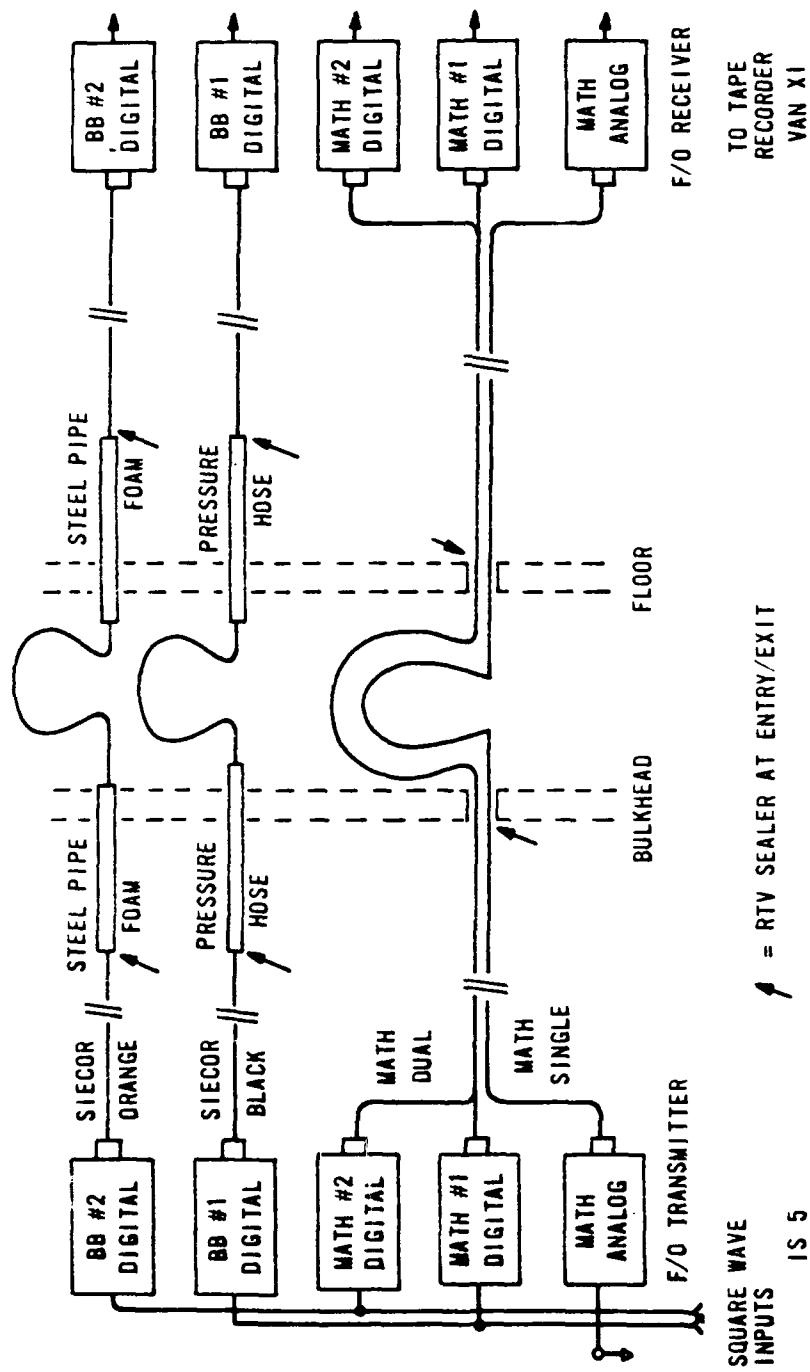


Figure 53. Cable protection detail.

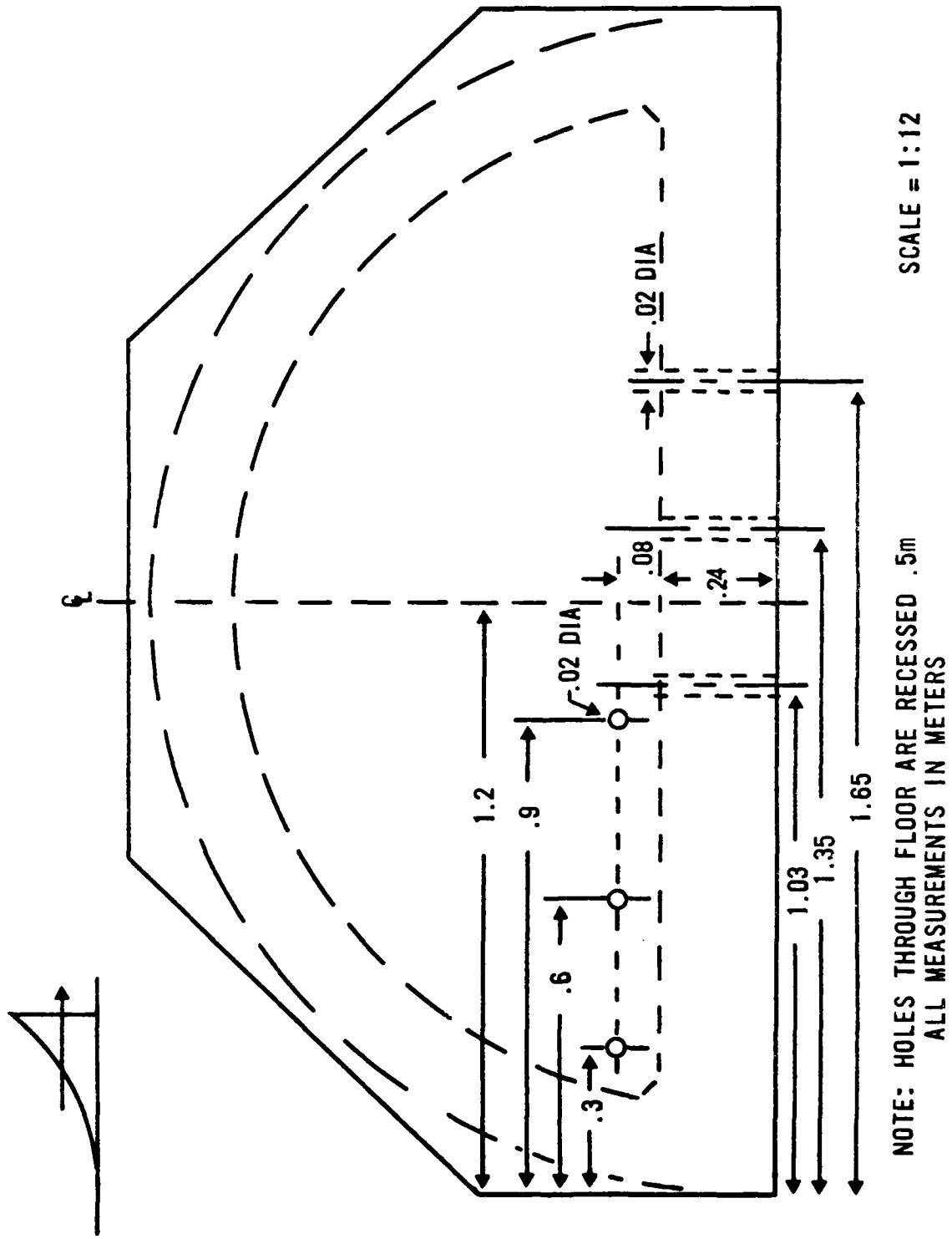


Figure 54. Cable penetration location, bulkhead view.

four were digital links. A square wave of approximately 10 kHz was applied to the digital links, two with 0-deg phase and the other two with 180-deg phase, so that at any one time two links always were in the ON-state. The analog link carried a zero signal and was set to the nominal operational full-scale level with a suitable calibration step provided. This analog setup was expected to show noise due to the physical environment of the cable (acceleration, pressure, strain), while the digital links would provide data on the amount of digital distortion resulting from this environment.

The signals generated in the IS5 shelter for input to the fibers were also fed to cable drivers for transmission to the instrumentation van (Fig. 55). The output of the respective cable receivers in the van was recorded on FM Tape tracks.

All cables were expected to survive the structure-media interface environment, and signal interference, if any, was expected to correlate to this environment.

ENVIRONMENT

Free Field--A central location for the free-field environment relative to the cable concentration is $x = 2$ m, $y = 10$ m, and $z = -2$ m, in global coordinates. The environment at this location is estimated below.

400-G peak vertical acceleration

7-m/s peak vertical velocity

0.2-m peak vertical displacement

75-G peak horizontal acceleration

0.9-m/s peak horizontal velocity

0.02-m peak horizontal displacement

The peak stress was estimated to be 1.2 MPa.

Structure--The A-5 structure was expected to stay intact. Fiber reactions to be recorded were to come from vibration and cable slap. But the midsection of structure caved in, covering all fibers (Fig. 52) with the full weight of the roof. The floor of the structure also ruptured and broke along the center line at the south end where the cable exits were located

STRUCTURE IS 5

VAN XI

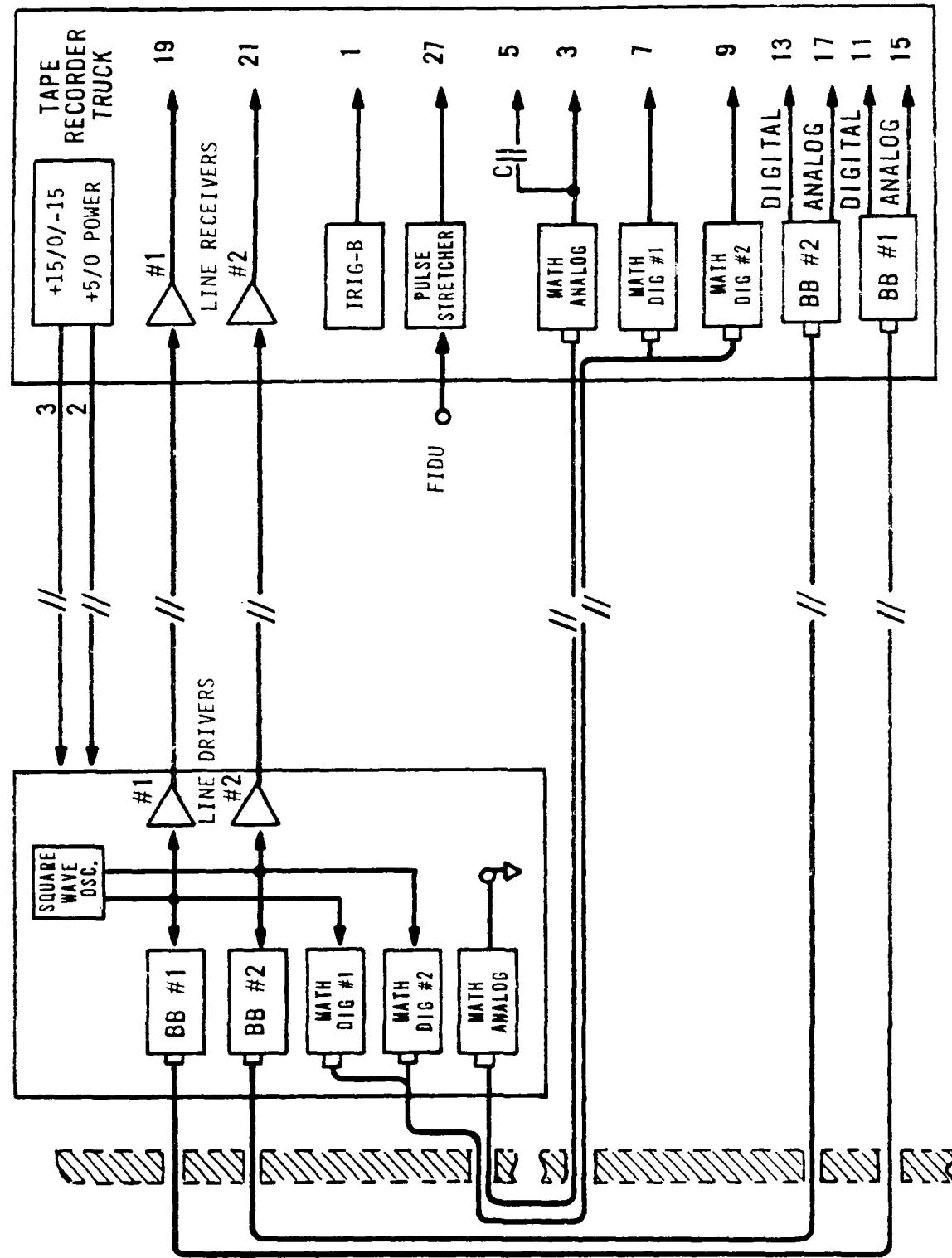


Figure 55. Instrumentation.

(Fig. 54). No vertical gage was close enough to the cable penetrations to obtain actual measurements.

RESULTS

All links dropped out between 20 and 30 ms after zero time, as shown in Table 15 and the accompanying figures (Figs. 56 through 60):

TABLE 15. FIBER OPTICS DATA SUMMARY

<u>Cable</u>	<u>Data</u>	<u>Protection</u>	<u>Dropout Time</u> (ms)	<u>Figure</u>
Siecor black (#1)	Digital	Pressure hose	28.7	56
Siecor orange (#2)	Digital	Steel pipe	22.3	57
Math Dual #1	Digital	None	21.7	58
Math Dual #2	Digital	None	22.3	59
Math Single	Analog	None	21.1	60

The dropout is complete and instantaneous in the Math cables, whereas a short transition period is observed in both Siecor cables. The "a" frame of the figures shows the dropout time from the fiducial point, while the "b" frame is a time expansion about the dropout incident.

The postmortem inspection showed that, at the bulkhead (outside), no damage was visible where it was most expected, at the unprotected exit. The cables were also intact at the outside exits from both pipes and hoses. All cables had continuity from the exits to the instrumentation shelters.

Continuity could not be found on any cable inside the structure. The cables penetrating from the underside of the structure bottom were as clean as those exiting through the bulkhead. The two Siecor cables that went through the bottom were pulled out for inspection. Both showed continuity.

AD-A171 212

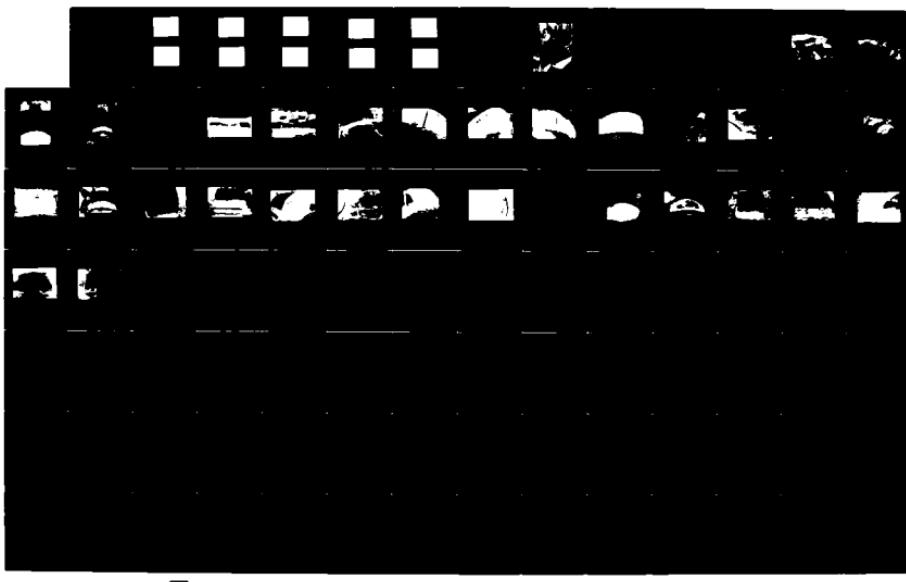
KACHINA TEST SERIES: DYNAMIC ARCH TEST THREE (DAT-3)
ANALYSIS REPORT(U) AIR FORCE WEAPONS LAB KIRTLAND AFB
NM J L SMITH ET AL. MAR 86 AFWL-TR-85-63

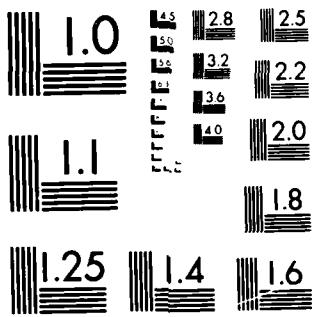
2/6

UNCLASSIFIED

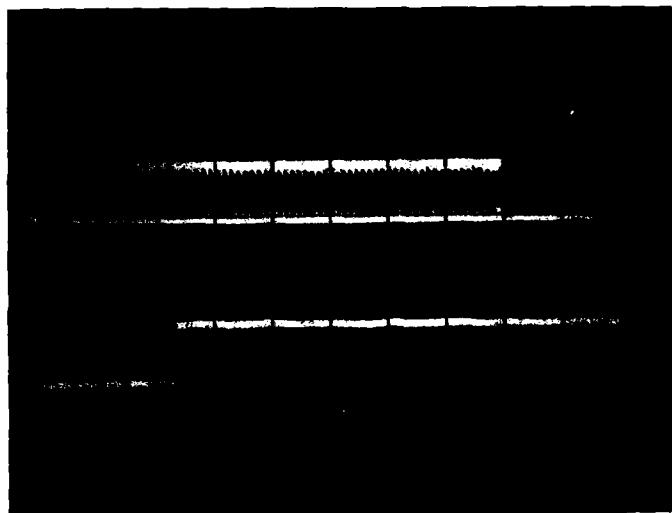
F/G 19/4

NL

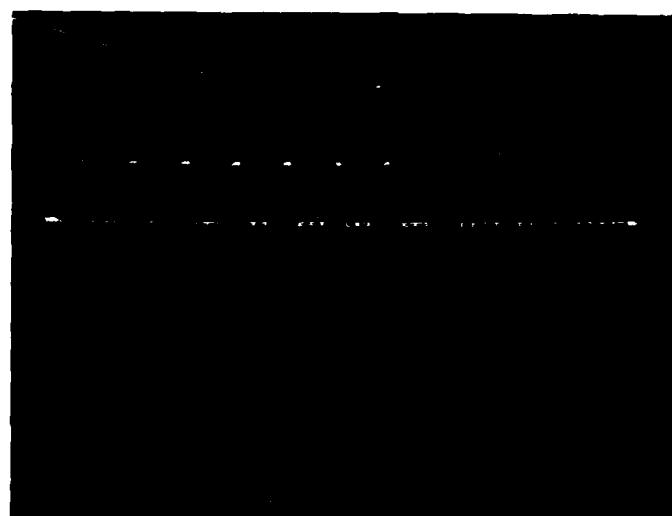




MICROCOPY RESOLUTION TEST CHART
NATIONAL BUREAU OF STANDARDS 1963-A

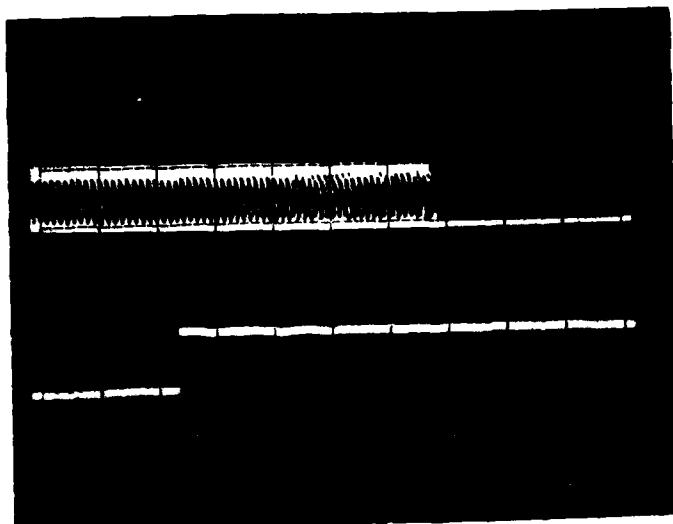


a. 5 ms/div.

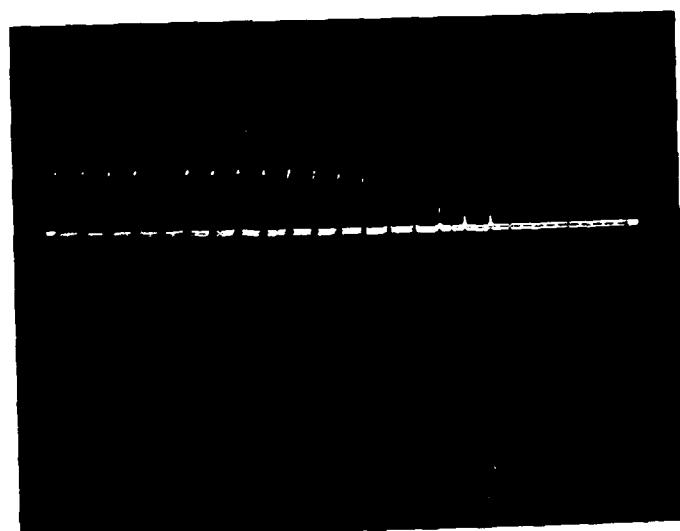


b. 0.1 ms/div.

Figure 56. Siecor Cable black (BB #1).

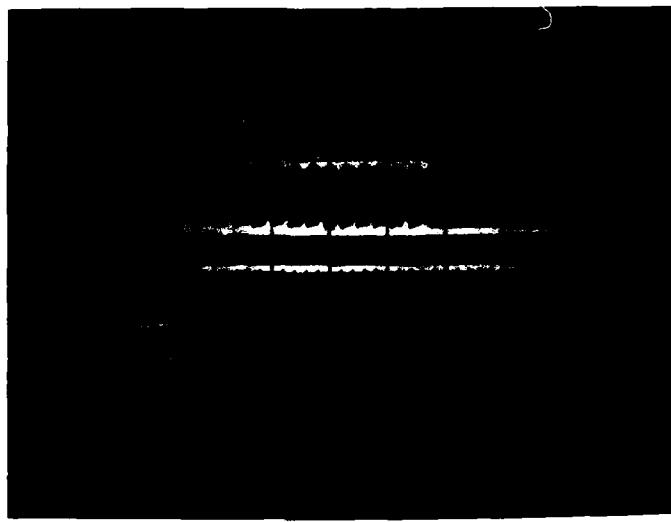


a. 5 ms/div.

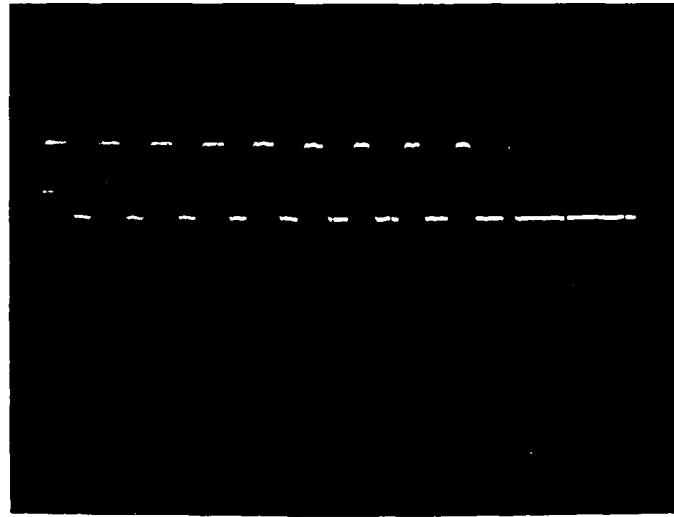


b. 0.2 ms/div.

Figure 57. Siecor Cable orange (BB #2).

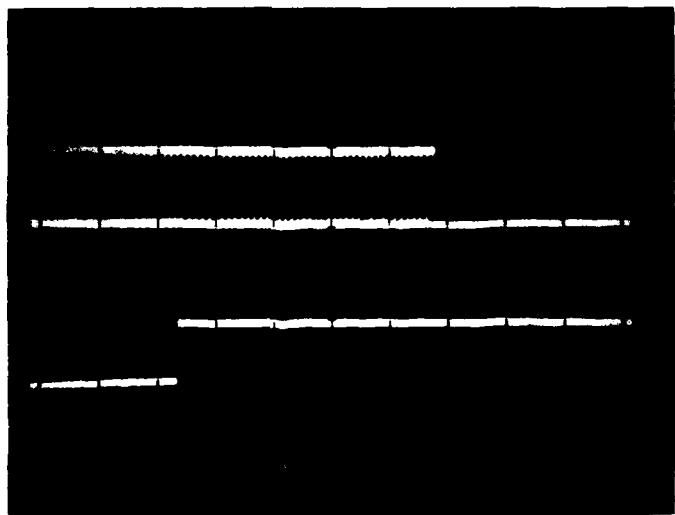


a. 5 ms/div.

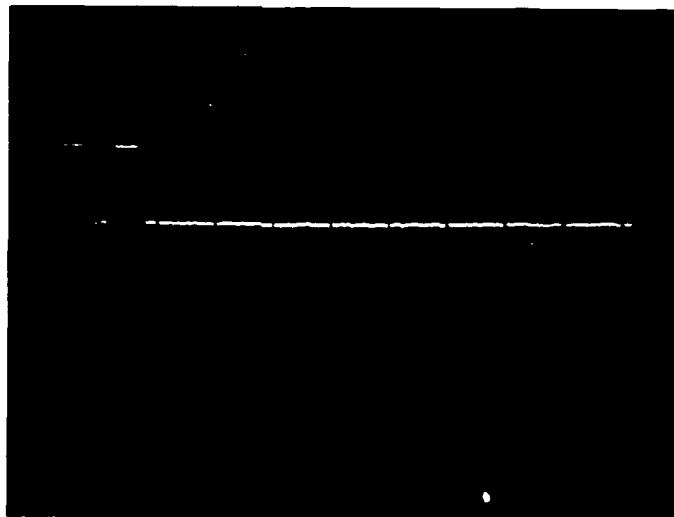


b. 0.1 ms/div.

Figure 58. Math Dual Cable #1.

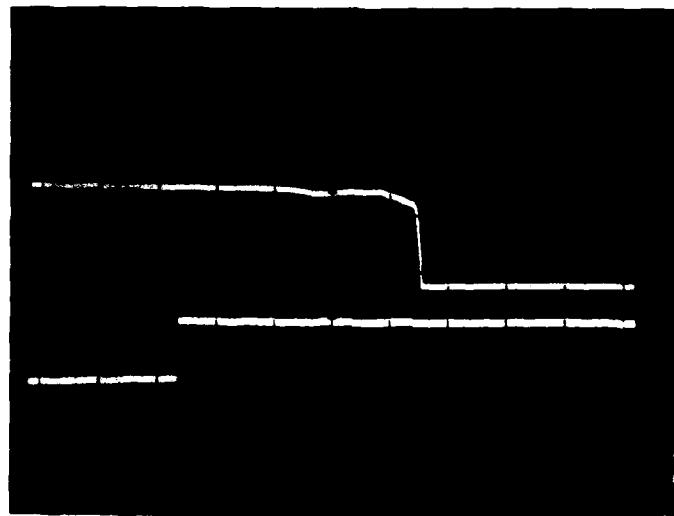


a. 5 ms/div.

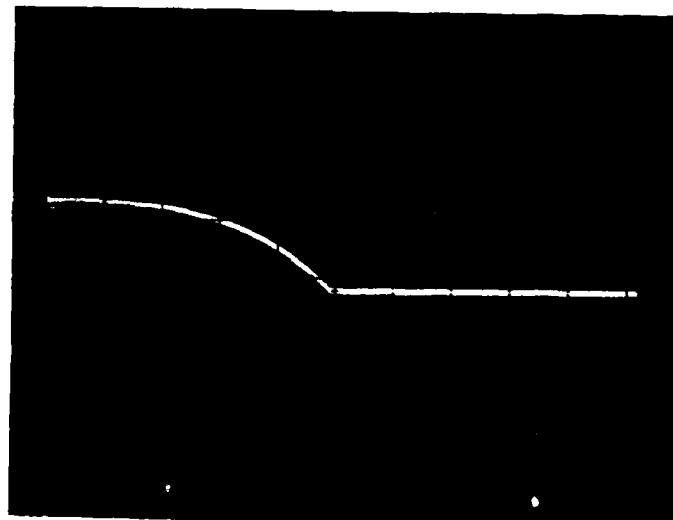


b. 0.1 ms/div.

Figure 5C. Math Dual Cable #2.



a. 5 ms/div.



b. 0.2 ms/div.

Figure 60. Math Single Cable.

DISCUSSION

The cable failures have to be correlated with structural events and an explanation of the failure mode has to be advanced. Three possible failure modes are being investigated in the following: Shearing at the inside surface of the bulkhead due to the bulkhead being pushed down relative to the floor, pinching at the outside surface of the floor due to buckling of the floor slab, and breakage due to the cave-in of the midsection.

By pushing down the bulkhead against the structure floor, the cables could have been sheared off. Floor and bulkhead have to move about 8 cm towards each other for the shearing action to begin. Lacking gages in the immediate area, arrival times have to be calculated from burn rate and stress propagation in the soil. This yields an arrival time of 18 ms at the bulkhead penetrations through the soil.

In Figure 60a, an early, slight disturbance in the analog amplitude can be seen at $t_a = 8.6$ ms. Calculating the stress propagation through the concrete material of the bulkhead, a time of arrival of the stress wave at the penetrations of 8.7 ms results. The amplitude disturbance at this time is approximately 4.5 percent or 6.5-dB attenuation of light energy. Stress values could not be obtained.

Since the steel pipe ended up flush with the bulkhead, the orange Siecor cable could have been sheared off in a similar way as might have been possible for the two Math cables. In fact, the times are very similar. All cables show a squeeze of the fiber of about 1-ms duration before the final break. The reason that the black Siecor cable took 6.5 ms longer to break might have been the pressure hose protection. It should take a little longer to shear through this material before the fiber is reached. The postmortem inspection does not support this theory, however.

The floor penetrations indicate a probability that the buckling of the floor plate could have pinched off the cables at the exit. The fact that the Math single cable still had continuity through the bulkhead, but broke at the same time as the others, suggests that the recorded break might have happened in the floor penetrations. Further breaks can be expected later in the center of the structure by the massive cave-in. Again, the postmortem inspection does not support this theory.



Figure 61. Posttest bulkhead inspection.

Although the structure analysts do not believe that the cave-in of the midsection could have happened as early as T+22 ms, some mechanism must have existed that could have broken cables in locations other than the penetration locations.

CONCLUSIONS AND RECOMMENDATIONS

Although the original objective could not be fully realized, the following can be established:

- a. The cable protection was adequate for the anticipated environment at the penetrations.
- b. The pressure hose protection was superior in this test to the other two means, i.e., steel pipe or loose tube construction.
- c. The analog signal transmission suffered from physical stress and/or strain on the fiber.
- d. The digital transmission can stand fairly large light intensity variations without effect on the transmission quality.

Since, due to the nature and circumstances of this particular test, the environment at the cables could not be obtained, a quantitative relationship between stress on the cable and its effect on transmission quality could not be established.

A fiber optic cable test that can provide these data should be designed.

VIII. STRUCTURAL RESPONSE

INTRODUCTION

The general intention of the DAT-3 test event and the KACHINA Test Series was to study the response of buried arches which underwent severe deformations and cracking under loading from a simulated nuclear surface burst. Test results met this expectation in that each arch responded well into the plastic region of behavior for reinforced concrete. This section will focus on characterizing the behavior of the structures: (1) In DAT-3 individually, (2) as a group, and (3) with respect to the KACHINA Butterfly Maiden (KBM) and KACHINA Eagle Dance (KED) tests.

Presentation of Data--Both active and passive instrumentation results will be used to define structure response during the test. Active gages from the test collected data on: (1) Normal stresses at the soil-structure interface around the arches, (2) accelerations along the principal X, Y and Z axes of each structure, and (3) reinforcing bar strains for bars oriented circumferentially and longitudinally in each arch. Passive relative displacement gages recorded the maximum vertical relative displacement between the inner crown and the center of the floor. Another source of data was the pictures taken of the excavated arches which showed the actual damage magnitudes and crack patterns on the arches. All of these sources will be used in the discussion of structural response.

Section Overview--Data from the aforementioned sources have been organized to allow the reader to develop an understanding of arch response and failure. First, the posttest photographs of the arches will be reviewed so that an image of failure planes and crack patterns for each arch relative to the others can be used as a foundation upon which the data results can be built. Loading on the arches will then be presented using normal stress data. Response of the arches to these loads will be presented in the form of velocity and strain graphs. This understanding of DAT-3 arch response will then be compared and contrasted with results from the KED and KBM tests to complete the KACHINA Test Series objective of understanding arch behavior as affected by parameter variations. All of these data will be condensed and presented as a short series of pertinent factors in the conclusion to this section.

With this understanding of the purpose of this section, the data used to develop the theory of response and the organization of presentation, the analysis of the DAT-3 arch response begins with pictorial data.

POSTTEST PICTORIAL REVIEW

General--The arches in the DAT-3 test experienced severe plastic deformation visible as cracking and spall over most of each cross section. Therefore, points of interest in the following photos are areas where cracking and failure are at a maximum and, also, areas where no visible cracks are present. These areas will be examined for each arch in detail.

A general examination of the test-bed from the upstream and downstream sides can be found in Figures 62 and 63, respectively. The excavated test-bed surrounding the arches illustrates the shallow-buried fielding of the arches during testing. The large chunks of concrete visible inside each structure are pieces of spalled concrete which would have had adverse effects on any unprotected contents within the arches. The vertical pipes visible in each arch are the passive relative displacement gages. Referring to Figure 62, the 1.7-m arch in the foreground is A7. Arch A6, resting on a foundation, is visible as the 1.7-m arch at the far right. Arch A5 is the four-segment arch, with the butt joint at the farthest red line, and the keyed joint at the middle red line; the closest red line is the butt joint with the elastomeric pad. While the midsections of A5 show a total collapse of the arch, the two end segments resemble their counterparts A6 and A7 upstream. Near-field and free-field soil analysis presented in Section VI indicates that vertical soil motions in the center of the test-bed may have contributed to the collapse of the middle sections in A5, but the findings require further study. More information about this contribution will be made in later discussions.

Arch A5--Figures 64 and 65 present end-on views of A5, highlighting the fairly symmetric failure of the arch in the middle sections. The upstream and downstream sides of the arch do not appear to differ as to the location or severity of the main fracture zone, with the exception of the south end segment of A5 which shows more failure on the downstream side. Each end cross section shows the focusing of the severe cracking at about ± 60 deg of angle from the crown of the arch and at the floor center. Unlike the KED



Figure 62. View of test-bed from upstream north side.



Figure 63. View of test-bed from downstream north side.

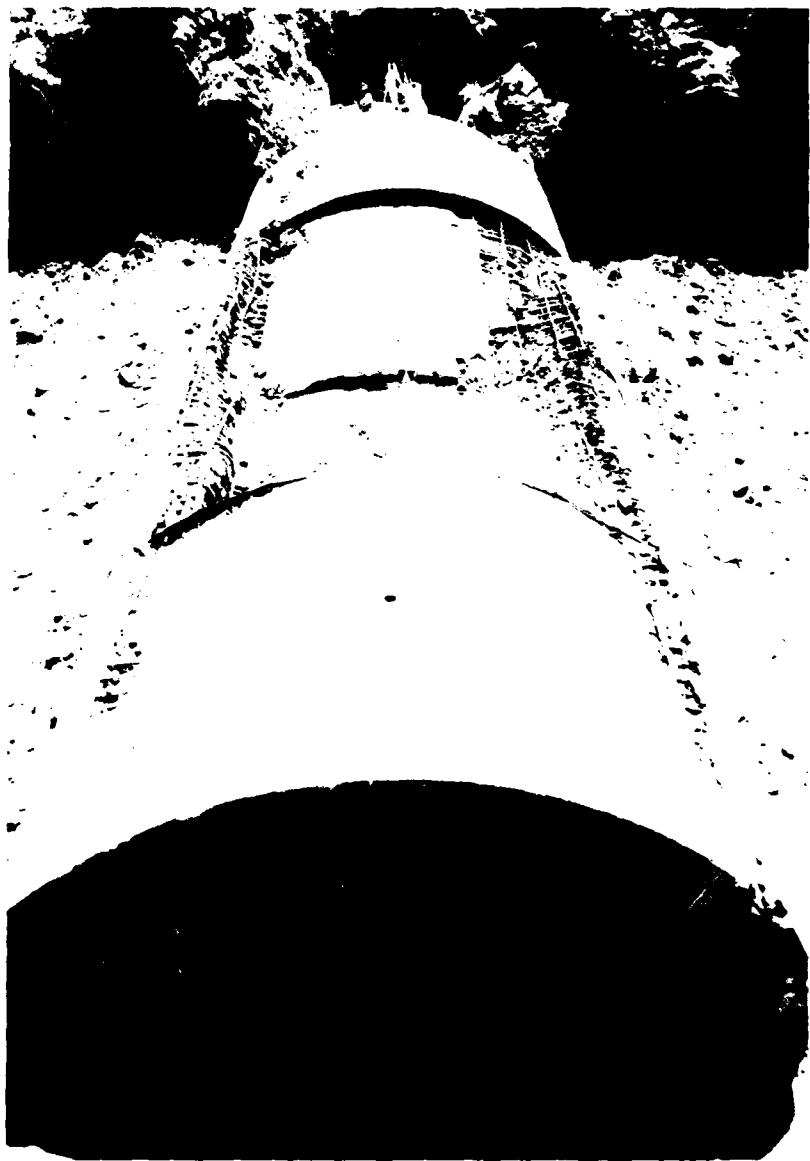


Figure 64. View of Arch A5 from north end (upstream on right).



Figure 65. View of Arch A5 from south side (upstream is left).

short arches, joint shear and beam shear cracking at the floor edges was not a major failure mode on DAT-3. The chamfer is intact, and relative deformation between the wall just above the floor and the floor is not apparent.

Exterior wall cracks in A5 are the focus of Figures 66 and 67. As seen in Figure 66, the upstream wall shows a major failure zone running longitudinally at about 45 to 60 deg from the crown, with a secondary failure zone along a line 75 deg from the crown running parallel to the first fractured zone. Figure 67 shows that the secondary crack zone is not as well defined on the downstream side, possibly due to a lower moment, but greater thrust is acting on the downstream wall relative to the upstream wall. This would indicate that the secondary cracking is due to moment in the wall. A major deviation from the KBM and KED arch response is seen by a total lack of circumferential failure at the bottom edge of the wall. Evidently, the joint reinforcement used in A5 on the DAT-3 test to minimize the joint shear failure which caused the external appearance in the KED and KBM events was successful.

A closeup of the crown area at the key joint at the center of A5 is shown in Figure 68. This is the point of maximum collapse of the crown of A5. The lower section of the key joint, in the foreground, is obviously more displaced than the upper section.

Figures 69 through 74 concentrate on the interior views of A5. Because of the collapse in the middle segments, documentation of the interior is limited to the north and south end segments of A5. Figure 69 shows the inside north segment of A5 before the spall chunks were removed. These sizable pieces of concrete pose a hazard for possible arch contents, even though the majority of the walls still protect an open space. Extreme distress is also visible on the passive relative displacement gages further in the interior of A5. Figure 70 shows the north segment upstream interior wall. Notice the integrity of the corner chamfer and the crack region focused between 60 and 80 deg from the crown in the wall. Tensile cracks are evident on the interior crown and the floor surface. These are cracks due to circumferential bending response of the arch. Cracking on the downstream interior wall of the north segment of A5 is seen in Figure 71. Here, spall is concentrated between 30 and 60 deg from the crown. Once again, the chamfer at the joint is undisturbed.

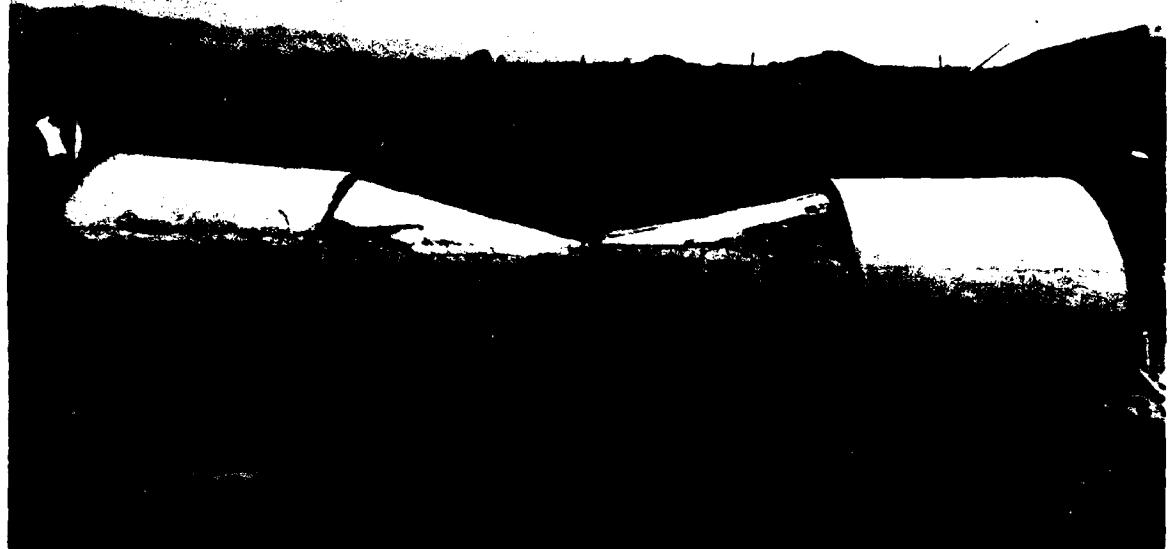


Figure 66. View of Arch A5 upstream exterior.



Figure 67. View of Arch A5 downstream exterior.



Figure 68. View of Arch A5 center key joint at crown.



Figure 69. Inside view of north end of Arch A5 (downstream at left).



Figure 70. View of upstream north end interior of Arch A5.



Figure 71. Downstream interior north end view of Arch A5.



Figure 72. Interior view of south end of Arch A5 (upstream is left).



Figure 73. Interior upstream south end wall of Arch A5.

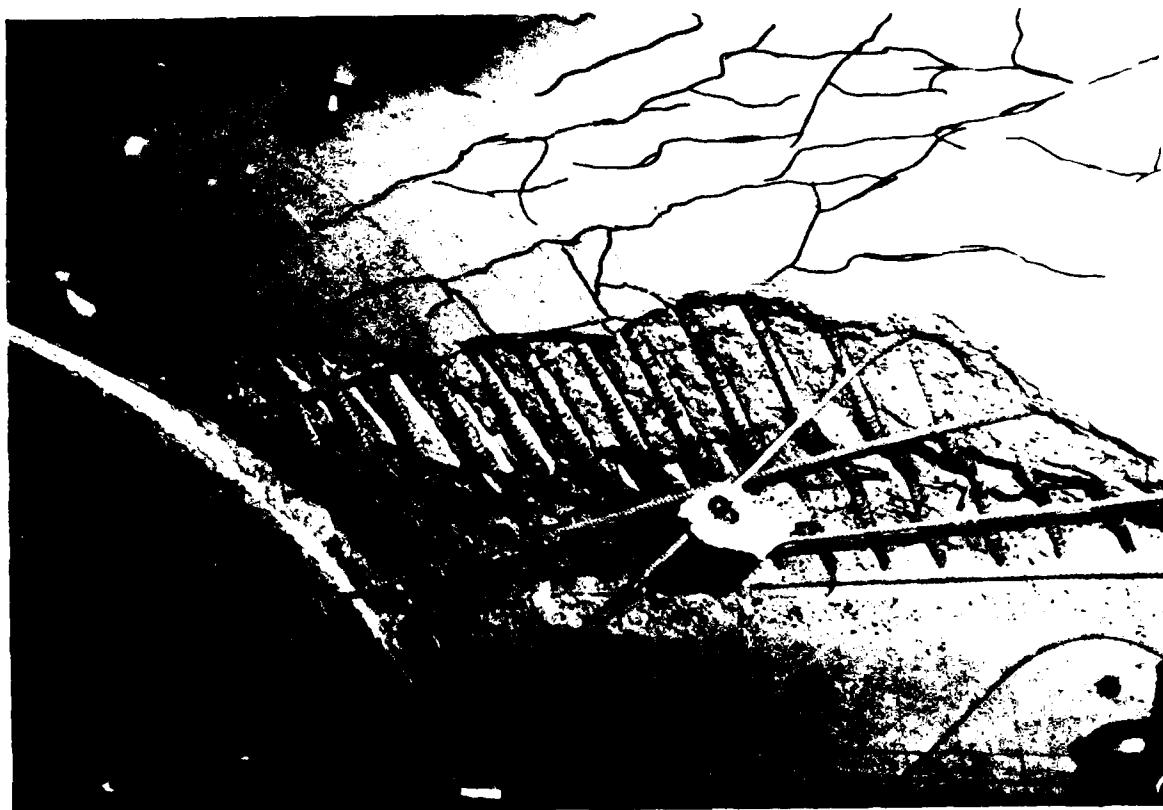


Figure 74. Interior downstream south end wall of Arch A5.

Figure 72 illustrates the interior of the south end segment of A5. Tensile cracks due to circumferential bending are seen at the inner crown and the floor surface as in the north end segment. Tensile cracks run deepest at the floor center, where bending moments are most severe. Spall, focused between 60 and 75 deg from the crown on the upstream wall, is shown in Figure 73, while Figure 74 presents the downstream interior wall, which shows a spall zone between 30 and 60 deg from the crown.

The overall failure trends in A5 indicate the spall zone is lower in the wall on the upstream side and in the middle of the wall (and wider) in general on the downstream side. Also, failure has been refocused to the floor center and the walls at about 60 deg from the crown, due to joint reinforcement relative to the KED test. These trends will be compared with those seen in the separate arch segments, A6 and A7, shown in Figure 75.

Arch A6--Arch A6 had the same cross-sectional dimensions and reinforcement as the other DAT-3 arches, but it sat on a continuous footing centered under each wall to examine the effects of the footing on response.

End views of A6, shown in Figures 76 and 77, highlight some failure modes not seen in the end segments of A5. Cracking in the floor is increased along the width, and beam shear failures at the floor edge on the upstream side have initiated, as seen in KED and A4. Failure planes in the walls still exist at 60 deg from the crown, but are less developed. The chamfer is fairly intact on both sides of the floor.

The exterior walls of A6 reflect less cracking at 60 deg from the crown than the other DAT-3 arches. As shown in Figures 78 and 79, the upstream side has major failure planes only at 30 and 50 deg from the crown (slightly higher than A5), while the downstream exterior shows the same major failure zone and an additional secondary crack zone at about 75 deg from the crown. This secondary crack zone has moved from the upstream side of A5 to the downstream side of A6. Photos of A7 will help to correlate this effect as a slight variation or a change in response caused by the footing.

Figures 80 through 83 show the interior of A6. The upstream wall shown in Figure 80 has a lower spall region above the floor and a more distressed zone between 45 and 60 deg from the crown. Figure 81 illustrates the



Figure 75. View of Arches A6 and A7 (foreground) from downstream north side.



Figure 76. North end of Arch A6 (upstream is right).

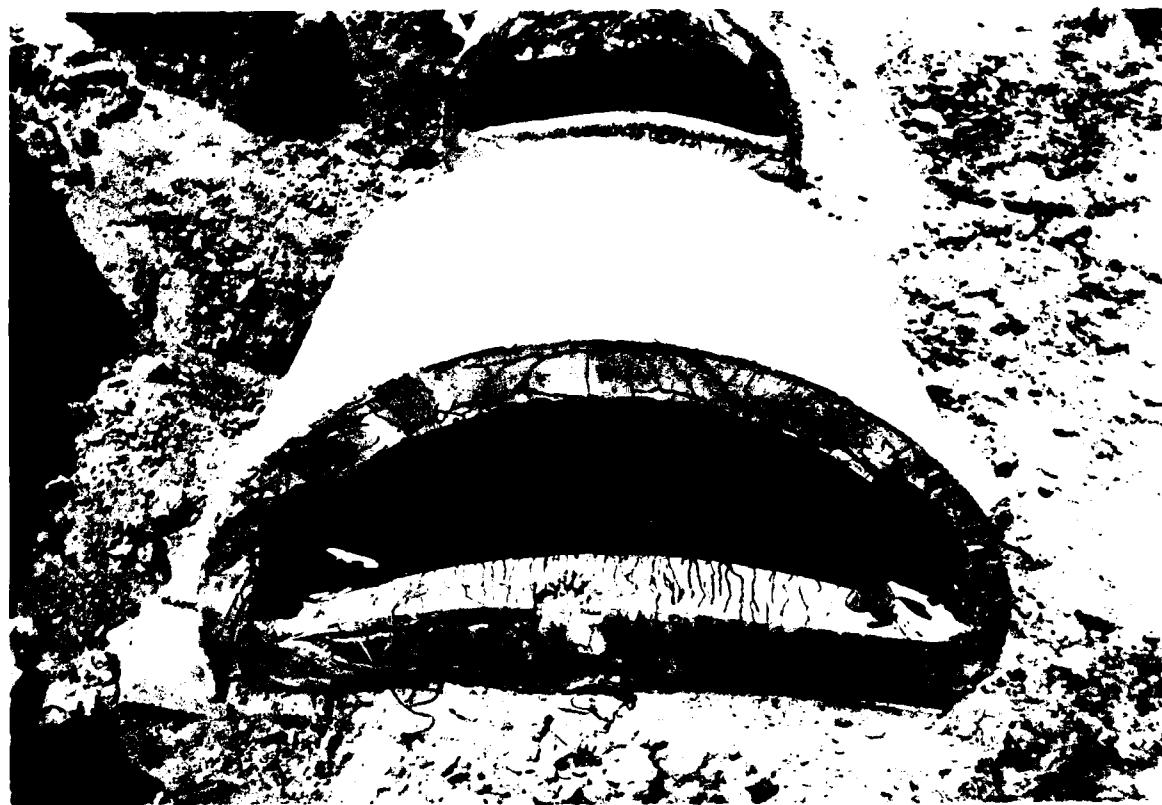


Figure 77. South end view of Arch A6 (upstream is left).



Figure 78. Upstream exterior of Arch A6.



Figure 79. Downstream exterior of Arch A6.



Figure 80. Upstream interior wall of Arch A6.



Figure 81. Closeup of Arch A6 upstream interior wall.



Figure 82. Downstream interior wall of Arch A6.



Figure 83. Closeup of Arch A6 downstream interior wall.

dominance of this shear plane formation in the wall. Figure 82 presents the downstream wall, which is quite similar to the upstream wall, but the spall region is larger and slightly further from the crown. The gage mount at 45 deg from the crown is atop the spall zone, shown in Figure 83.

Relative to A5, Arch A6 appears to have been affected by the footing which directed the failure into the floor of the arch and the lower walls. Relief of the shear failure zone at 45 to 60 deg from the crown is apparent in the photographs, although the character and location of the spall is not significantly affected. Evidence from A7 will complete this review of the visual data from DAT-3 on general arch response and the effects of footings on arch response.

Arch A7--Arch A7 is, for the most part, similar to Arch A4 in the KED test with respect to its location in the test-bed, length, and lack of support (free standing, no footing). The major difference between the two arches is the reinforcement percentage (higher for A7) and the corner reinforcement details (better confinement and shear reinforcement in A7).

End views of A7 are presented in Figures 84 and 85. This arch is similar to the end sections in A5, whereas failure is concentrated at the 45- to 60-deg points in the walls and at the floor center. Very little cracking is evident at the edges of the floor relative to A6. Tensile cracking is evident in the interior crown and inner floor surface in the same pattern as that seen in A5. Both the upstream and downstream side chamfers, at the edge of the floor, are undisturbed.

Exterior wall surfaces are fairly symmetric for A7. Figures 86 and 87 show the extensive longitudinal crack patterns due to circumferential bending, with major cracking at the shear failure centered 45 to 60 deg from the crown of the arch. Secondary crack zones at about 75 deg from the crown are evident on both sides of the arch.

Interior walls show spall zones similar to those in A5 and A6. Figures 88 through 90 show the spall regions, which extend from 45 to 60 deg from the crown, with a minor spall zone on the upstream wall just above the floor seen in Figure 88.



Figure 84. North end of Arch A7 (upstream is right).



Figure 85. South end of Arch A7 (upstream is left).

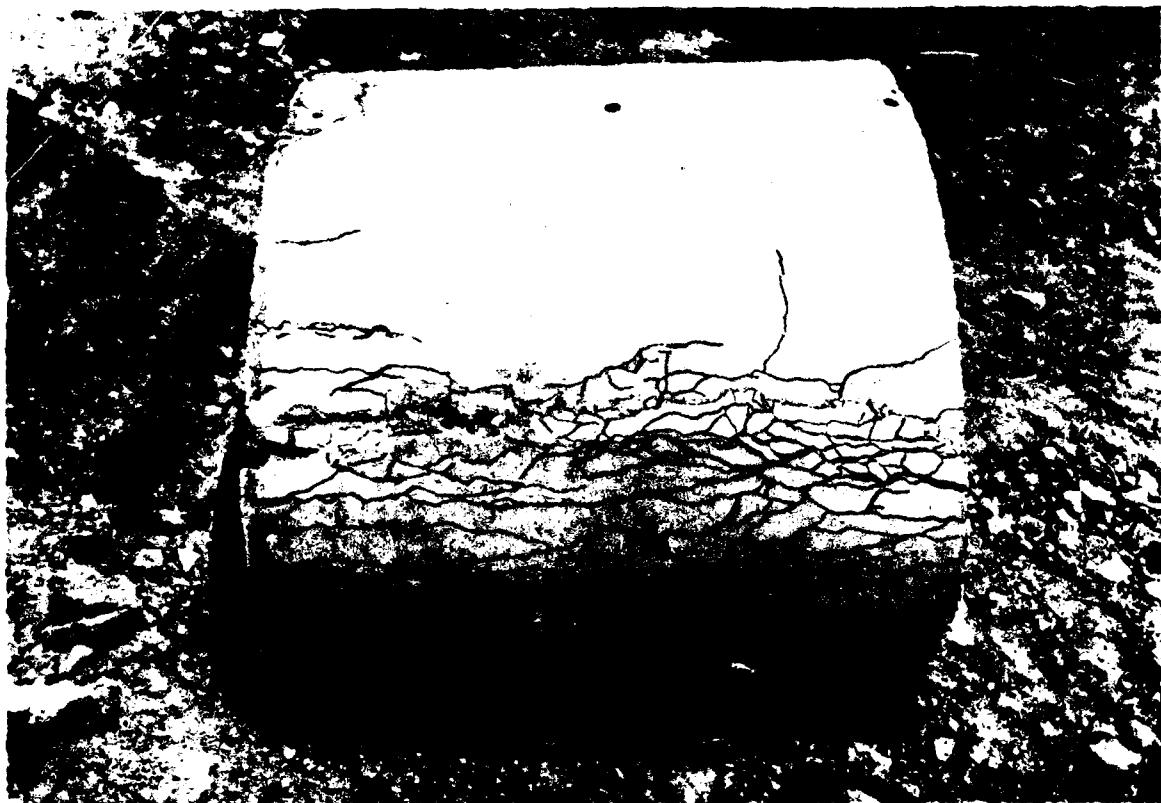


Figure 86. Upstream exterior wall of Arch A7.

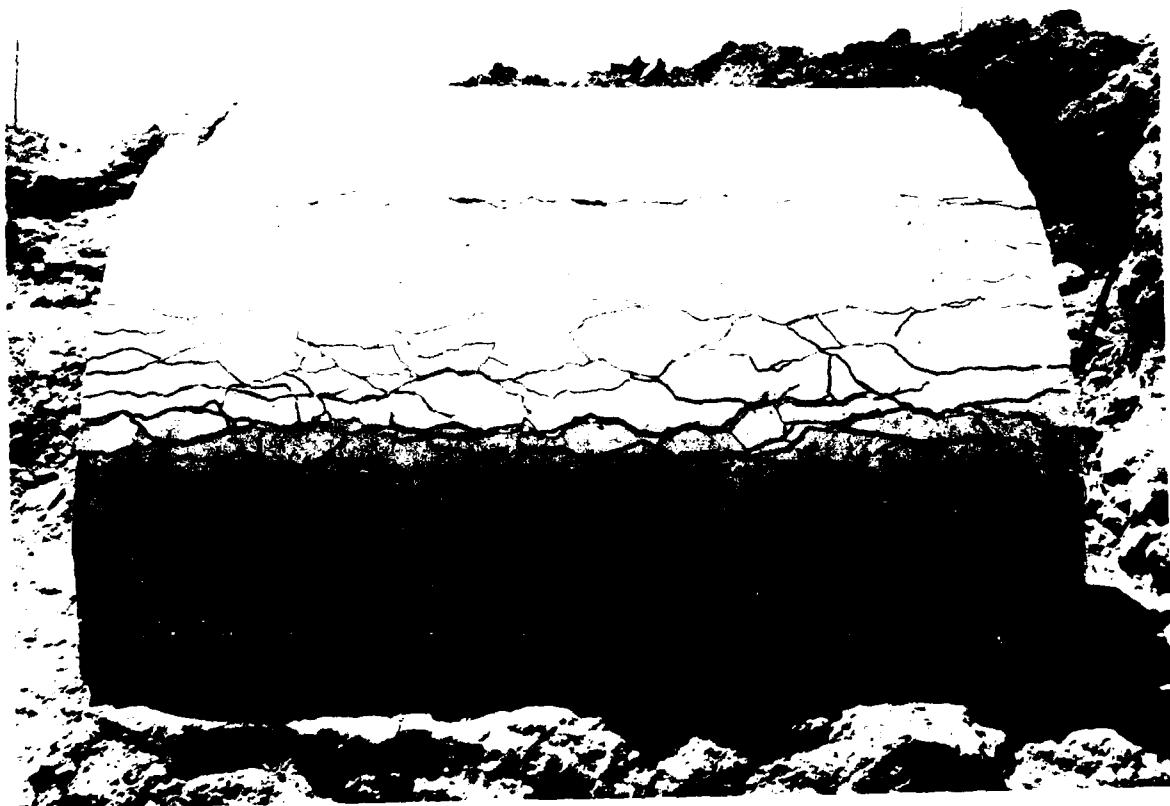


Figure 87. Downstream exterior wall of Arch A7.



Figure 88. Upstream interior wall of Arch A7.

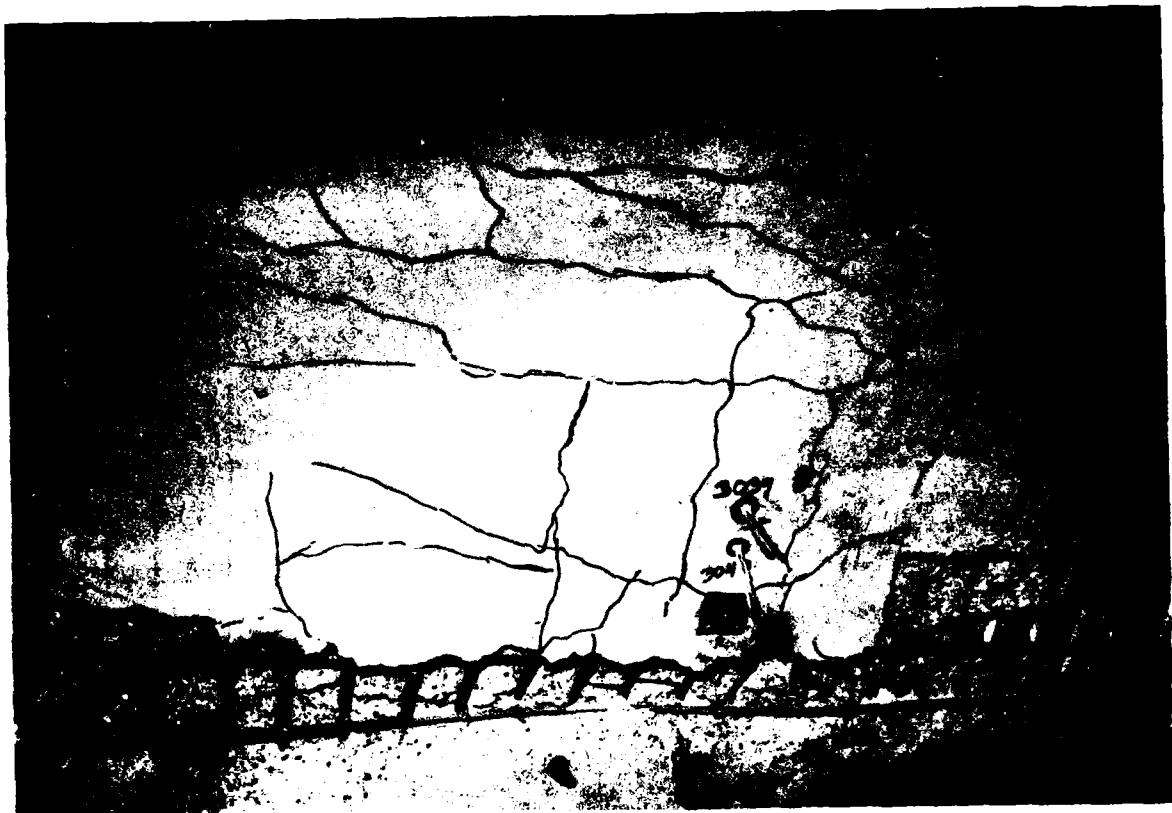


Figure 89. Closeup of Arch A7 upstream interior wall.



Figure 90. Closeup of Arch A7 downstream interior wall.

The general consensus of these results indicates that the unsupported arches, A5 and A7, are similar in response character. Both displayed hinge formations at 45 to 60 deg from the crown on the upstream and downstream walls and at the floor center. Exterior wall tensile cracks and interior spall regions existed generally between 45 and 85 deg from the crown of each arch. Severe tensile cracks formed in the floor of each arch extending from the floor surface down, due to extreme downward displacement of the floor edges relative to the center. Foundation effects on A6 most visibly altered failure zones by increasing failure in the lower walls and floor and relieving cracking in the upper portion of the arch.

Active data will lend insight to the timing of these mechanisms and verify the response theories in gaging footing effects on A6. The photographs will aid in the evaluation of the data records because the final result of arch responses will be known.

GAGE RESULTS

Active gages in the DAT-3 event performed well and provided a great deal of valuable information on loads and response. While some gages were not actually placed in their planned locations because of the placement problems mentioned in Sections II and III, generally, the symmetric gage layouts in each arch and between arches helped to form a fairly complete picture of arch loading and response. This portion of the structural response section will first discuss loads, then the motion response to the loading conditions, and finally the strains generated in the arches during response (and failure).

Normal Stresses--Normal stress magnitudes in the arches were a direct result of the applied airblast loading on the surface of the soil, and thus were predominantly a vertical phenomenon. Since the soil was stiffer in DAT-3, as discussed in Section VI, the horizontal loads applied around the arch were reduced from what was expected, and tended to be negligible relative to the vertical loads.

For example, the normal stresses recorded in A5 are presented in Figure 91. Vertical load at the crown is over 6 MPa (870 psi), but because of a gage problem, the gage did not record the peak value. By the time the load reaches 45 deg from the crown, the load has attenuated to approximately

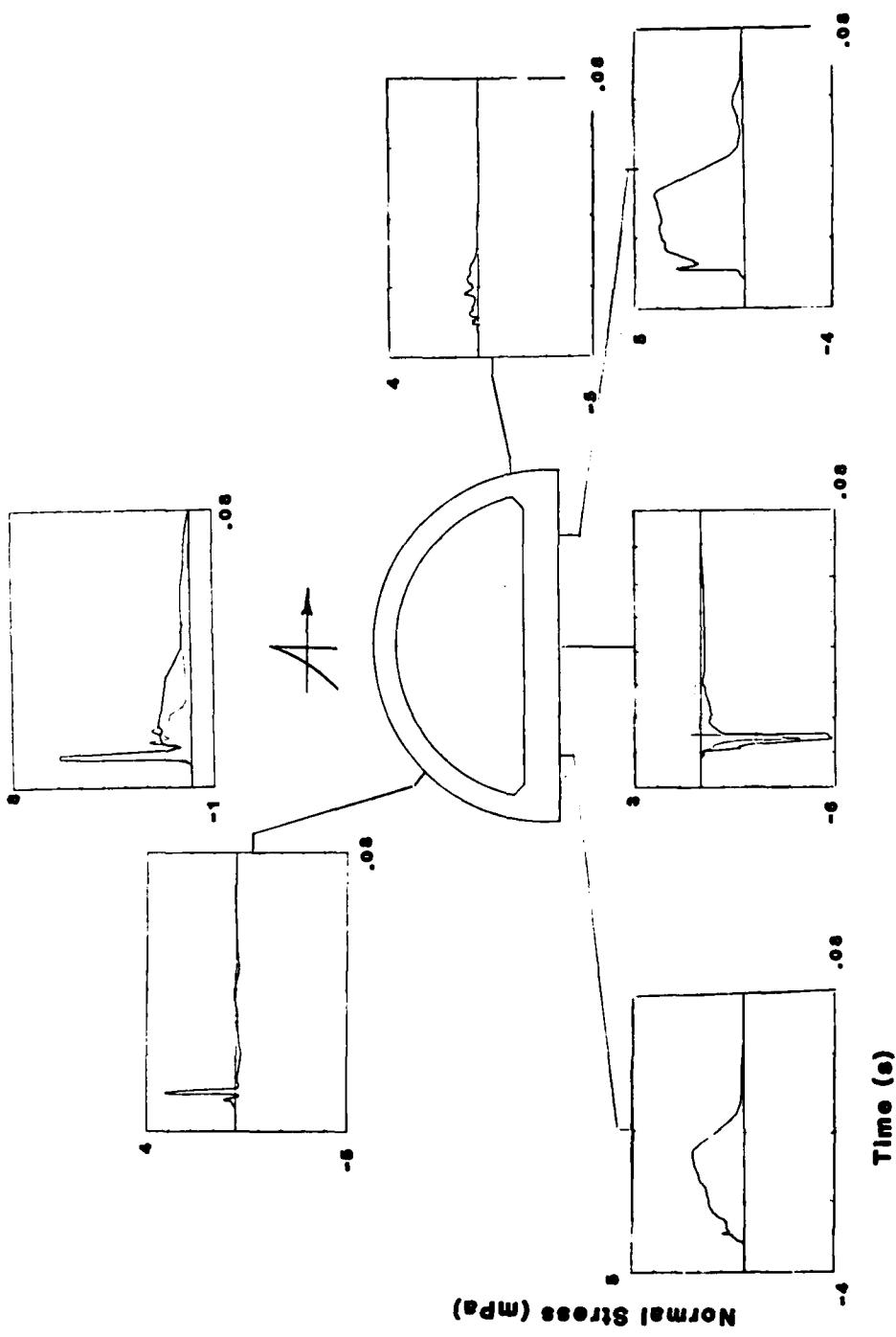


Figure 91. Normal stresses on Arch A5.

3 MPa (435 psi), and at 90 deg from the crown the horizontal stress measured at the interface is only approximately 0.5 MPa (73 psi). Vertical stresses under the walls, where the soil is attempting to support the arch, reach 4 MPa (580 psi) on the downstream side. The additional thrust on the downstream side causes the greater normal stress measured under the wall.

Interesting facets of these data include the visible peak at locations below the crown, which occur before soil loads arrive at each location. These early peaks, observed clearly at 8 ms at 45 deg from the crown, 10 ms at 90 deg, and 11 ms at the gages under the walls, are caused by structural response into the soil, not soil stresses transmitted from the airblast loading on the surface. Also, a tensile stress is consistently recorded at the floor center as the middle of the floor heaves upward initially as structural response begins. These tensile stresses are quite high in magnitude and end at later times as soil stresses propagate to depth.

These same phenomena were recorded on A6, as shown in Figure 92. Gage inadequacies were partially responsible for these data being so poor, but these questionable data are presented because the phenomena shown cannot be ignored. The general trends of rapid attenuation with depth and a large ratio between vertical and horizontal stress are evident by the low magnitude stresses at 45 deg and 90 deg from the crown. The lower magnitude normal stresses recorded here relative to A5 could be caused in part by the footing under the arch, which could change the arch response to loading. Rapid relief, such as that seen at the crown of A5 in Figure 91, is due to arch response as the crown of the arch moves downward upon application of the loading, which then relieves the load. The vertical stress recorded under the center of the floor in Figure 92 is in agreement with the waveform from A5 in the same location, but, once again, is much lower in magnitude. Tentatively, the footing seemed to redistribute the loads on the arch as measured by these gages.

Finally, the normal stresses on A7 are presented in Figure 93. These magnitudes and waveforms are in good agreement with those seen in A5. The vertical stress peaks at almost 8 MPa (1,160 psi) at the crown, but at 90 deg from the crown, the norizontal stress peaks below 0.5 MPa (73 psi).

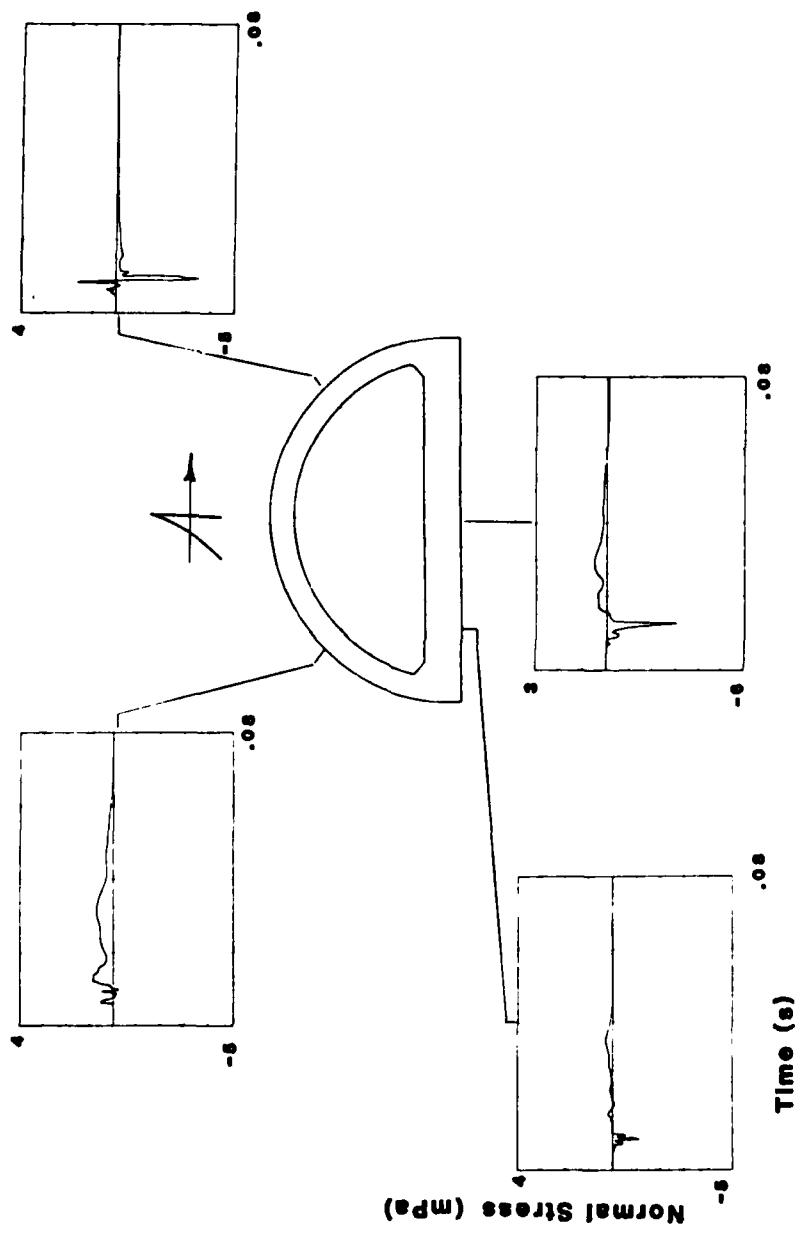


Figure 92. Normal stresses on Arch A5.

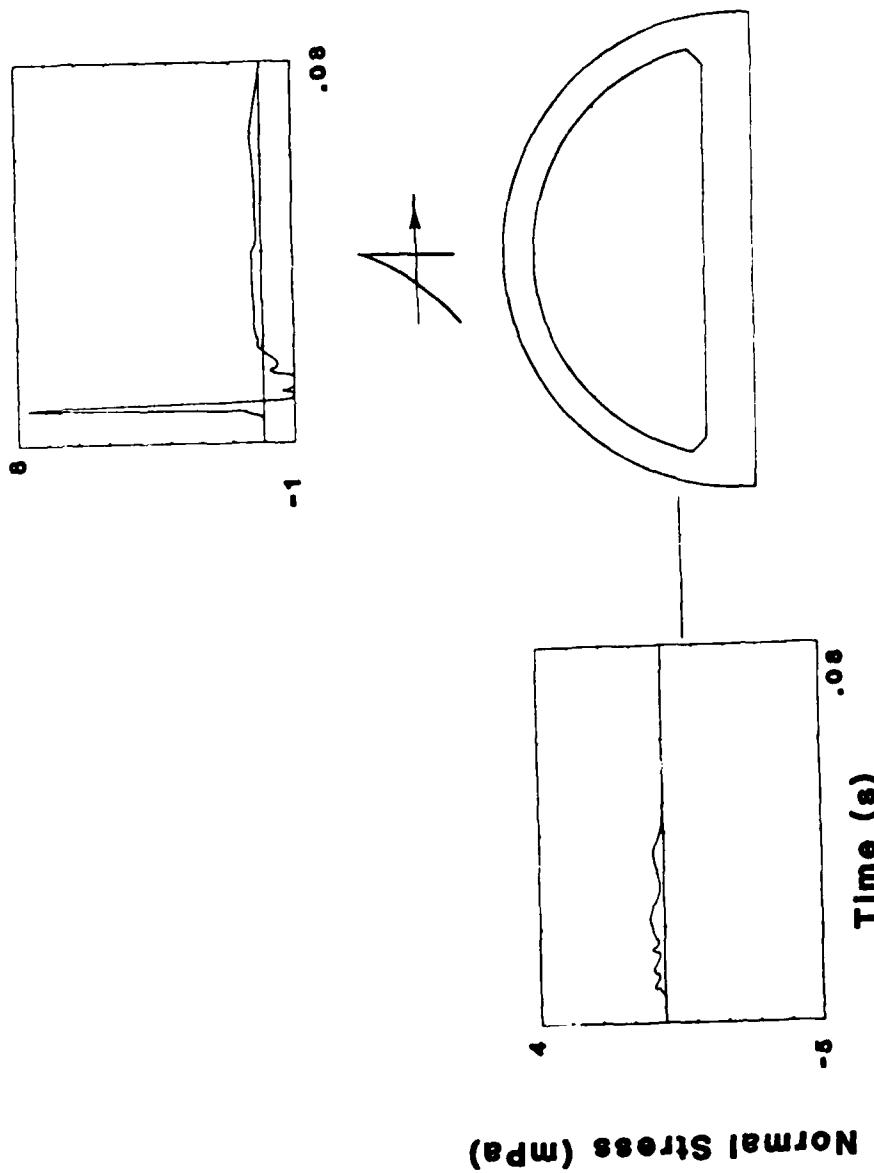


Figure 93. Normal stresses on Arch A7.

Crown motions in A7 seem to be so great that a tensile stress is recorded during relief of the incoming soil stress load.

Overall, the normal stress measured on the arches shows a dominant vertical load acting on the structures. Structural motions seem to slightly preload the soil below the crown as the structure moves into the as-yet-unloaded soil during initial response. Vertical loads are transmitted mostly to the soil under the walls, while structural response causes a separation between the floor center and the soil as indicated by soil tensile stress before the loading wave propagates through the soil. Finally, the footing seems to redistribute soil loading at the interface, but in an undetermined amount due to the questionable interface data recorded in the test.

This understanding of the primarily vertical orientation of the loading, and the response of the structure into (and away from) the soil prior to soil stress loading wave arrival, will help in translating the results of the structural accelerometer and strain data which follow.

Structural Velocity--Accelerometers were placed to record motions in the three primary axes directions. Longitudinal (x) velocities were recorded for A5 only, since only that structure could experience collisions between segments due to differences in longitudinal velocity. Lateral (y) and vertical (z) velocities were measured for all three arch structures on DAT-3.

Figure 94 presents a compilation of the longitudinal velocities for A5. The first arch segment moves toward the middle, then away from the middle, and at late times moves back toward the middle. This segment does not collide with its neighbor until late time (after 50 ms), because the second segment moves towards the middle with more thrust before moving away. There is a definite collision between the second and third segments at around 5 to 8 ms as they move towards each other and then separate at between 15 and 20 ms. This could have been a factor in the collapse of these two segments. No contact occurs between the third and fourth segments until a very late time, because the fourth segment moves away from the third segment, and the third segment does not overtake the fourth segment until well after 60 ms.

Vertical velocities in the end segments of A5 are compiled in Figure 95. A very dominant downward vertical velocity pulse is recorded at the crown,

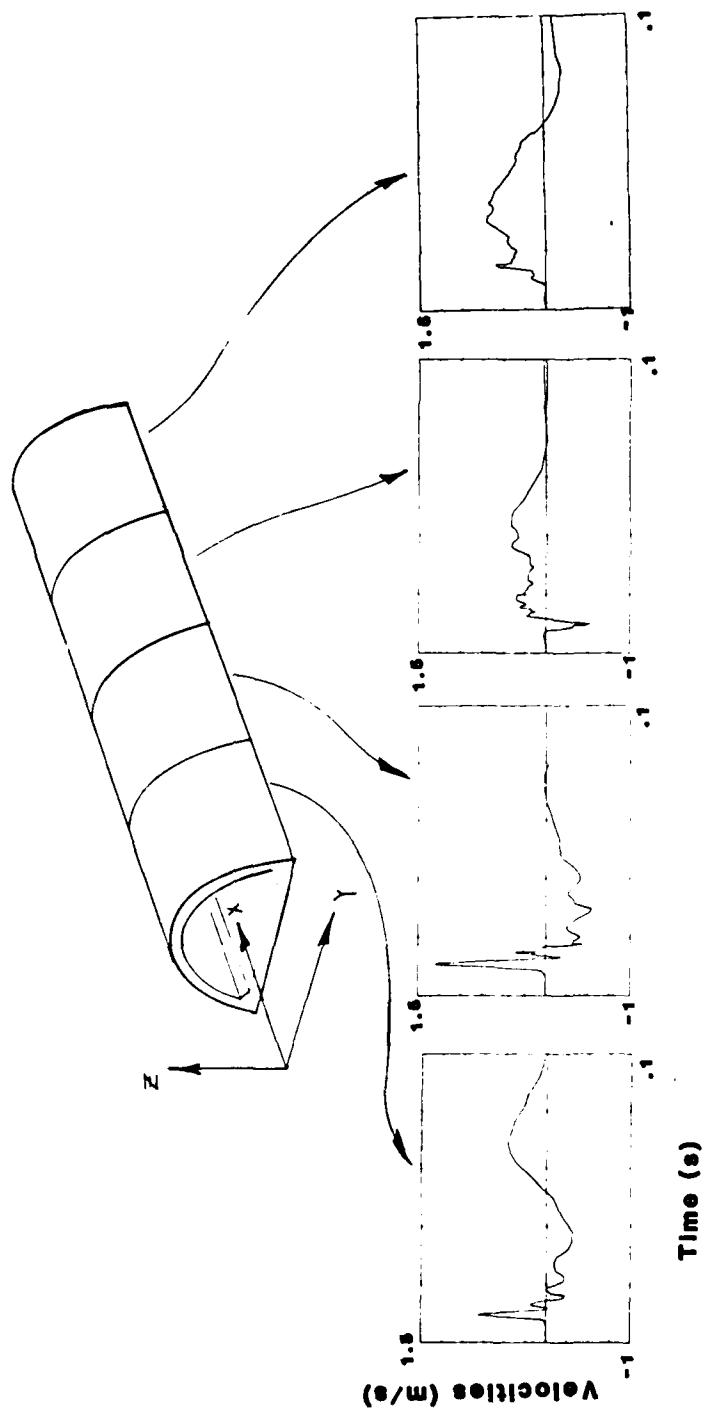


Figure 94. Longitudinal velocities in Arch A5 segments.

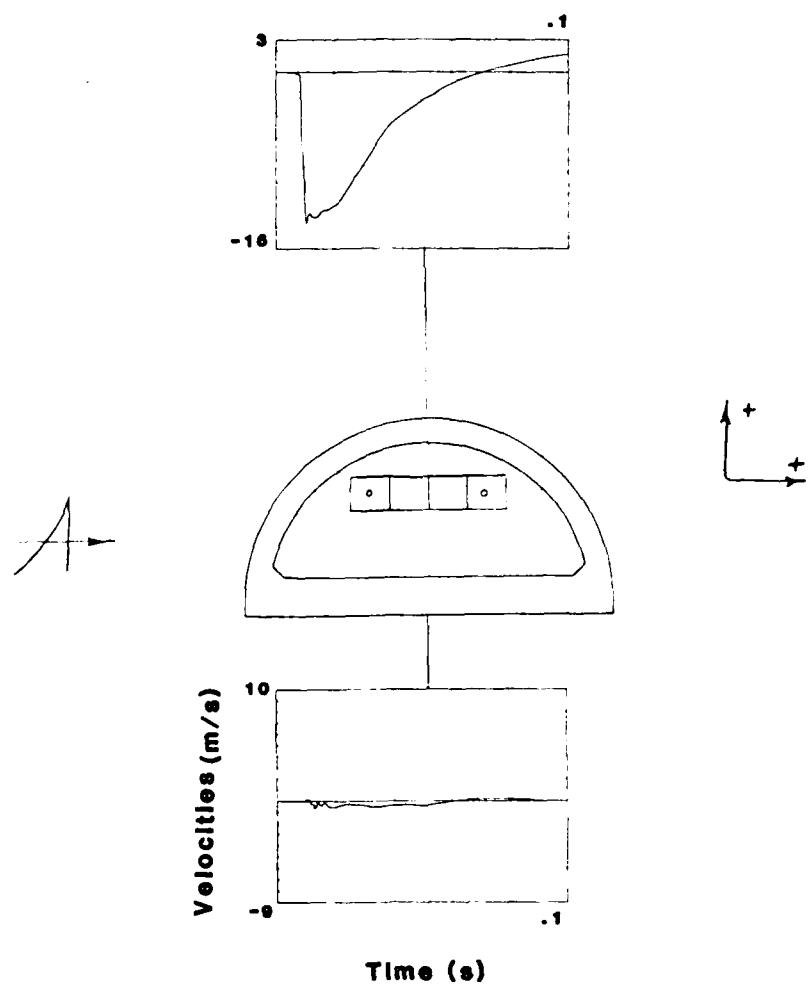


Figure 95. Vertical velocities in Arch A5 end segments.

while the magnitude of the floor vertical motion is relatively small and consists of an initial upward pulse followed by a generally downward drift of the floor center. This could be an edge effect of the HEST, but the soil data do not support that theory.

Vertical and horizontal velocities in the middle segments of A5 are collected in Figure 96. Vertical velocities are recorded on each side of the arch at 45 deg from the crown and at the floor center, while horizontal velocities are presented at the crown and on each wall at 45 deg from the crown. Vertical velocities on the walls show a stronger downward motion than that observed in the end segments with far less recovery. This is to be expected, since the arch collapsed. Judging from the gage break times and the general waveform, collapse was probably initiated at 50 to 60 ms. Vertical velocity recorded in the floor center clearly shows the initial upward thrust of the middle of the floor, followed by a downward motion as the near-field soil begins to move downward and the floor edges drag the middle down as well.

Horizontal velocities are not of the same magnitudes as the vertical velocities, but they are more dominant than expected from the horizontal soil loads because of circumferential response of the arch. The crown horizontal motion is a low magnitude drift downstream, as would be expected from a side-on loading situation as was simulated in the KACHINA Series. Both arch walls thrust outward under the initial structural response as the crown normal stress loading was applied [upstream wall moved upstream (-), downstream wall moved downstream (+)], then a reversal of motion to a low magnitude followed as the soil normal stress loading arrived at each location. These data velocity histories are consistent with the data recorded in KBM and KED and generally typify arch response in this fielded state and cross-section design. From these data, however, the effect of soil motions on the collapse of the middle segments cannot be determined.

Far greater definition of sectional vertical velocities was obtained for the individual arch segments. Vertical velocities at 45 deg from the crown and immediately above the floor on each wall are measured, along with crown, floor center, and both floor edge vertical velocities. For Arch A6, a horizontal velocity at the crown was measured also, but the vertical

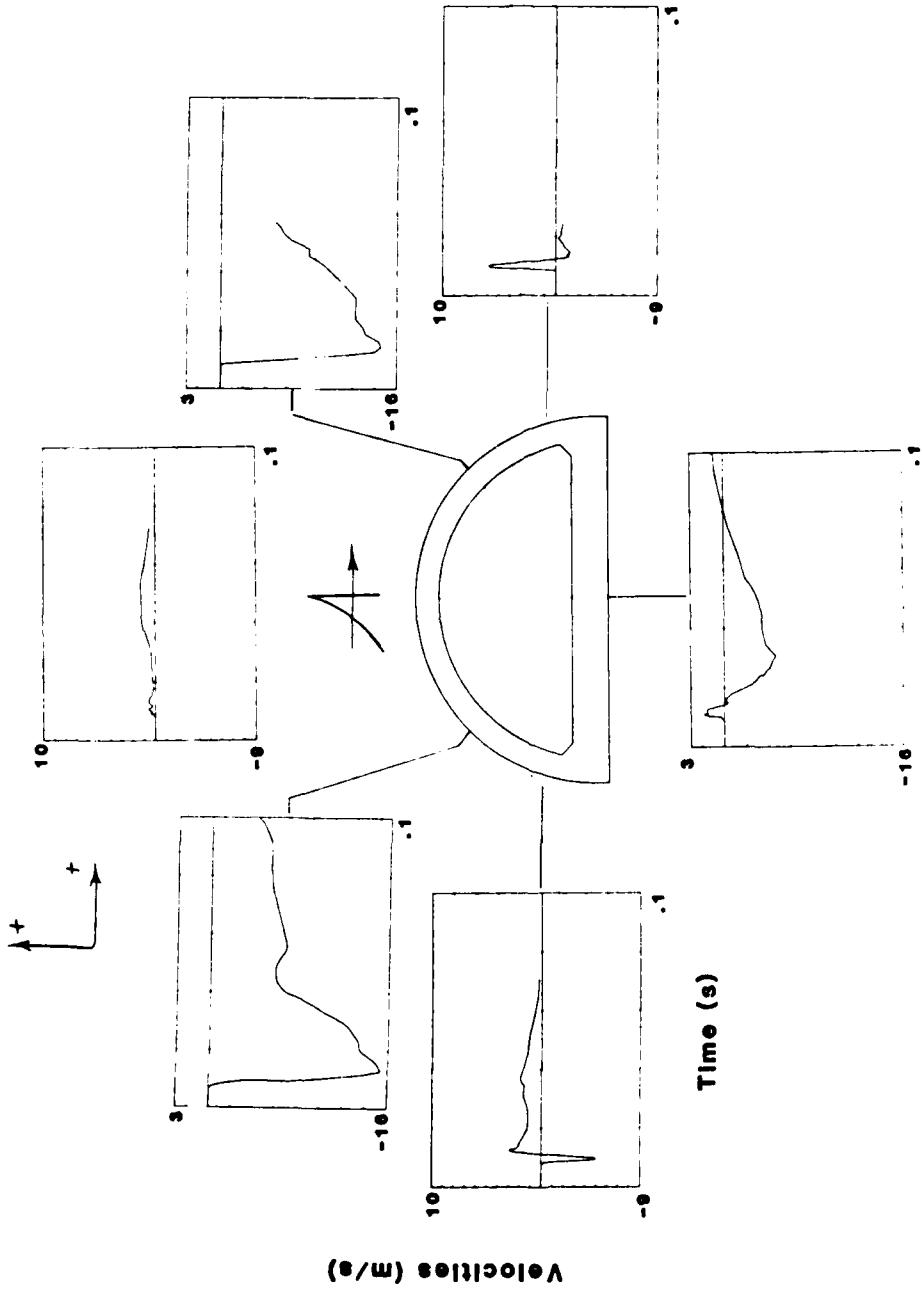


Figure 96. Vertical and horizontal velocities in Arch 5 middle segments.

accelerometer on the downstream wall at 45 deg from the crown did not transmit data.

Figure 97 shows the velocities measured on Arch A6. The horizontal velocity at the crown is generally negligible, with a small initial movement downstream followed by occasional oscillatory motions after 10 ms. Vertical velocities generally match with a decrease in vertical motion between the crown and the edge of the floor. The overlay between the floor edge and the bottom of the wall in each case shows close agreement, although the upstream waveforms differ in magnitude. The fact that the downstream waveforms parallel each other indicates, to some extent, a difference in gage drift which overemphasizes the difference between the readings. However, the overall good agreement indicates no significant failure between the floor and the wall. The vertical floor motions were lagging behind those in the floor edges, causing a bend which cracked the floor.

In comparison with the velocities of the middle sections of A5, vertical velocities in A6 were of less peak magnitude and had better recovery in the walls, while the floor experienced greater downward motions in A6. Both of these differences are due to the collapse of the arch segments in A5, which increased upper wall velocities while relieving floor velocities.

Vertical velocities in Arch A7 are shown in Figure 98. The general character of these waveforms is the same as those presented for A6, but with some important differences. The magnitudes of the vertical velocities at 45 deg are greater for A7, caused by the increased failure in the middle of the walls. A6 had wall failure relieved by the foundation, as seen in the photographs. Further, reinforcement of the trends seen in the photographs (that is, the foundation under A6 tended to increase the stress in the lower walls and floor) can be observed in the magnitudes of the vertical velocities in the lower wall and floor. There is better agreement between the lower wall and floor edge gages in A7 than in A6, and there are greater downward motions in the center of the floor in A7 compared to A6. Both of these facts indicate that a greater stress due to bending was in the floor of A6 than in A7.

An examination of the velocity data contains four major observations: First, the A5 middle segments collapsed around 60 ms, or about 50 ms after

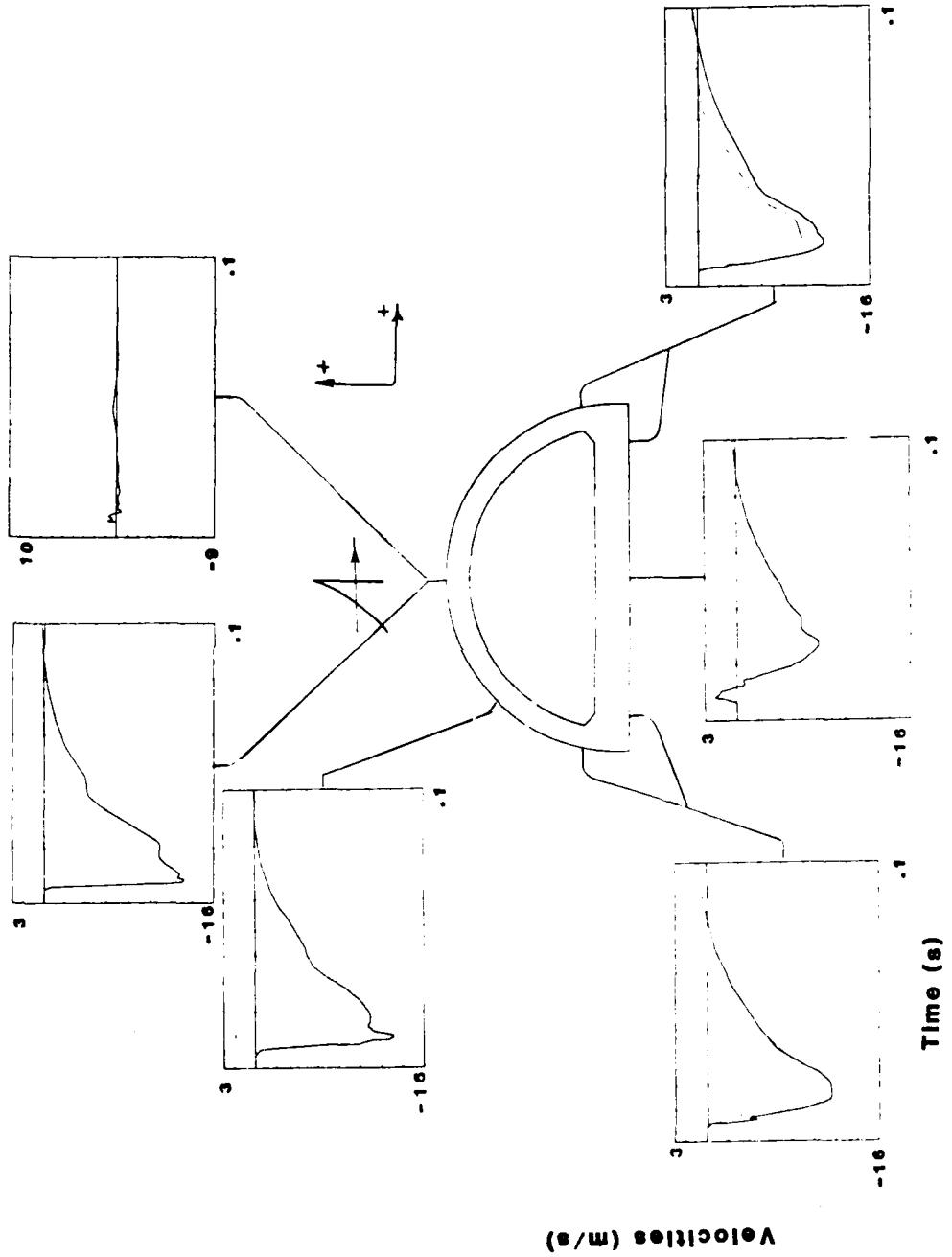


Figure 97. Vertical and horizontal velocities in Arch A6.

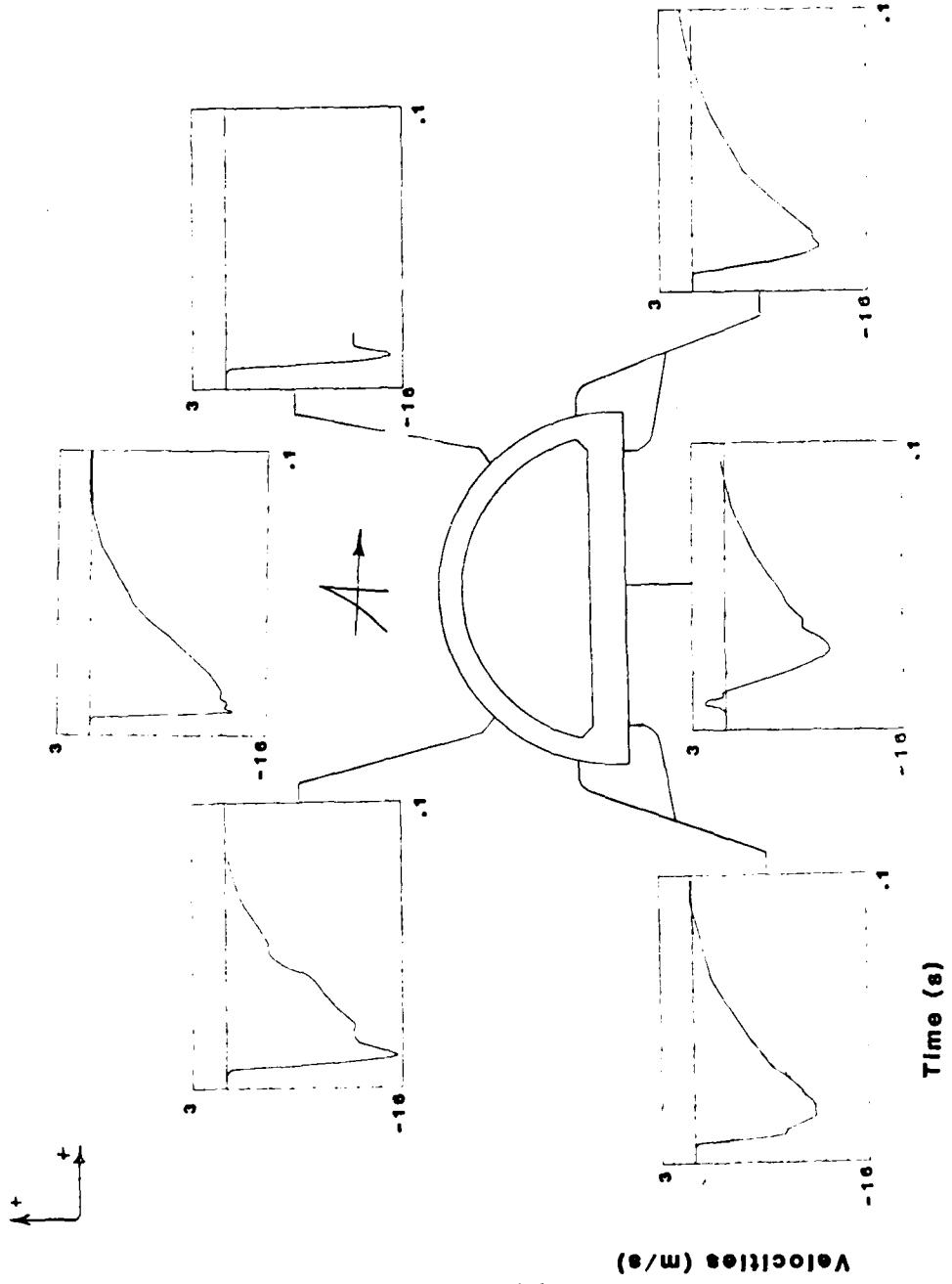


Figure 98. Arch 7 vertical velocities.

load application at the crown. Second, vertical velocities dominate response relative to horizontal and longitudinal velocities. Third, the floor center heaves upward as initial structural response occurs. Fourth, the velocity data support the observed pattern that the footing under A6 increased stresses on the lower portions of the arch.

Strain Data--Structural strain results will further enhance the understanding of failure mechanisms and stress concentrations experienced on Dat-3. When examining the following strain data (Figures 99 through 104), note that the scales of each plot vary depending on the values. Strain histories are presented at three different scales, depending on the severity of the stress in a section. Circumferential strains will be presented first, followed by longitudinal strains and the chamfer reinforcing bar strain histories. Tensile strains over 0.5 millistrain and compressive strains over 2 millistrains indicate failure of the concrete (microcracks), while strains over 6 millistrains are clearly visible.

Circumferential strains in the south end segment of A5 are detailed in Figure 99. Large moments are found at the crown which is in overall tension, but experience bending as the load flattens the crown inward. At a much greater scale, severe bending moments in the center of the floor create failure strains that exceed the largest scale used for strains in this section. Finally, at the expanded scale, slight tensile strains are registered in the bottom of the floor at the edges after an initial small compressive strain. These tensile strains in the bottom edges of the floor are negligible relative to the tensile strains at the top center of the floor.

Figure 100 shows circumferential strains in a middle segment of A5. Relative to the end segments of A5, the crown experiences less bending moment, although the compressive strains on the outer surface of the crown and the end segments agree almost exactly. Strain readings on the downstream wall at 45 deg from the crown indicate that the outer surface failed at 30 ms (or 20 ms after load application at the crown), although the inner reinforcement does not record distress until after 55 ms. Floor strains are still severe, although there is some relief of the strains in the center of the floor (the bottom surface experiences less compression). The strains at the downstream edge of the floor indicate the joint has opened, so that the inner surface

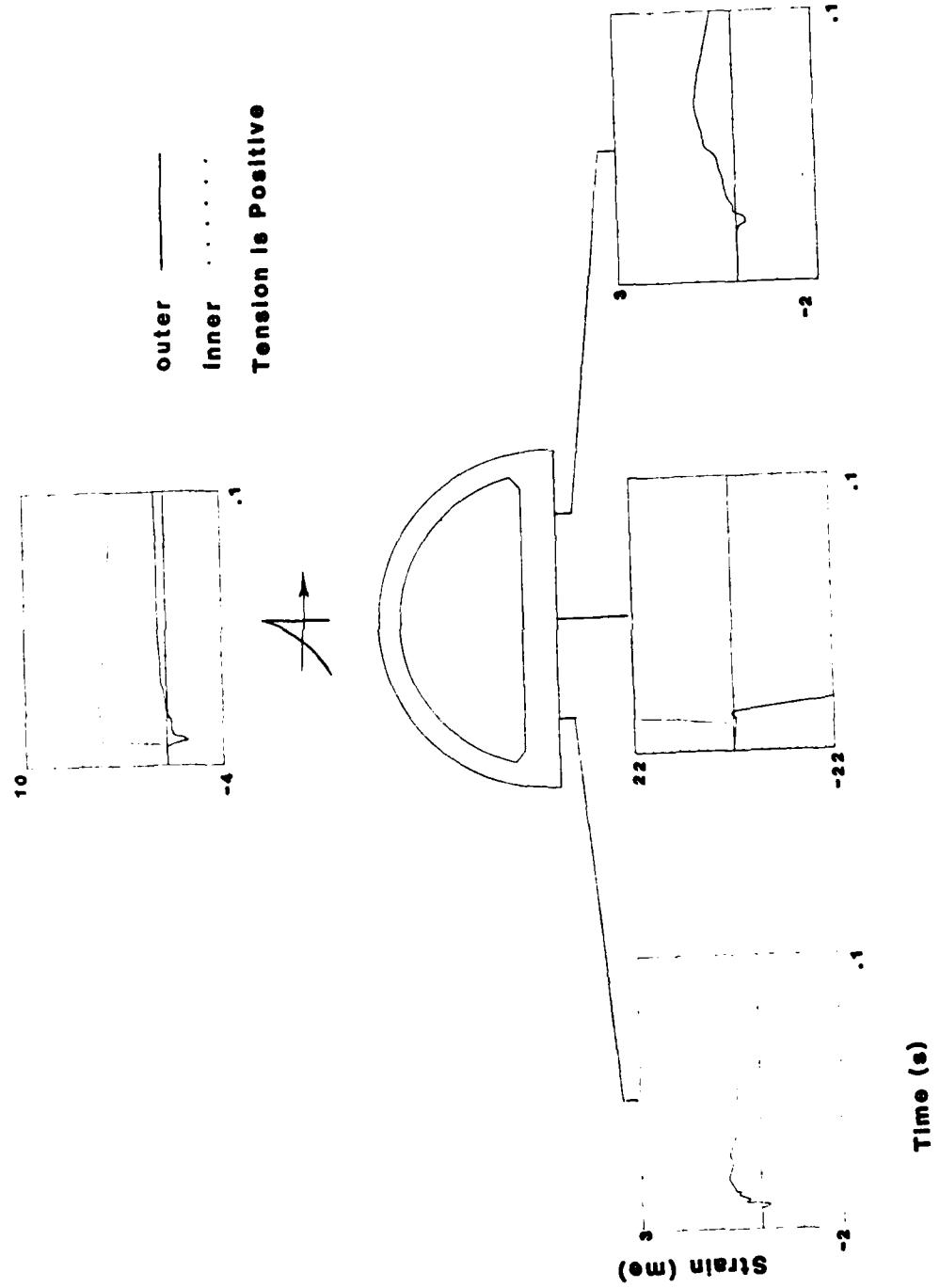


Figure 99. Circumferential strains in south end segment of Arch A5.

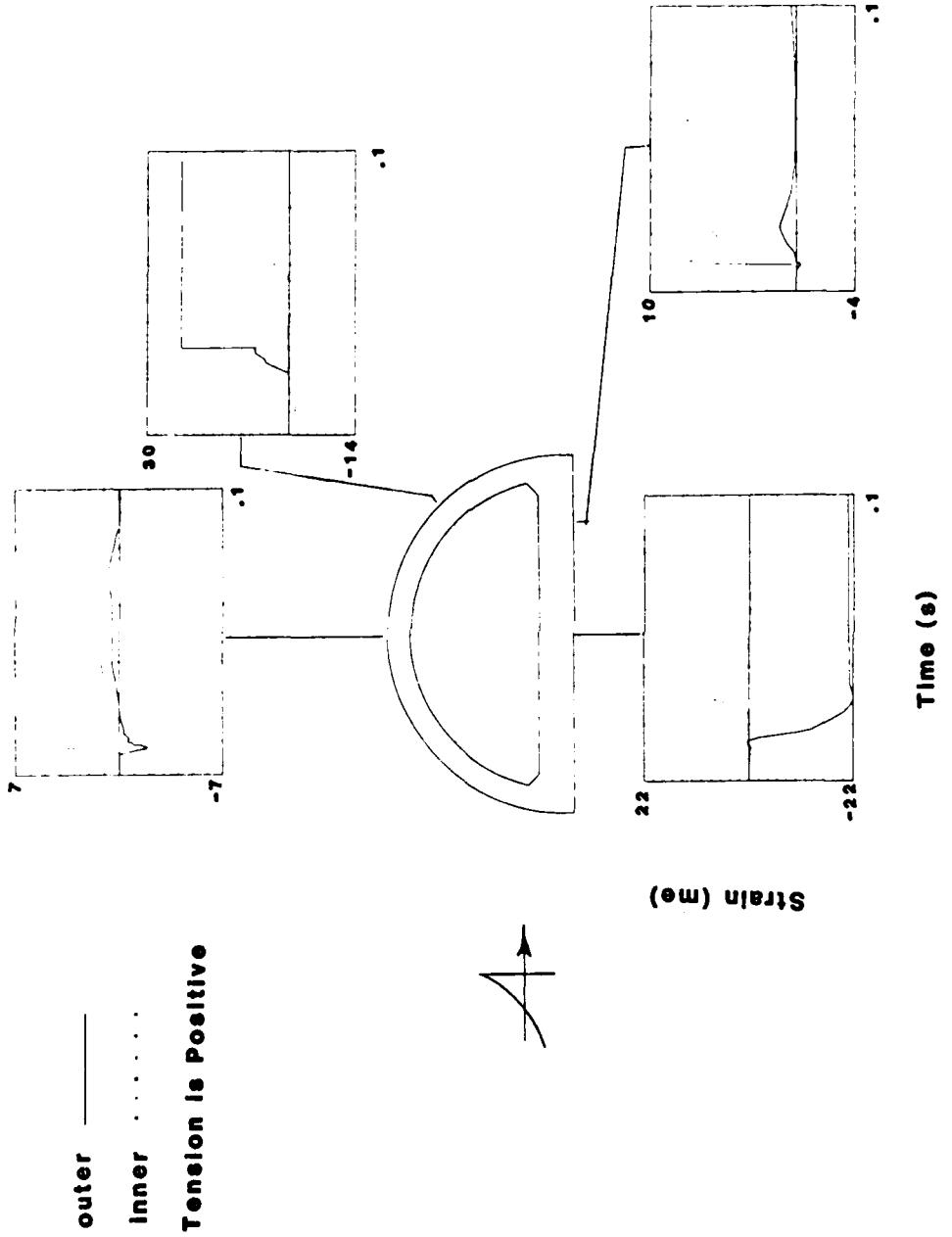


Figure 100. Circumferential strains in northern middle segment of Arch A5.

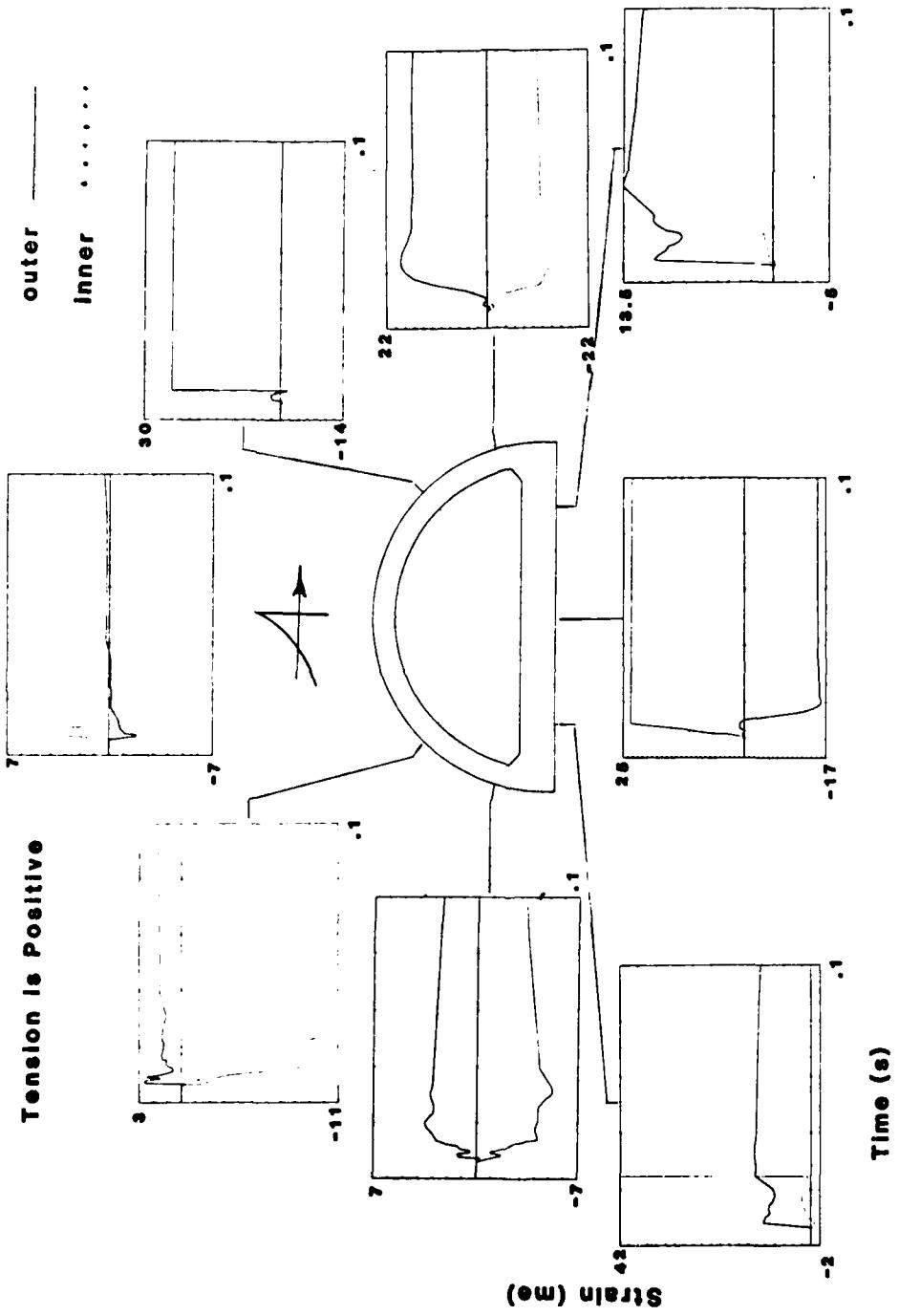


Figure 101. Circumferential strains in Arch A6.

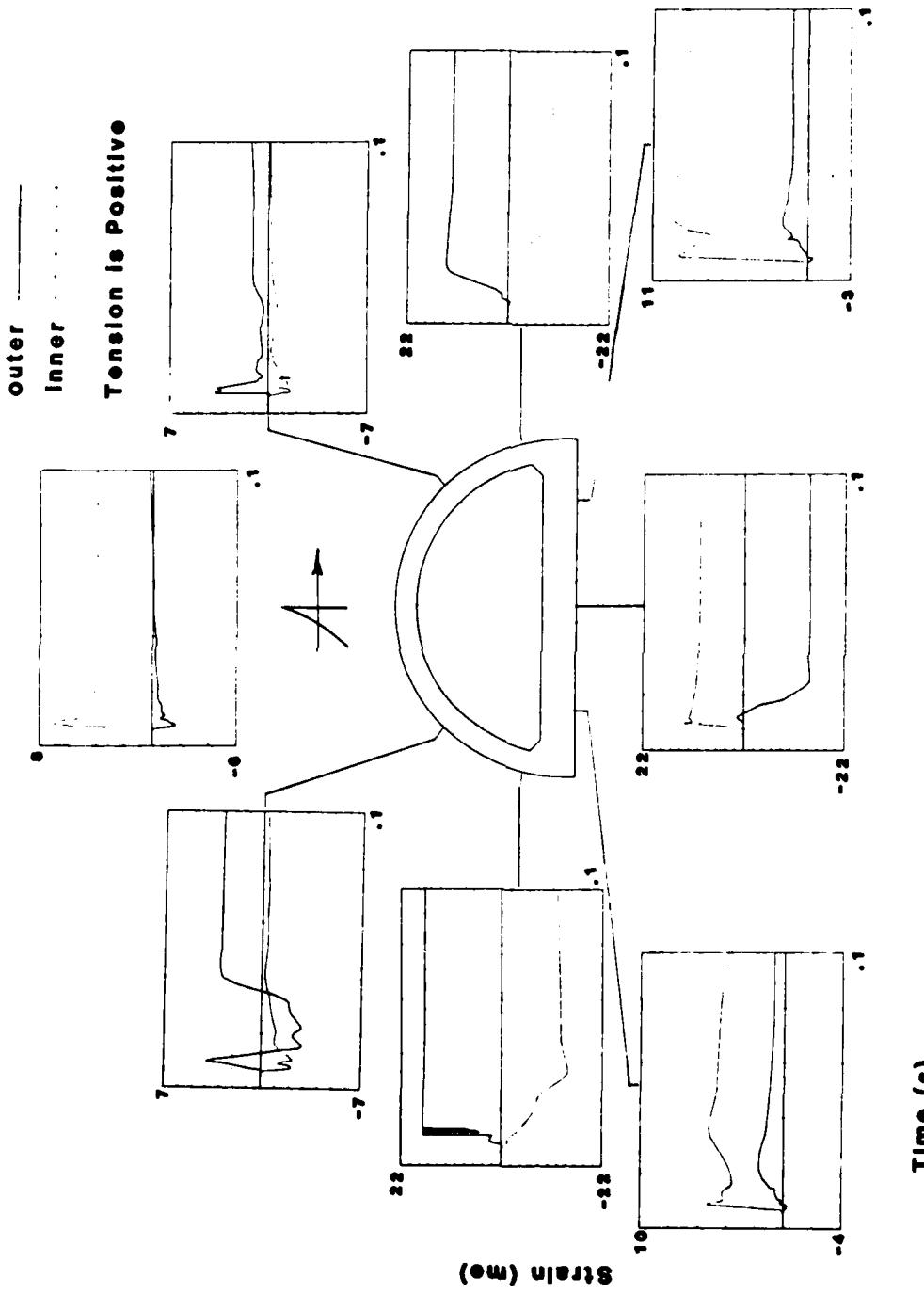


Figure 102. Circumferential strains in Arch A7.

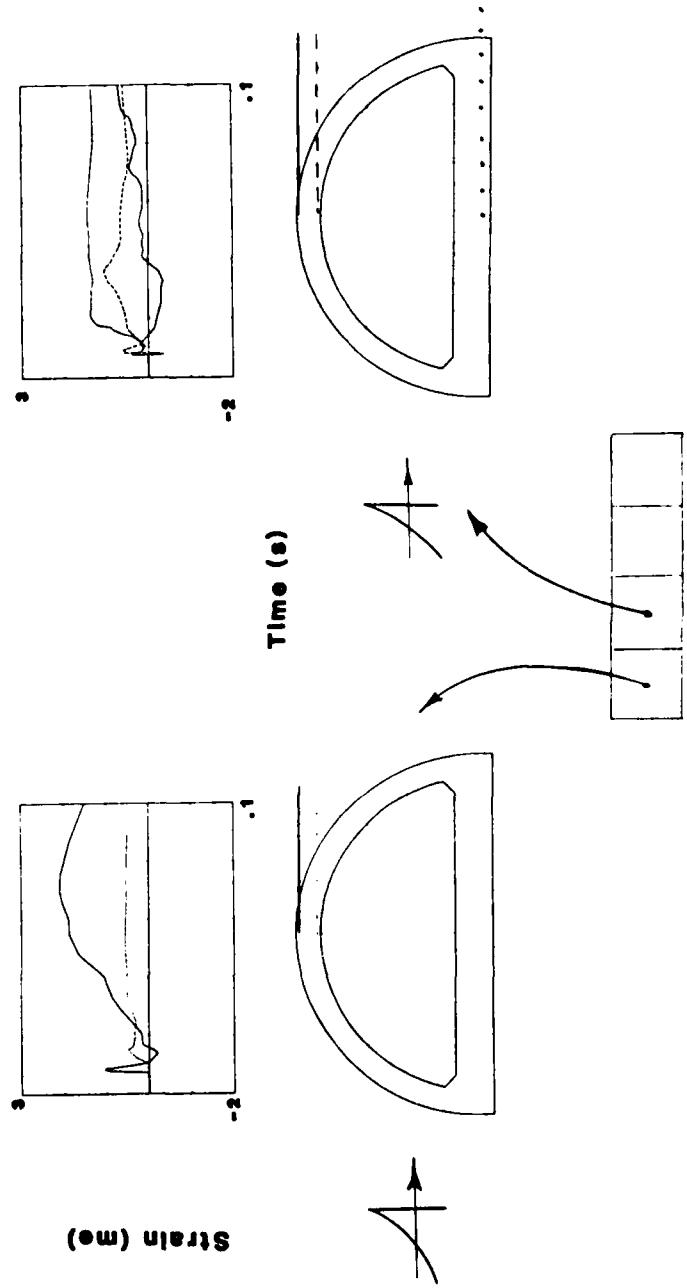


Figure 103. Longitudinal strains in Arch A5 northern segments.

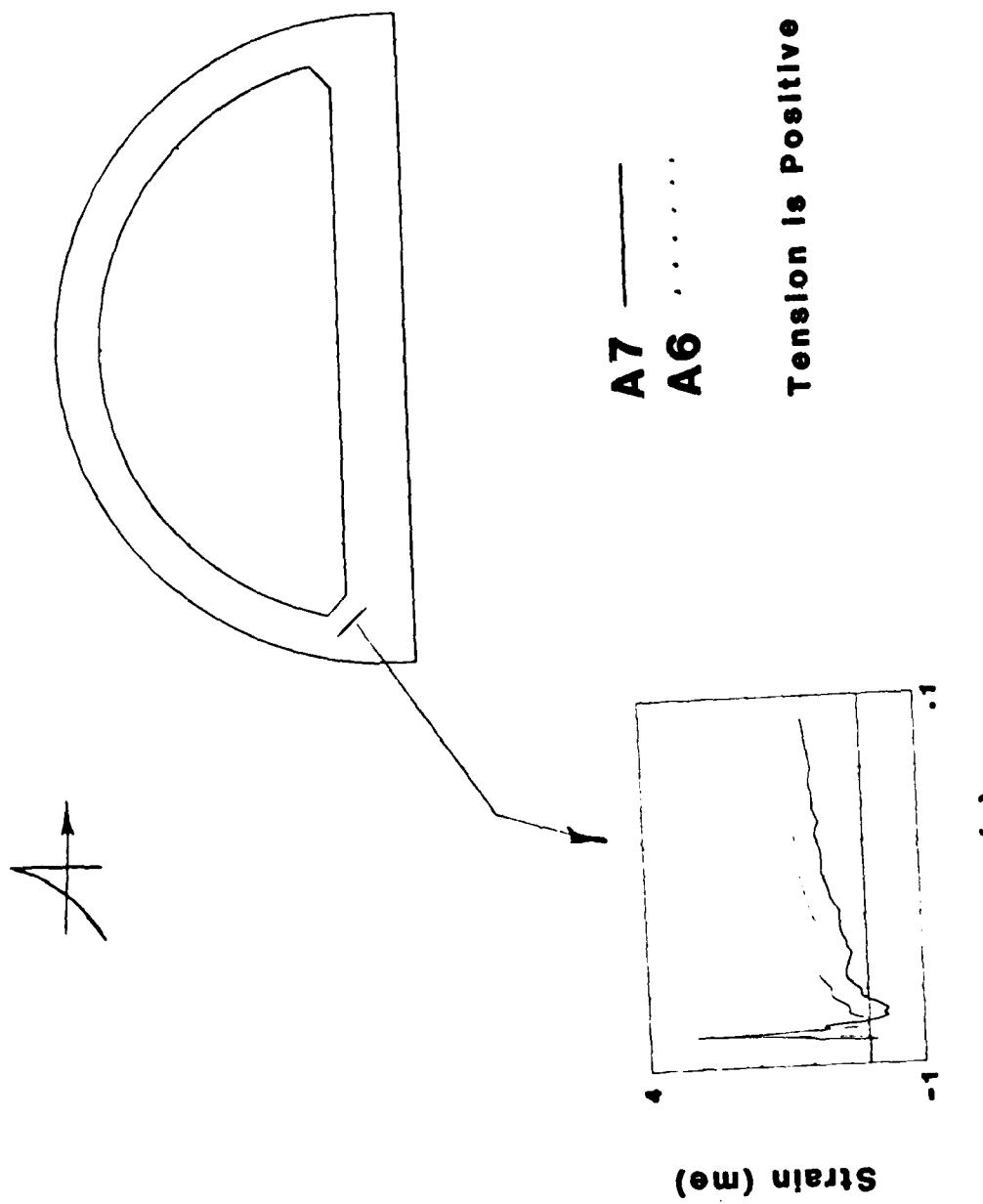


Figure 104. Strains in chamfer shear rebar in Arches A5 and A7.

experiences more tension than the outer surface. This means that, as the load travels down the wall to the joint, the wall spreads the joint open, causing the floor side of the joint to close. This opening of the joint was also observed in the KED test.

Therefore, in comparing the end section of A5 with a middle segment, apparently the collapse of the roof, or the early formation of severe failure planes at mid-wall on each side of the crown, relieved the bending moment at the crown and at the center of the floor.

Strains in Arch A6 are presented in Figure 101. As expected by the indications thus far, circumferential strains in the crown of A6 are the lowest of any of the arches, and the orientation of the moment is the same as that seen in A5. Severe cracking is recorded on the downstream wall at mid-height, but only medium scale strains are recorded at the same level on the upstream wall. The orientation of the strains is reversed for both walls from the crown, indicating that the walls were bending outward while the crown was bending inward. Failure in the walls was accompanied by high bending moments, suggesting that bending is at least a contributing mechanism, if not the main one, in forming the failure plane. Joint closure is evident in both corners of the arch, as the inner surfaces of the walls were in compression to resist further closing of the joint as the floor buckled inward. Strain values in the floor are higher than those seen in A5, with the floor center in more overall tension. In Arch A6, during examination of all the floor gages, the floor was closing the joint, as opposed to the case in A5, when the wall acted to open the joint.

Examining the circumferential strains in Arch A7, the magnitude of the crown strains, shown in Figure 102, are in agreement with Arch A5. Strains at the mid-wall are lower than those in A6, because the failure plane has moved upward above the strain gages, so they have been relieved by the formation of the failure plane. However, the severity of the moments in the wall above the floor have not been diminished. The difference is that the joint was not being opened or closed; rather, both the wall and floor acted to rotate the joints lowering the floor. Finally, floor moments in the center are the least of all the arch data.

Strain gage data from this series of gages did not follow as reasonable a pattern as the rest of the data and the photos, but strain gage results are dependent on their location in heavily cracked structures such as these. Gages which happen to lie on a crack will measure more strain than nearby gages on rebars that do not cross a crack at that location. The general trends were supported in the circumferential strain data, but the correlation was not as definite as anticipated.

Longitudinal strain data for Arch A5 is presented in Figure 103. These strain plots are all presented on an expanded scale relative to the circumferential strain data. Generally, the results from longitudinal strain gages indicate that longitudinal response of the long arch structure is unimportant. No saddling of the crown on the end segment takes place throughout the first 10 ms, whereas the response of the midsection exhibits a slight vertical longitudinal bend. These values could be affected as much by the angled collapse of the crown on Arch A5 midsection or the keyed joint in the middle as by a true vertical longitudinal bending mode. Regardless of the cause, the longitudinal bending response is not a dominant mode on DAT-3.

Figure 104 compares the strain recorded in the chamfer reinforcement for Arches A6 and A7. While these strains are also at a low magnitude relative to the circumferential strain, the A6 footing and its resultant focusing of load in the lower half of the arch is seen by the comparison of the strain in A6 relative to A7. The confinement and reinforcement provided by the chamfer rebar is also important at later times (after 30 to 40 ms), when the load attenuation is occurring at the base of the wall.

Active data have aided in the analysis of the DAT-3 arch responses by backing up pictorial evidence with parameter histories which show the responses as they progress as a function of time. Normal stress data shaped a predominantly vertical load picture and gave evidence that the floor center heaved upward during initial structural response while the floor edges were driving downward. Accelerometer data showed this to be real behavior and gave further evidence of the concentration of stress in the lower half of the A6 structure due to the footing. Strain data clarified the general circumferential response, proved longitudinal response to be negligible in the four-segment arch, and proved the necessity of chamfer splice bars.

KACHINA SERIES FINDINGS

An overall comparison of arch behavior between the three KACHINA tests is useful as a review of the conditions and response in each test relative to one another. While no figures will be used in this discussion, the figures can be referenced in the KBM (Ref. 5) and KED (Ref. 6) Quick Look Reports.

Normal stresses measured on the arches varied. The arches on the KBM series had the highest overall normal stresses recorded from the three tests, followed by the KED series, with the lowest normal stress measurements recorded on the DAT-3 test. Some of the peaks on the DAT-3 test were as high as those in KED, but DAT-3 experienced relief of the load and did not accumulate a matching amount of impulse.

Vertical velocities were not as comparable, since the KBM tests had only an 8.5-m arch and no short arch segments. However, the KBM arch remained fairly intact as far as vertical velocity comparisons throughout the structure. In rating velocity output, DAT-3 had the highest vertical velocities at all measurement locations, and very little relative displacement took place between the lower wall and floor. This was offset by the failure in the wall midsection which allowed relative displacement in the walls. The KBM arch also held its shape. Despite failure, it maintained the best post-yield integrity in the test series, especially in light of the high loads on the structure. Maximum relative displacement between the arch walls and floor occurred in the KED test, although the most severe failure was in the collapsed inner segments of DAT-3 Arch A5.

The KBM arch held together because it had low relative displacements under the greatest interface loads. This is due more to the size of the rebar used in the KBM arch than the slightly higher percentage of circumferential steel. Relative displacements between the arch walls and floor were greatest in the KED test due to the small rebar size and the inadequate confinement of the concrete in the joint due to poor reinforcing bar detailing. Relative displacement between the arch and the floor was minimized by properly confining the concrete in the joint. However, this forced failure to move up the arch wall where bending and shear stresses combined to fail the arch as a small circumferential section on a supporting wall. This type of failure is less

desirable than the failures at the joint region connecting the wall and the floor, since failures on the wall as seen on DAT-3 are more catastrophic.

Strain data from the three tests generally reflect the degree of fixity in the sections. The KBM arch had the largest rebar and the best fixity, so that in areas of stress concentrations, like the lower wall, high magnitude moments were carried by the rebar as the corner remained fairly rigid in spite of joint shear failure of the concrete. The smaller rebars in KED allowed more flexibility in the section after the concrete cracked; therefore, the moments were lower in the joint area but higher at the crown and the floor center. Finally, the fixity was recovered in the DAT-3 test by arranging the steel in the joint region to maximize rebar development; but the failure, subjected to stress concentrations, was relocated to the weakest section which was on the wall.

Table 16 compares peak relative displacement estimates for the three test events. Minimum relative displacements occurred in the KBM arch, as expected. The difference between the long and short arches in the KED test was due to longitudinal bending effects in the long arch which had a low enough longitudinal bending frequency to cause a definite effect on the failure mode. Finally, the KED shorter arches (A3 and A4) are generally comparable to the DAT-3 arches because, although the reinforcement in the joint was rearranged to prevent failure in that region, the increased stiffness of the DAT-3 arch floor regions was offset by the failure in the walls of the arch.

All of these comparisons are too complex to be understood in this short discourse. The best approach would be to examine each of the aforementioned reports which provide background material for the preceding discussion. The major points developed in each test can now be presented to conclude this section.

CONCLUSIONS

Rebar Size Effects (KBM)--The size of the reinforcing bars used in the arch structures influenced the integrity and stiffness of the section. Larger rebars contributed a greater section modulus to a fully cracked concrete section than an equivalent area of smaller rebars in the same configuration. This additional stiffness moderated relative displacements due to concrete

TABLE 16. KACHINA ARCH RELATIVE DISPLACEMENTS

		<u>Peak Relative Displacements (mm)</u> (Approximate)	<u>Crown-to-Floor</u>
KBM	A2	120	(All figures approximate)
KED	A2	330	
	A3	180	
	A4	190	
DAT-3	A5	235	
	A6	205	
	A7	210	

failure, although the resultant spall regions for larger bars (at resultant greater spacing) must be considered.

Length Effects (KED)--The length of an arch (that is, the length over which full longitudinal moments can be transmitted along a wall) determines how bending modes interact to produce failure. Longer arch structures are more likely to experience a longitudinal bending mode of response, which imparts an additional outward thrust to the walls of the arch. This thrust can aggravate a joint shear failure and increase relative displacements between the crown and floor center.

Scaling (KED)--This factor really is derived from the consequences of length changes mentioned above. By scaling a structure to a smaller scale, higher mode frequencies result which cannot be driven by a simulator lacking more energy proportioned into the same higher frequencies. This may delete response modes which will affect the behavior of the full-scale structure. The ability to scale power with frequency may not be possible, but attention should be given to matching the scaling with the full-scale structure. This was accomplished in DAT-3 by constructing a long arch from four short segments with no moment capacity across the joints.

Joint Designs (DAT-3)--Joints should be designed in light of what forces are to be transmitted from component to component. While it is not a clear factor in the failure, the ability of the keyed joint at the midsection of Arch A5 to transmit axial forces may have contributed to the failure seen in the middle two segments. Collapse halted at the butt joints which transmitted only longitudinal axial forces.

Foundation Effects (DAT-3)--As seen in comparing Arch A6 to A5 and A7, the continuous footing under each wall of the arch served to relieve loads on the upper portions of the structure at the expense of floor integrity. Despite added reinforcement in the joint, A6 had the closest formation of a beam shear failure in the floor of all the DAT-3 arches. This negative effect was not limited to the floor immediately above the footings, but ran through the entire floor.

Failure Design (KACHINA Test Series)--A major consideration in design is failure. A proper design is essential so that, in the event of a failure, it is not a catastrophic event. Results from the arch tests point to the

desirability of a controlled failure zone at the edges of the floor, especially in light of the unattractive choice of arch collapse due to shear and moment failure in the upper wall. Thus, arches should have a distinct weak area inside the joint, or the floor should be placed separately from the arch and the footing for the arch. This is the current method of constructing arch shelters, and all KACHINA data point to that as the optimum choice for a failure zone.

IX. FINDINGS AND CONCLUSIONS

This report documents the posttest recovery and analysis efforts for the DAT-3 event. Model construction, test site operations and instrumentation were discussed in Sections II through IV, and Sections V through VIII presented the analyses of simulation performance, ground shock, the fiber optics experiment, and structural response. Each of these sections presented in detail the results and important conclusions of the various aspects of the DAT-3 event. Especially enlightening are the KACHINA Series findings and conclusions presented at the end of Section VIII. To repeat all of the conclusions and observations documented in this report would be redundant. Rather, the following selected list of findings and conclusions represent the highlights and major points of interest in the first eight sections.

a. The simulator performance in this test was excellent. The HEST design yield was achieved and the peak pressure was within 16 percent of design. This represents a vast improvement in performance of the thin high-pressure HEST design over the previous two tests, Butterfly Maiden and Eagle Dancer. The best estimate of the DAT-3 simulation is a 1.56-kt nuclear surface detonation at a range of 42.53 m with a peak pressure of 14 MPa and airblast shock velocity of 3348 m/s.

b. Of the 171 active gages fielded in this event, 158 provided useful data. Many channels survived for the full duration of the test. This represents successful data recovery from approximately 93 percent of all the active channels fielded.

c. As discussed in Sections II and III, the inner two segments of Arch A5 were reversed when placed in the field. Due to the symmetric arch design, this error did not significantly affect the results of the test. However, this error does point to the need for extreme care and on-site inspections, especially during critical phases of field work.

d. In construction of the DAT-3 arches, it was discovered that, although weldable strain gages have a higher unit cost than bondable strain gages, significant savings in both time and money can be obtained by using the weldable gages. On the average, using the weldable gages saved approximately 3 manhours per gage.

e. Analysis of the ground shock data indicates the relief effects produced by the finite-sized simulator did not significantly degrade the desired environment during the simulation time. There is evidence, however, that relief was probably significant late in time.

f. Analysis of the free-field vertical motion records below a depth of 2 m show clear evidence of spall. This phenomenon was also observed in the KED and KBM test events.

g. While it is not a clear factor in the failure, the ability of the keyed joint at the midsection of Arch A5 to transmit axial forces may have contributed to the failure of the middle two segments.

h. By comparing the response of Arch A6 to A5 and A7, it is apparent that the continuous footing under each wall of the arch served to relieve loads on the upper portions of the structure at the expense of floor integrity.

Overall, the DAT-3 event was successful in meeting all of its objectives.

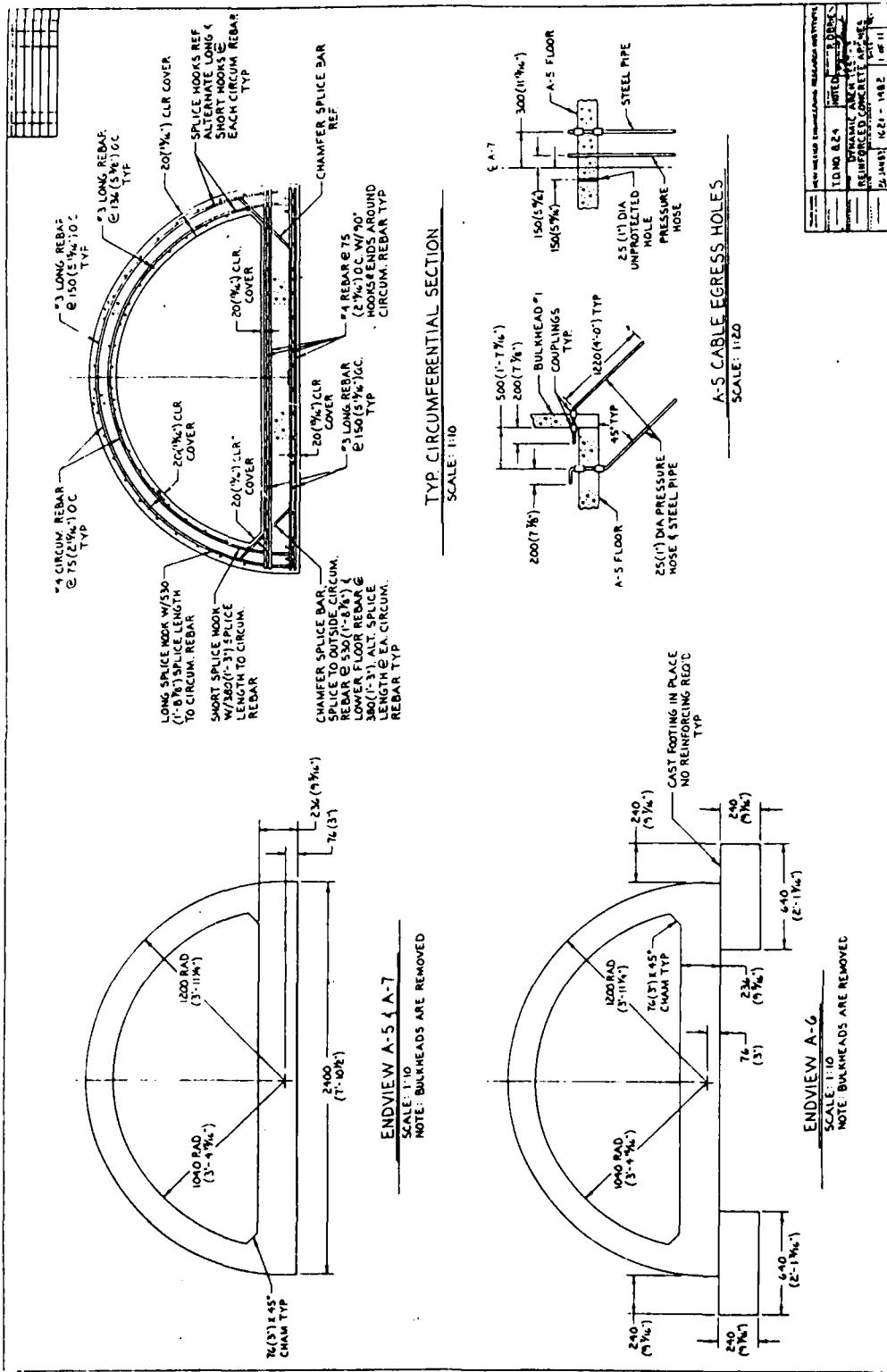
REFERENCES

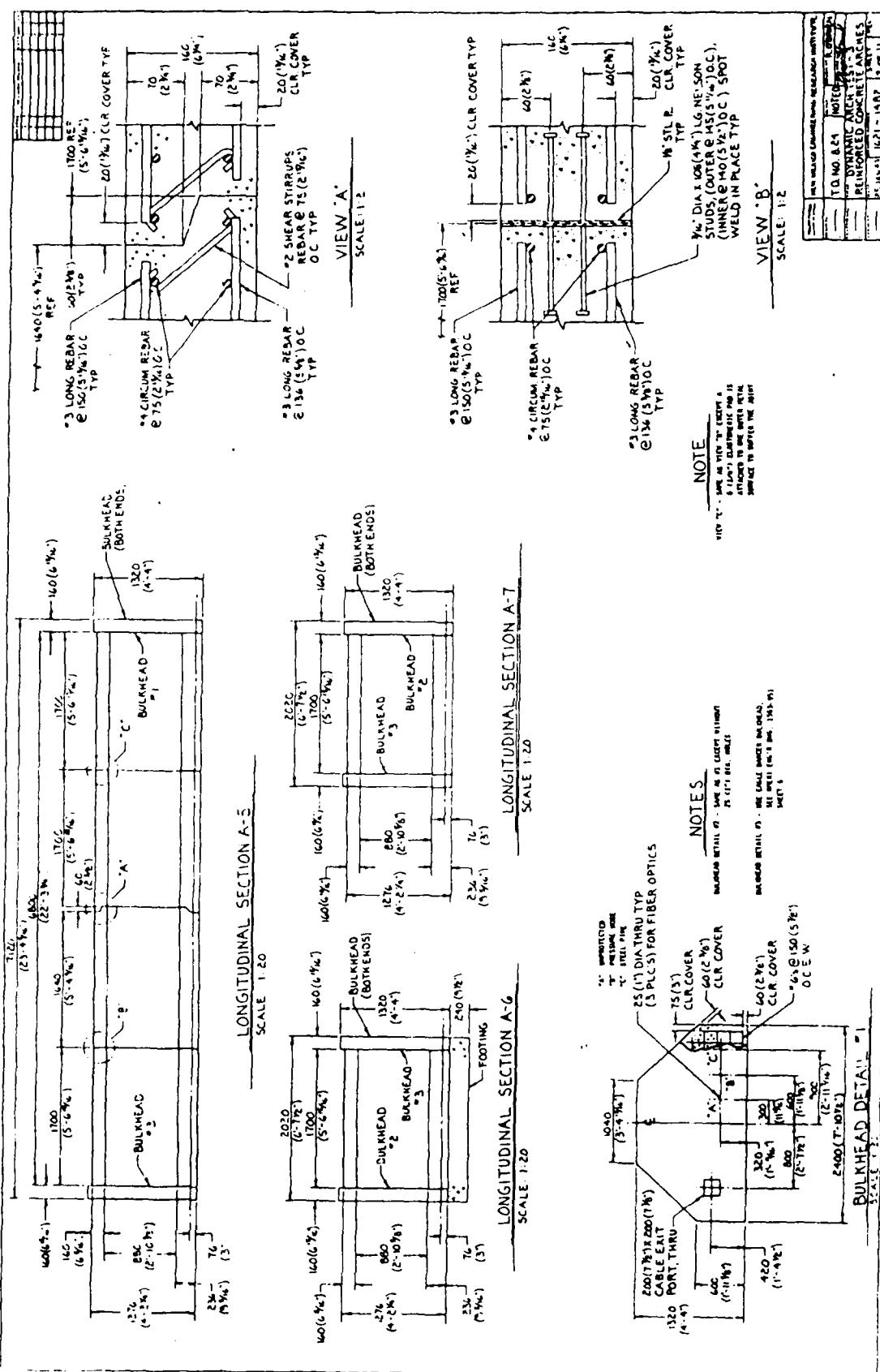
1. Bedsun, David A., and Callahan, John A., "Geotechnical Investigations for the Dynamic Arch Test at McCormick Ranch," Letter Report, Air Force Weapons Laboratory, Kirtland AFB, NM, December 1982.
2. Baird, Glenn T., Backfill and HEST Overburden Material Properties for the DAT-3 Test Event, New Mexico Engineering Research Institute Task Report to AFWL, Kirtland AFB, NM, June 1983.
3. Smith, Joseph L., et al., KACHINA Test Series: Dynamic Arch Test - 3 Pretest Report, AFWL-TR-83-56, Air Force Weapons Laboratory, Kirtland AFB, NM, September 1983.
4. Crawford, Robert E., et al., The Air Force Manual for Design and Analysis of Hardened Structures, AFWL-TR-74-102, Air Force Weapons Laboratory, Kirtland AFB, NM, October 1974, p. 236.
5. Parsons, Roger and Rinehart, Eric, KACHINA Test Series: Butterfly Maiden, Quick Look Report, AFWL-TR-82-132, Air Force Weapons Laboratory, Kirtland AFB, NM, June 1983.
6. Betz, John F., Smith, Joseph L., et al., KACHINA Test Series: Eagle Dancer, Quick Look Report, AFWL-TR-83-35, Air Force Weapons Laboratory, Kirtland AFB, NM, July 1983.

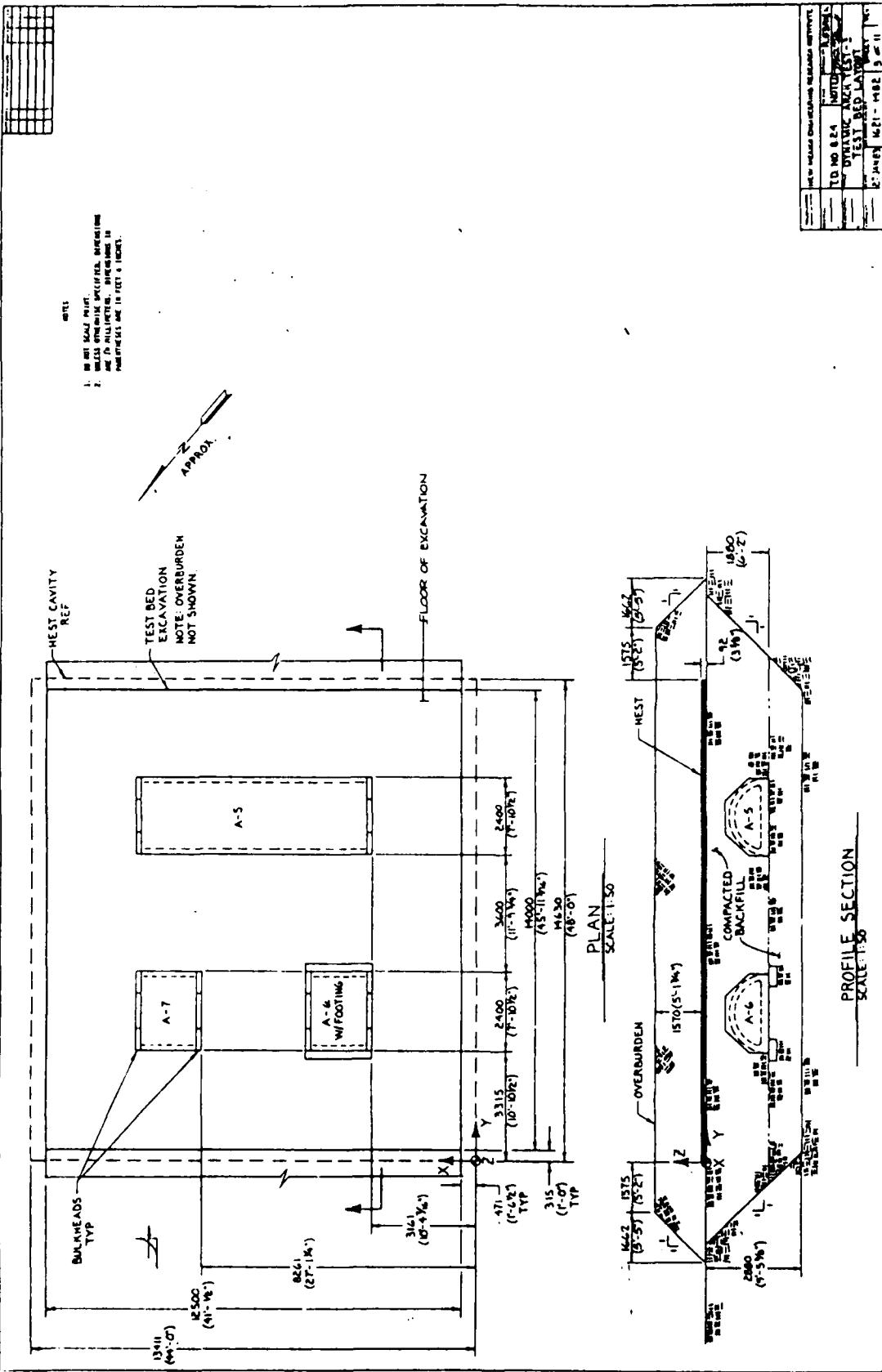
APPENDIX A

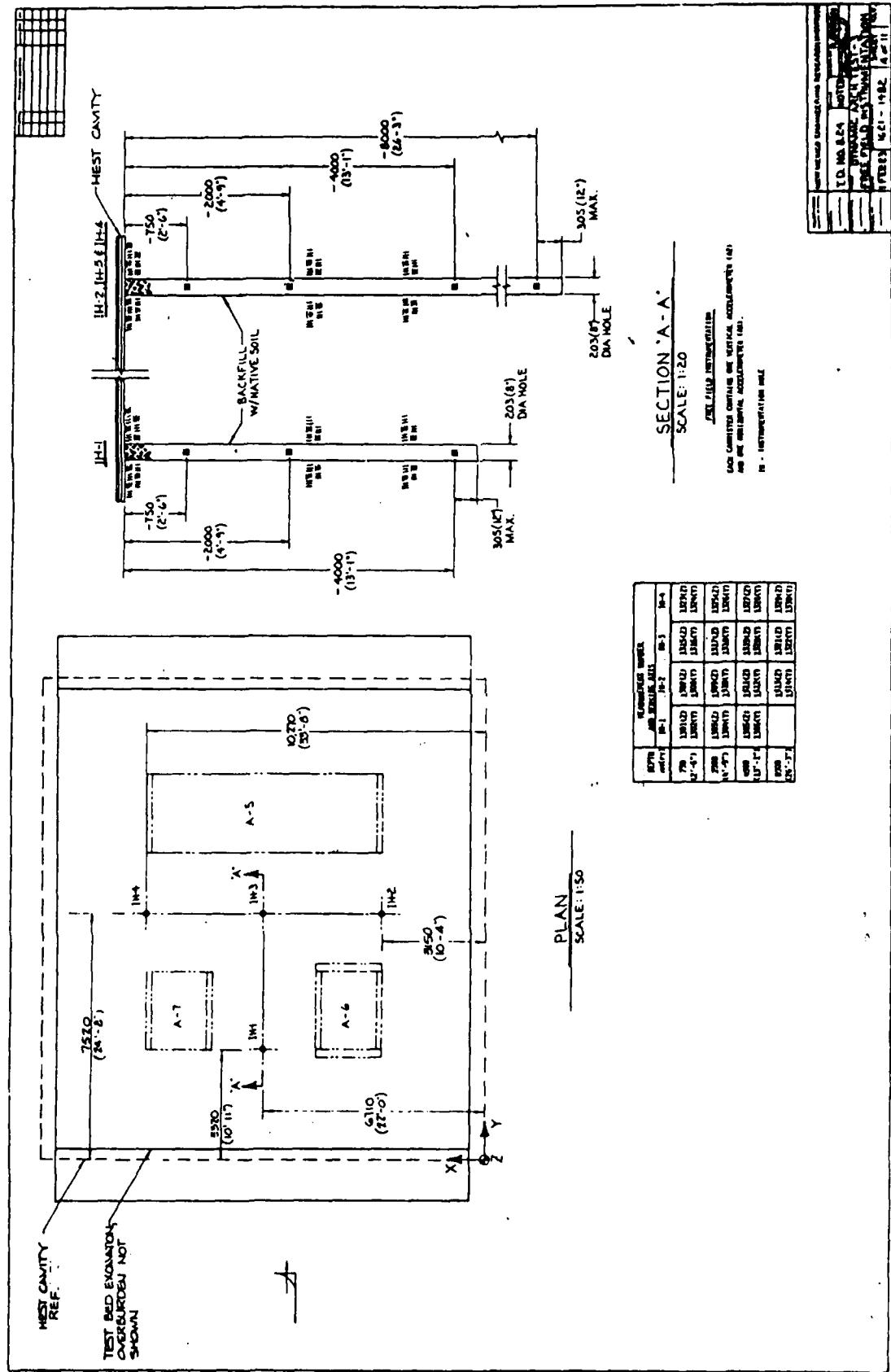
STRUCTURAL DETAIL AND CONSTRUCTION DRAWINGS

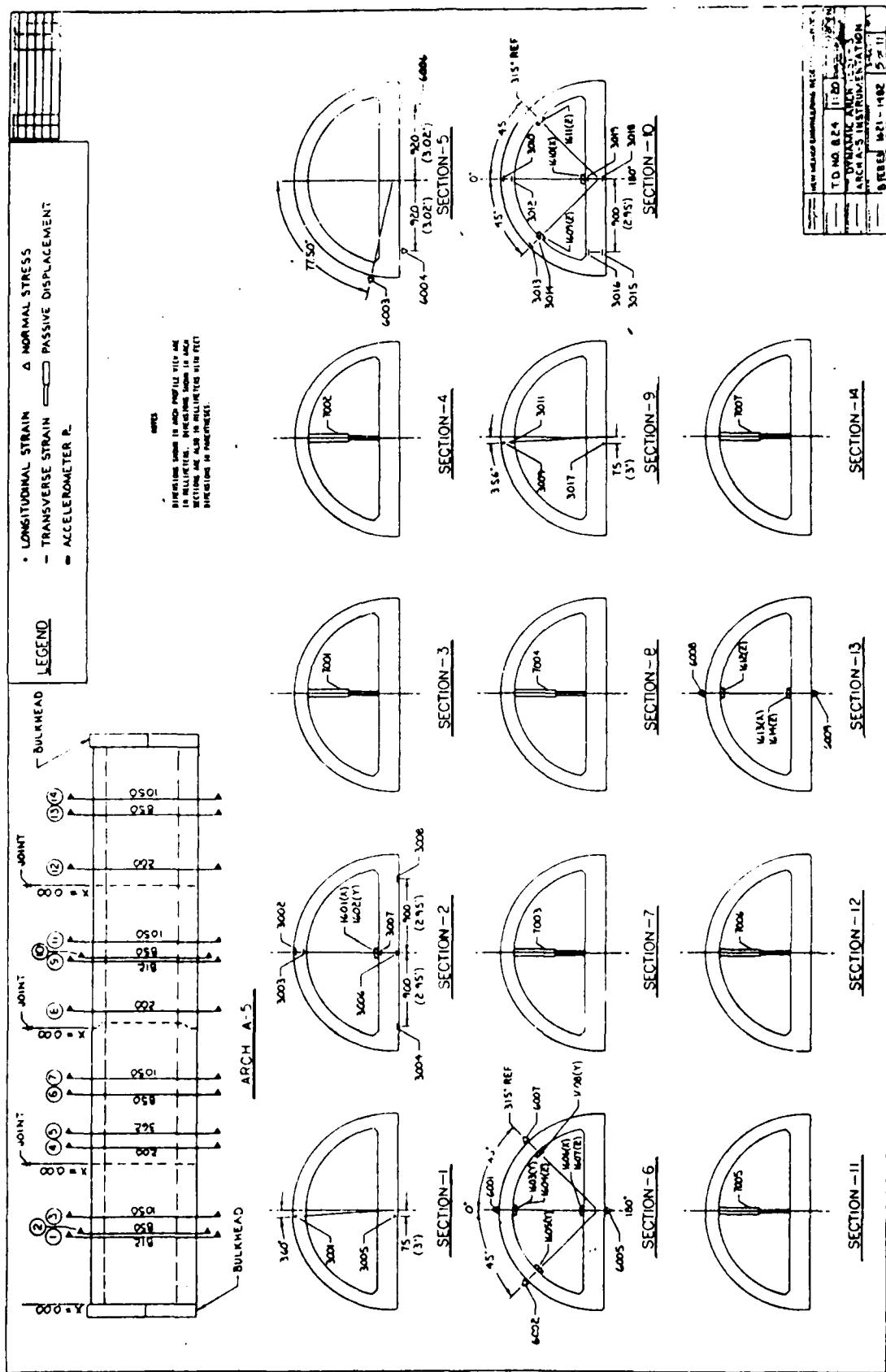
The engineering drawings shown in this appendix are reductions of New Mexico Engineering Research Institute drawings 1621-1482. Copies of the full-size drawings may be obtained from the New Mexico Engineering Research Institute, University of New Mexico, P.O. Box 25, Albuquerque, New Mexico 87131. Point of contact: Mr Glenn Baird.

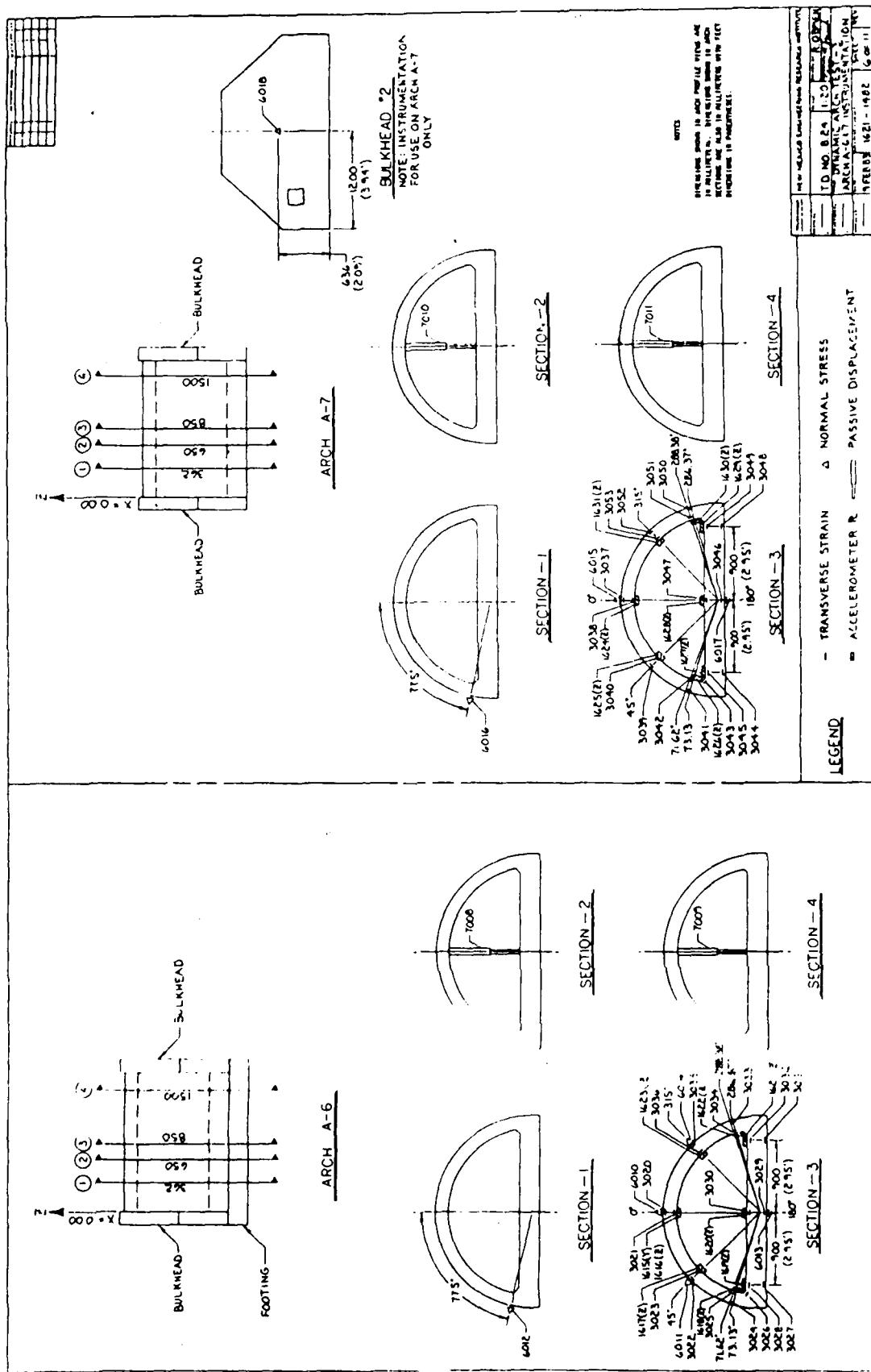


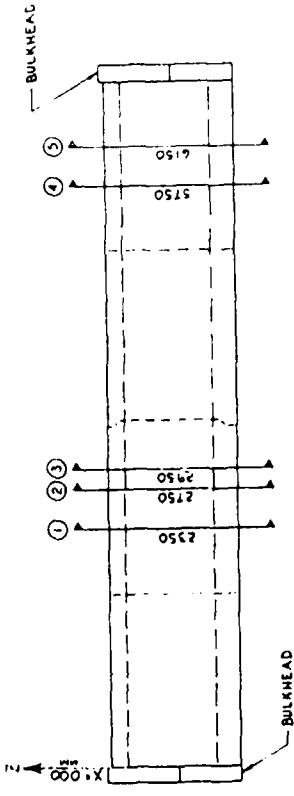




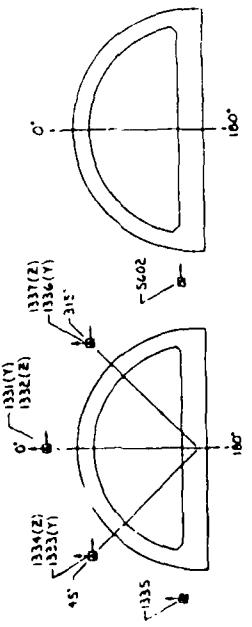




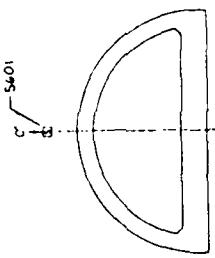




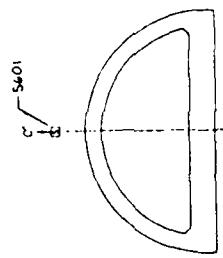
ARCH A-5



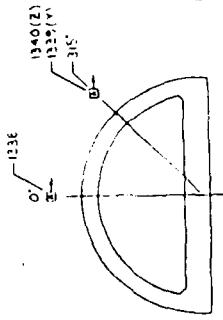
SECTION - 1



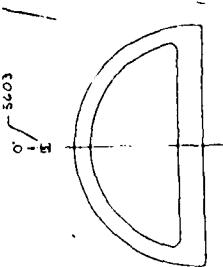
SECTION - 2



SECTION - 3



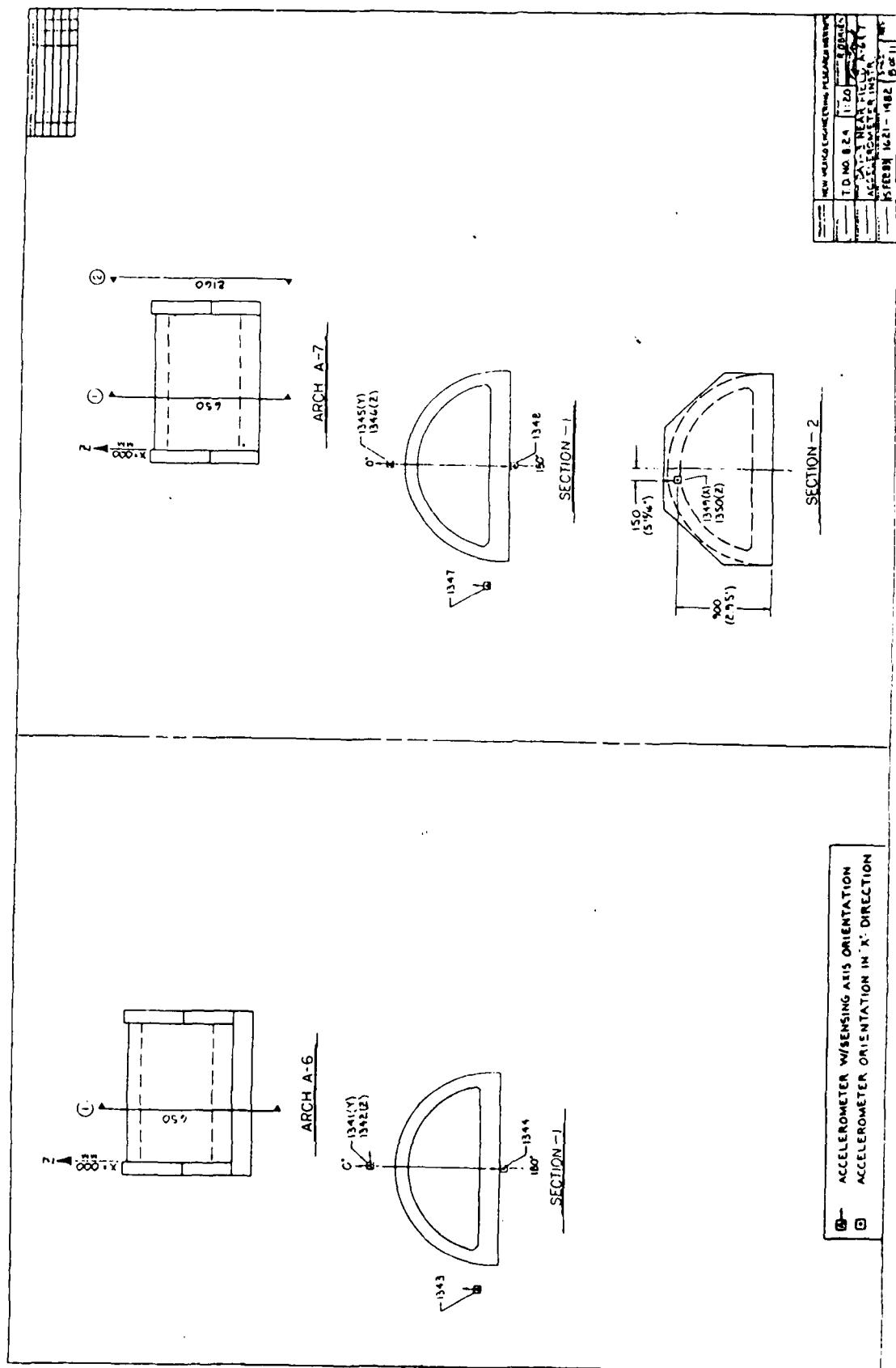
SECTION - 4

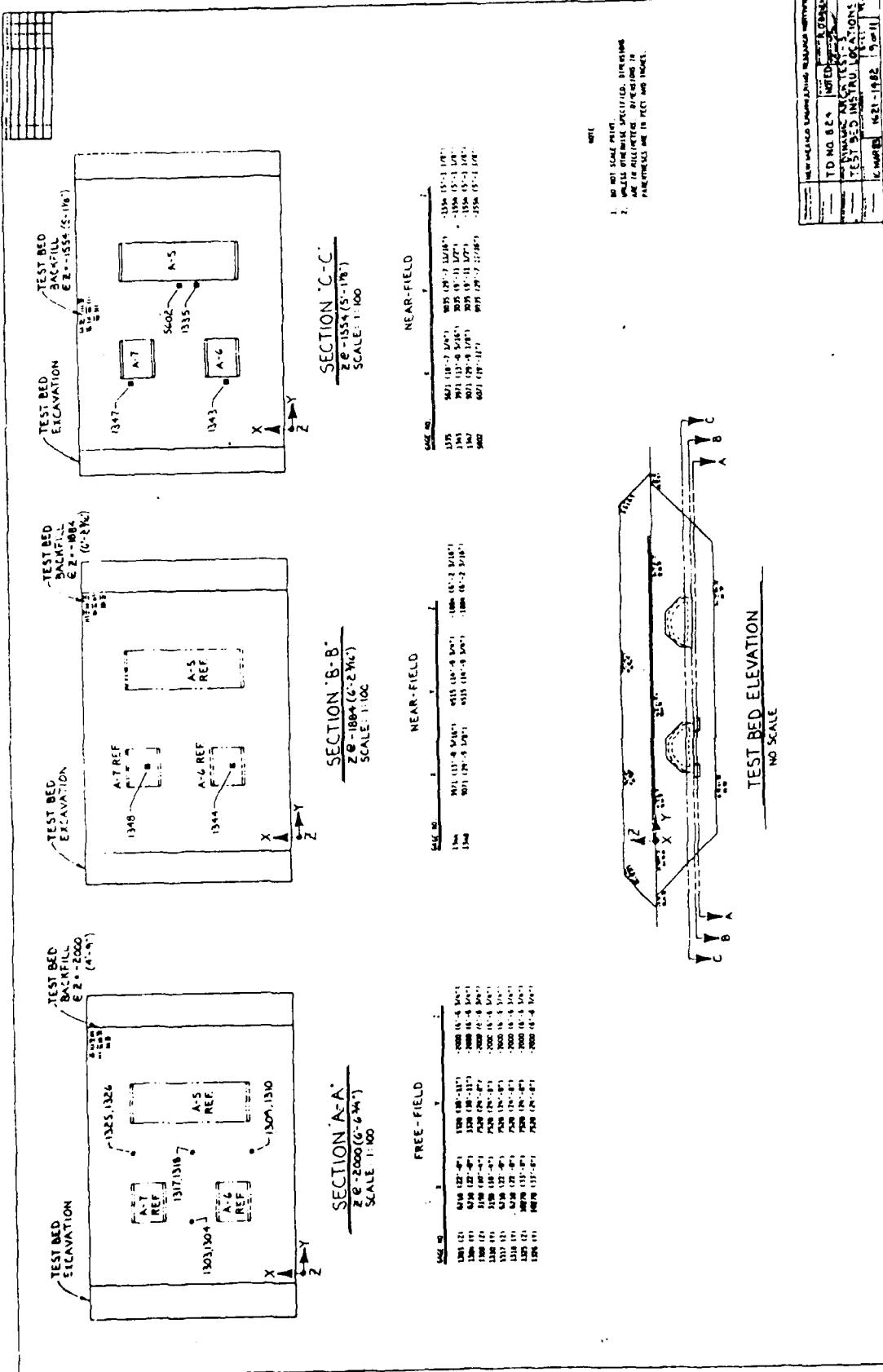


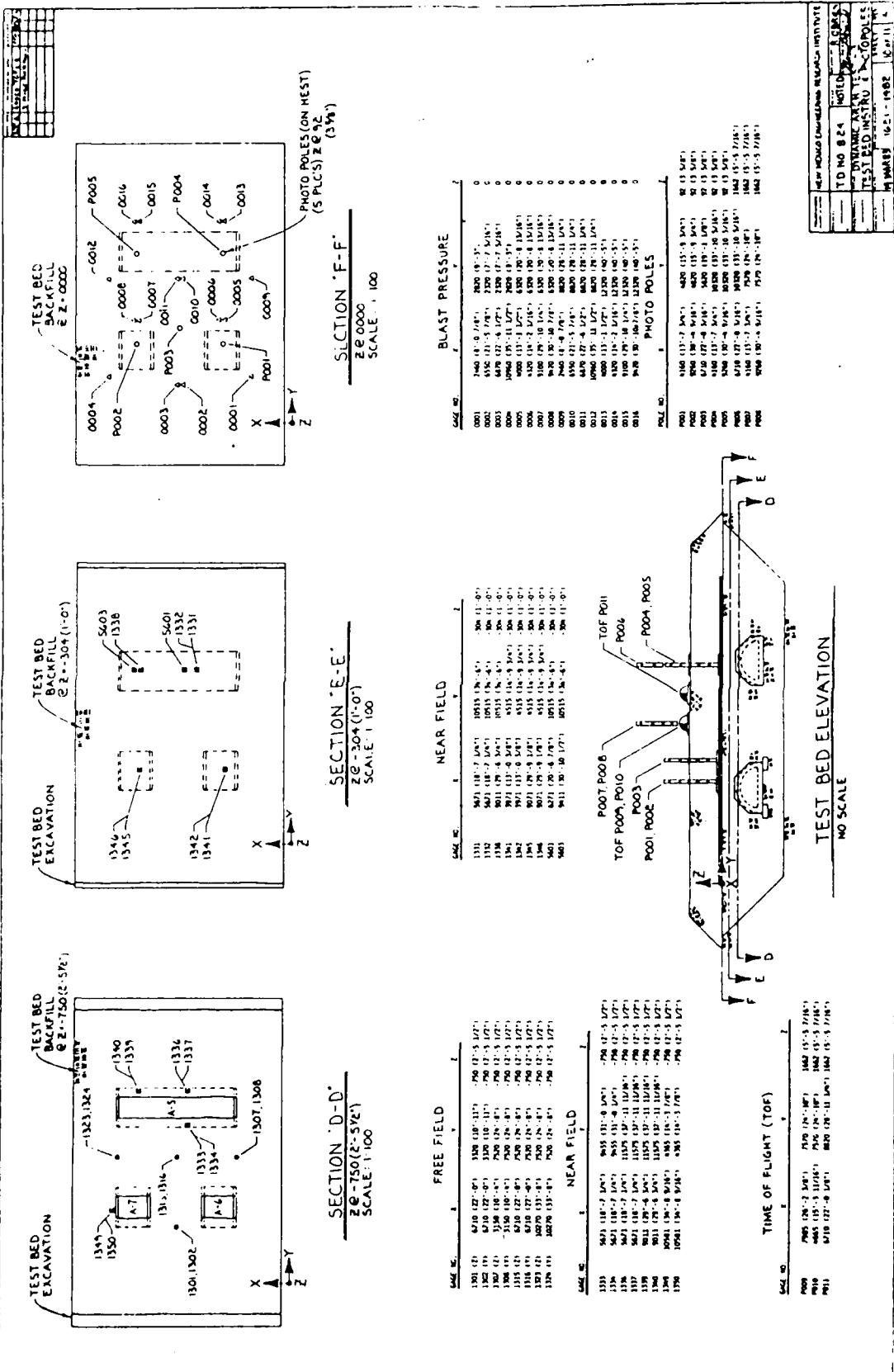
SECTION - 5

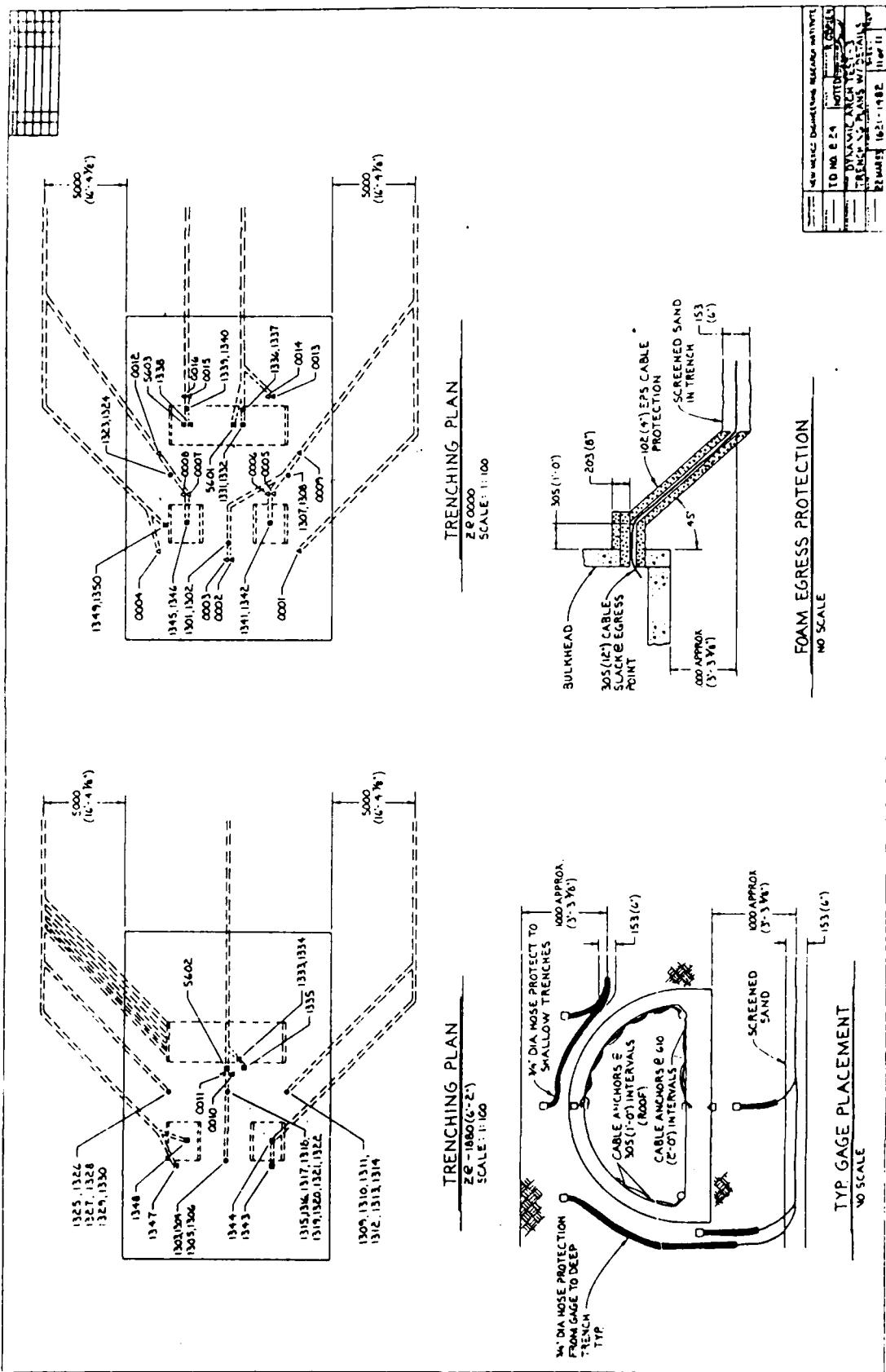
TEST NUMBER		TEST DIRECTION	TEST DURATION
TD NO.	6.24	1 : 10	0.000
ACCEL. X	3.00	NEAR	0.000
ACCEL. Y	3.00	STRAINS	0.000
ACCEL. Z	3.00	STRESS	0.000
WAVELET	1021 - 1082	7 sec	0.000

(1) ACCELEROMETER WISENSING AXIS ORIENTATION
 (2) SOIL STRESS WISENSING AXIS ORIENTATION









APPENDIX B

MEASUREMENT AND INSTRUMENTATION LIST

MEASUREMENT LIST DAT-3 TEST

MEASUREMENT LIST CODE DESIGNATION

General Location

FF - Free Field
A(n) - On Arch (n)
NF(n) - Near Arch (n)

Sensing Axis

X - Parallel to axis of arches
Y - Perpendicular to axis of arches
Z - Vertical

Polarity

Pressure Measurements

- + Compression
- Tension

Motion Measurements

- + Motion in +coordinate axis direction
- Motion in -coordinate axis direction

Measurement Number Assignment

<u>Numbers</u>	<u>Type Measurement</u>	<u>Location</u>
0001-0999	Airblast Pressure	Free Field
1301-1599	Acceleration	Free Field
1601-1899	Acceleration	Structure
3001-3599	Steel Strain	Structure
5601-5899	Soil Stress	Free Field
6001-6599	Interface Pressure	Structure
7001-7599	Displacement	Structure
8000-8999	TOA	Free Field
P001-P999	Passive RD	Free Field

COORDINATE SYSTEM

DAT-3 had four separate coordinate systems. The free-field (FF) measurements were referenced to the west corner of the test-bed. Measurements on or near the arches are designated A-5, A-6, A-7 for "on the arches" and NF5, NF6, and NF7 for "near the arches." The four coordinate systems are thus FF, A-5, A-6, and A-7. The Z-coordinate for all four systems is chosen as positive-up.

The origin of A-5 is 3.31, 10.52, -1.65 referenced to FF; A-6 is 3.31, 4.52, -1.65, and A-7 is 8.25, 4.52, -1.65 (Fig. B1). The coordinate system used for each measurement is shown in the upper left-hand corner of the data plots shown in Appendixes D through I.

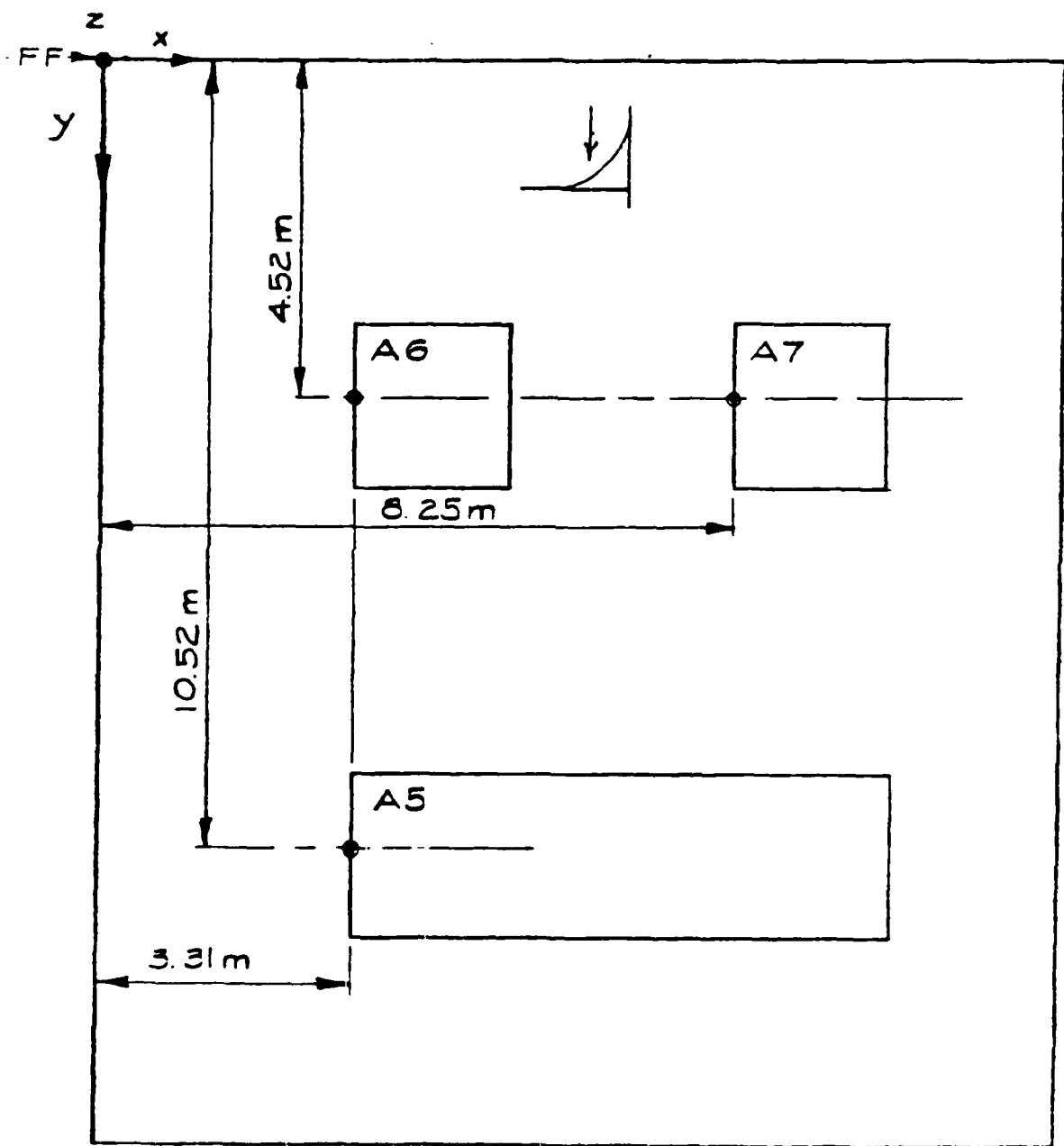


Figure B1. DAT-3 coordinate system (z is positive, oriented up).

STANDARD MEASUREMENT DESIGNATION

The Measurement Designation consists of eight coded sets of letters and numbers which tell: (1) the organization establishing the measurement requirement, (2) how the data are recorded, (3) the exact sensing location of the transducer (using either Cartesian or cylindrical coordinates), (4) the type of transducer, and (5) the sensing axis orientation of the transducer.

To prevent confusion from different designations on different field tests, this Standard Measurement Designation is hereby established. All of the presently known entries that make up the Measurement Designation are covered, and each project officer selects only those that apply to a particular field test. The Measurement Designation used in each test will still be included in the Instrumentation Plan. If additional entries are required, such as one for another organization which is not already listed, they can readily be added. The important factor is that the format of the Measurement Designation remain the same.

STANDARD MEASUREMENT DESIGNATION

X - X - XXXX - XX.XXX - XX.XXX - XX.XXX - XXX - XX

ITEM: 1 2 3 4 5 6 7 8

Item 1. The first character indicates the organization establishing the measurement requirement:

- A - AFWL/NTED-S (Effects Simulation)
- S - AFWL/NTES-R (Structural Response)
- G - AFWL/NTED-E (Earth Phenomenology)
- C - AFWL/NTED-A (Atmospheric Phenomenology)
- I - AFWL/NTEO-I (Instrumentation Systems Engineering)
- F - AFWL/NTES-A (System Assessment)
- T - AFESC/RD (Engineering Services Center)

Item 2: The second character denotes the method of data recording:

- E - Electronic
- M - Mechanical
- O - Optical

Item 3. The third set of characters describes where, in which structure or free field, the particular measurement is located.

a. For structures only, use: S01, S02, etc.

b. For structures with subsystems only, use: SOIL, SO1E, etc.

(The last letter will designate a particular subsystem such as the launch silo or the launch equipment room.)

c. For free-field only, use: L01, L02, etc. The L indicates a free-field location which can be either a hole or just a surface point where a measurement is being made.

Item 4. The fourth set of characters indicates either D, the angle in degrees, from the reference axis or X, the longitudinal distance in meters from the reference plane.

Item 5. The fifth set of characters indicates either R, the radial distance in meters from the reference axis, or Y, the transverse distance in meters from the reference plane.

Item 6. The sixth set of characters indicates Z, the vertical distance in meters from the reference plane.

Item 7. The seventh set of characters specifies the type of measurement being made.

A - Acceleration
V - Velocity
AC - Acoustic Pressure
BP - Blast Pressure
HP - Hydraulic Pressure
SP - Stagnation Pressure
FE - Free-field Strain
CE - Concrete Strain
SE - Steel Strain
AD - Absolute Displacement
RD - Relative Displacement
CS - Concrete Stress
FS - Free-field Stress
SS - Steel Stress
L - Electrical Noise
TA - Time of Arrival
IP - Interface Pressure
IS - Interface Shear
CP - Cavity (Structural) Pressure
S - Slip Measurement
T - Temperature

Item 8. The last set of characters indicates the sensing axis of the transducer:

R or T (Radial or Tangential)
+ or -X (Horizontal Longitudinal)
+ or -Y (Horizontal Transverse)
+ or -Z (Vertical)
0 - Omnidirectional

TABLE B1. MEASUREMENT AND INSTRUMENTATION LIST

Measurement number	Design location, m			As-built location, m		
	X	Y	Z	X	Y	Z
0001	2.46	2.82	0.00	2.45	2.84	0.00
0002	6.55	2.32	0.00	6.535	2.332	0.00
0003	6.87	2.32	0.00	6.857	2.317	0.00
0004	10.96	2.82	0.00	10.957	2.848	0.00
0005	4.00	6.32	0.00	3.981	6.327	0.00
0006	4.32	6.32	0.00	4.304	6.305	0.00
0007	9.10	6.32	0.00	9.066	6.292	0.00
0008	9.42	6.32	0.00	9.407	6.313	0.00
0009	2.46	8.82	0.00	2.436	8.834	0.00
0010	6.55	8.82	0.00	6.549	8.783	0.00
0011	6.87	8.82	0.00	6.876	8.785	0.00
0012	10.96	8.82	0.00	10.961	8.835	0.00
0013	4.00	12.32	0.00	4.005	12.328	0.00
0014	4.32	12.32	0.00	4.326	12.336	0.00
0015	9.10	12.32	0.00	9.068	12.358	0.00
0016	9.42	12.32	0.00	9.384	12.327	0.00

TABLE B1. (Continued)

Measurement number	Design location, m			As-built location, m		
	X	Y	Z	X	Y	Z
1301	6.71	3.32	-0.75	6.71	3.32	-0.75
1302	6.71	3.32	-0.75	6.71	3.32	-0.75
1303	6.71	3.32	-2.00	6.71	3.32	-2.00
1304	6.71	3.32	-2.00	6.71	3.32	-2.00
1305	6.71	3.32	-4.00	6.71	3.32	-4.00
1306	6.71	3.32	-4.00	6.71	3.32	-4.00
1307	3.15	7.52	-0.75	3.15	7.52	-0.75
1308	3.15	7.52	-0.75	3.15	7.52	-0.75
1309	3.15	7.52	-2.00	3.15	7.52	-2.00
1310	3.15	7.52	-2.00	3.15	7.52	^a -4.00
1311	3.15	7.52	-4.00	3.15	7.52	-4.00
1312	3.15	7.52	-4.00	^a 10.27	7.52	-4.00
1313	3.15	7.52	-8.00	3.15	7.52	-8.00
1314	3.15	7.52	-8.00	3.15	7.52	-8.00
1315	6.71	7.52	-0.75	6.71	7.52	-0.75
1316	6.71	7.52	-0.75	6.71	7.52	-0.75
1317	6.71	7.52	-2.00	^a 3.15	7.52	-2.00
1318	6.71	7.52	-2.00	6.71	7.52	-2.00
1319	6.71	7.52	-4.00	6.71	7.52	-4.00
1320	6.71	7.52	-4.00	6.71	7.52	^a -4.00

^aAs-built gage locations adjusted by Instrumentation Officer and Technical Director.

TABLE B1. (Continued)

Measurement number	Design location, m			As-built location, m		
	X	Y	Z	X	Y	Z
1321	6.71	7.52	-8.00	6.71	7.52	-8.00
1322	6.71	7.52	-8.00	6.71	7.52	-8.00
1323	10.27	7.52	-0.75	10.27	7.52	-0.75
1324	10.27	7.52	-0.75	10.27	7.52	-0.75
1325	10.27	7.52	-2.00	10.27	7.52	-2.00
1326	10.27	7.52	-2.00	10.27	7.52	-2.00
1327	10.27	7.52	-4.00	^a 6.71	7.52	^a -2.00
1328	10.27	7.52	-4.00	10.27	7.52	-4.00
1329	10.27	7.52	-8.00	10.27	7.52	-8.00
1330	10.27	7.52	-8.00	10.27	7.52	-8.00
1331	2.35	0.00	1.34	2.35	0.00	1.34
1332	2.75	0.00	1.34	2.35	0.00	1.34
1333	2.35	-1.06	0.90	2.35	-1.06	0.90
1334	2.75	-1.06	0.90	2.35	-1.06	0.90
1335	2.35	-1.48	0.09	2.35	-1.48	0.09
1336	2.35	1.06	0.90	2.35	1.06	0.90
1337	2.75	1.06	0.90	2.35	1.06	0.90
1338	5.69	0.00	1.34	5.75	0.00	1.34
1339	5.69	1.06	0.90	5.75	1.06	0.90
1340	6.09	1.06	0.90	5.75	1.06	0.90
1341	0.65	0.00	1.34	0.65	0.00	1.34
1342	1.05	0.00	1.34	0.65	0.00	1.34
1343	0.65	-1.48	0.09	0.65	-1.48	0.09
1344	0.65	0.00	-0.24	0.65	0.00	-0.24
1345	0.65	0.00	1.34	0.65	0.00	1.34

^aAs-built gage locations adjusted by Instrumentation Officer and Technical Director.

TABLE B1. (Continued)

Measurement number	Design location, m			As-built location, m		
	X	Y	Z	X	Y	Z
1346	1.05	0.00	1.34	0.65	0.00	1.34
1347	0.65	-1.48	0.09	0.65	-1.48	0.09
1348	0.65	0.00	0.24	0.65	0.00	0.24
1349	2.16	-0.15	0.90	2.16	-0.15	0.90
1350	2.16	0.15	0.90	2.16	-0.15	0.90
1601	0.85	0.00	0.00	0.85	0.00	0.00
1602	0.85	0.00	0.00	0.85	0.00	0.00
1603	2.55	0.00	0.88	4.250	0.00	0.88
1604	2.55	0.00	0.88	4.250	0.00	0.88
1605	2.55	-0.74	0.57	4.250	-0.74	0.57
1606	2.55	0.00	0.00	4.250	0.00	0.00
1607	2.55	0.00	0.00	4.250	0.00	0.00
1608	2.55	0.74	0.57	4.250	-0.74	0.57
1609	4.19	-0.74	0.57	2.55	0.74	0.57
1610	4.19	0.00	0.00	2.55	0.00	0.00
1611	4.19	0.74	0.57	2.55	-0.74	0.57
1612	5.89	0.00	0.88	6.01	0.00	0.88
1613	5.89	0.00	0.00	6.01	0.00	0.00
1614	5.89	0.00	0.00	6.01	0.00	0.00
1615	0.85	0.00	0.88	0.85	0.00	0.88
1616	0.85	0.00	0.88	0.85	0.00	0.88
1617	0.85	-0.74	0.57	0.85	-0.74	0.57
1618	0.85	-1.00	0.13	0.85	-1.00	0.13
1619	0.85	-0.94	0.00	0.85	-9.25	0.00
1620	0.85	0.00	0.00	0.85	0.00	0.00

TABLE B1. (Continued)

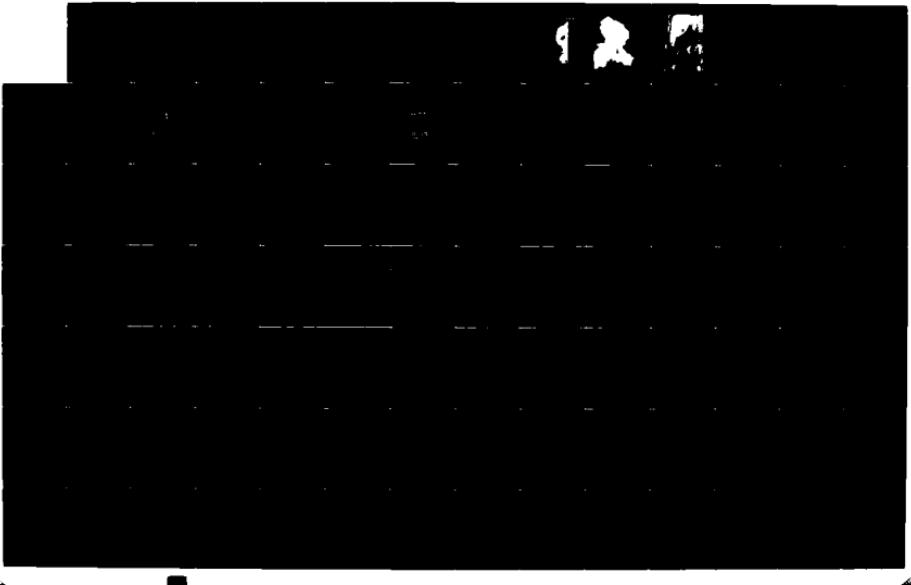
Measurement number	Design location, m			As-built location, m		
	X	Y	Z	X	Y	Z
1621	0.85	0.94	0.00	0.85	0.925	0.00
1622	0.85	1.00	0.13	0.85	1.00	0.13
1623	0.85	0.74	0.57	0.85	0.74	0.57
1624	0.85	0.00	0.88	0.85	0.00	0.88
1625	0.85	-0.74	0.57	0.85	-0.74	0.57
1626	0.85	-1.00	0.13	0.85	-1.00	0.13
1627	0.85	-0.94	0.00	0.85	-0.925	0.00
1628	0.85	0.00	0.00	0.85	0.00	0.00
1629	0.85	0.94	0.00	0.85	0.925	0.00
1630	0.85	1.00	0.13	0.85	1.00	0.13
1631	0.85	0.74	0.57	0.85	0.74	0.57
3001	0.85	0.00	1.02	0.812	-0.075	1.015
3002	0.85	0.00	1.01	0.85	0.00	1.164
3003	0.85	0.00	0.91	0.85	0.00	0.916
3004	0.85	-0.94	-0.21	0.85	-0.900	-0.209
3005	0.85	0.00	-0.22	0.812	-0.075	-0.199
3006	0.85	0.00	-0.21	0.85	0.00	-0.209
3007	0.85	0.00	-0.03	0.85	0.00	-0.026
3008	0.85	0.94	-0.21	0.85	0.900	-0.209
3009	4.19	0.00	1.02	2.528	0.075	1.015
3010	4.19	0.00	1.01	2.490	0.00	1.164
3011	4.19	0.00	0.90	2.528	0.068	0.902
3012	4.19	0.00	0.91	2.490	0.00	0.916
3013	4.19	-0.83	0.67	2.490	0.823	0.663
3014	4.19	-0.76	0.60	2.490	0.648	0.452

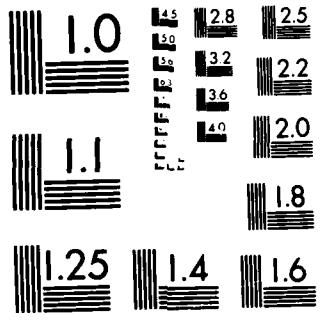
AD-A171 212 KACHINA TEST SERIES: DYNAMIC ARCH TEST THREE (DAT-3) 3/6
ANALYSIS REPORT(U) AIR FORCE WEAPONS LAB KIRTLAND AFB
NM J L SMITH ET AL. MAR 86 AFWL-TR-85-63

UNCLASSIFIED

F/G 19/4

ML





MICROCOPY RESOLUTION TEST CHART
NATIONAL BUREAU OF STANDARDS 1963-A

TABLE B1. (Continued)

Measurement number	Design location, m			As-built location, m		
	X	Y	Z	X	Y	Z
3015	4.19	-0.94	-0.21	2.490	0.900	-0.209
3016	4.19	-0.94	-0.03	2.490	0.900	-0.026
3017	4.19	0.00	-0.22	2.528	0.075	-0.199
3018	4.19	0.00	-0.21	2.490	0.00	-0.209
3019	4.19	0.00	-0.03	2.490	0.00	-0.026
3020	0.85	0.00	1.01	0.85	0.00	1.01
3021	0.85	0.00	0.91	0.85	0.00	0.91
3022	0.85	-0.83	0.67	0.85	0.83	0.67
3023	0.85	-0.76	0.60	0.85	-0.76	0.60
3024	0.85	-1.12	0.16	0.85	-1.12	0.16
3025	0.85	-1.03	0.13	0.85	-1.03	0.13
3026	0.85	-1.04	0.03	0.85	-1.04	0.03
3027	0.85	-0.94	-0.21	0.85	-0.900	-0.21
3028	0.85	-0.94	-0.03	0.85	-0.900	-0.03
3029	0.85	0.00	-0.21	0.85	-0.00	-0.21
3030	0.85	0.00	-0.03	0.85	-0.00	-0.03
3031	0.85	-0.94	-0.21	0.85	-0.900	-0.21
3032	0.85	-0.94	-0.03	0.85	-0.900	0.03
3033	0.85	1.12	0.16	0.85	1.12	0.16
3034	0.85	1.03	0.13	0.85	1.03	0.13
3035	0.85	0.83	0.67	0.85	0.83	0.67
3036	0.85	0.76	0.60	0.85	0.76	0.60
3037	0.85	0.00	1.01	0.85	0.00	1.01
3038	0.85	0.00	0.91	0.85	0.00	0.91
3039	0.85	-0.83	0.67	0.85	-0.83	0.67
3040	0.85	-0.76	0.60	0.85	-0.76	0.60

TABLE B1. (Continued)

Measurement number	Design location, m			As-built location, m		
	X	Y	Z	X	Y	Z
3041	0.85	-1.12	0.16	0.85	-1.12	0.16
3042	0.85	-1.03	0.13	0.85	-1.03	0.13
3043	0.85	-1.04	0.03	0.85	-1.04	0.03
3044	0.85	-0.94	-0.21	0.85	-0.900	-0.21
3045	0.85	-0.94	-0.03	0.85	-0.900	-0.03
3046	0.85	0.00	-0.21	0.85	0.00	-0.21
3047	0.85	0.00	-0.03	0.85	0.00	-0.03
3048	0.85	0.94	-0.21	0.85	0.900	-0.21
3049	0.85	0.94	-0.03	0.85	0.900	-0.03
3050	0.85	1.12	0.16	0.85	1.12	0.16
3051	0.85	1.03	0.13	0.85	1.03	0.13
3052	0.85	0.83	0.67	0.85	0.83	0.67
3053	0.85	0.76	0.60	0.85	0.76	0.60
5601	2.95	0.00	1.34	2.95	0.00	1.34
5602	2.75	-1.48	0.09	2.75	-1.48	0.09
5603	6.09	0.00	1.34	6.150	0.00	1.34
6001	2.55	0.00	1.04	2.495	0.00	1.04
6002	2.55	0.85	0.69	2.495	0.85	0.69
6003	2.55	1.18	0.04	2.062	1.18	0.04
6004	2.55	-1.10	-0.24	2.062	0.92	-0.236
6005	2.55	0.00	-0.24	2.495	0.00	-0.236
6006	2.55	1.10	-0.24	2.062	-0.920	-0.236
6007	2.55	-0.85	0.69	2.495	-0.85	0.64

TABLE B1. (Continued)

Measurement number	Design location, m			As-built location, m		
	X	Y	Z	X	Y	Z
6008	5.89	0.00	1.04	5.955	0.00	1.04
6009	5.89	0.00	-0.24	5.955	0.00	-0.236
6010	0.85	0.00	1.04	0.795	0.00	1.04
6011	0.85	-0.85	0.69	0.795	-0.85	0.69
6012	0.85	-1.18	0.04	0.362	-1.18	0.020
6013	0.85	0.00	-0.24	0.795	0.00	-0.236
6014	0.85	0.85	0.69	0.795	0.85	0.69
6015	0.85	0.00	1.04	0.795	0.00	1.04
6016	0.85	-1.18	0.04	0.340	-1.18	0.02
6017	0.85	0.00	-0.24	0.795	0.00	-0.236
6018	1.86	0.00	0.40	1.86	0.00	0.40
7001	1.05	0.00	0.88 - 0.00	1.05	0.00	0.88 - 0.00
7002	1.90	0.00	0.88 - 0.00	2.350	0.00	0.88 - 0.00
7003	2.75	0.00	0.88 - 0.00	3.200	0.00	0.88 - 0.00
7004	3.54	0.00	0.88 - 0.00	4.050	0.00	0.88 - 0.00
7005	4.39	0.00	0.88 - 0.00	4.900	0.00	0.88 - 0.00
7006	5.30	0.00	0.88 - 0.00	5.42	0.00	0.88 - 0.00
7007	6.15	0.00	0.88 - 0.00	6.27	0.00	0.88 - 0.00
7008	0.65	0.00	0.88 - 0.00	0.65	0.00	0.88 - 0.00
7009	1.50	0.00	0.88 - 0.00	1.50	0.00	0.88 - 0.00
7010	0.65	0.00	0.88 - 0.00	0.65	0.00	0.88 - 0.00
7011	1.50	0.00	0.88 - 0.00	1.50	0.00	0.88 - 0.00

TABLE B1. (Continued)

Measurement number	Design location, m			As-built location, m		
	X	Y	Z	X	Y	Z
8000		Detonator				
8001	2.68	0.00	0.051			
8002	5.36	0.00	0.076			
8003	8.04	0.00	0.051			
8004	10.72	0.00	0.076			
8005	2.68	1.63	0.051			
8006	5.36	1.63	0.076			
8007	8.04	1.63	0.051			
8008	10.72	1.63	0.076			
8009	2.68	3.26	0.051			
8010	5.36	3.26	0.076			
8011	8.04	3.26	0.051			
8012	10.72	3.26	0.076			
8013	2.68	4.89	0.051			
8014	5.36	4.89	0.076			
8015	8.04	4.89	0.051			
8016	10.72	4.89	0.076			
8017	2.68	6.52	0.051			
8018	5.36	6.52	0.076			
8019	8.04	6.52	0.051			
8020	10.72	6.52	0.076			
8021	2.68	8.15	0.051			
8022	5.36	8.15	0.076			
8023	8.04	8.15	0.051			
8024	10.72	8.15	0.076			
8025	2.68	9.78	0.051			

TABLE B1. (Concluded)

Measurement number	Design location, m			As-built location, m		
	X	Y	Z	X	Y	Z
8026	5.36	9.78	0.076			
8027	8.04	9.78	0.051			
8028	10.72	9.78	0.076			
8029	2.68	11.41	0.051			
8030	5.36	11.41	0.076			
8031	8.04	11.41	0.051			
8032	10.72	11.41	0.076			
8033	2.68	13.04	0.051			
8034	5.36	13.04	0.076			
8035	8.04	13.04	0.051			
8036	10.72	13.04	0.076			
P001	4.16	4.82	0.092	4.16	4.82	0.092
P002	9.26	4.82	0.092	9.26	4.82	0.092
P003	6.71	5.82	0.092	6.71	5.82	0.092
P004	4.16	10.32	0.092	4.16	10.32	0.092
P005	9.26	10.32	0.092	9.26	10.32	0.092
P006	6.71	10.32	1.57	6.71	10.32	1.57
P007	4.16	7.57	1.57	4.16	7.57	1.57
P008	9.26	7.57	1.57	9.26	7.57	1.57
P009	7.985	7.57	1.57	7.985	7.57	1.57
P010	4.665	7.57	1.57	4.665	7.57	1.57
P011	6.71	8.82	1.57	6.71	8.82	1.57

APPENDIX C

MISCELLANEOUS PHOTOGRAPHS AND STRUCTURAL DAMAGE DRAWINGS

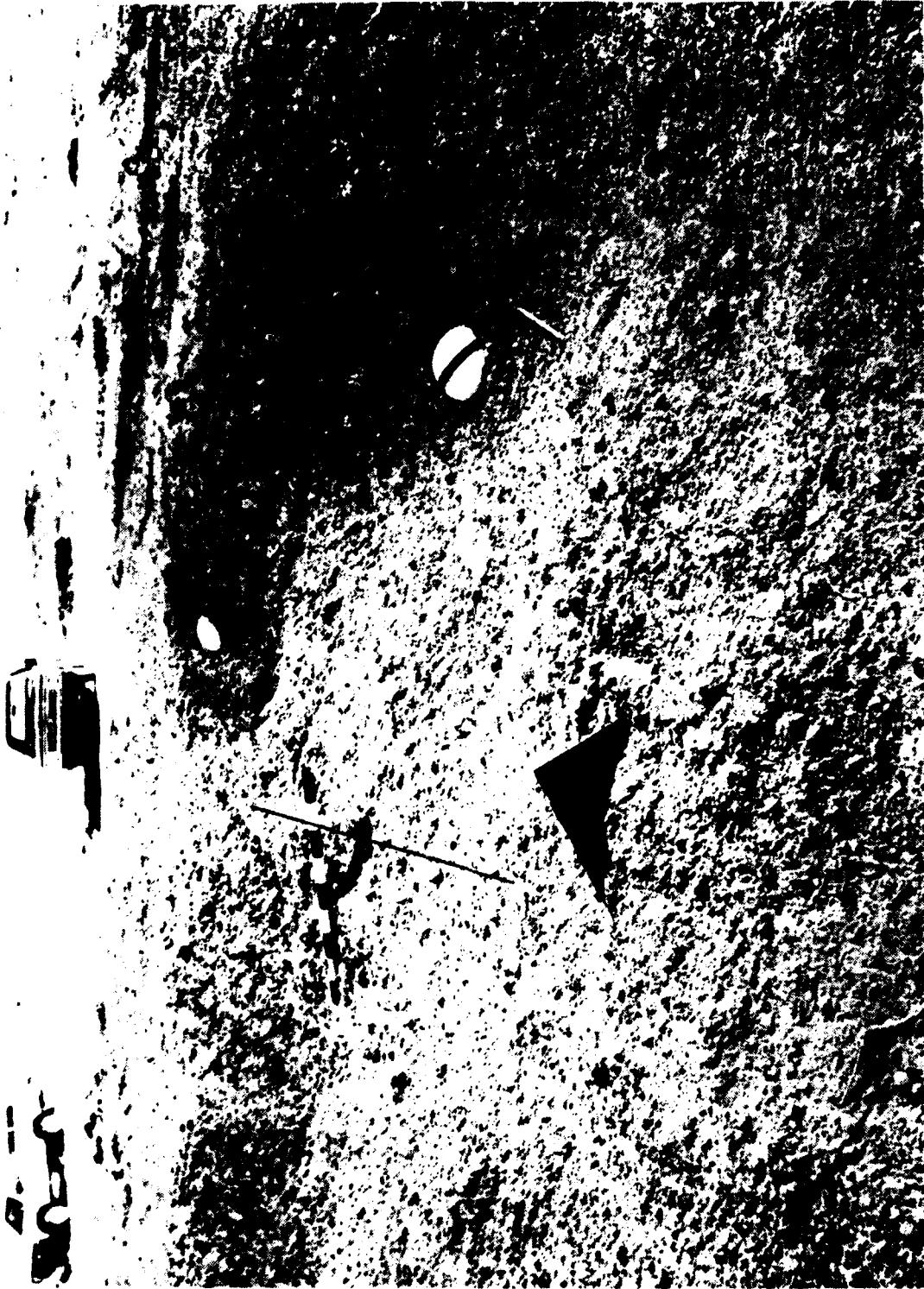
HEST detonation.

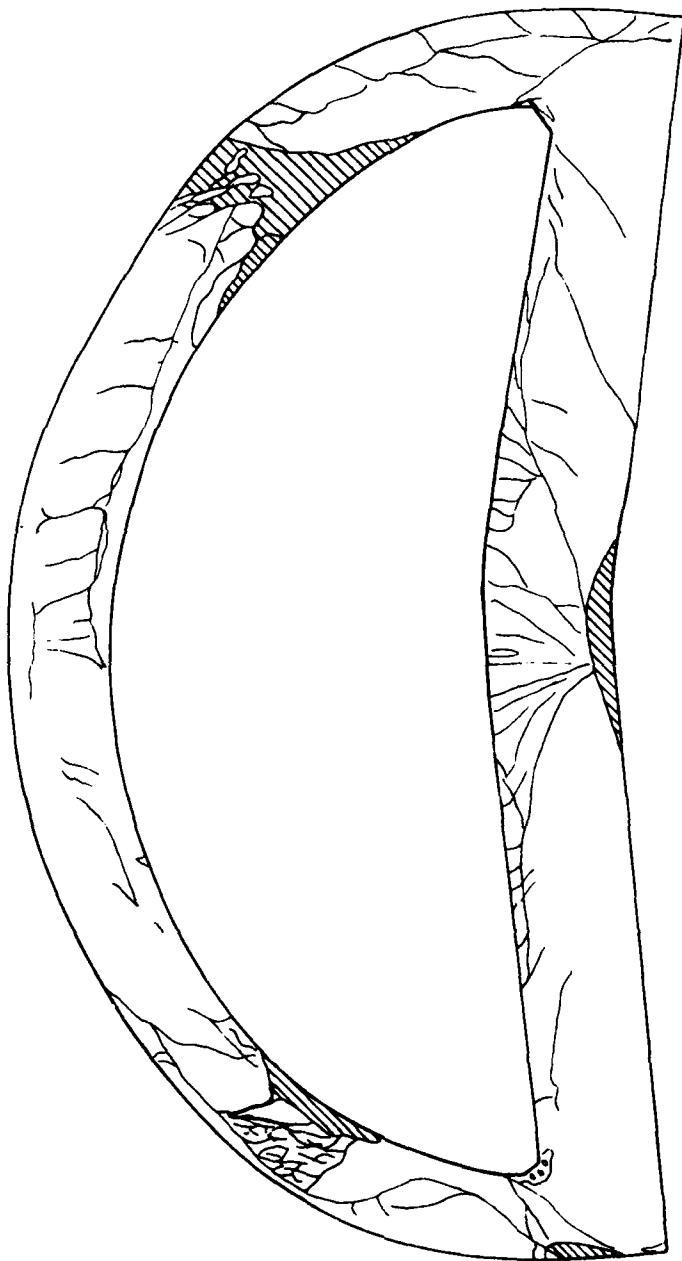




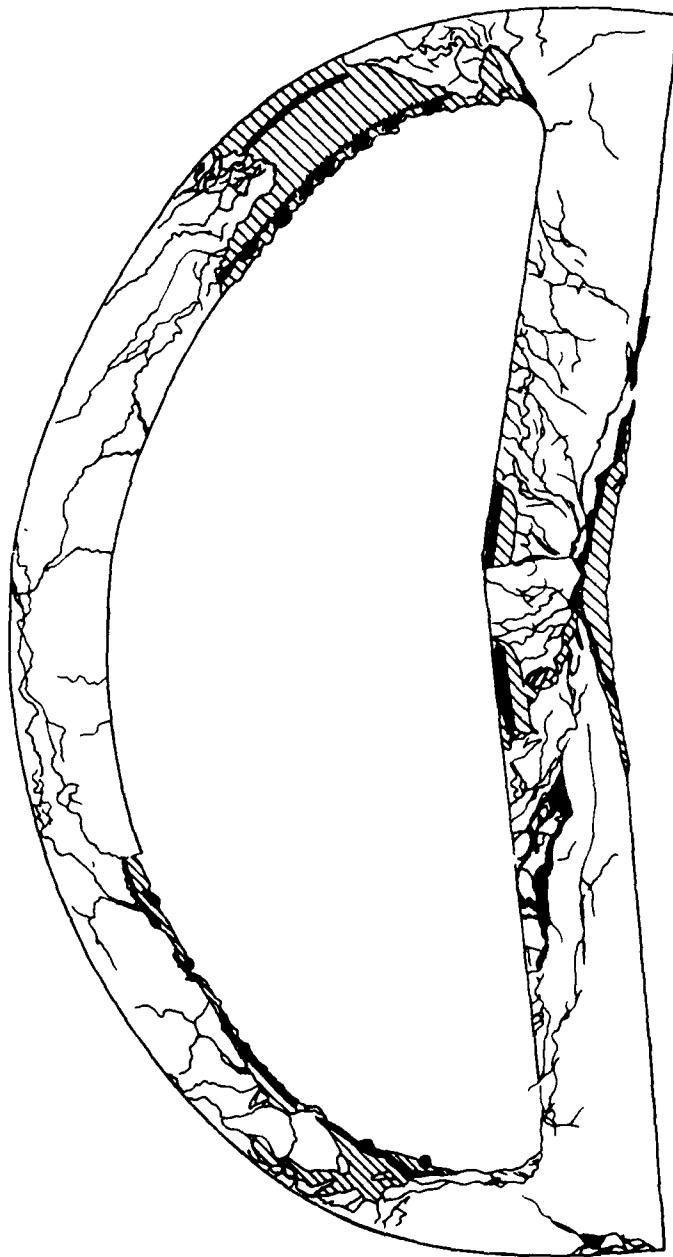
HEST detonation continued.

HEST overburden fallback material.

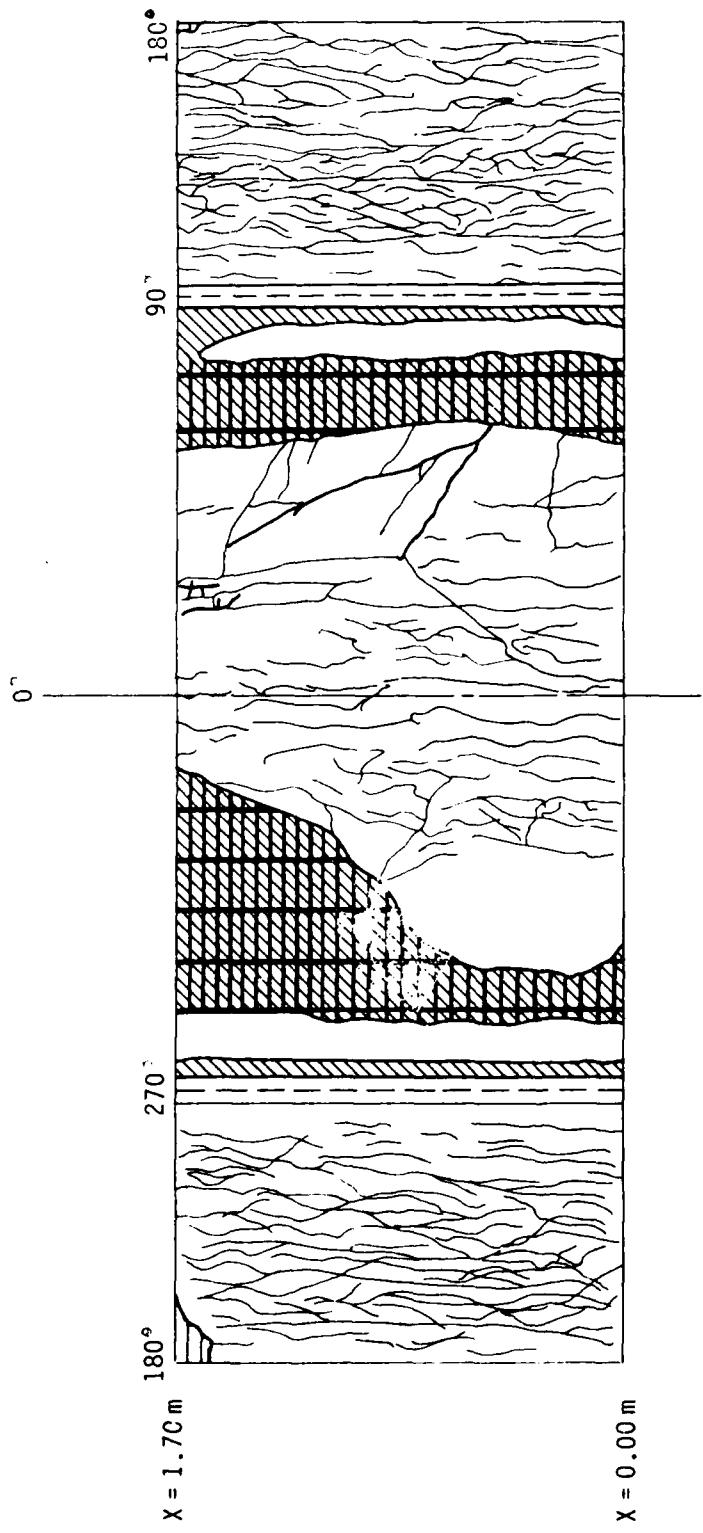




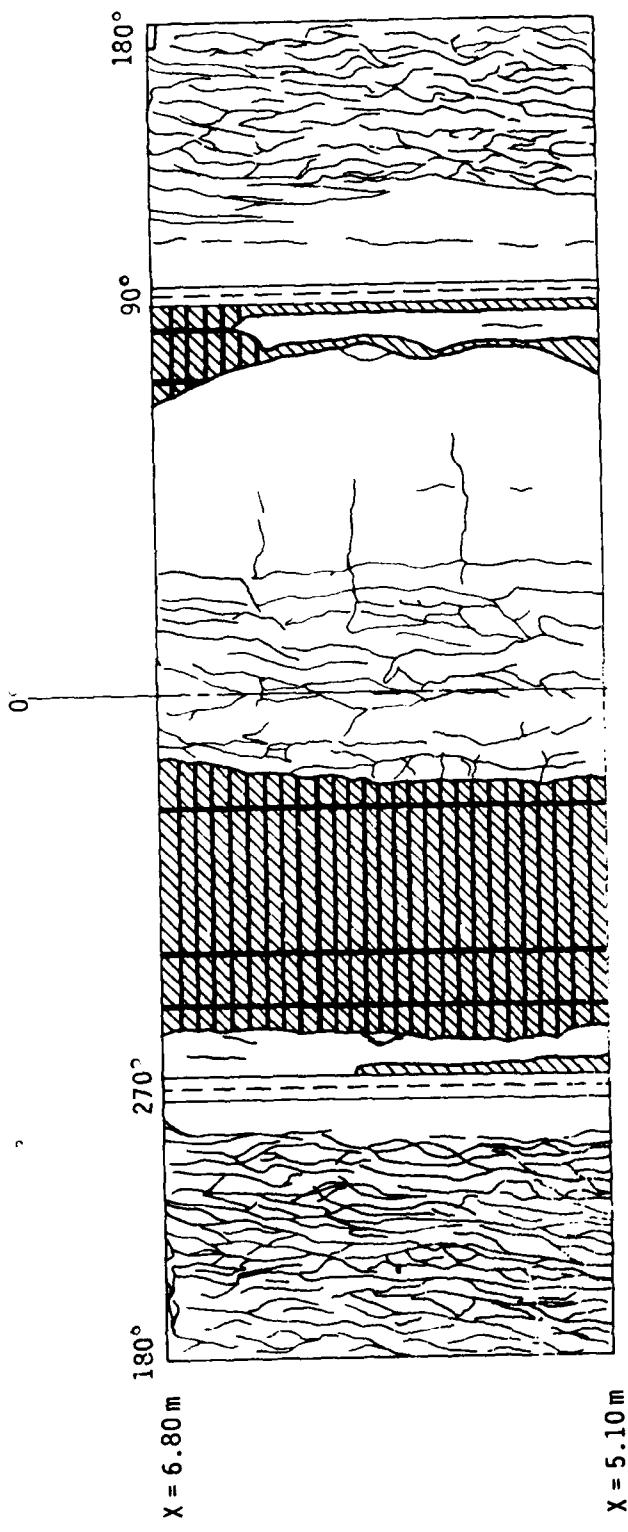
A5-1 cross section, station 0.00 m.



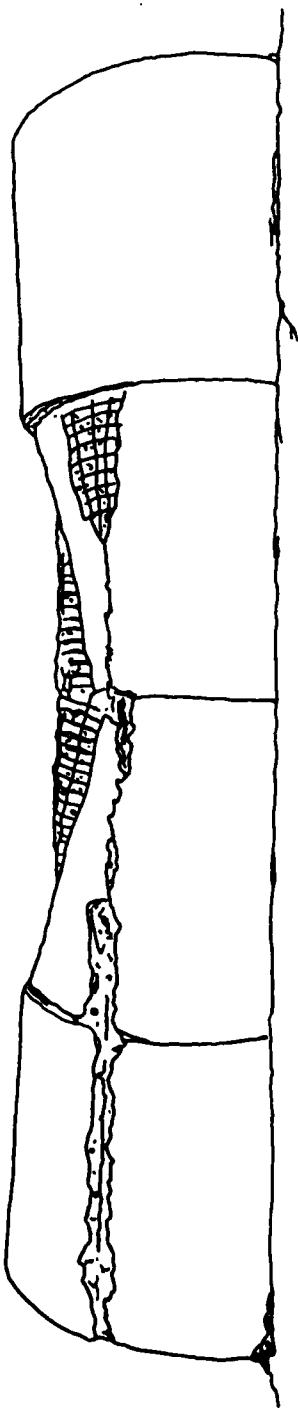
A5-4 cross section, station 6.80 m.



A5~1 interior.



A5-4 interior.



A5 profile, viewed from upstream side (90 deg).

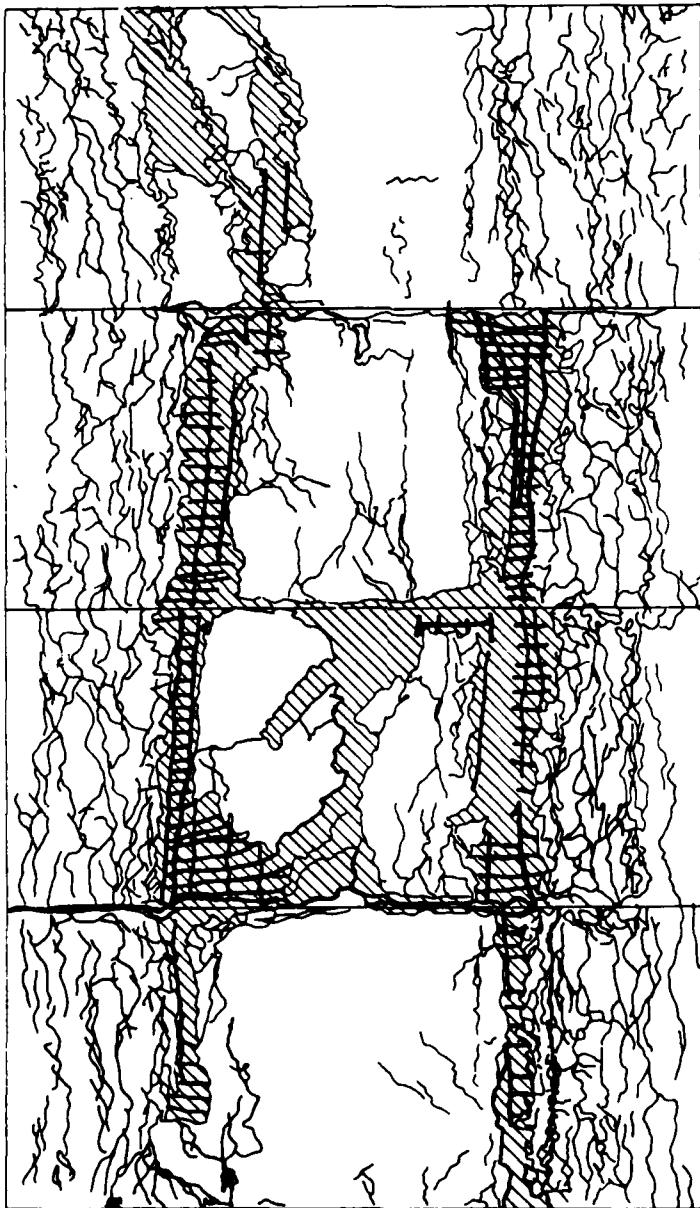
270°

0°

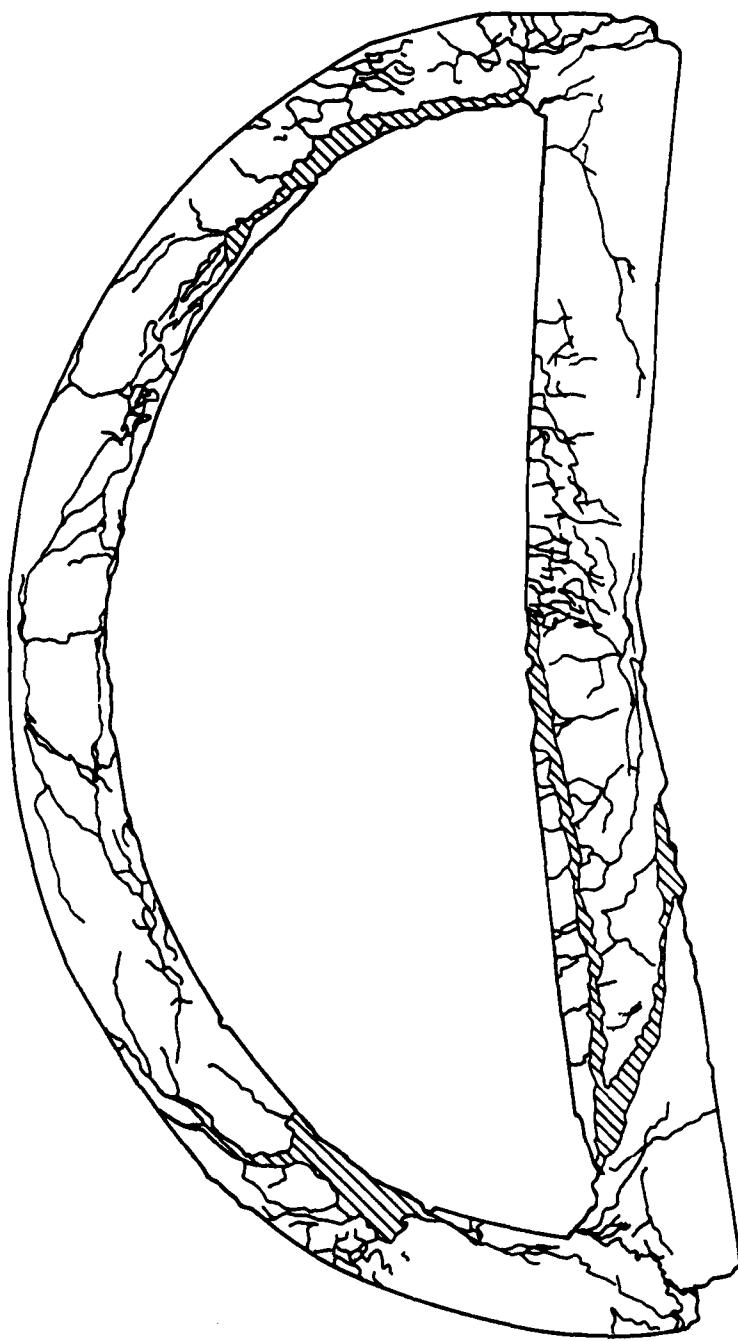
90°

X = 0.00 m

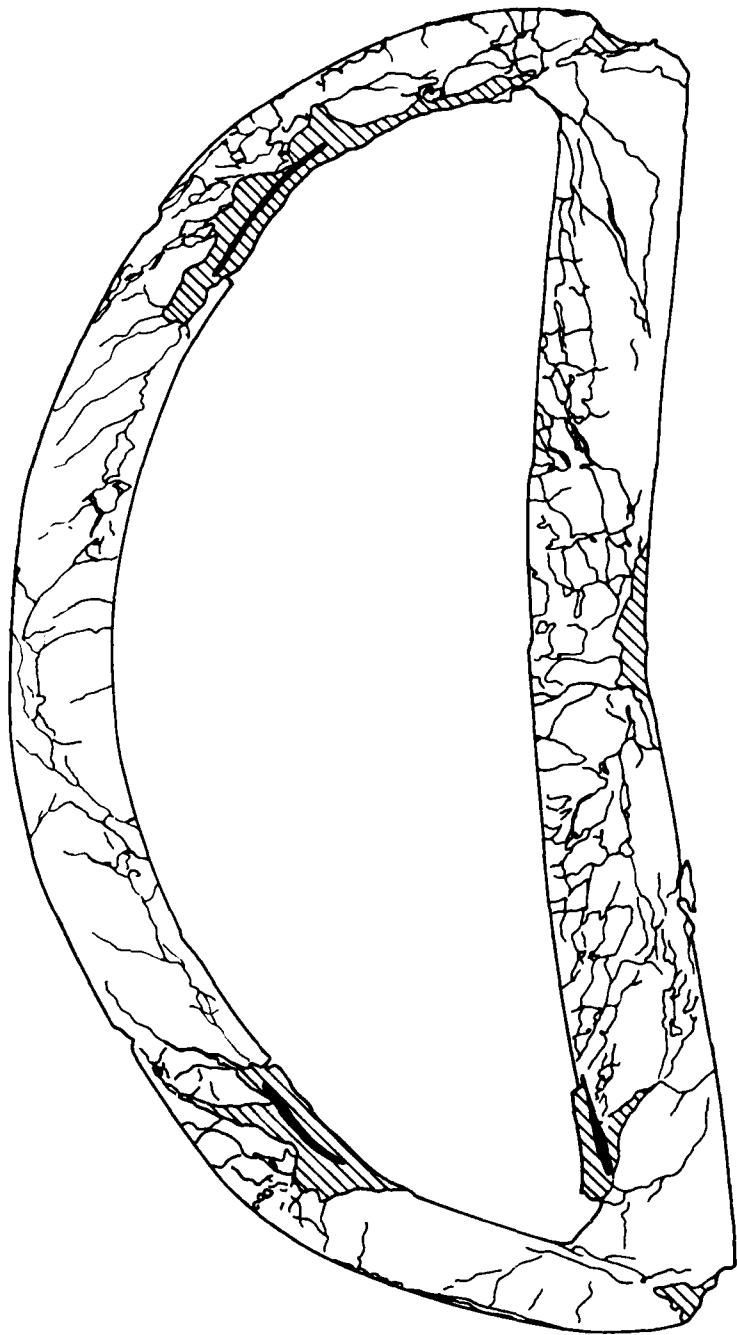
X = 6.80 m



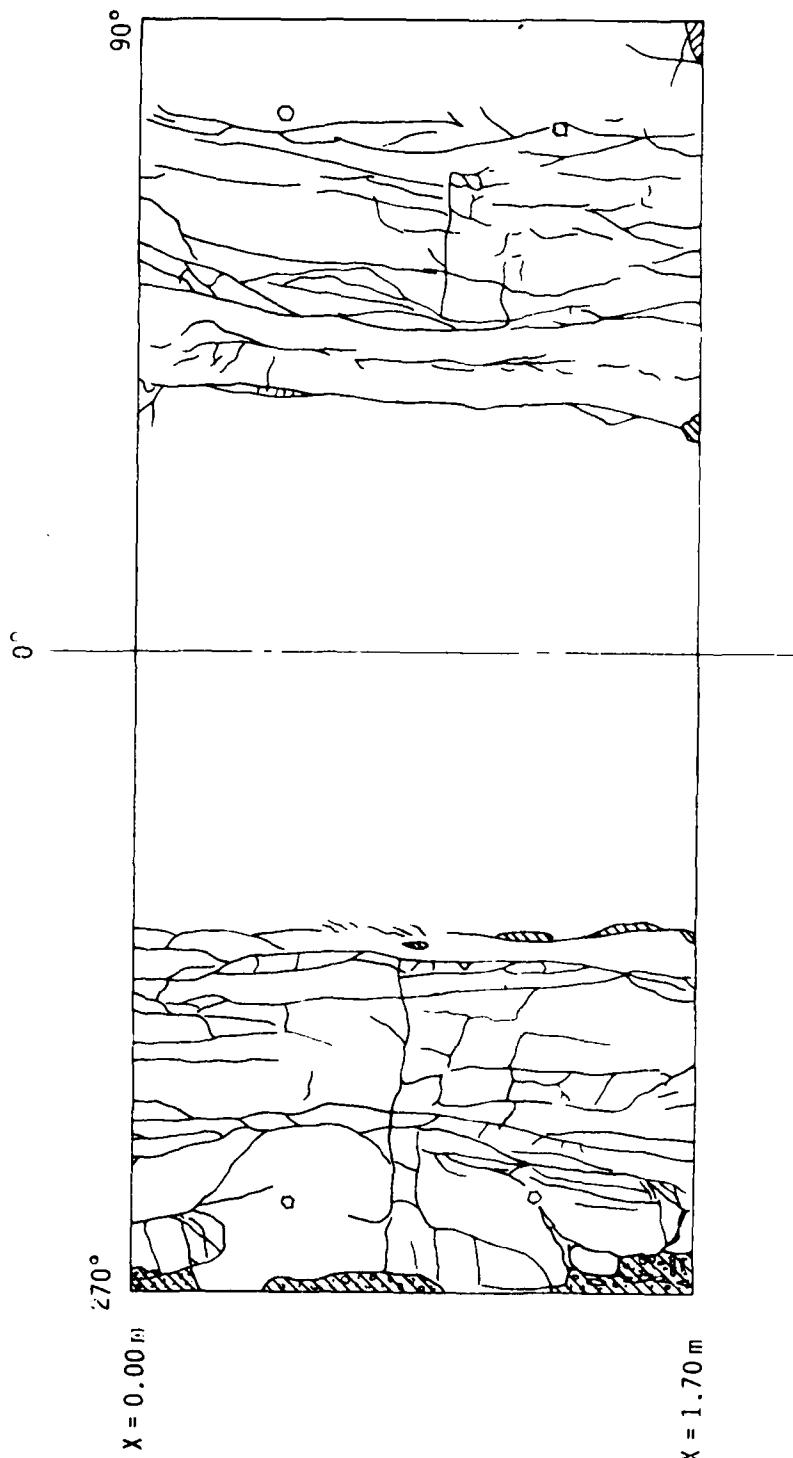
A5 exterior.



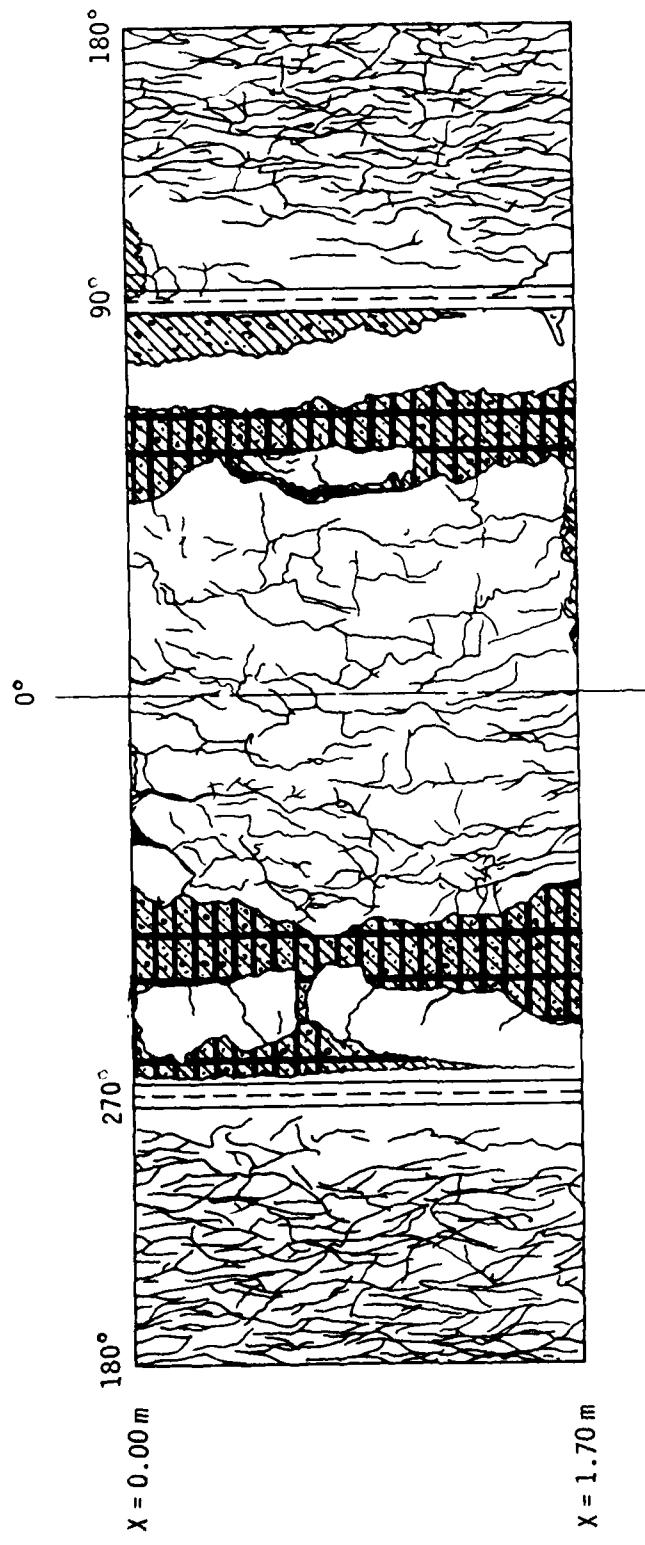
A6 cross section, station 0.00 m.



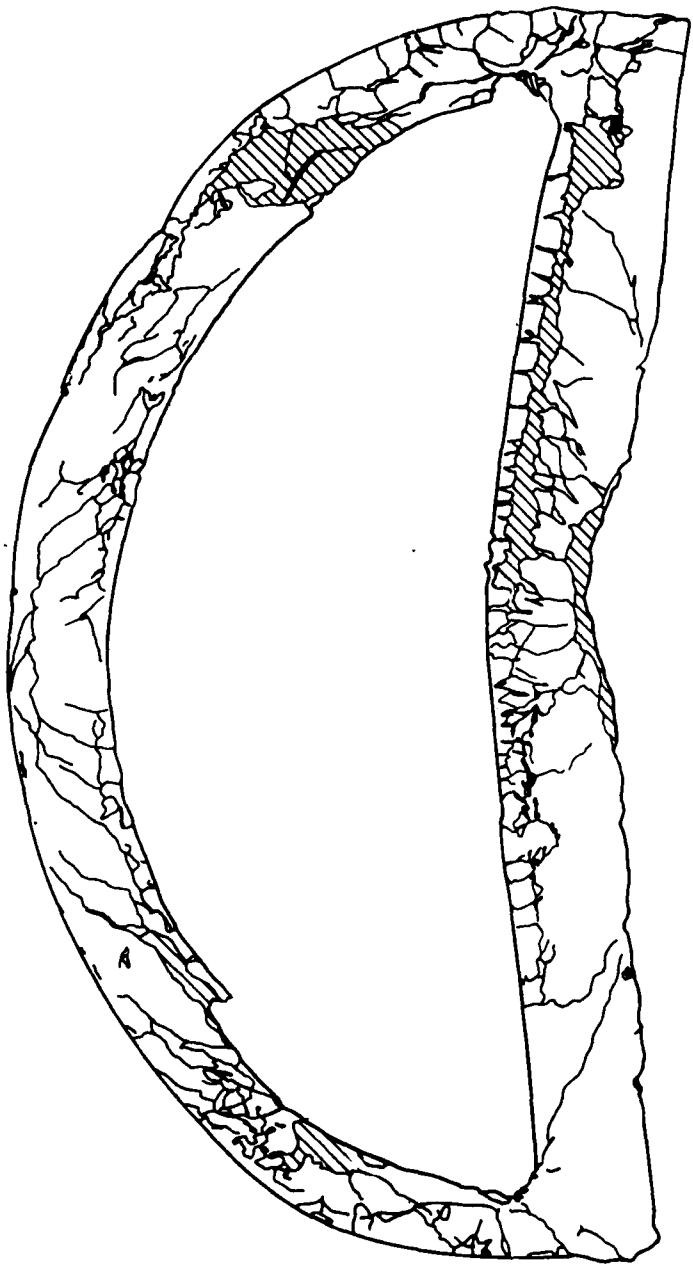
A6 cross section, station 1.70 m.



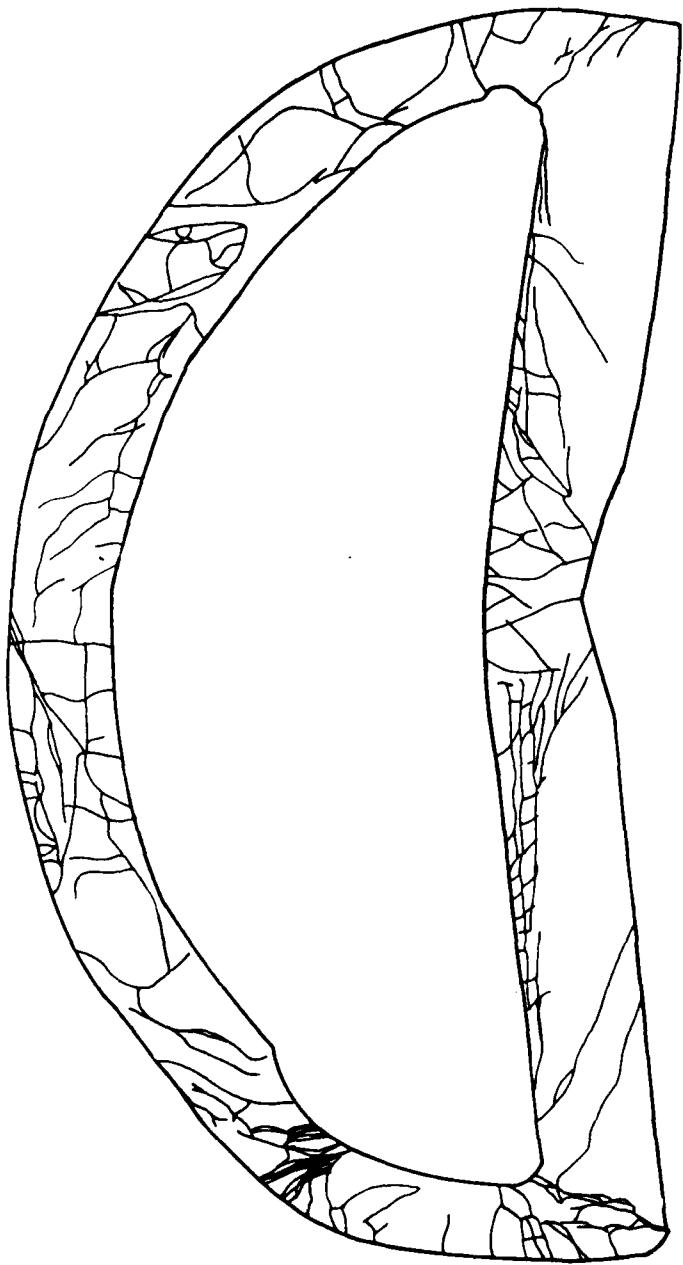
A6 exterior.



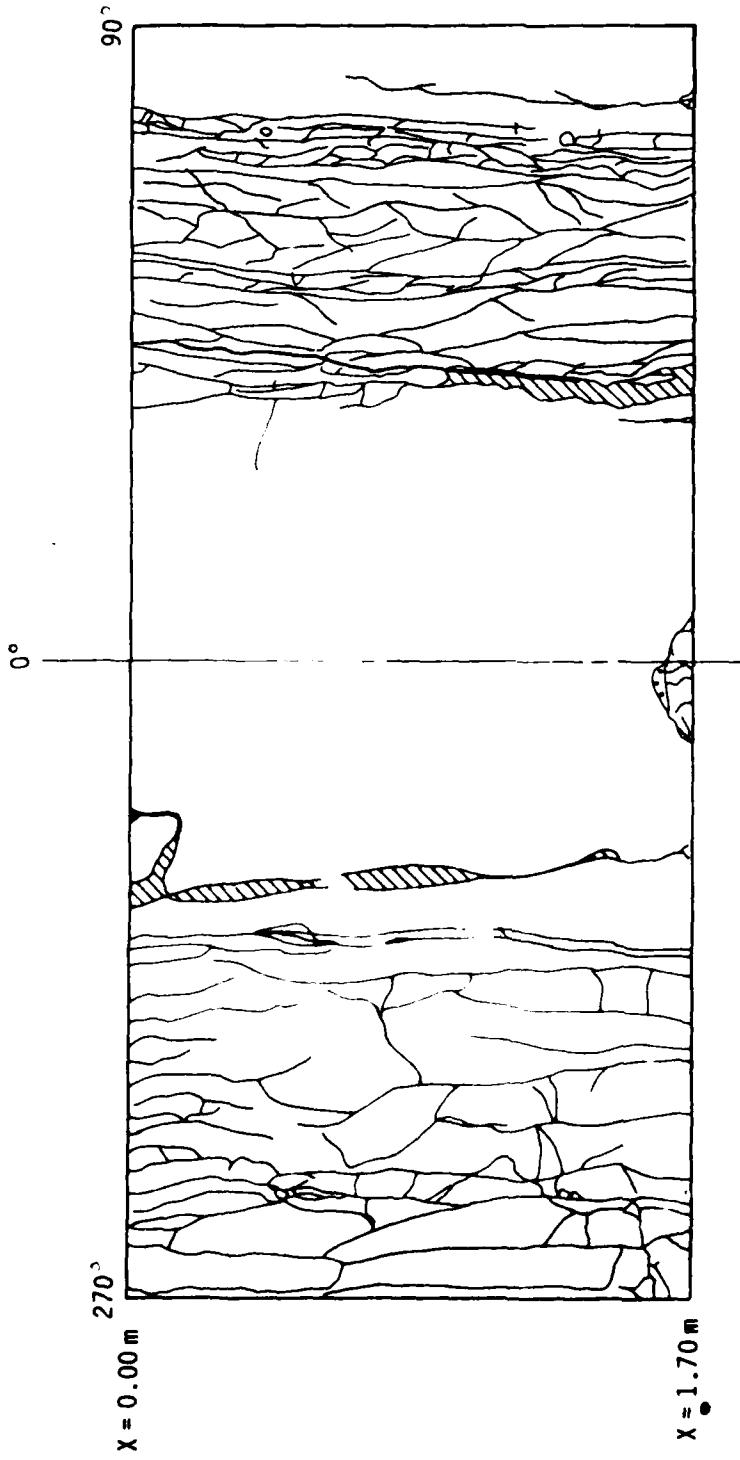
A6 interior.



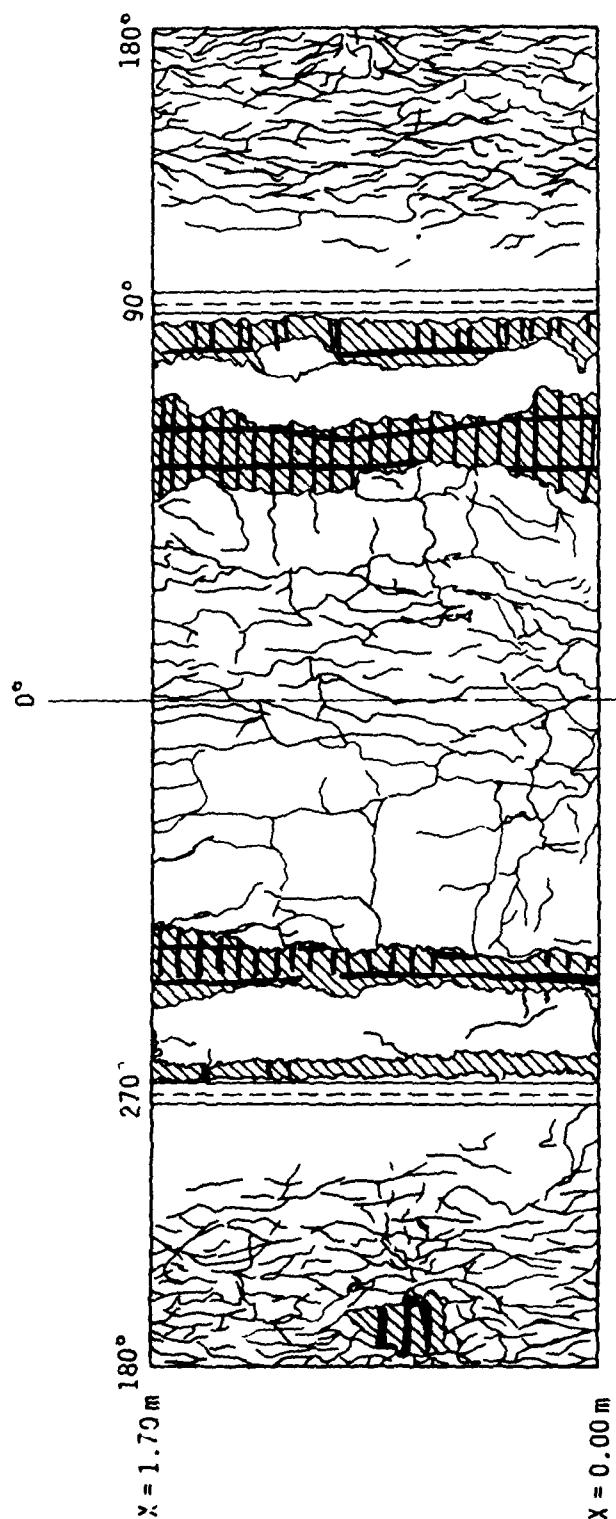
A7 cross section, station 0.00 m.



A7 cross section, station 1.70 m.

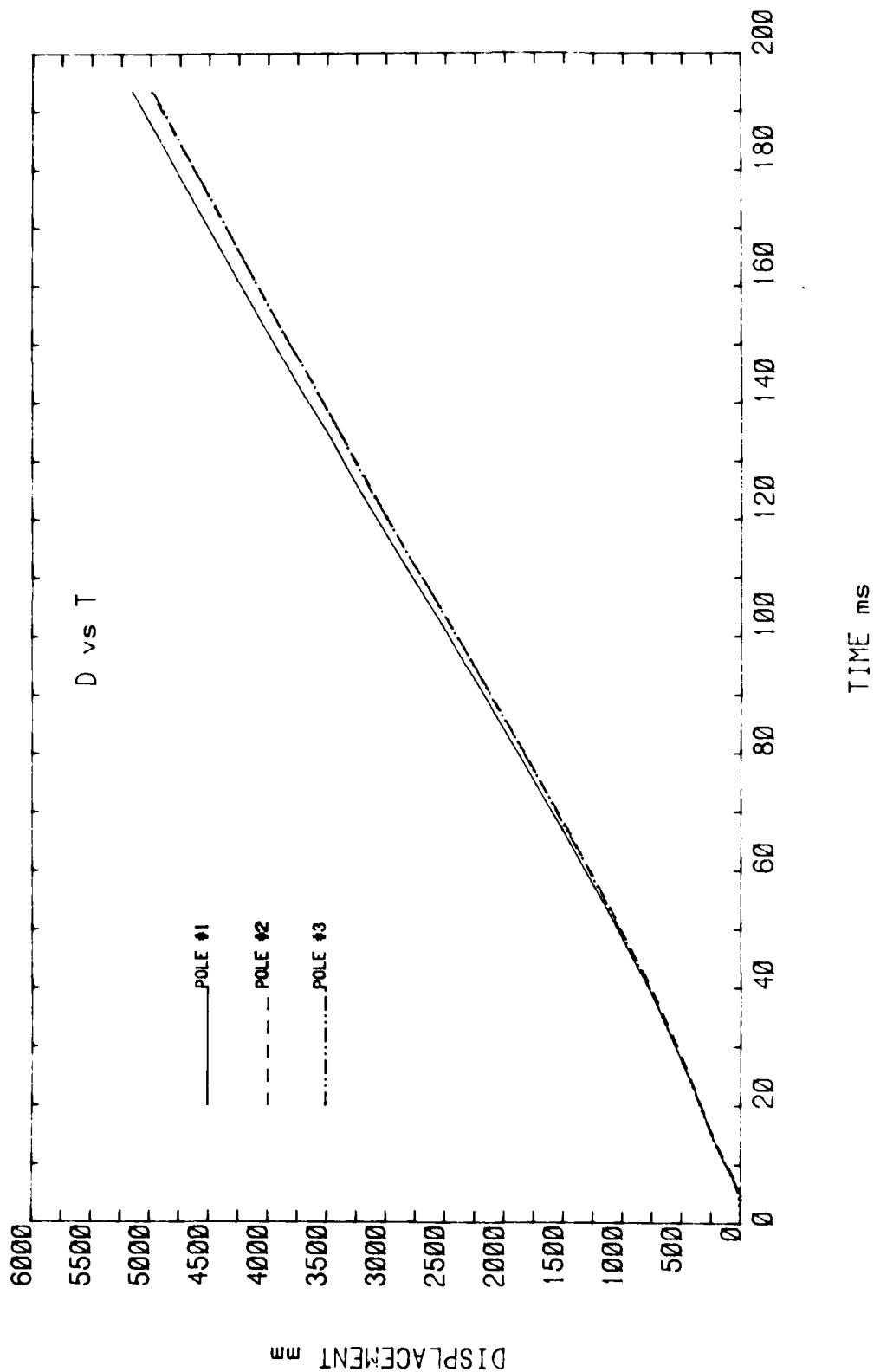


A7 exterior.

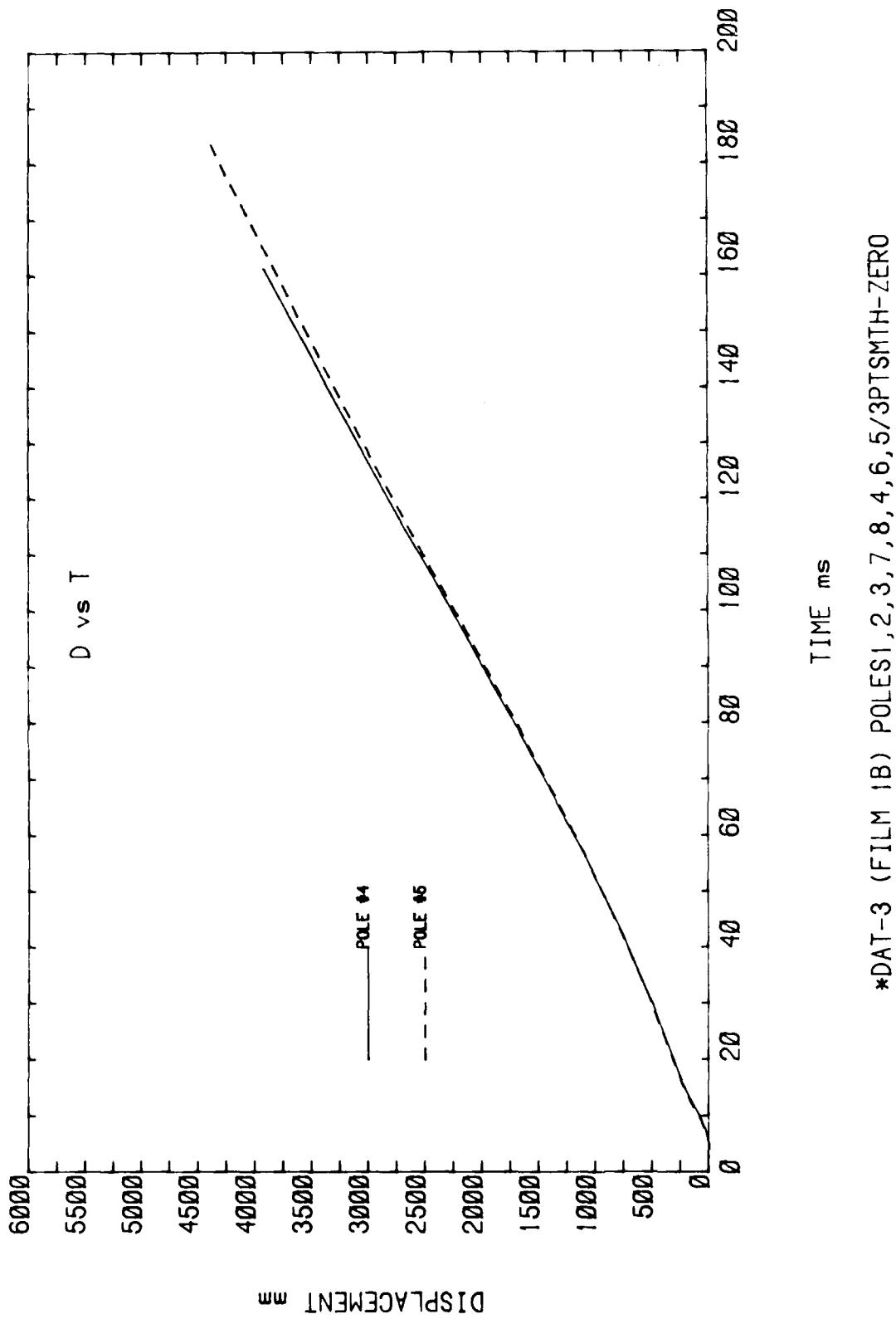


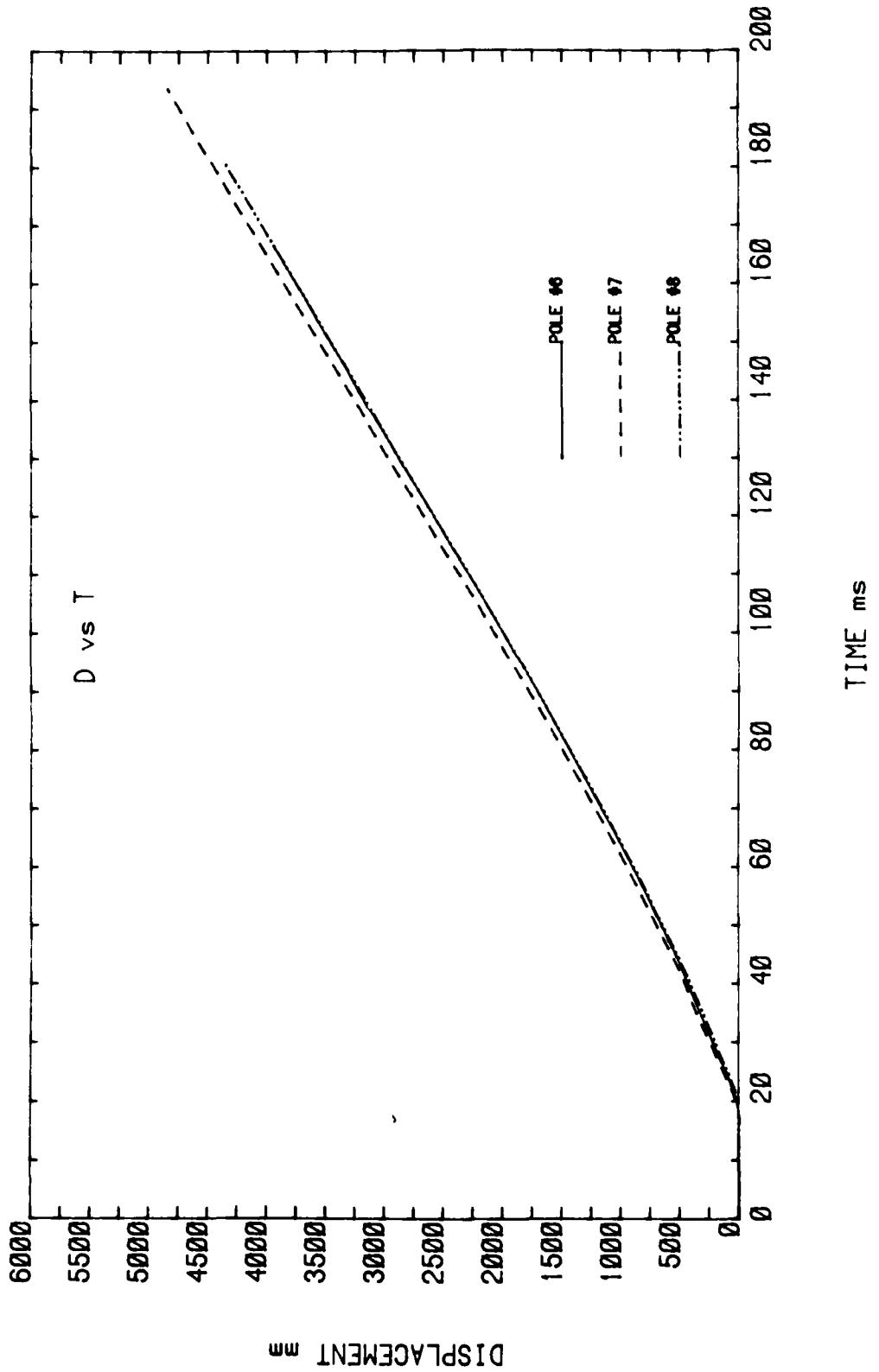
APPENDIX D

PHOTOPOLE DATA

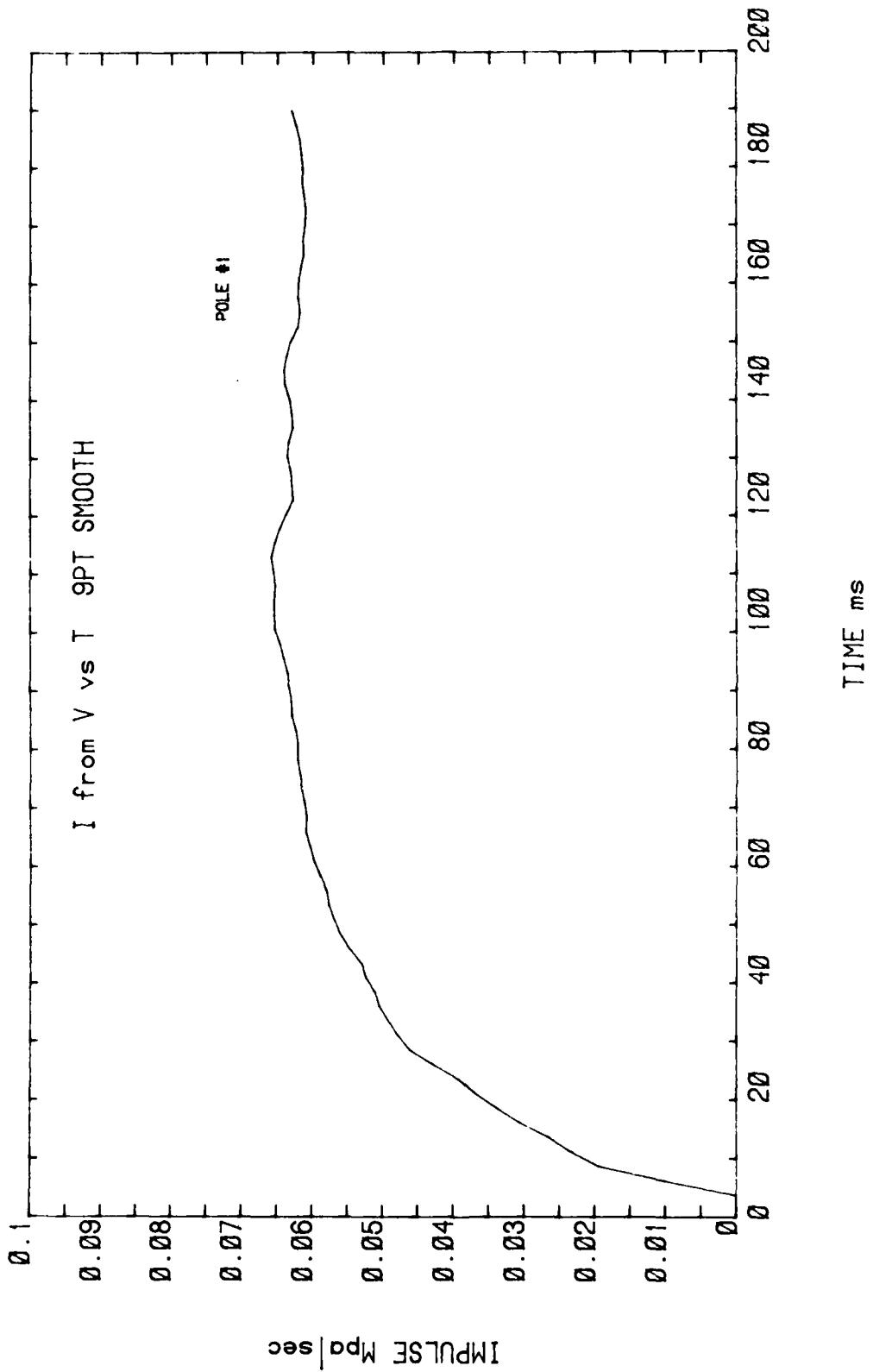


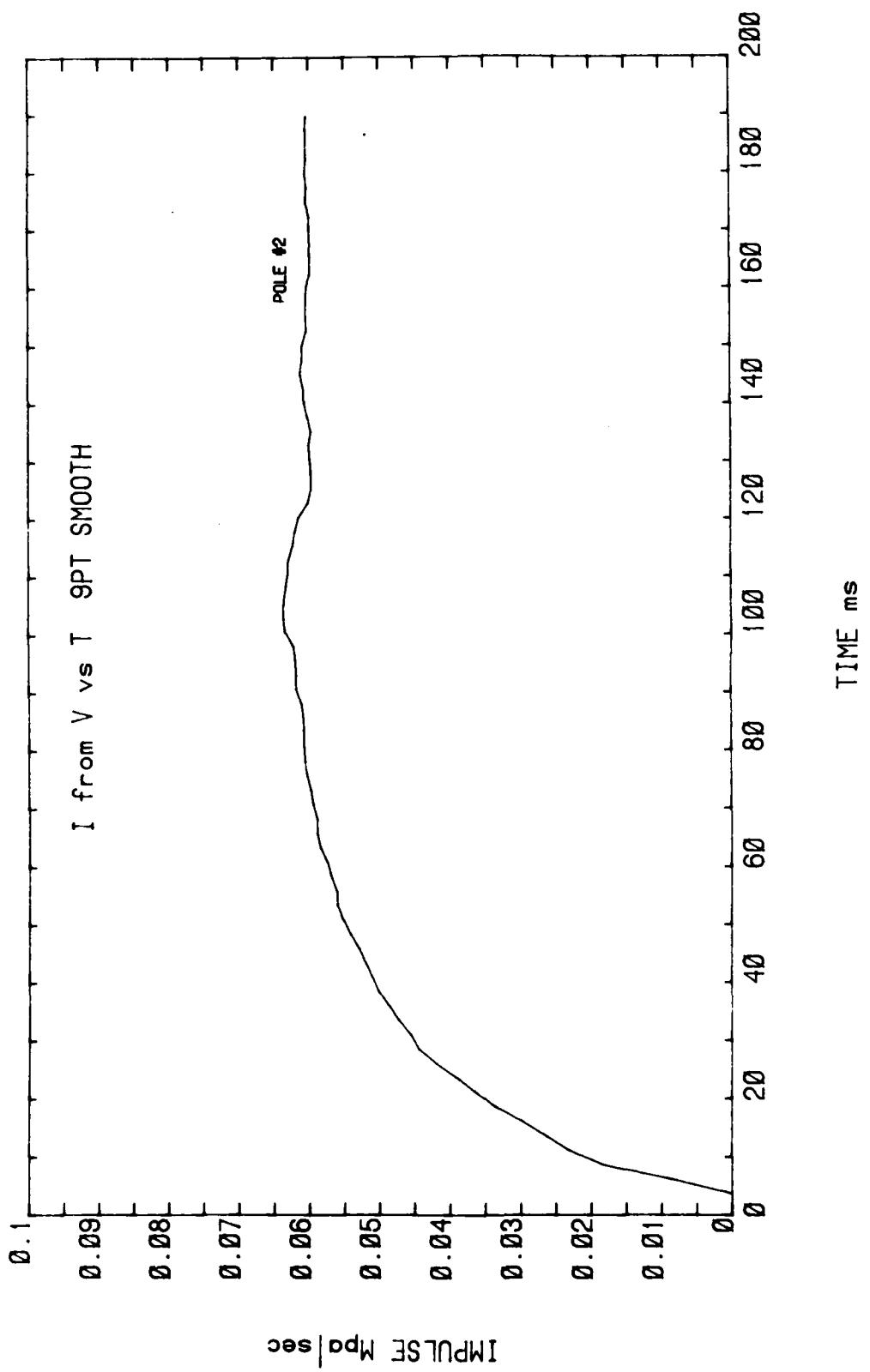
*DAT-3 (FILM 1B) POLES1,2,3,7,8,4,6,5/3PTSMTH-ZERO



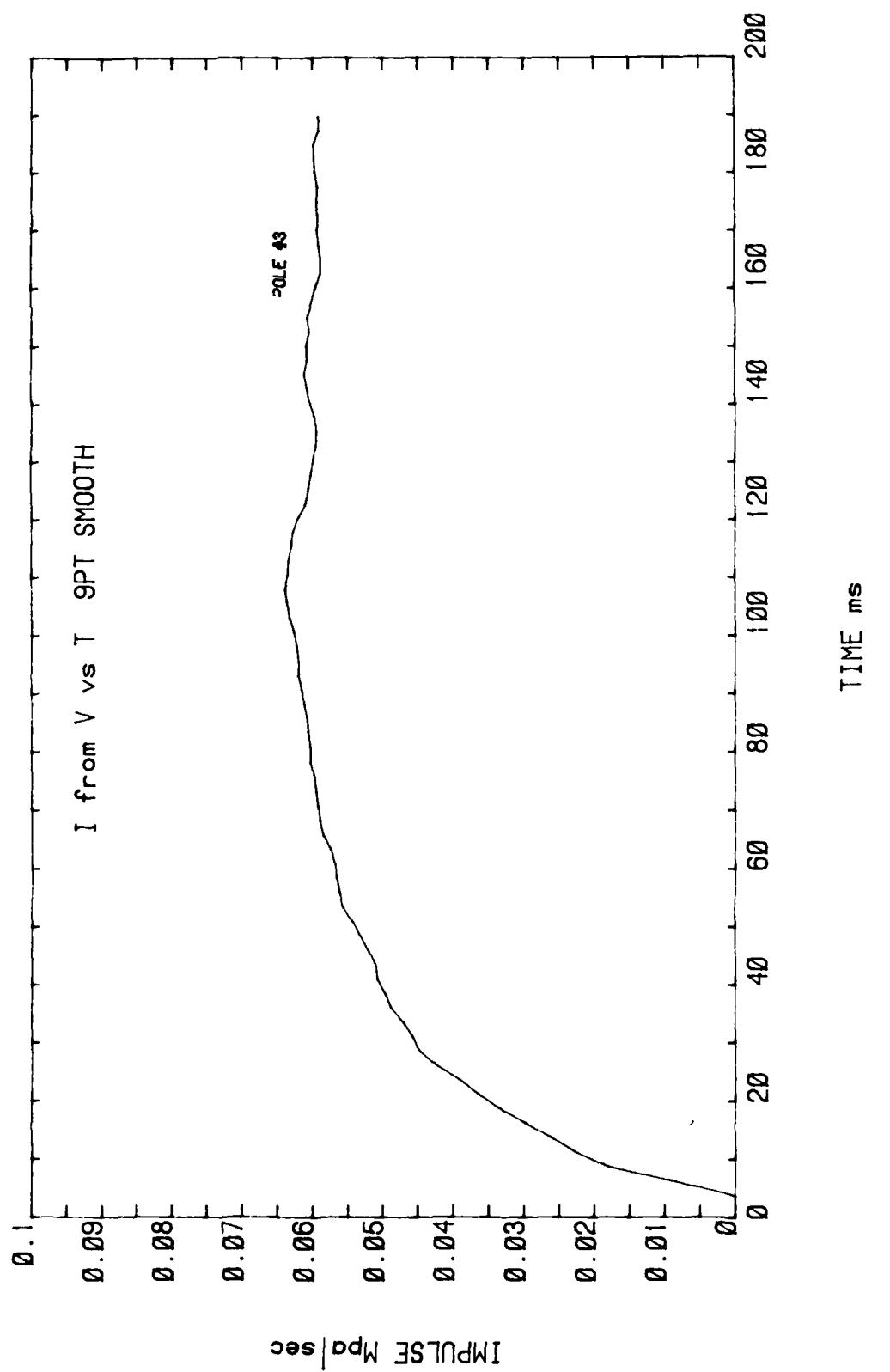


*DAT-3 (FILM 1B) POLES 1, 2, 3, 7, 8, 4, 6, 5/3PTS MTH-ZERO

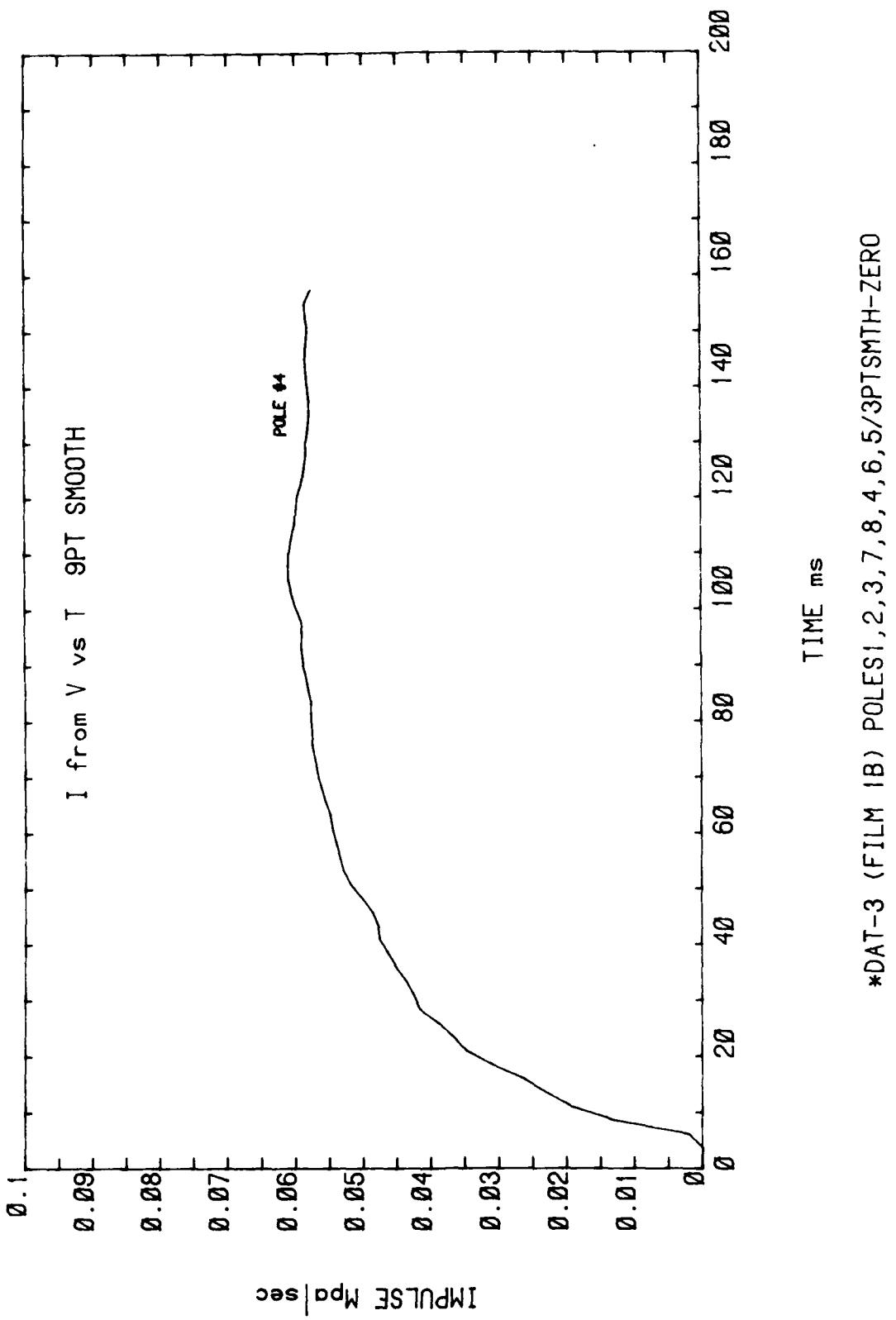




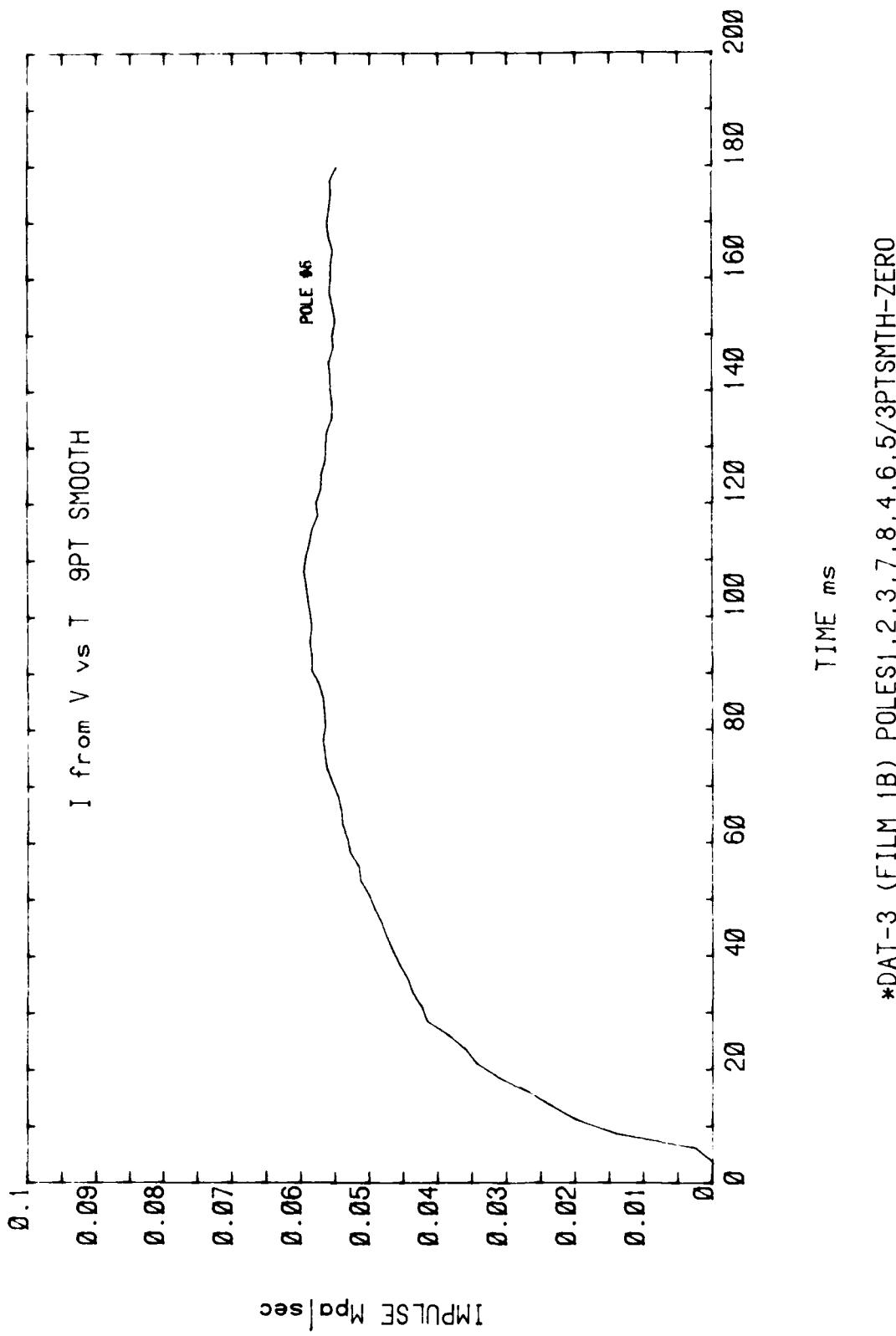
*DAT-3 (FILM 1B) POLES1,2,3,7,8,4,6,5/3PTSMTTH-ZERO



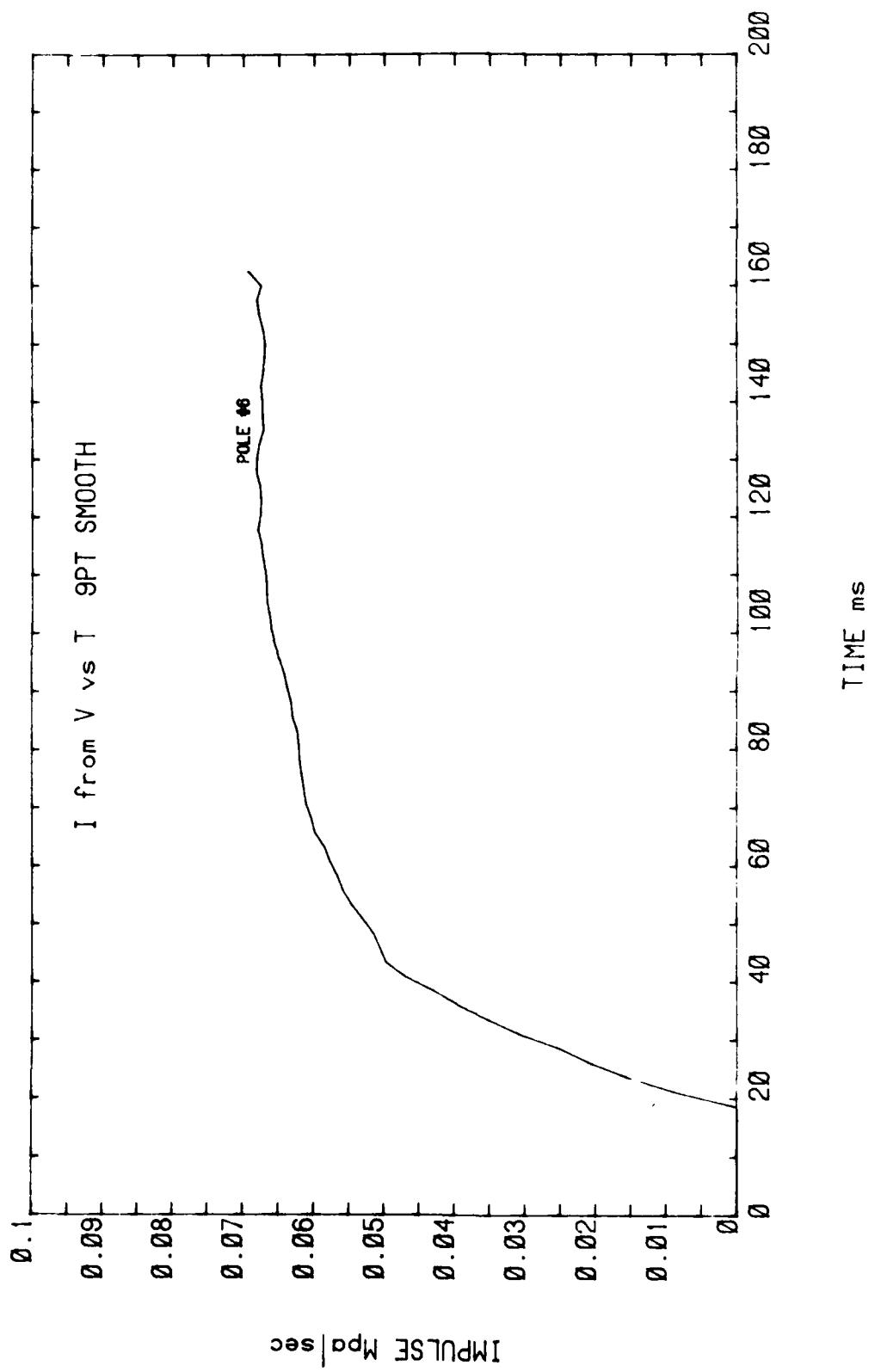
*DAT-3 (FILM 1B) POLES1,2,3,7,8,4,6,5/3PTSMTZ-ZERO



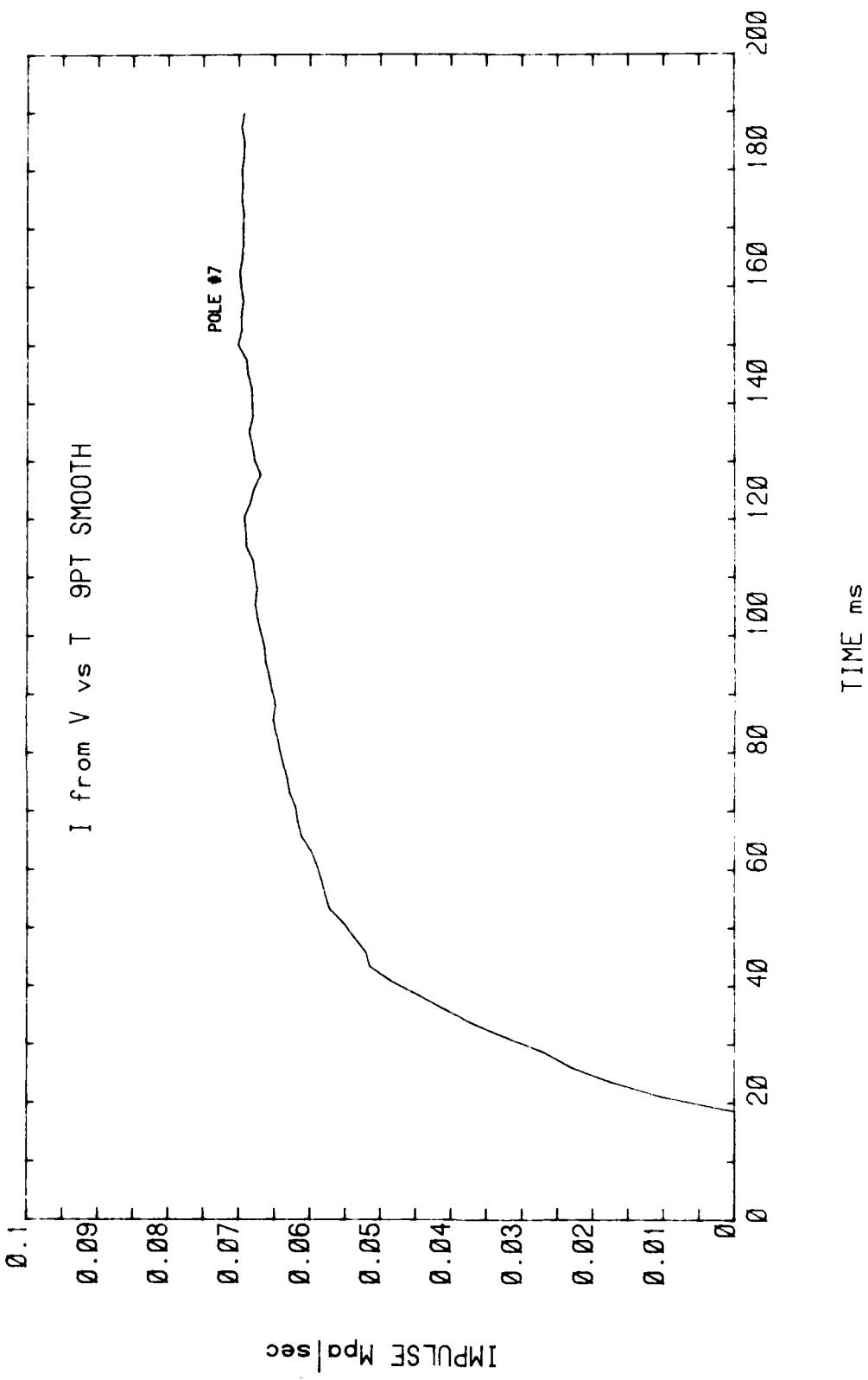
*DAT-3 (FILM 1B) POLES1,2,3,7,8,4,6,5/3PTSMTH-ZERO



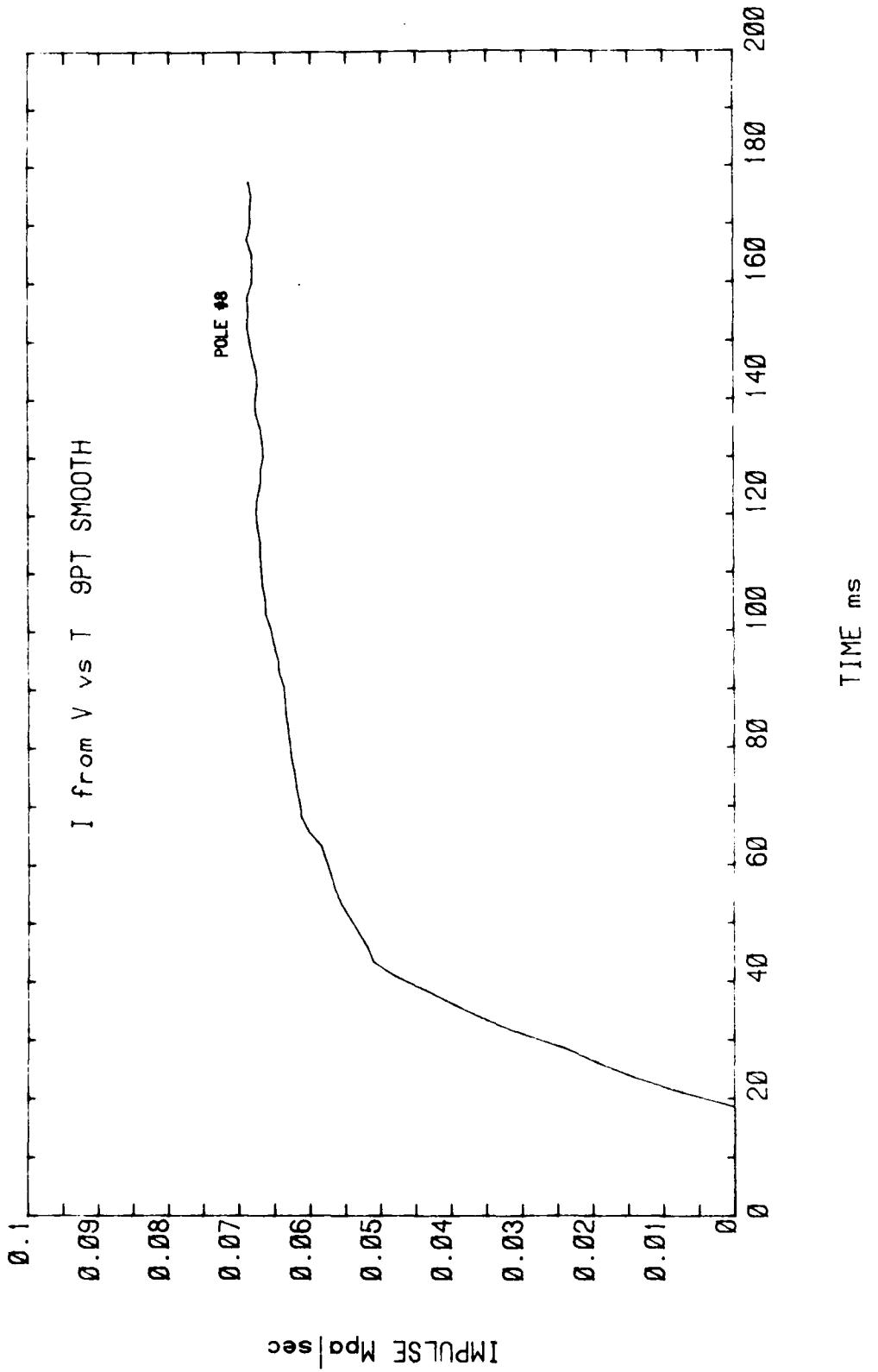
*DAT-3 (FILM 1B) POLES1,2,3,7,8,4,6,5/3PTSMTH-ZERO



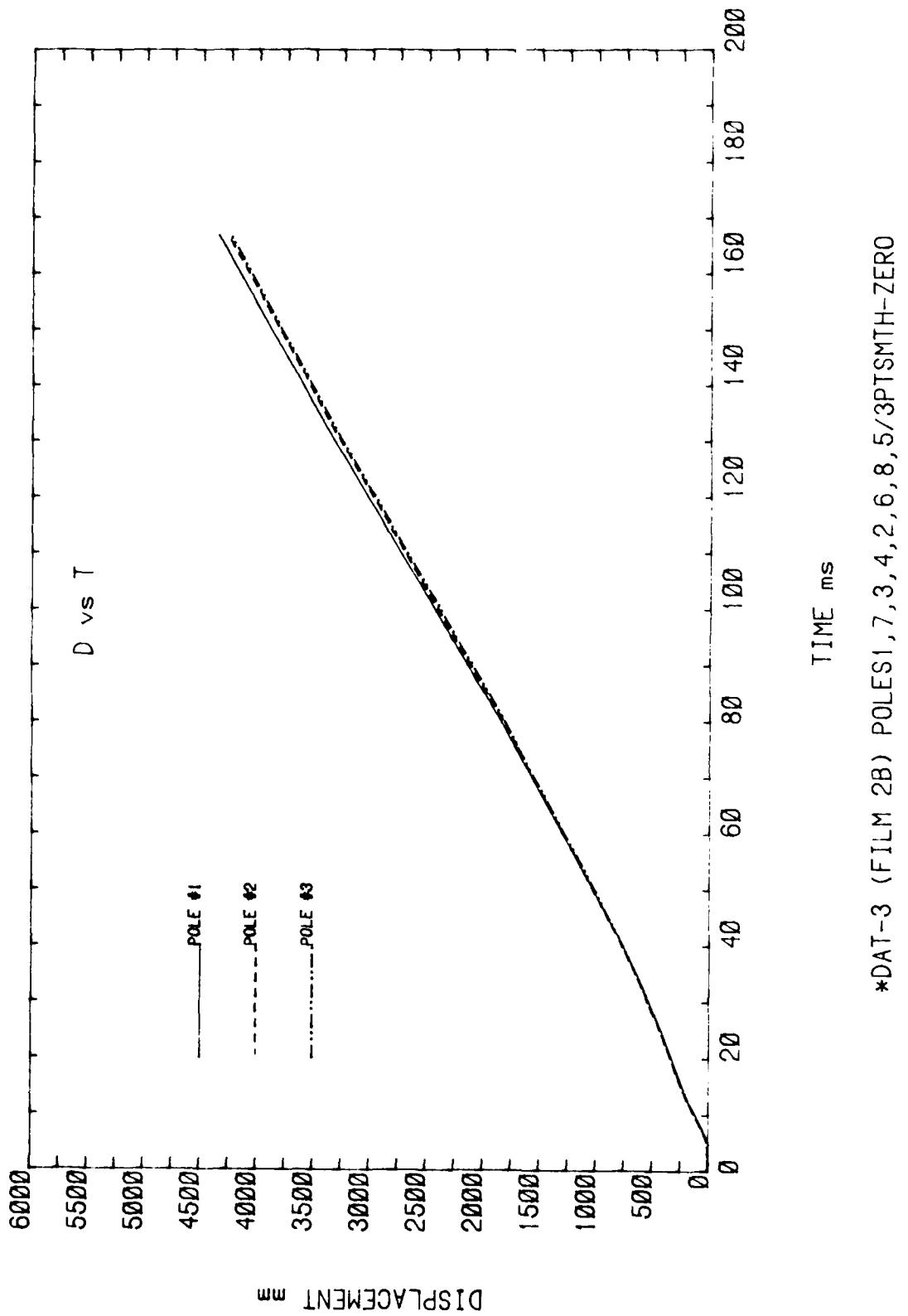
*DAT-3 (FILM 1B) POLES1,2,3,7,8,4,6,5/3PTSMTH-ZERO



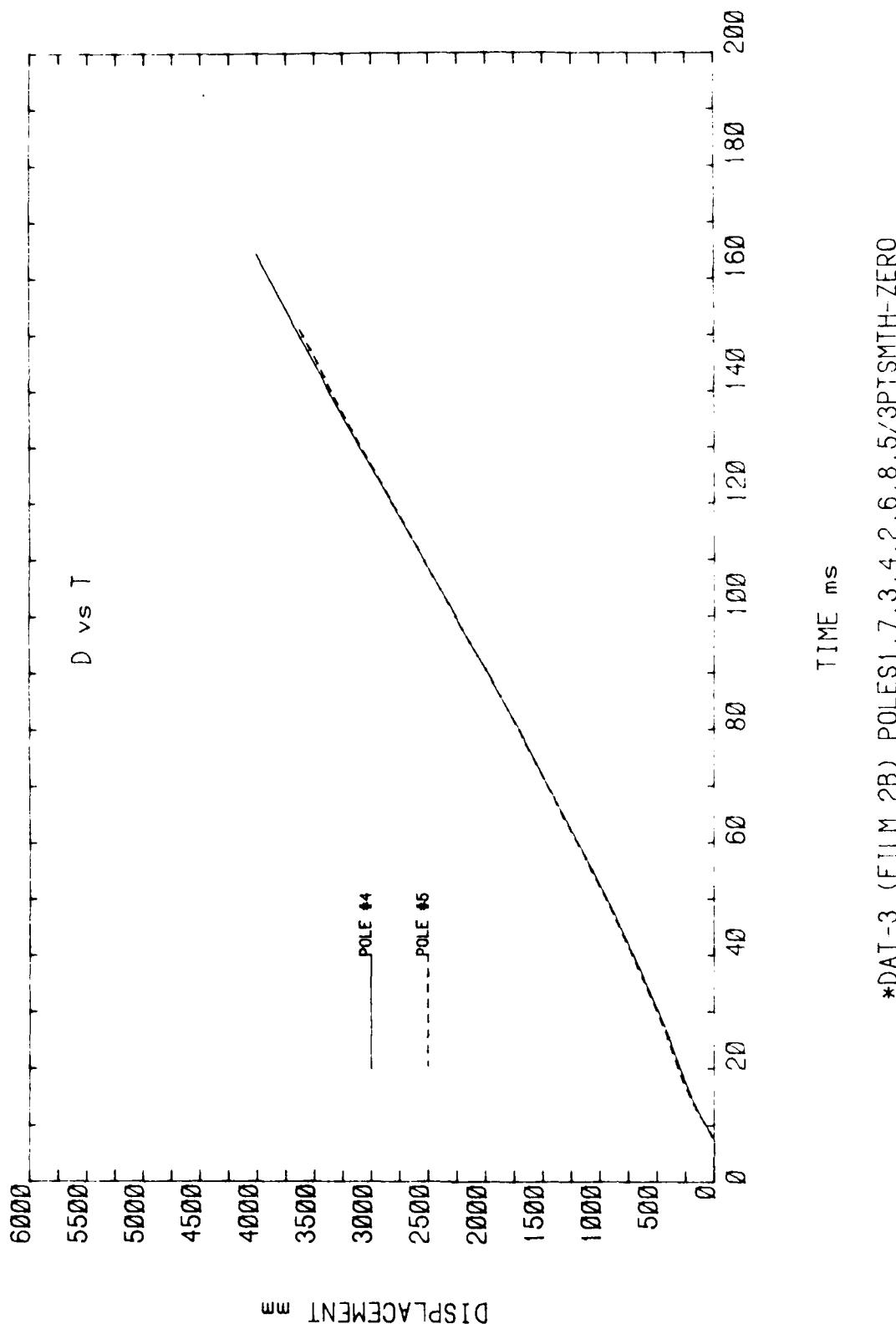
*DAT-3 (FILM 1B) POLES: 1, 2, 3, 7, 8, 4, 6, 5/3PTS SMTH-ZERO

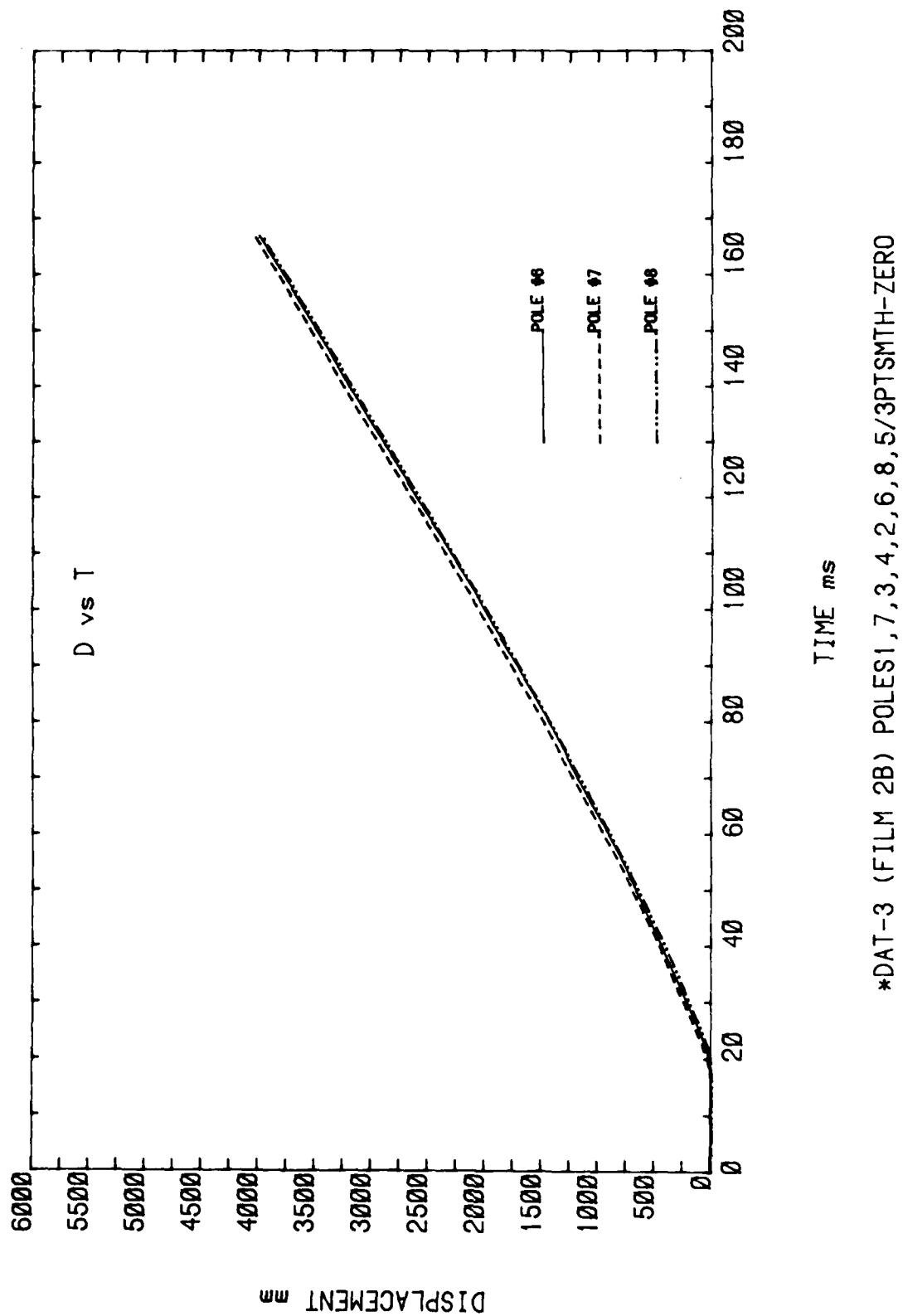


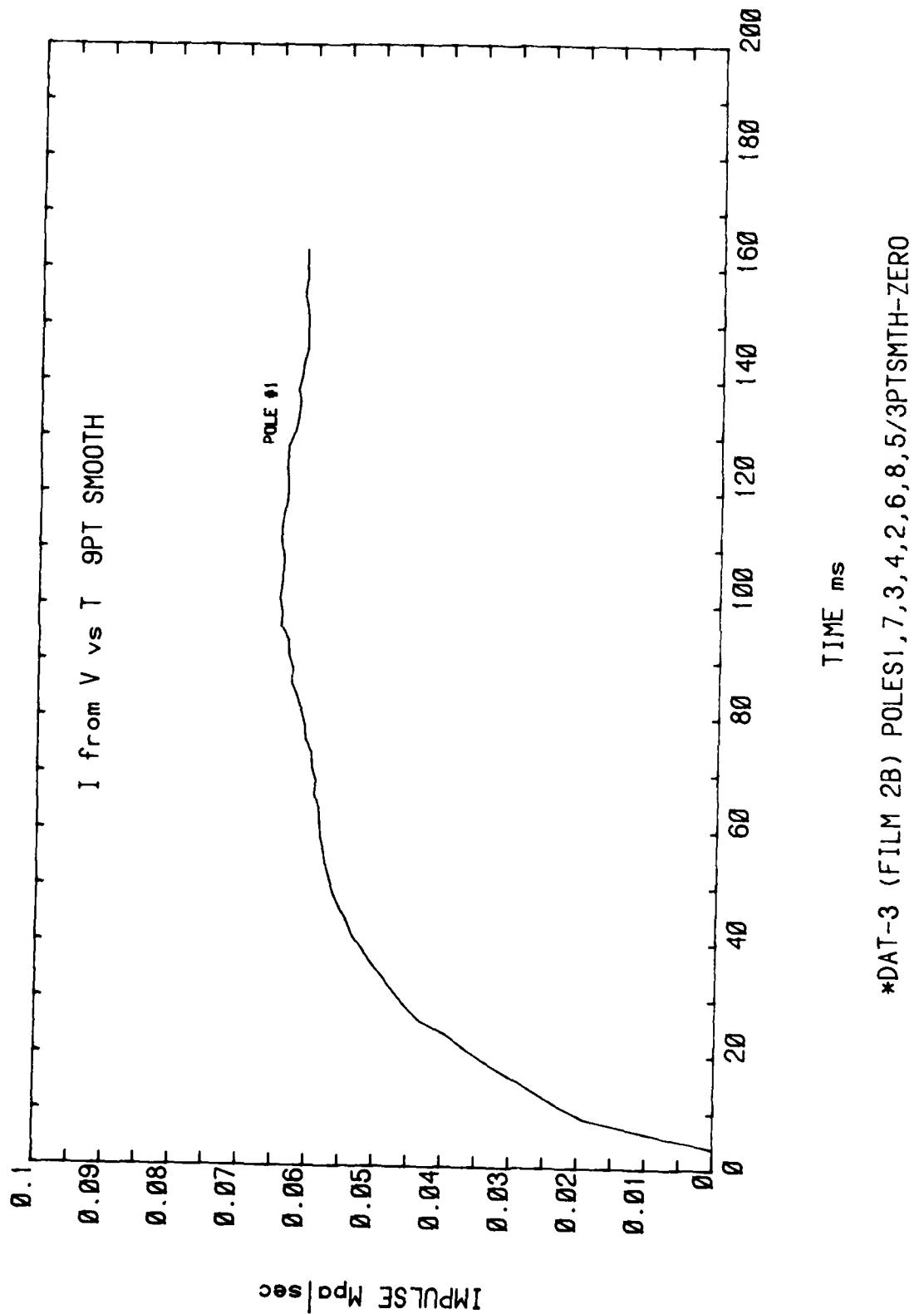
*DAT-3 (FILM 1B) POLES1,2,3,7,8,4,6,5/3PTSMTH-ZERO

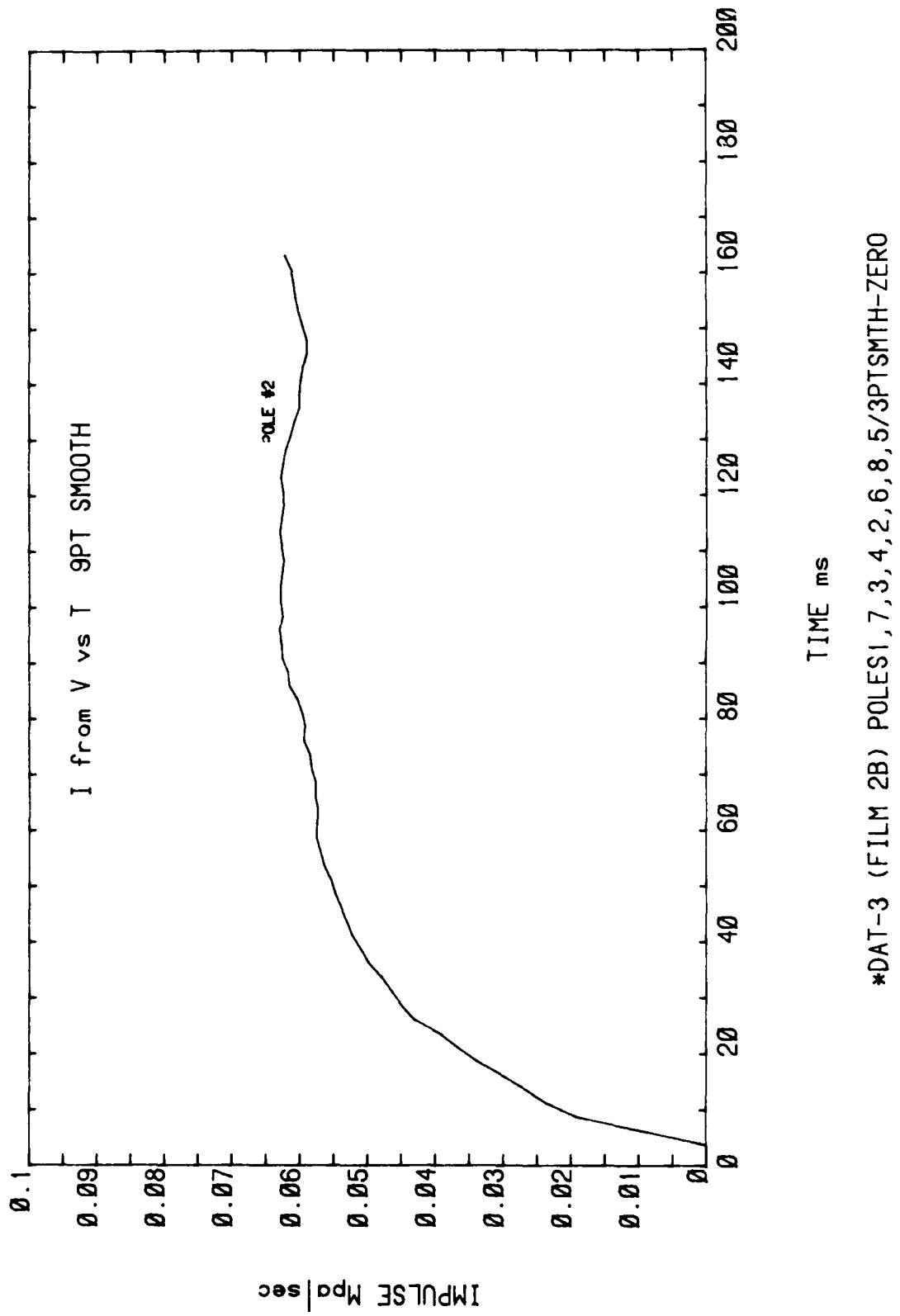


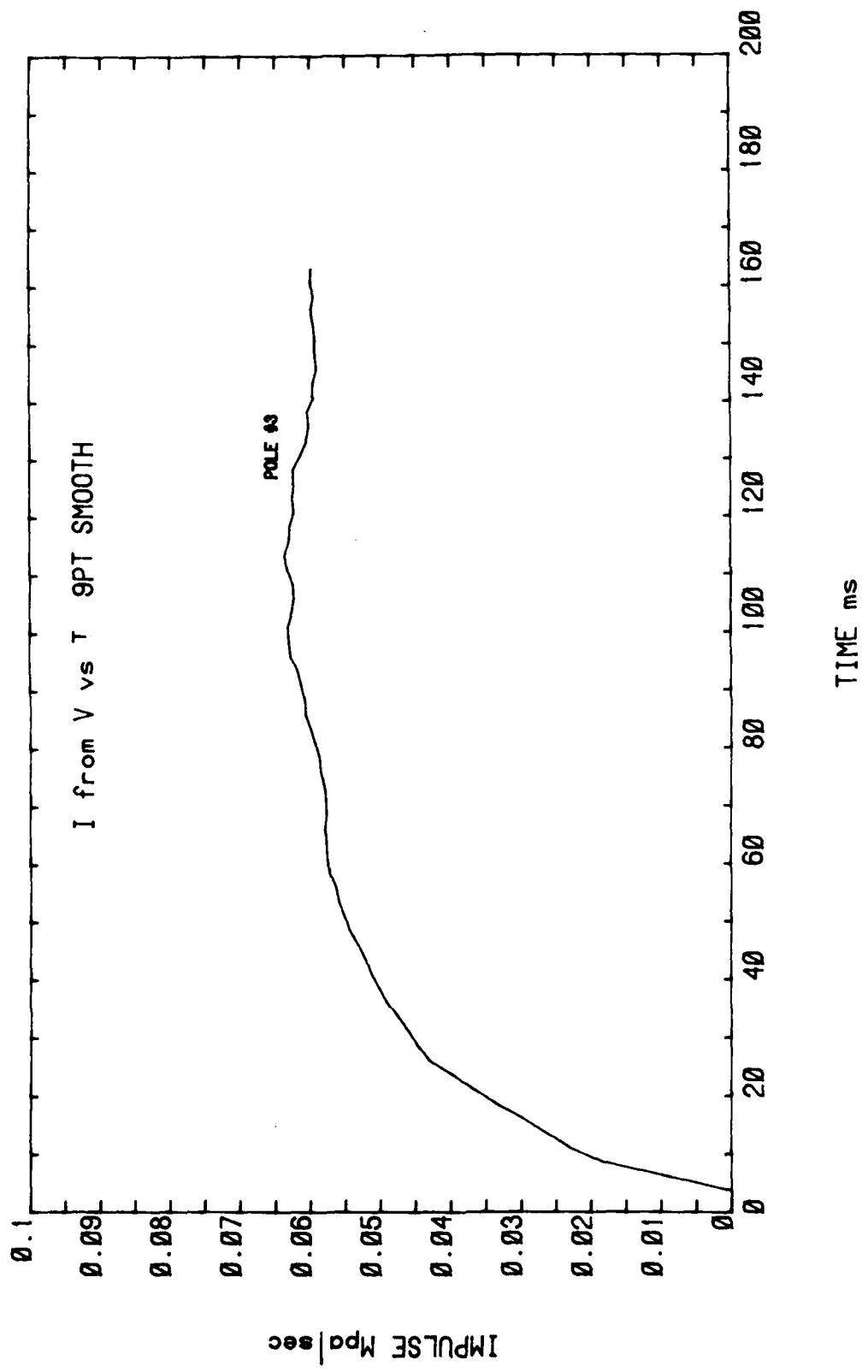
*DAT-3 (FILM 2B) POLES1,7,3,4,2,6,8,5/3PTS MTH-ZERO



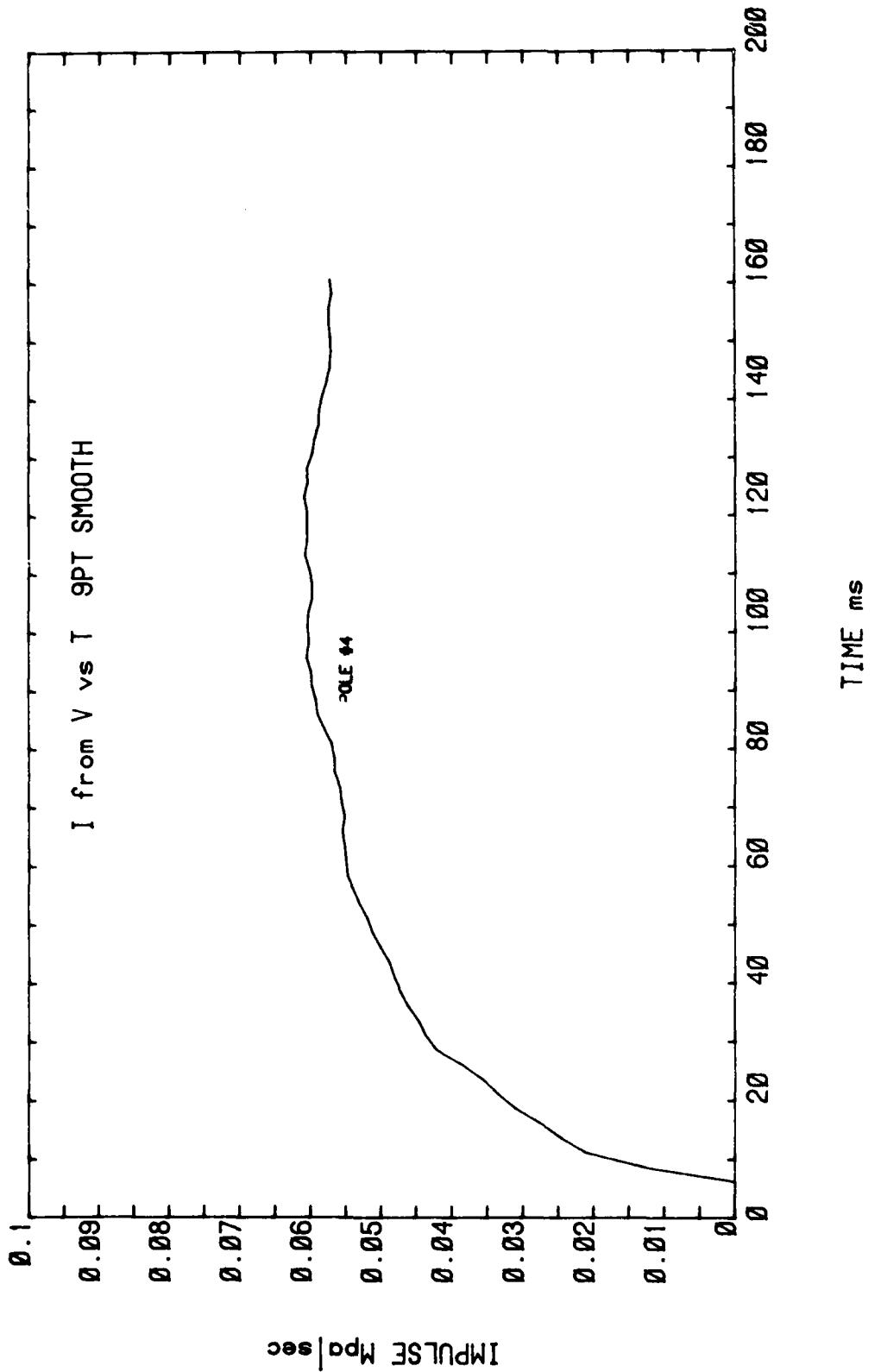




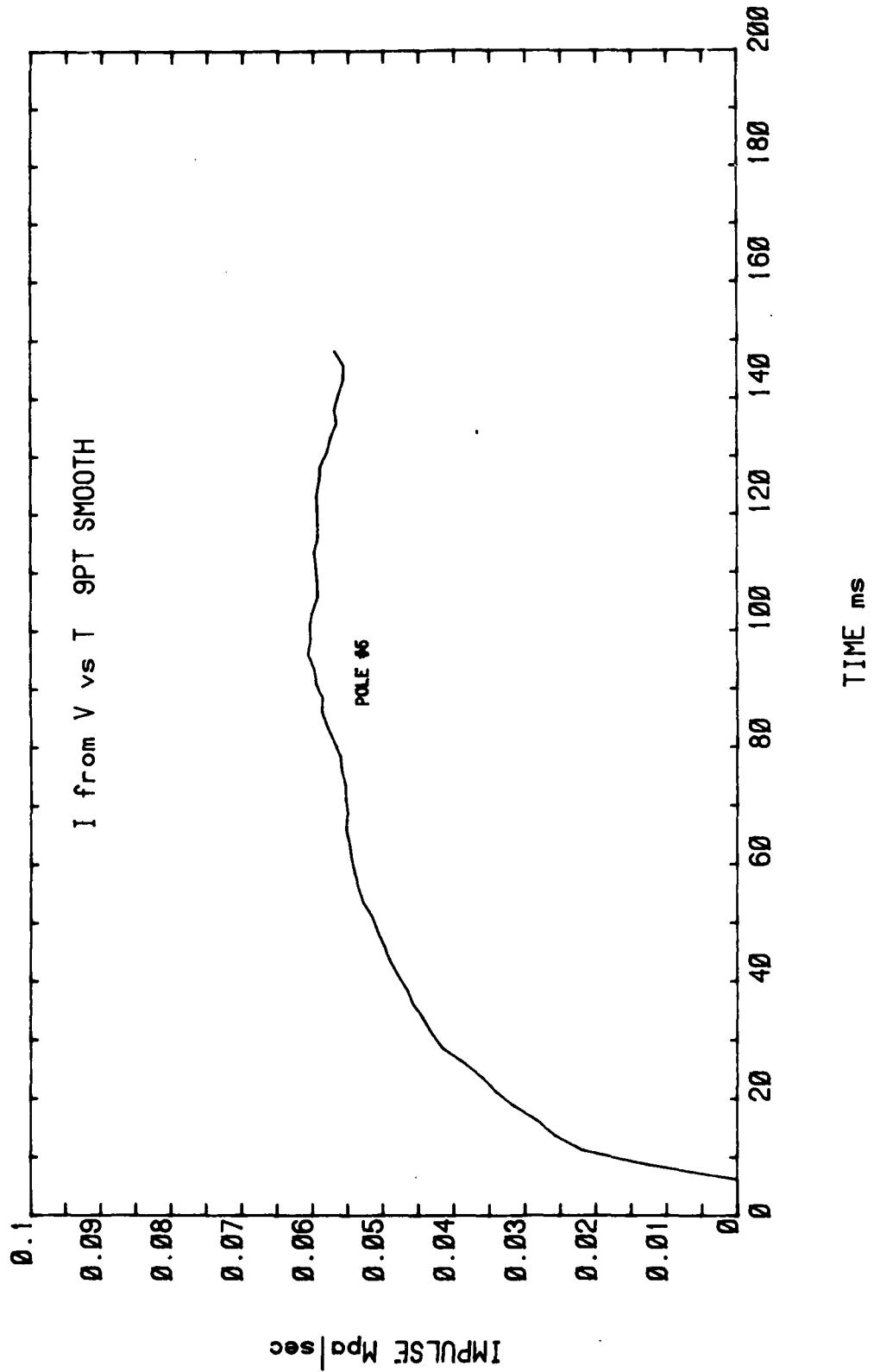




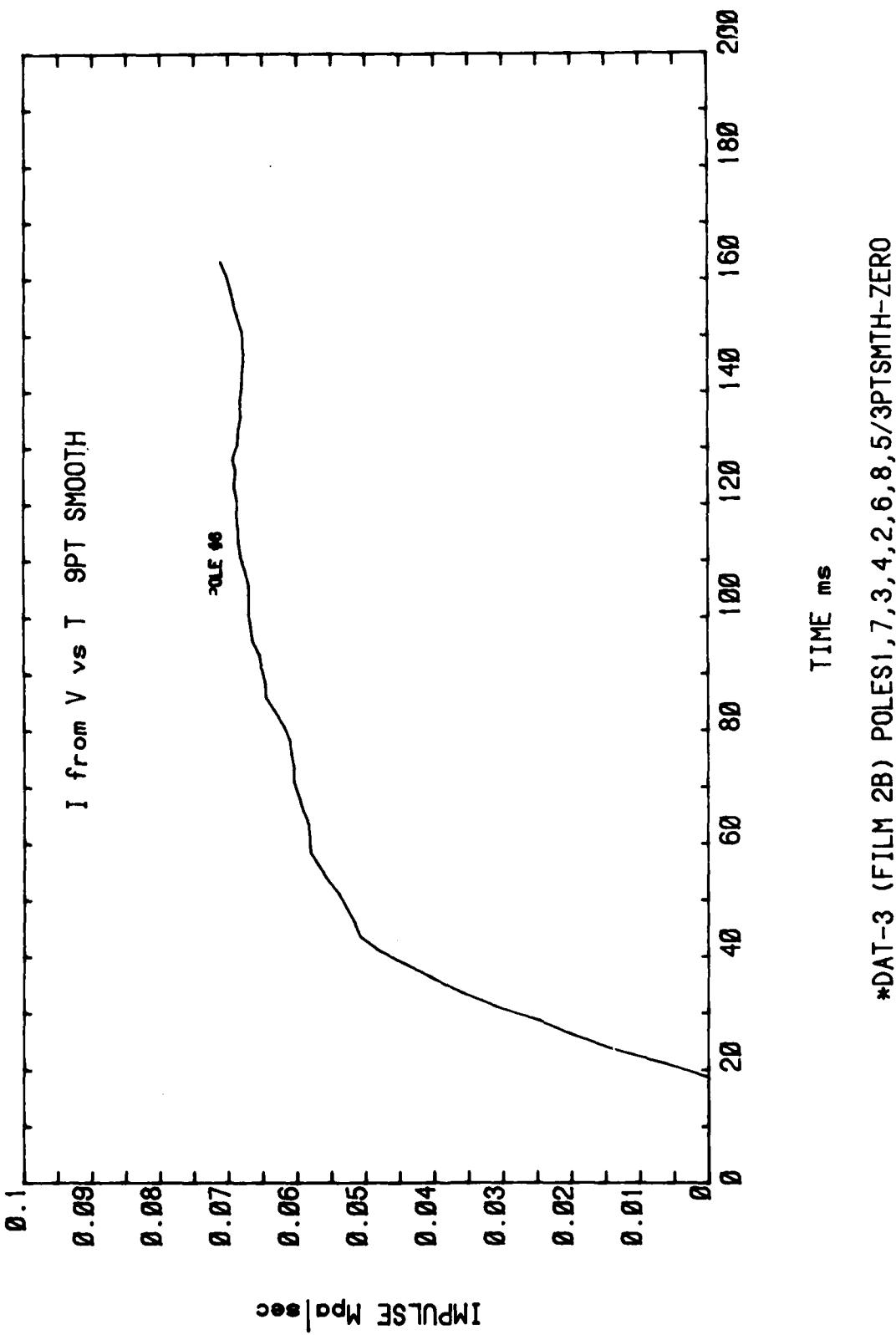
*DAT-3 (FILM 2B) POLES1,7,3,4,2,6,8,5/3PTSMTH-ZERO



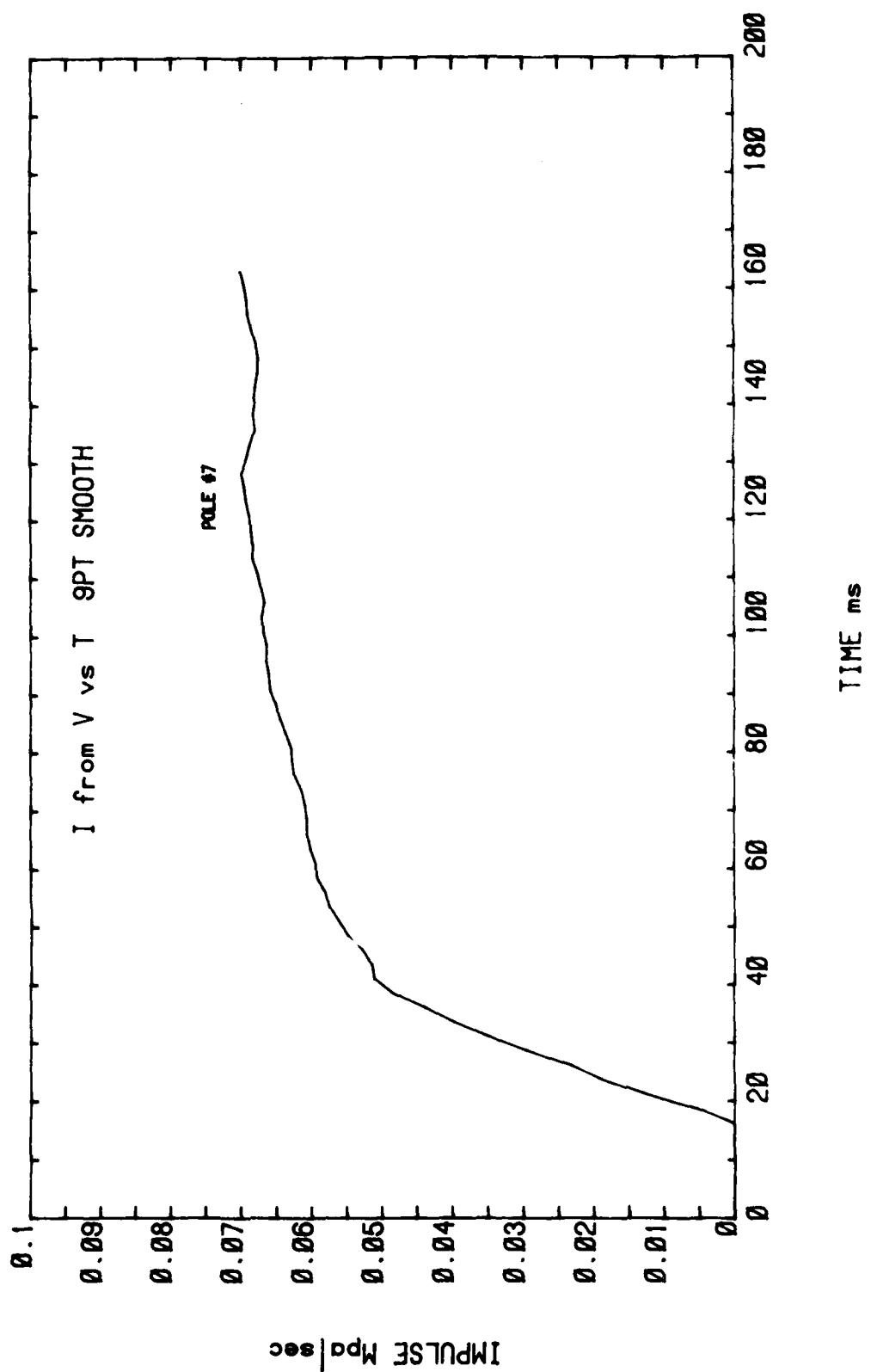
*DAT-3 (FILM 2B) POLES1,7,3,4,2,6,8,5/3PTSMTH-ZERO



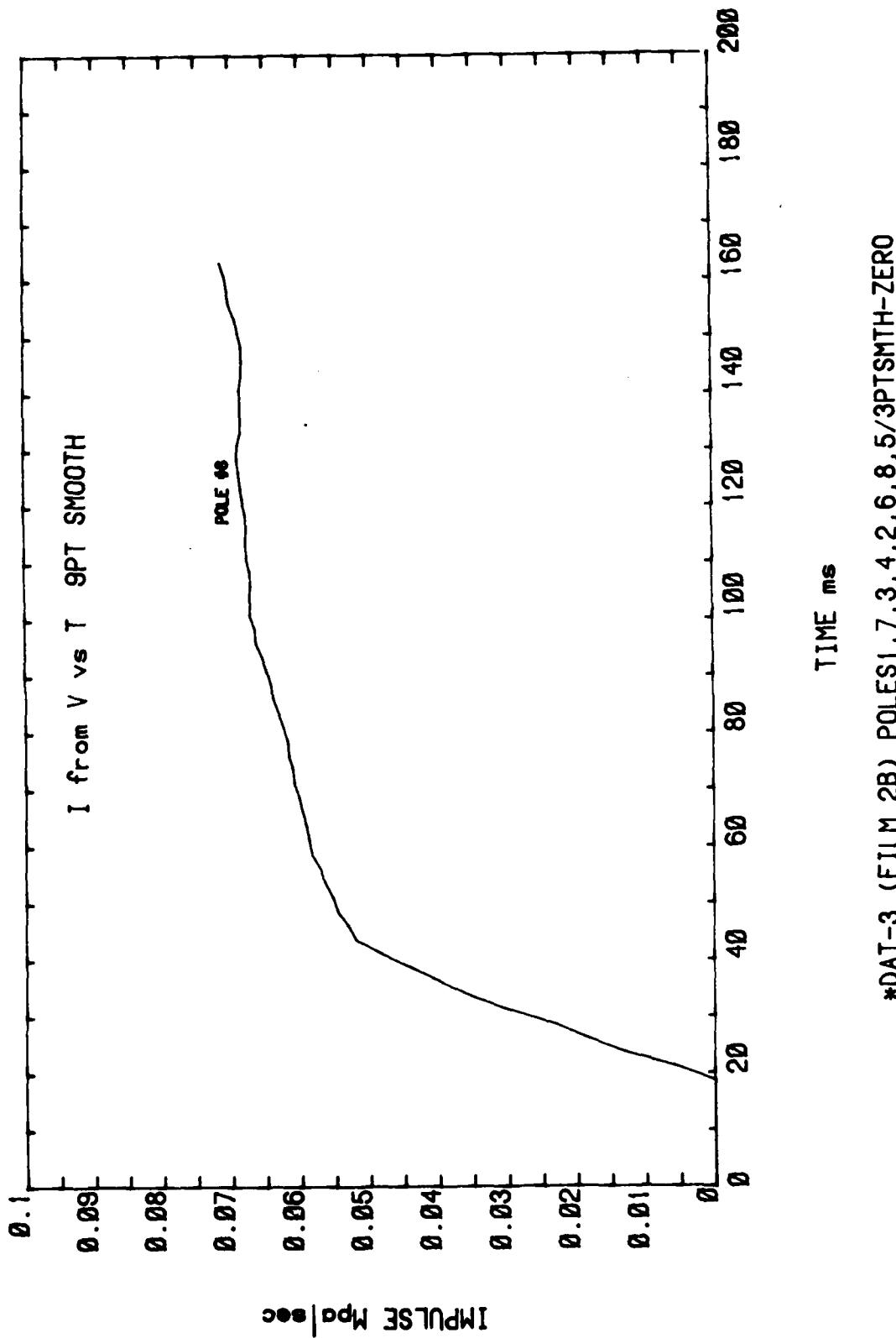
*DAT-3 (FILM 2B) POLES1,7,3,4,2,6,8,5/3PTSMTH-ZERO

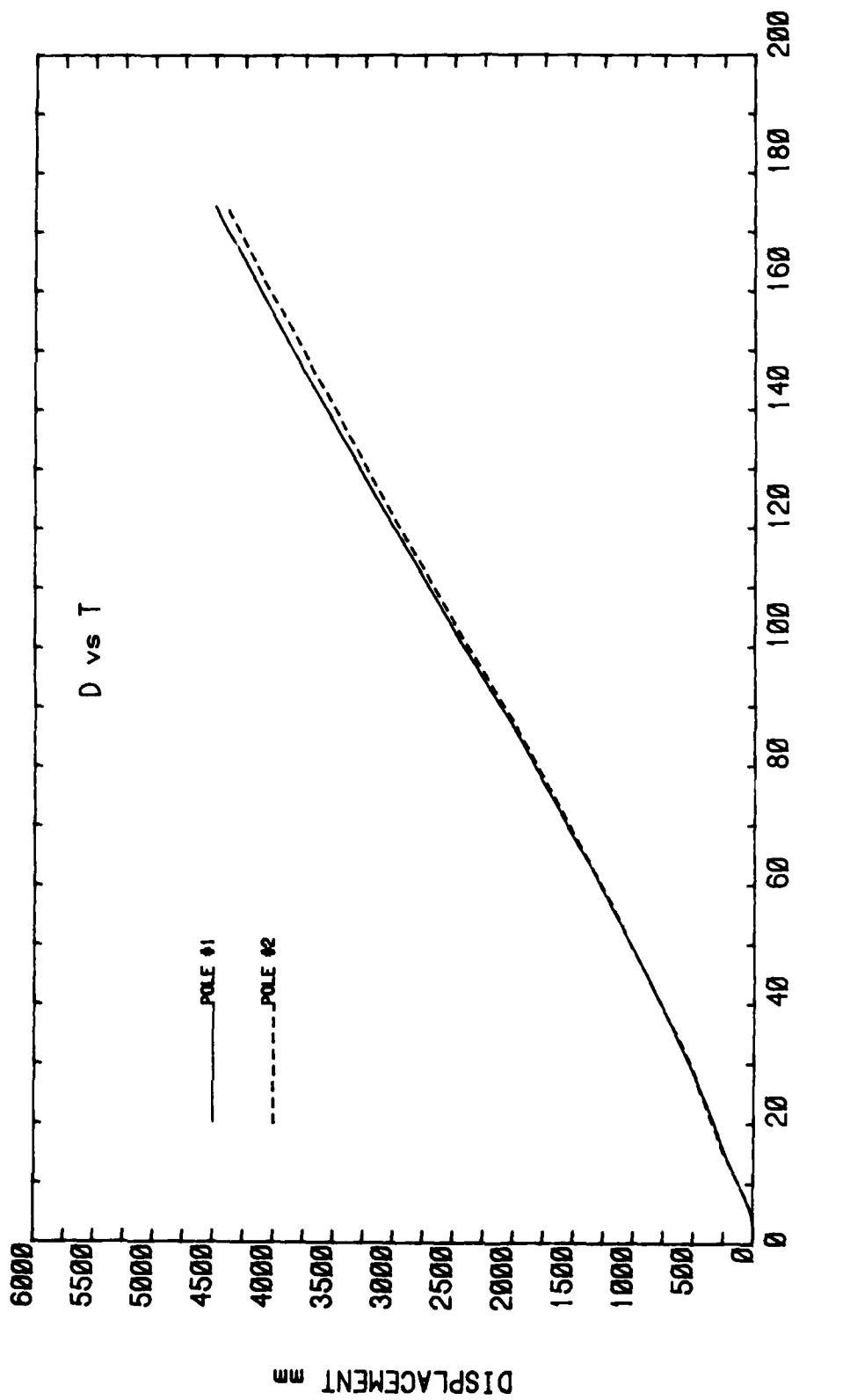


*DAT-3 (FILM 2B) POLES1,7,3,4,2,6,8,5/3PTS MTH-ZERO

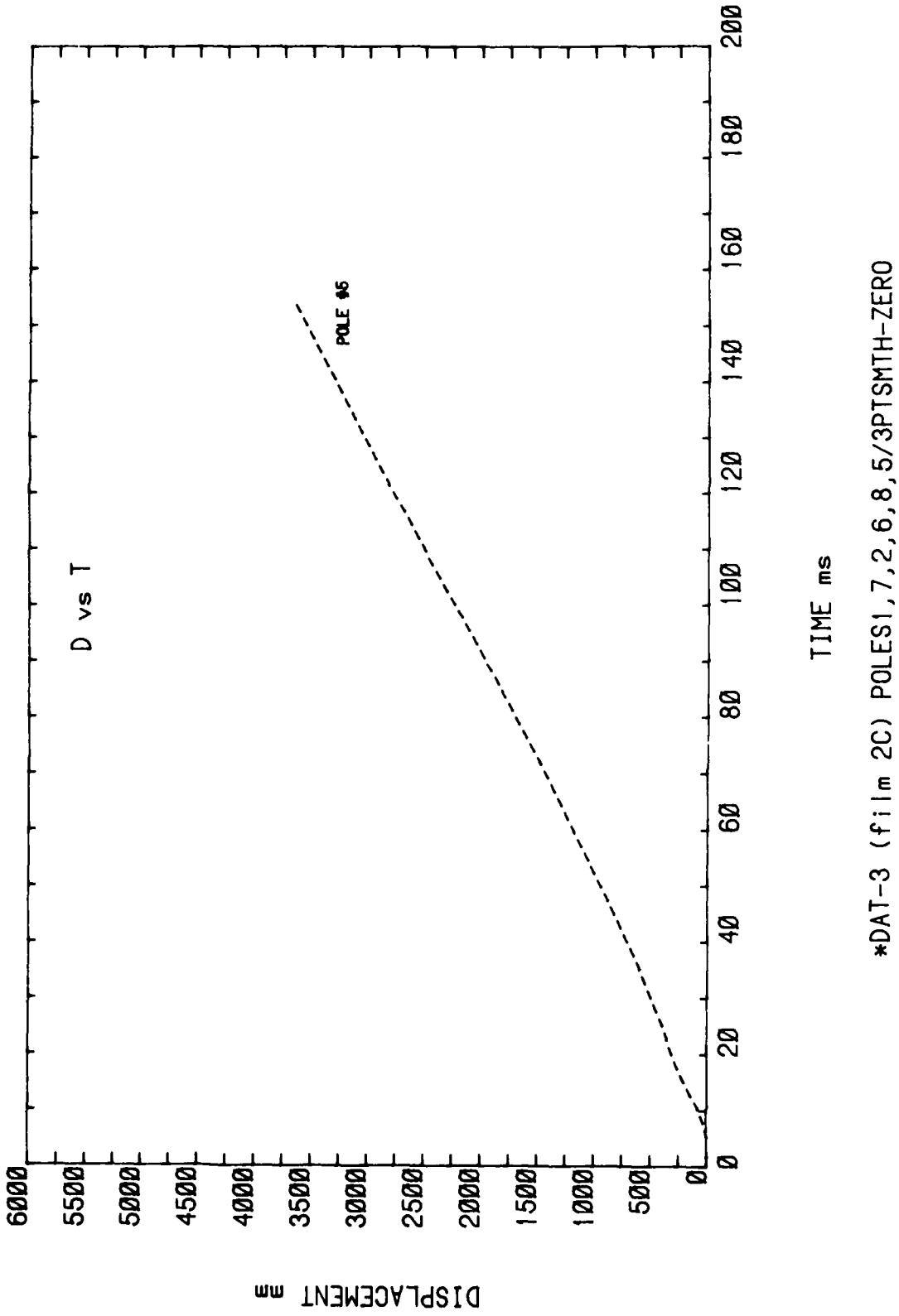


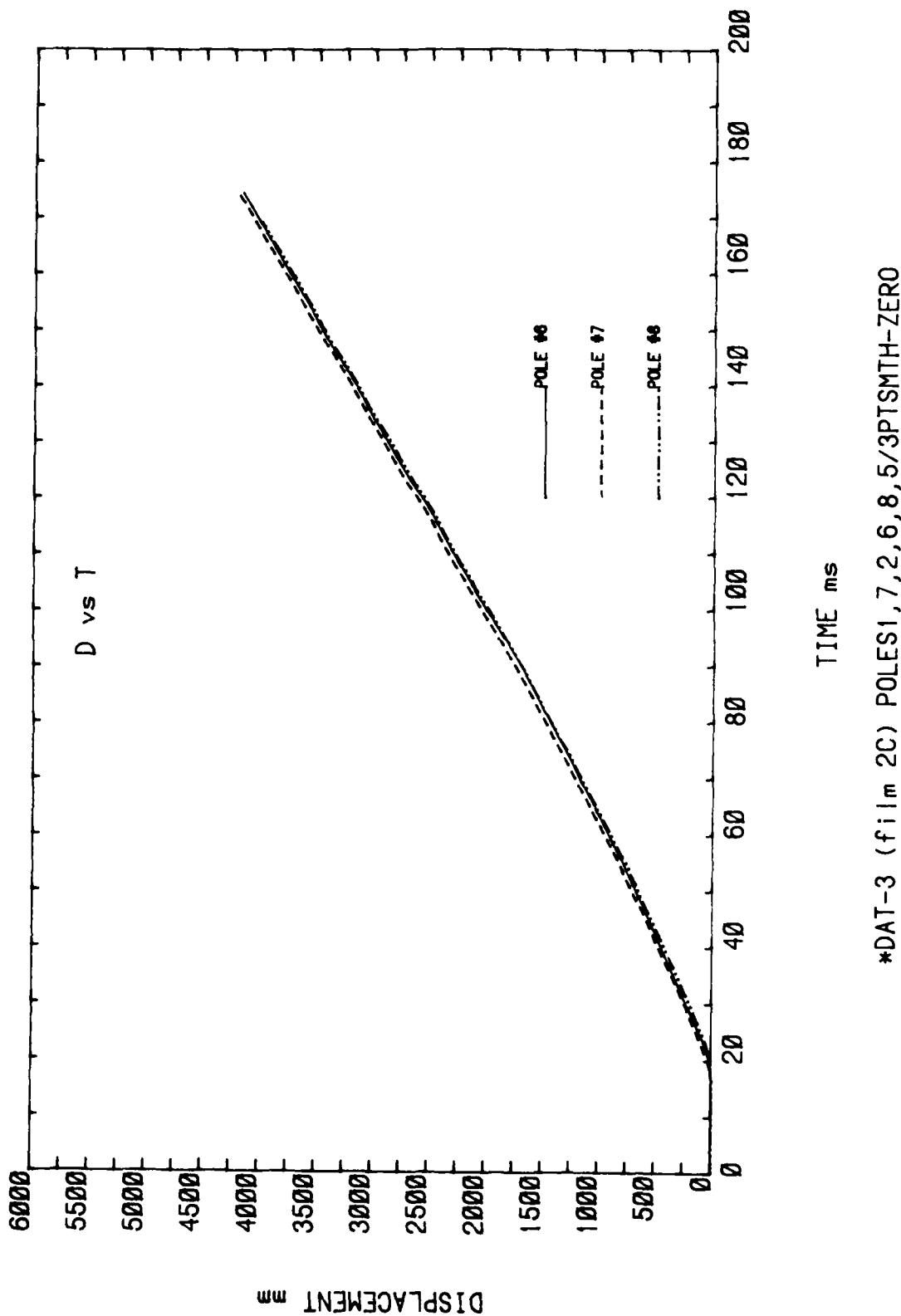
*DAT-3 (FILM 2B) POLES1,7,3,4,2,6,8,5/3PTSMTH-ZERO

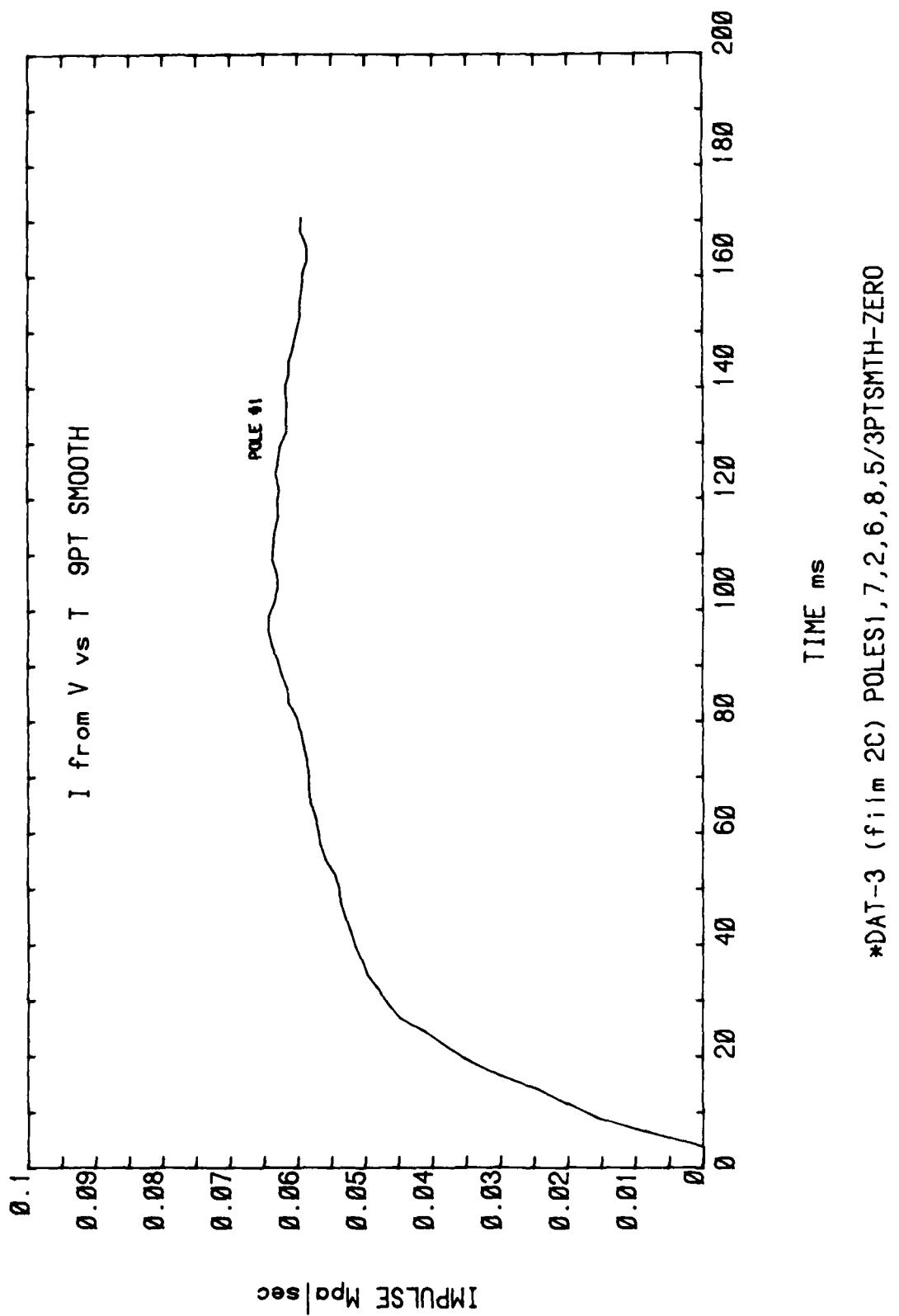


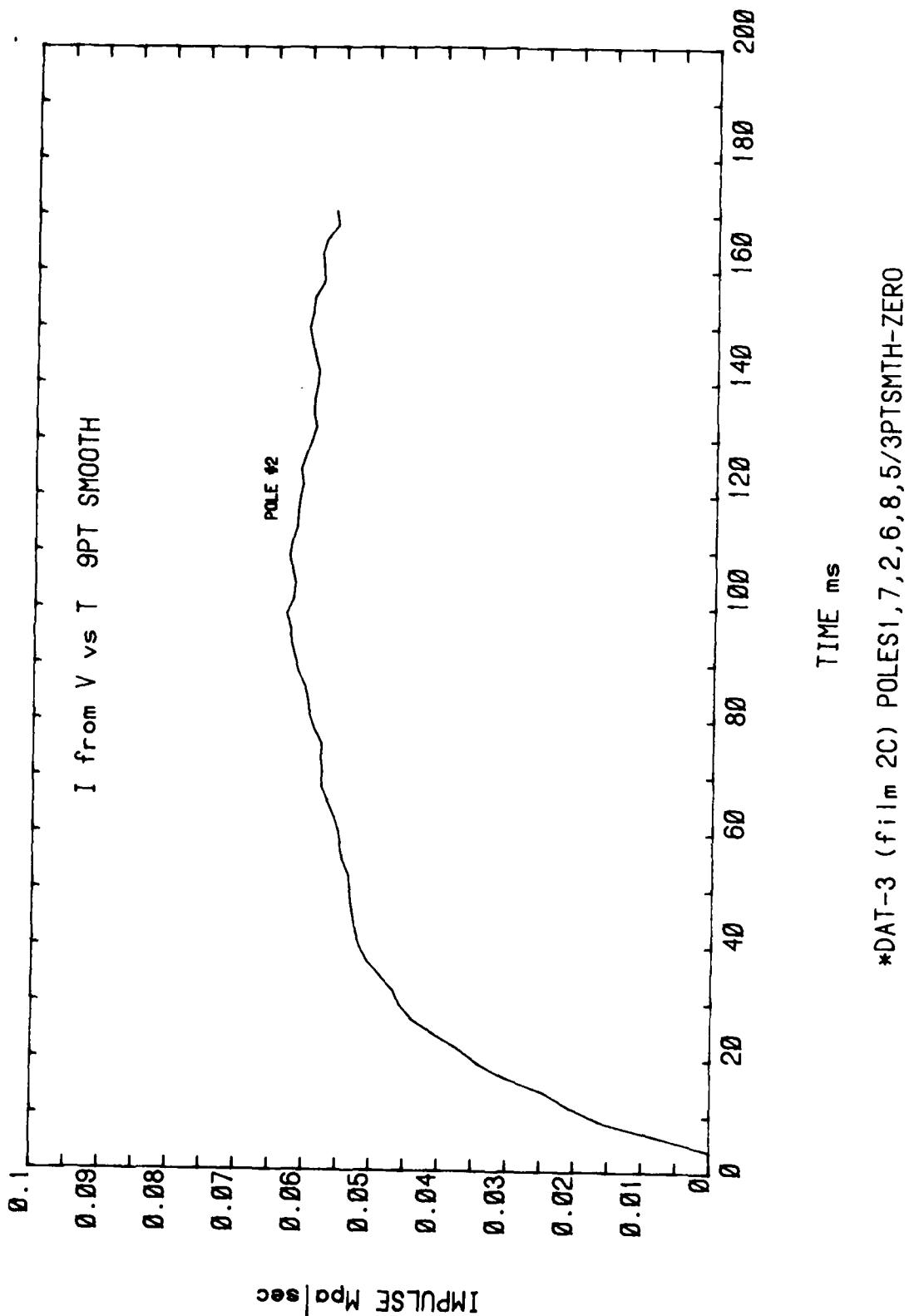


*DAT-3 (film 2C) POLES1,7,2,6,8,5/3PTSMTZ-ZERO

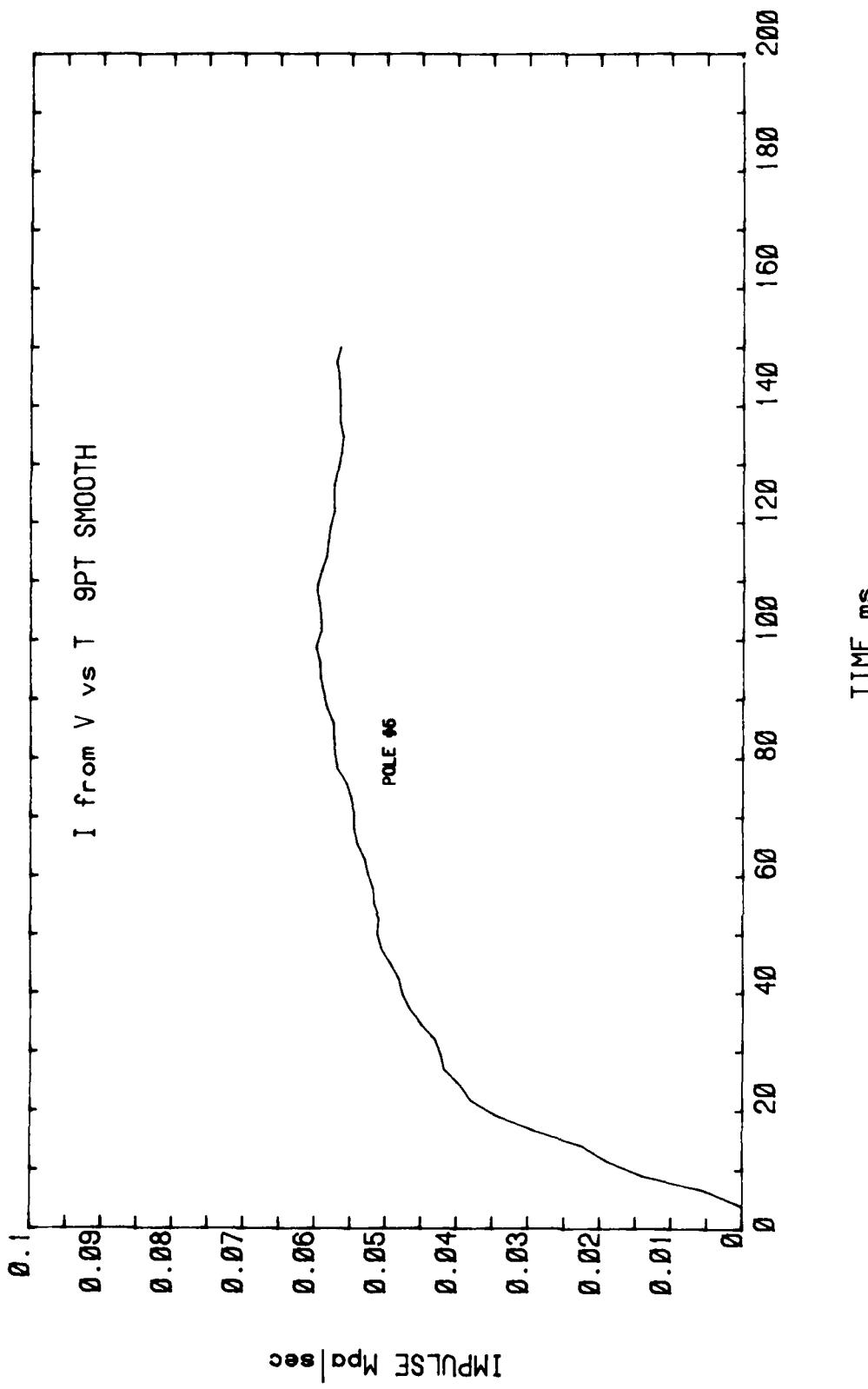




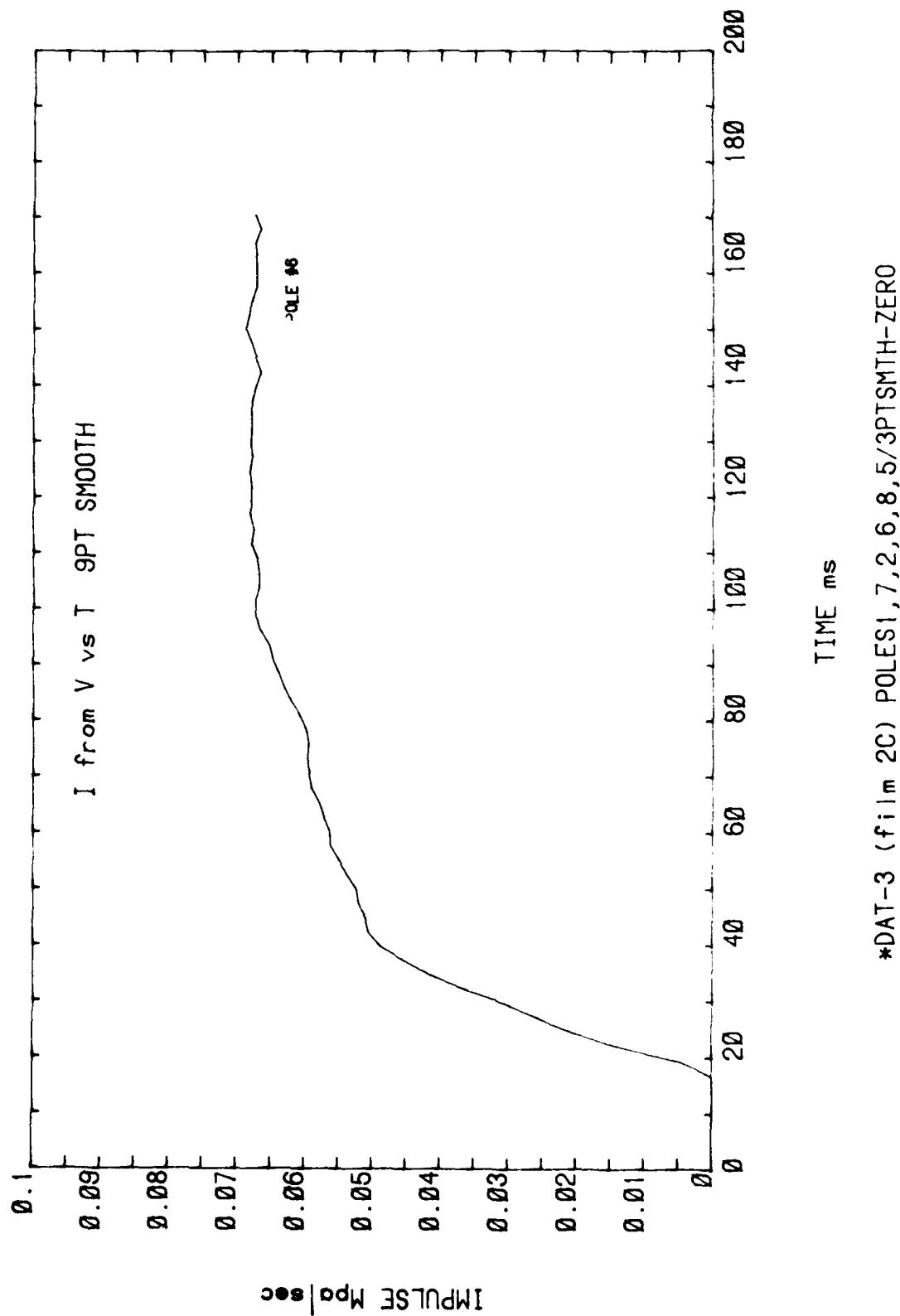




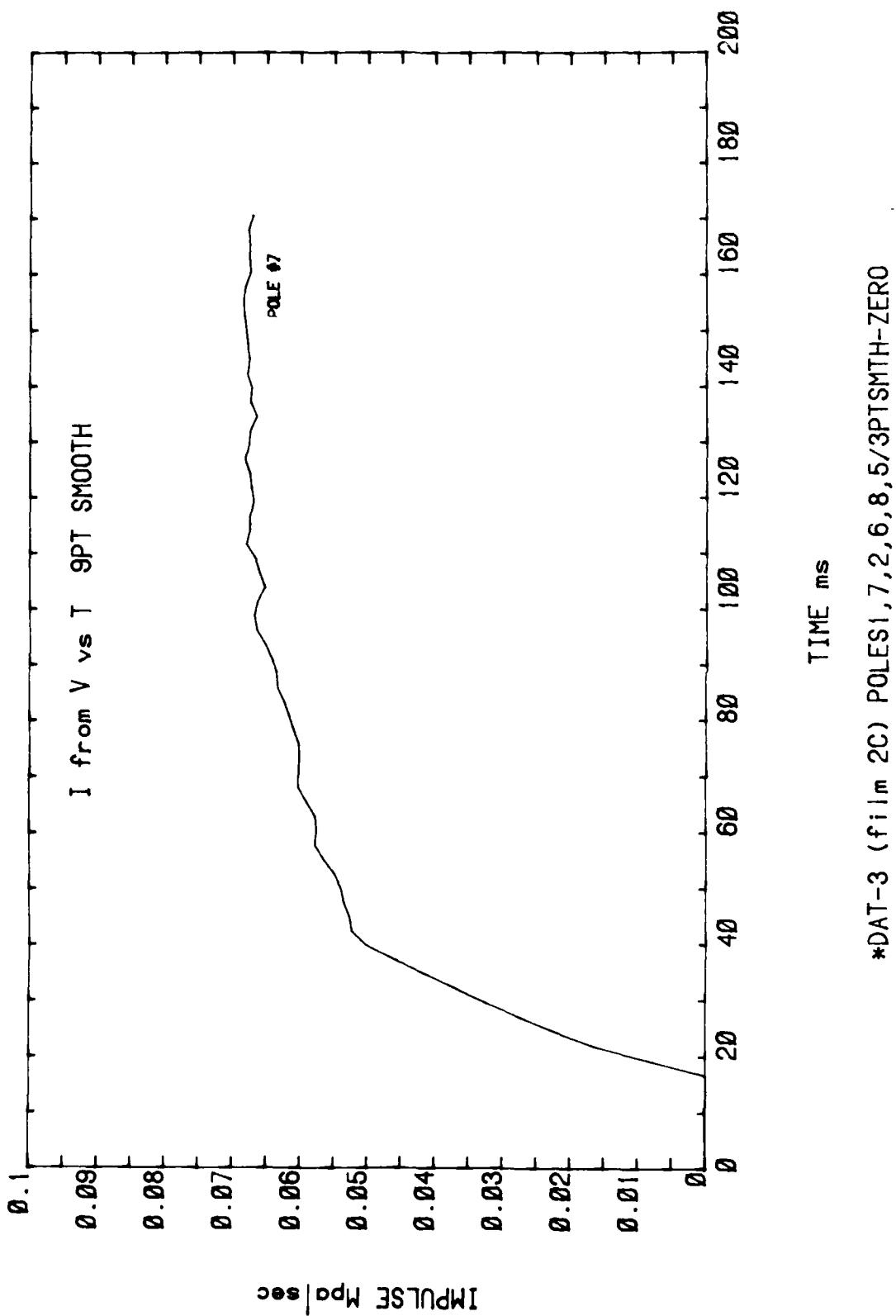
*DAT-3 (film 2C) POLES1,7,2,6,8,5/3PTSMT-ZERO

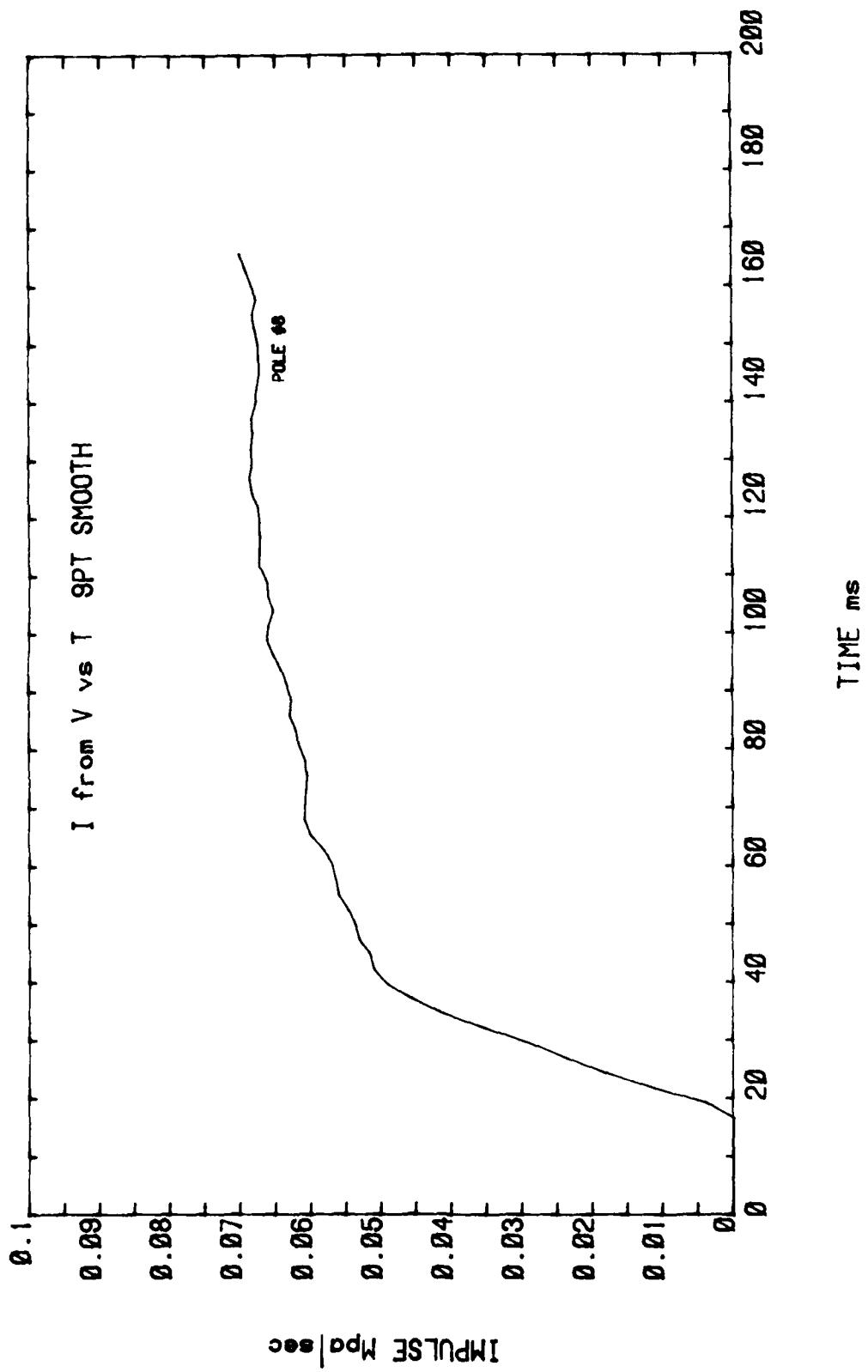


*DAT-3 (film 2C) POLES! ,7,2,6,8,5/3PTSMTZ-ZERO



*DAT-3 (film 2C) POLES1,7,2,6,8,5/3PTSMTH-ZERO

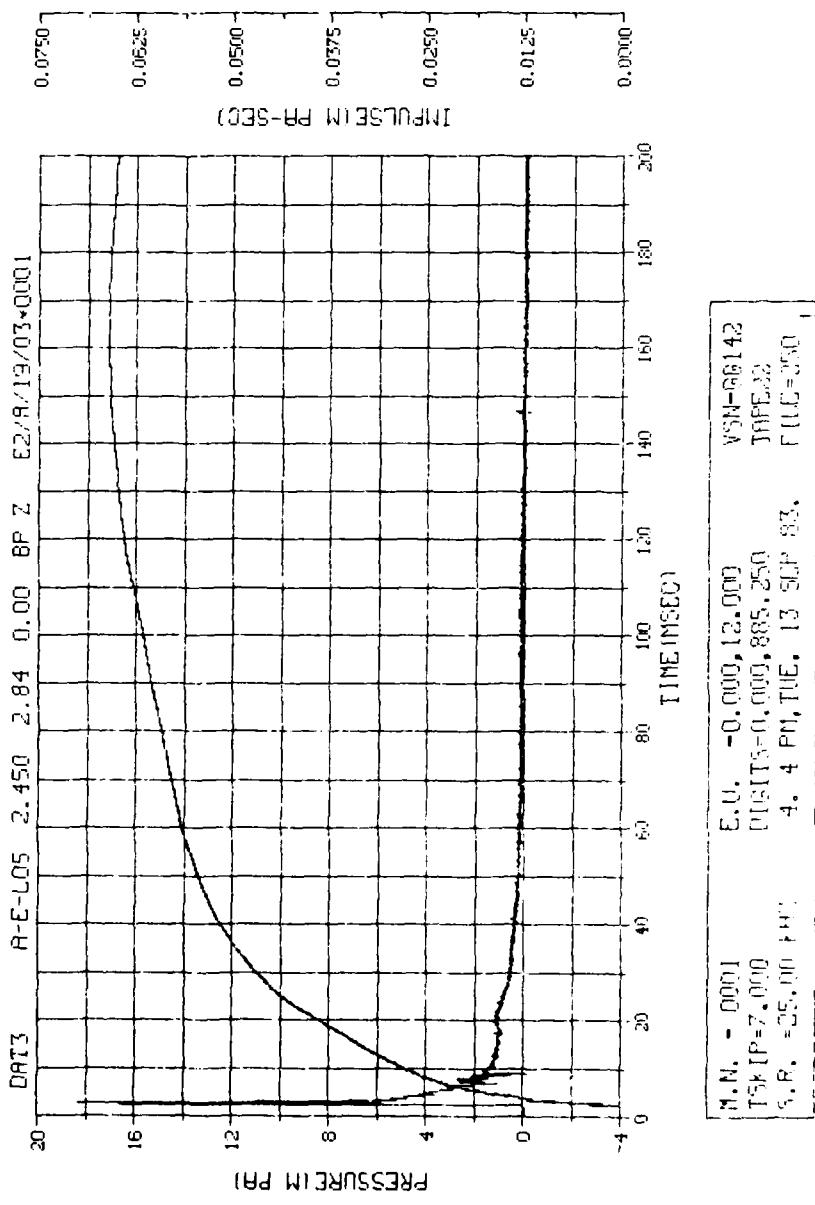


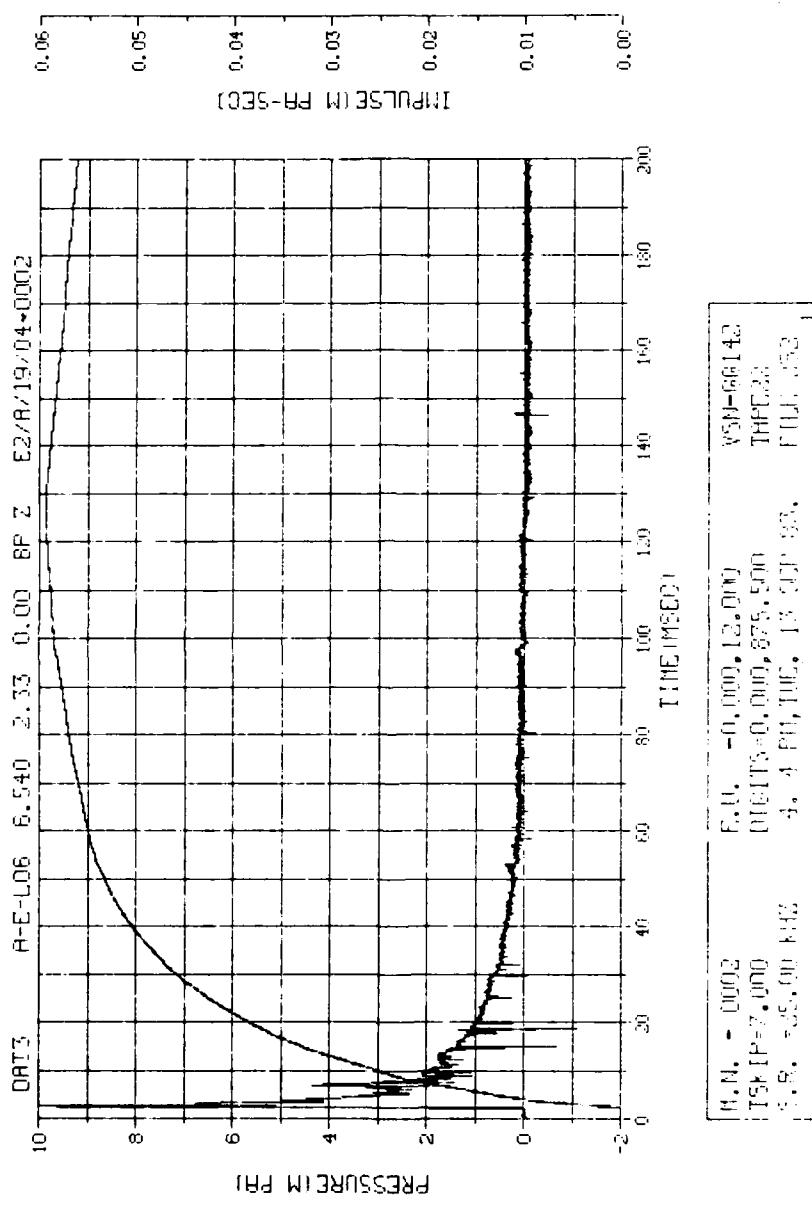


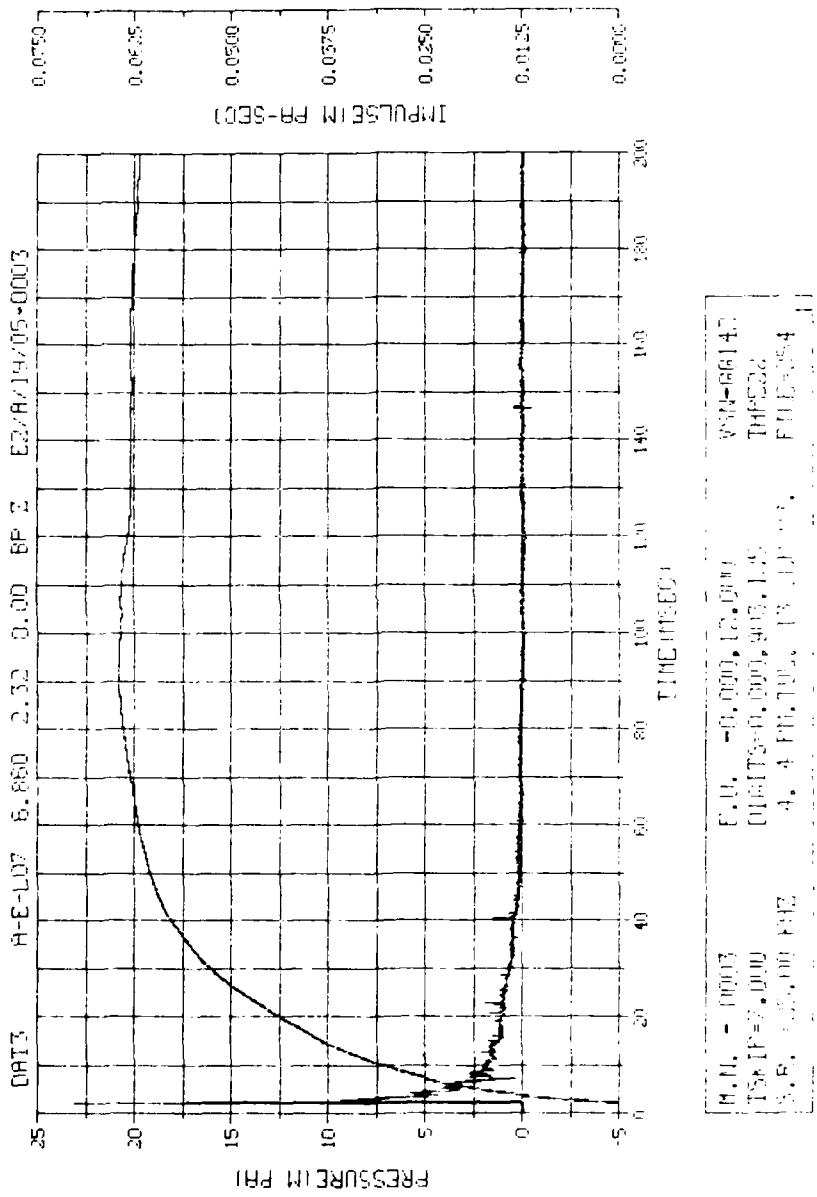
*DAT-3 (film 2C) POLES1,7,2,6,8,5/3PTSMTH-ZERO

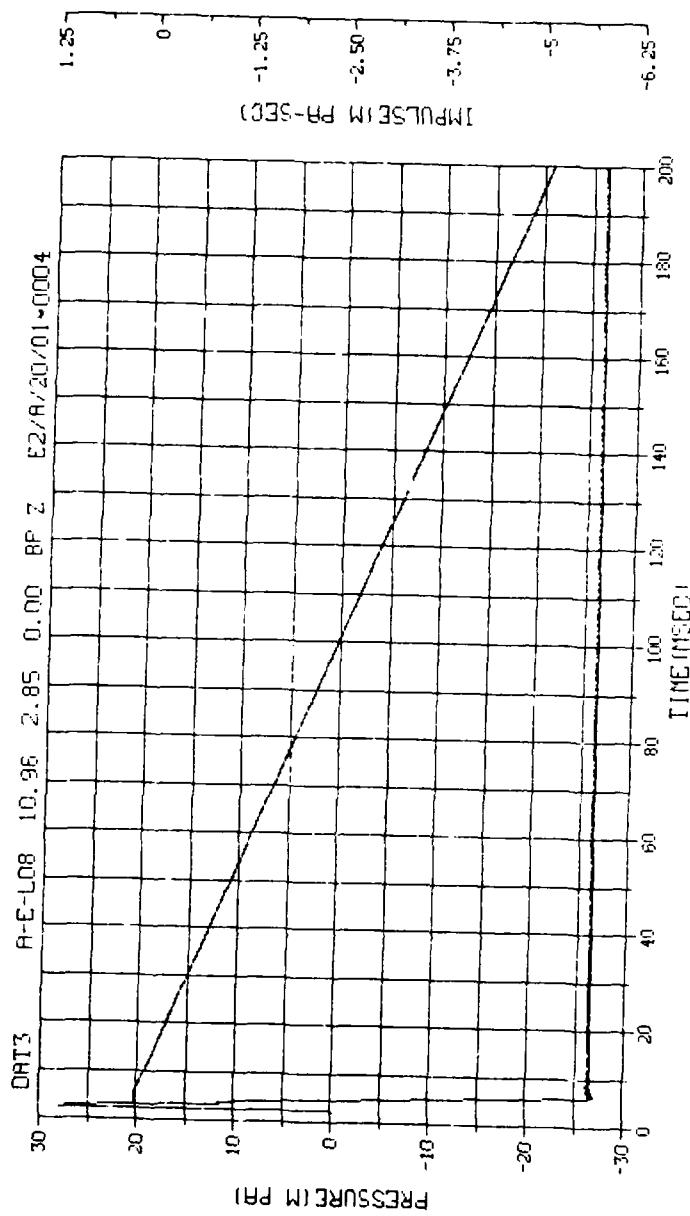
APPENDIX E

AIRBLAST PRESSURE DATA

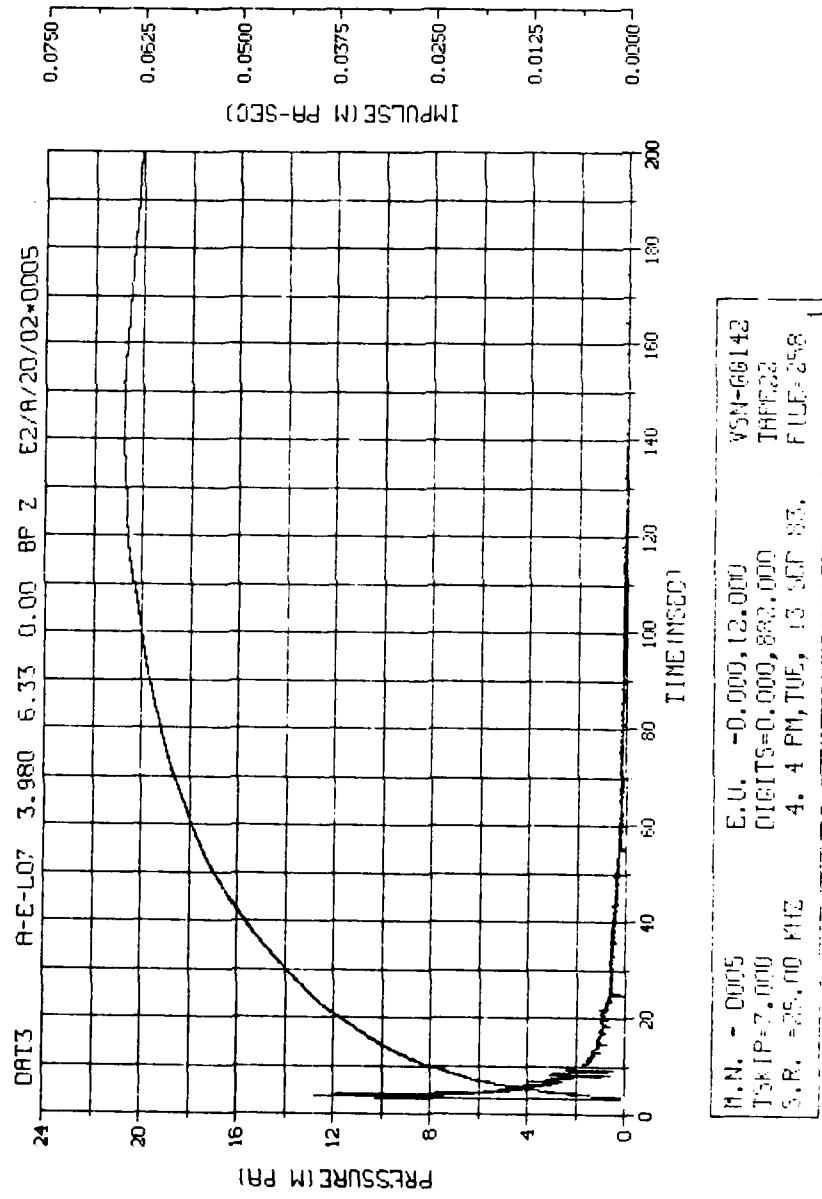


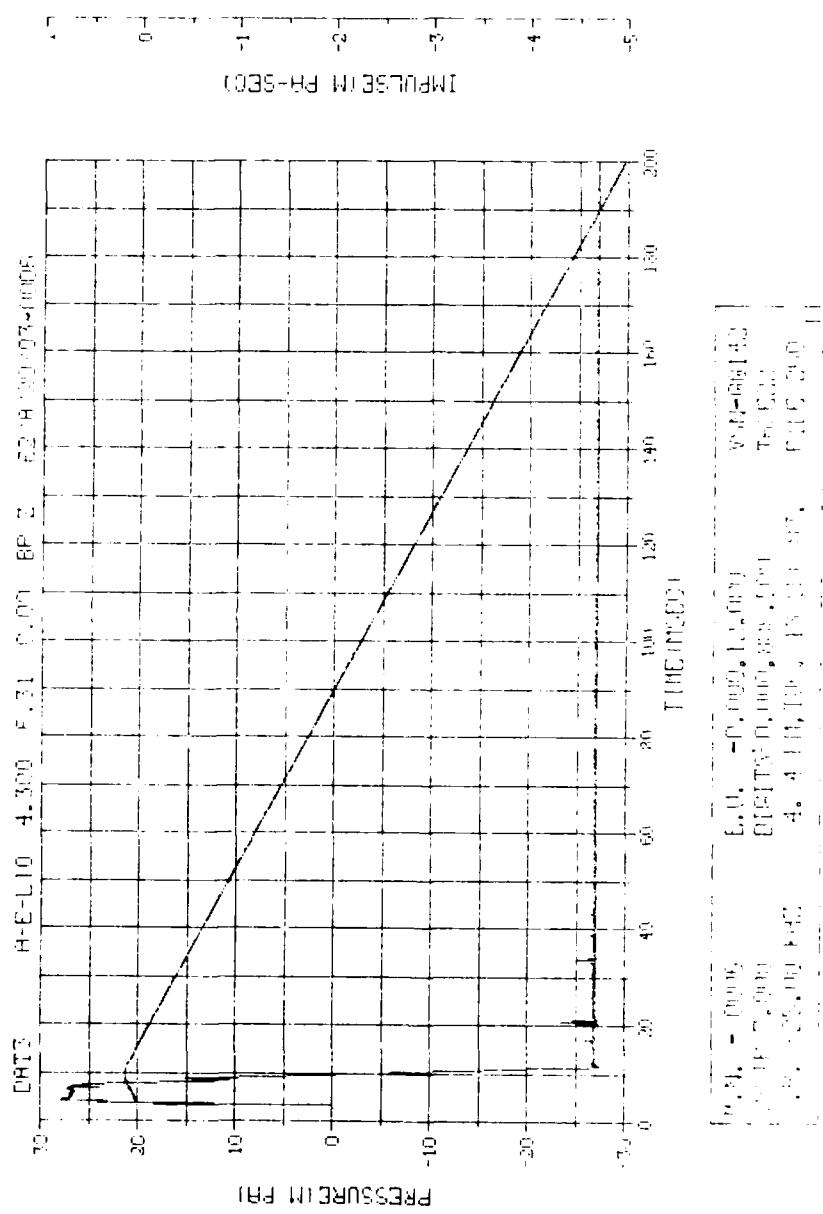


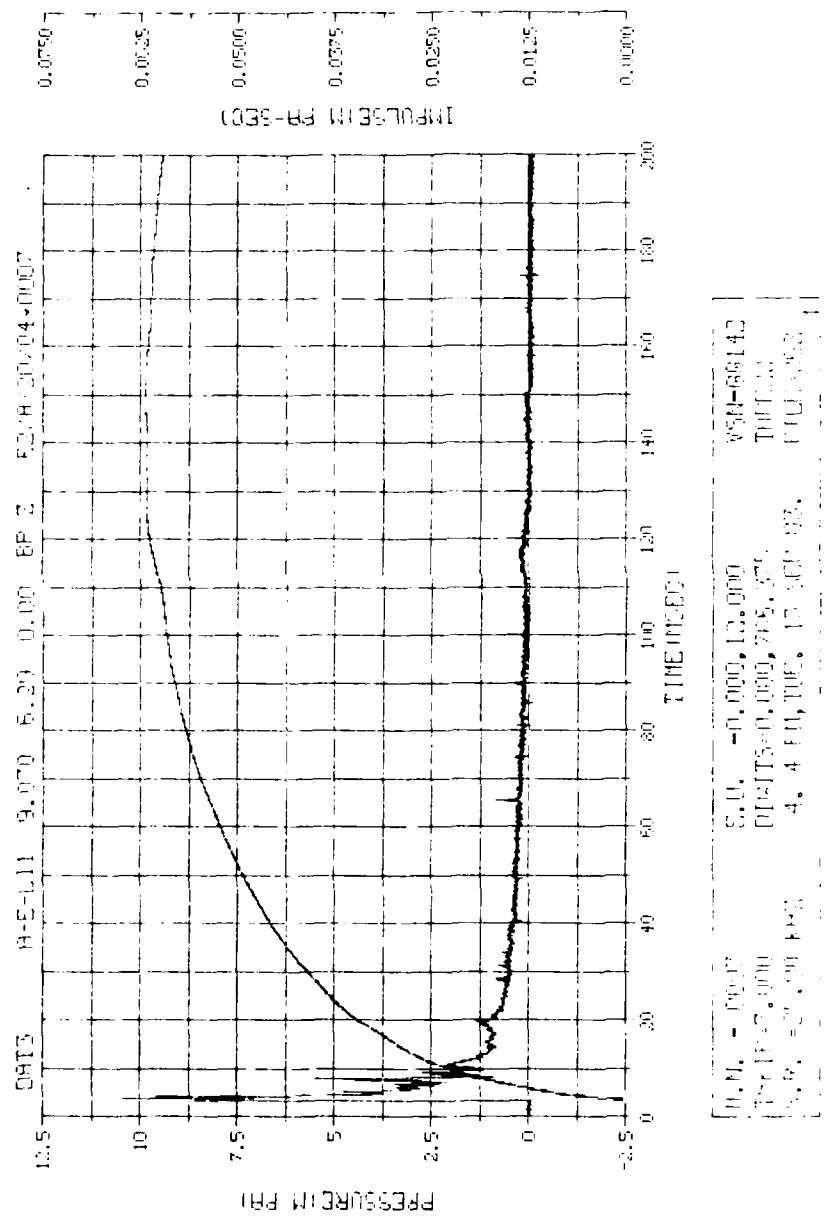


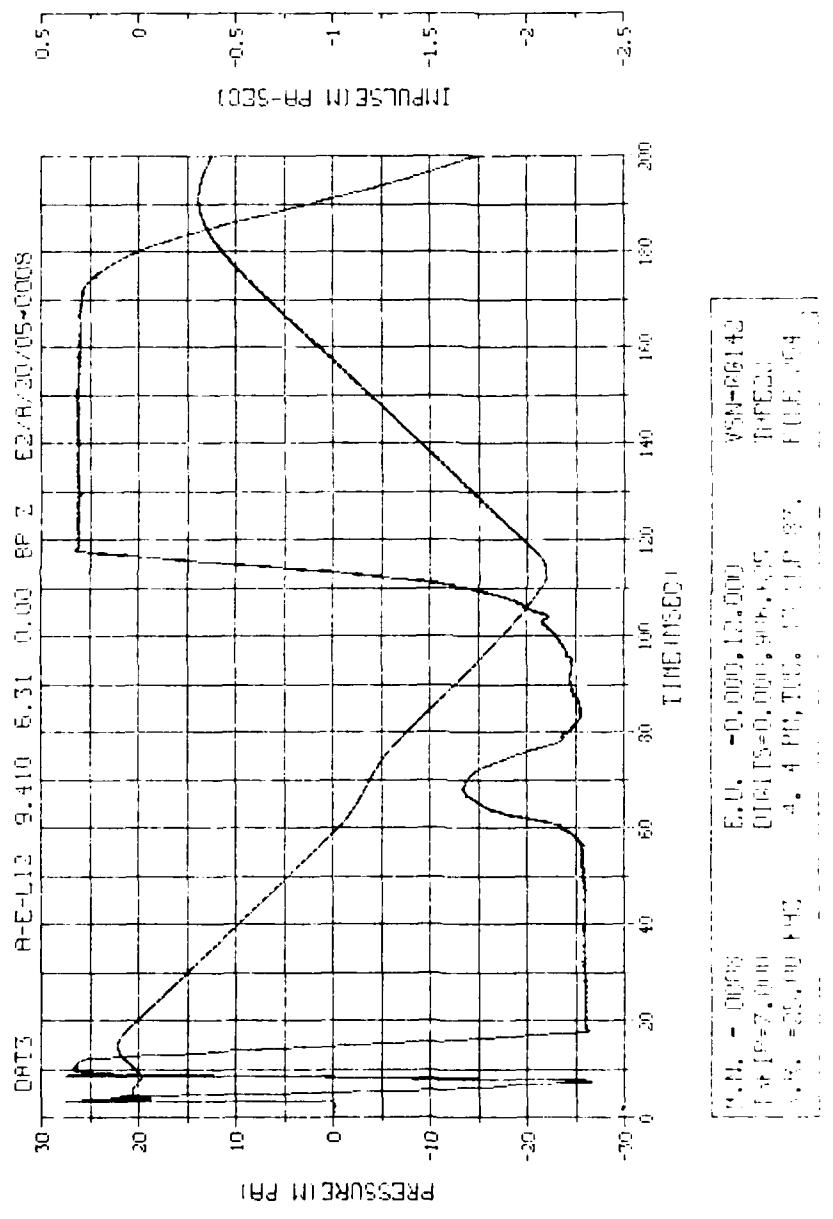


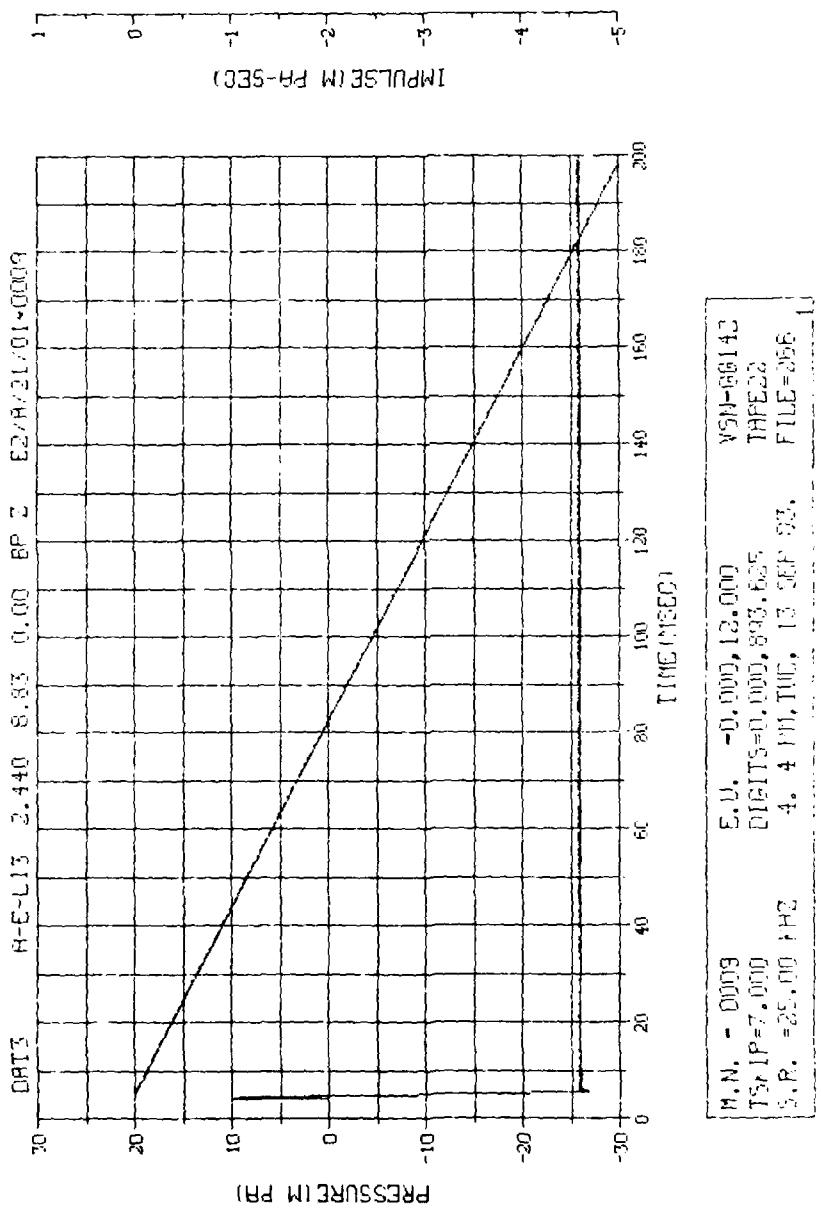
M.N. = 0004	E.U. = 0.000, 12.00	VSN=66142
TSKIP=7.000	DIGITS=0,000,894.375	TAPE22
S.R. = 25.00 KHZ	4. 4 PH, TUE, 13 SEP 93,	FILE=356

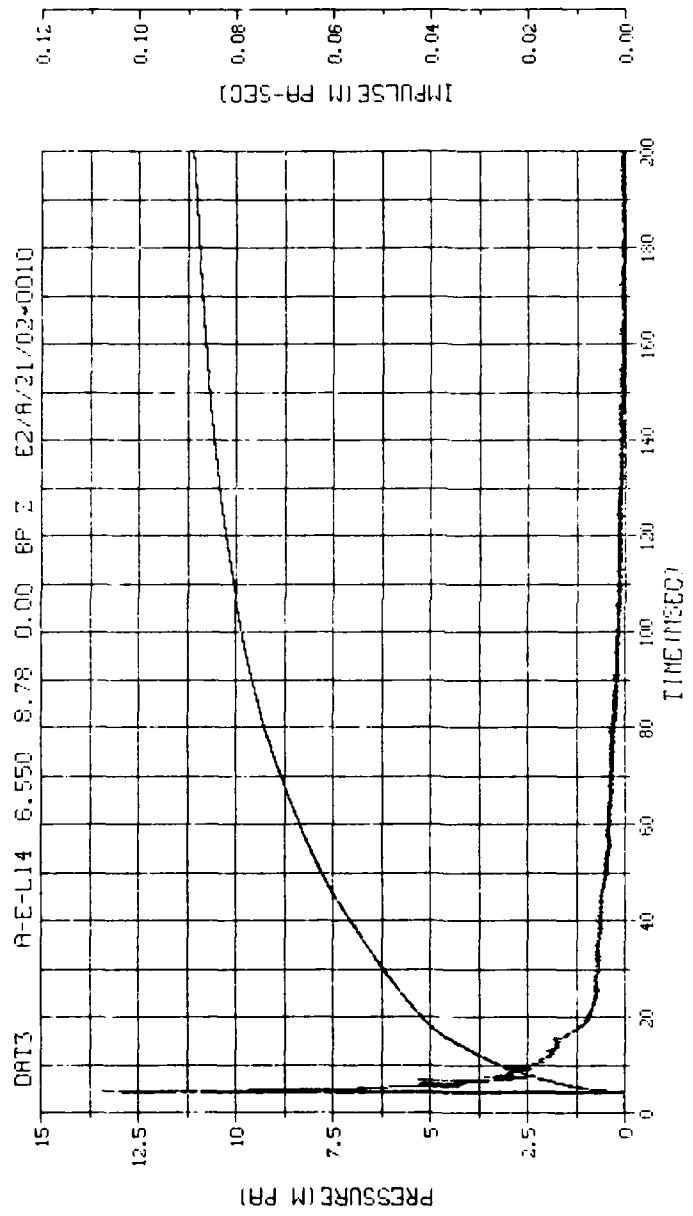




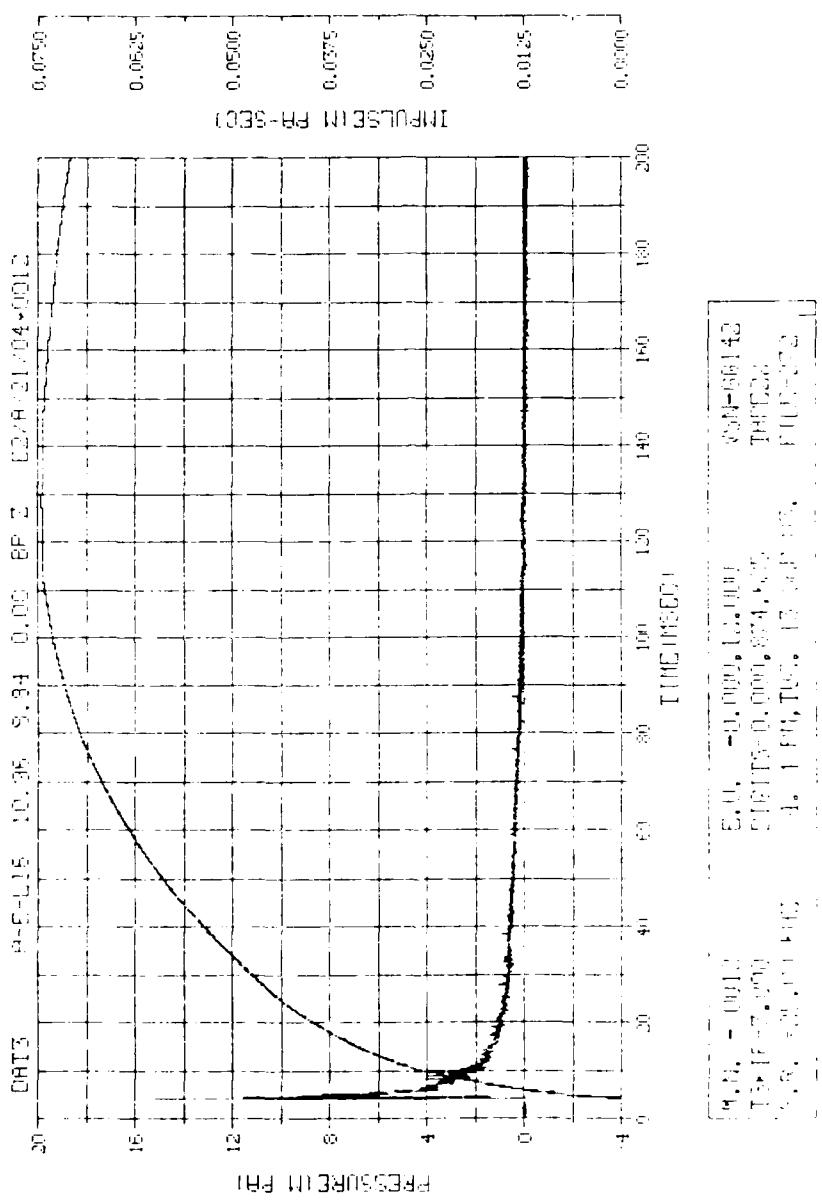


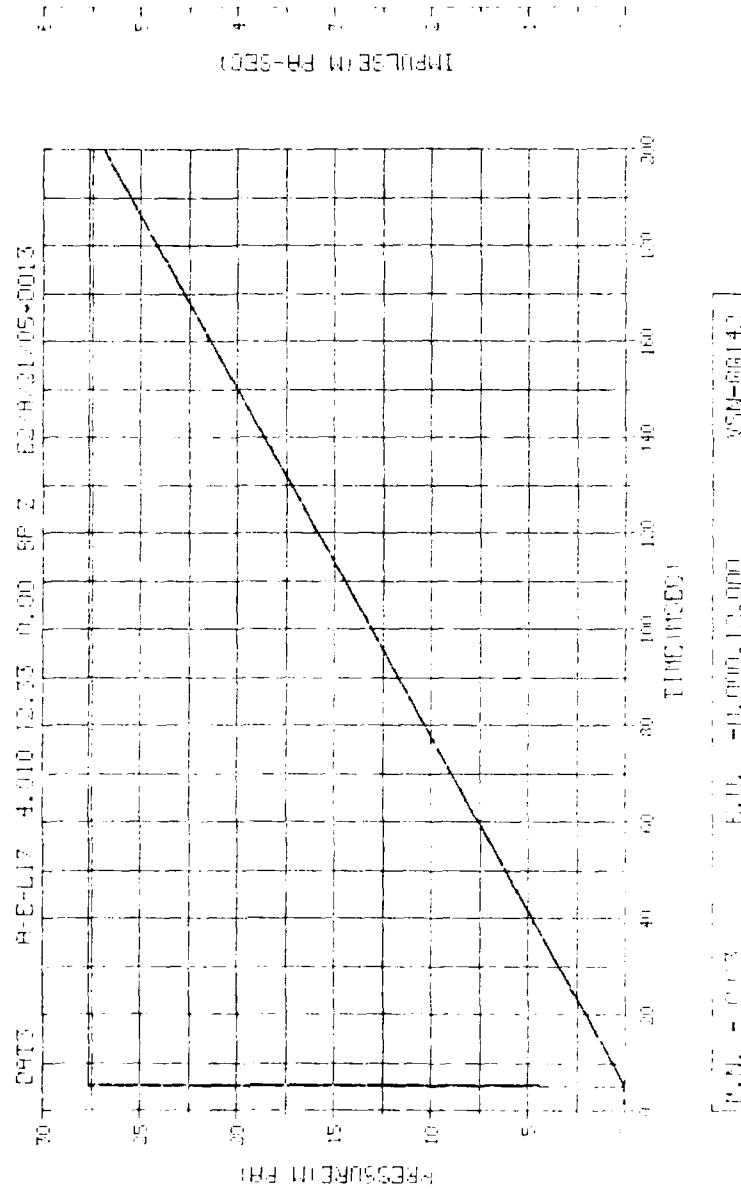


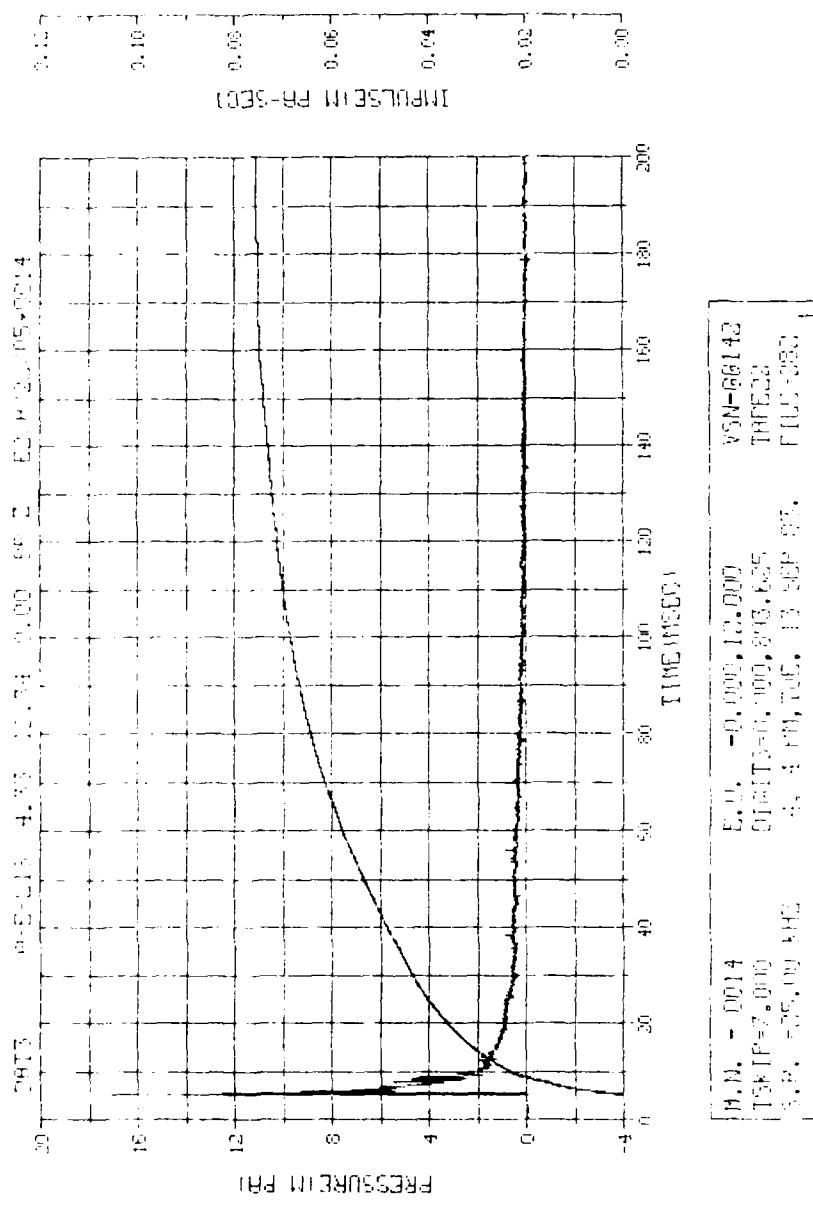




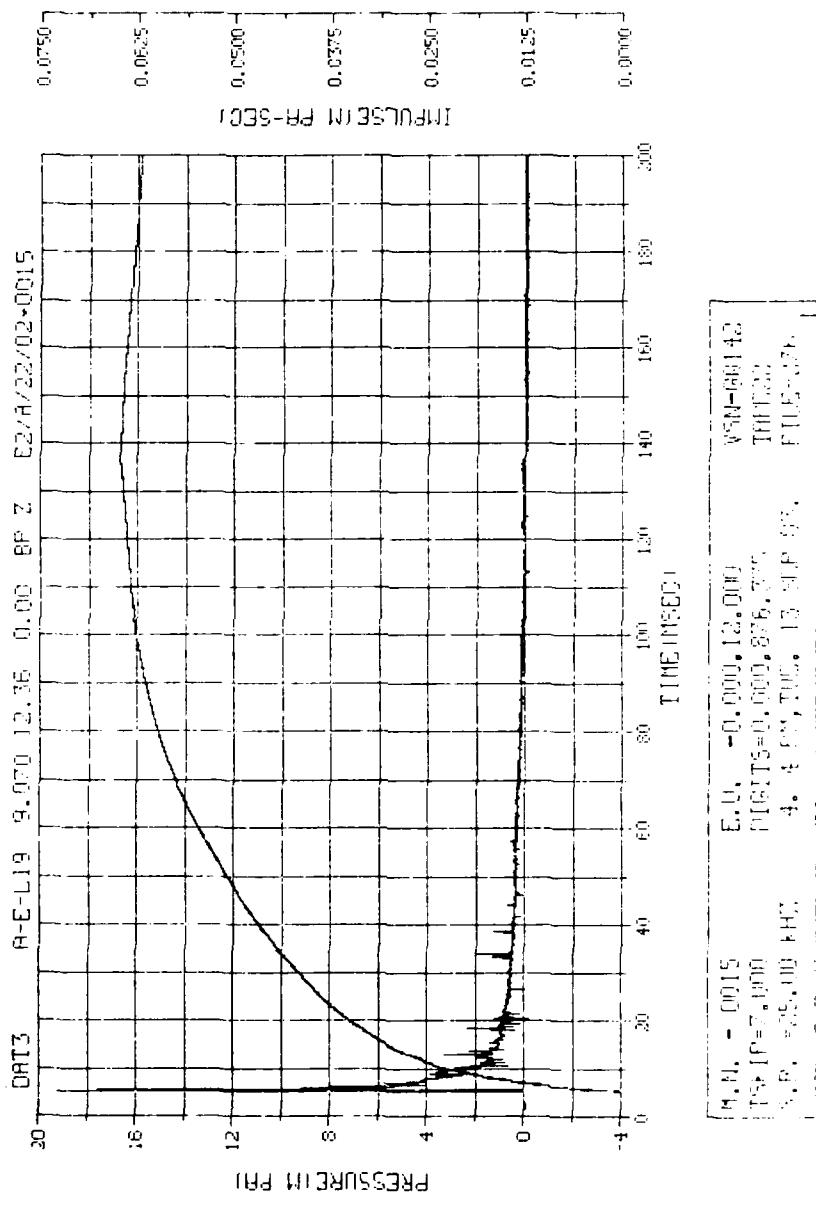
M.N. = .0010	E.H. = -0.000, 12.000	VSN-66142
Tsk IP=7.000	DIGITS=0.000, 878.635	TYPE 2
S.R. = 25.00 kHz	4. 4 PM, TUE, 13 SEP 97,	f1Lc= 358

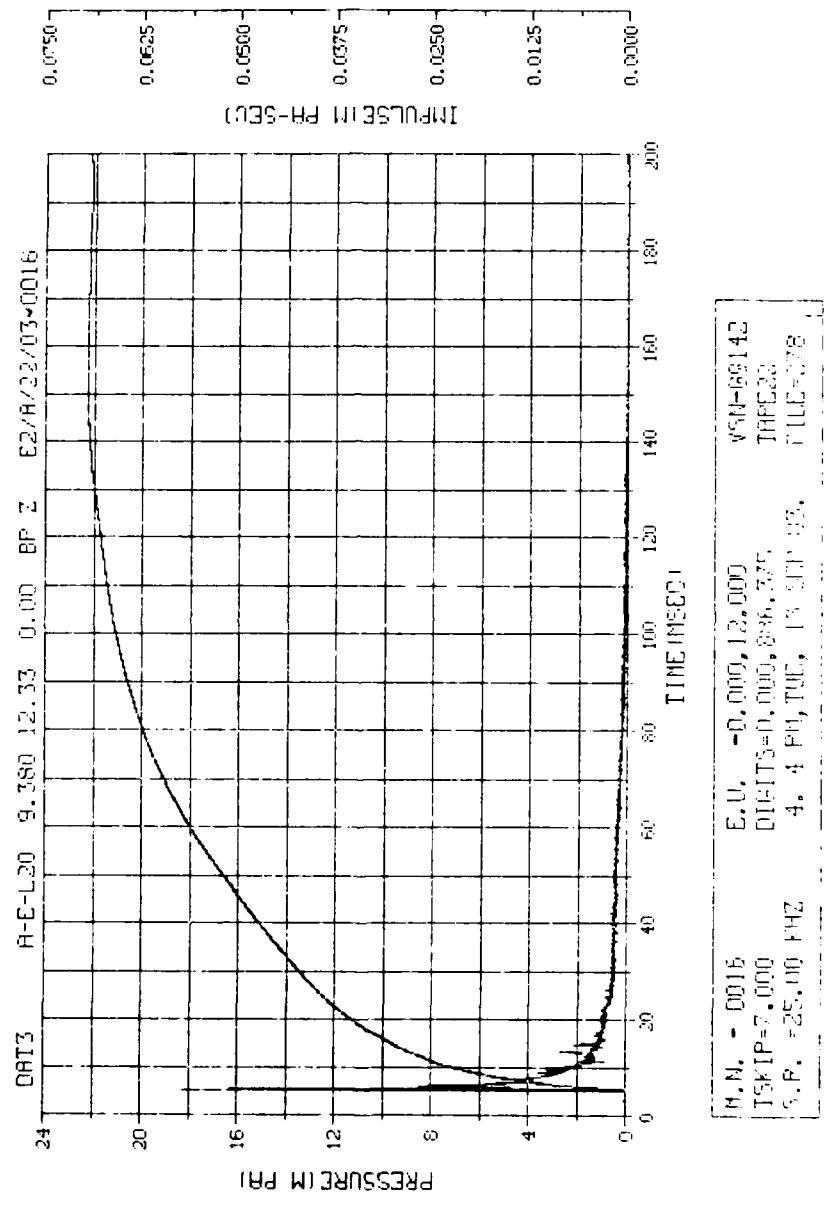






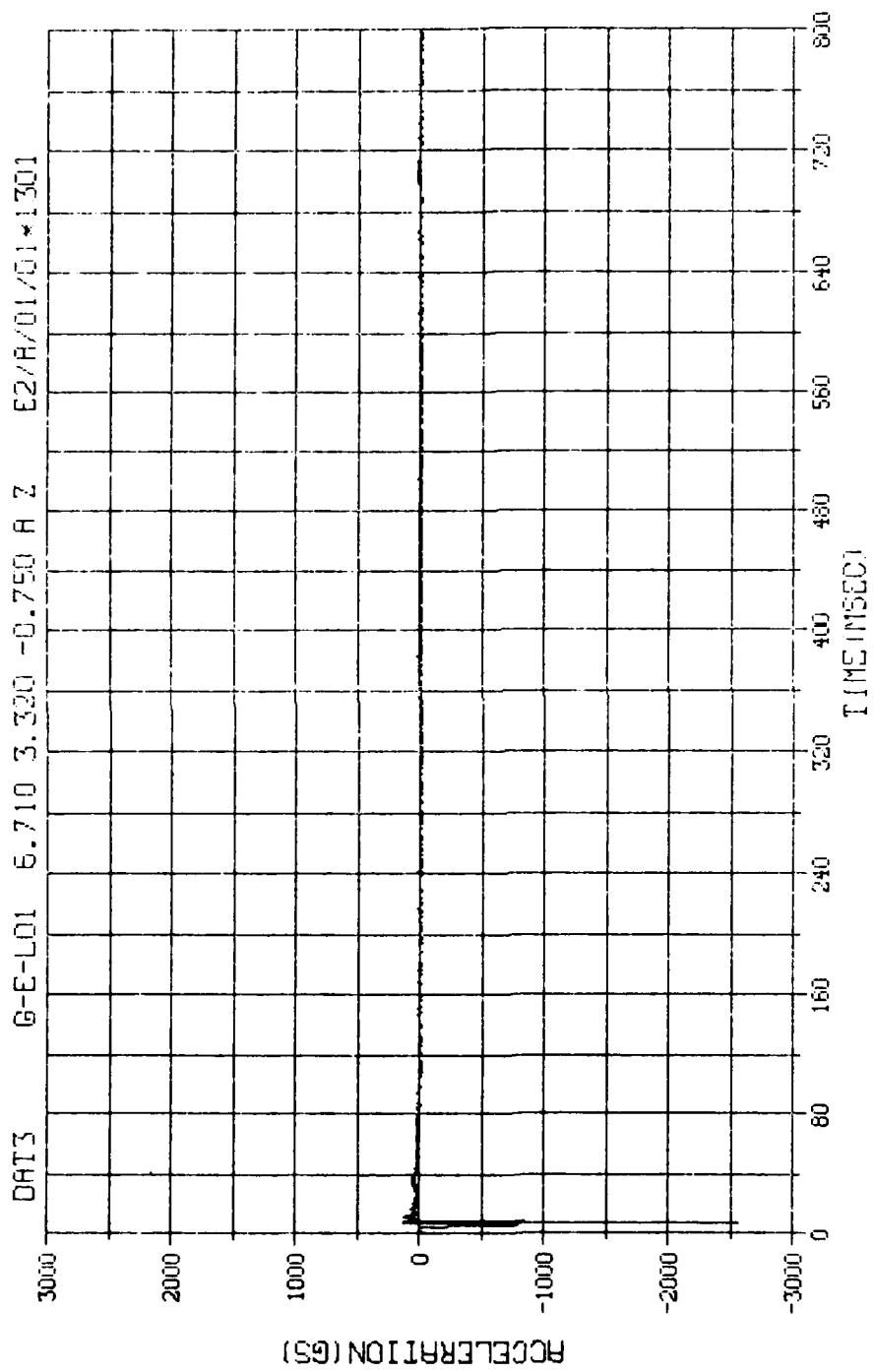
P.M. = 0014	E.O. = +0.0000 12.0000	VSN-86142
TSP = 7.000	CHARGE = 0.000 03.035	THREE
S.P. = 35.00 KPSI	4 PIV, 15. 13 SEP 87.	FILE 350



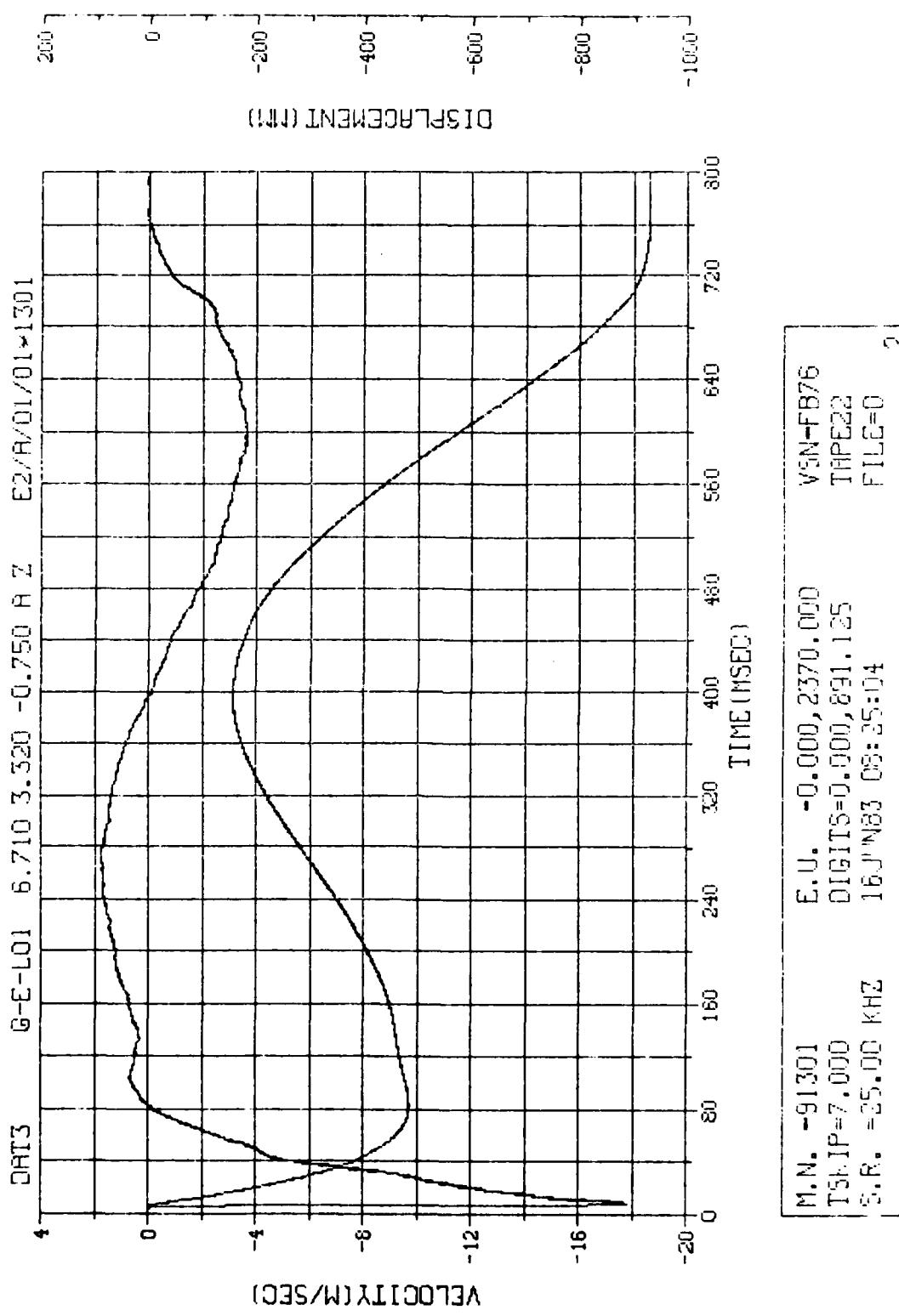


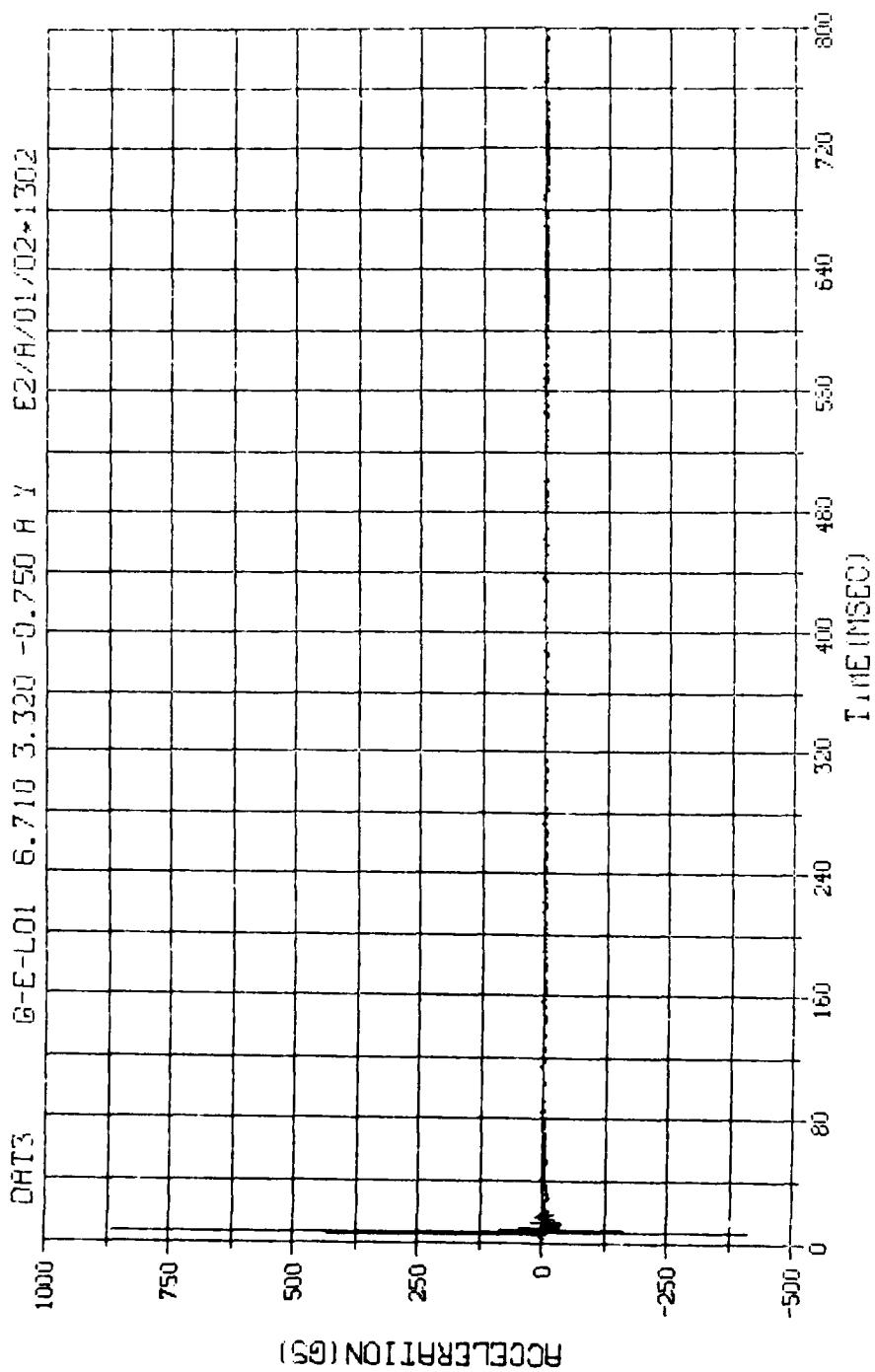
APPENDIX F

FREE-FIELD SOIL DATA

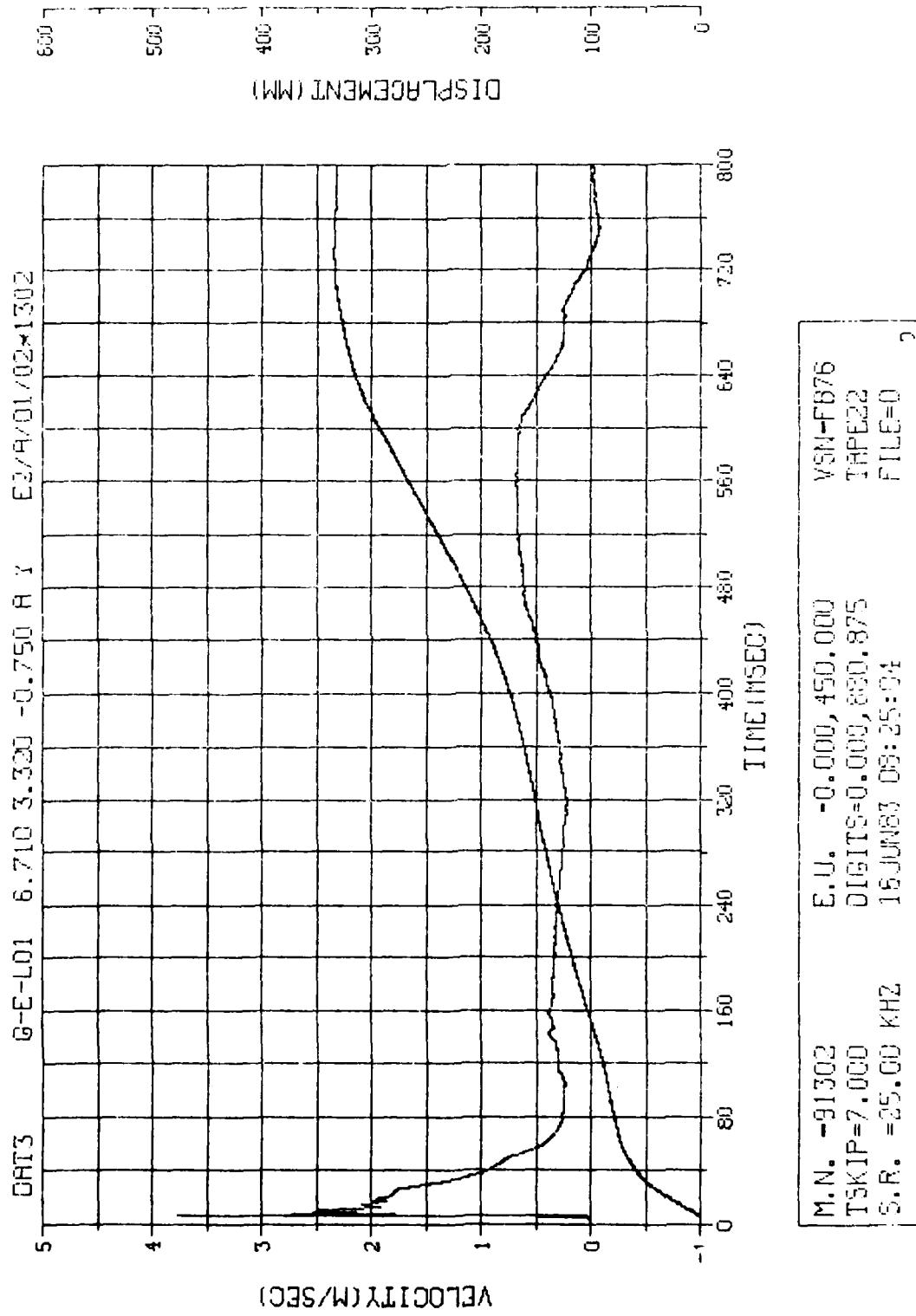


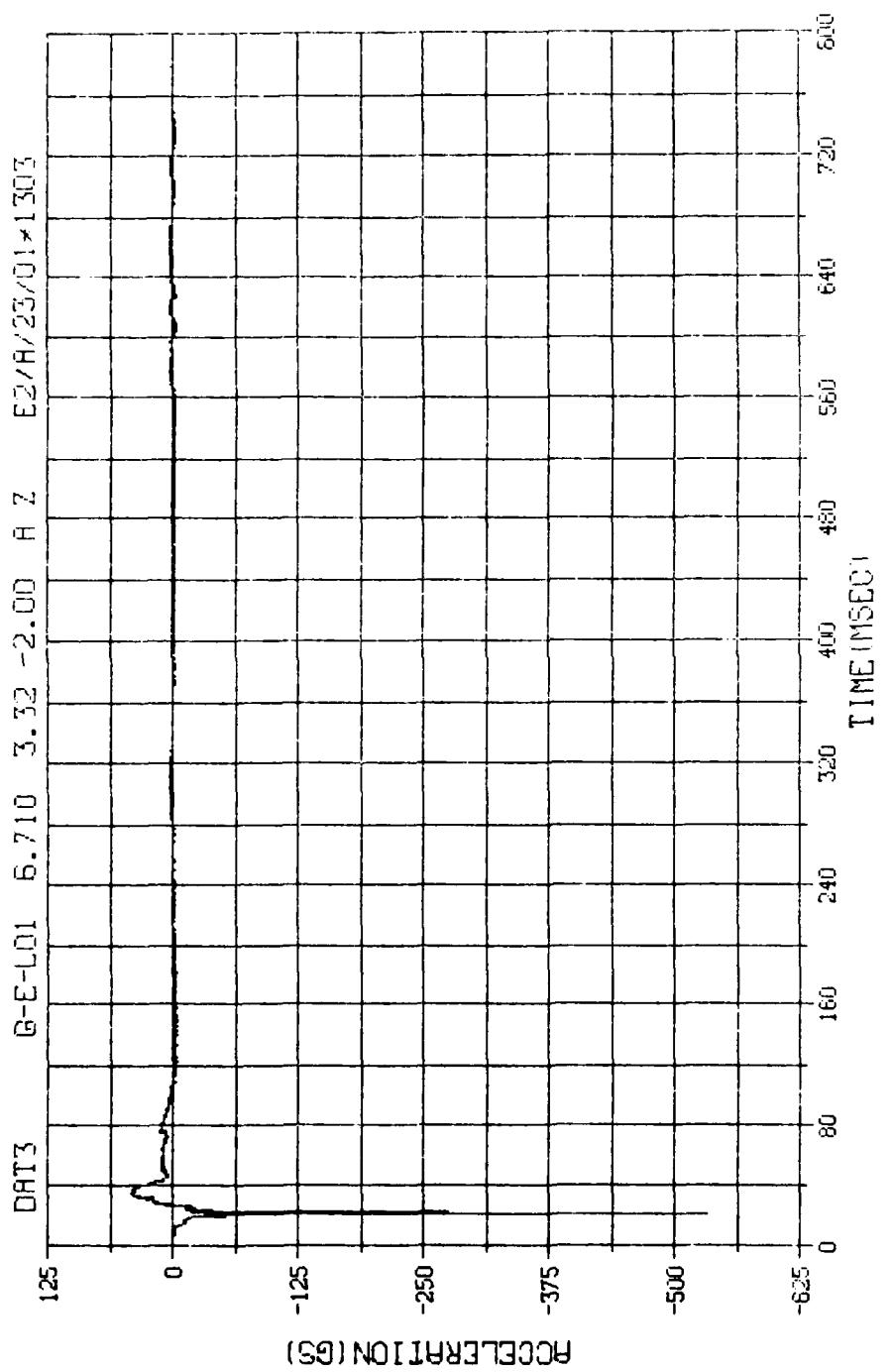
N. N. -91301	E.U. -0.000,2370.000	VSN-FE76
SKIP=7,000	DIGITS=0,000,891,125	TRIP22
S.R. =25,00 kHz	16-JUN-83 08:25:04	FILE=0
		1



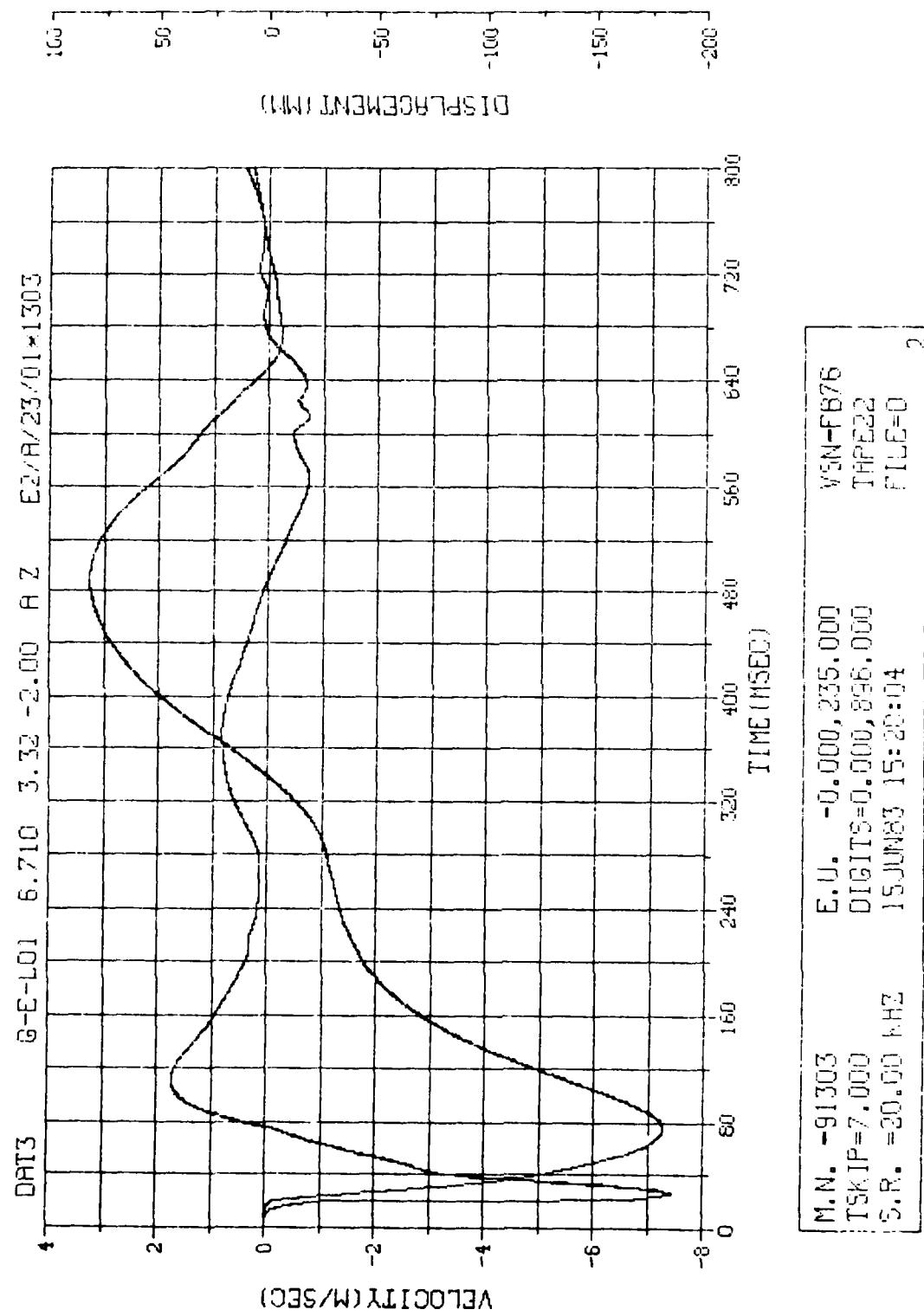


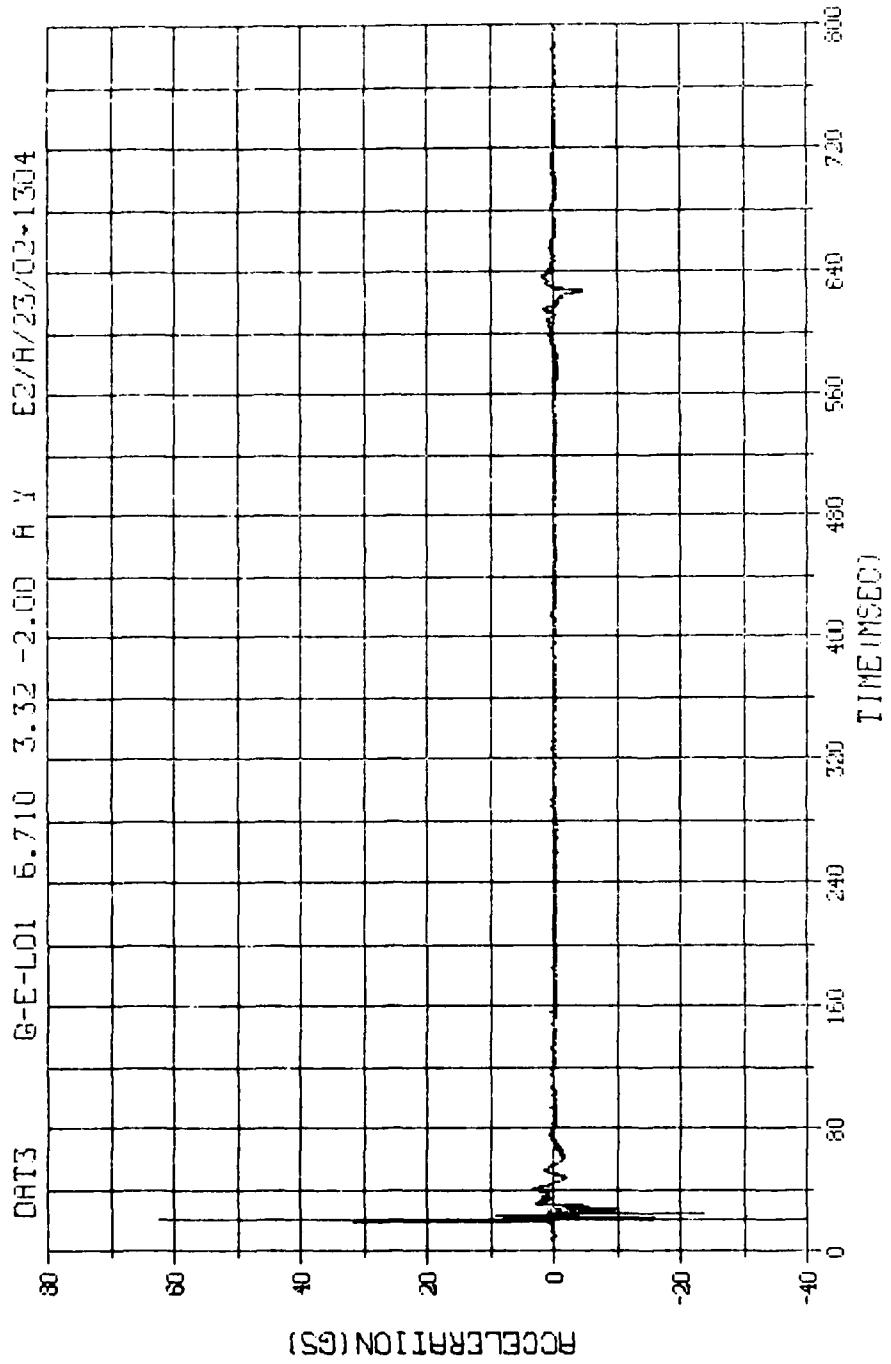
M.N. -91302	E.U. -0.000, 450.000	VSN-FB76
TSKIP=7.000	DIGITS=0.000, 880.875	TYPE22
S.R. =25.00 KHZ	16 JUNE 93 08:25:04	FILE=0
		1



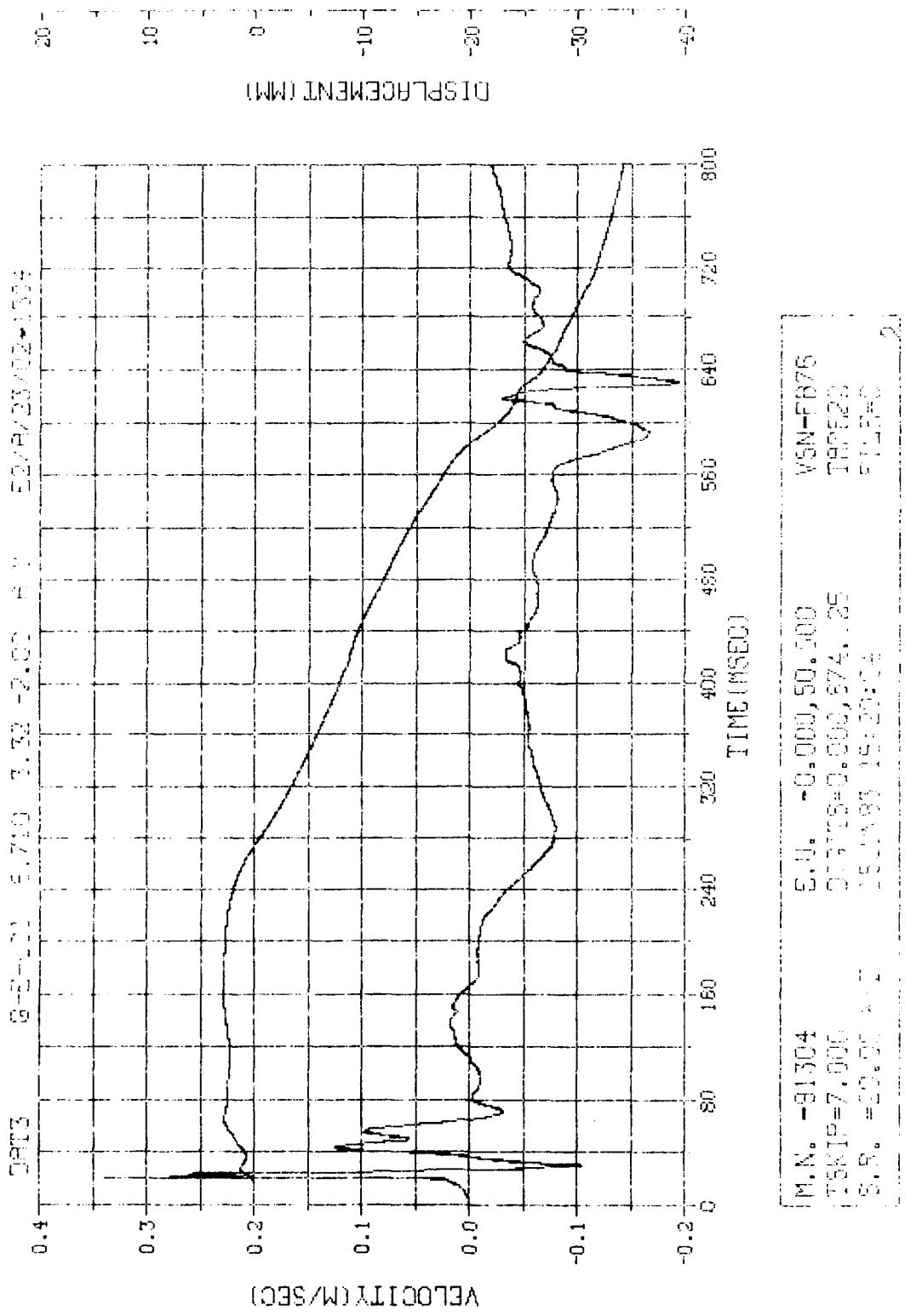


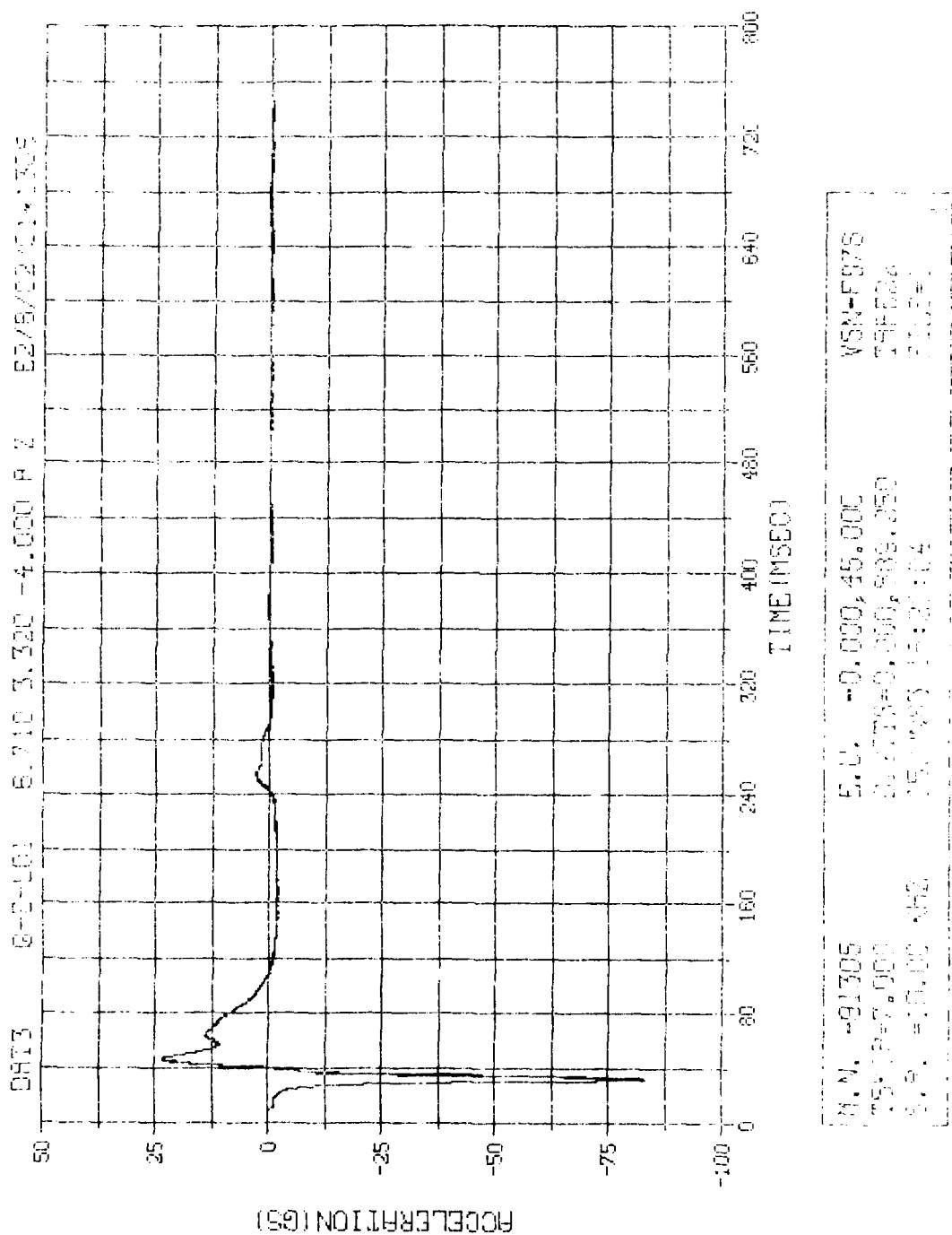
N.N. -91303	E.U. -0.000, 235.000	VSN-F876
TSKIP=7.000	DIGIT5=0.000, 896.000	TRPE22
S.R. =20.00 KHZ	15.00N83 15:20:04	FILE=0
		1

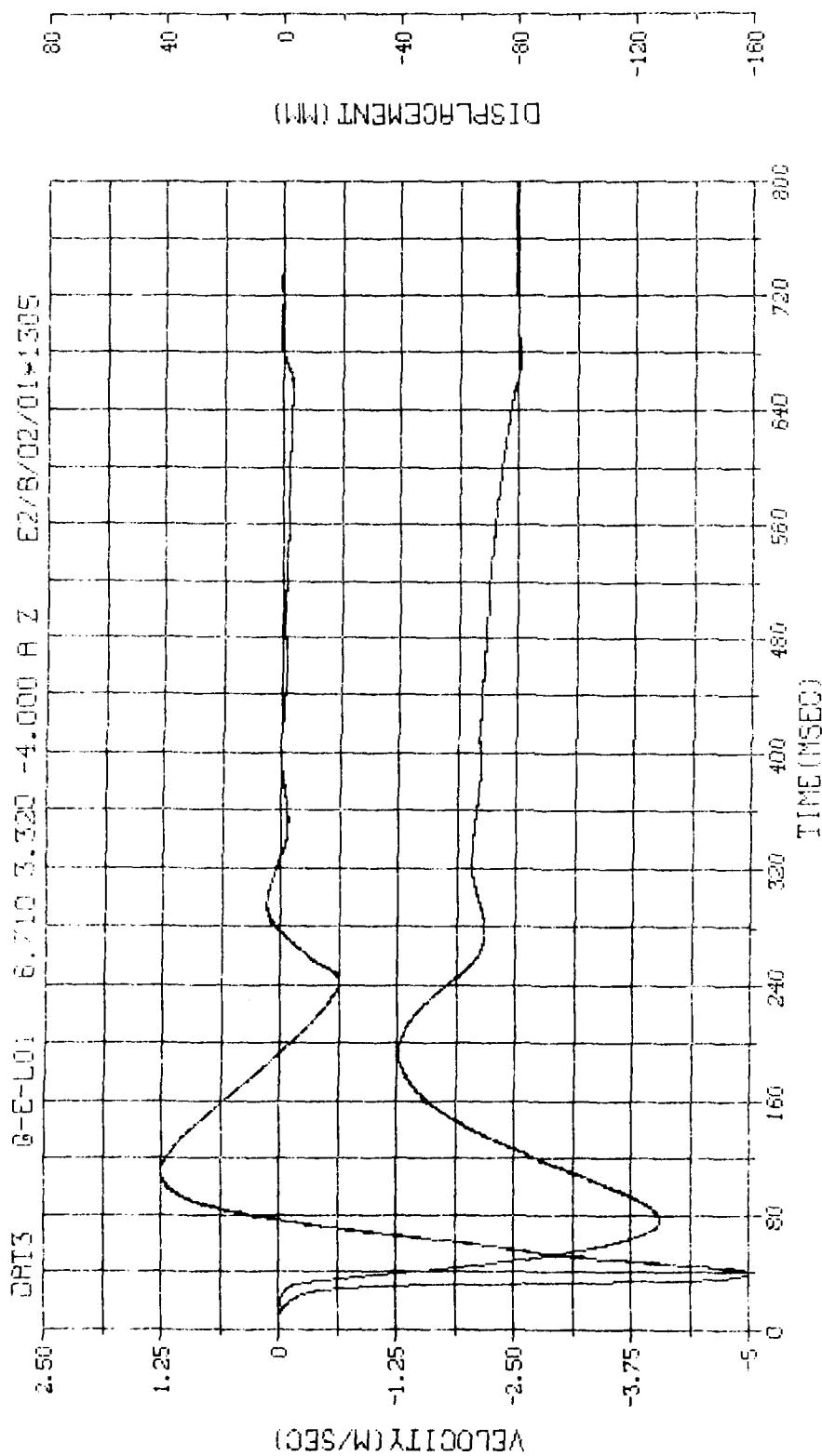




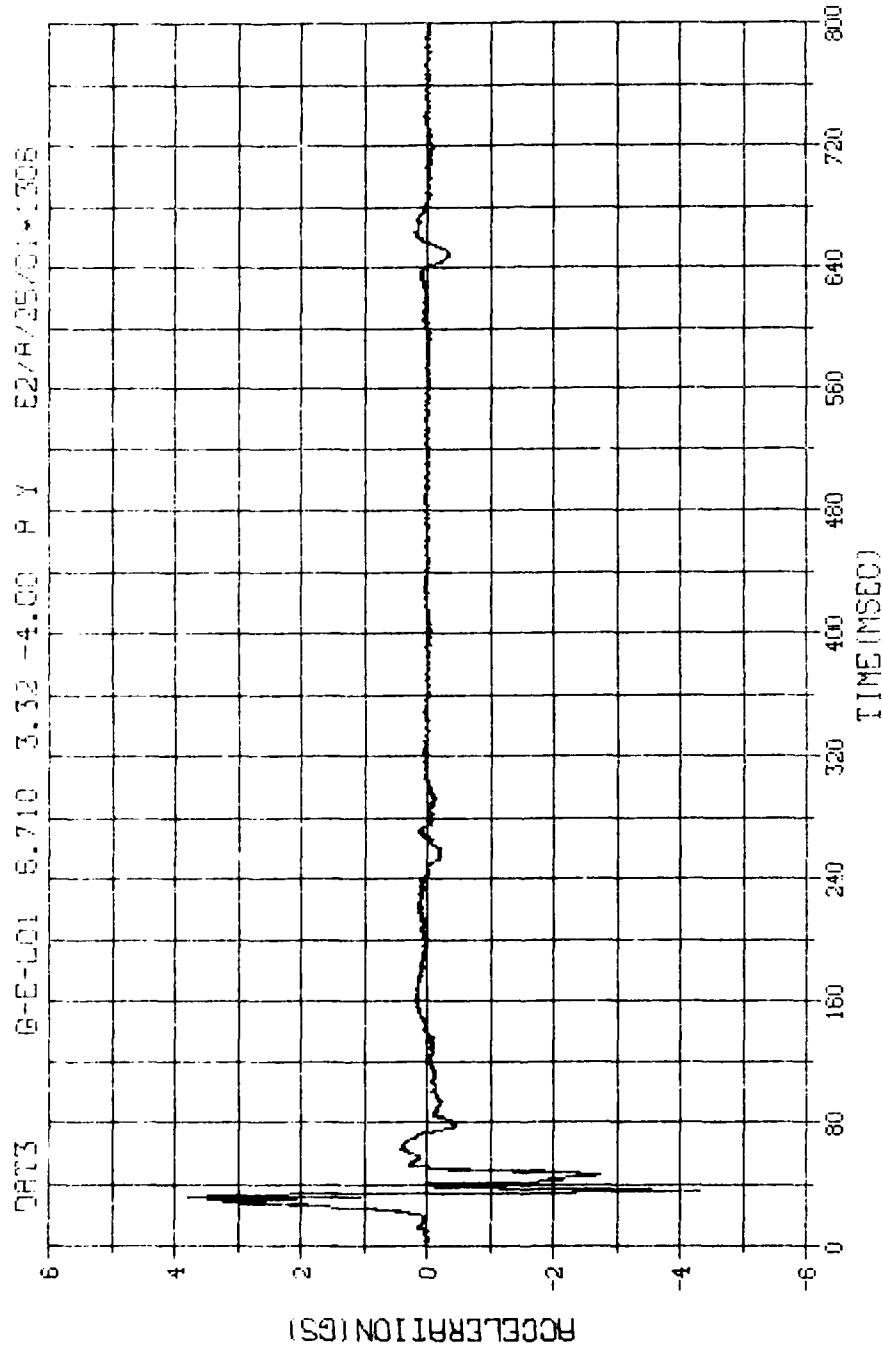
M.N. -91304	E.U. -0.000, 50.000
TSKIP=7.000	DIGITS=0.000, S74.125
S.R. =20.00 KHZ	15 JUN 83 15:20:04
	VSN-F876
	TAPE22
	FILE=0
	1





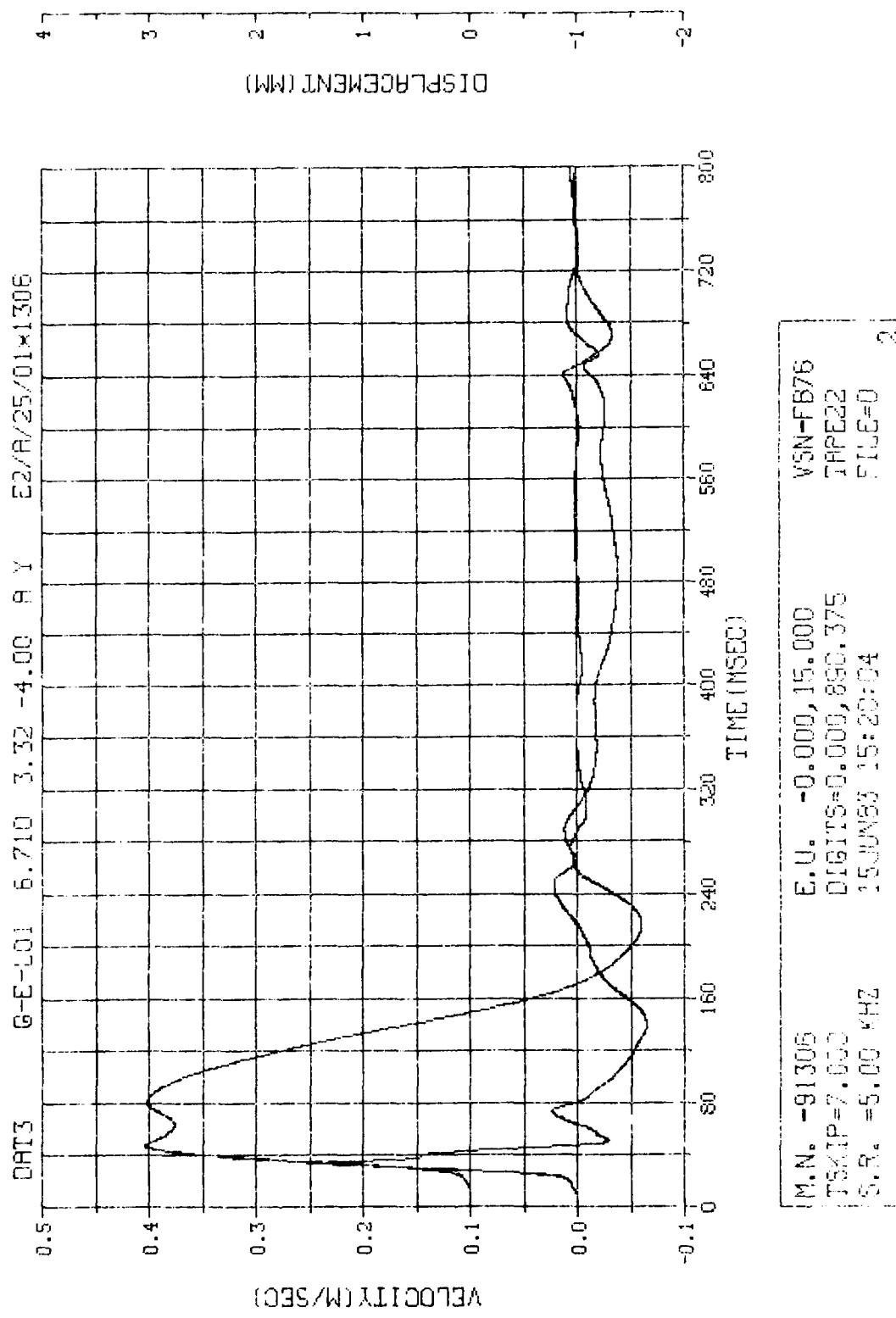


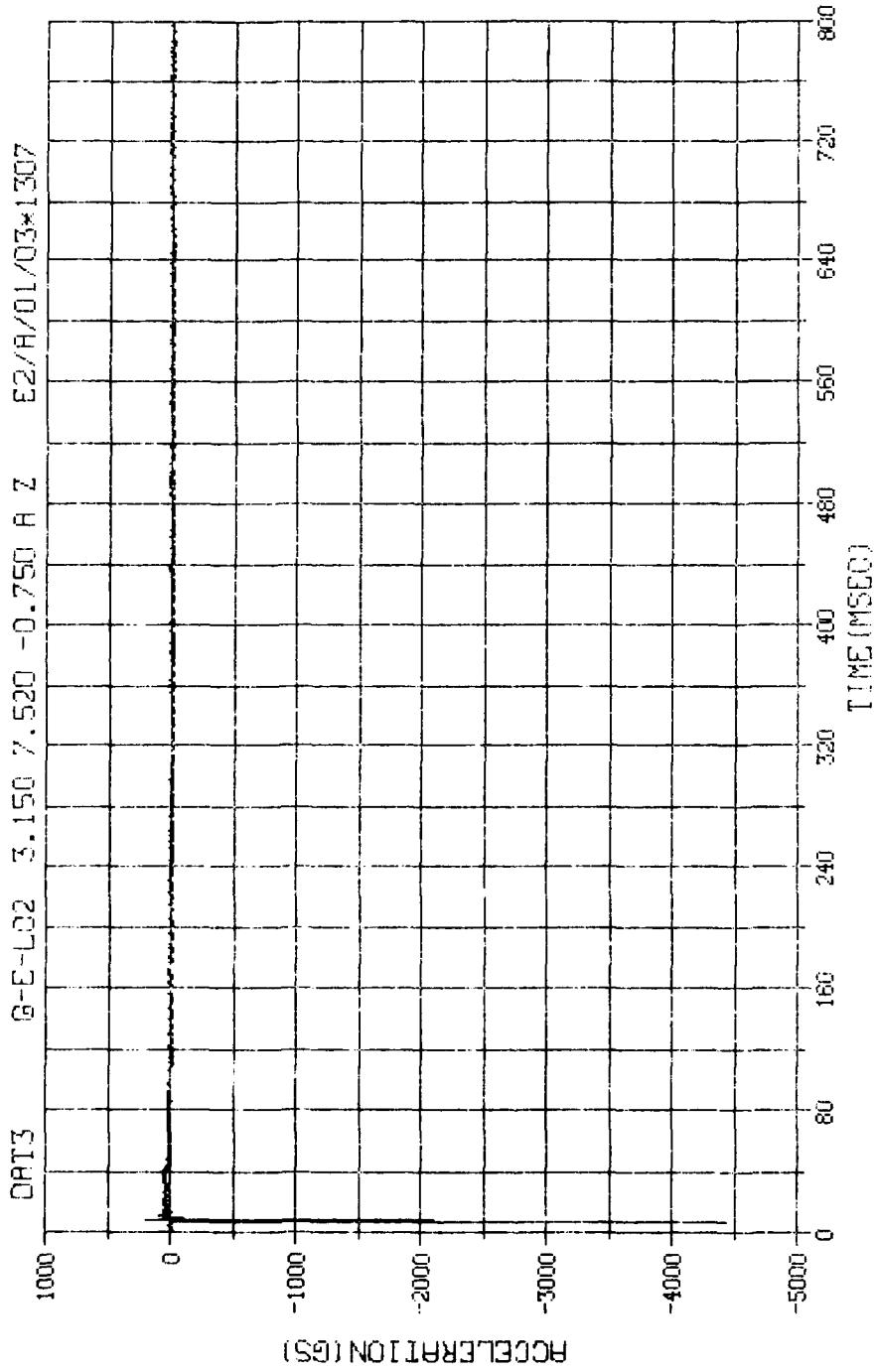
M.N. = 81305	E.U. = -0.000, 45.000	WSN-FB76
TENIP = 7.000	WAVEFORM = 5.000, 888.200	TAPE22
G.R. = 13.00	15-JUN-93 15:25:04	FIL 5=2



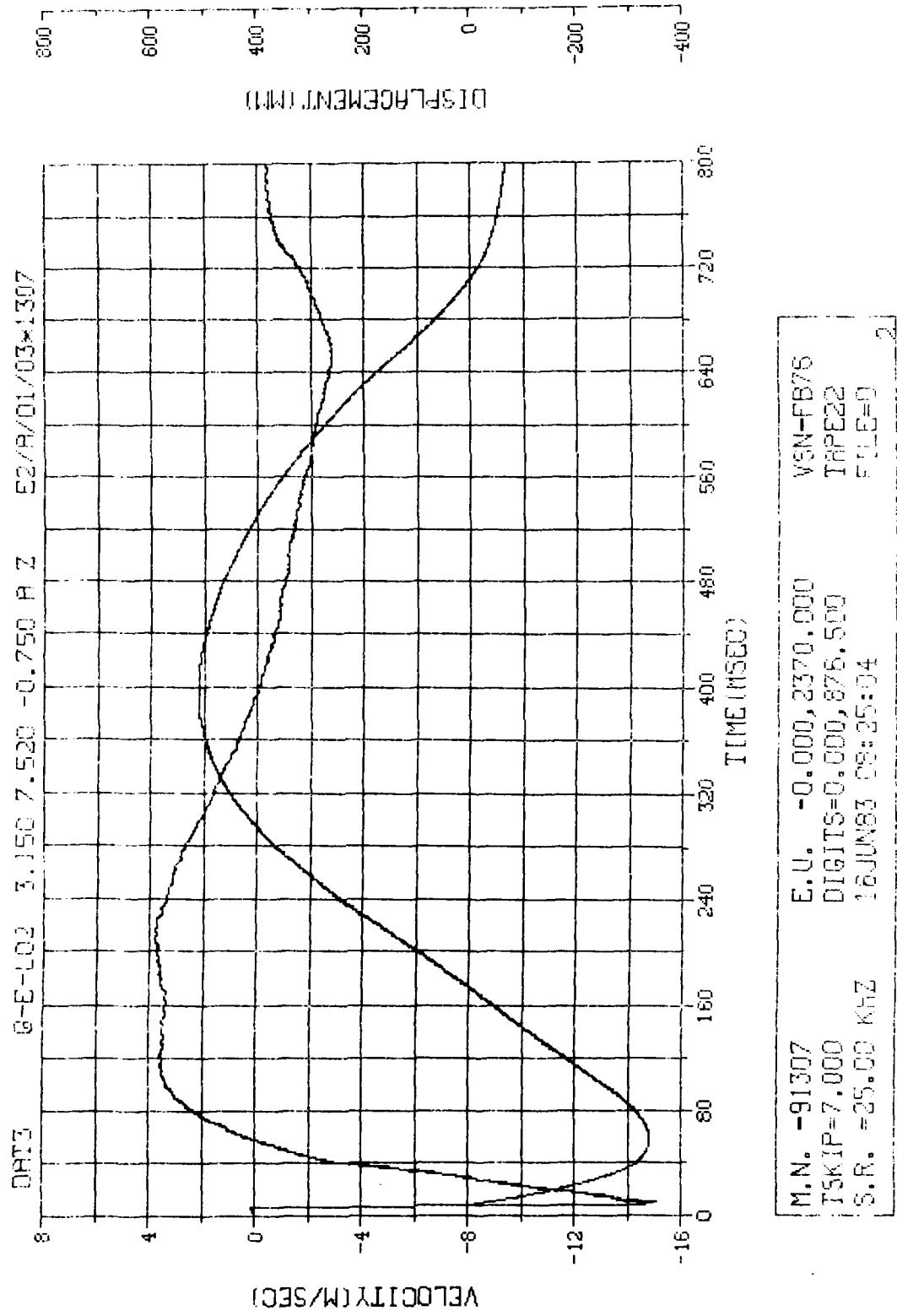
M.N.	-91306	E.U.	-0.000, 15.000
TSKTP	=7.000	DATAFS	=0.000, 890, 375
S.R.	=1.00 KHZ	TAPE22	
		FILE=0	
			1

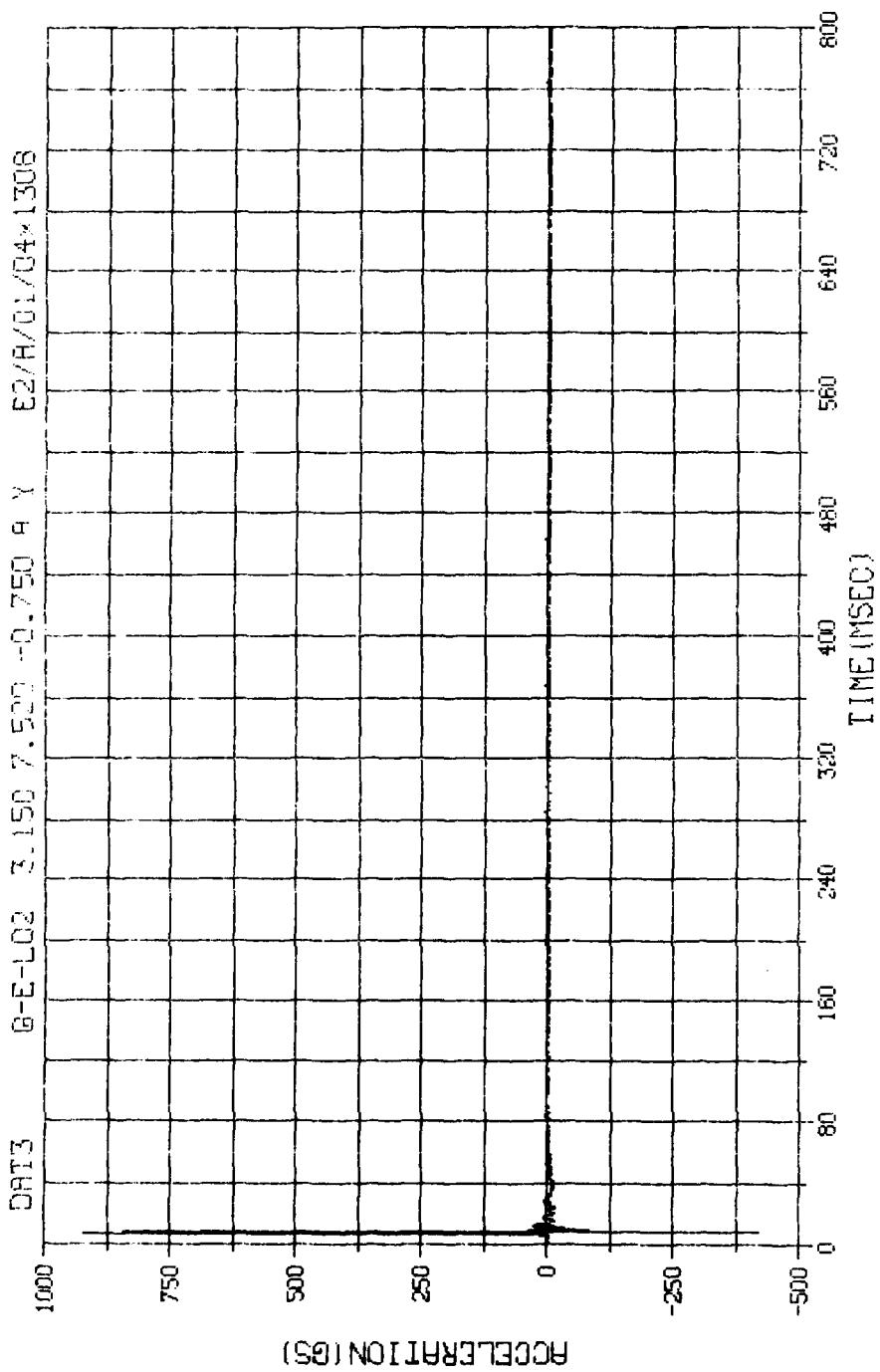
15-JUN-83 15:20:04



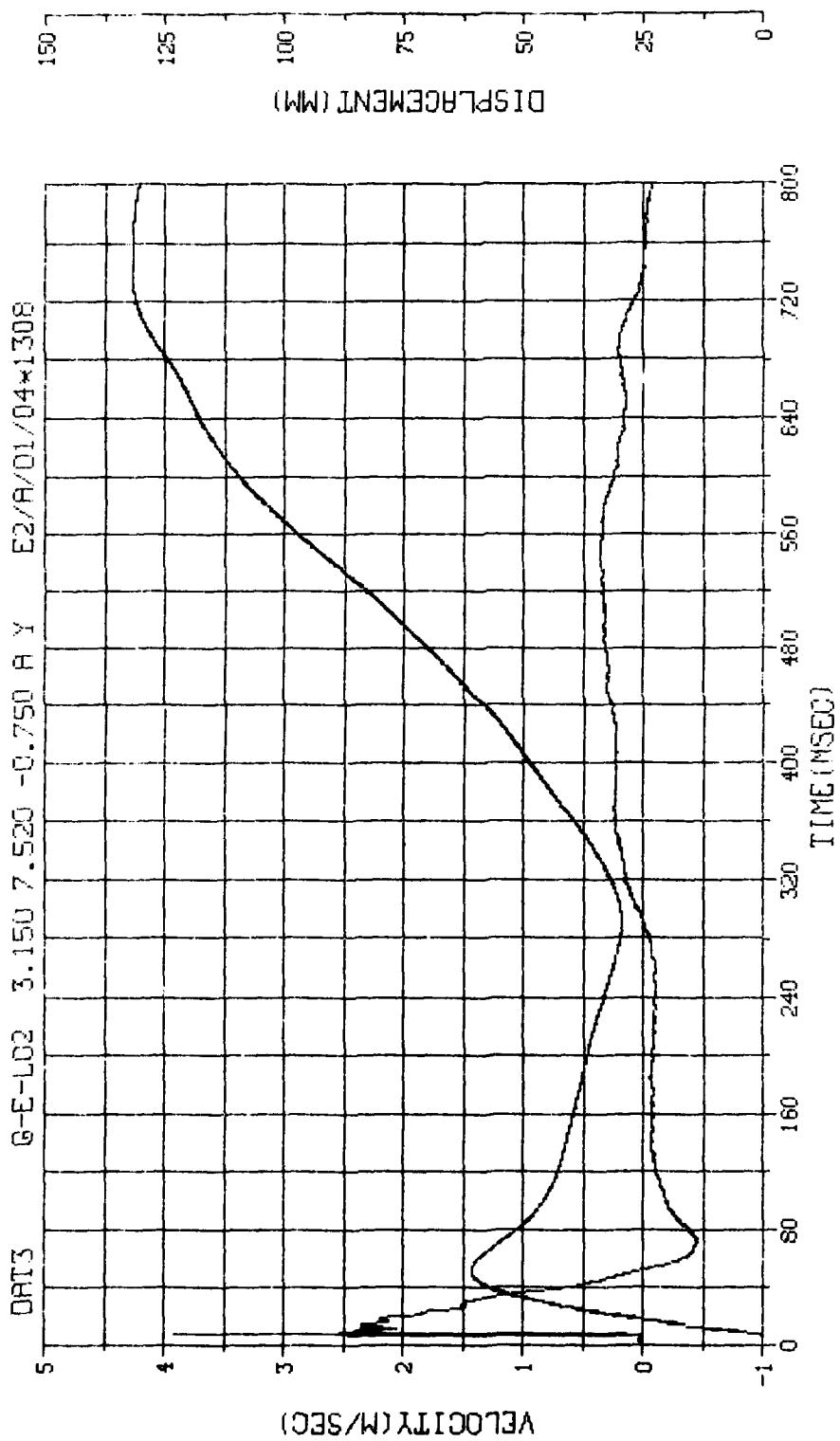


H.N. -91307	E.U. -0.000, 2370.000	VSN-FB76
TSKIP=7.000	DIGITS=0.000, 876.500	TRPS22
S.R. =25.00 KHZ	16 JUN 23 08:25:04	FILE=0
		1

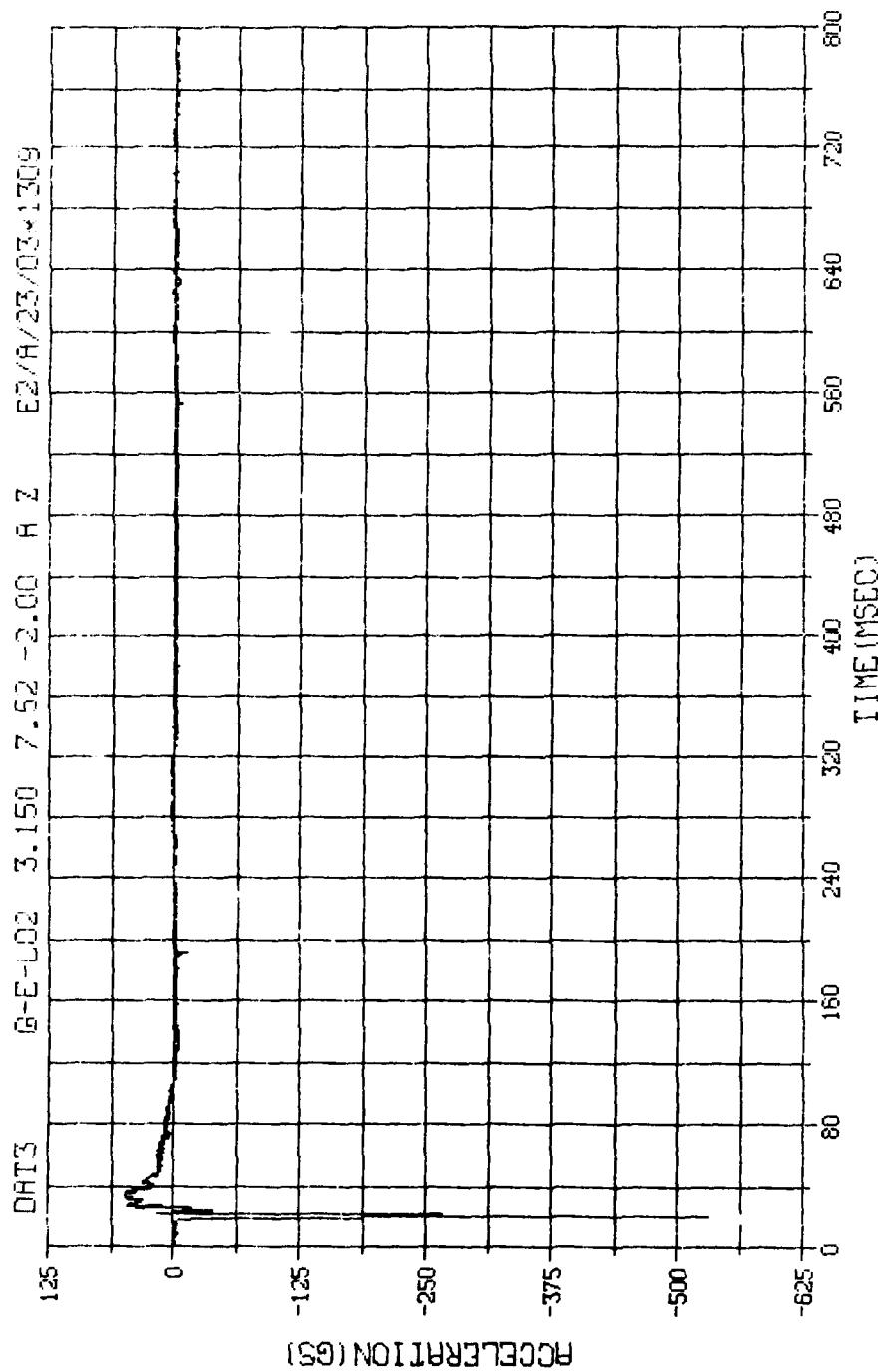




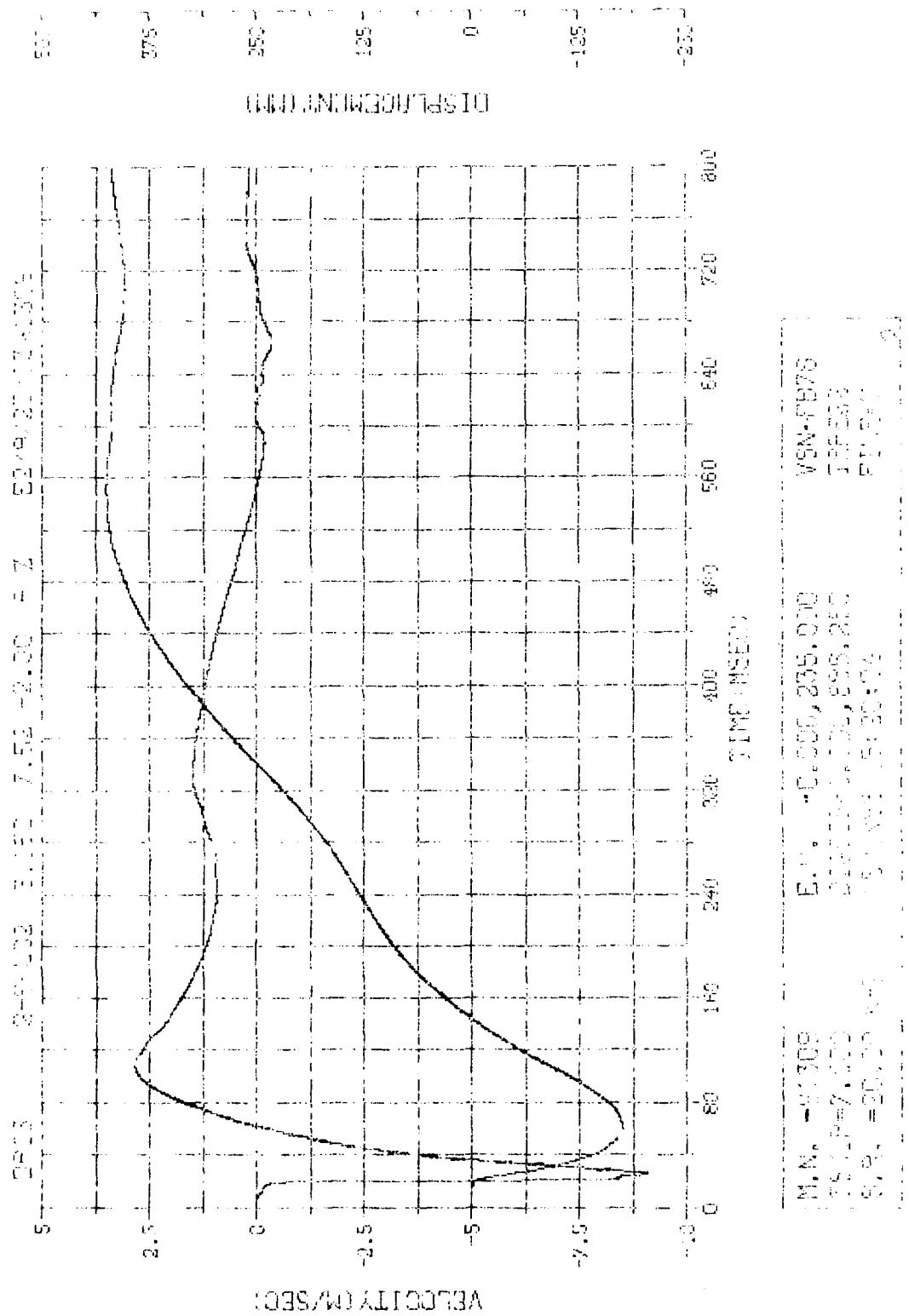
R.N.	-91308	E.U.	-0.000, 450.000
TSKIP	=7.000	DIGITS	=0.000, 868.000
S.R.	=25.00	TRAPEZ	
		FILE	=0

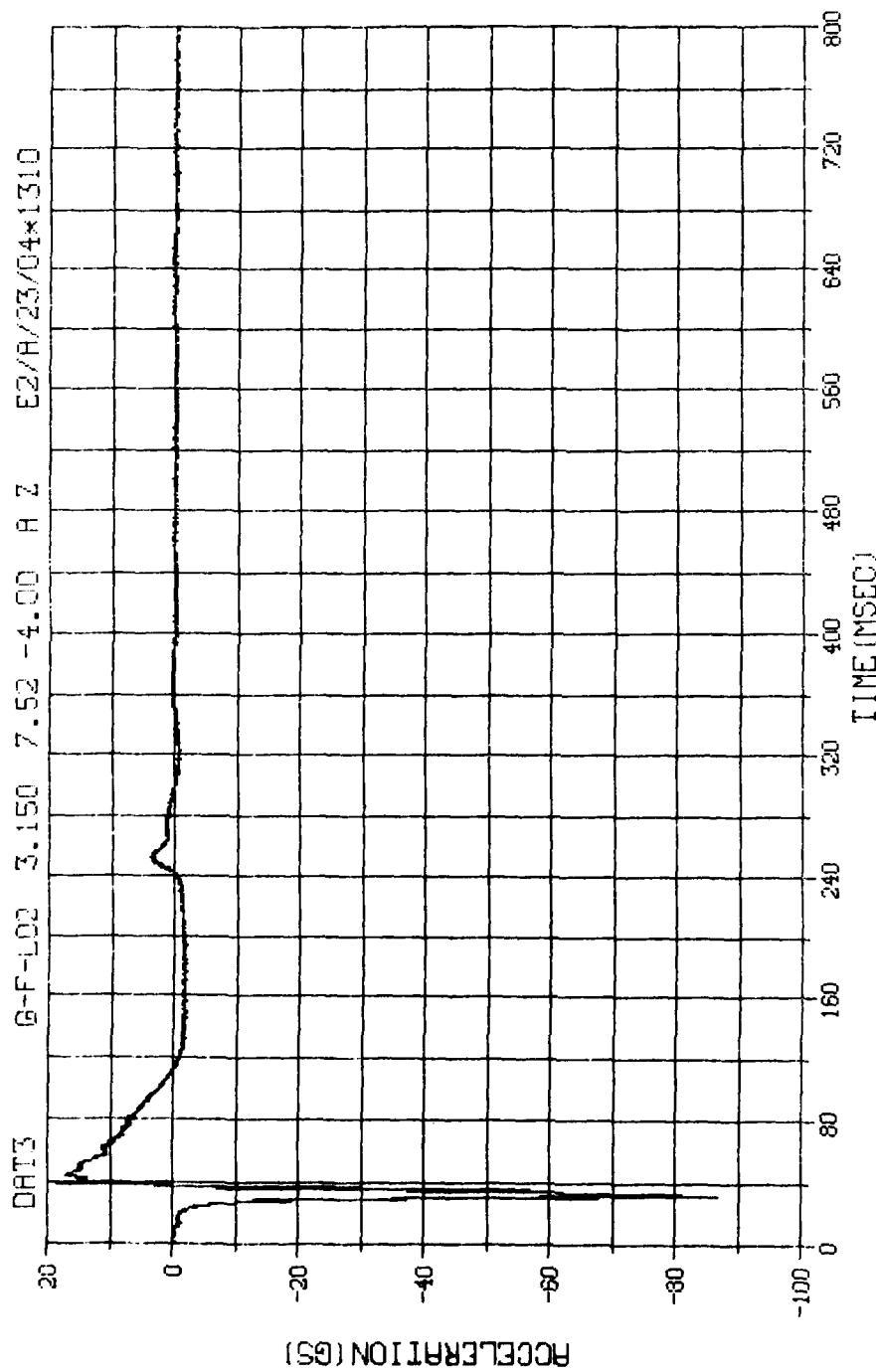


M. N. -91308	E.U. -0.000, 450.000
TSKIP=7.000	DIGITS=0.000, 868.000
S.R. =25.00 KHZ	TAPE22
	FILE=0 2
VSN-FB76	
16 JUN 63 06:25:04	

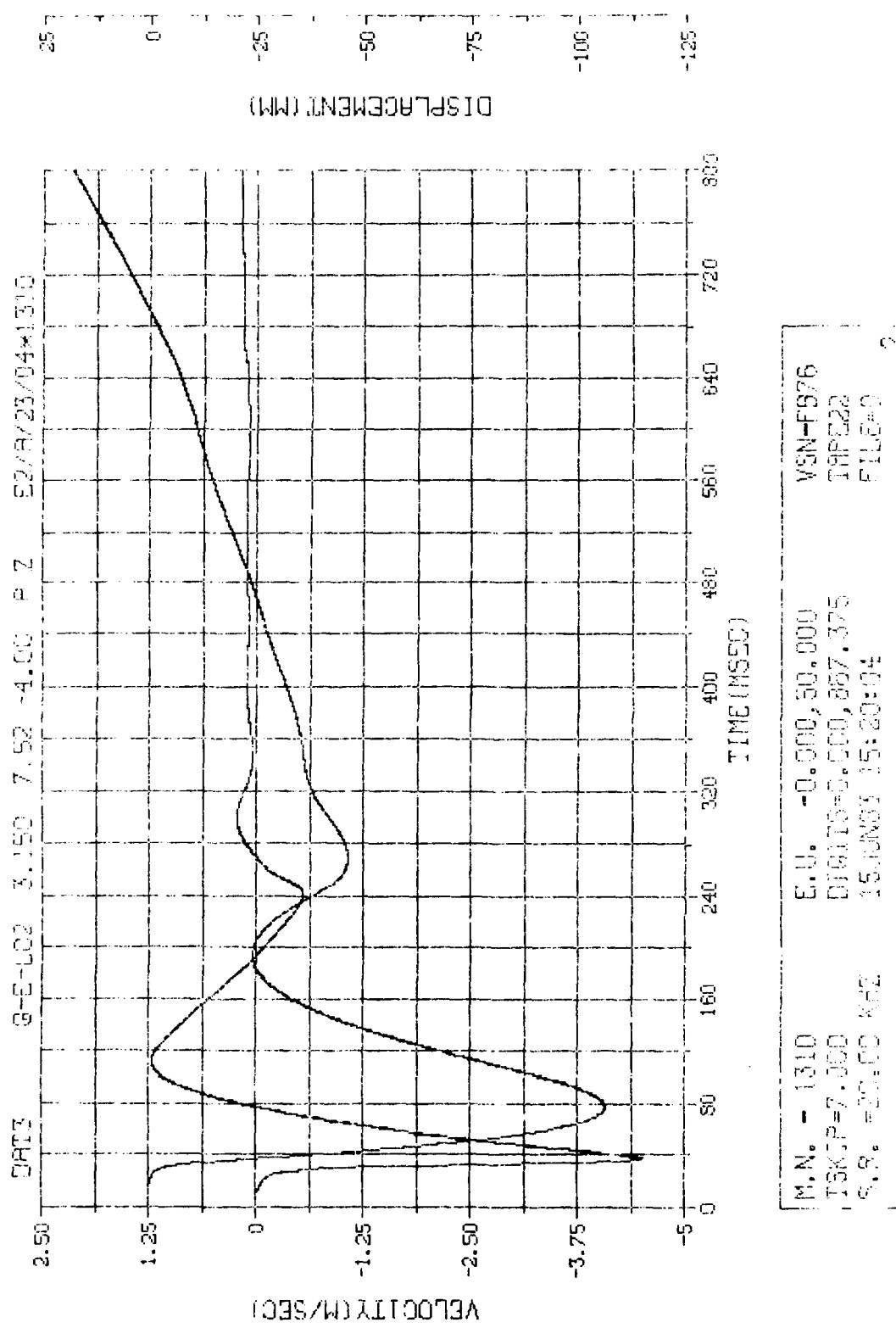


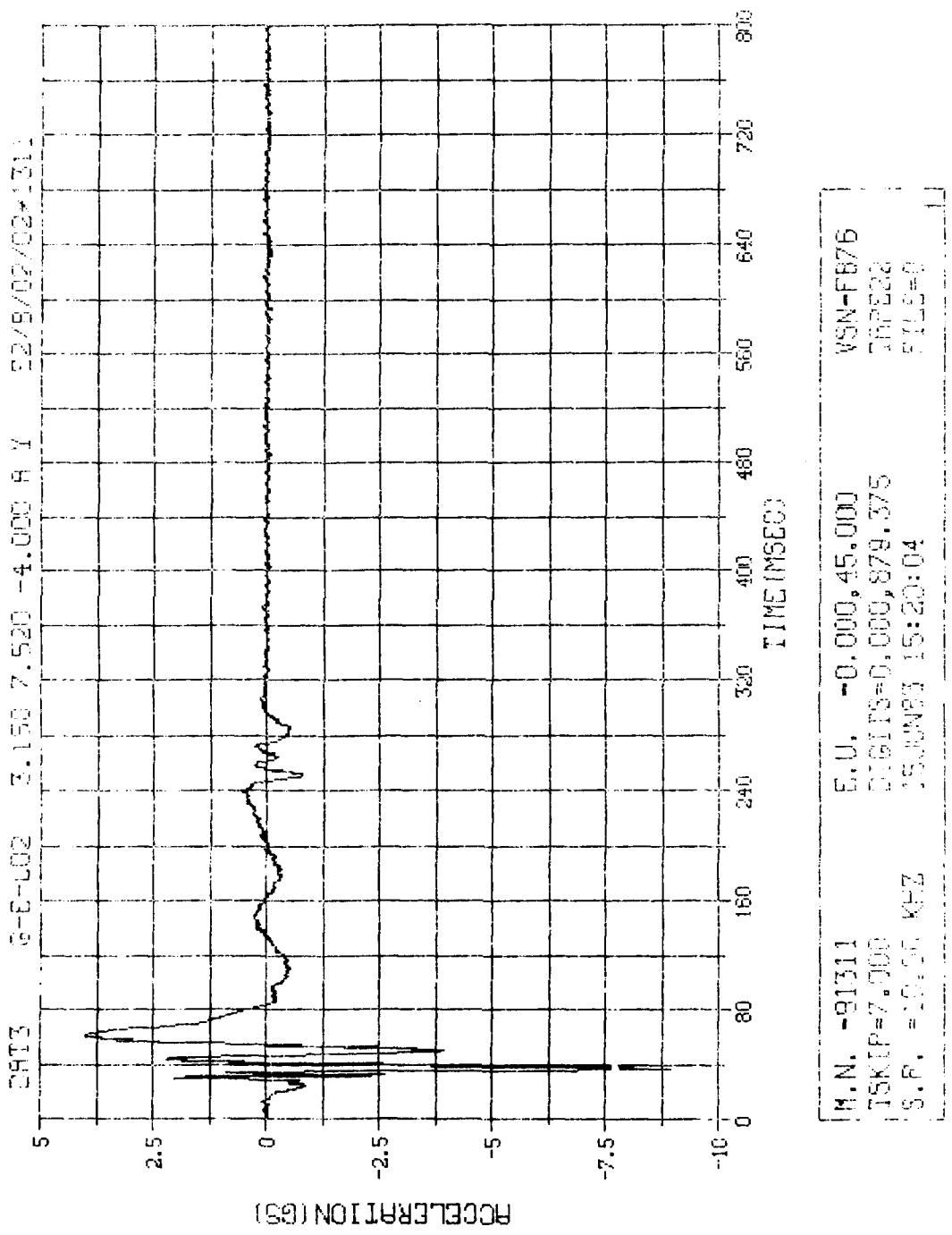
M.N. -91309	E.U. -0.000,235.000	VSN-F876
SKIP=7.000	DIGITS=0.000,886,250	TAPE22
S.R. =20.00 KHZ	15JUN83 15:20:04	FILE=0

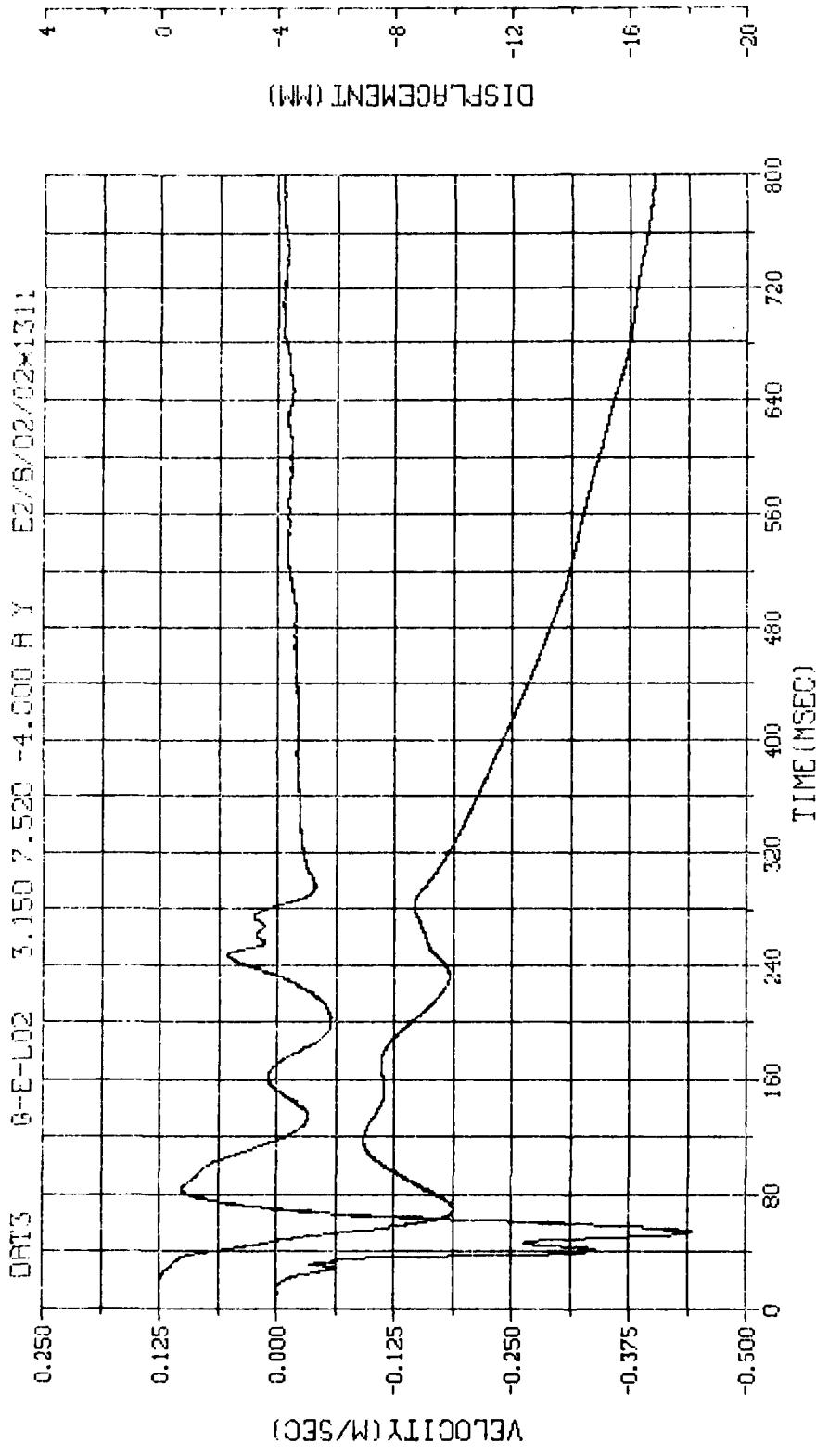




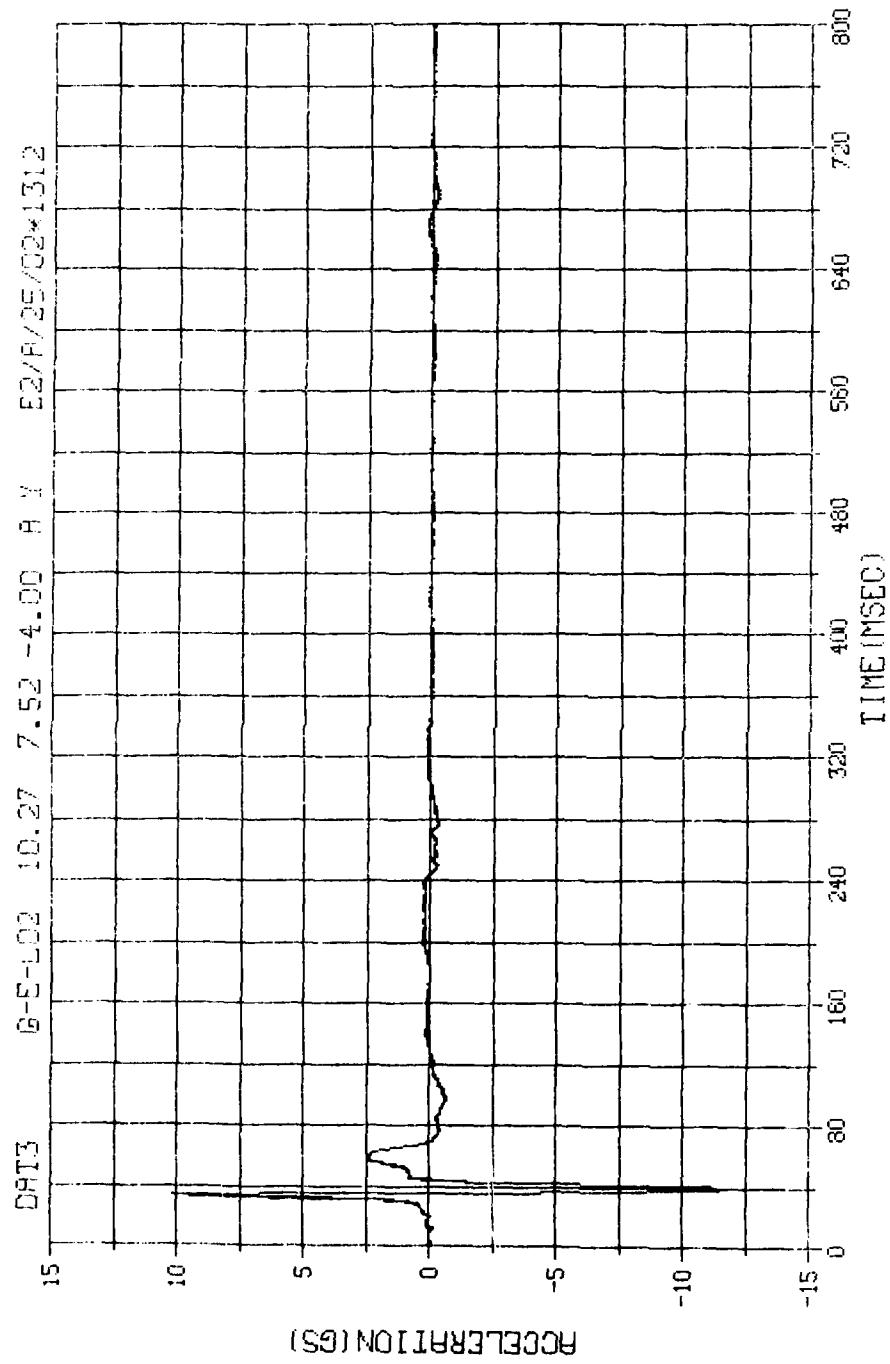
M.N. - 1310	E.U. -0.000,50.000	VSN-FB76
SKIP=7.000	DIGITS=0.000,867.375	TAPE22
S.R. =20.00 KHZ	15 JUNE 83 15:20:04	FILE=0 1

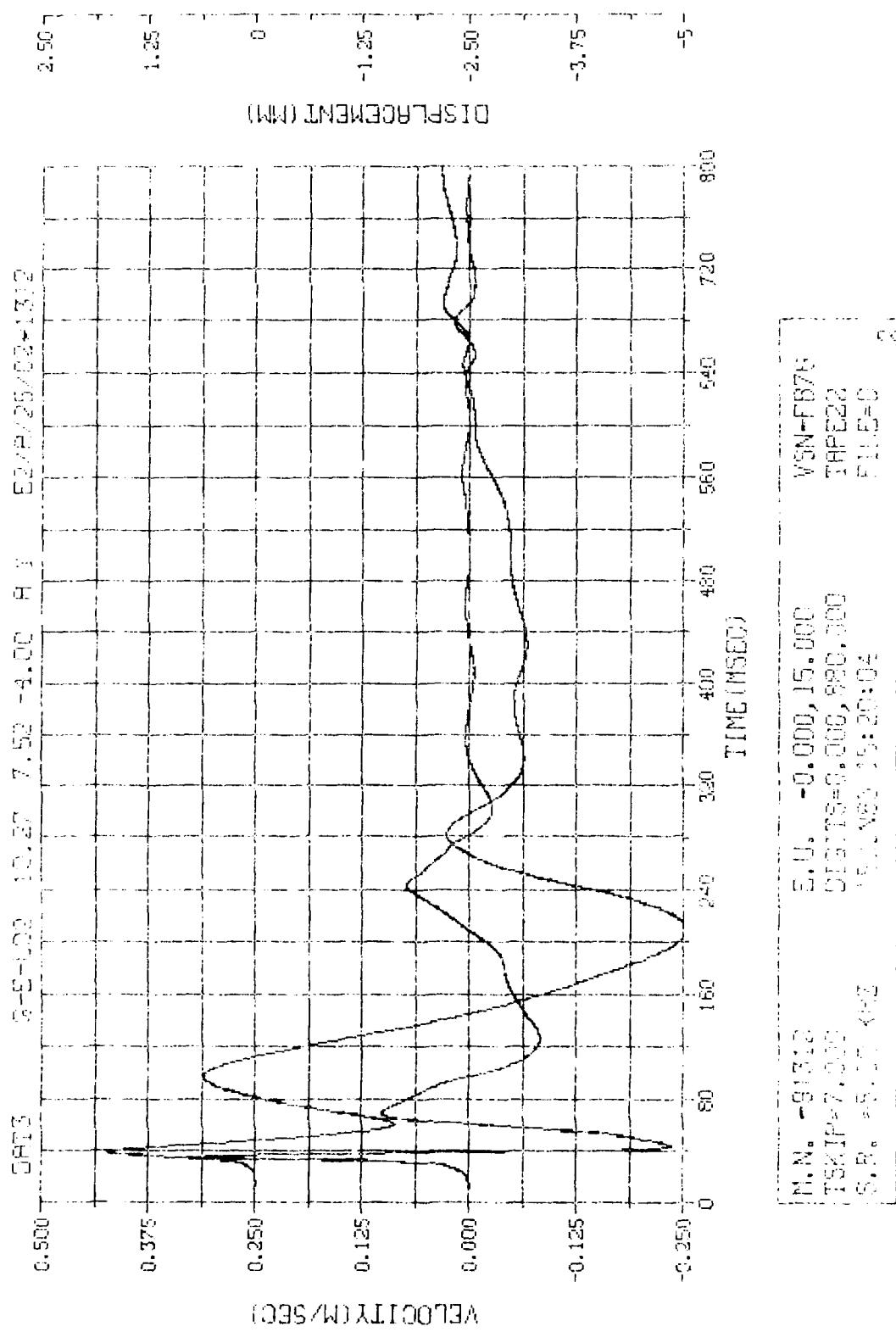






M.N. -91311	E.U. -0.000,45.000	VSN-FB76
TSKIP=7.000	DIGITS=0.000,879.375	TAPE22
S.R. =10.00 KHZ	15JUN83 15:20:54	FILE=0
		21





AD-A171 212

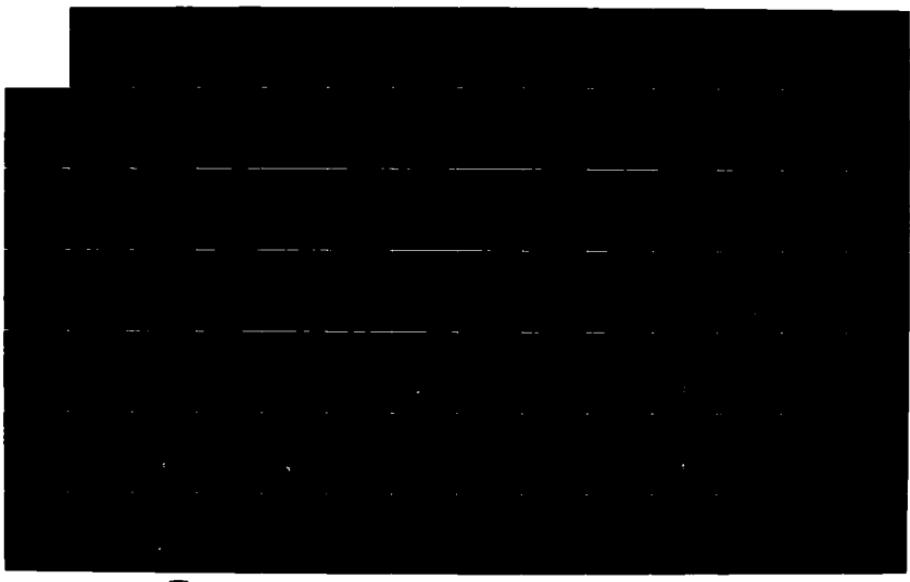
KACHINA TEST SERIES: DYNAMIC ARCH TEST THREE (DAT-3)
ANALYSIS REPORT(U) AIR FORCE WEAPONS LAB KIRTLAND AFB
NM J L SMITH ET AL. MAR 86 AFWL-TR-85-63

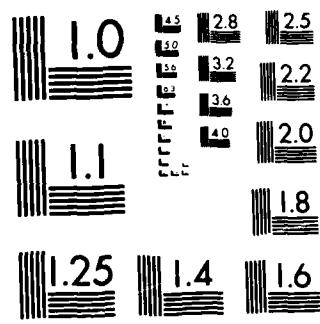
4/6

UNCLASSIFIED

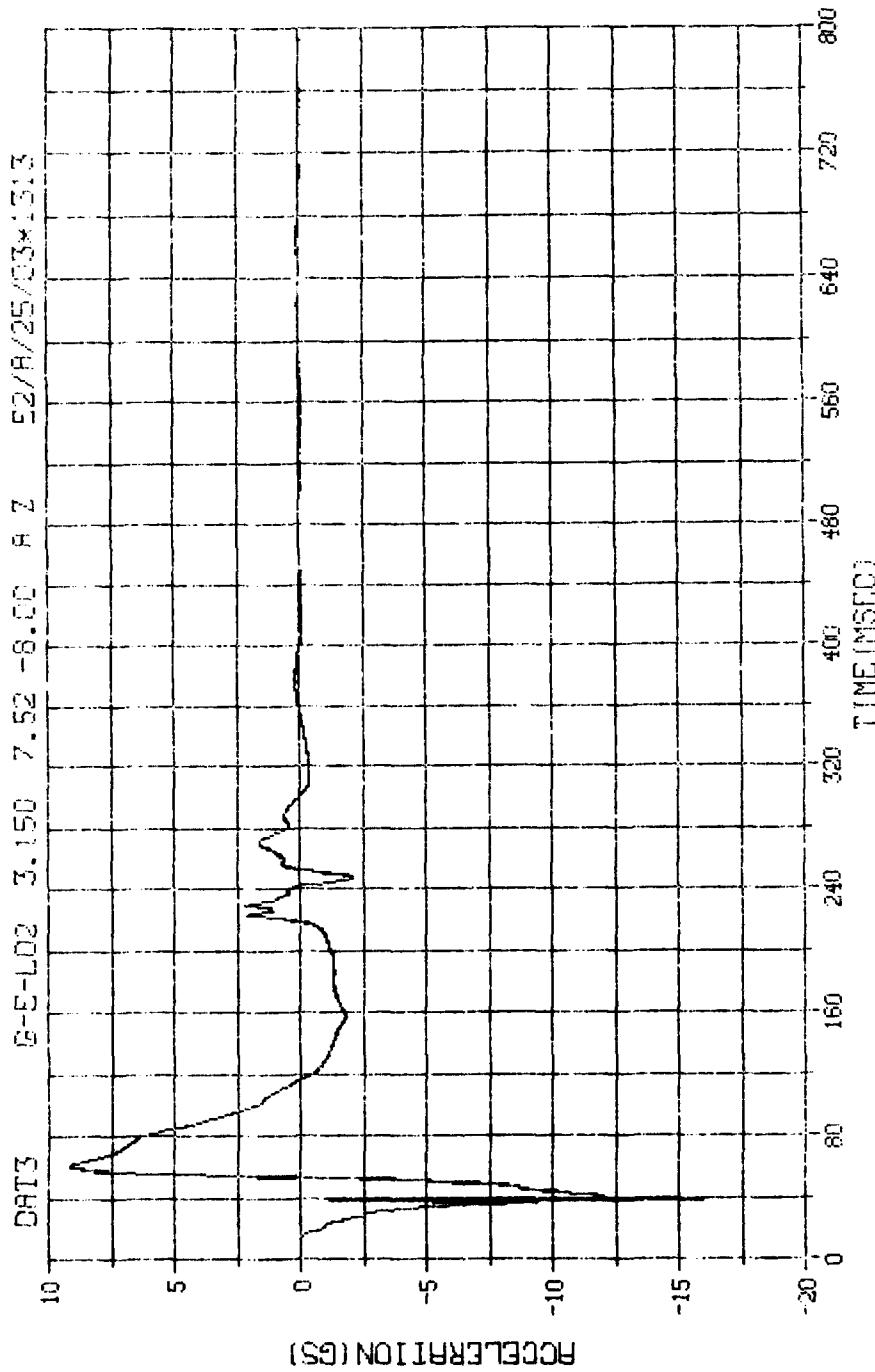
F/G 19/4

NL

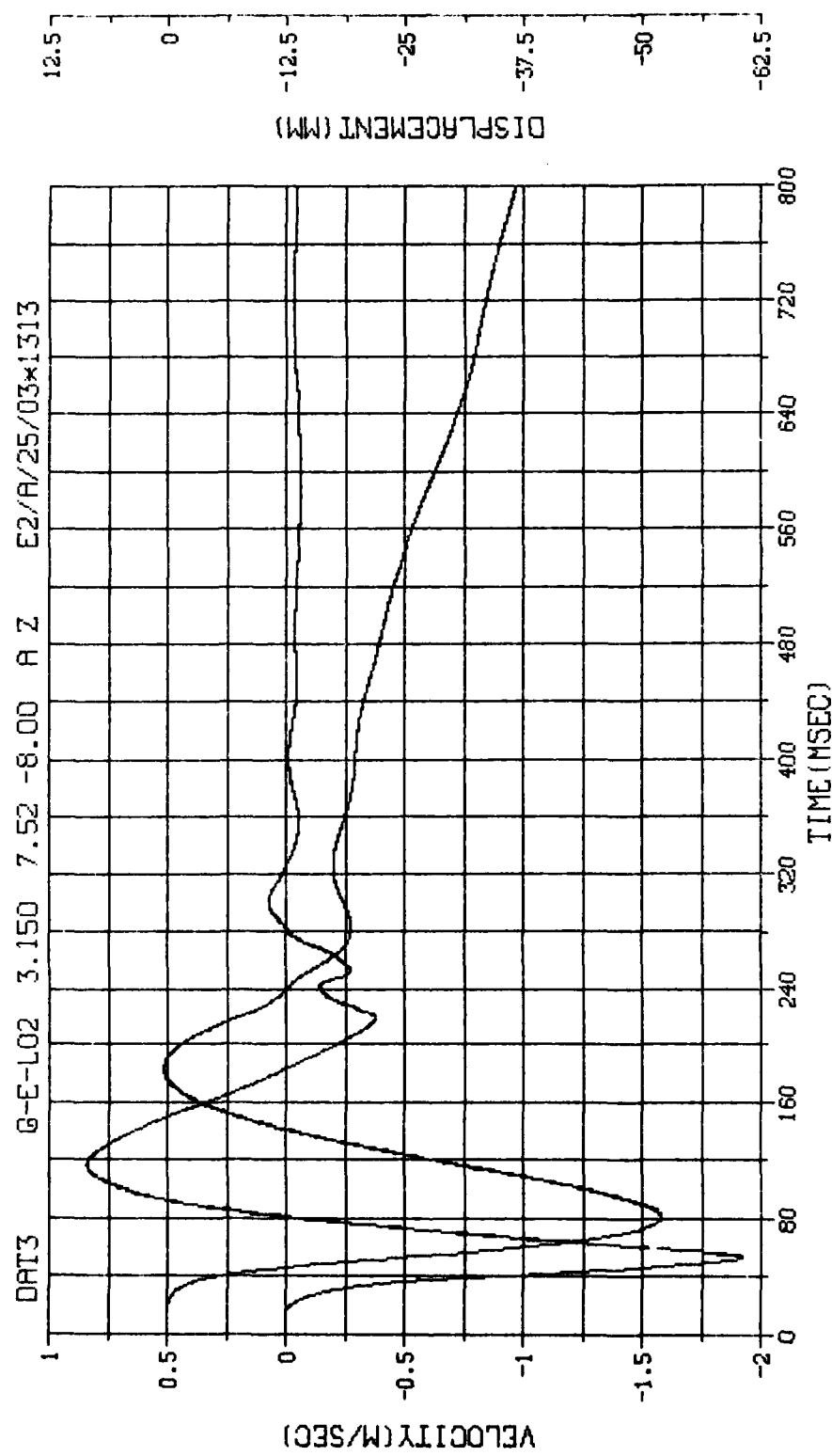




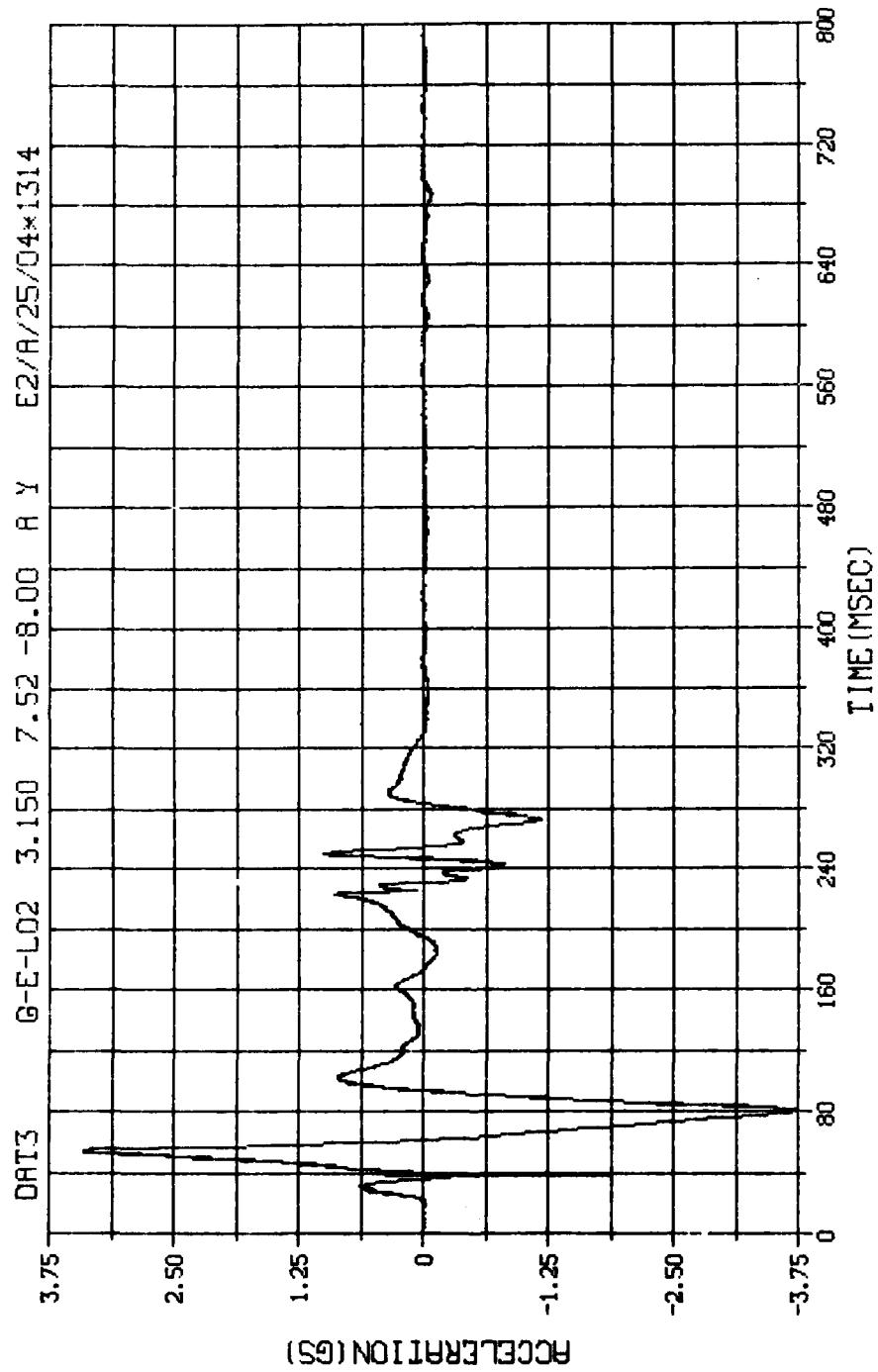
MICROCOPY RESOLUTION TEST CHART
NATIONAL BUREAU OF STANDARDS-1963-A



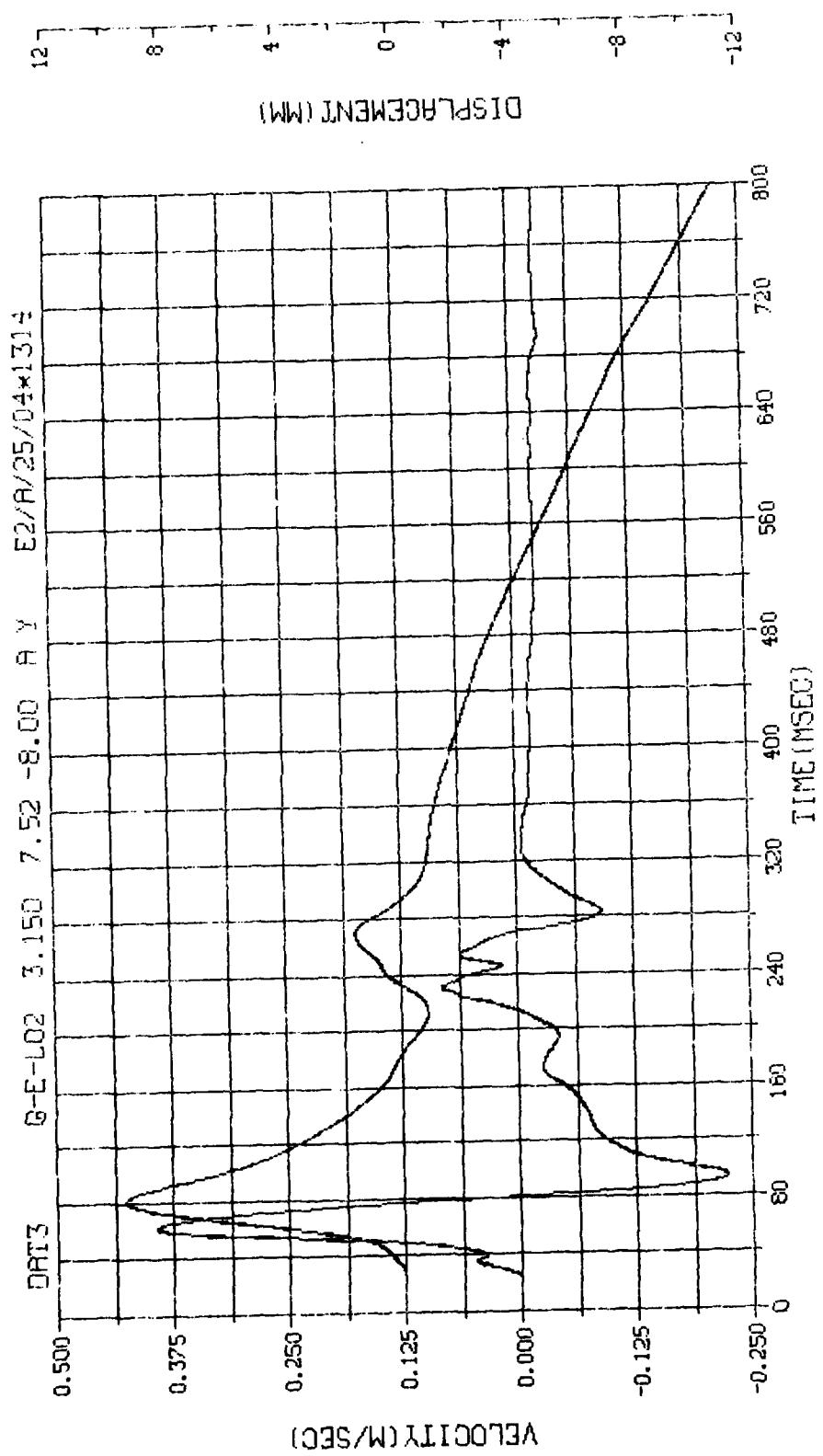
M.N. - 1313	E.U. -0.000, 9.000	VSN-FB76
SKIP=7.000	DIGITS=0.000,882.125	TRIG22
S.R. = 5.000	ISDNG3 15:23:54	P115=0



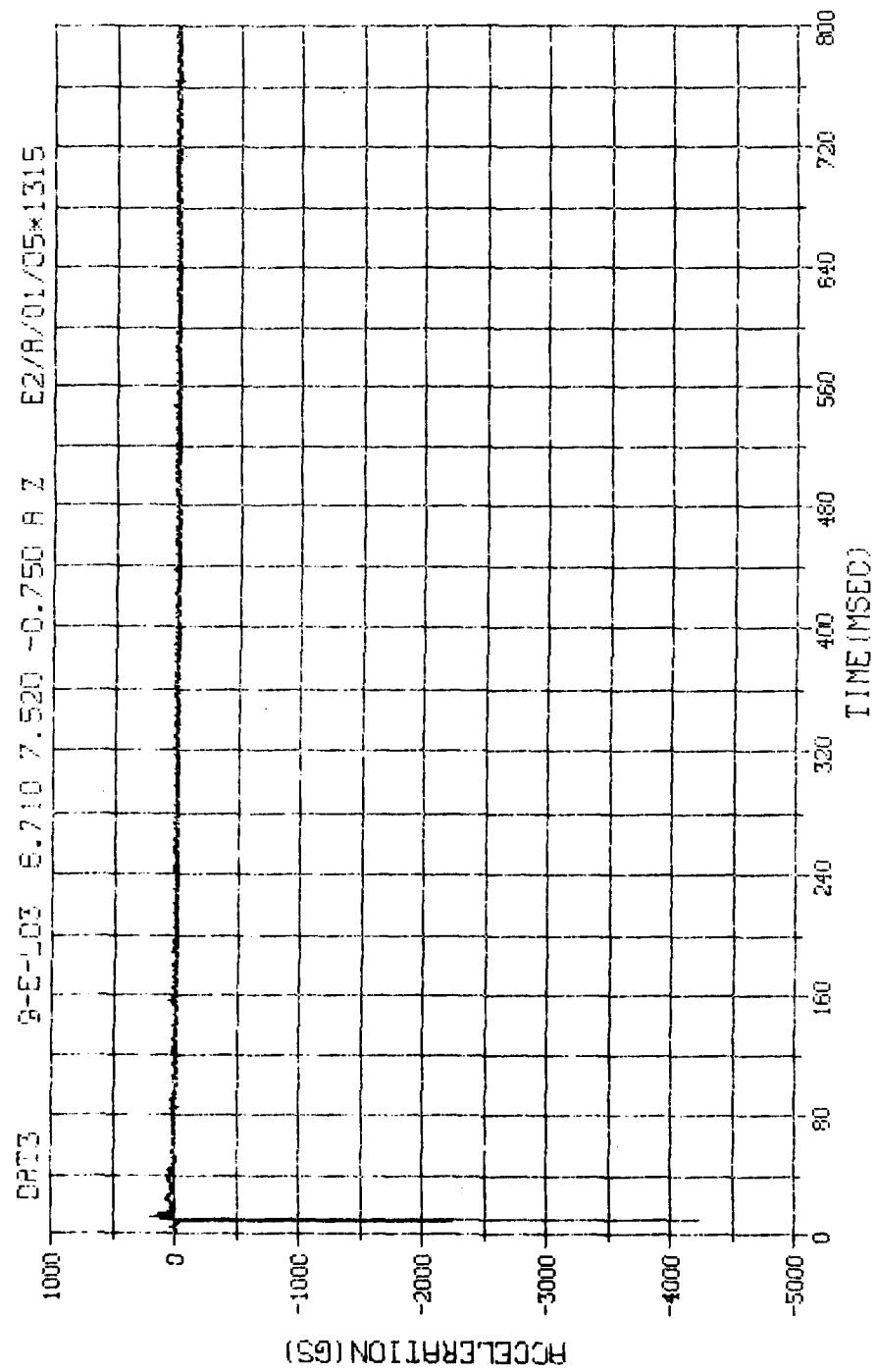
M. N. = 1313	E. U. = -0.000, 9.000	YSN-FB76
TSKIP=7.000	DIGITS=0.000, 882, 125	TAPE22
S.R. =5.00 KHZ	15JUN83 15:20:04	FILE=0
		2



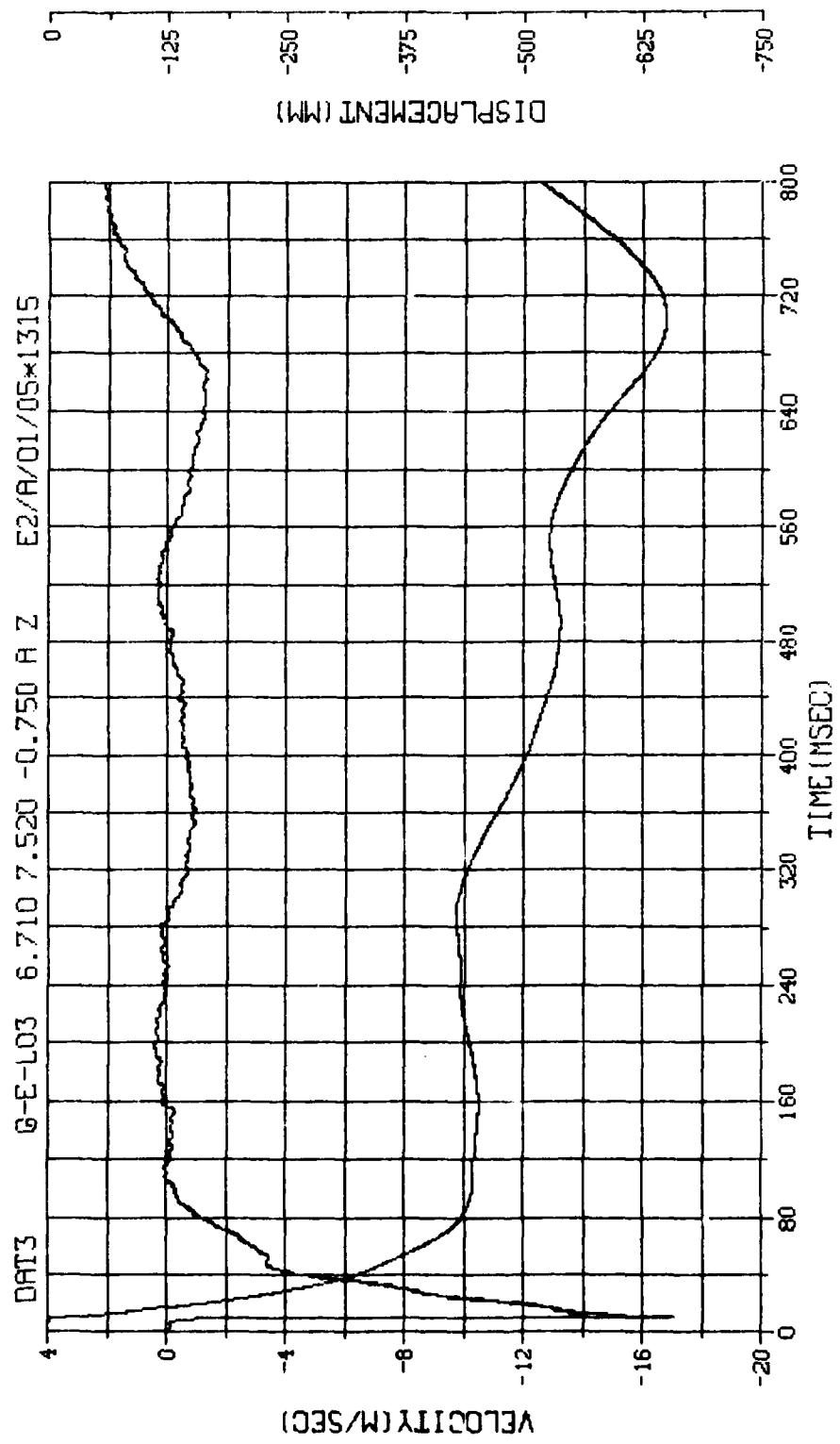
M.N. -71314	E.U. -0.000,4.000	VSN-FB76
SKIP=7.000	DIGITS=0.000,871.875	TAPE22
S.R. =5.00 KHZ	15JUN83 15:20:04	FILE=0
		1



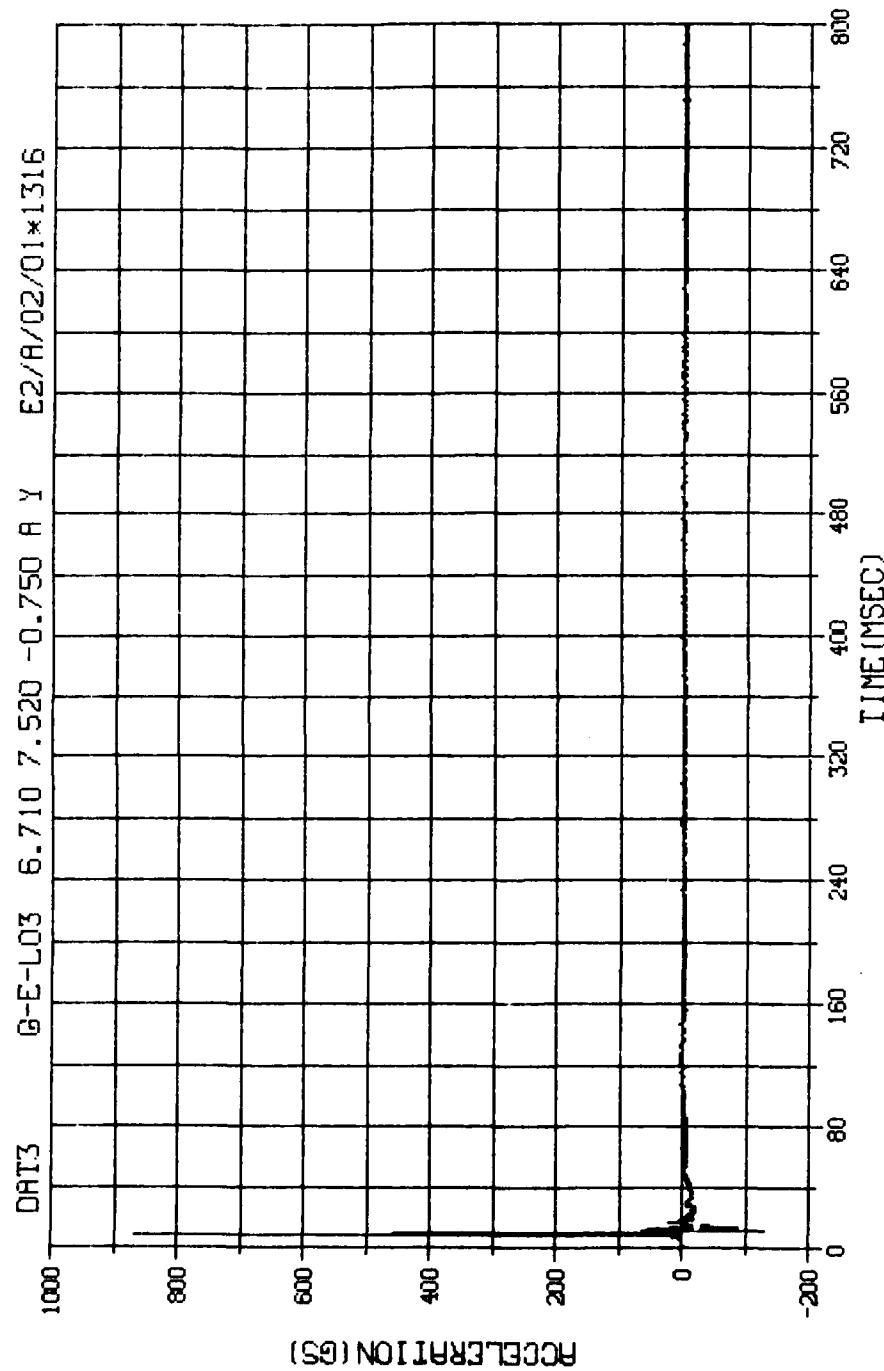
M. N.	-71314	E.U.	-0.000, 4.000
TSKIP	=7.000	DIGITS	=0.000, 871, 875
S.R.	=5.00 KHZ	TAPE22	
		FILE=0	2



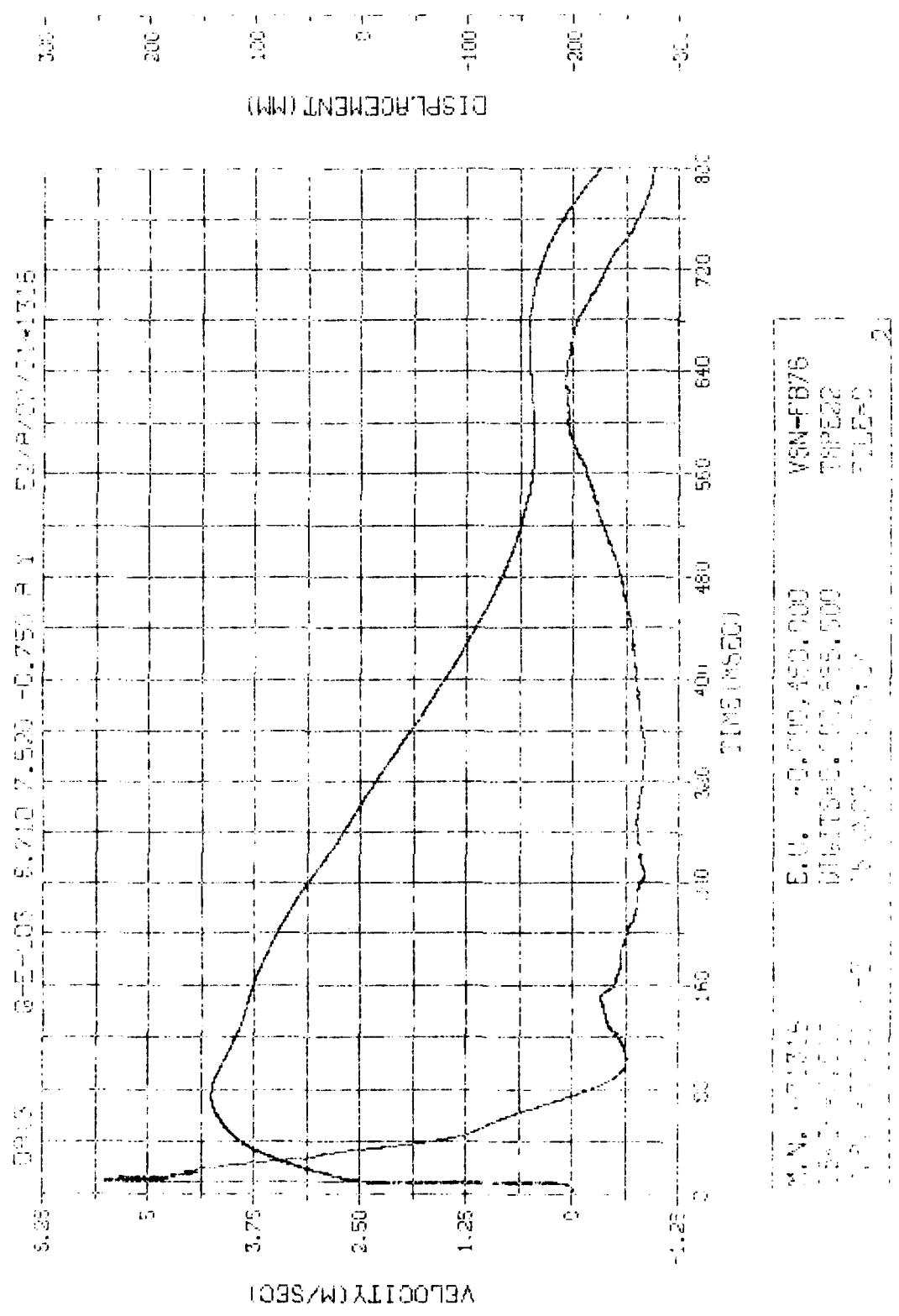
N.N. -91315	E.U. -0.000, 2370.000	VSN-FB76
TSKIP=7.000	SIGITS=0.000, 901.125	TRAPEZ2
S.R. = 25.00 kHz	16JUN83 08:25:04	FILE=0

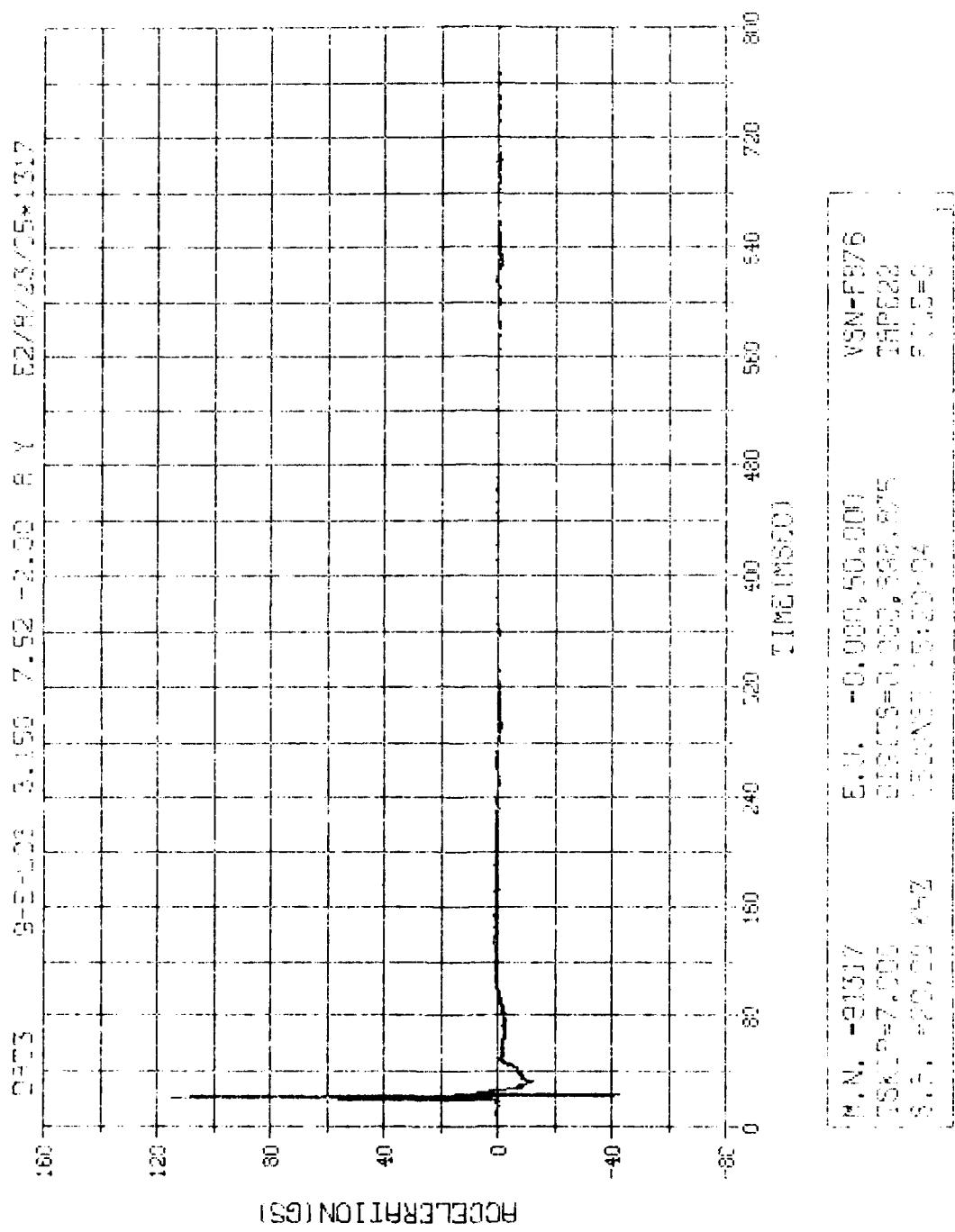


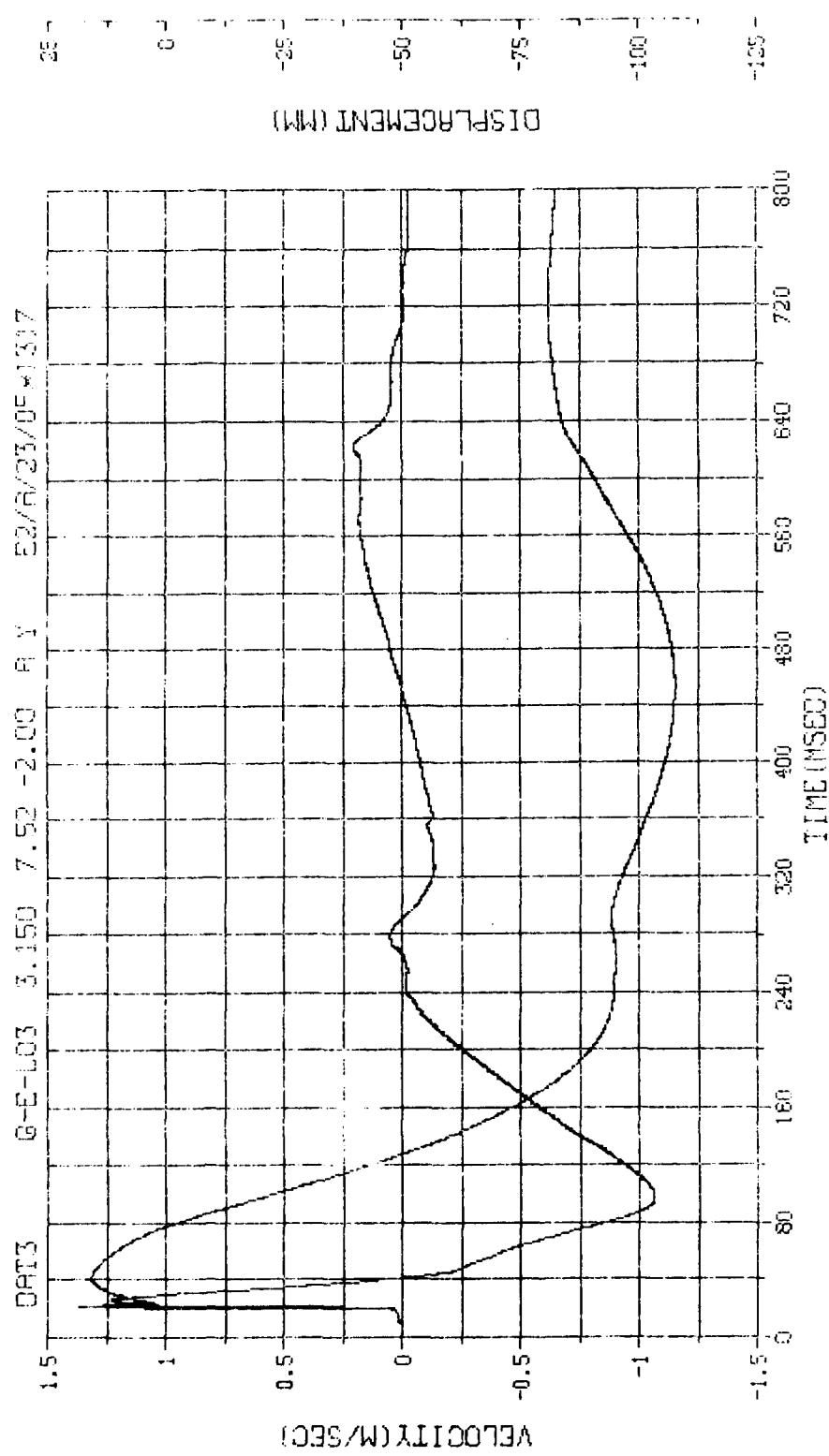
M.N.	-91315	E.U.	-0.000, 2370.000	VSN-FB76
TSKIP	=7.000	DIGITS	=0.000, 901.125	TPPE22
S.R.	=25.00 KHZ		16 JUN 83 08:25:04	FILE=D
				2



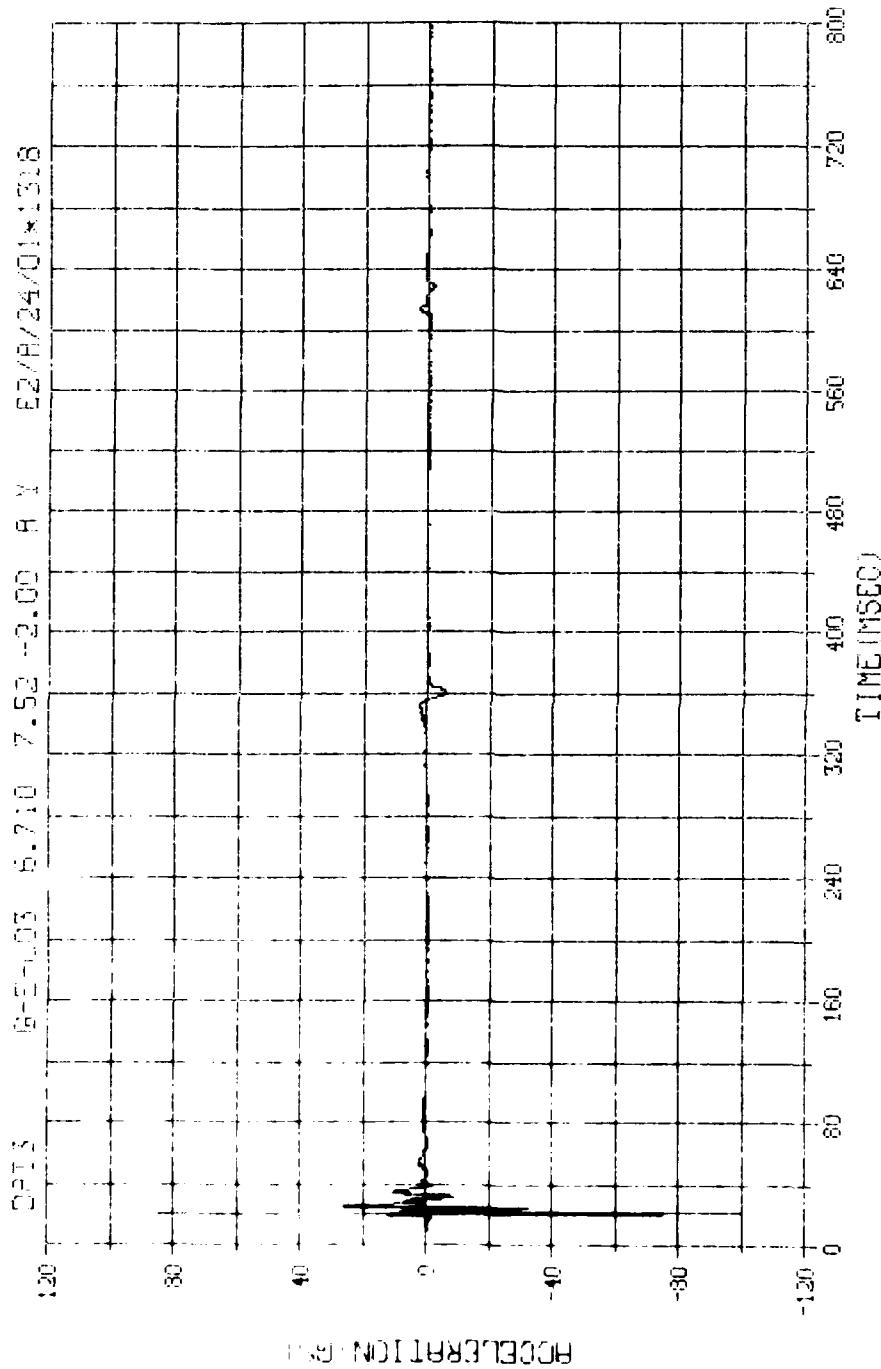
M.N. -71316	E.U. -0.000,450.000	VSN-FB76
SKIP=7.000	DIGITS=0.000,885.500	TAPE22
S.R. =25.00 KHZ	15JUN83 15:20:04	FILE=0
1		



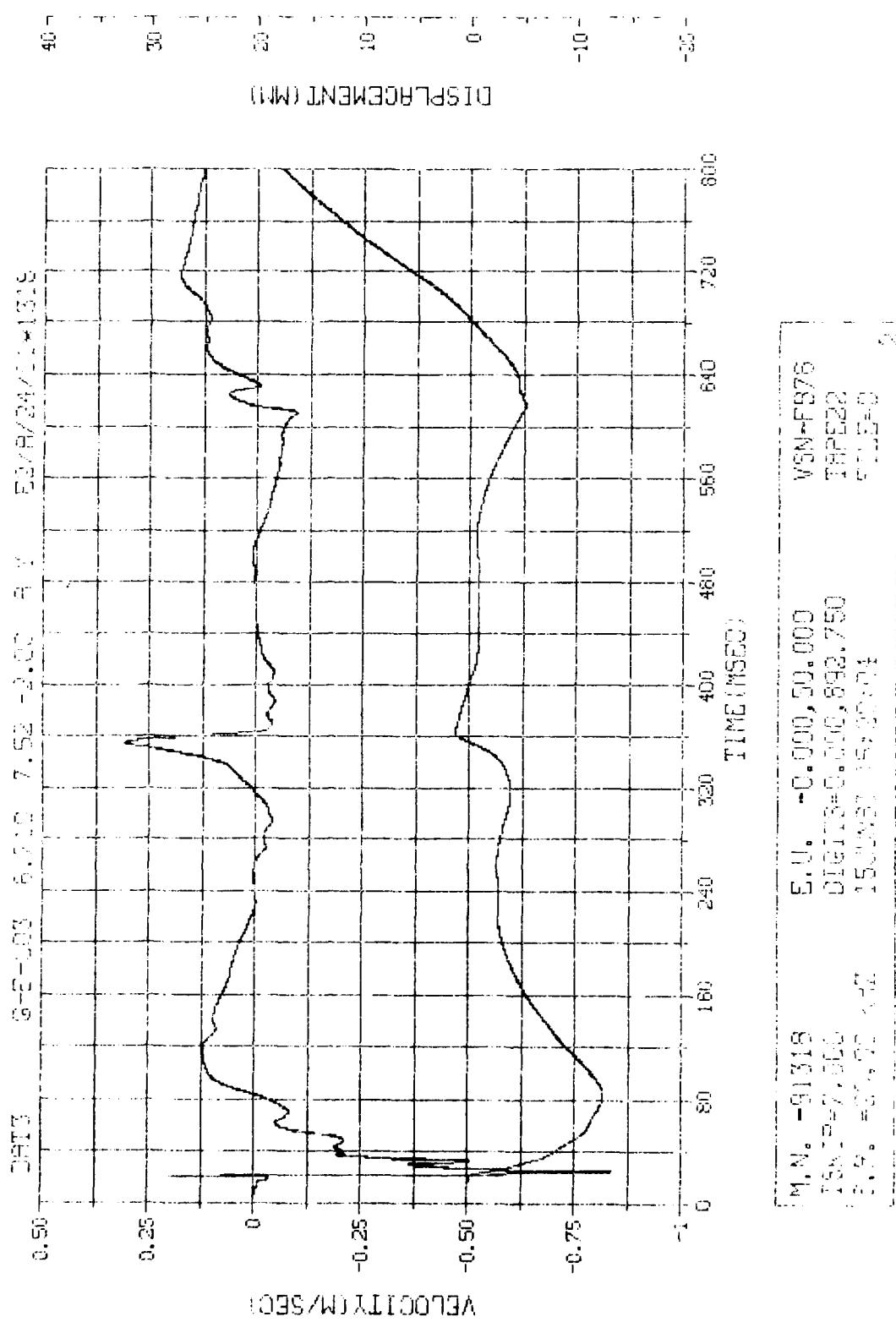


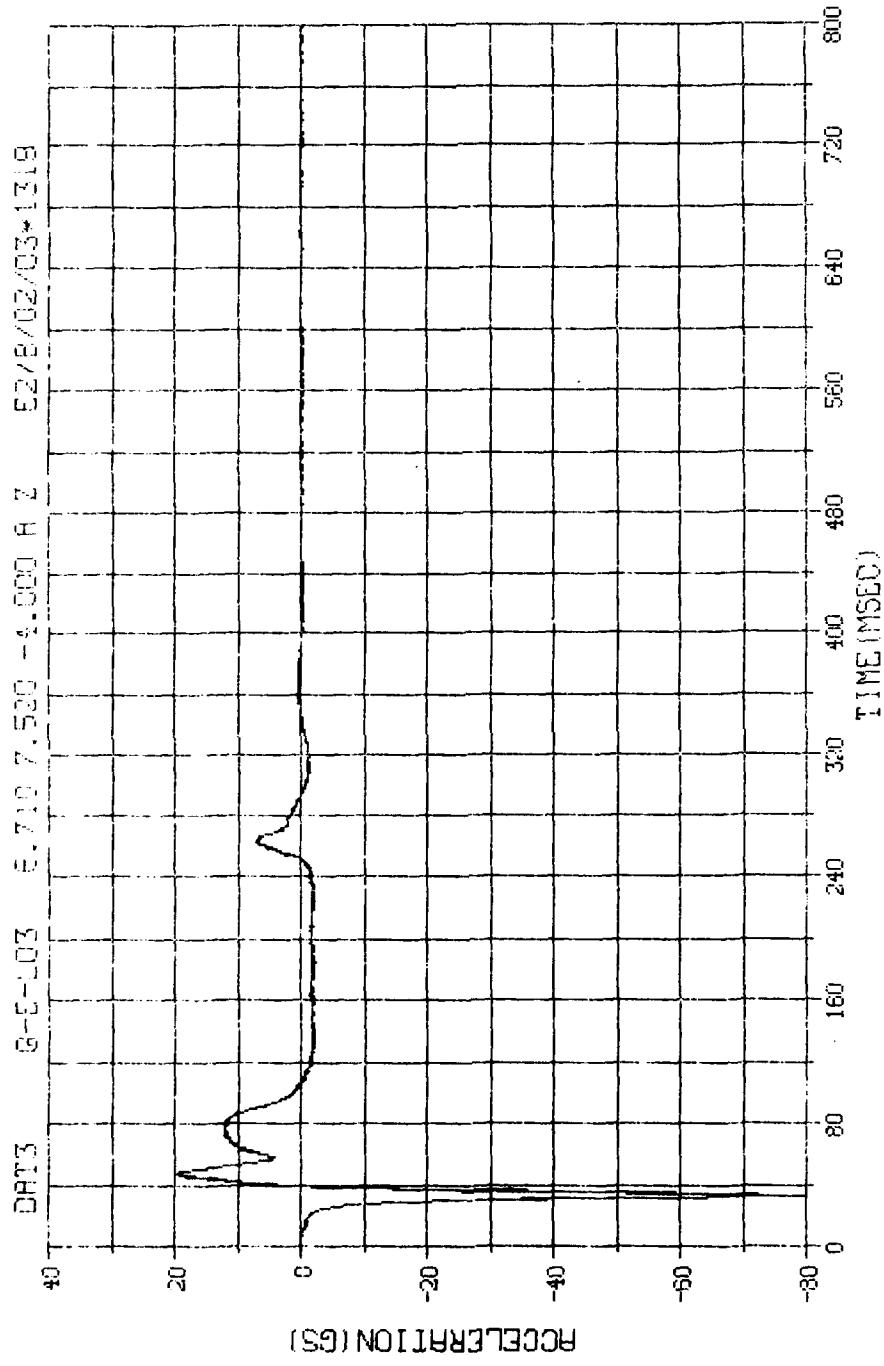


M.N. -91317	E.U. -0.300, 50.000	VSN-FB76
TEST P=7.000	DIGITS=0.000, 998.975	TRP522
$\rho = 20.00$	15.000	TEST=2

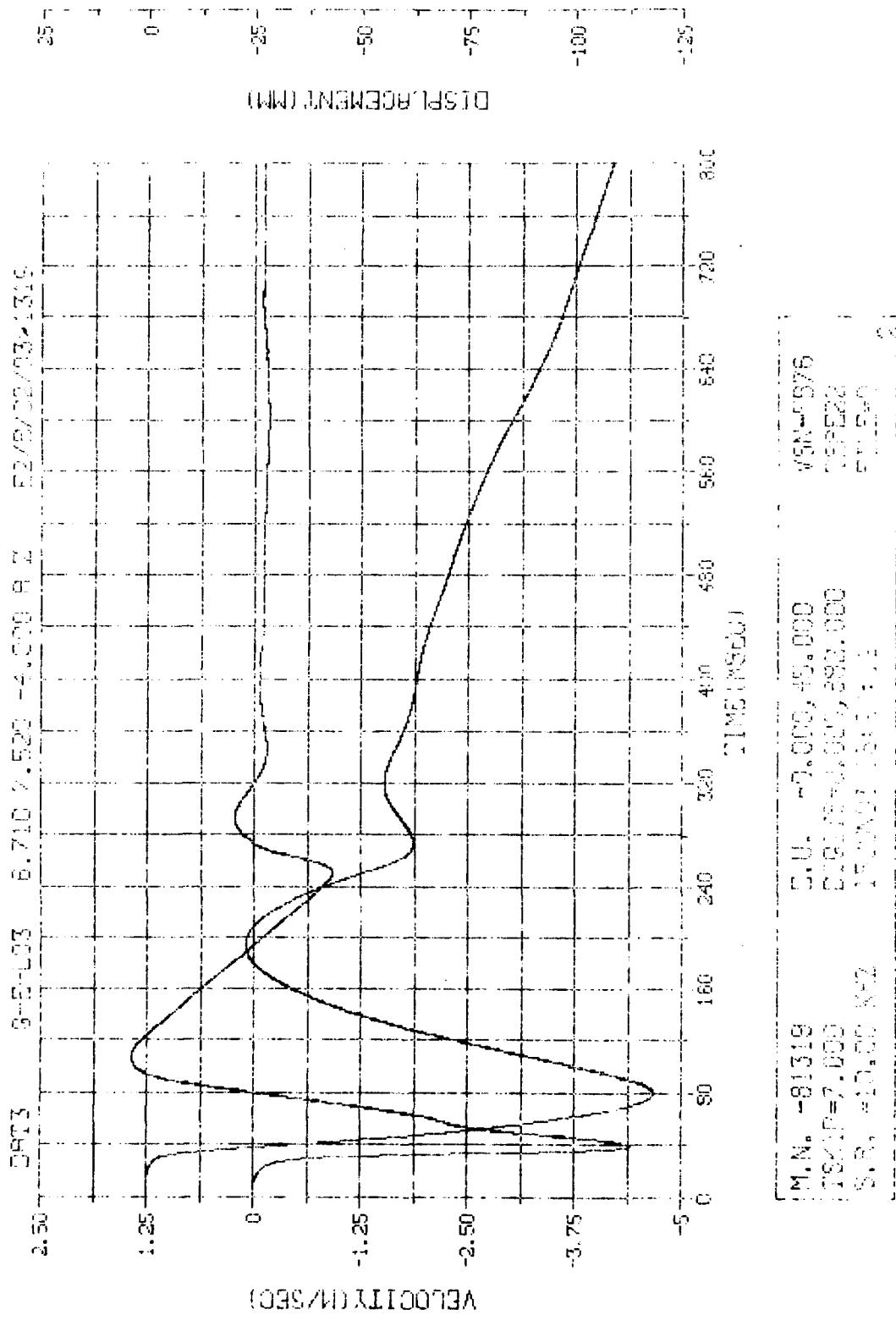


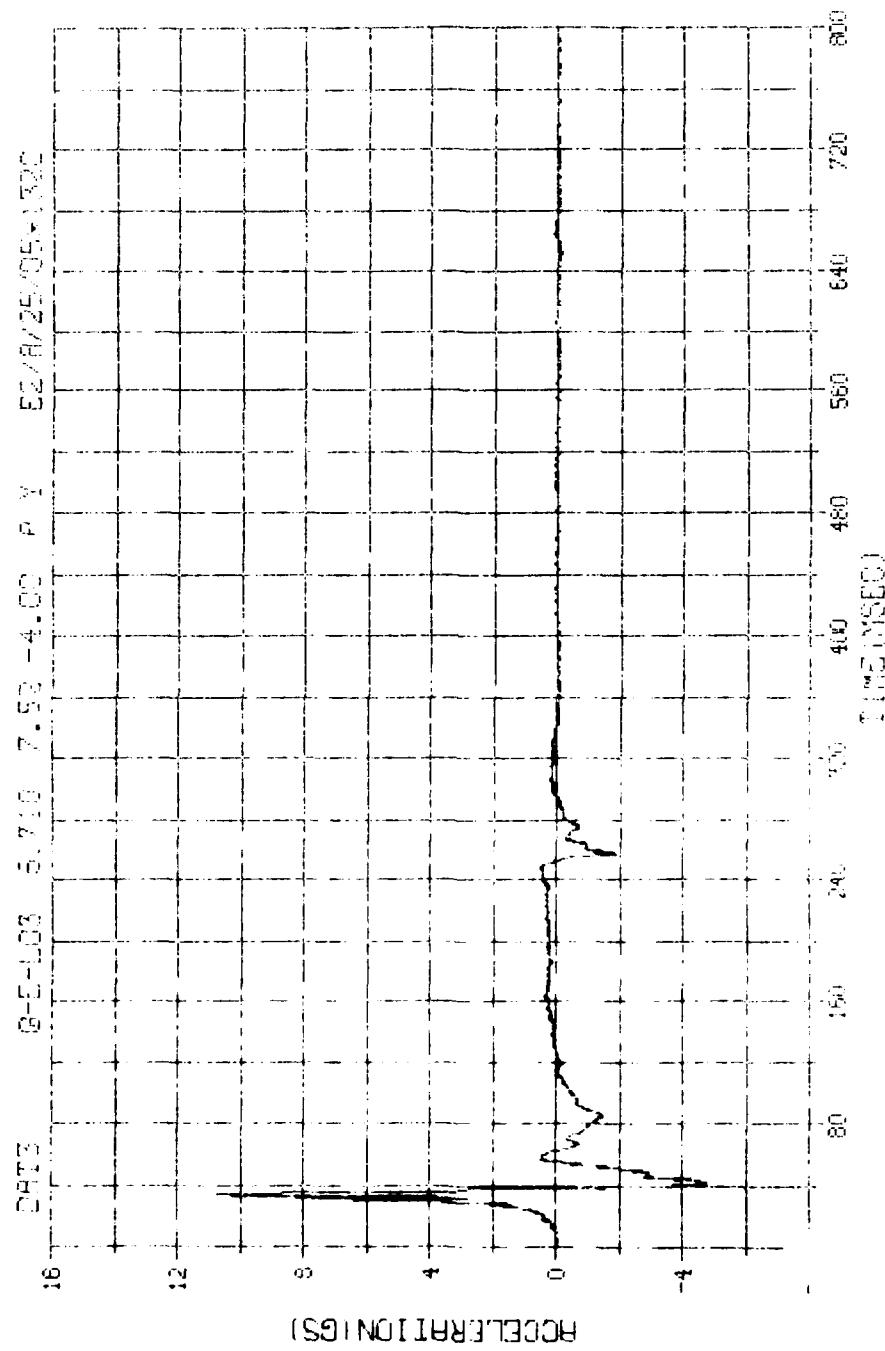
IP, N. = 91318	E.I. = 0.000, 50.000	VSN-FB75
z, S, IP=7.000	DATA175=0.000, 892.750	TYPE22
z, S, = 350.0, k=2	15.0, XN=315, ZD=04	PULSE=5



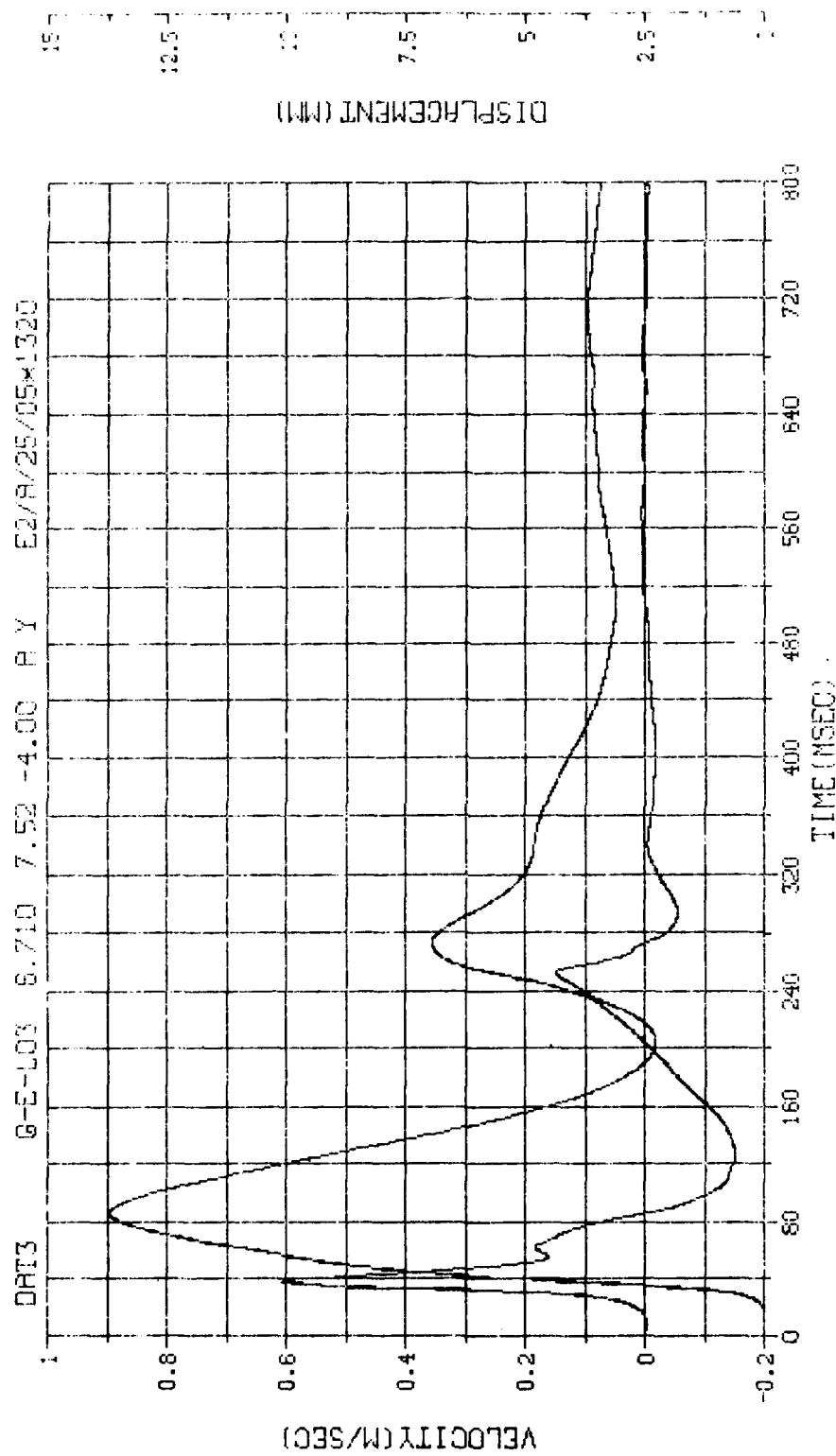


M. N.	-81319	E.U.	-0.000, 45.000	VSN-FB76
TSKIP	=7.000	SIGHTS	=0.000, 860, 011	THE E2c
S.R.	=10.00	TIME	15:20:04	END S=6

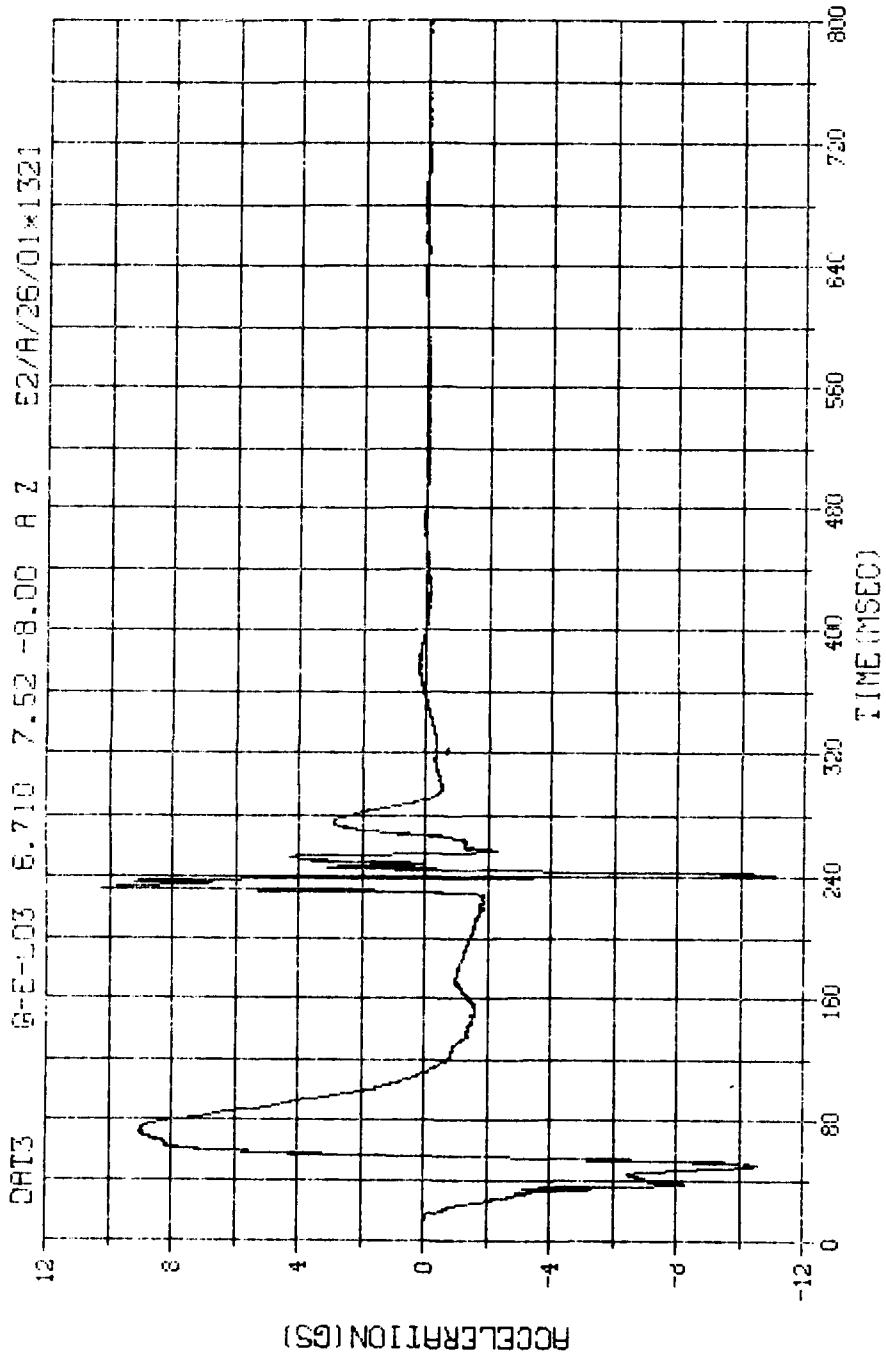




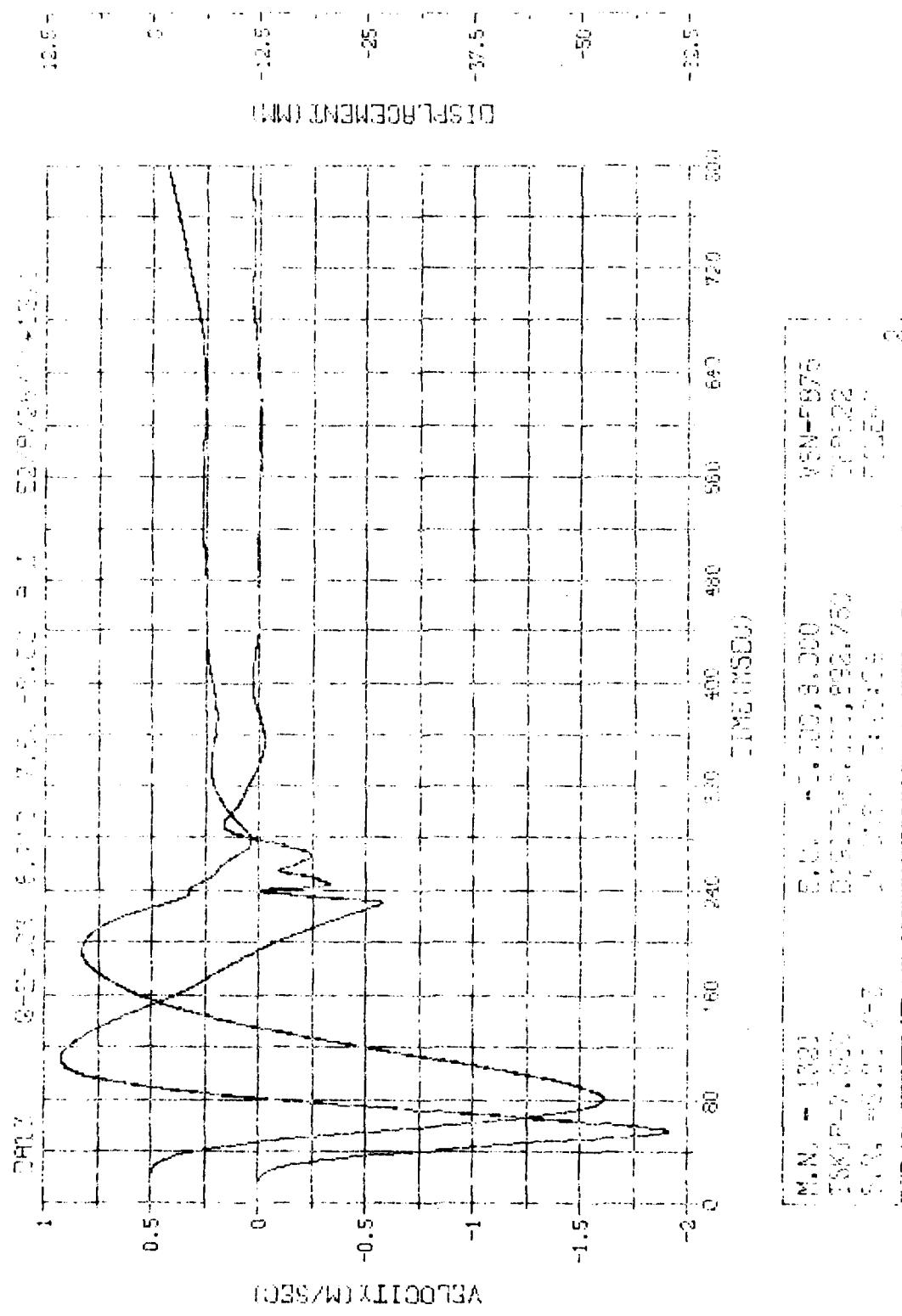
H.M. - 01720
 E.M. - 01720
 TPE22
 WSN-E76
 5, 30, 300, 15, 000
 35, 350, 350, 350, 350
 35, 350, 350, 350, 350

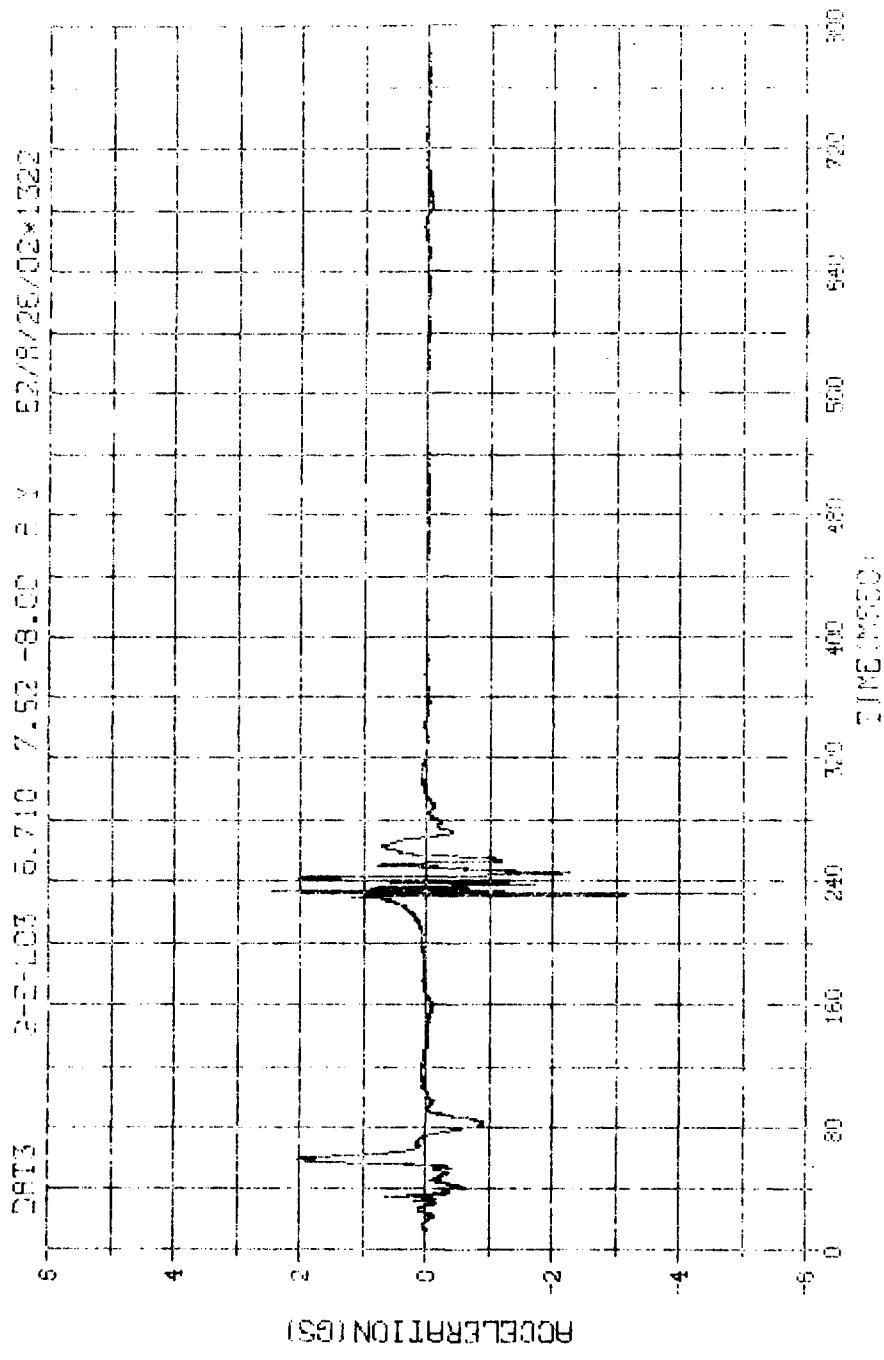


M.N. -91320	E.U. -0.000, 15.000	VSN-FB76
SKIP=7,000	DIGITS=0,000,857,375	TYPE22
S.R. =5.00 K=2	15JUN83 15:20:04	FILED=
		2

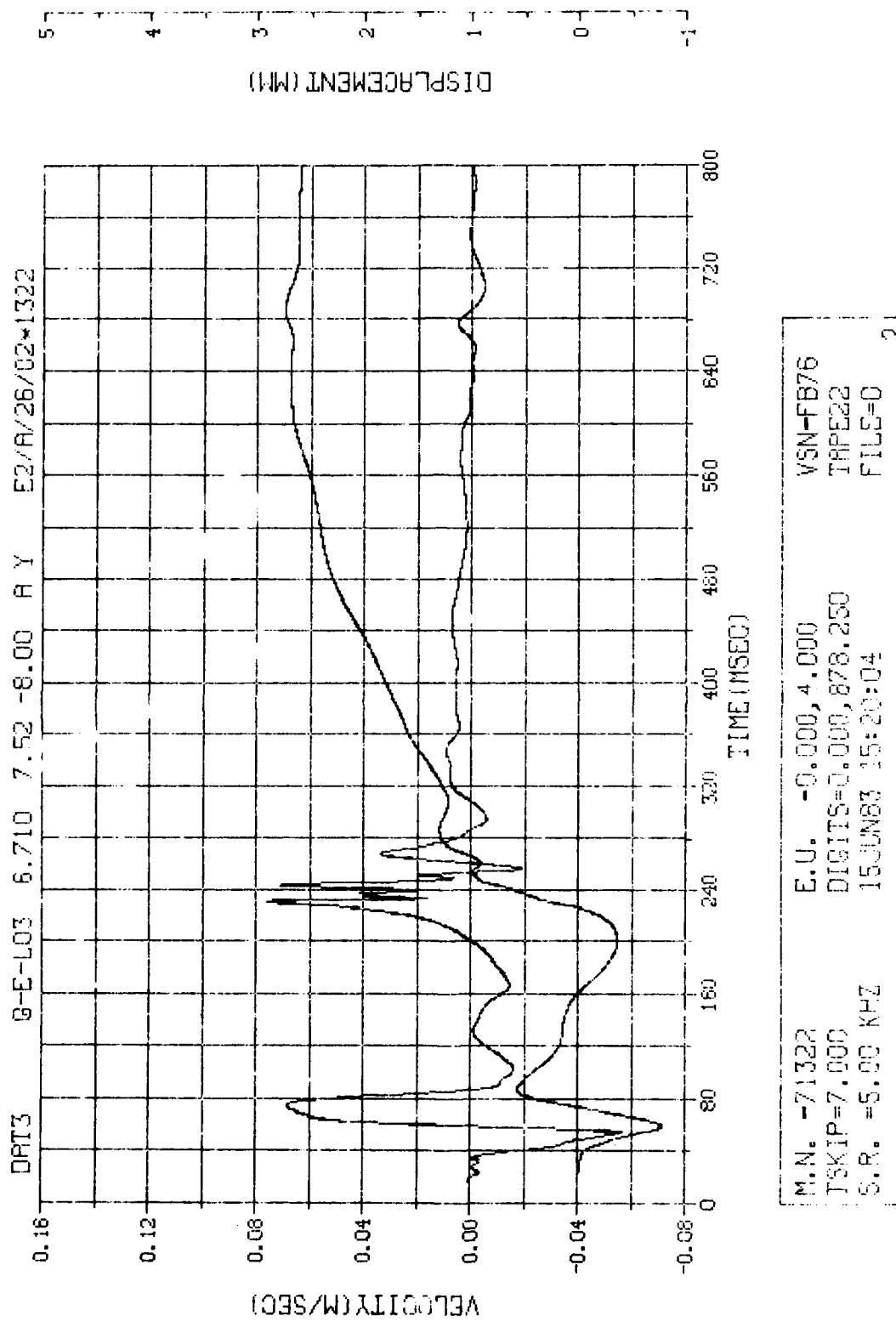


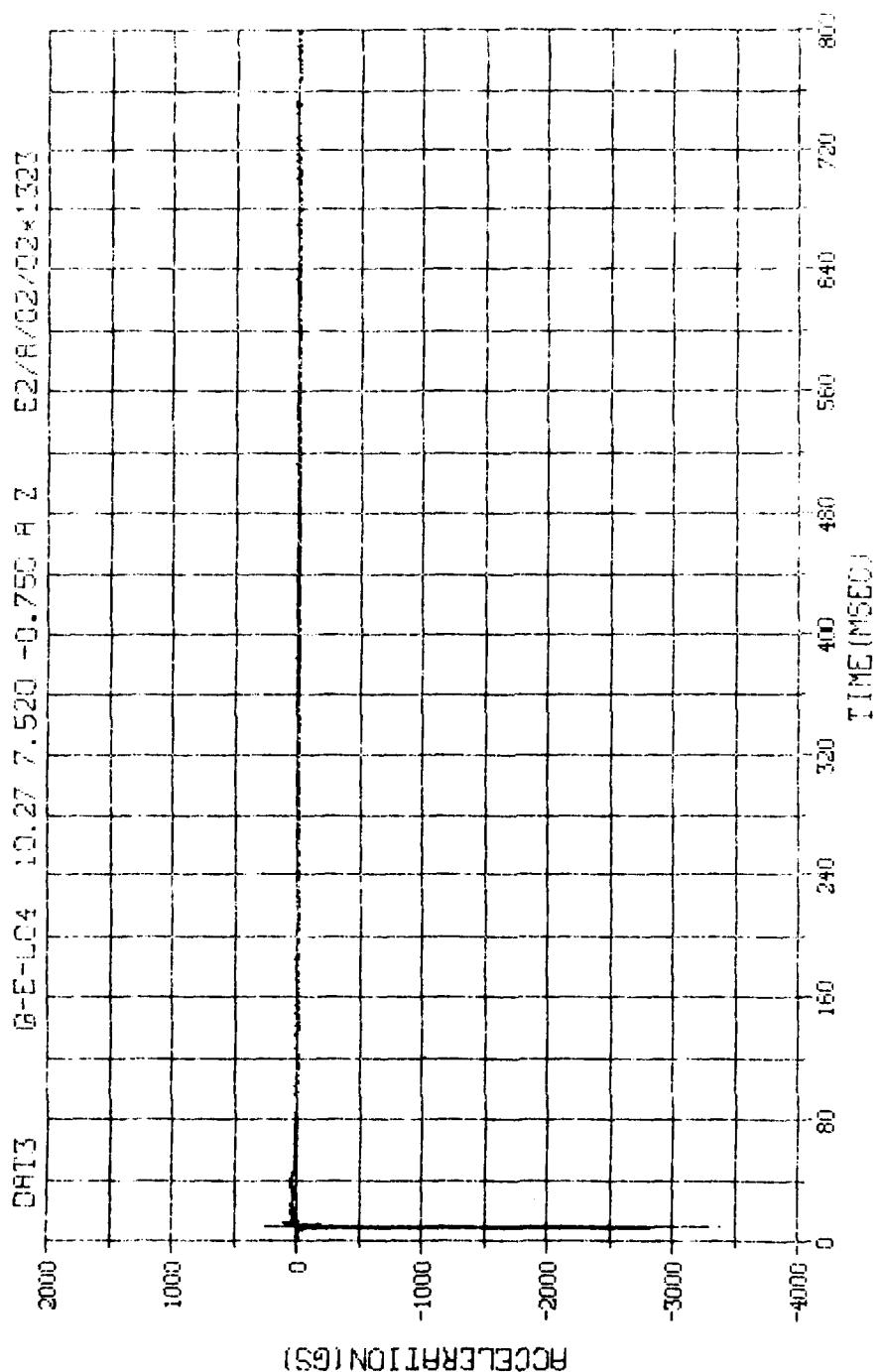
N.N. = 1321	E.U. = 0.000, 9.000	VSN-F875
SKIP=7,000	DATAIT5=0,000,892,750	TRPE22
S.R. =5,00 X42	15,00,47,15,30,34	F1,L2=0



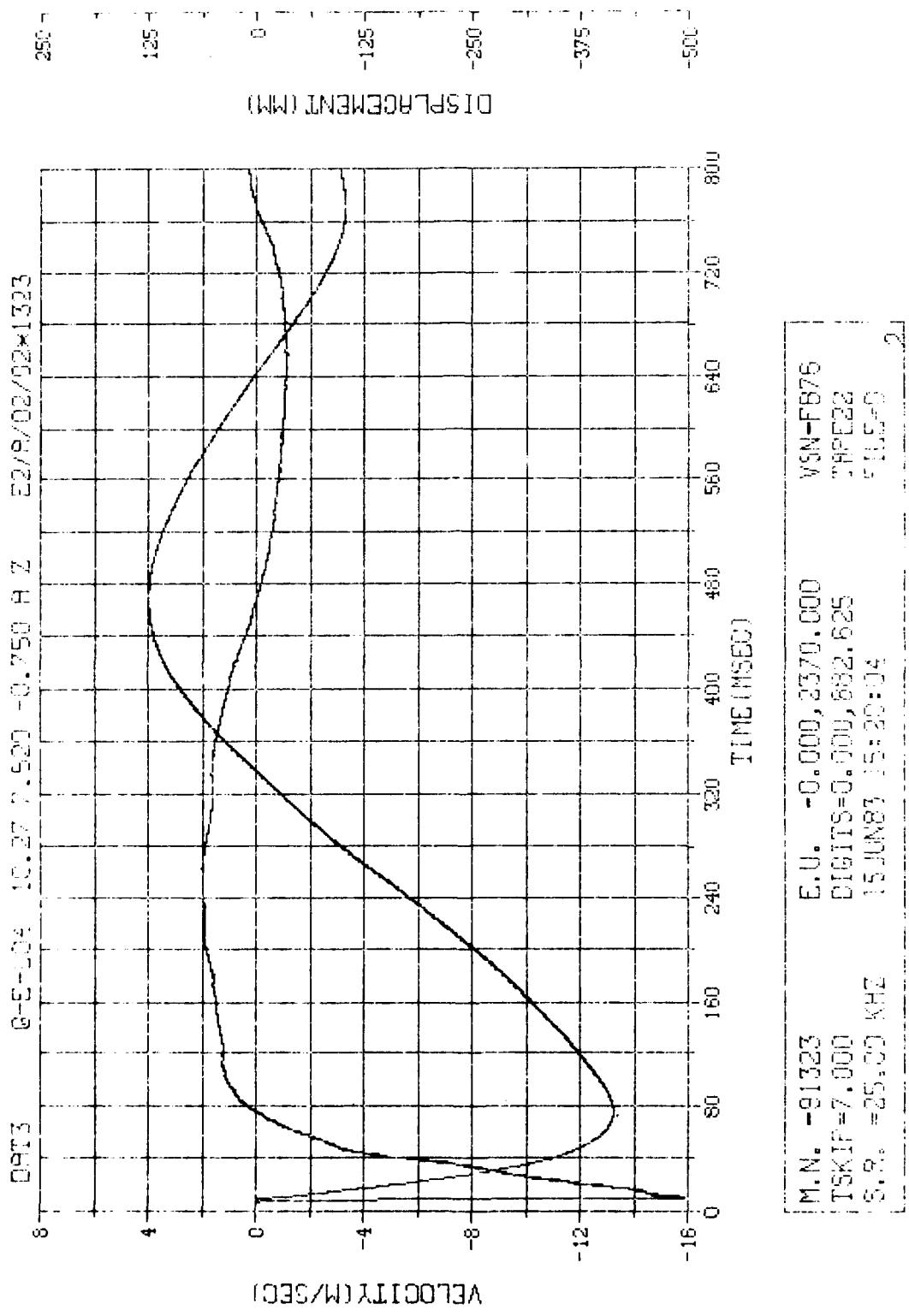


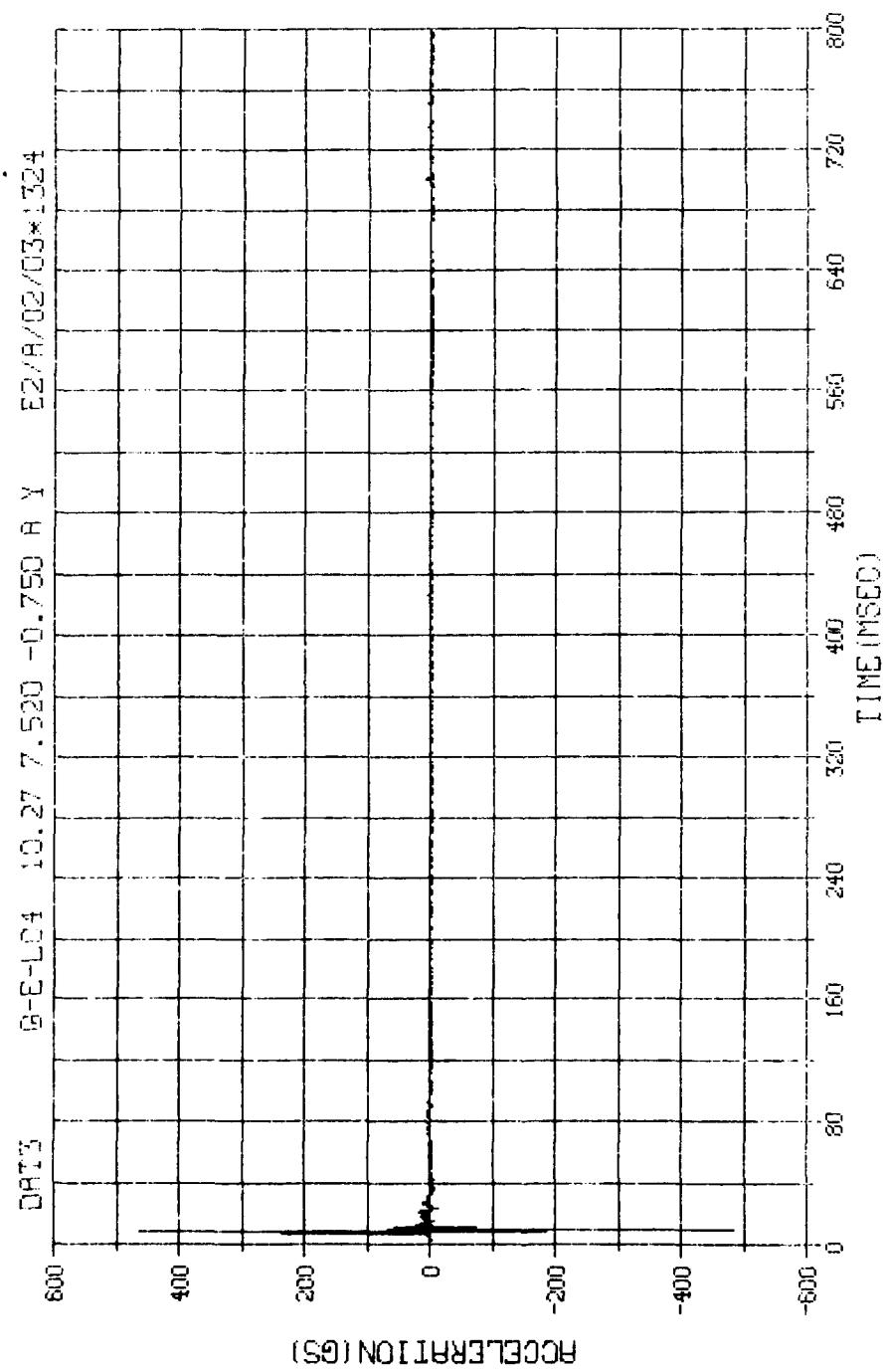
296



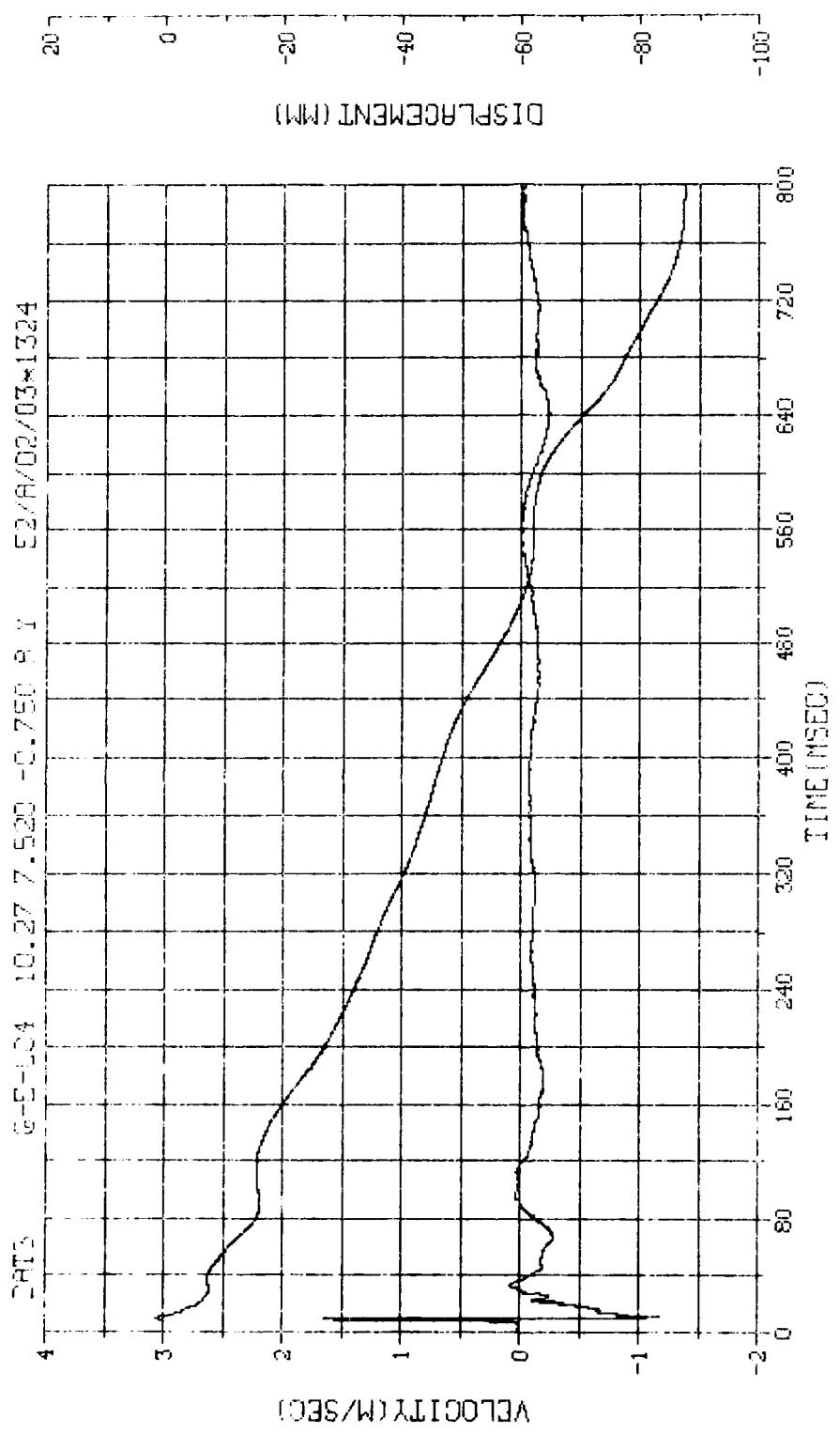


R.N.	-91323	E.U.	-9.000, 2370.000	VSN-FG75
1SKIP	7.000	TIME=0.000, 582.625	TAPE22	
S.R.	=25.00	RECORD=15:30:04	DATA=0	

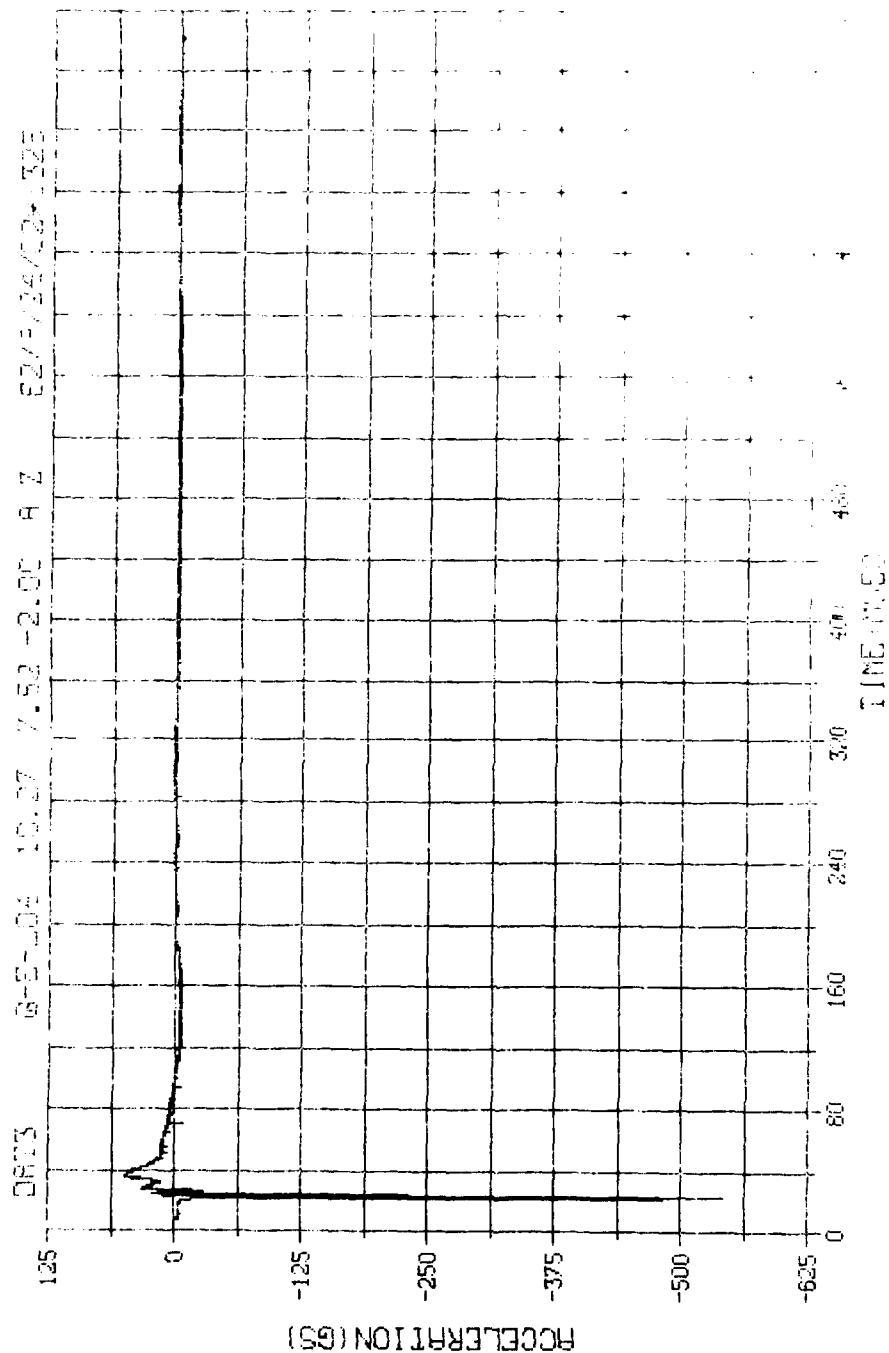




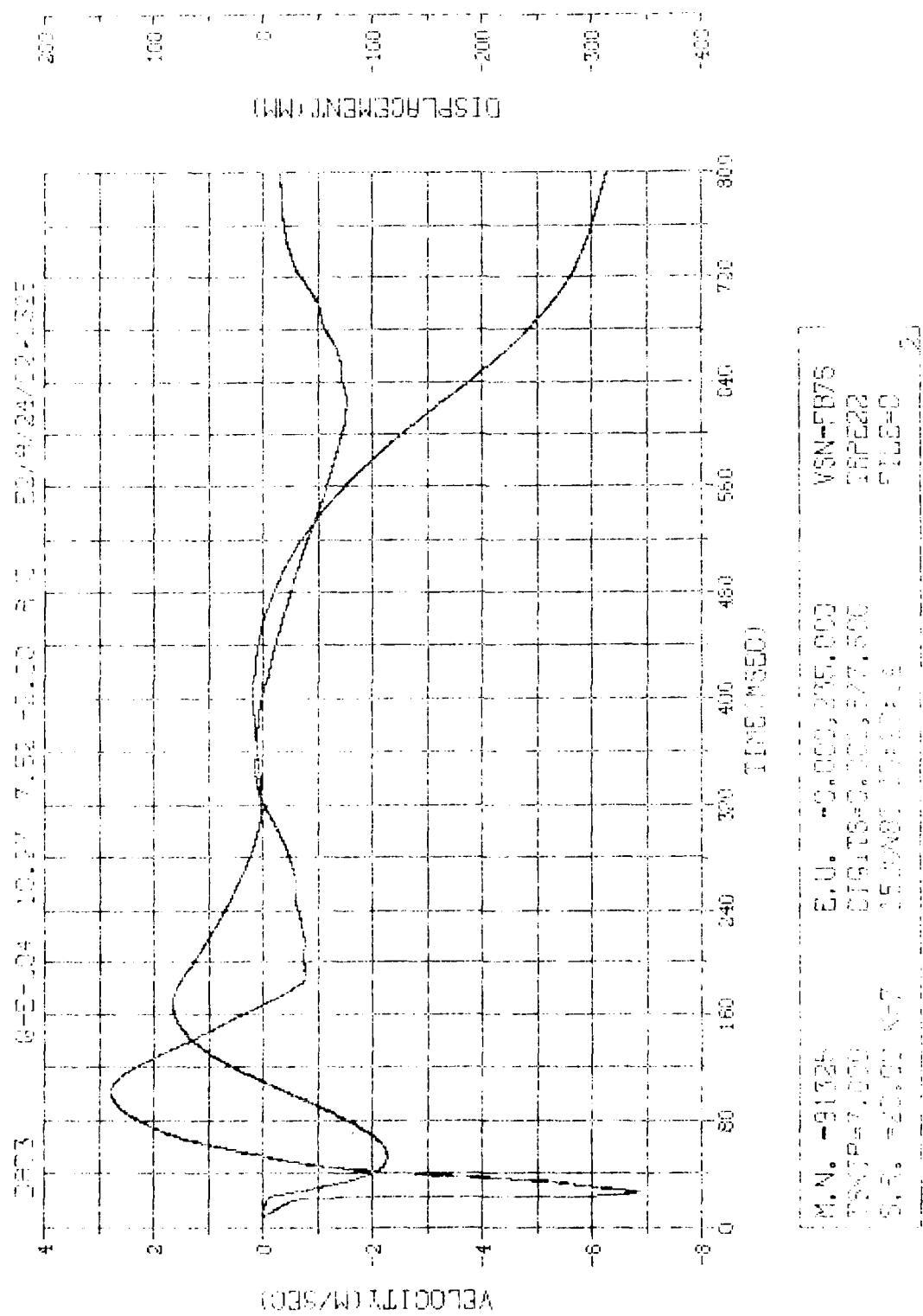
M.N.	-91324
TSKIP	=7.000
STARTS	=0, 000, 865, 750
ENDTIME	=15:20:04
S.R.	=25.00 kHz
	VSN-FB76
	78822
	21.8=0
	1

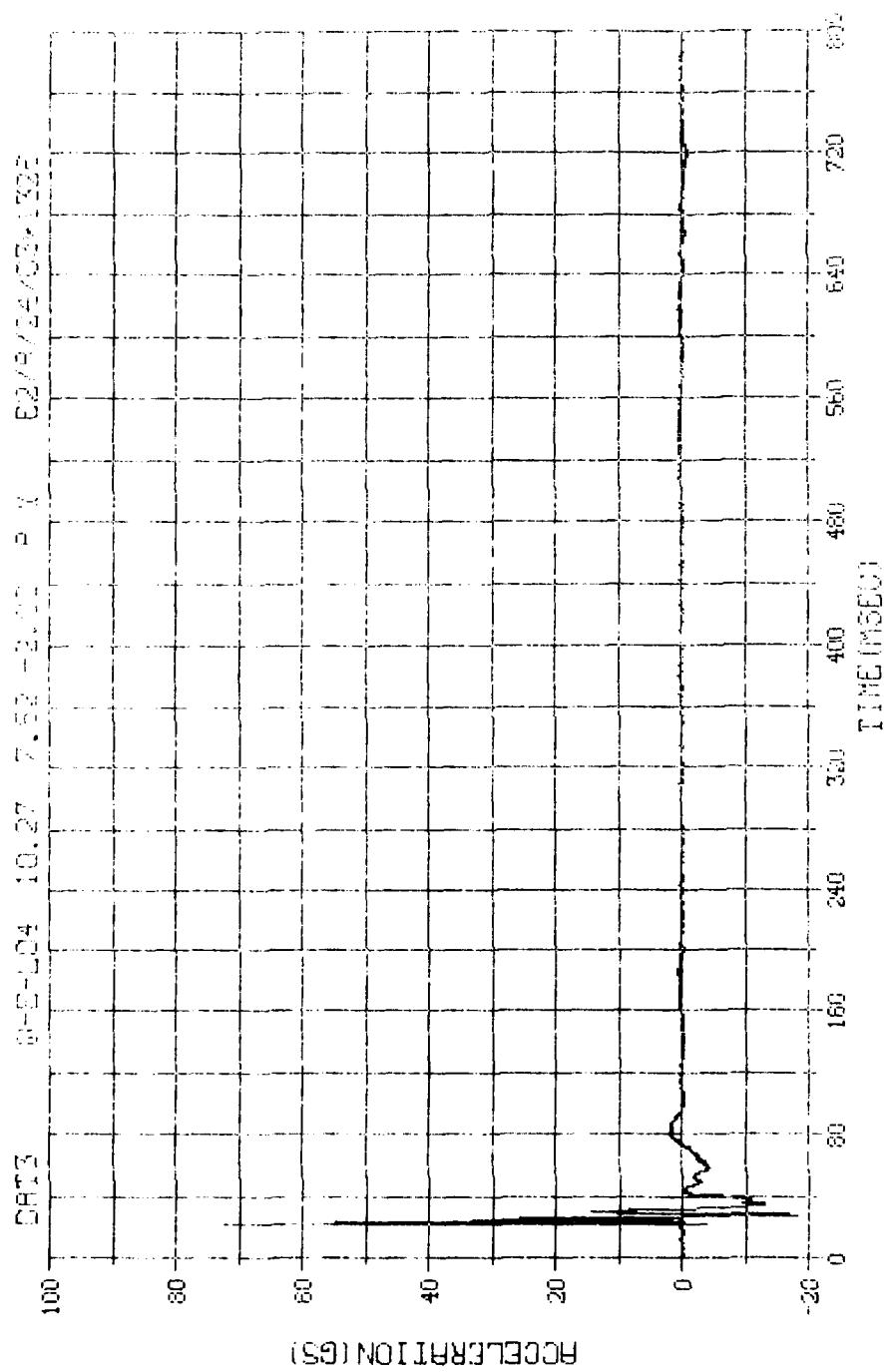


W.N. -91324 S.U. -0.000,450,000 VSN-FB76
 15SK1P=7,000 Starts=6,300,600,750 TAPE22
 6,300 15,000 15,000 15,000 TAPE23
 15,000 15,000 15,000 15,000 TAPE24

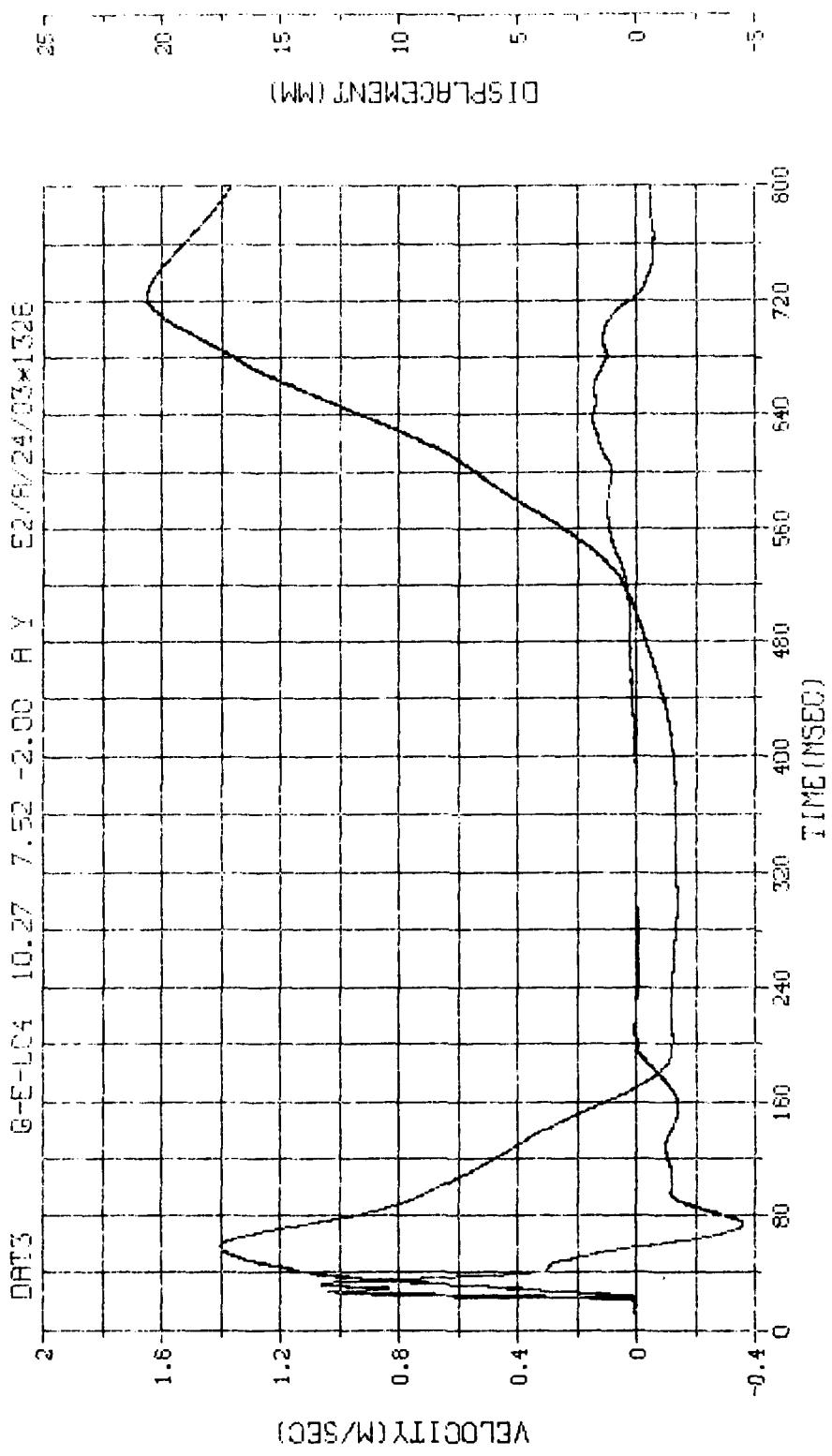


N.N. = 91325
 $\sigma_{\text{N}} = 0.0001335$, $\sigma_{\text{L}} = 0.0001335$, $\sigma_{\text{C}} = 0.0001335$
 $\sigma_{\text{E}} = 0.0001335$, $\sigma_{\text{R}} = 0.0001335$, $\sigma_{\text{S}} = 0.0001335$
 $\sigma_{\text{D}} = 0.0001335$, $\sigma_{\text{F}} = 0.0001335$, $\sigma_{\text{G}} = 0.0001335$
 $\sigma_{\text{H}} = 0.0001335$, $\sigma_{\text{I}} = 0.0001335$, $\sigma_{\text{J}} = 0.0001335$
 $\sigma_{\text{K}} = 0.0001335$, $\sigma_{\text{L}} = 0.0001335$, $\sigma_{\text{M}} = 0.0001335$
 $\sigma_{\text{N}} = 0.0001335$, $\sigma_{\text{O}} = 0.0001335$, $\sigma_{\text{P}} = 0.0001335$
 $\sigma_{\text{Q}} = 0.0001335$, $\sigma_{\text{R}} = 0.0001335$, $\sigma_{\text{S}} = 0.0001335$
 $\sigma_{\text{T}} = 0.0001335$, $\sigma_{\text{U}} = 0.0001335$, $\sigma_{\text{V}} = 0.0001335$
 $\sigma_{\text{W}} = 0.0001335$, $\sigma_{\text{X}} = 0.0001335$, $\sigma_{\text{Y}} = 0.0001335$
 $\sigma_{\text{Z}} = 0.0001335$, $\sigma_{\text{A}} = 0.0001335$, $\sigma_{\text{B}} = 0.0001335$
 $\sigma_{\text{C}} = 0.0001335$, $\sigma_{\text{D}} = 0.0001335$, $\sigma_{\text{E}} = 0.0001335$
 $\sigma_{\text{F}} = 0.0001335$, $\sigma_{\text{G}} = 0.0001335$, $\sigma_{\text{H}} = 0.0001335$
 $\sigma_{\text{I}} = 0.0001335$, $\sigma_{\text{J}} = 0.0001335$, $\sigma_{\text{K}} = 0.0001335$
 $\sigma_{\text{L}} = 0.0001335$, $\sigma_{\text{M}} = 0.0001335$, $\sigma_{\text{N}} = 0.0001335$
 $\sigma_{\text{O}} = 0.0001335$, $\sigma_{\text{P}} = 0.0001335$, $\sigma_{\text{Q}} = 0.0001335$
 $\sigma_{\text{R}} = 0.0001335$, $\sigma_{\text{S}} = 0.0001335$, $\sigma_{\text{T}} = 0.0001335$
 $\sigma_{\text{U}} = 0.0001335$, $\sigma_{\text{V}} = 0.0001335$, $\sigma_{\text{W}} = 0.0001335$
 $\sigma_{\text{X}} = 0.0001335$, $\sigma_{\text{Y}} = 0.0001335$, $\sigma_{\text{Z}} = 0.0001335$

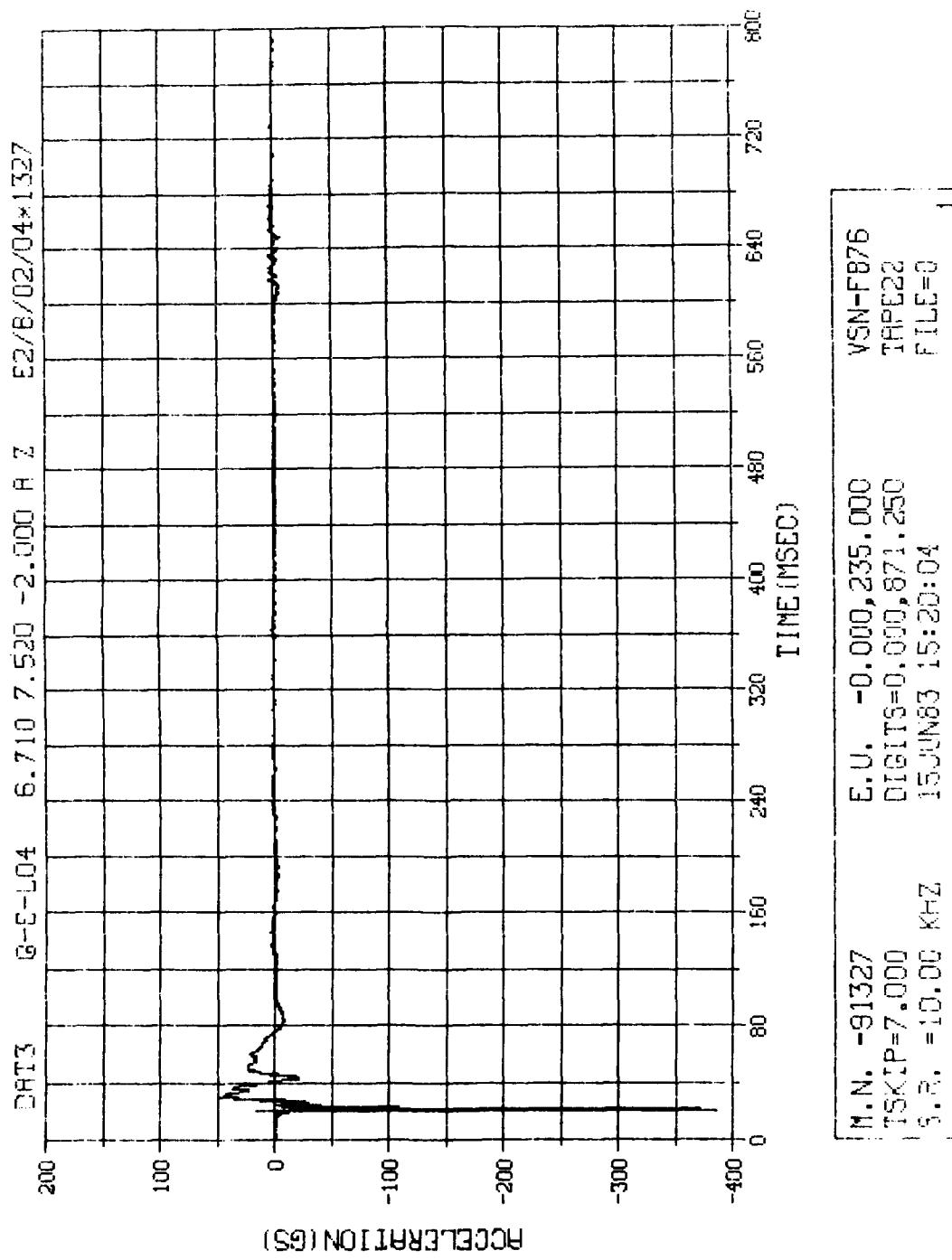


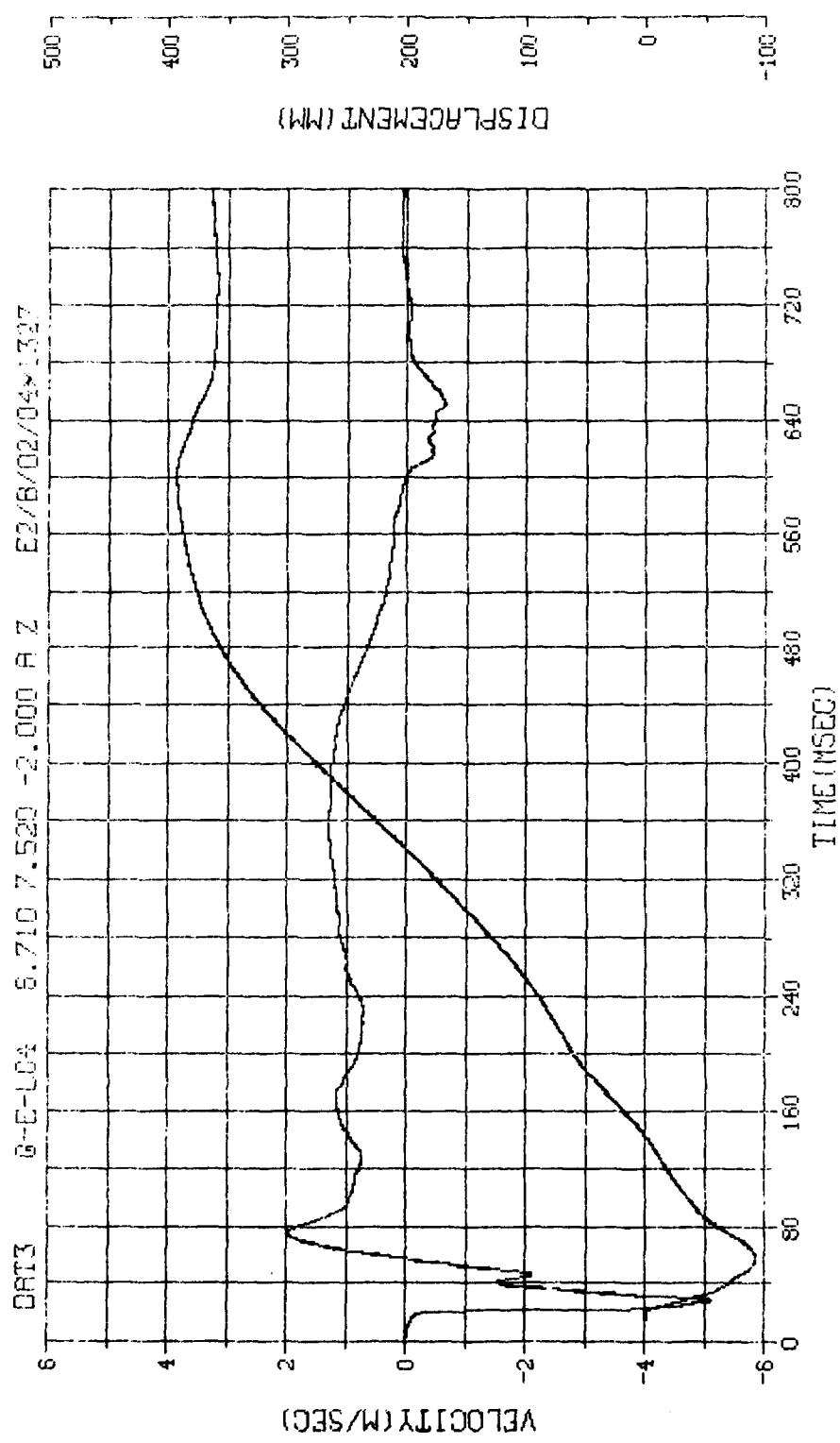


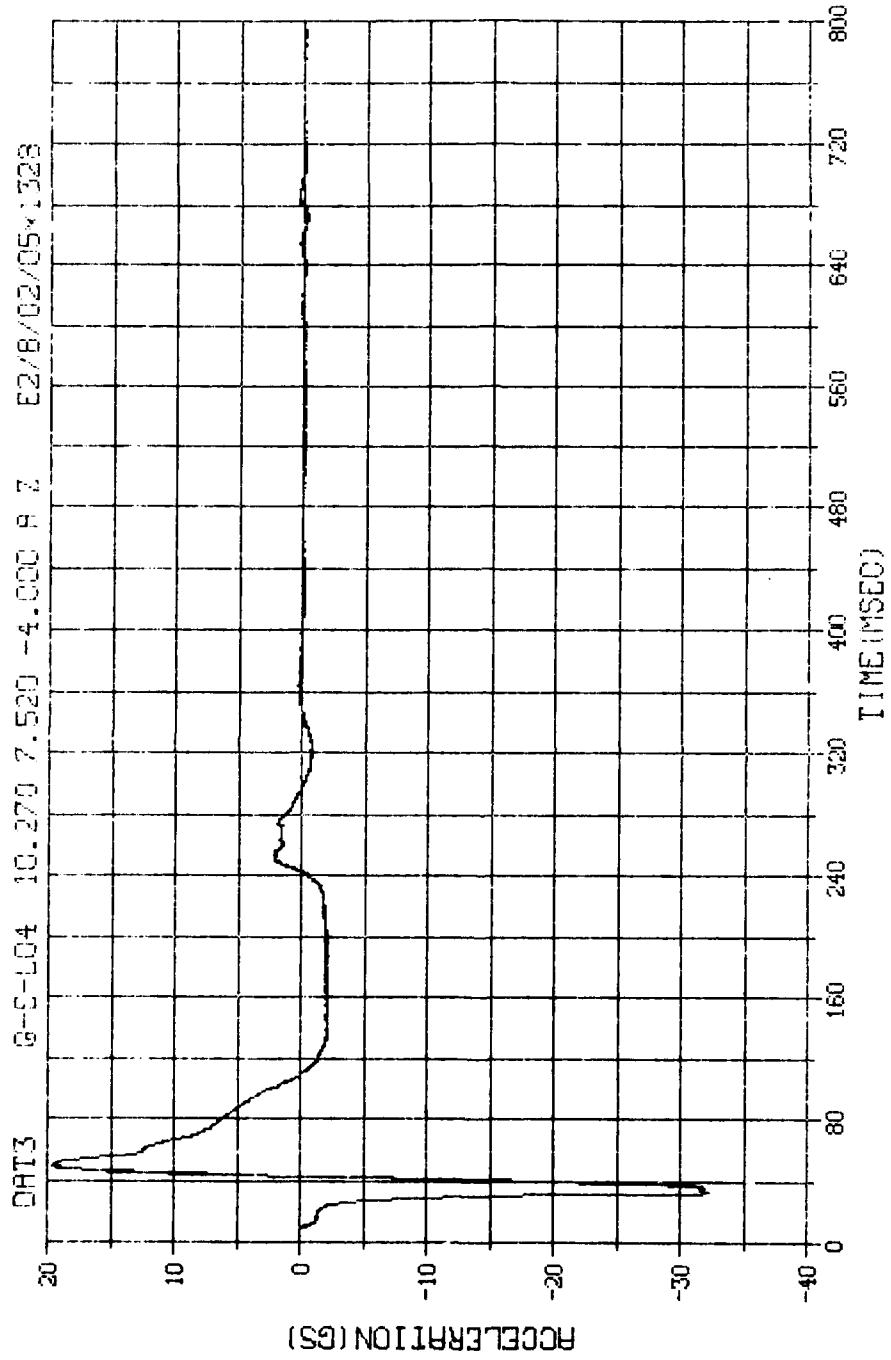
R.N. 21326	E.U. -6.000, 53.000
TEST P=7.500	DIGIT=6.000, 882, 750
F.R. = 27.00 kHz	15.000, 15.000, 15.000
	VSN-F675 TYPE26 FILE=5



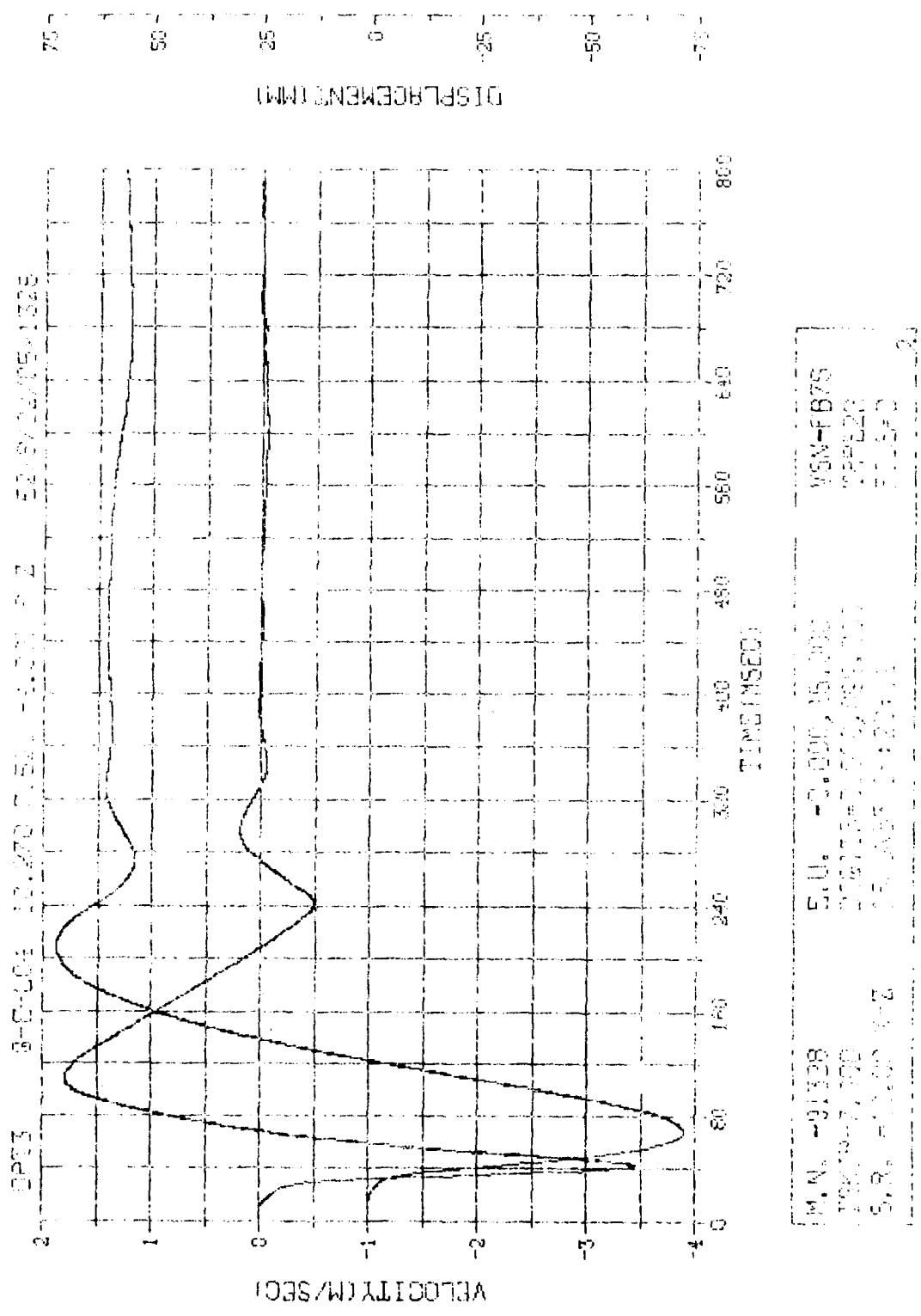
M.N. -91326	E.U. -0.000, 50.100	VSN-FB76
TSKIP=7.000	NGTTS=C, CCO, G82, 750	750522
S.R. =20.30 kHz	15.0msec	PLATE=2

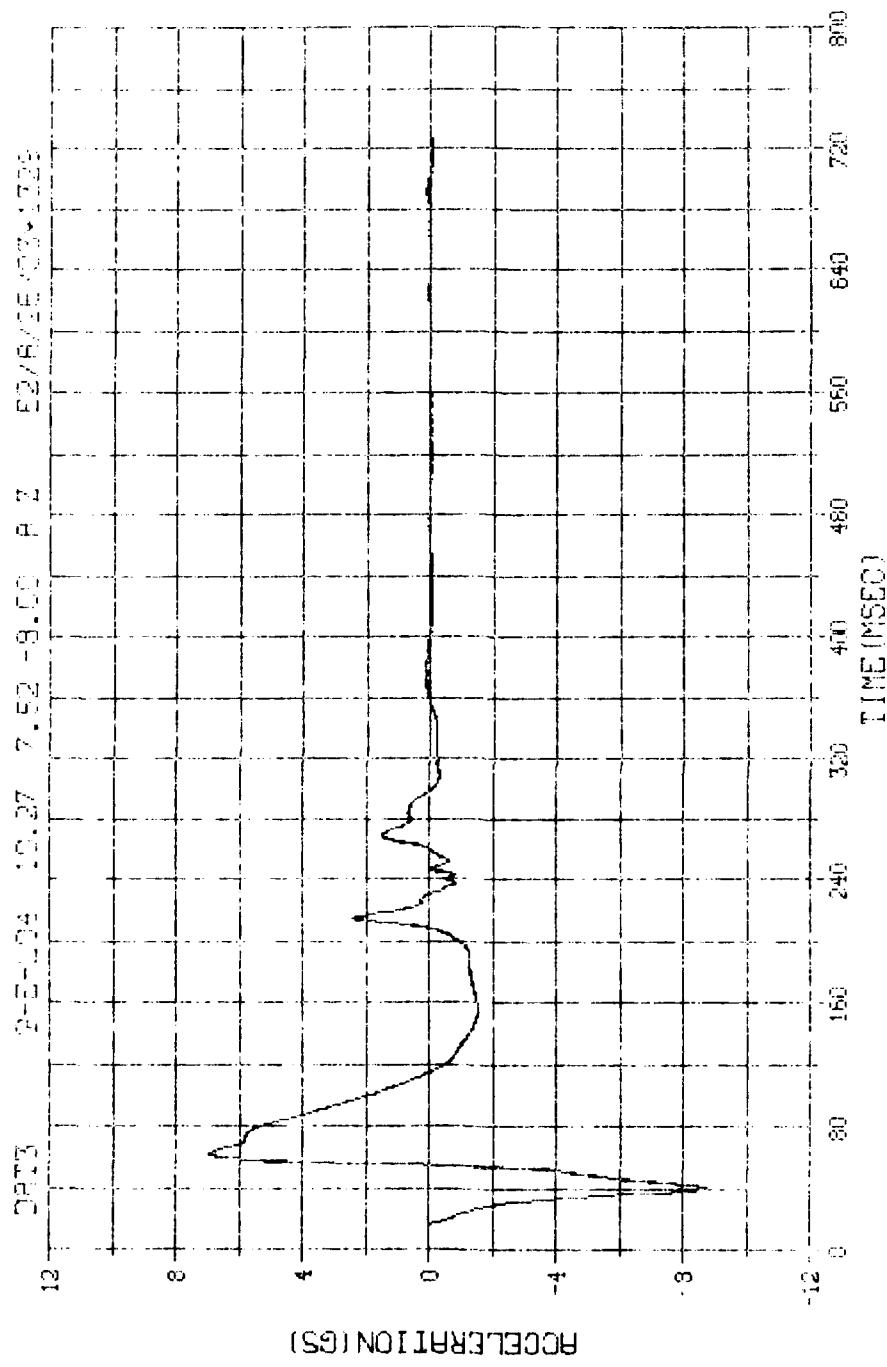


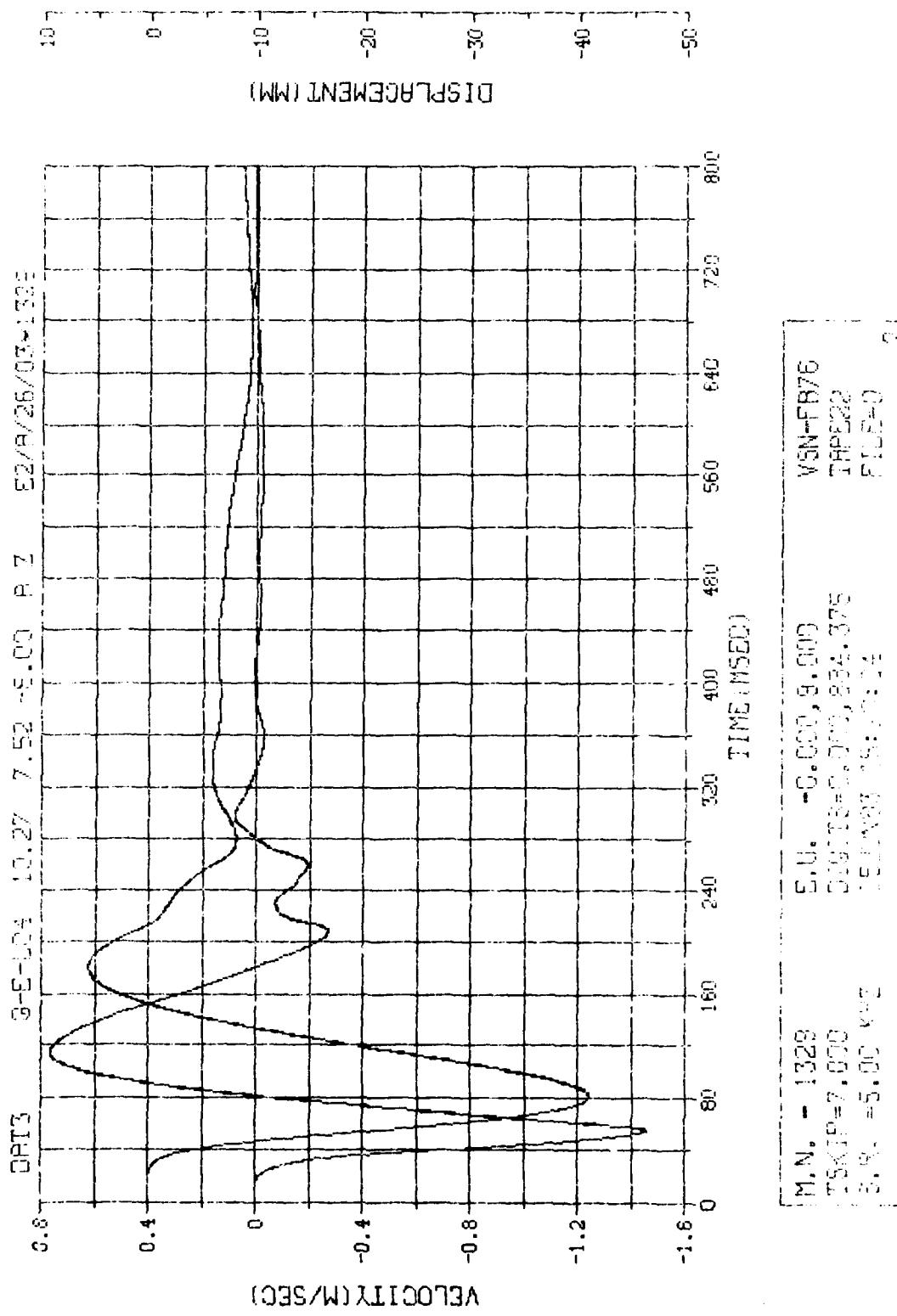


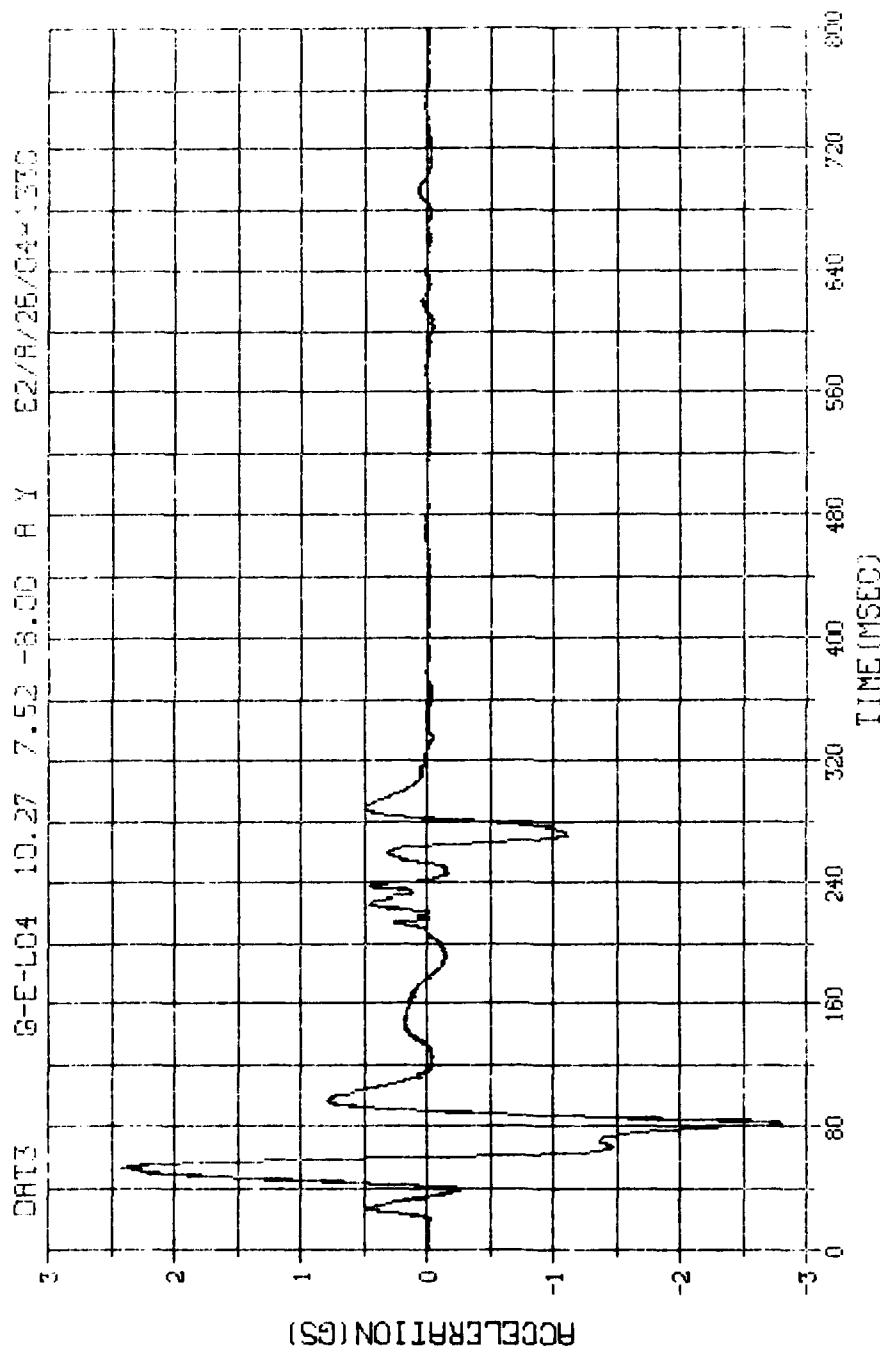


M.N. -91328	E.U. -0.000, 15.000	VSN-FB76
TSKIP=7.000	DIGITS=0.000,800,000	TRAP22
S.R. =10.00 KHZ	15.0003 15:20:34	FILE5.C

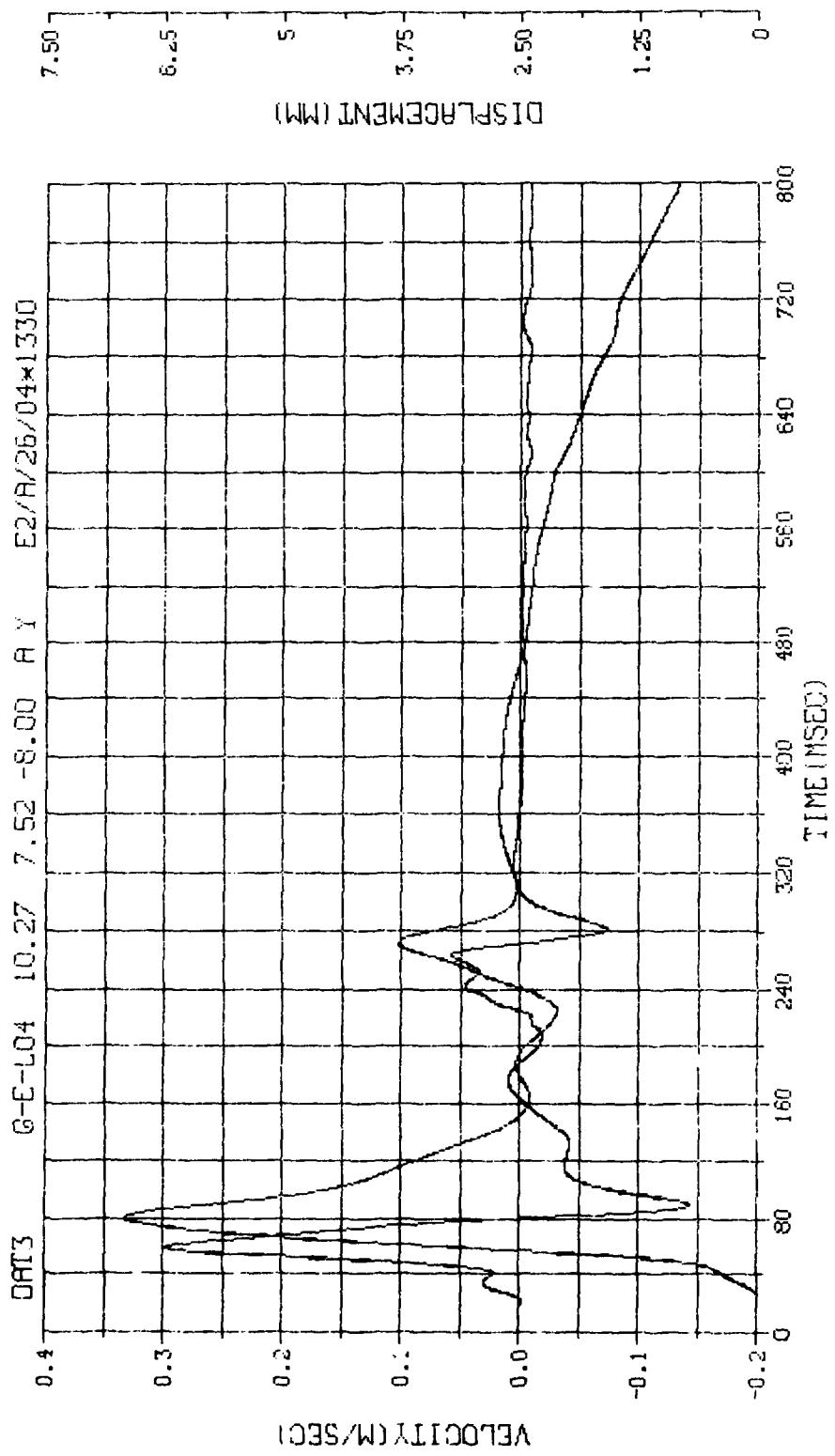








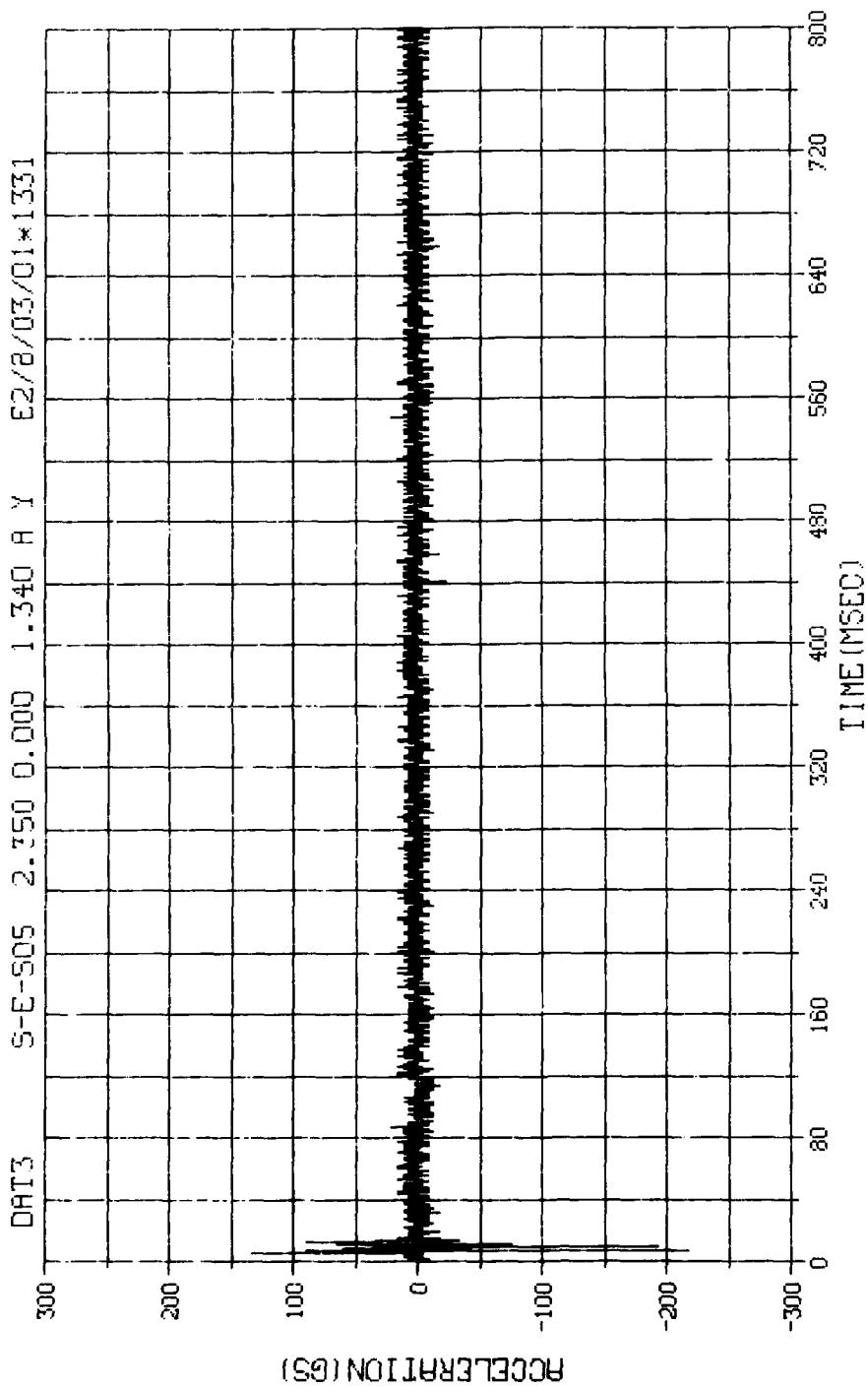
M.N. = 1330	E.U. = -0.000, 4.000	VSN-FB75
TSKIP=7,000	DIGITS=0,000,875,100	TRIP22
S.R. = 5.00 KHZ	15 JUNE 1964 16:50:04	STL20



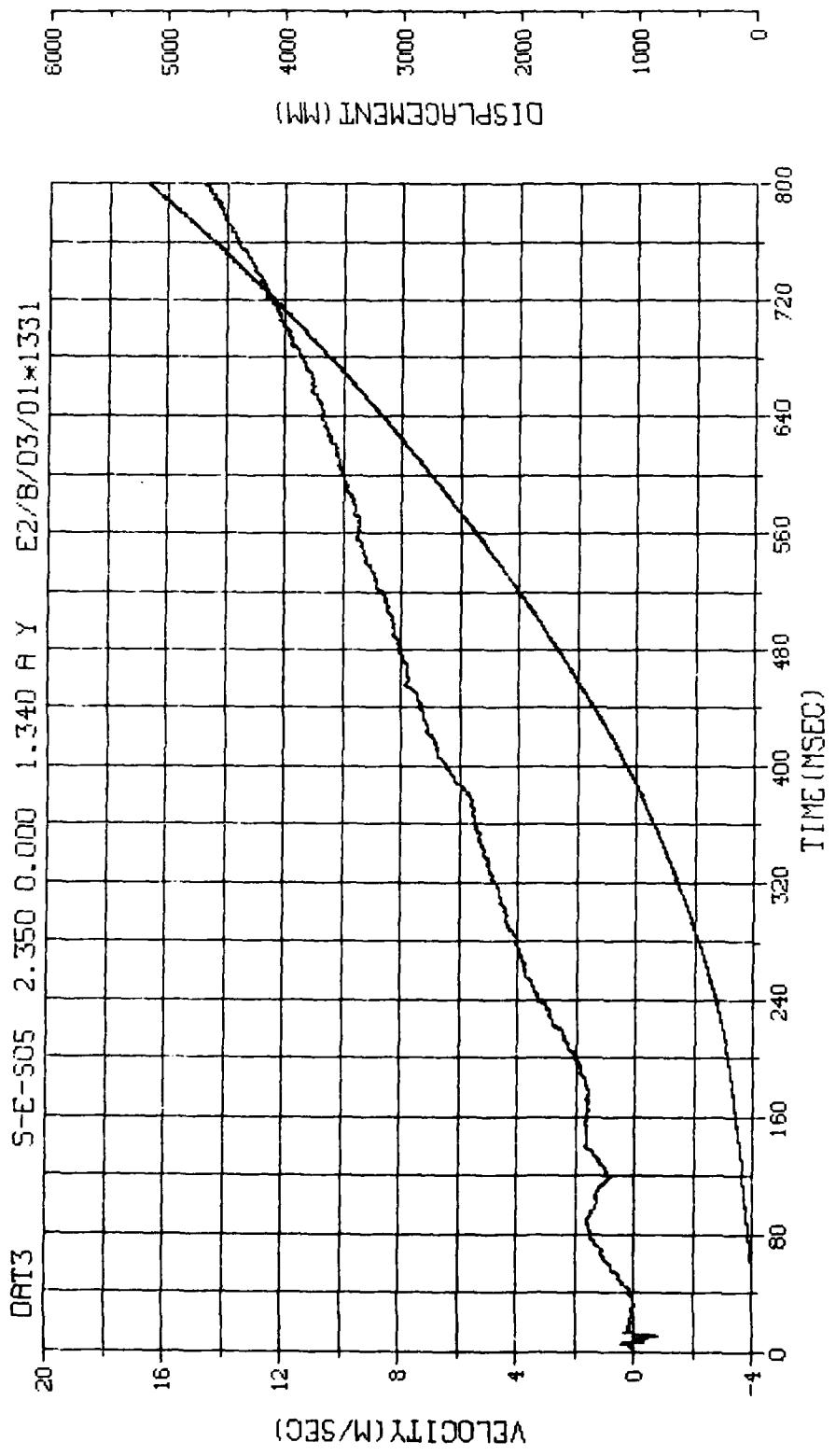
M. N. = 1330	E. U. = -0.000, 4.000	VSN-F676
TSK1P=7.000	DIGITS=0.000,875.500	TAPE22
S. R. = 5.00 KHZ	15JUN83 15:20:04	FILE=0
		2

APPENDIX G

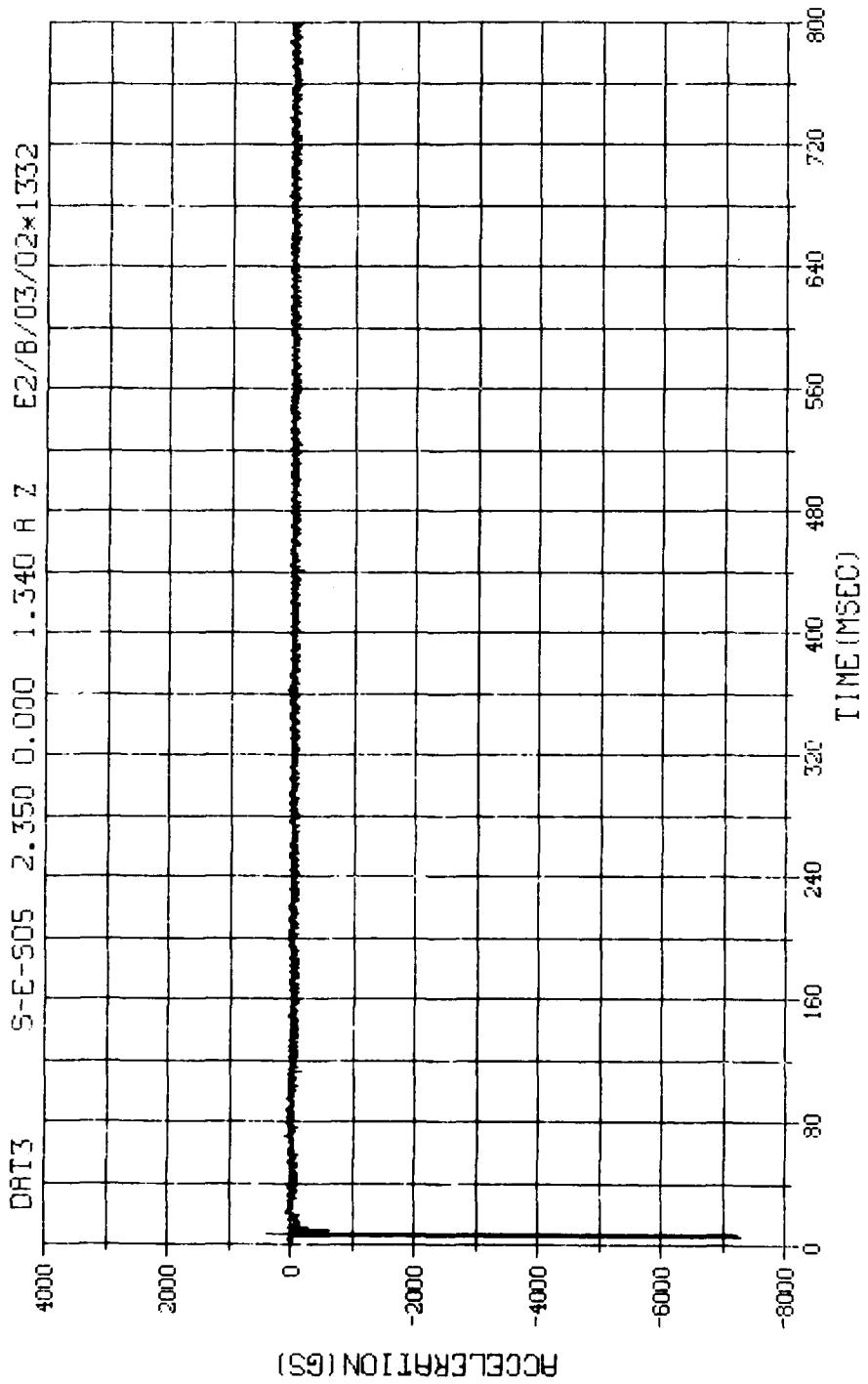
NEAR-FIELD AND STRUCTURAL DATA ARCH A-5



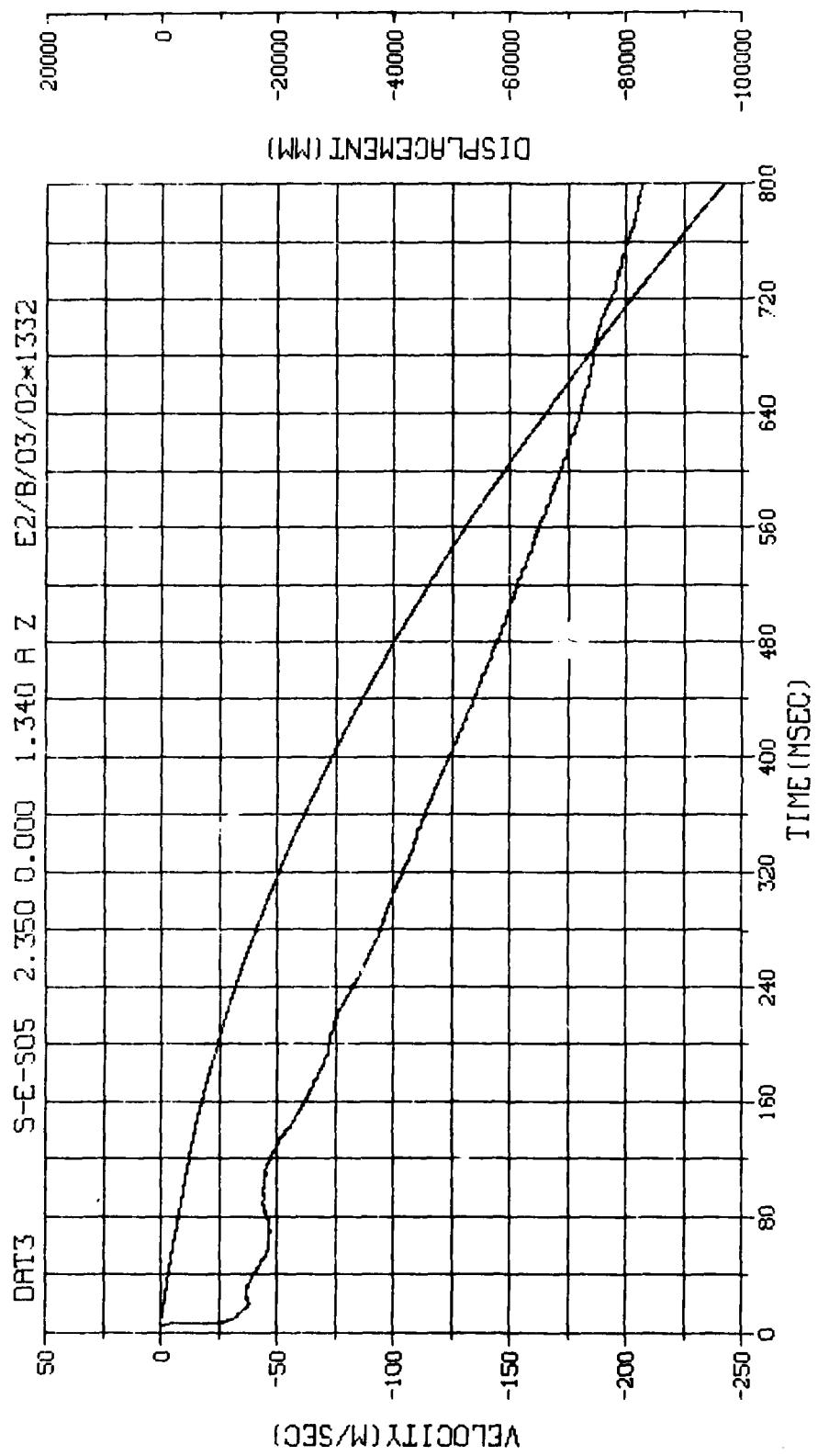
R.N. - 1331	E.U. -0.000,4500.000	VSN-66142
TSKIP=7.009	DIGITS=0.000,927.125	TAPE22
S.R. =10.00 KHZ	4. 4 FM, TUE, 13 SEP 83.	FILE=336 1



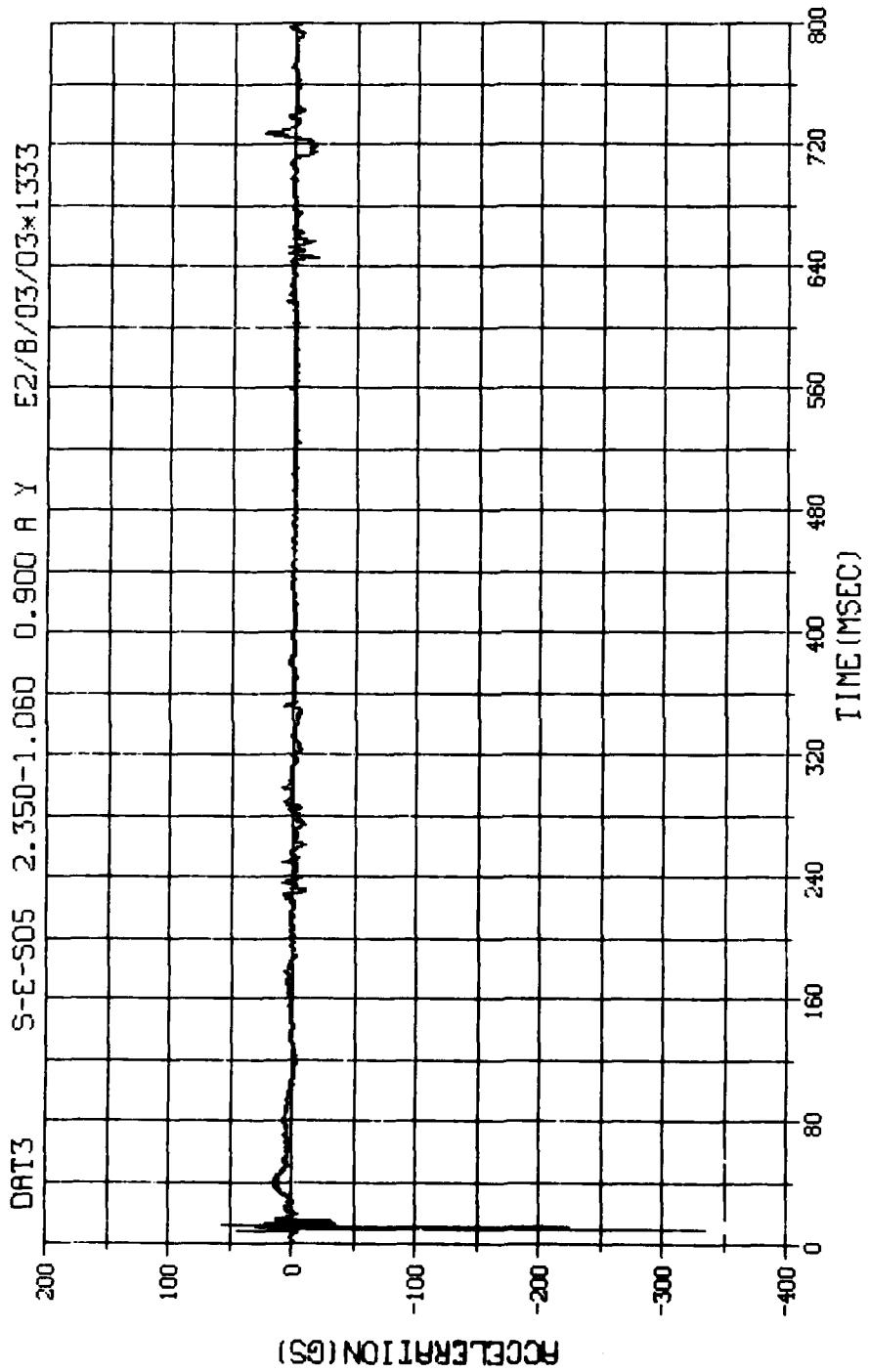
M.N. = 1331	E.U. = 0.000, 4500.000	VSN=00142
TSKIP=7.000	DIGITS=0.000, 927.125	TAPE22
S.R. = 10.00 KHZ	4. 4 PM, TUE, 13 SEP 83.	FILE=3356 2



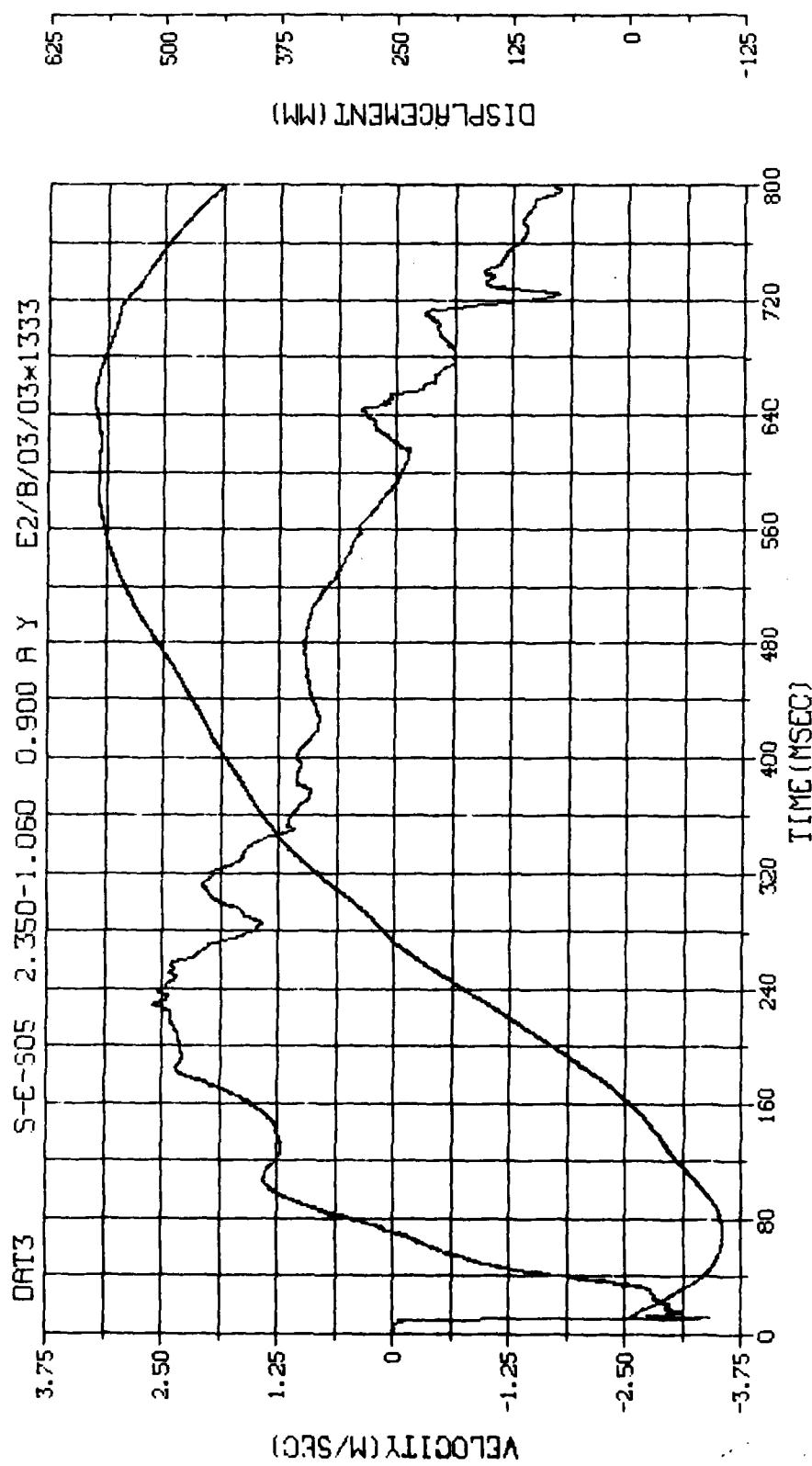
M.N. = 1332	E.U. = 0.000, 20000.000	VSN=00142
SKIP=7.000	DIGITS=0.000, 883.750	TAPE22
S.R. =10.00 KHZ	4. 4 PM, TUE, 13 SEP 83.	FILE=338 1



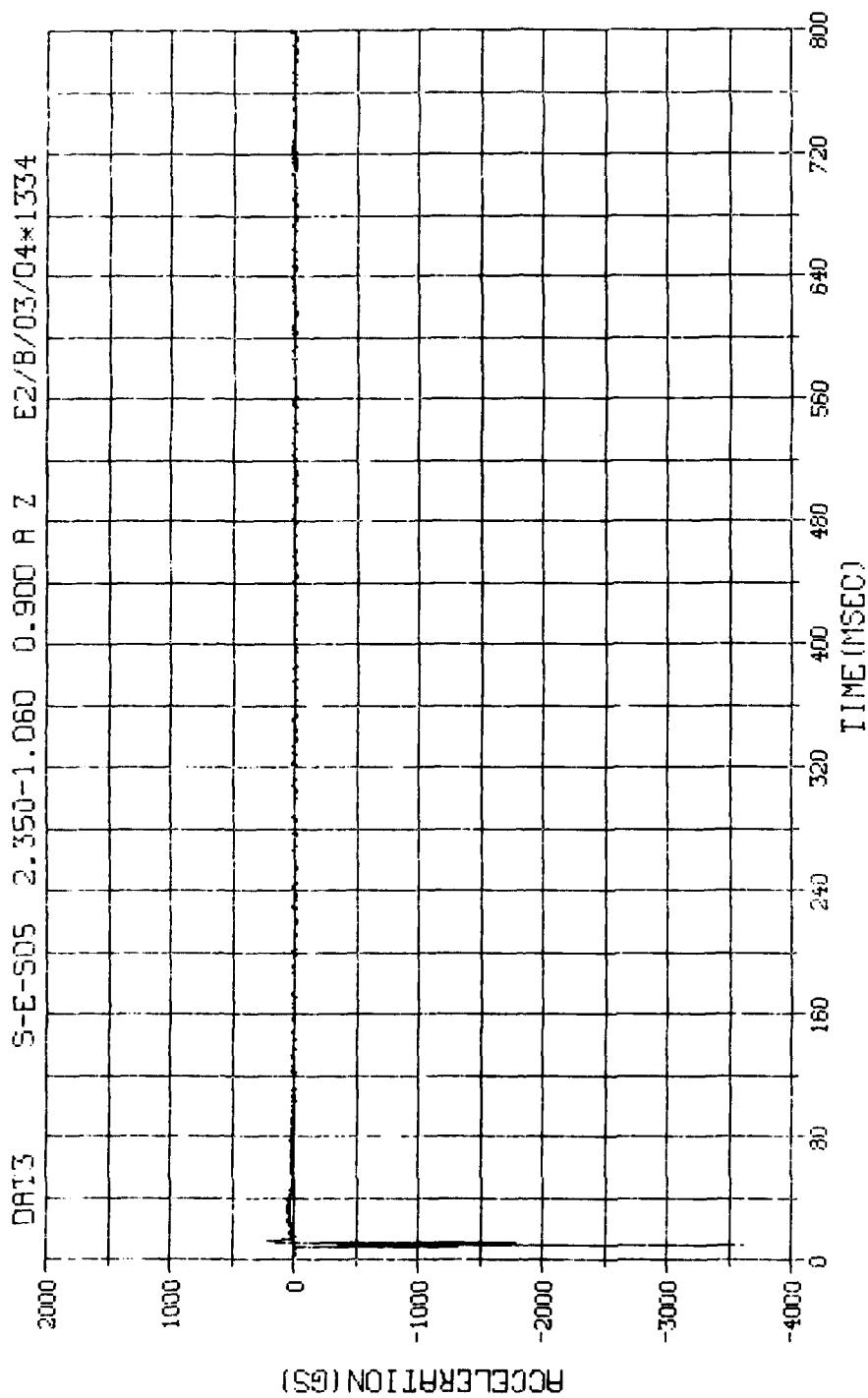
M.N. = 1332 E.U. = -0.000, 20000.000 VSN-GG142
 TSKIP=7.000 DIGITS=0.000, 883.750 TAPE22
 S.R. =10.00 KHZ 4. 4 PM, TUE, 13 SEP 83. FILE=338 2



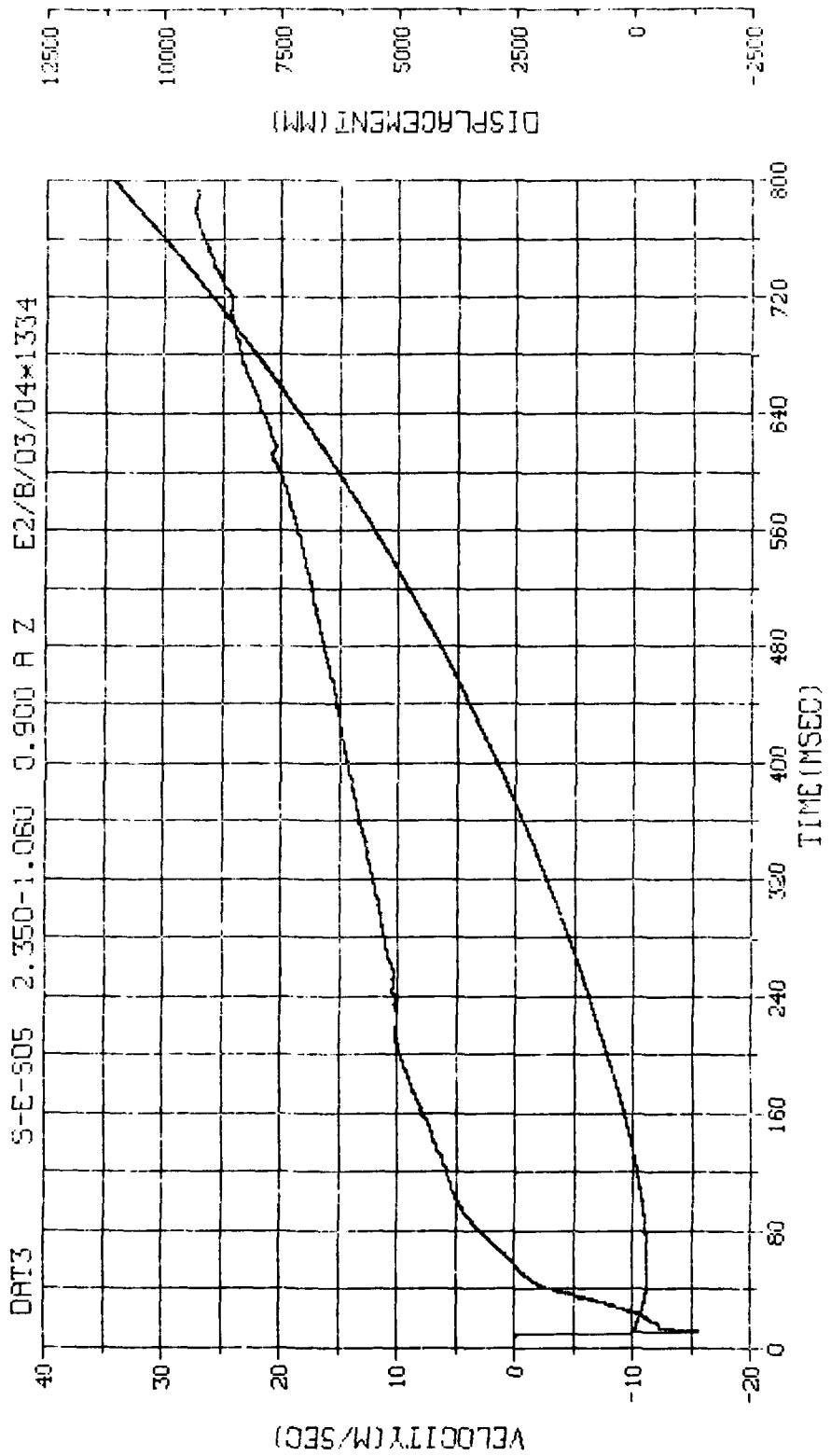
M.N. - 1333	E.U. -0.000,450.000	VSN-00142
TSKIP=7.000	DIGITS=0.000,886.625	TAPE22
S.R. =10.00 KHZ	4. 4 PM,TUE, 13 SEP 83.	FILE=340 1

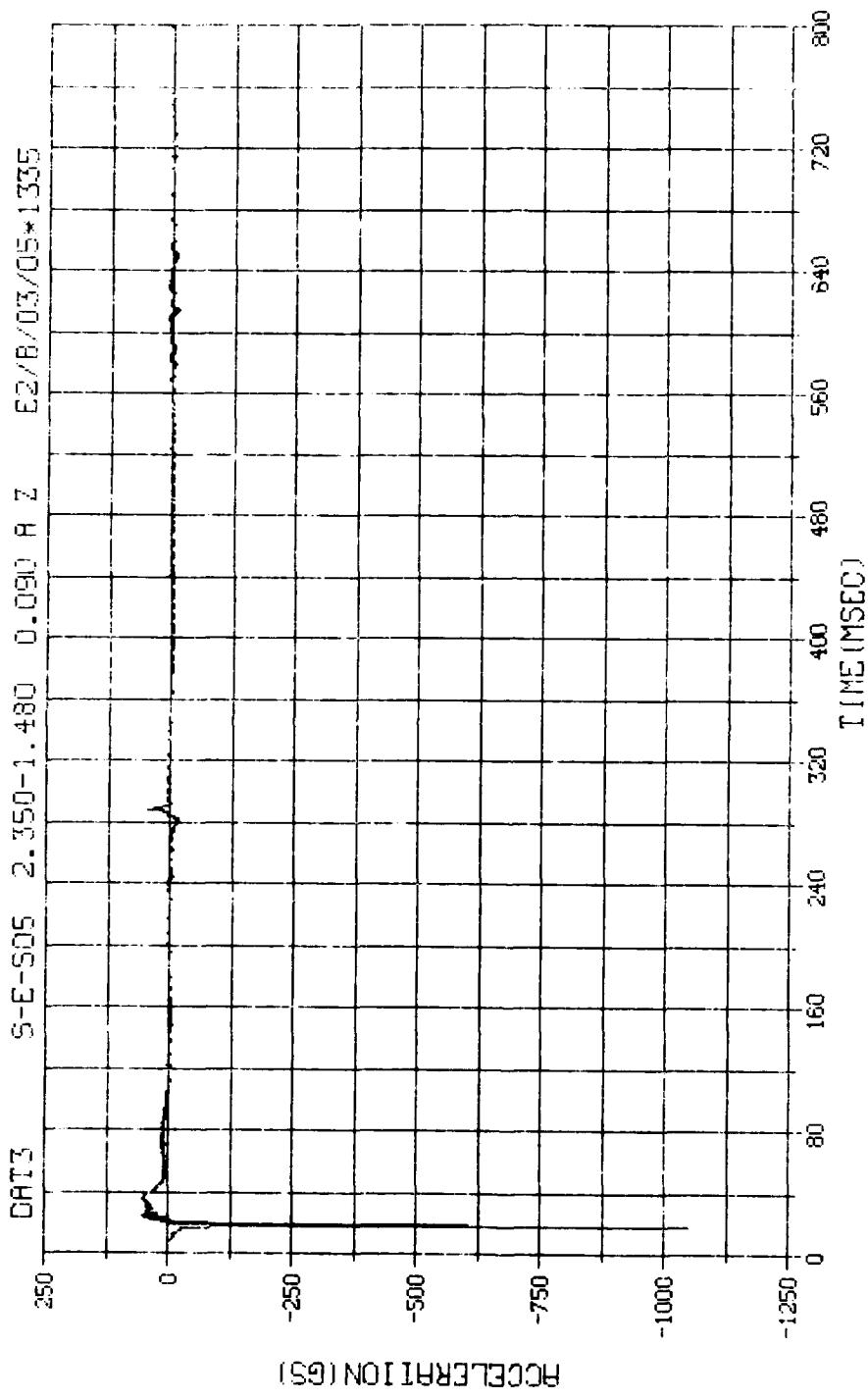


M.N. - 1333	E.U. -0.000, 450.000	VSN-66142
TSKIP=7.000	DIGITS=0.000, 886.625	TAPE22
S.R. =10.00 KHZ	4. 4 PM, TUE, 13 SEP 83.	FILE=340 2

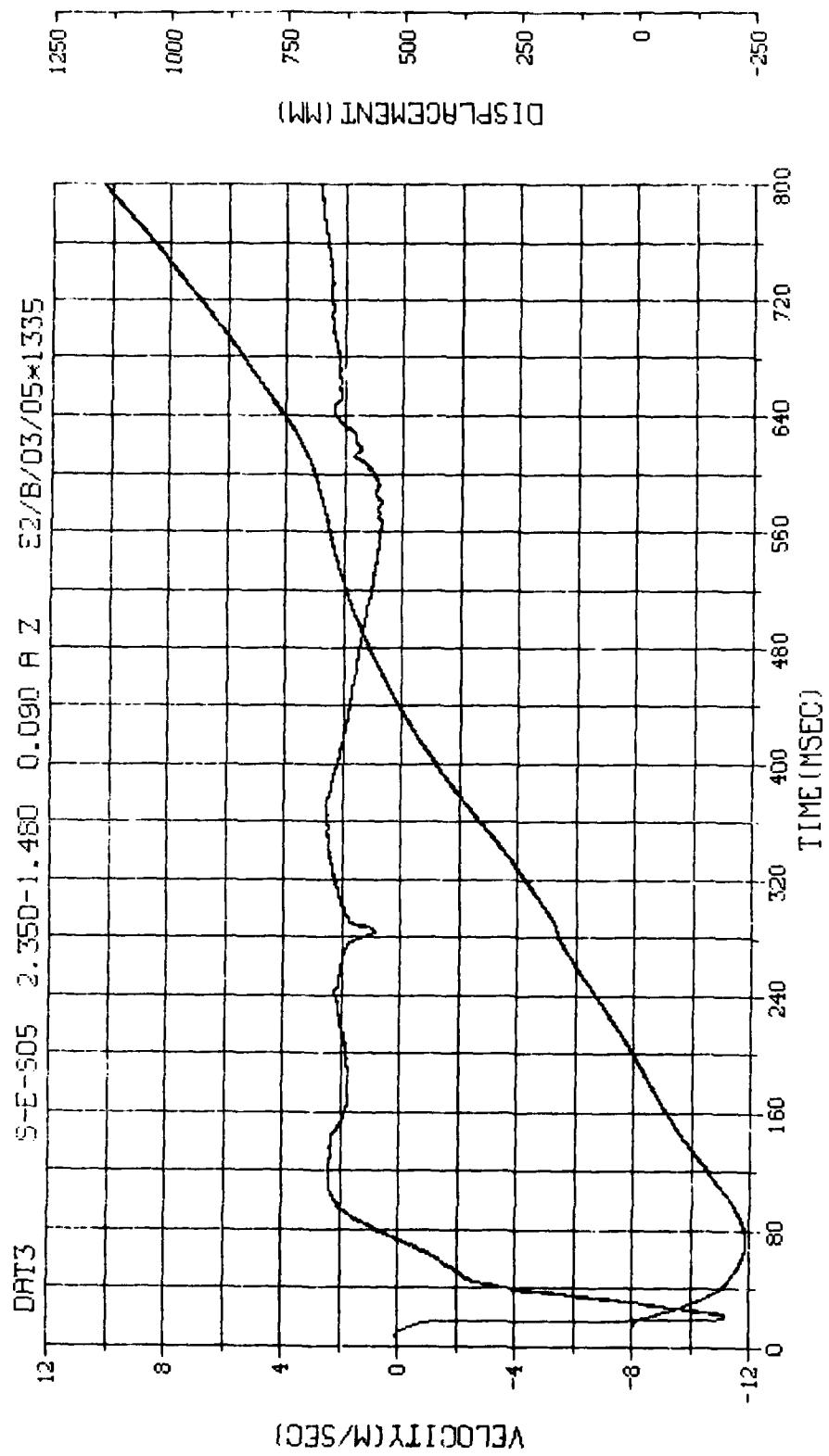


N.N. = 1334	E.U. = 0.000, 2400.000	VSN-66142
SKIP=7.000	DIGITS=0.000, -873.000	TAPE22
S.R. =10.00 KHZ	4. 4 PM, TUE, 13 SEP 83.	FILE=342 1

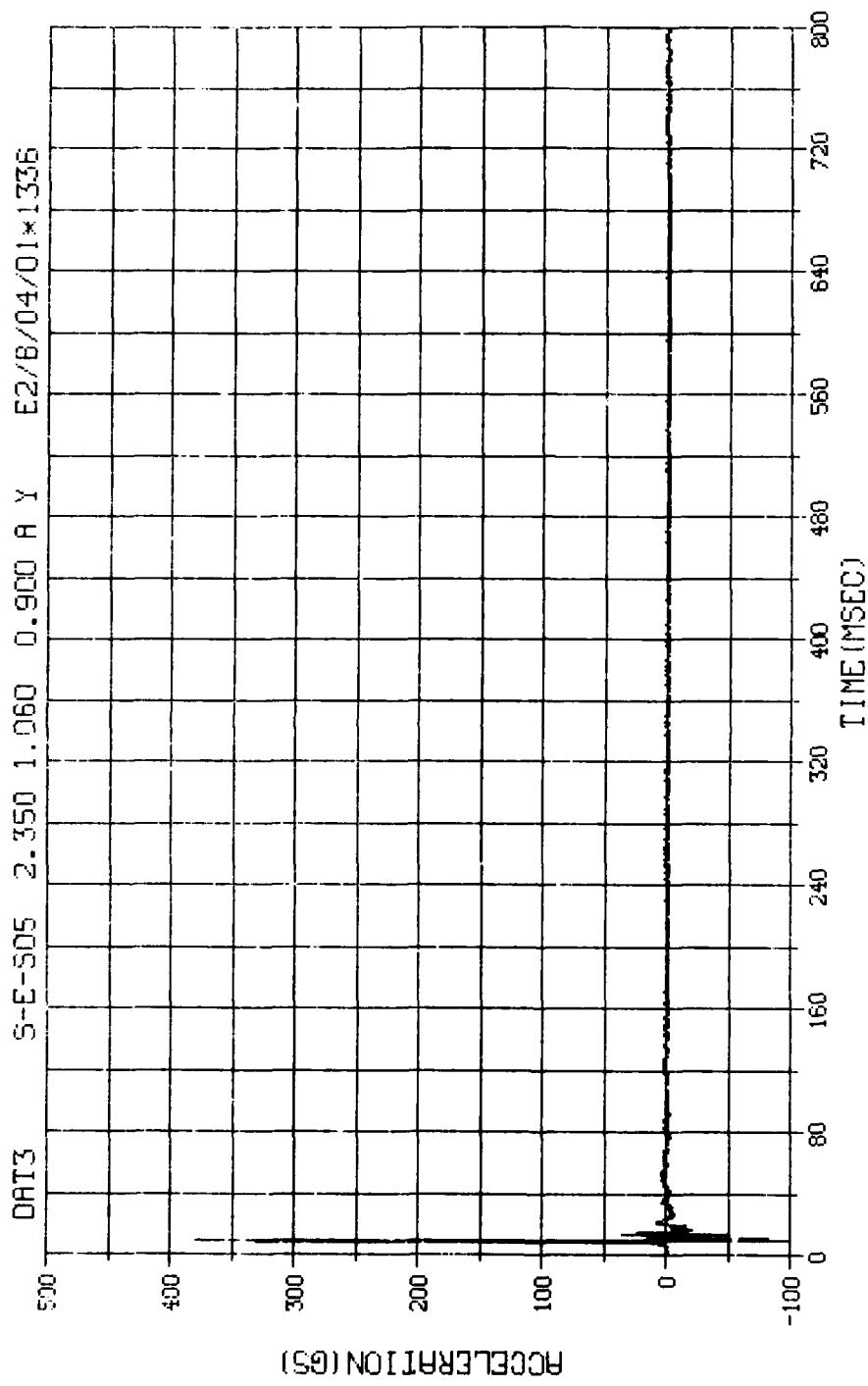




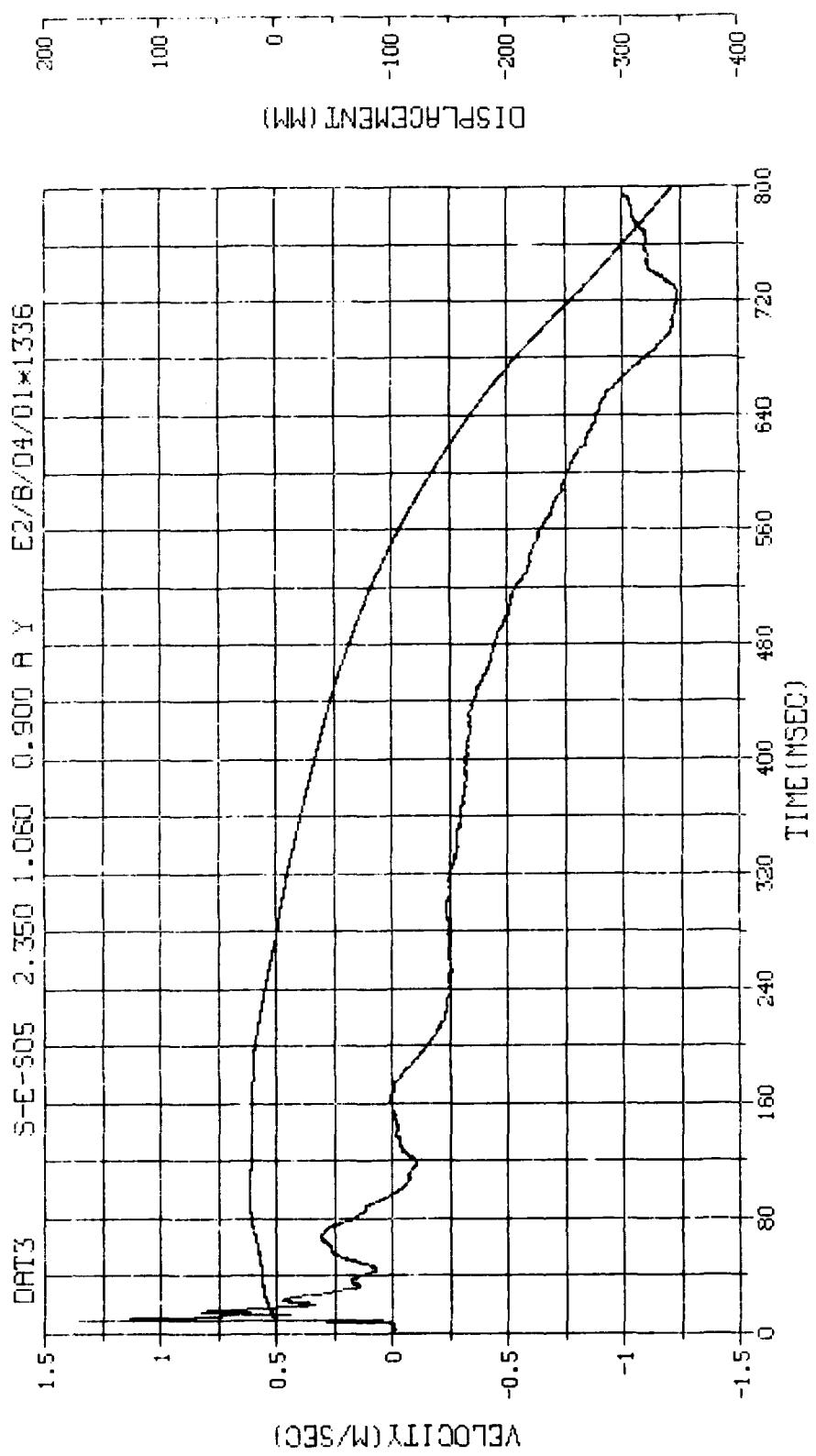
M.N. = 1335	E.U. = -0.090, 450.000	VSN-00142
TSKIF=7.000	DIGITS=0.000, -892.375	THPE22
S.R. = 10.00 KHZ	8.47 AM, W.D., 14 SEP 83.	FLLC-3+4, 1



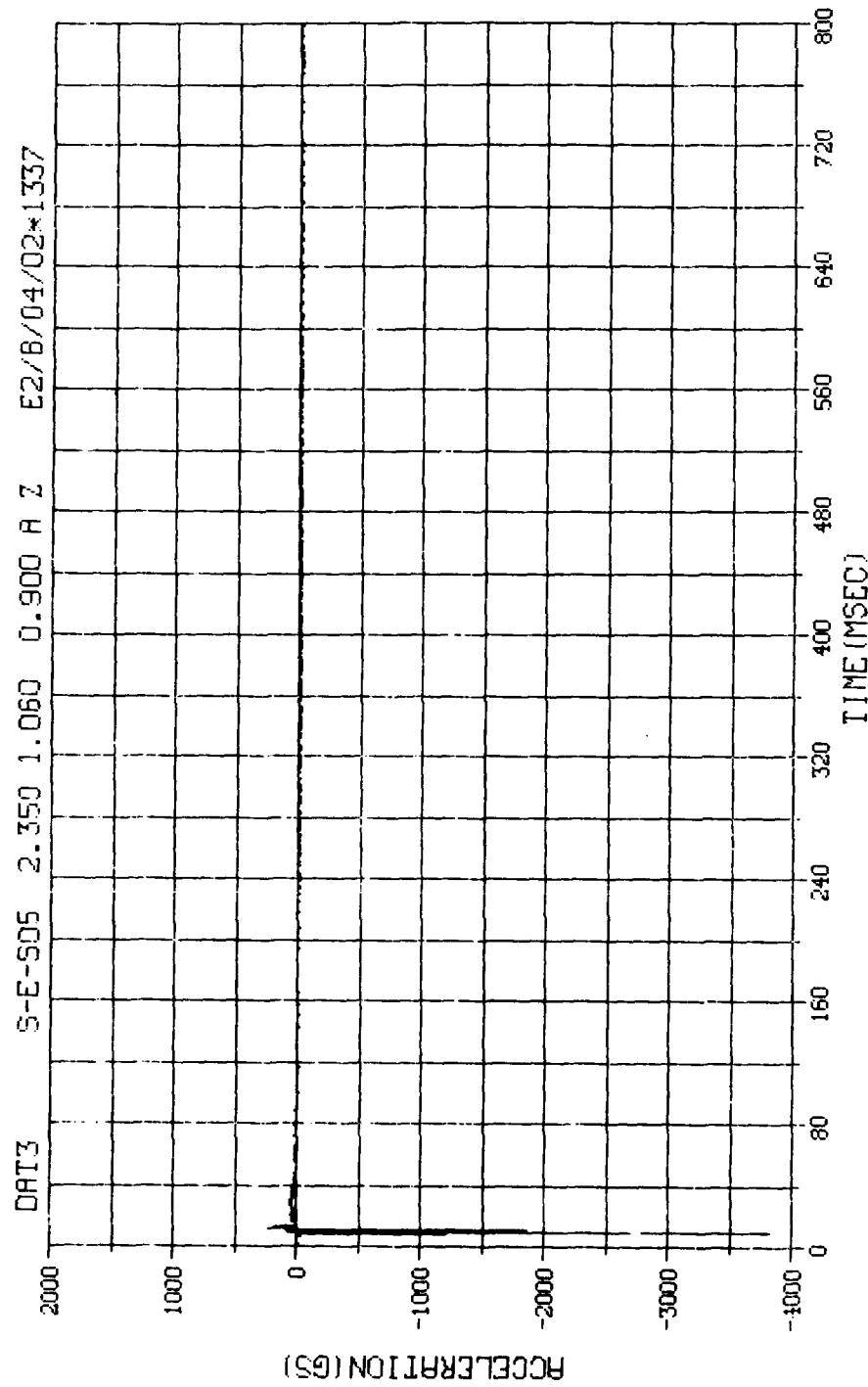
M. N. = 1335	E.U. = 0.000, 450.000	VSN-66142
TSKIP=7.000	DIGITS=0.000, -892.375	TYPE22
S.R. =10.00 KHZ	8.47 AM, WED, 14 SEP 83.	FILE=344 2



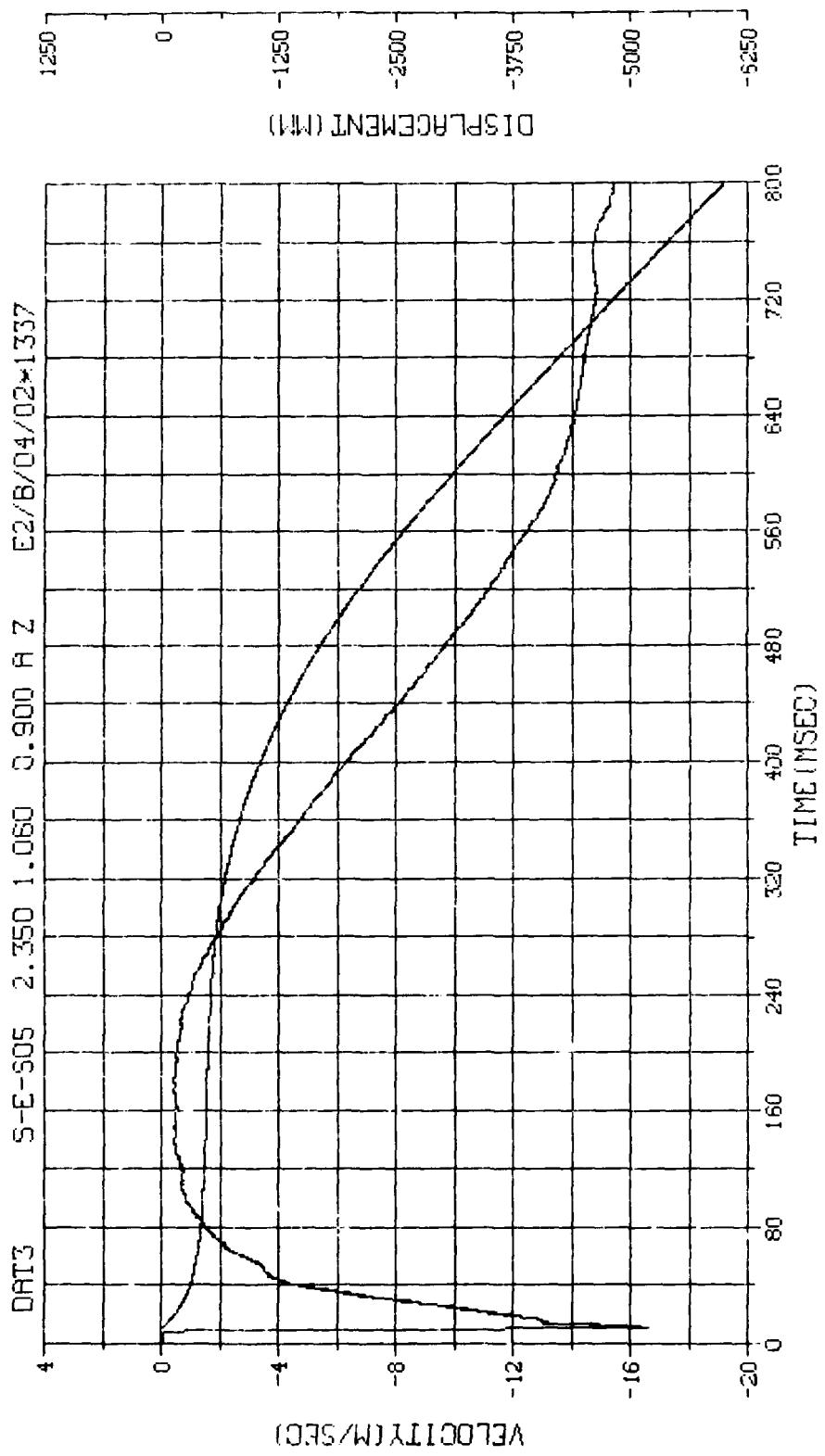
N.N. = 1336	E.U. = 0.000, 450.000	VSN-00142
SKIP=7.000	DIGITS=0.000, -893.375	TAPE22
S.R. = 10.00 KHZ	8.47 AM, WED, 14 SEP 83.	FILE=346



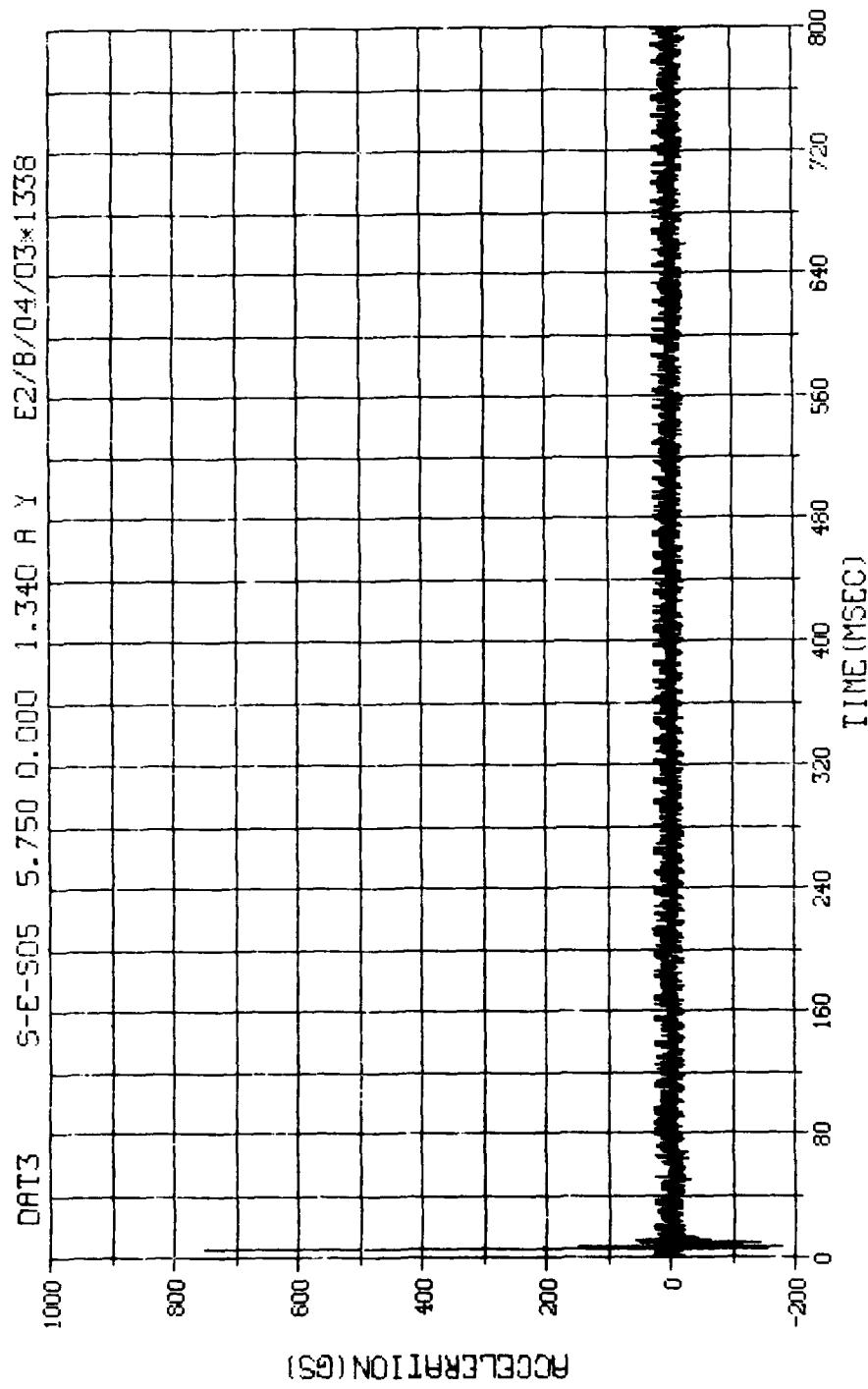
M.N. = 1336	E.U. = 0.000, 450.000	VSN=06142
TSKIP=7.000	DIGITS=0.000, -893.375	TAPE22
S.R. =10.00 KHZ	8.47 AM, WED, 14 SEP 83.	FILE=345_2



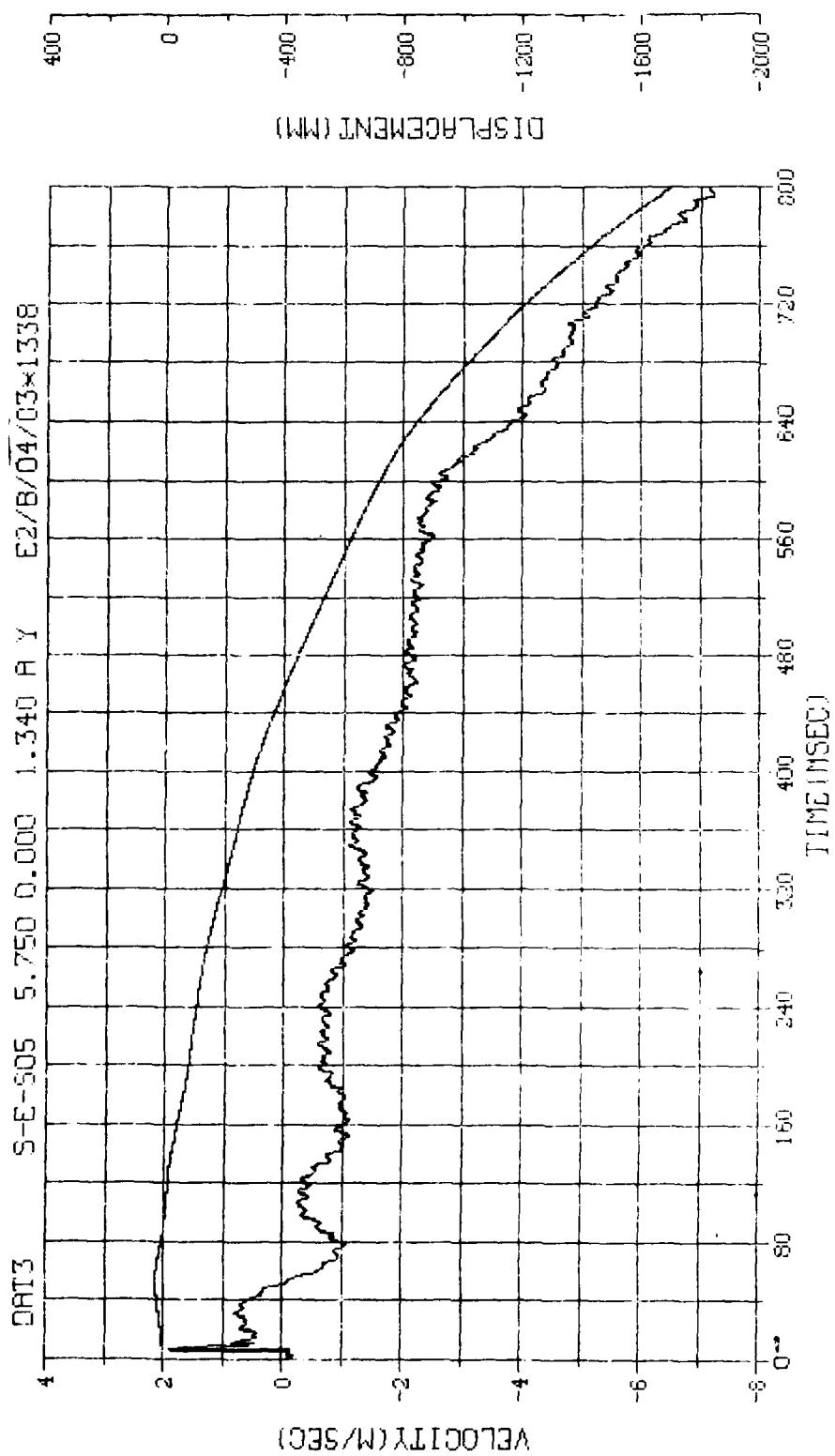
N.N. - 1337 S.U. -0.000, 2400.000 VSN-66142
TSKIP=7.000 DIGITS=0.000, -877.500 TAPE22
S.R. =10.00 KHZ 4. 4 PM, TUE, 13 SEP 83. FILE=348 1



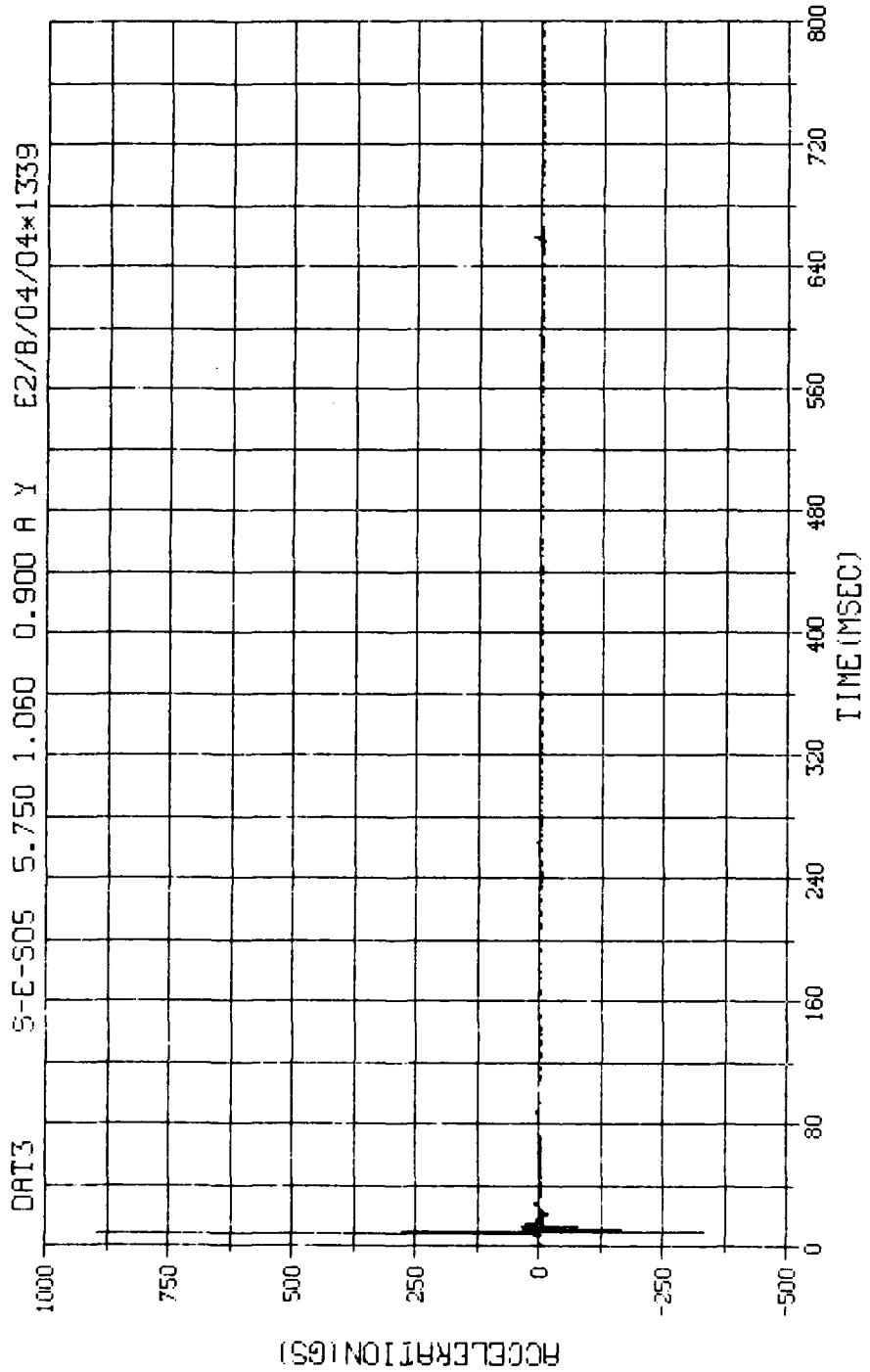
M.N. = 1337	E.U. = 0.000, 2400.000	VSN=06142
SKIP=7.000	DIGITS=0.000, -877.500	TAPE22
S.R. = 10.00 KHZ	4. 4 FM, TUE, 15 SEP 83.	FILE=348_2



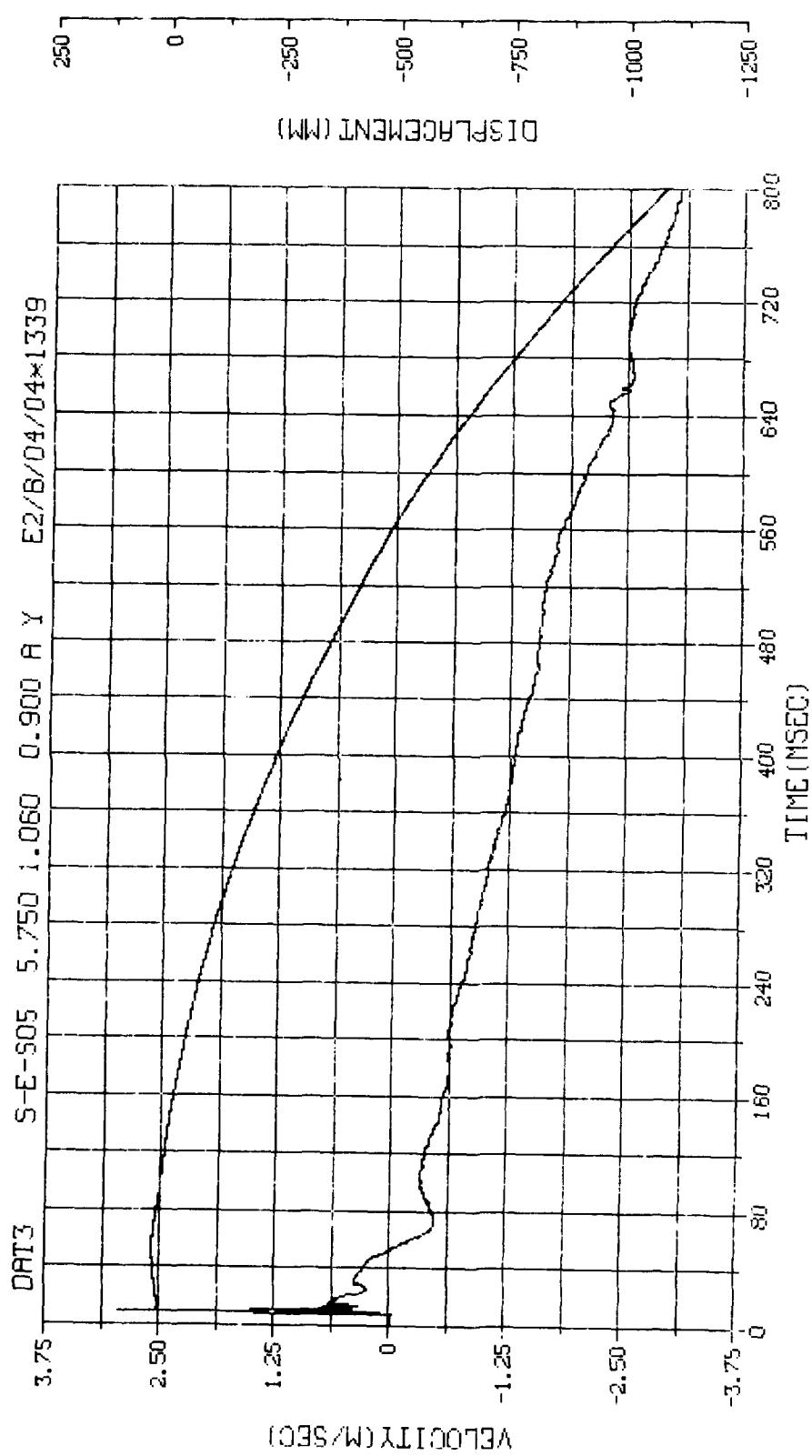
N.N. = 1338	E.U. = 0.000, 4500.000	VSN=66142
TSKIF=7.000	DIGITS=0.000, -884.875	TAPE22
S.R. = 10.00 KHZ	4. 4 PM, TUE, 13 SEP 83.	FILE=350 1



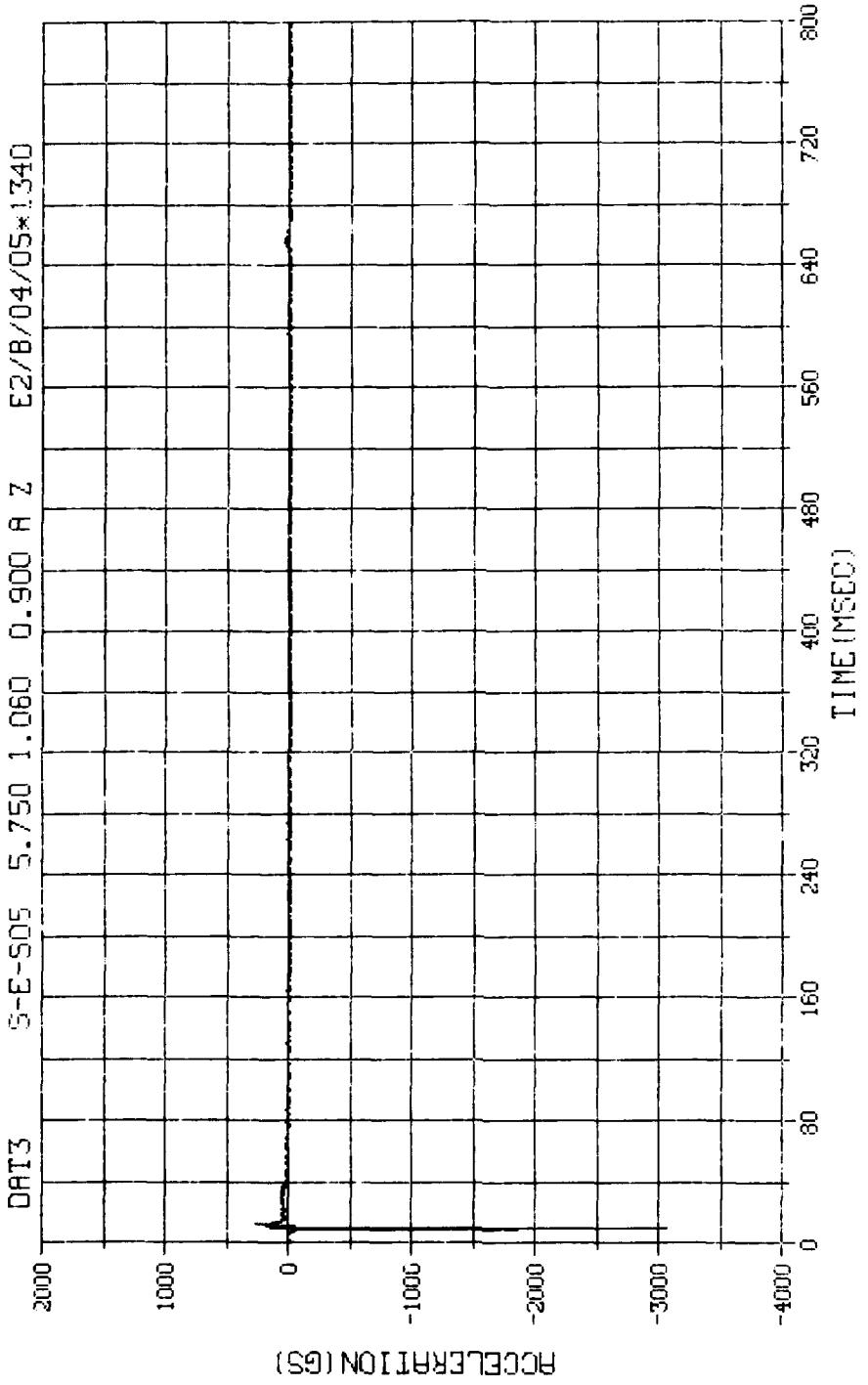
M.N. = 1338	E.U. = 0.000, 4500.000	VSN-GG142
T5KIP=7.000	DIGIT3=0.000, -884.875	THFE22
S.R. = 10.00 KHZ	4, 4 P.P.TUE, 13 SEP 03.	FILE=350
		2



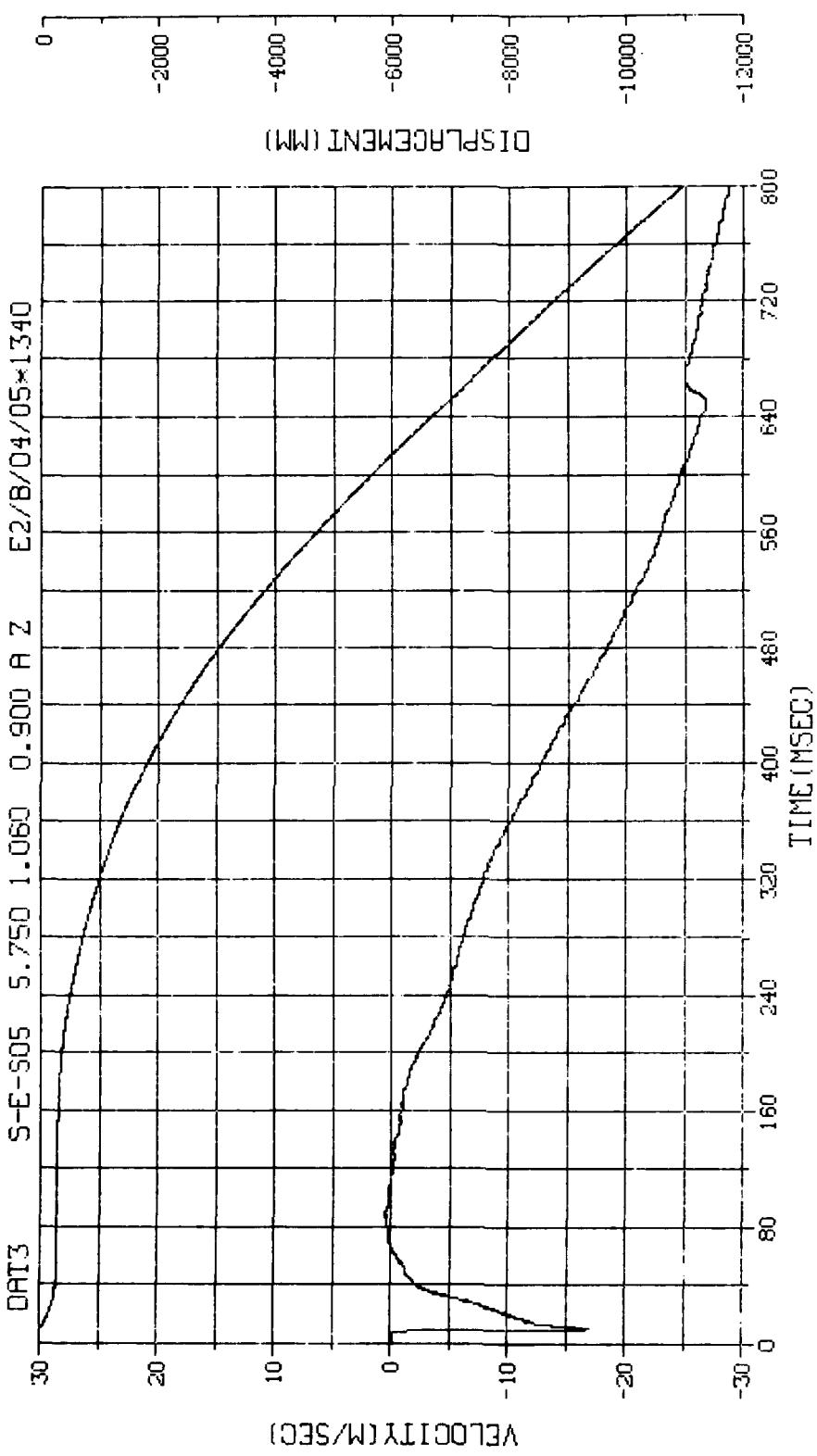
N. N. = 1339	E. U. = -0.000, 450.000	VSN-66142
SKIP=7.000	DIGITS=0.000, -876.875	TAPE22
S. R. = 10.00 KHZ	4. 4 PM, TUE, 13 SEP 83.	FILE=352 1



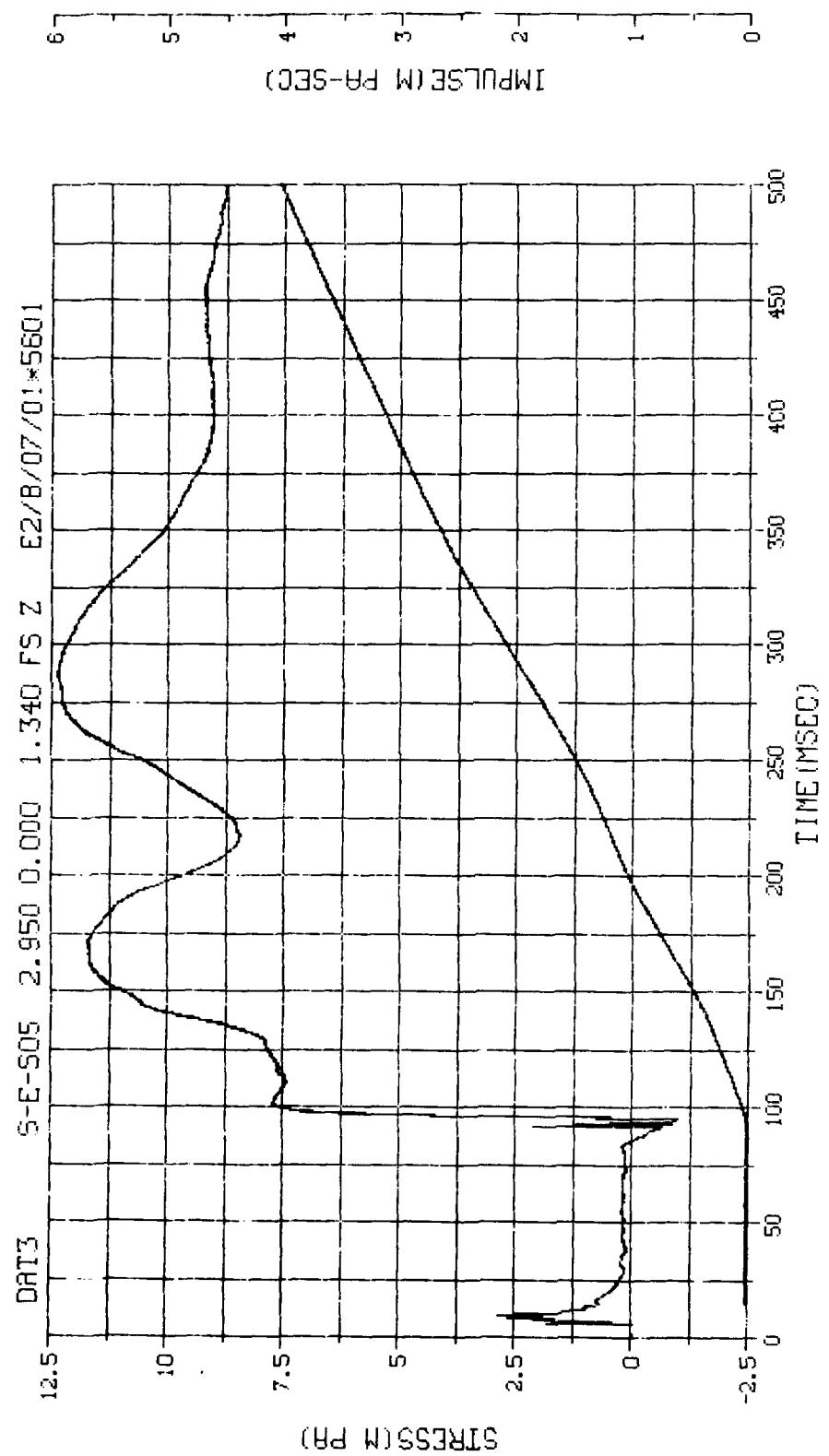
M. N. = 1339	E. U. = 0.000, 450, 000	VSN-66142
TSKIP=7,000	DIGITS=0,000,-876,875	TAPE22
S. R. = 10.00 KHZ	4. 4 P1, 100, 13 SEP 83.	FILE=352 2



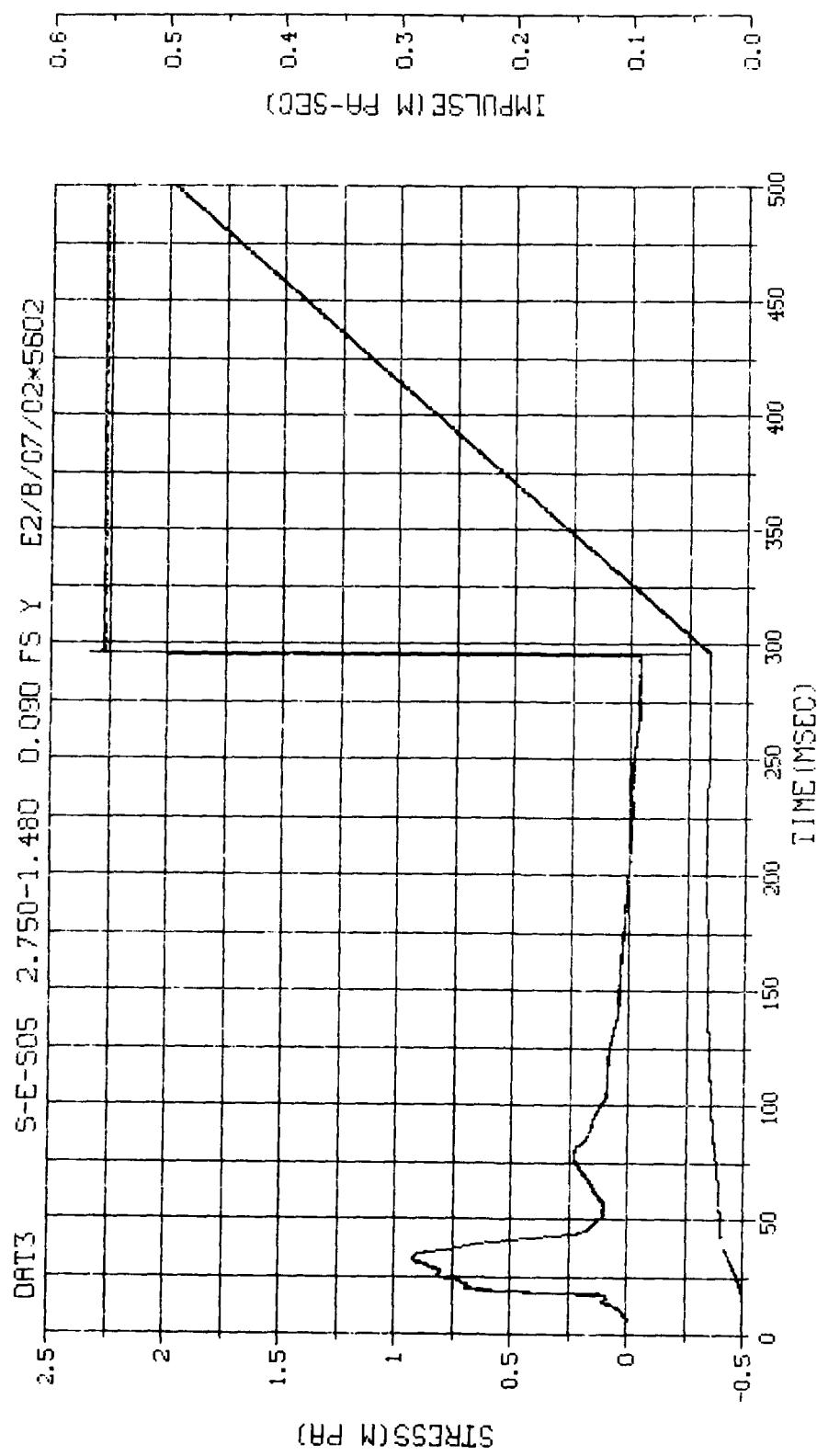
M.N. - 1340	E.U. -0.000, 2400.000	VSN-66142
TSKIF-7.0000	DIGITS-0.000, -899.500	TAPR22
S.R. = 10.00 kHz	4, 4 PH, TUE, 13 SEP 83,	FILE=354
		1



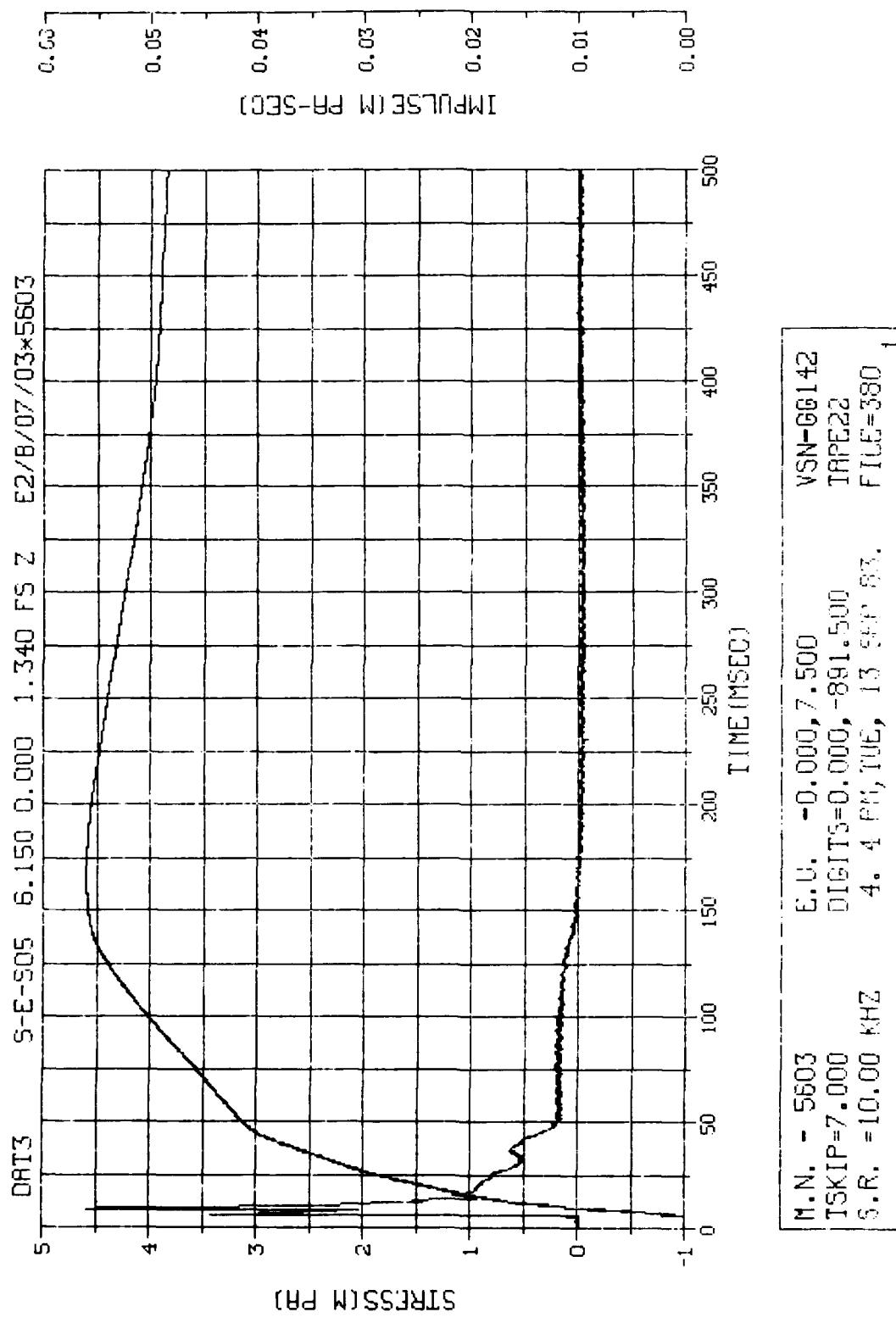
M.N. = 1340	E.U. = 0.000, 2400.000	VSN-00142
TSKIP=7.000	DISPLS=0.000, -898, 500	TAPE22
S.R. = 16.00 KHz	4, 4 PM, 13 SEP 83,	FILE=154 2

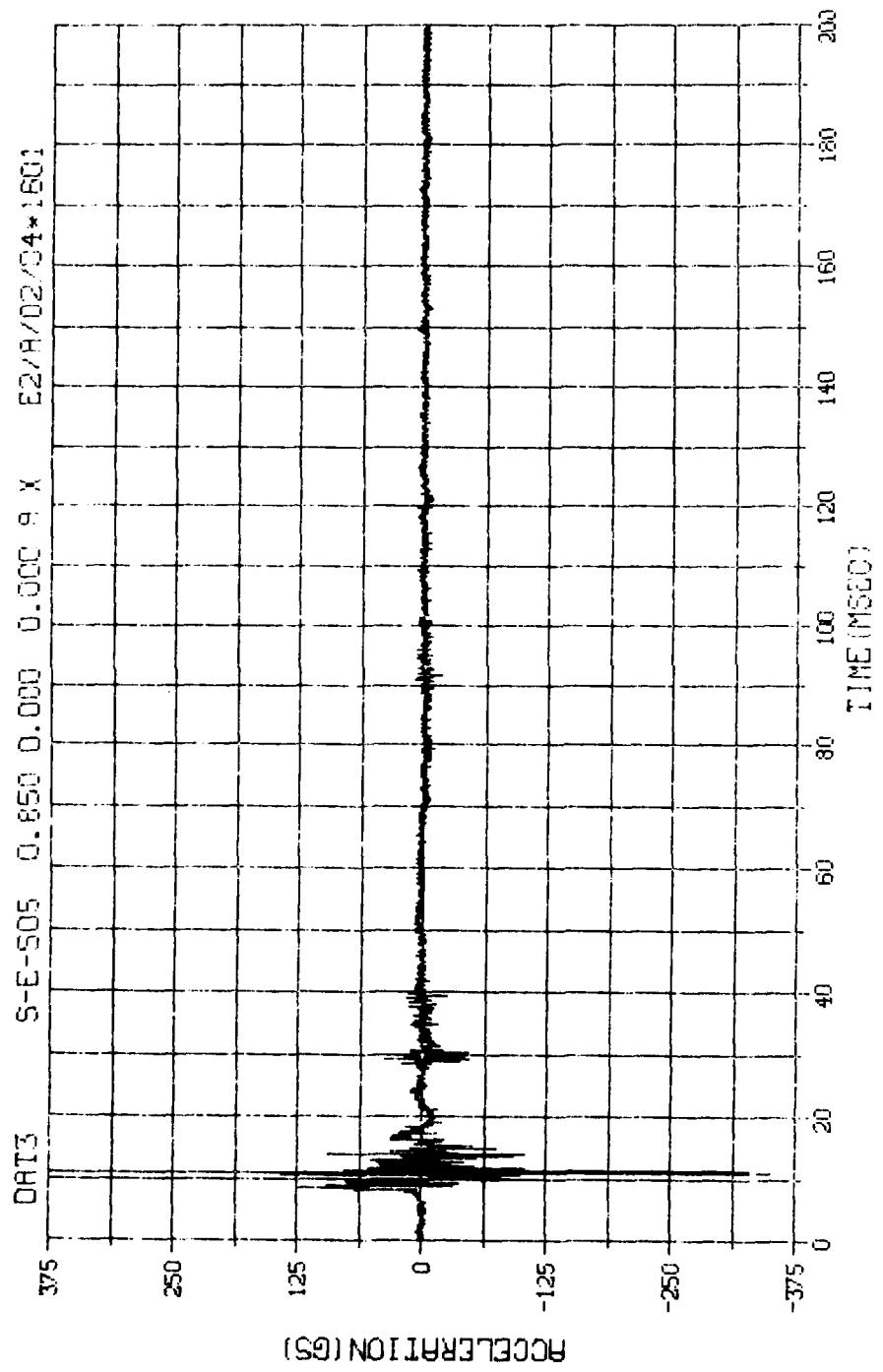


M.N. = 5601	E.U. = 0.000, 7.500	VSN=60142
SKIP=7.000	DIGITS=0,000, -909.125	TAPE22
S.R. = 10.00 KHZ	4. 4 PM, TUE, 13 SEP 83.	FILE=376 1]

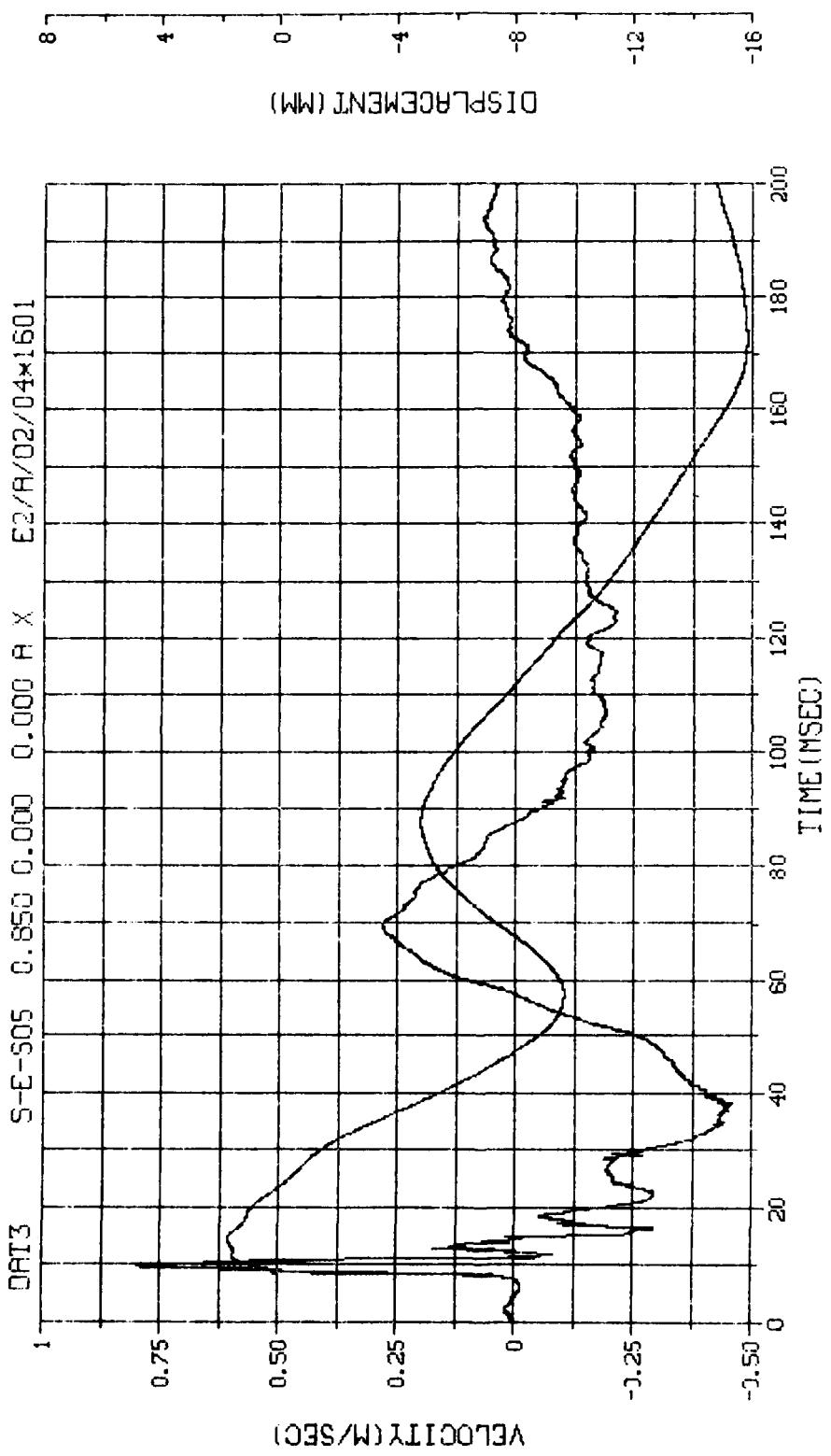


M.N. - 5602	E.U. -0.000, 1.000	VSN-66142
SKIP=7.000	DIGITS=0.000, -872.250	TAPE22
S.R. =10.00 KHZ	4. 4 PH, TUE, 18 SEP 83.	FILE=370_1]

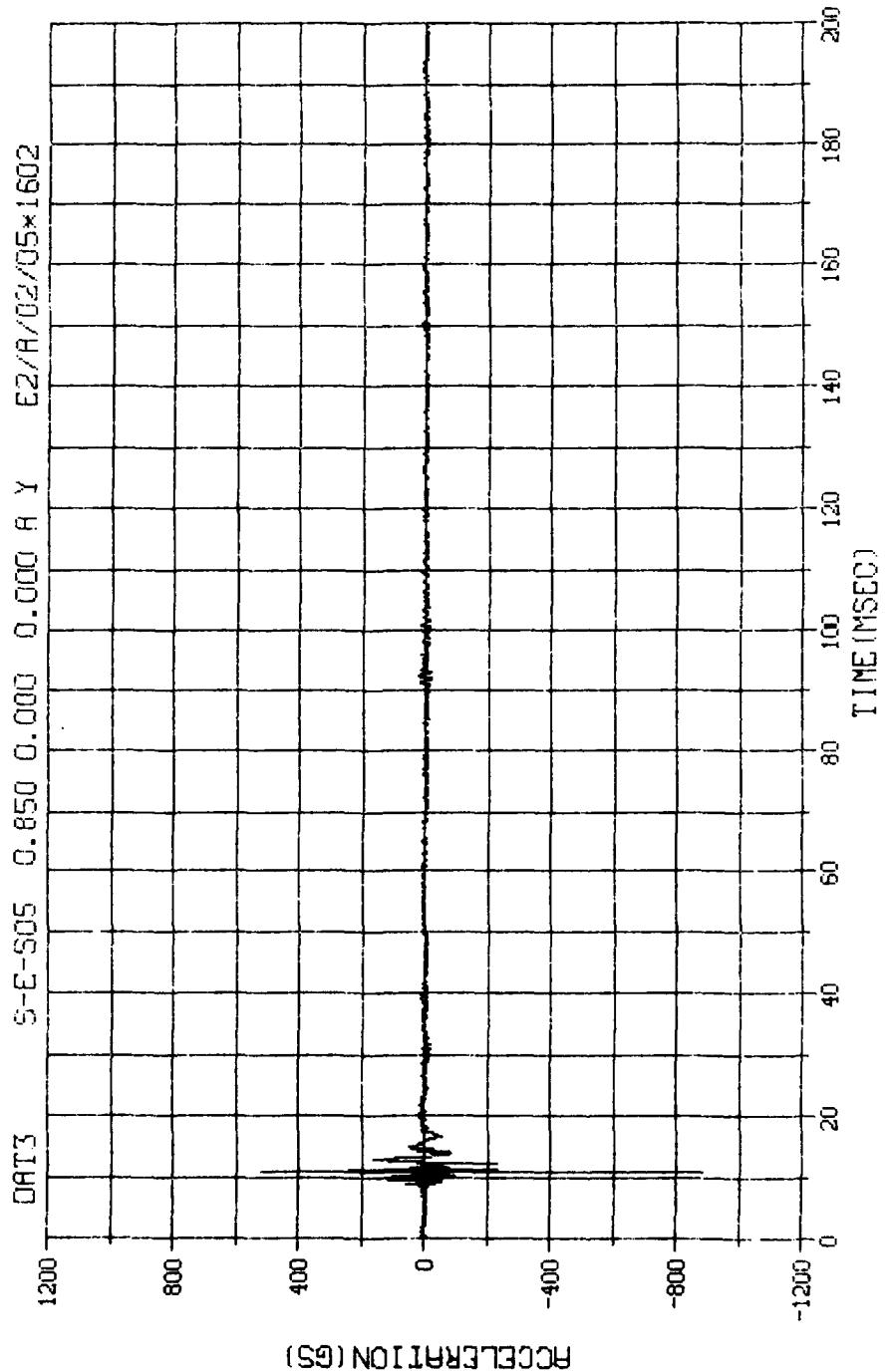




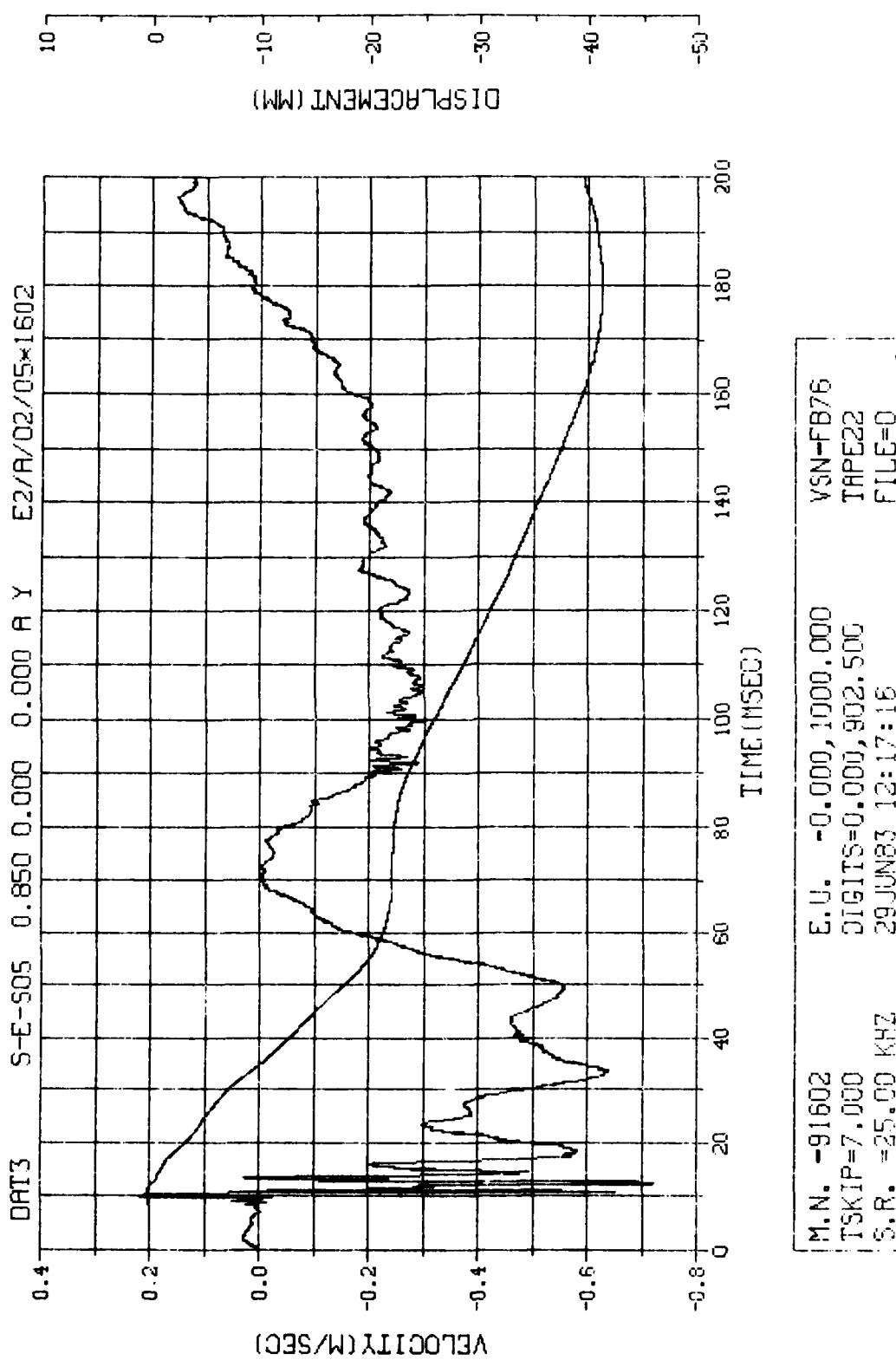
M.N. -91601 E.U. -0.000, 1000.000 VSN-FB76
TSKIP=7.000 DISITS=0.000, 867.125 TAPE22
S.R. =25.00 KHZ 29 JUN 83 12:17:16 FILE=0

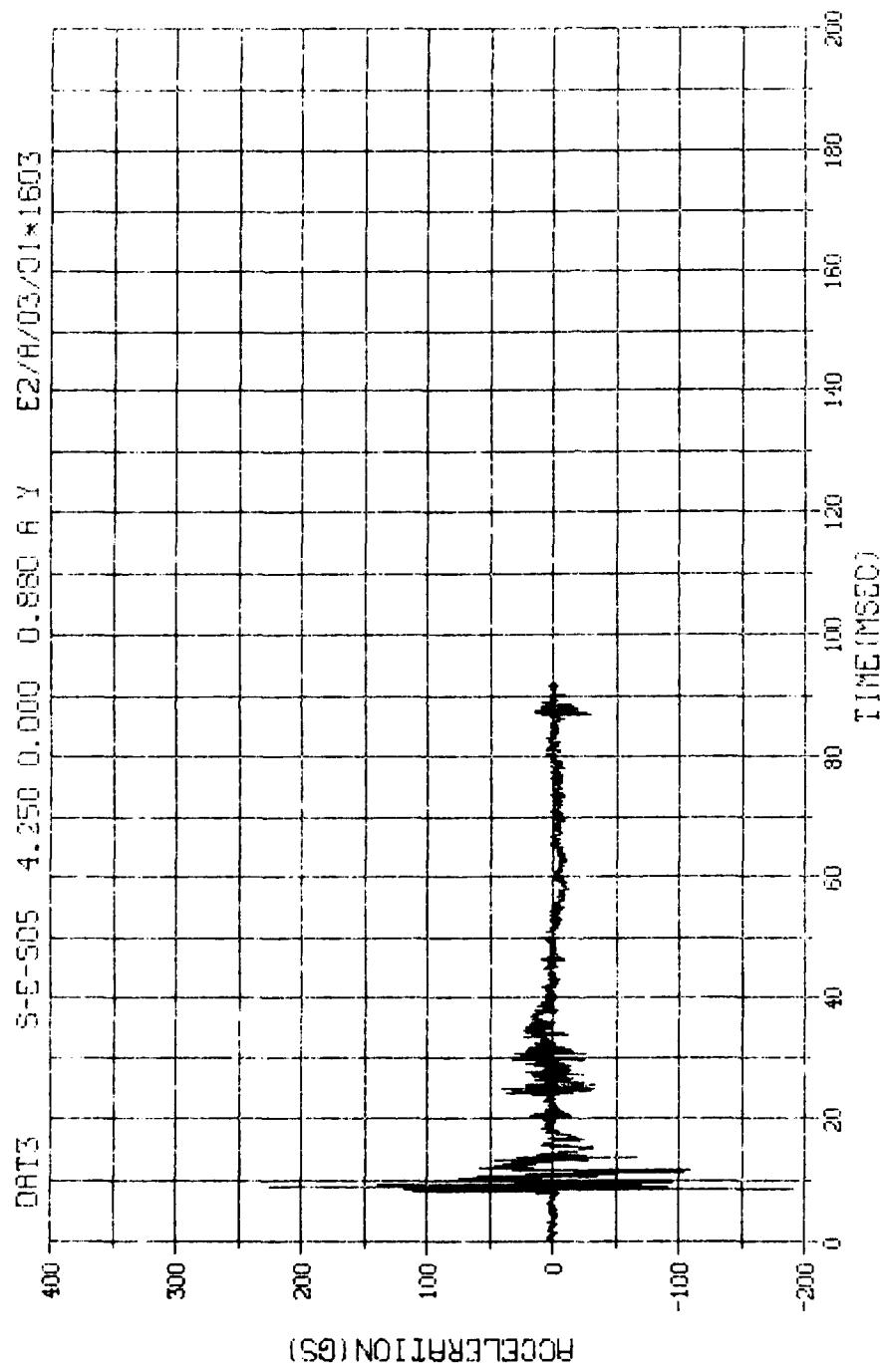


M.N.	-91601	VSN-FB76
E.U.	-0.000, 1000.000	DIGIT5=0.000, 867.125
TSKIP	=7.000	THPE22
S.R.	=25.00 KHZ	FILE=0
		2

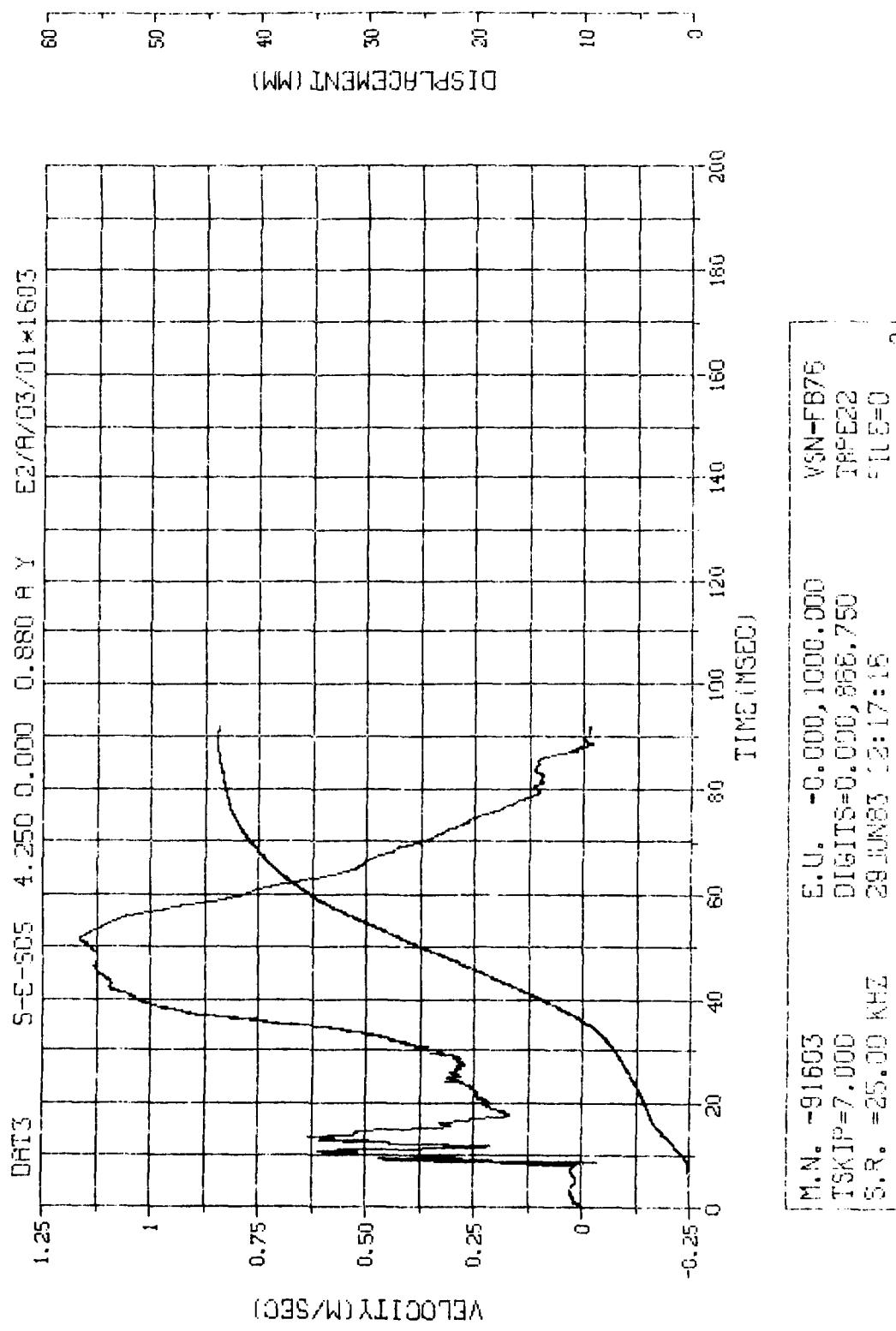


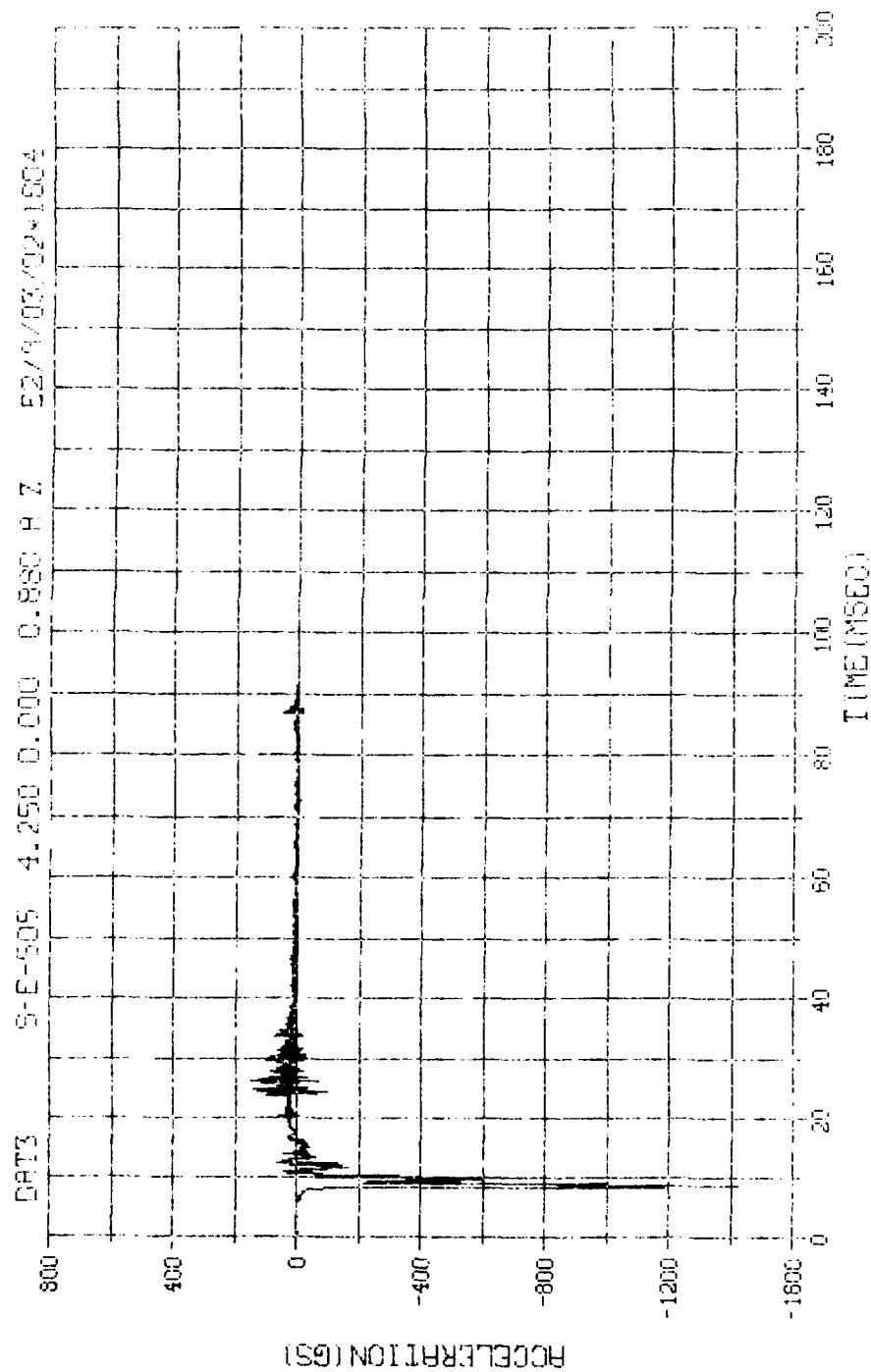
H.N. -91602	E.U. -0.000 1000.000	SEQUENC 13:17:16
TSKTP=7.000	DIGITS=0,000,902,500	TRPES2
S,A. =25.00 KHz	VSN-FE75	F1L5=0



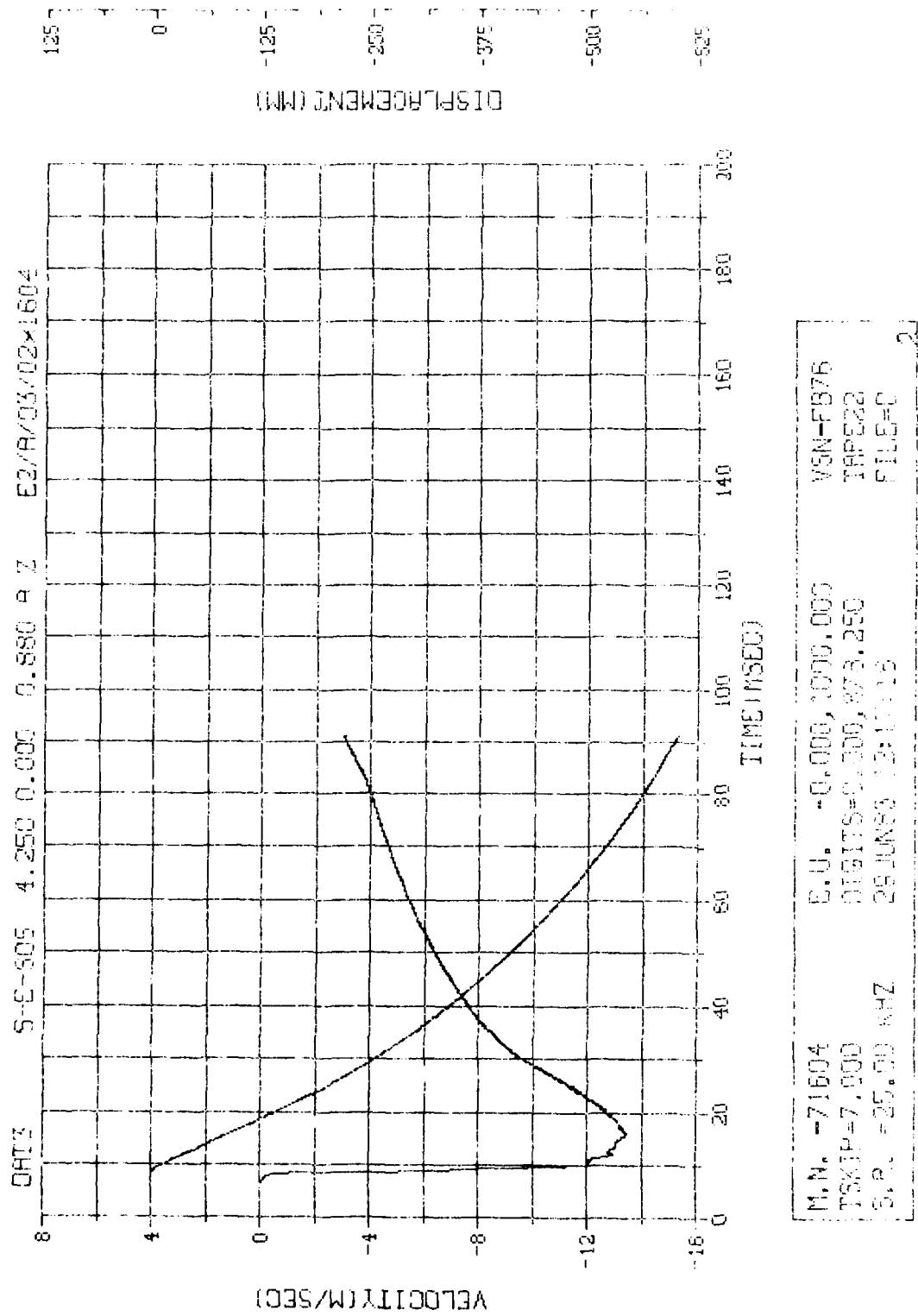


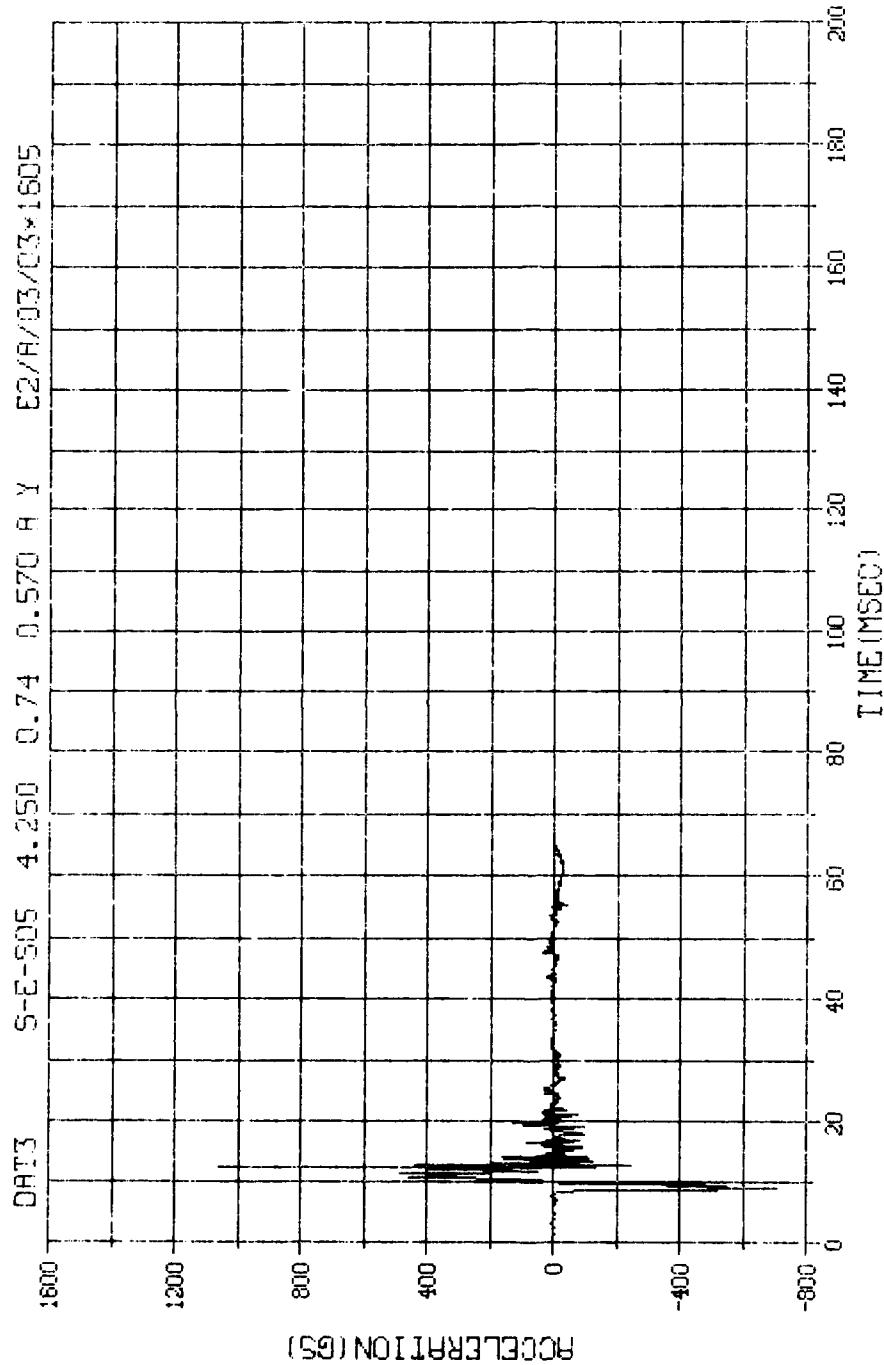
M.N. -91503	E.U. -0.000,1000.000	VSN-FB75
TSKIP=7.000	DISITS=0.000,866.750	THRE22
S.R. =25.00 KHZ	29.JUN83 12:17:16	FILE=0
		1



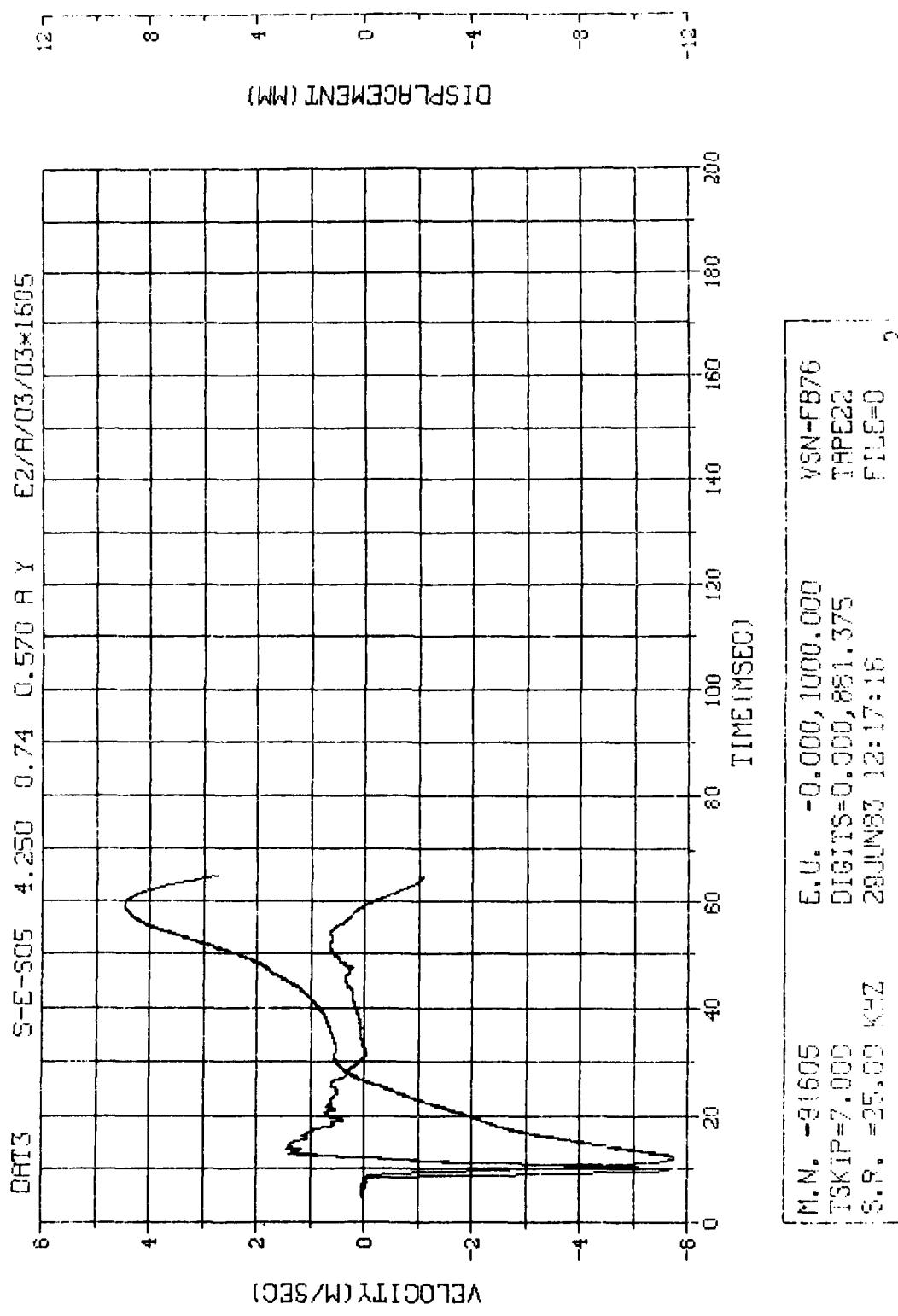


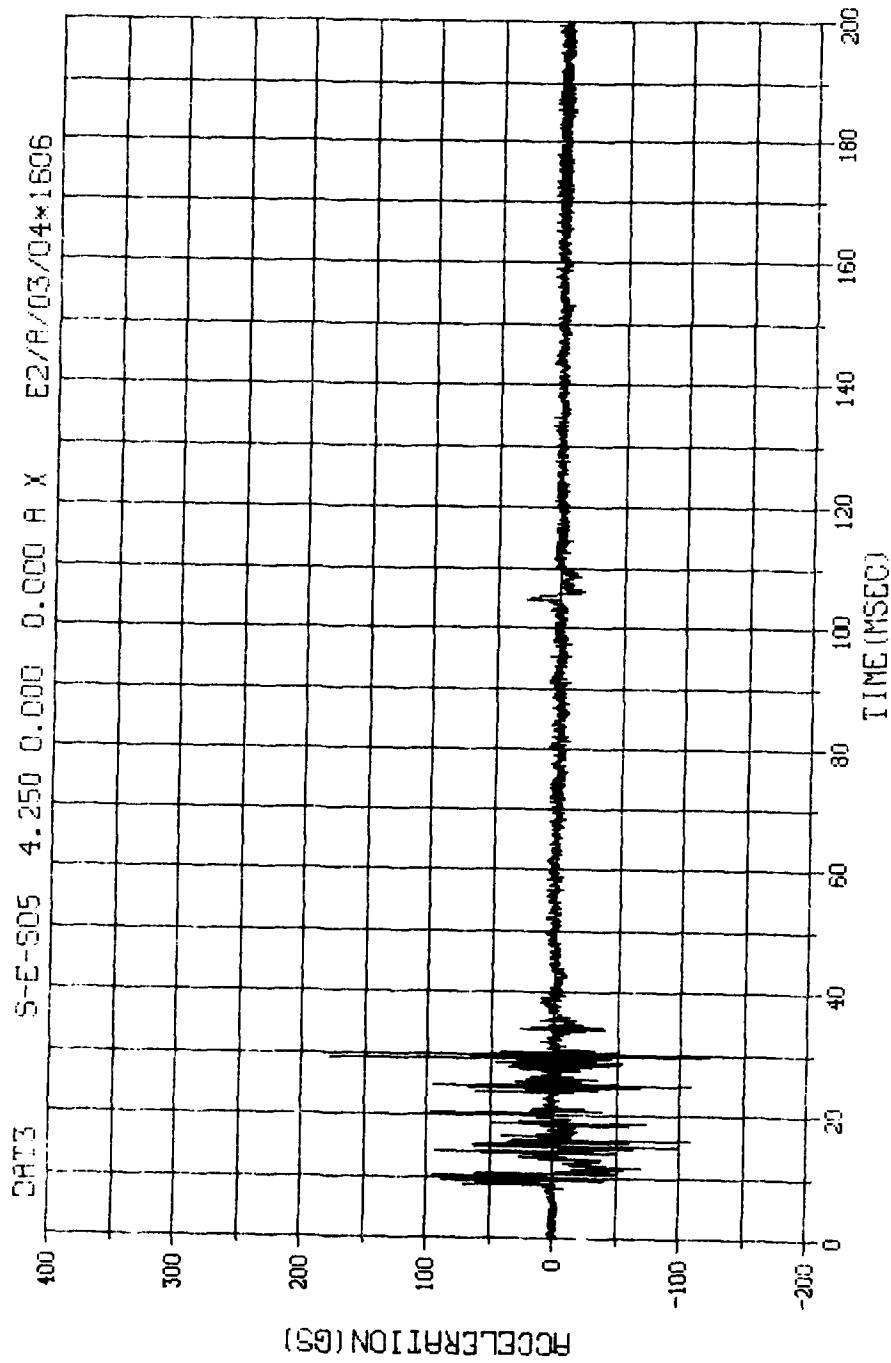
N. N.	-7.0004	5.0,	-0,000,1000,000	VSN-15B/6
7.0002	0.000	0.000,000,276,250	765522	
15.000	0.000,000	0.000,000,276,16	710E=0	



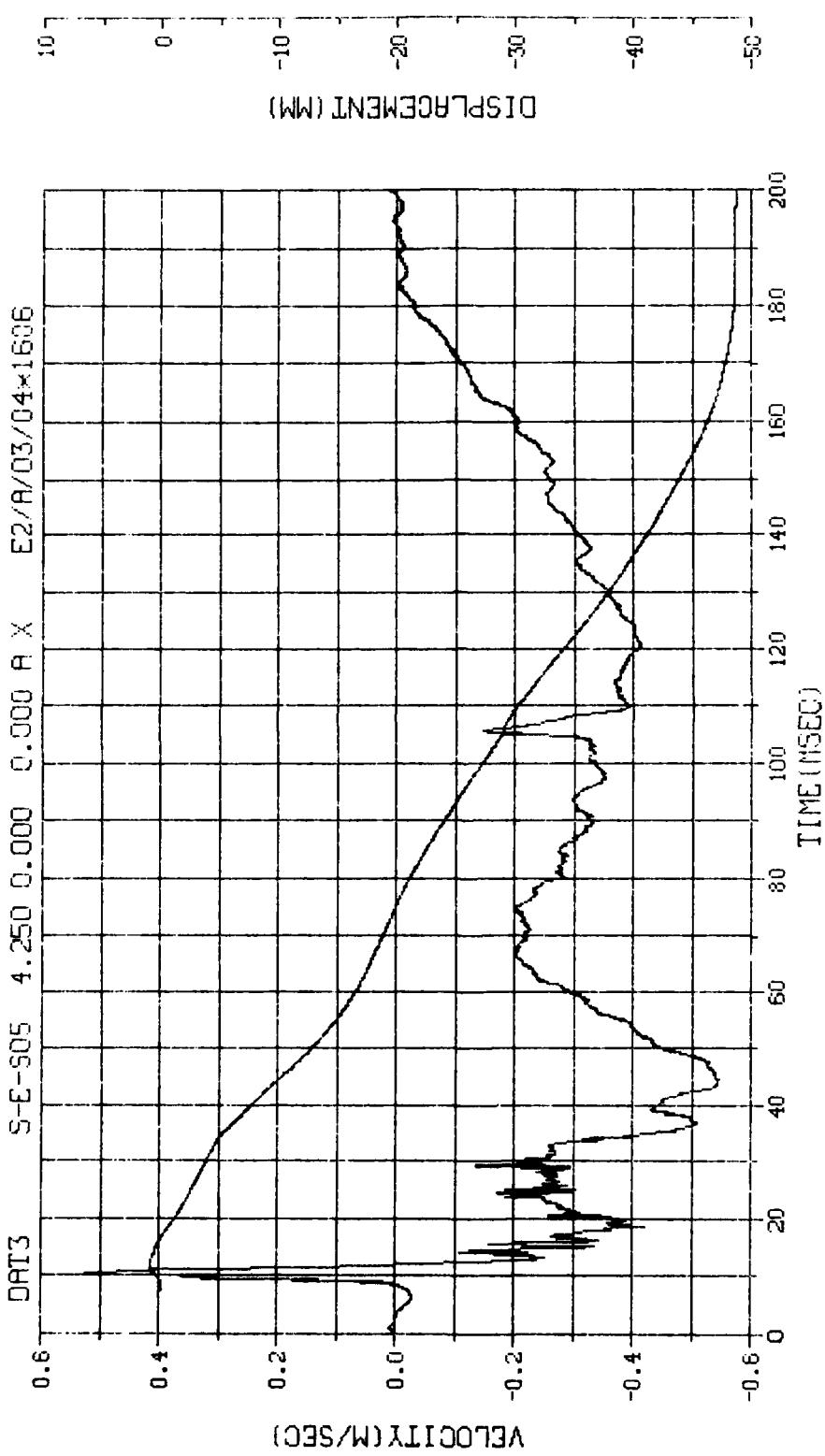


M.N. -91605 E.U. -0.000,1000.000 VSN-F875
TSKTP=7.000 DIGITS=0.000,881.375 TAPE22
S.R. =25.00 KHZ FILE=0
29JUN83 12:17:16

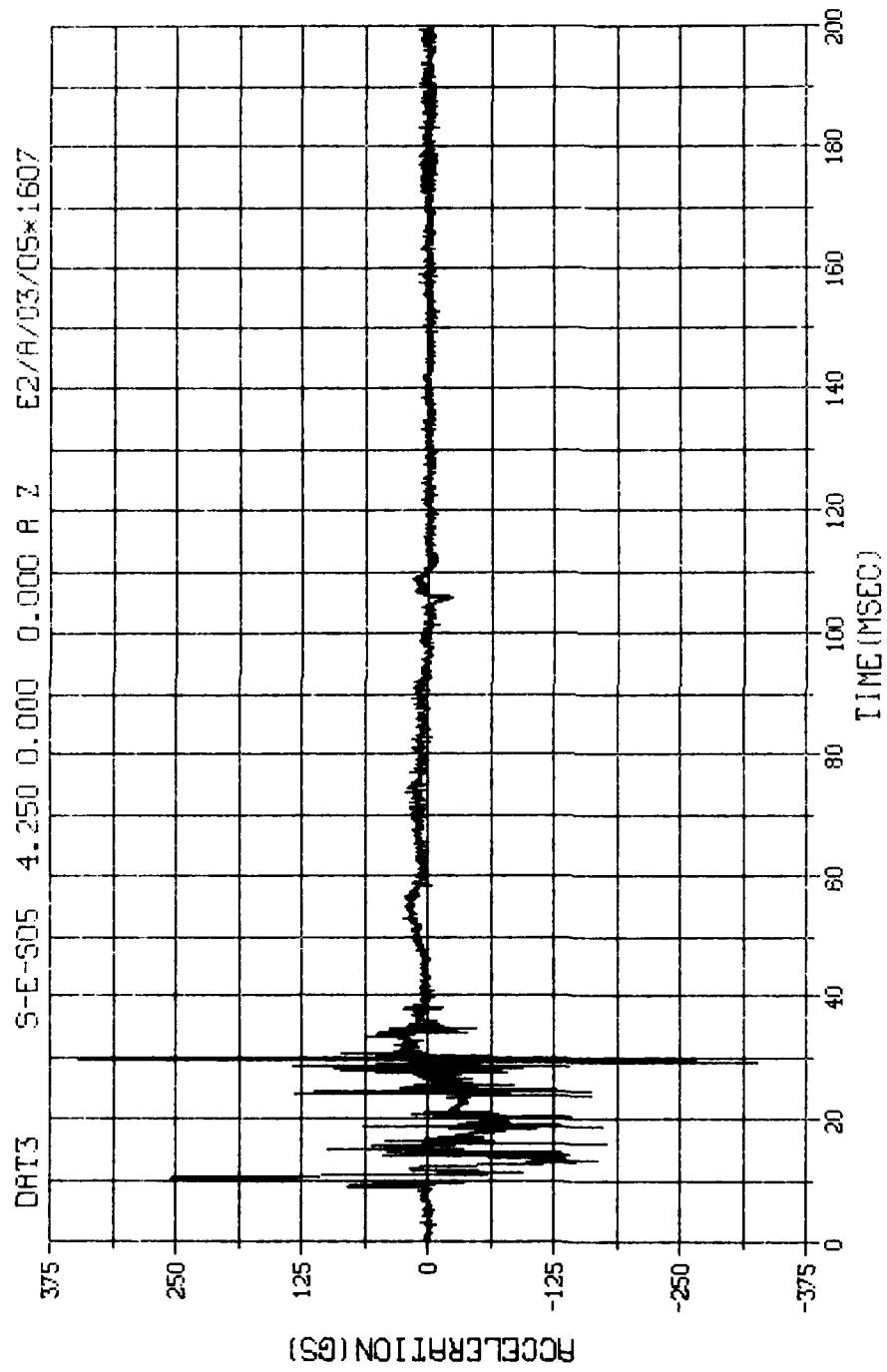




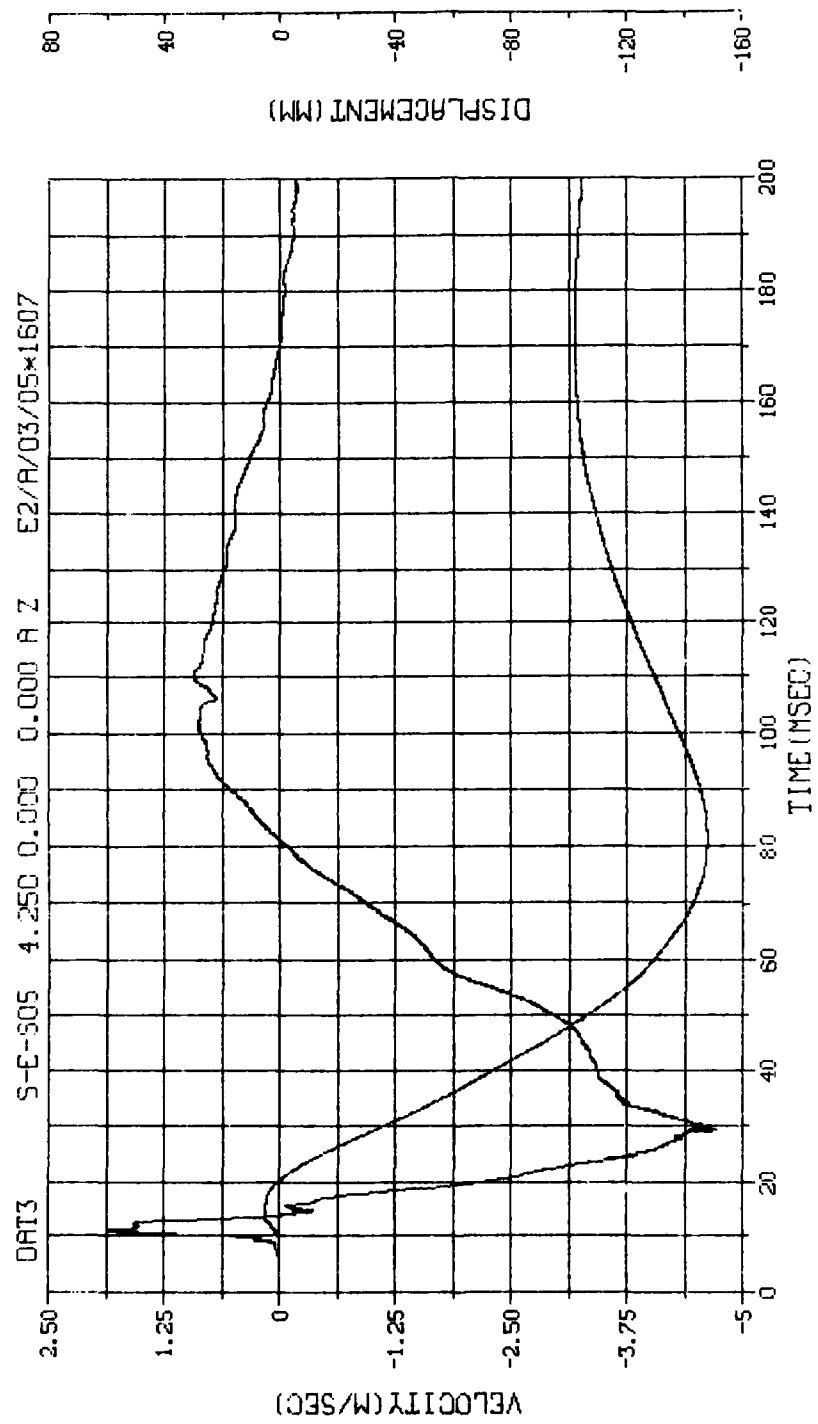
M.N. -91606	E.U. -0.000,1000.000
FSKTP=7.000	VSN-FB75
DIGITS=0.000,87.8,250	TRPE22
S.R. =25.00 KHZ	FILE=0
29 JUN 83 12:17:16	



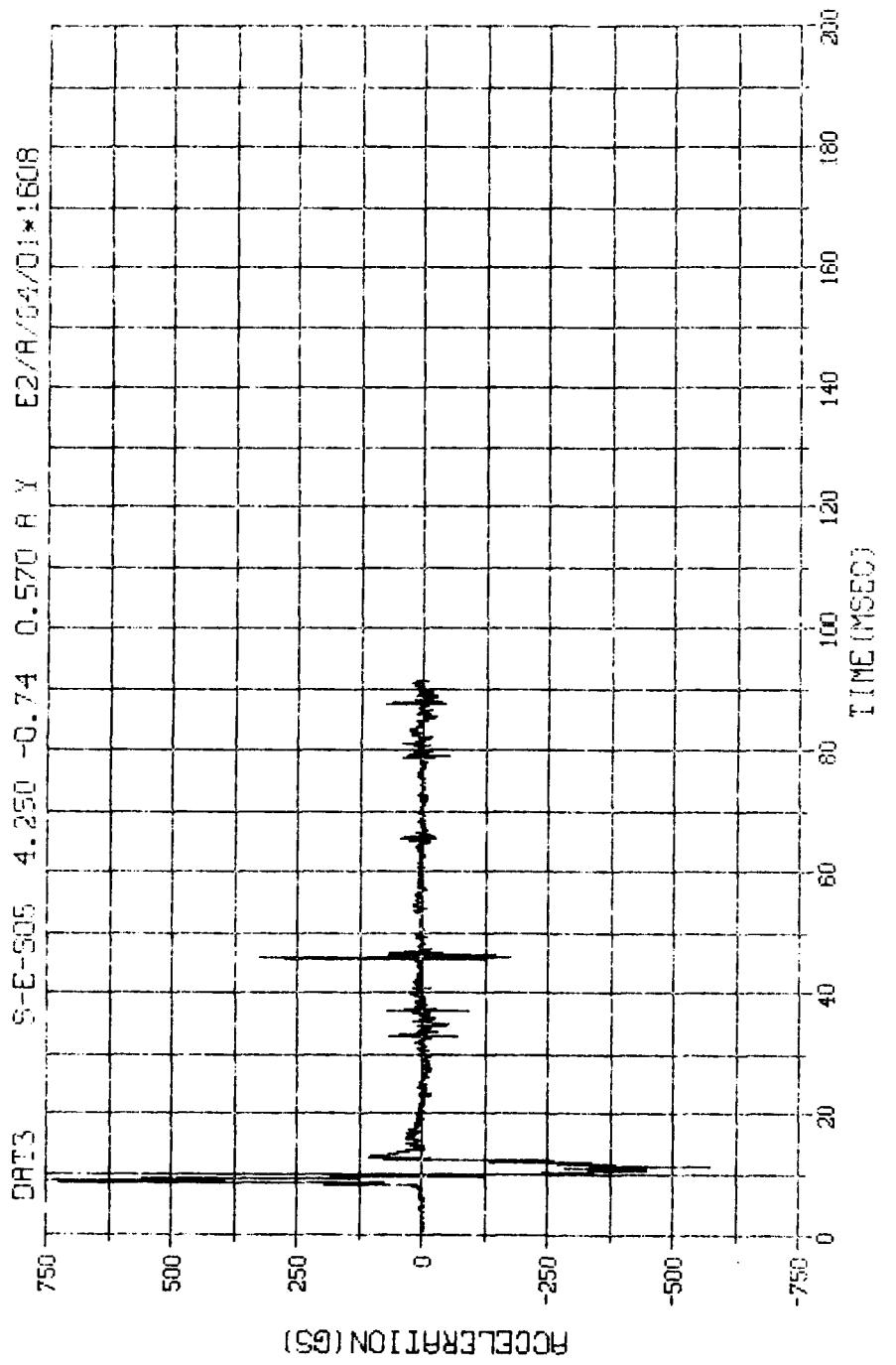
M.N. -91606	E.U. -0.000,1000.000	VSN-FB76
TSKIP=7,000	DIGITS=6,000,878.250	TAPE22
S.R. = 25.66 kHz	29-JUN-73 12:17:16	FILE=C
		21



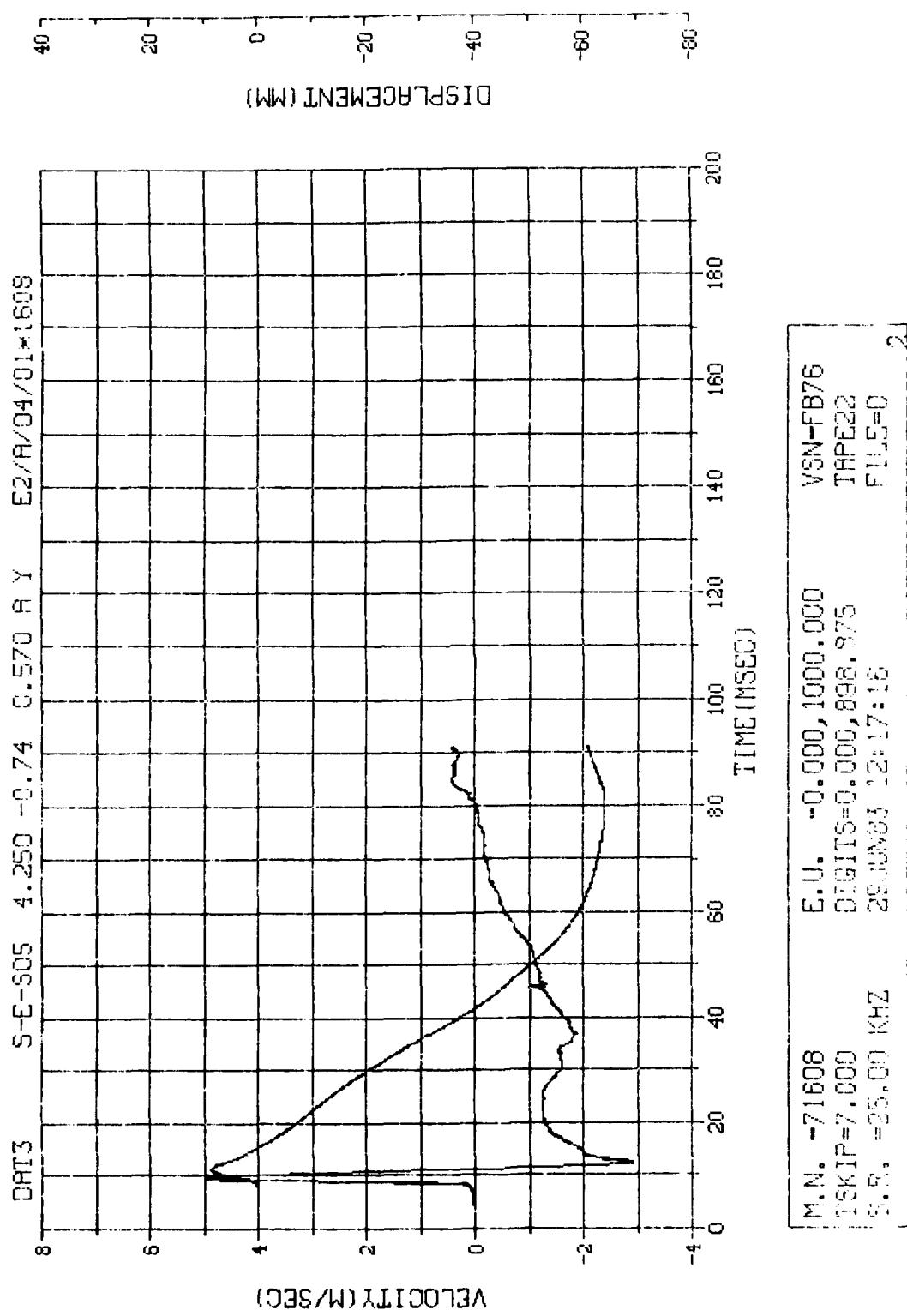
H.N. -91607 E.U. -0.000,1000.000
TSKIP=7.000 DIGITS=0.000,901.875
S.R. =25.00 KHZ TAPE22
29 JUN 83 12:17:16 FILE=6
1

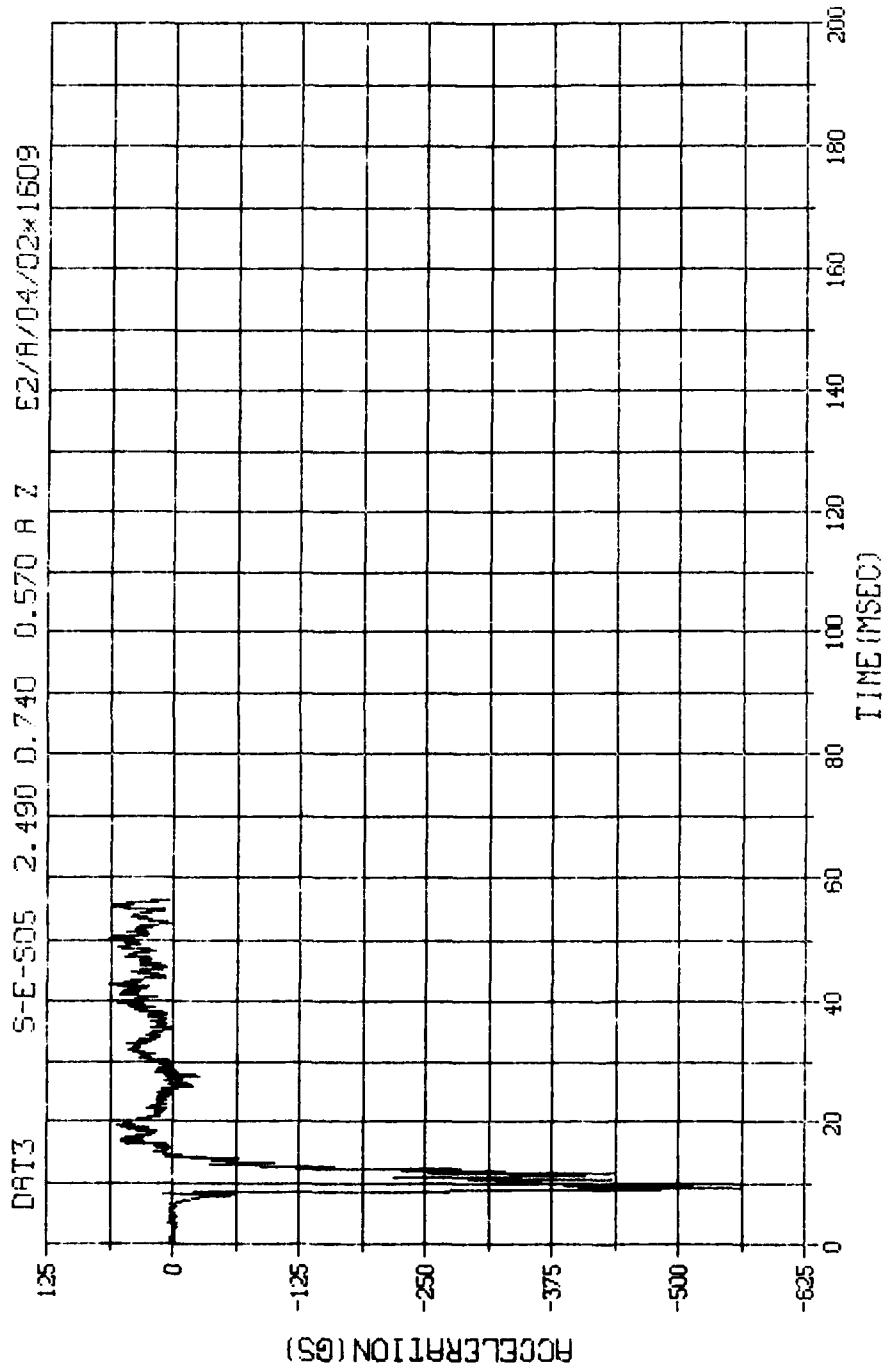


M.N. -91607	E.U. -0.000,1000.000	VSN-FB76
SKIP=7.000	DIGITS=0.000,901.875	TAPE22
S.R. =25.00 KHZ	28JUN83 12:17:16	FILE=0
		2

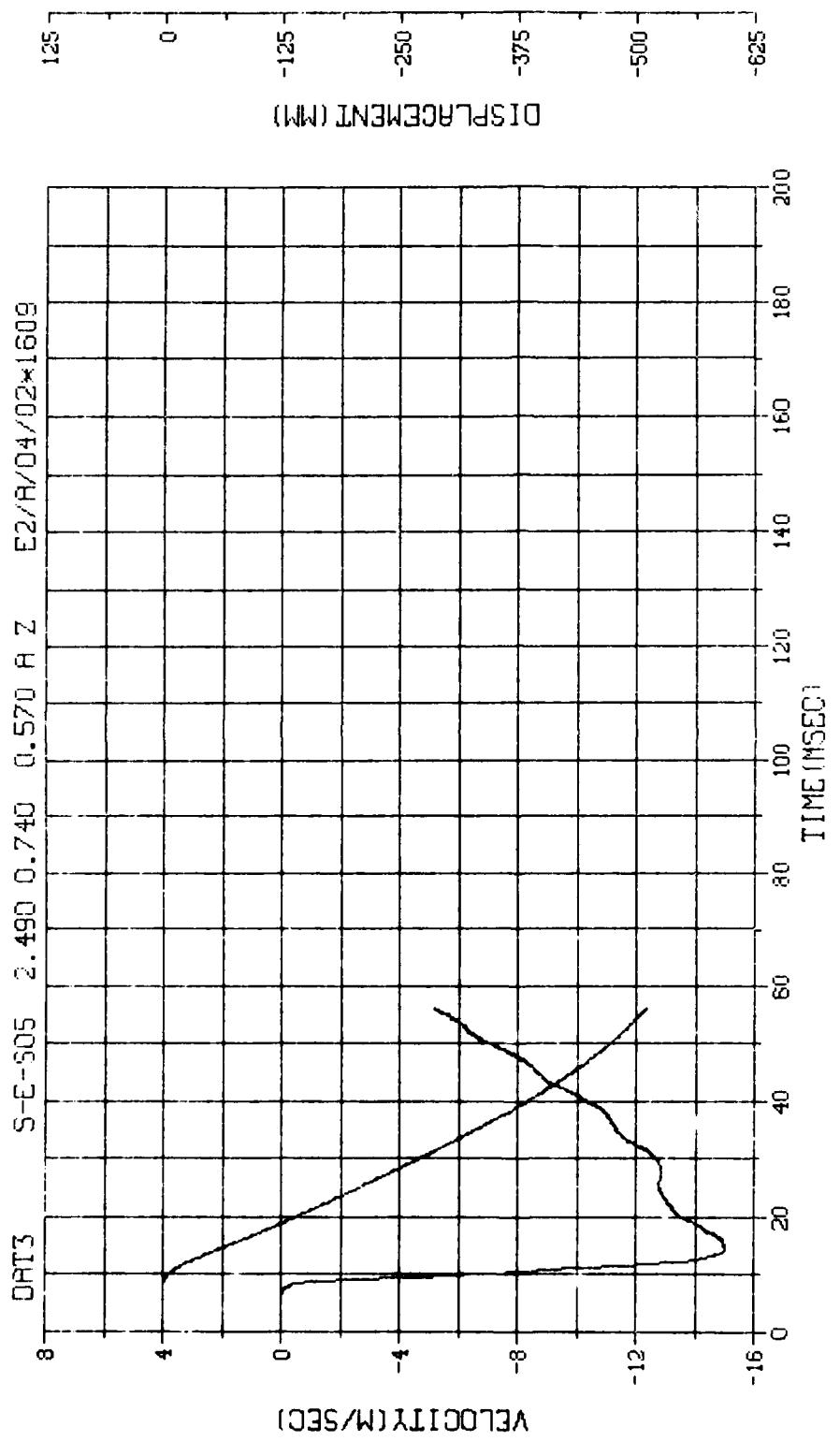


M.N. -71608	S.U. -0.000,1000.000	VSN-FB76
TSKIP=7.000	DIGITS=0,000,898,875	TGP522
S.R. =35.00 K=2	SCALING=1.0E+16	FILE=S

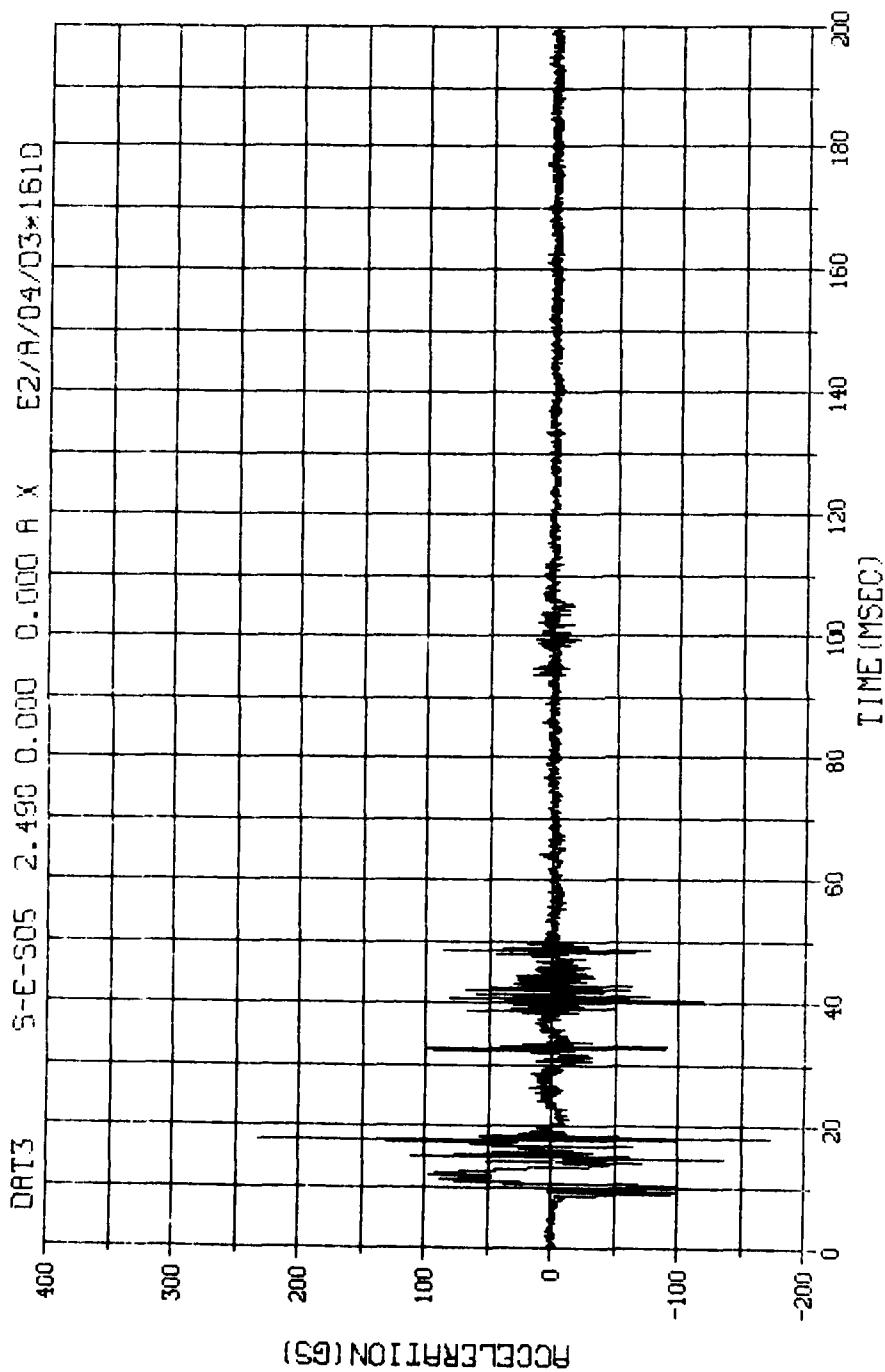




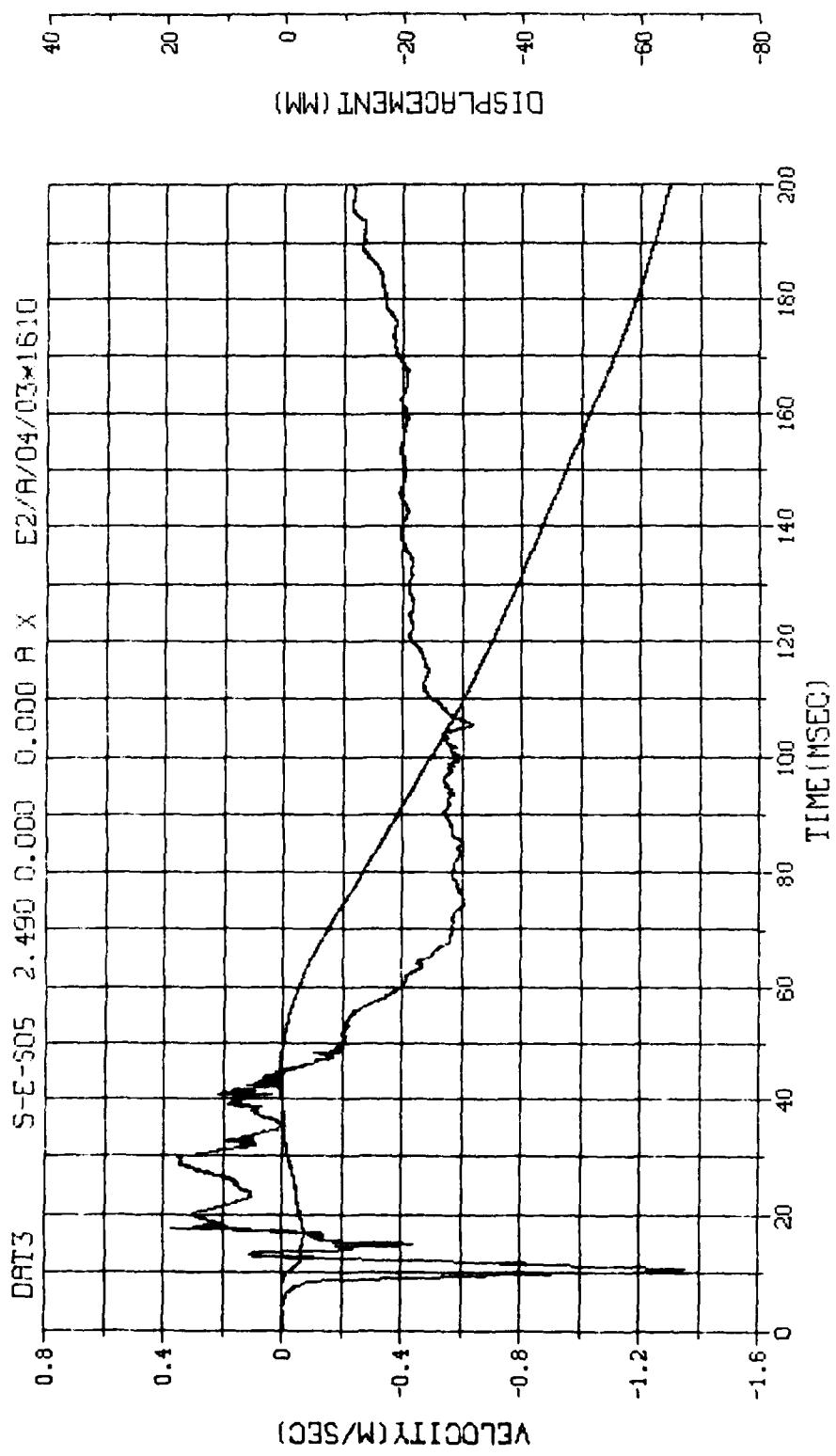
M.N. -71609 E.U. -0.000,1000.000 VSN-F875
TSKIP=7.000 DIGITS=0.000,875.875 TRPE22
S.R. =35.00 KHZ 26JUN83 12:17:16 FILE=9



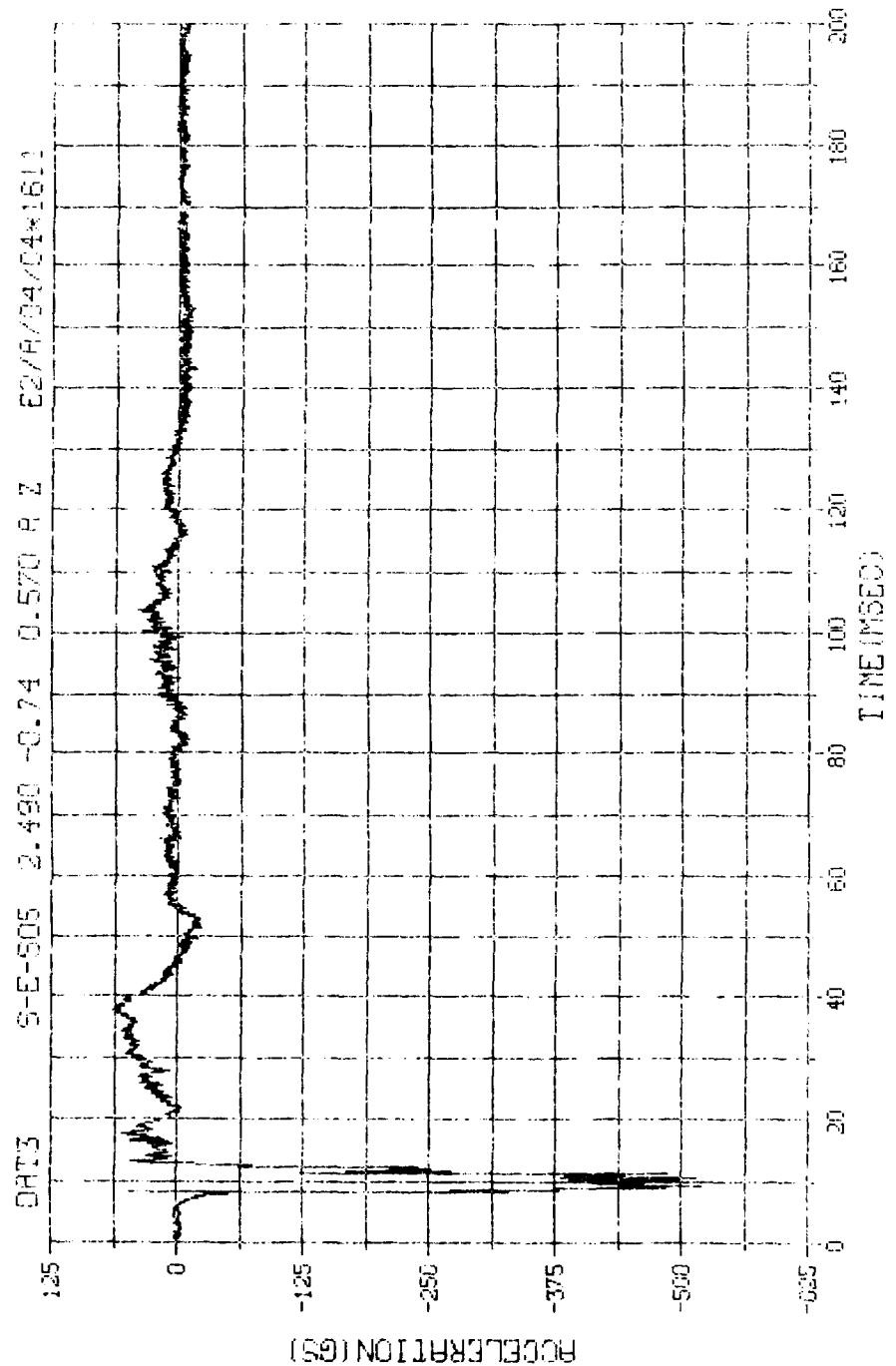
M. N. -71609	E.U. -0.000, 1000.000	VSN-FB76
SKIP=7.000	DIGITS=0.000, 075, 875	TAPE22
S.R. =35.00 kHz	29 JUN 83 12:17:16	FILE=0
		2]



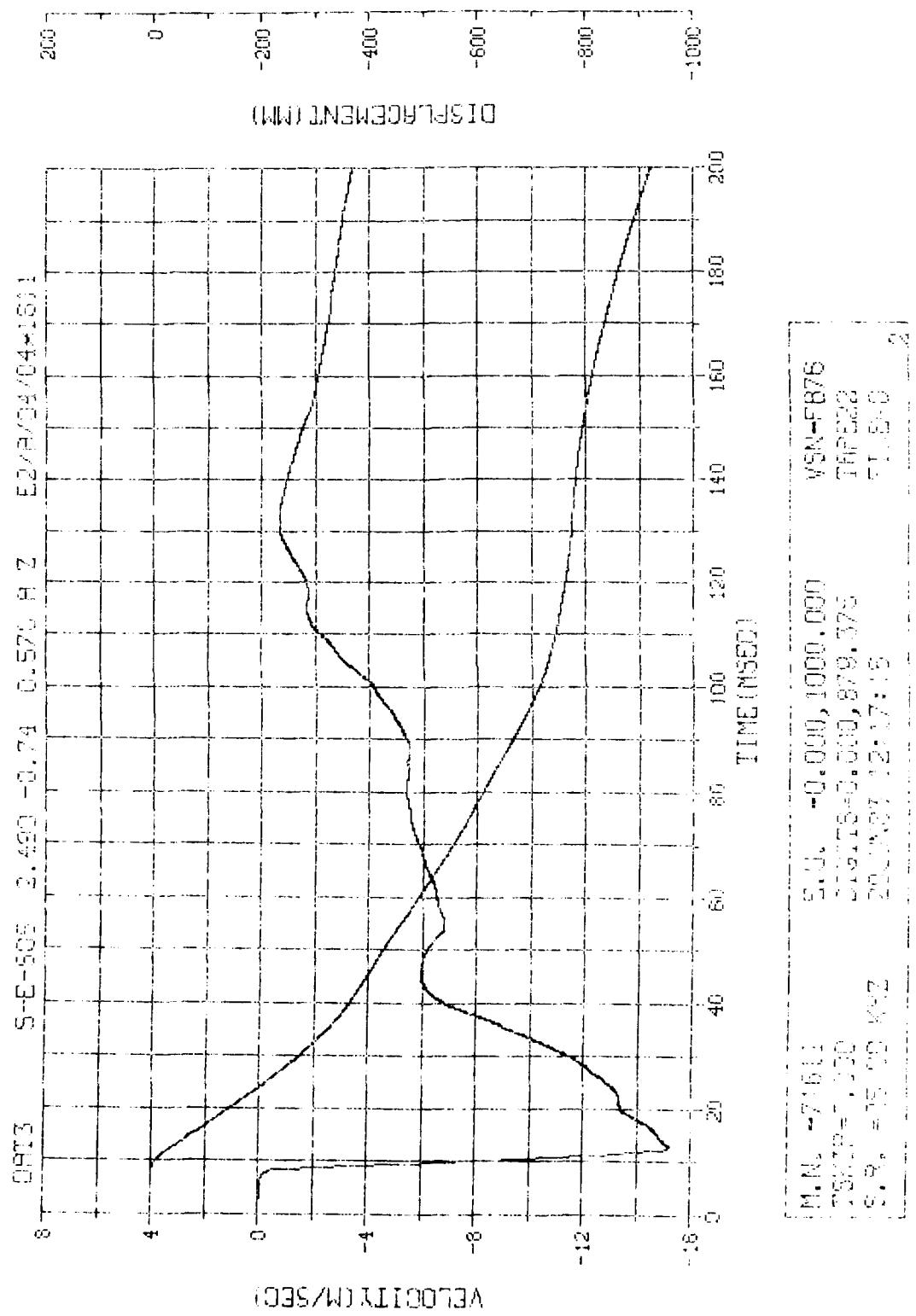
N.N. -91610 E.U. -0.000,1000.000 VSN-F876
SKIP=7.000 DIGITS=0.000,885,125 TAPE22
S.R. =25.00 KHZ 20JUN83 12:17:16 FILE=0

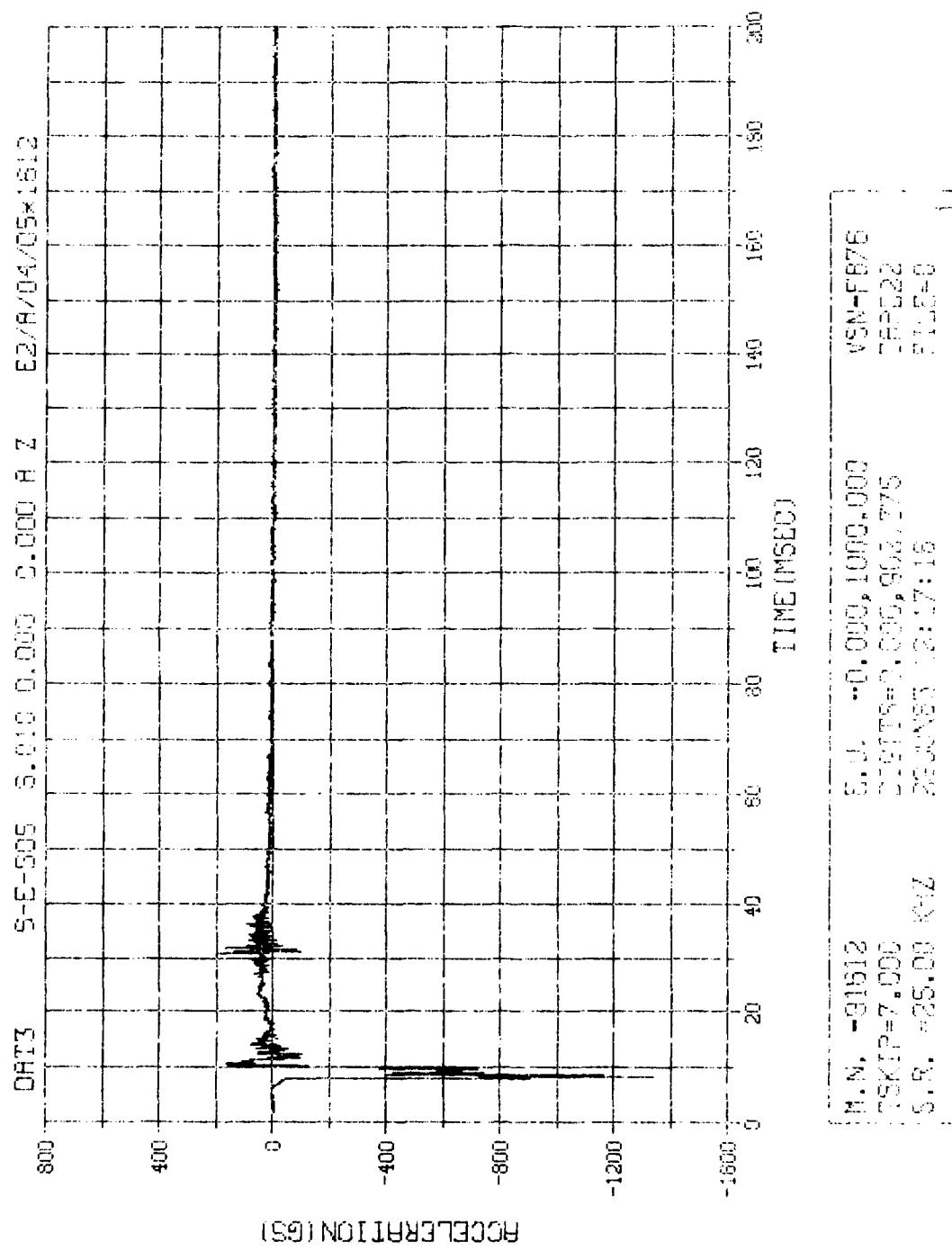


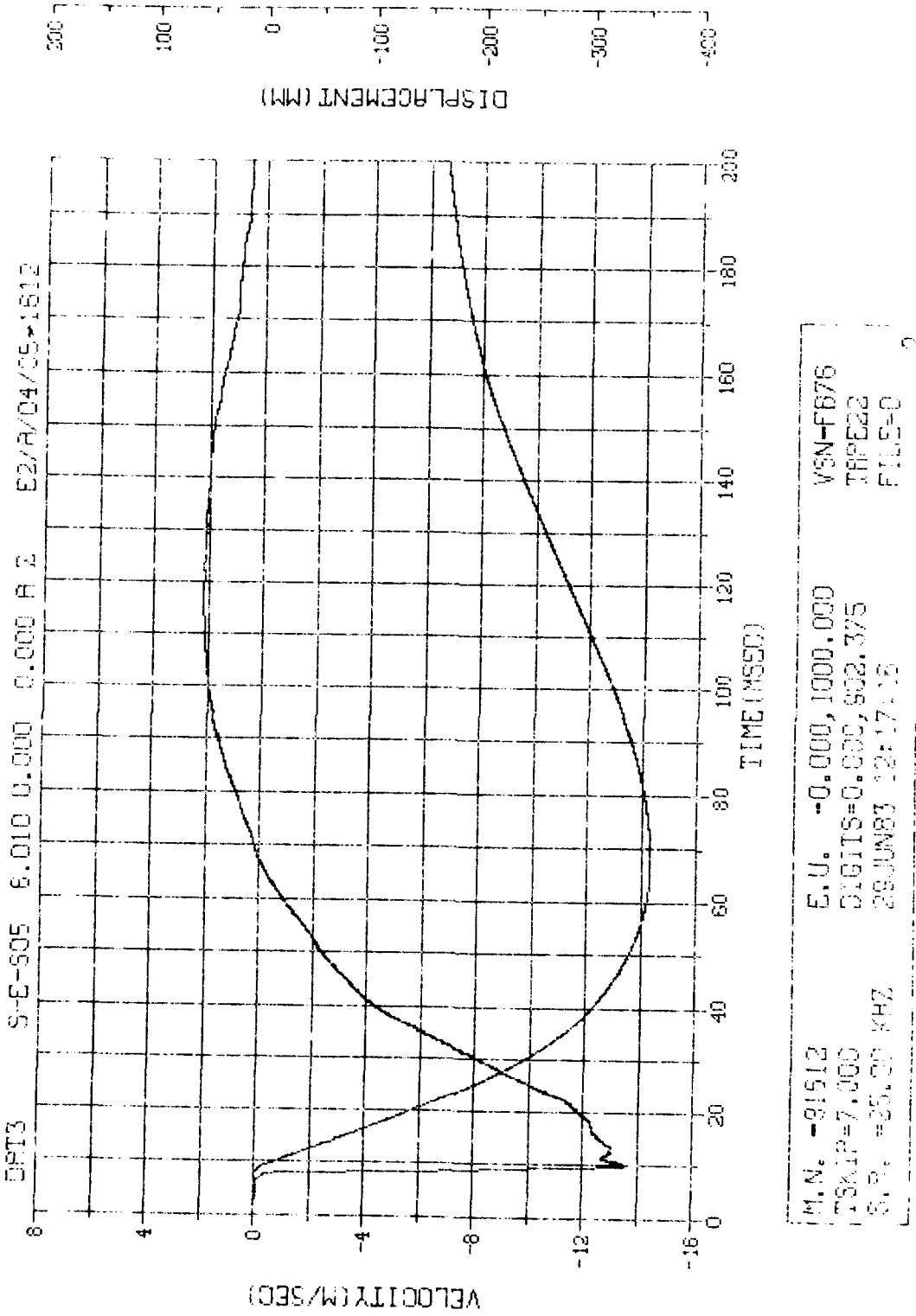
M.N. -91610	E.U. -0.000,1000.000	VSN-F676
TSKIP=7.000	DIGITS=0.000,885.125	TAPE22
S.R. =25.00 KHZ	29 JUN 83 12:17:16	FILE=0 2

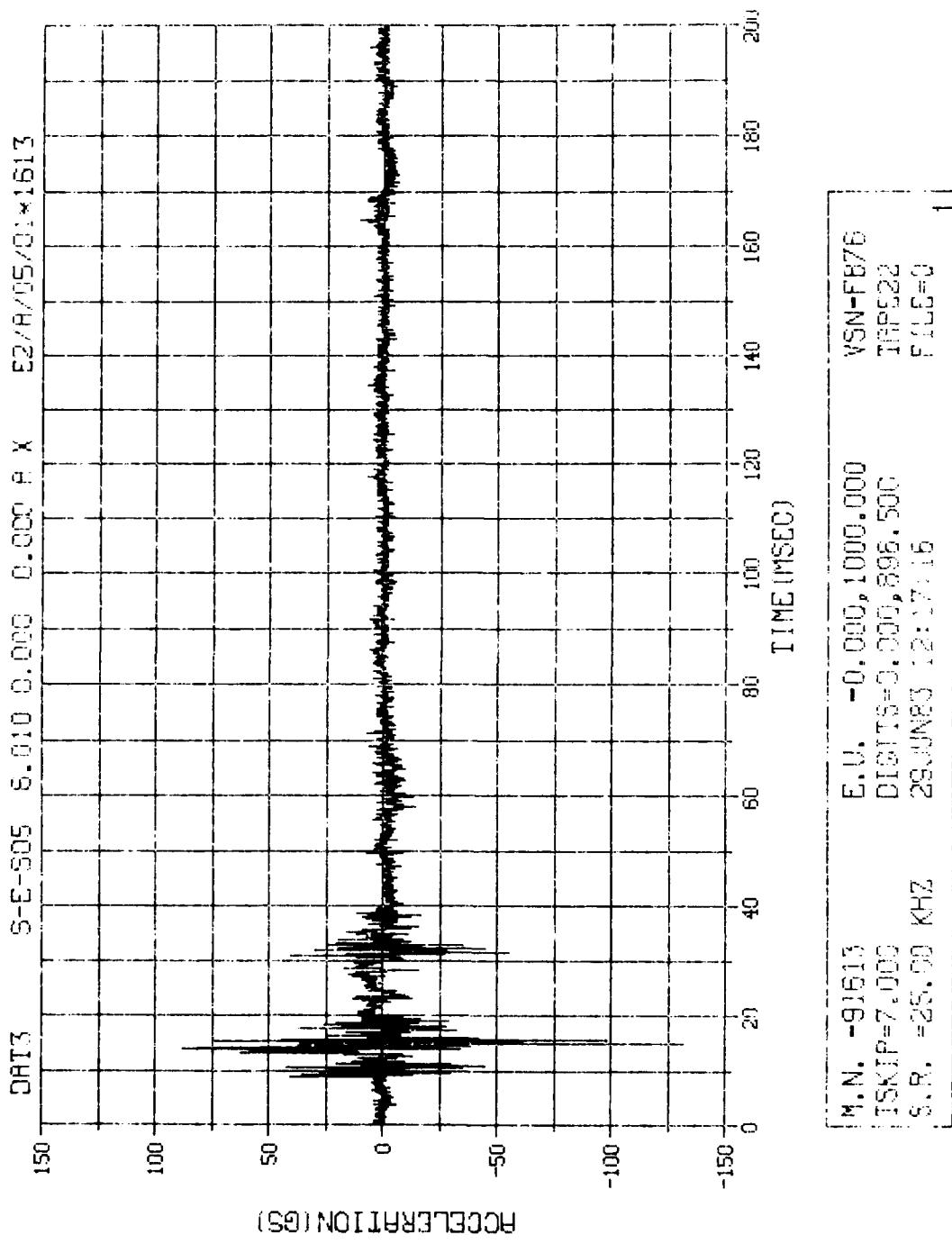


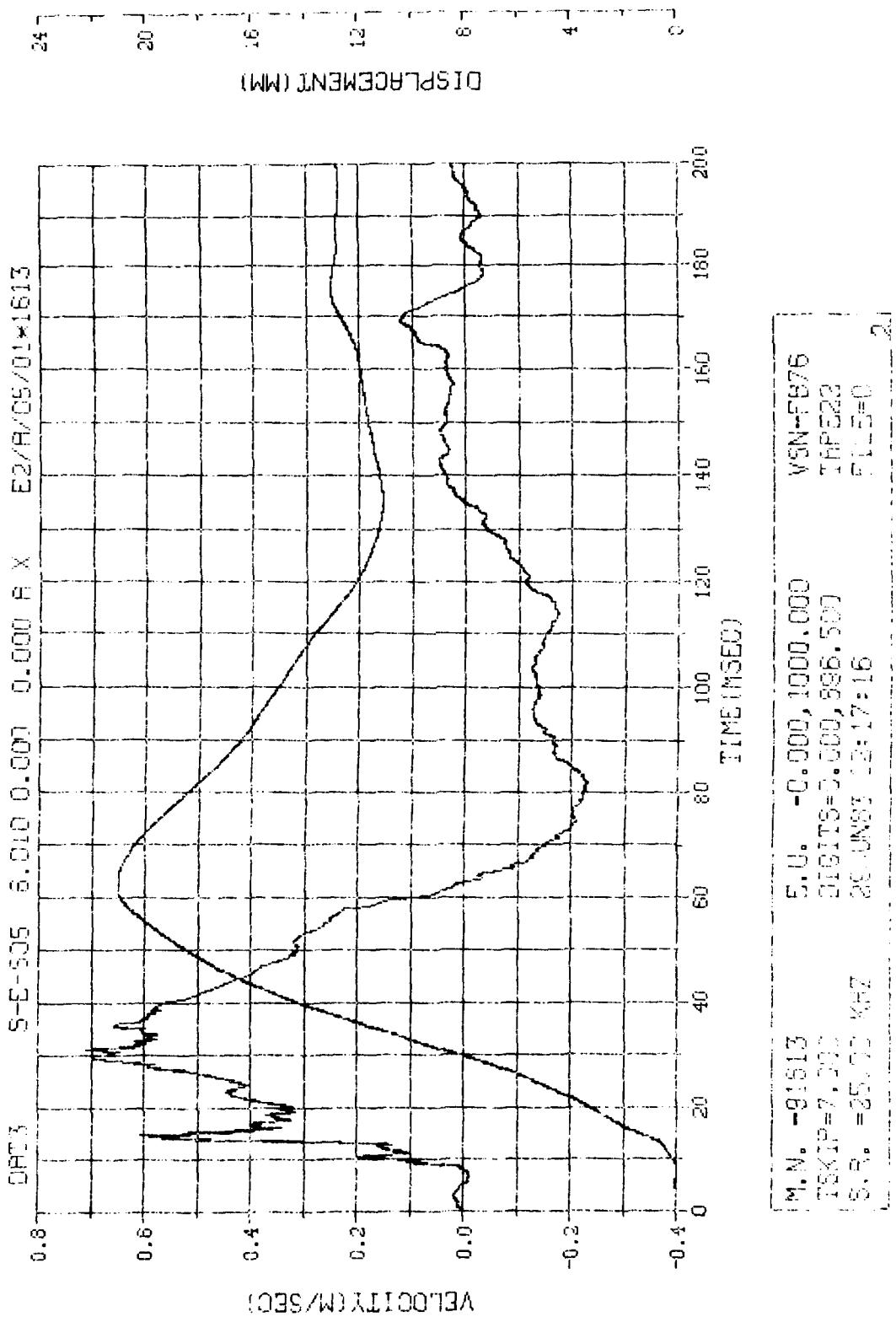
H.N. -71611	S.O. -9.800, 1000.000	VSN-F876
TSK T=7,000	1121125=9,000, 875, 375	199222
S.P. -20,00 812	39-4983 12,171.6	PLATE 2

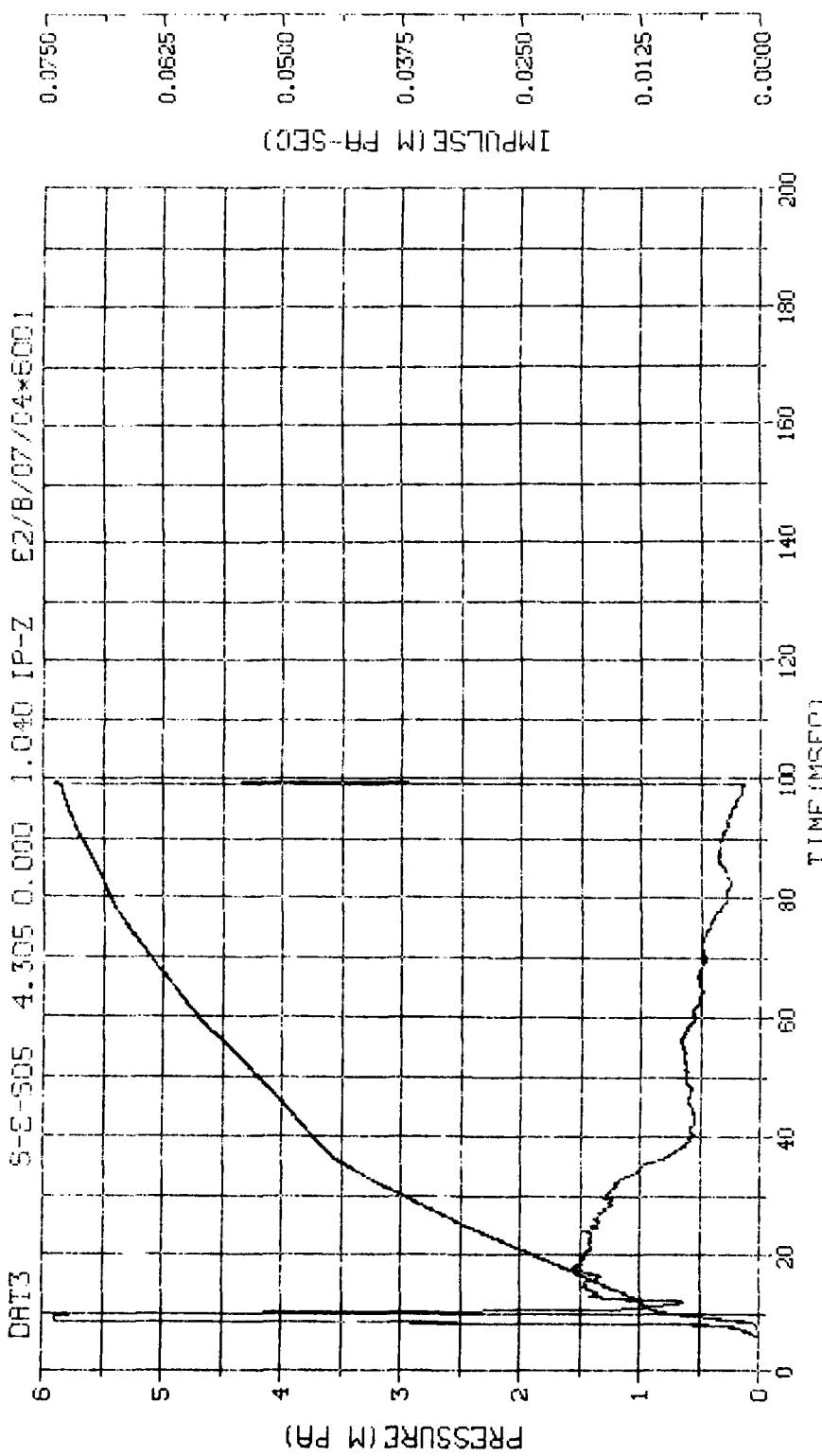




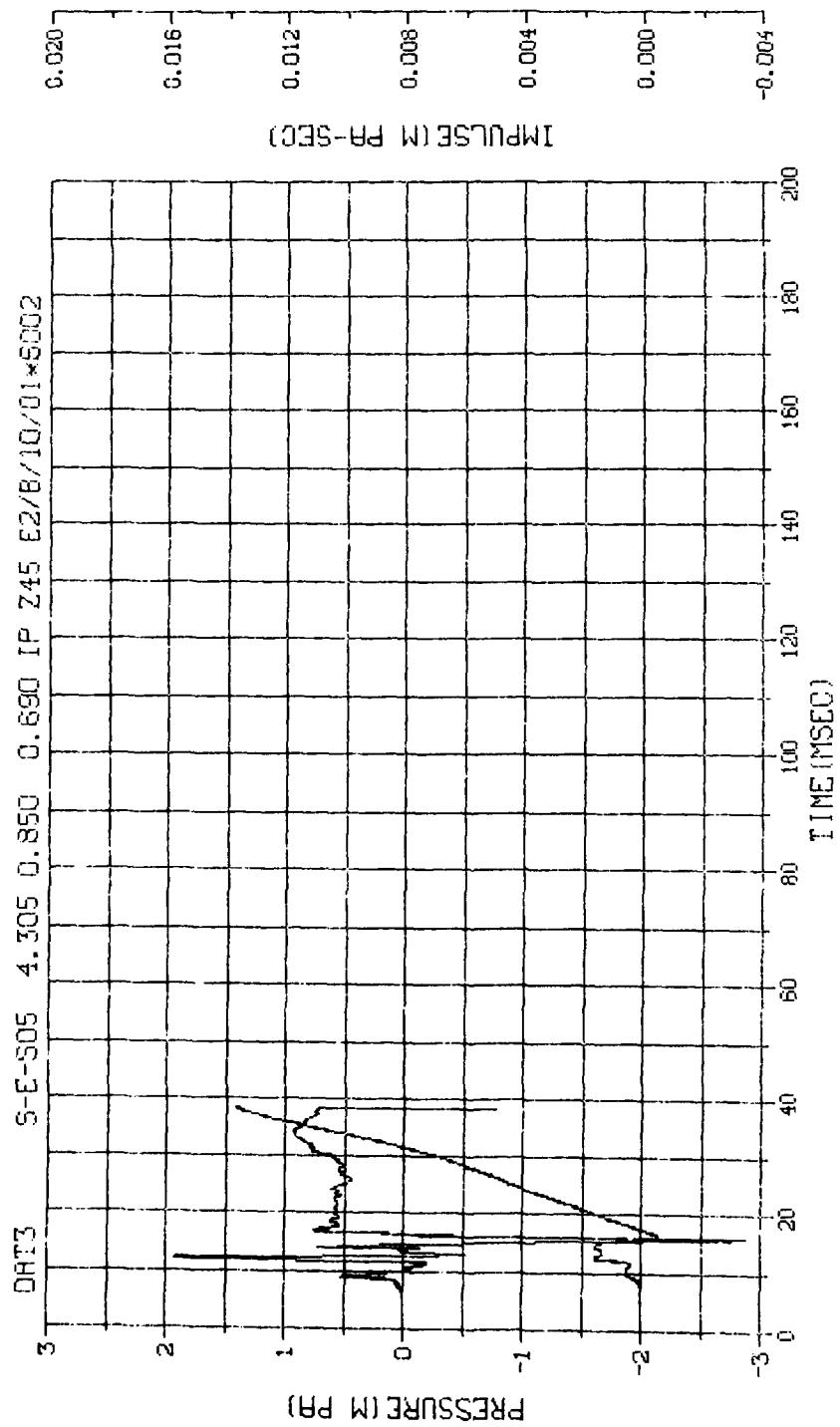




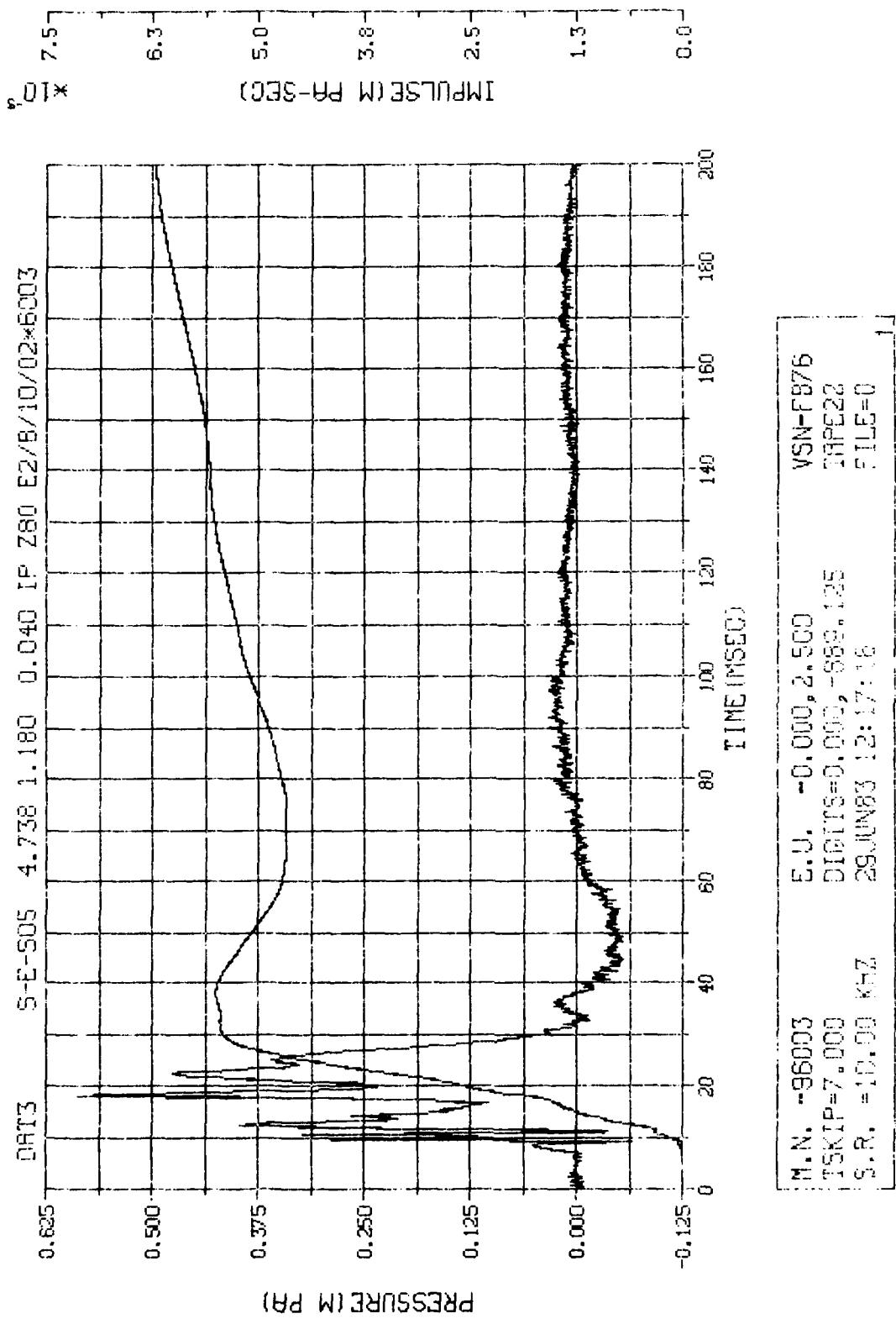


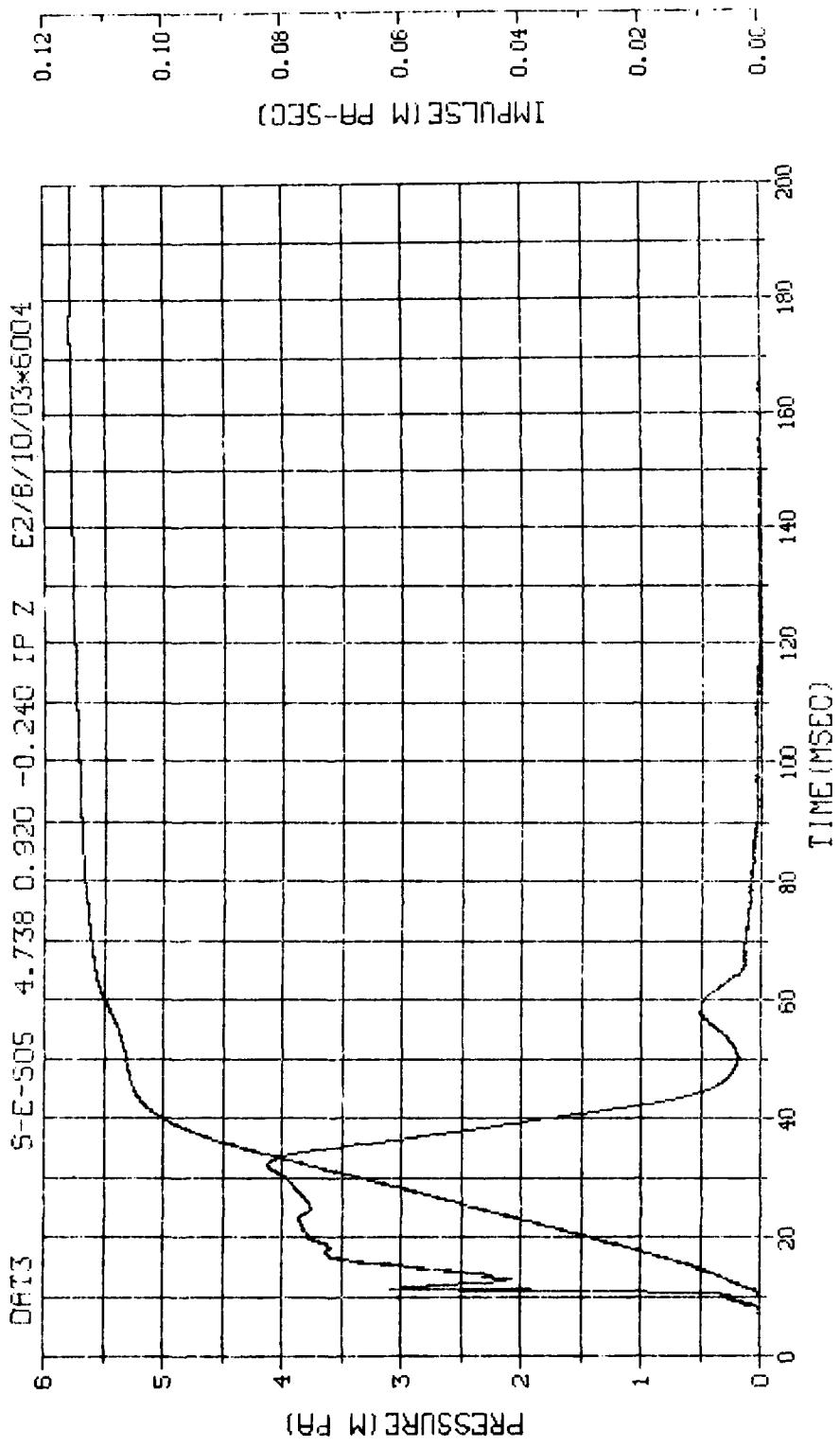


N.N.	-7600!	E.U.	-0.000, 2.500	WSN-FB76
TSKIP	=7.000	DIGITS	=0.000, -854.875	TAPE22
S.R.	=10.00	KHZ		FILE=0
		28.JUN.03	12:17:16	

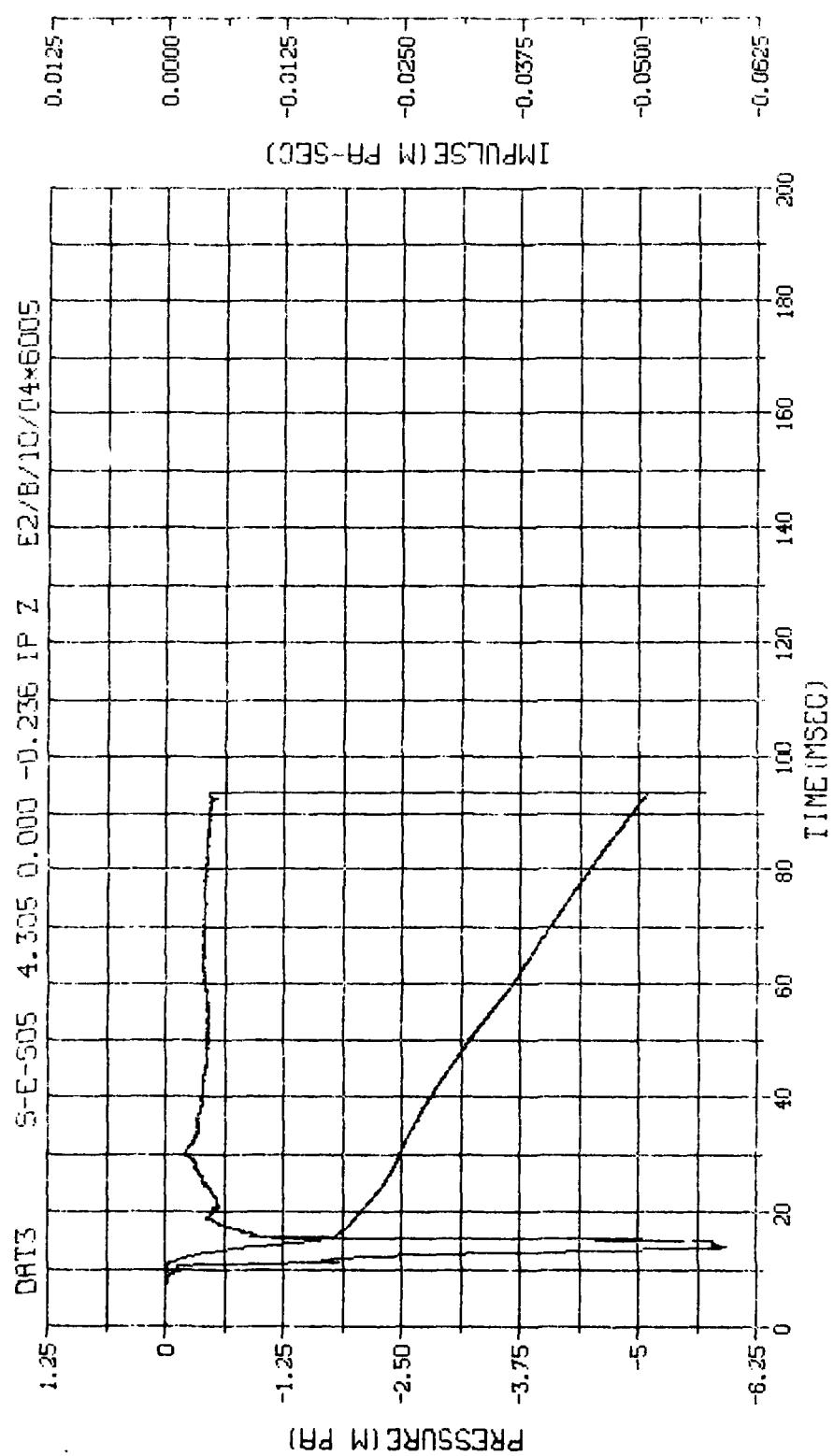


M.N. -76002	E.U. -0.000, 2.500	VSN-FB76
TSKIP=7.000	DIGITS=0.000, -872.500	TRPC22
S.R. =10.00 KHz	29JUN87 12:17:16	FILE=0

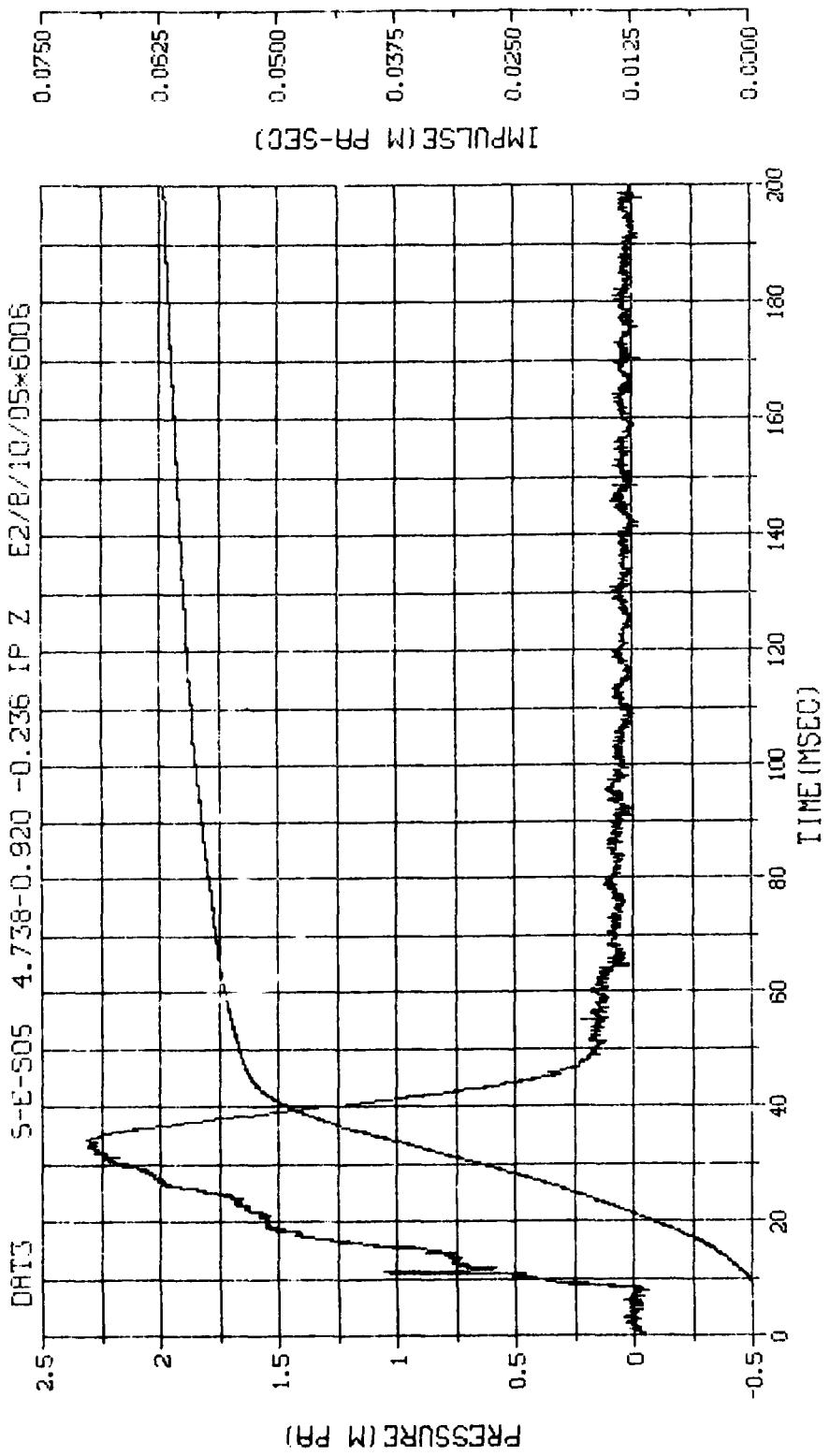




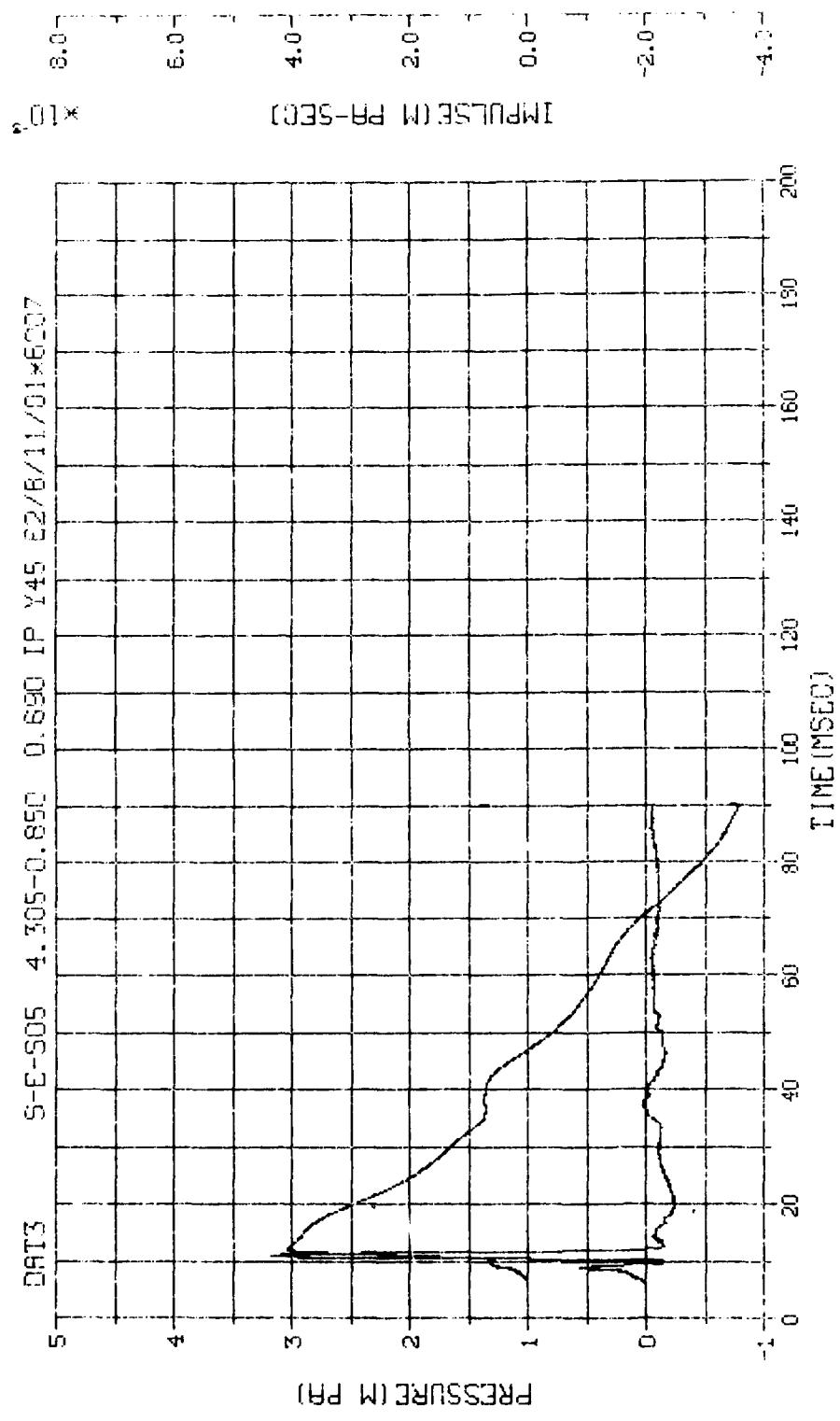
M.N. = 6004	E.U. = 0.000, 2.000	VSN-FB76
TSKIP=7.000	DIGITS=0.000, -603, 125	TRPE22
S.R. = 10.00 KHZ	29 JUN 83 12:17:15	FILE=0



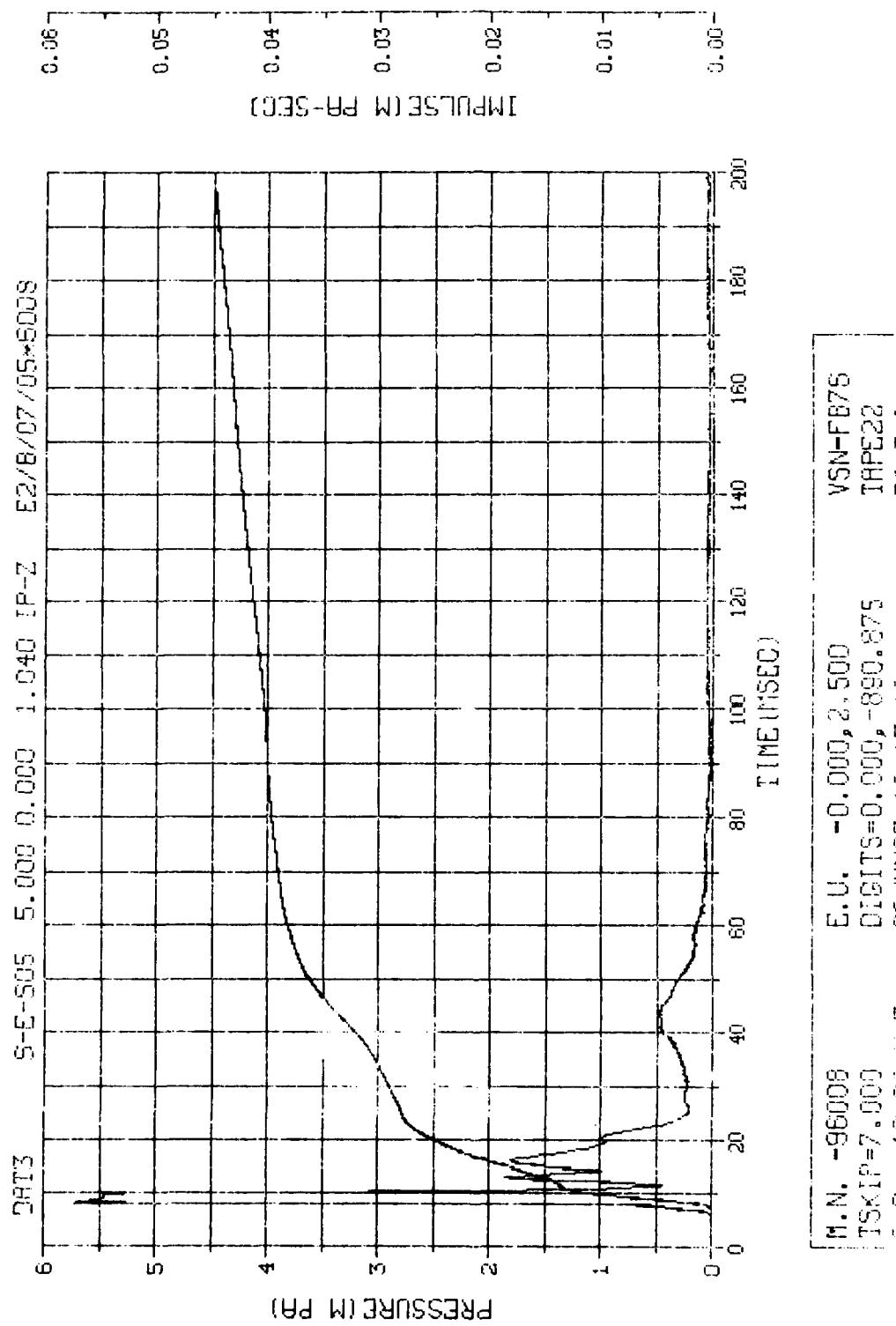
N.N.	-76005	E.U.	-0.000, 2.500	VSN-FB76
TSKIP=7.000		DIGITS=5.000, -651.875	TRPZ2G	
S.R. = 10.00 KHZ		29 JUN 87 12:17:16	FILE=U	

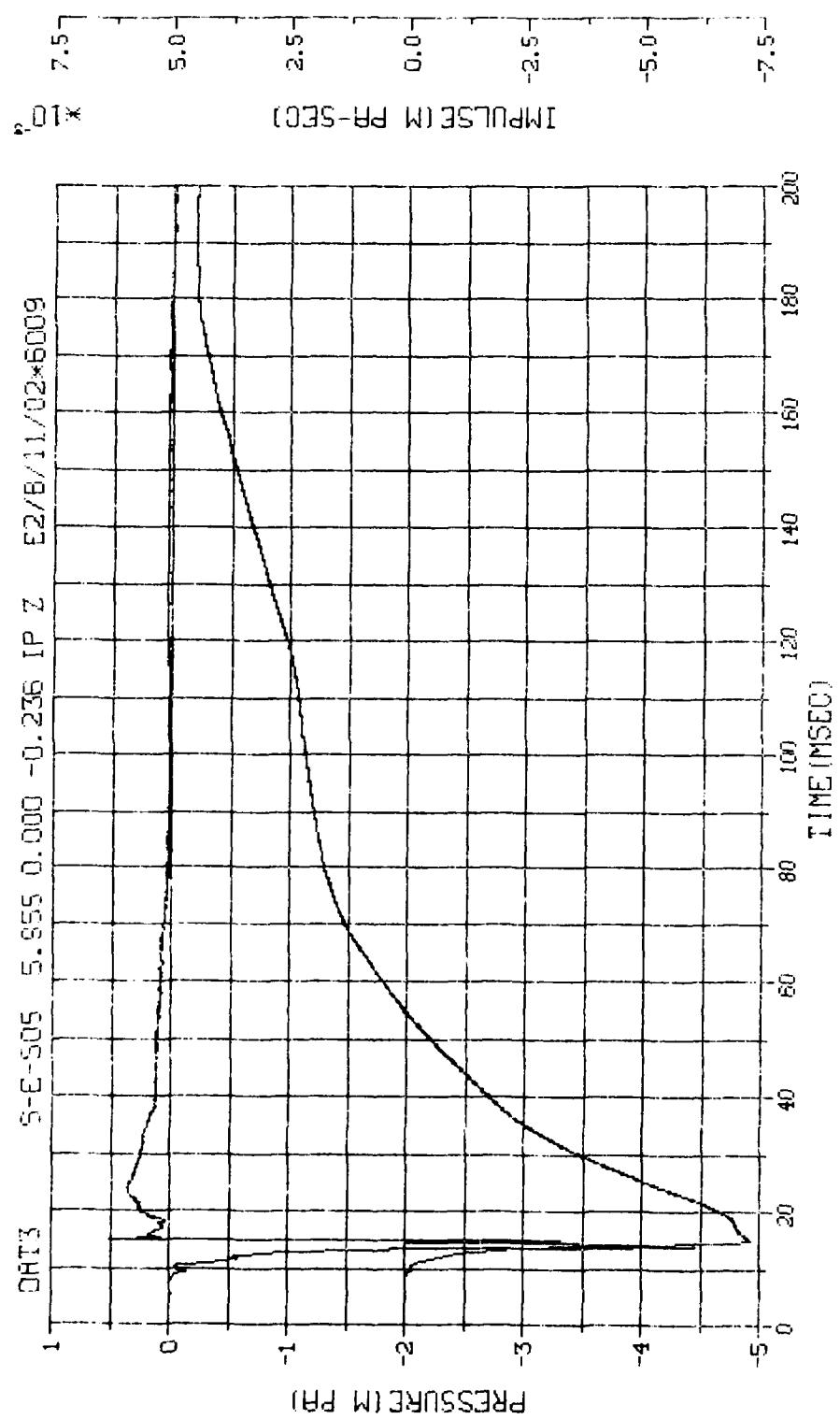


M. N. = 6006	E. U. = 0.000, 10.000	VSN-FB75
SKIP=7.000	DIGITS=0.000, -866.875	TAPE22
S. R. = 10.00 KHZ	29 JUN 83 12:17:16	FILE=U

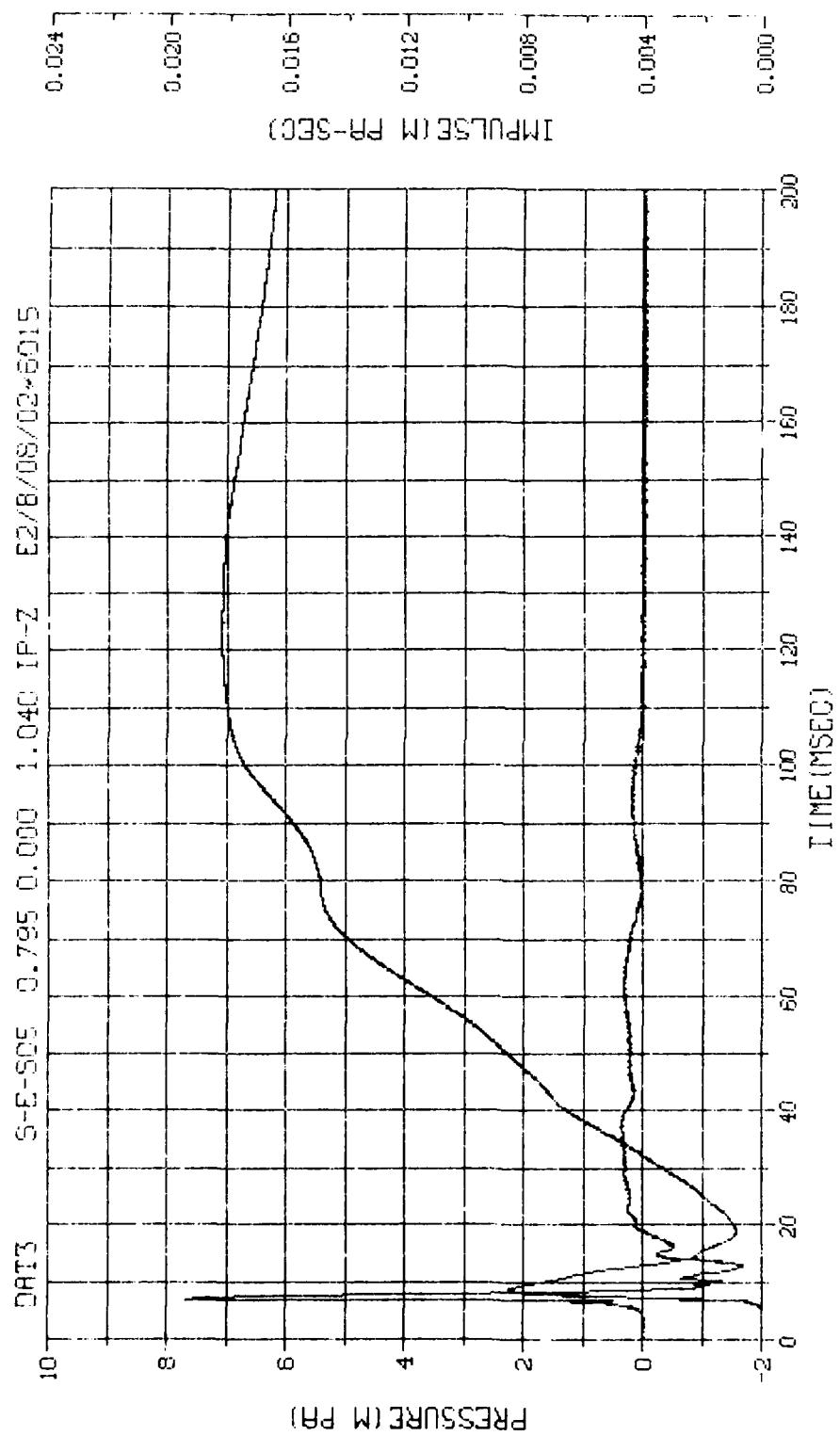


M.N. -76007	E.U. -0.000, 2.500	VSN-FB76
TSKIP=7.000	DIGIT5=0.000, -853.250	THPE22
I.S.R. =10.00 KHZ	26.JUN93 12:17:16	FIL1E=0
		4





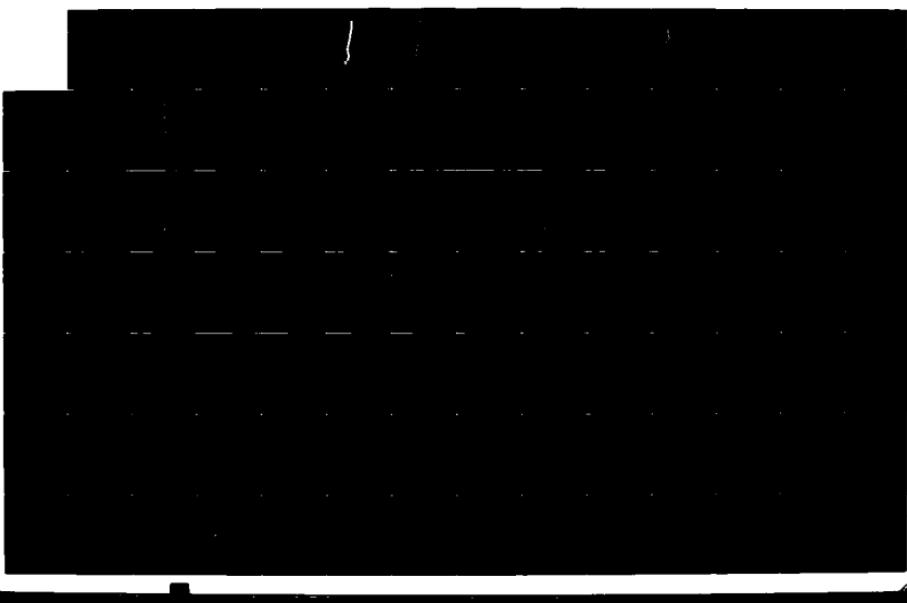
M.N. = 6009	E.U. = 0.000, 2,500
SKIP=7,000	RIGHTS=0,000,-851,250
S.R. = 10,00 KHZ	REC'D 12:17:15
	FILE=6 1]

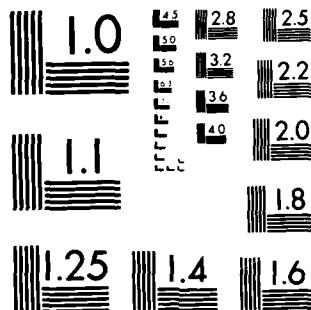


M.N. -96015	E.U. -0.000, 10.000	VSN-F876
TSKIP=7,000	DIGITS=6,000,-850,750	THRE22
S.Q. =10.00 X72	282000, 1347, 16	FILE22
		FILE=0

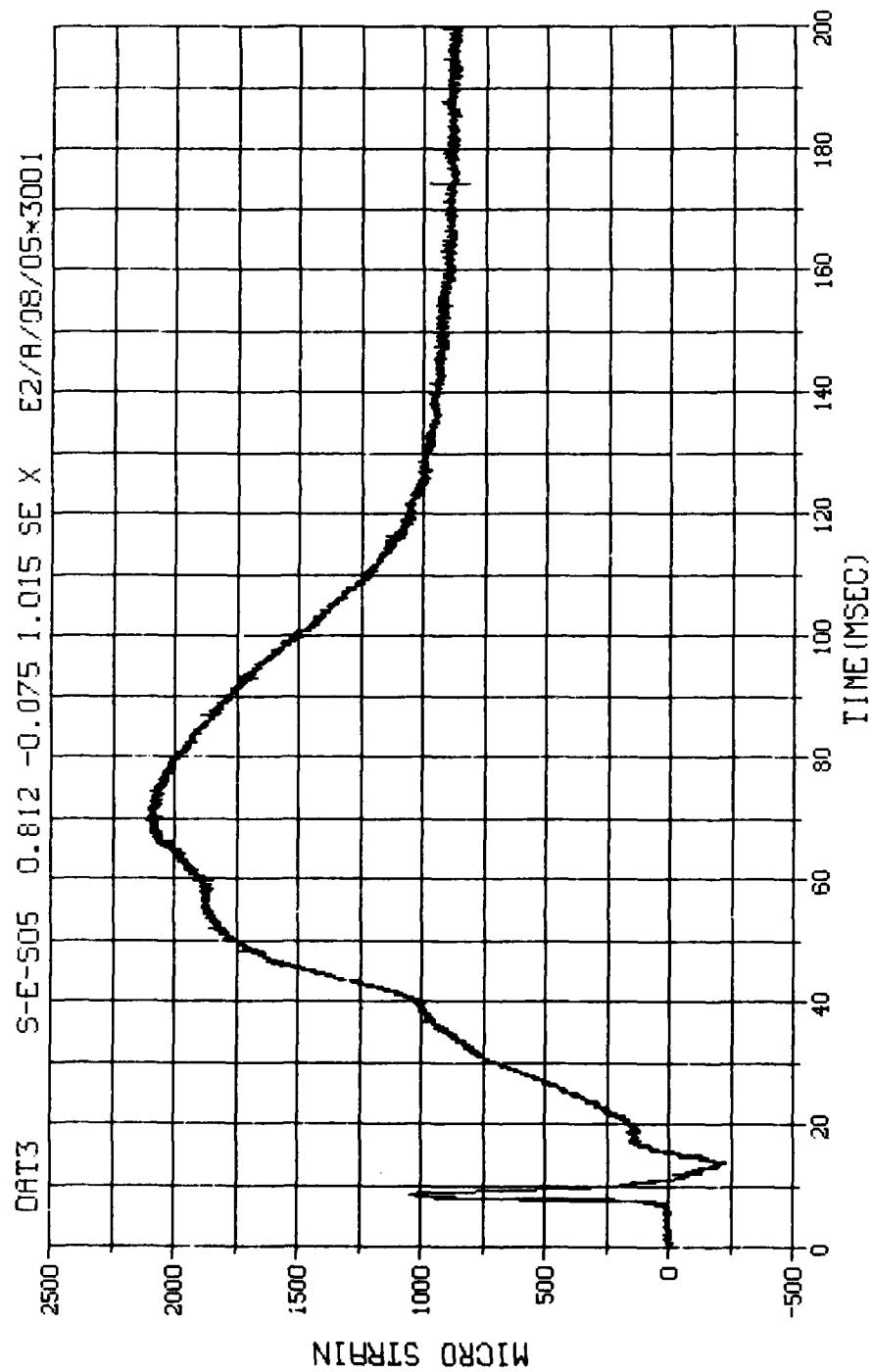
AD-A171 212 KACHINA TEST SERIES: DYNAMIC ARCH TEST THREE (DAT-3) 5/6
ANALYSIS REPORT(CU) AIR FORCE WEAPONS LAB KIRTLAND AFB
NM J L SMITH ET AL MAR 86 AFWL-TR-85-63 F/G 19/4 NL

UNCLASSIFIED

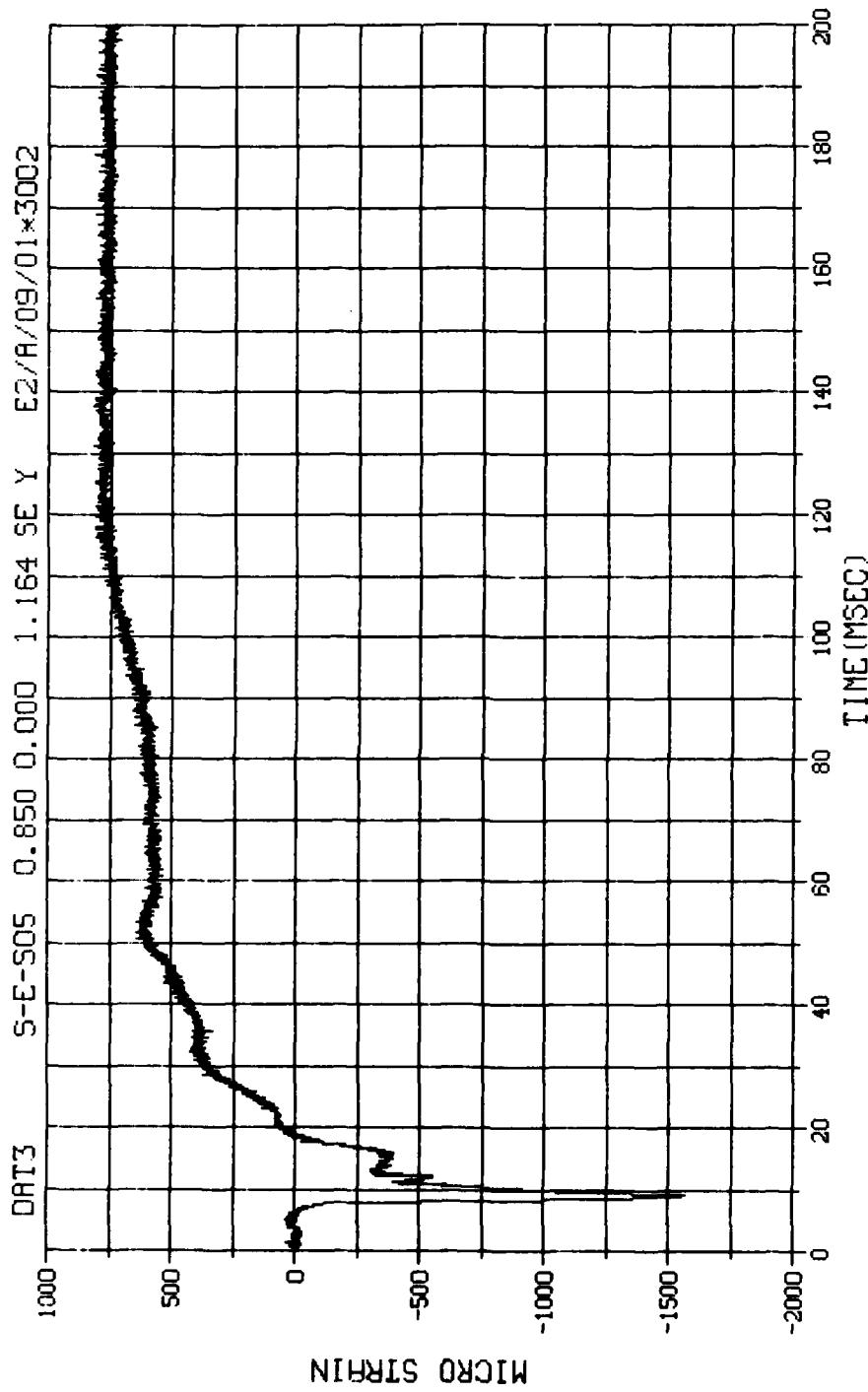




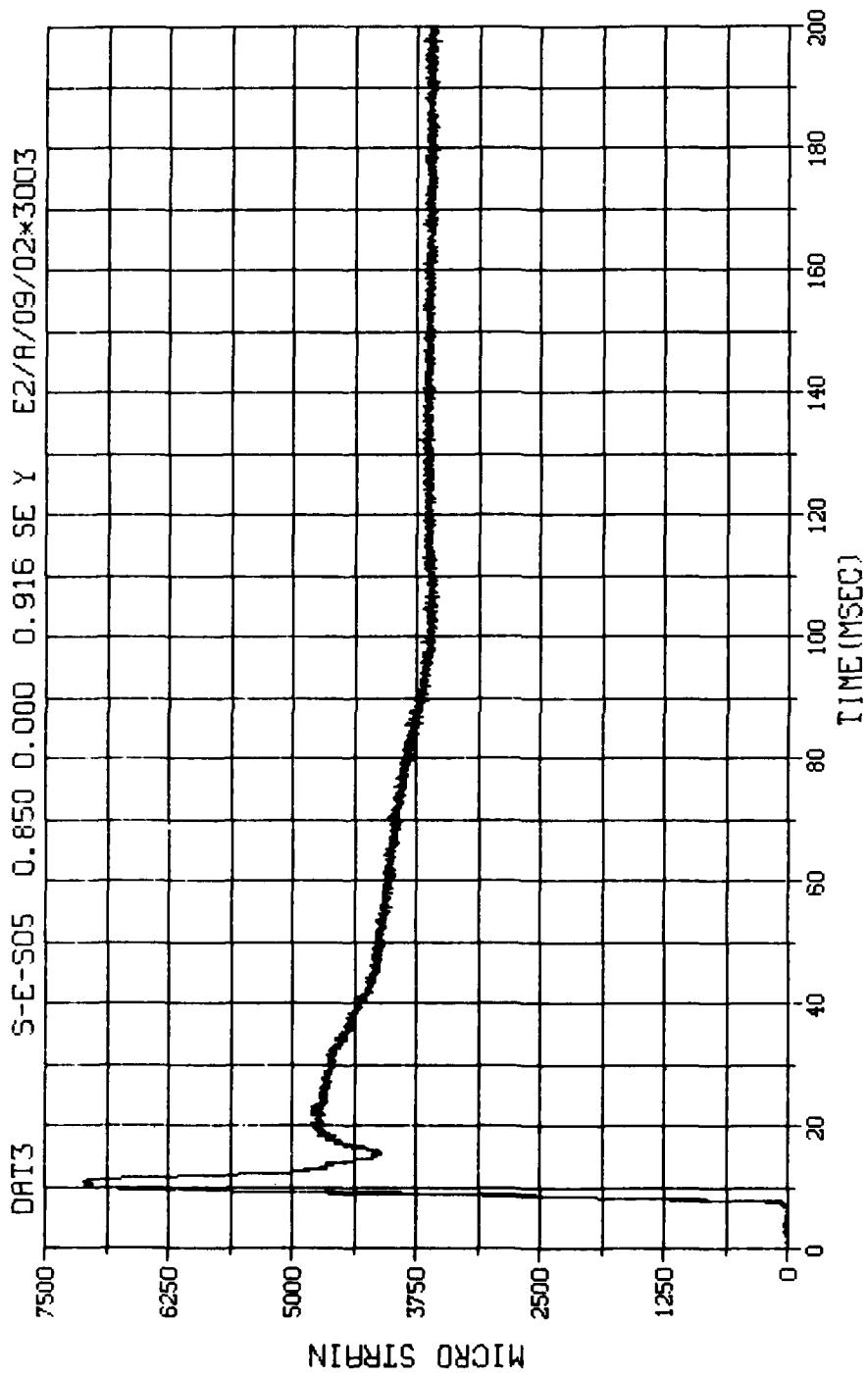
MICROCOPY RESOLUTION TEST CHART
NATIONAL BUREAU OF STANDARDS 1963-A



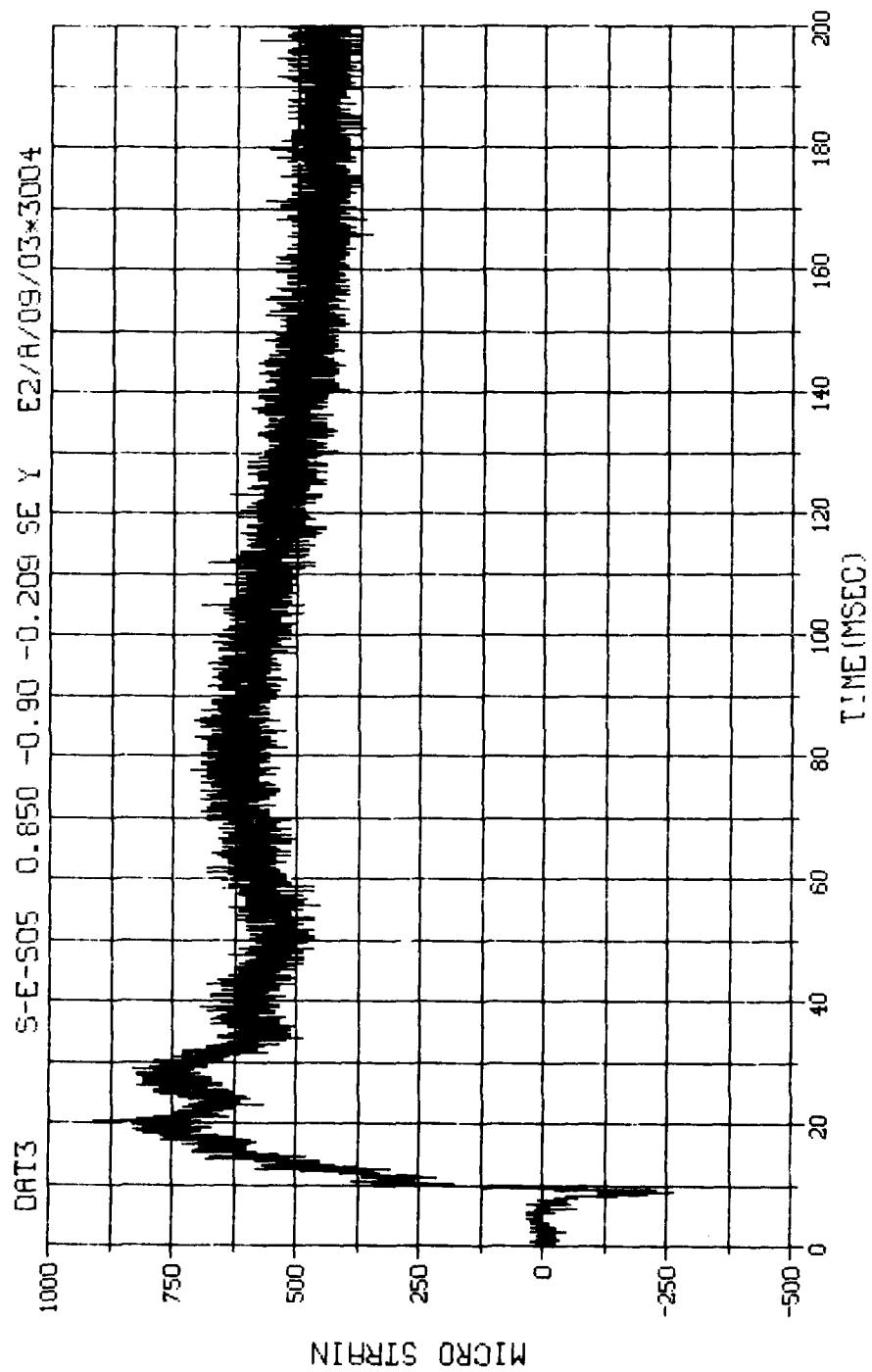
M.N. = 3001 E.U. = 0.000, 4000.000 VSN=66142
T SKIP=7.000 DIGITS=0.000, 891.500 TAPE22
S.R. =25.00 KHZ 4. 4 PM, TUE, 13 SEP 83. FILE=144 1



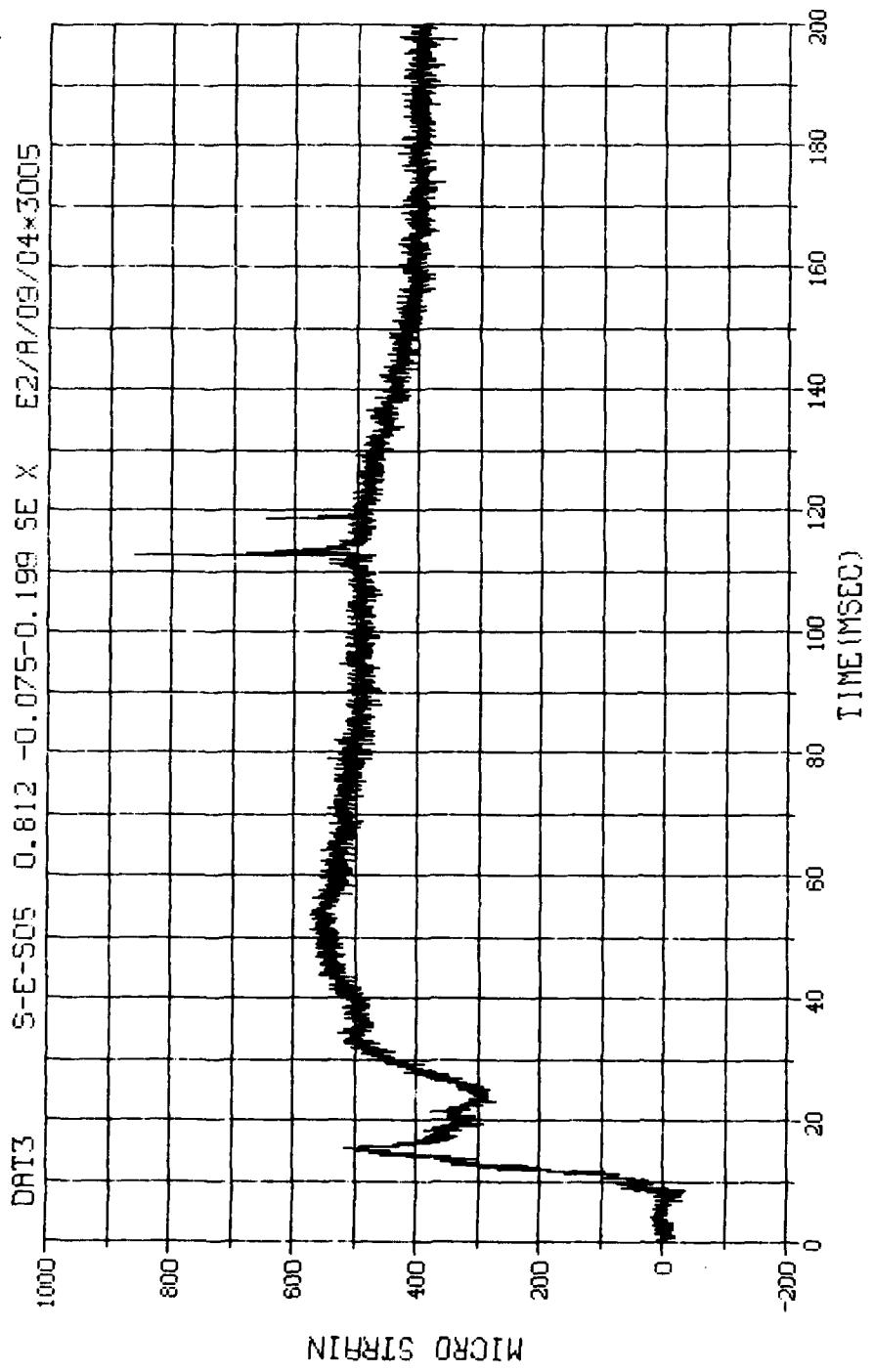
M.N. - 3002	E.U. -0.000, 7500.000	VSN-60142
TSKIP=7.000	DIGITS=0.000, 878.125	TAPE22
S.R. =25.00 KHZ	4. 4 PM, TUE, 13 SEP 83.	FILE=146 1



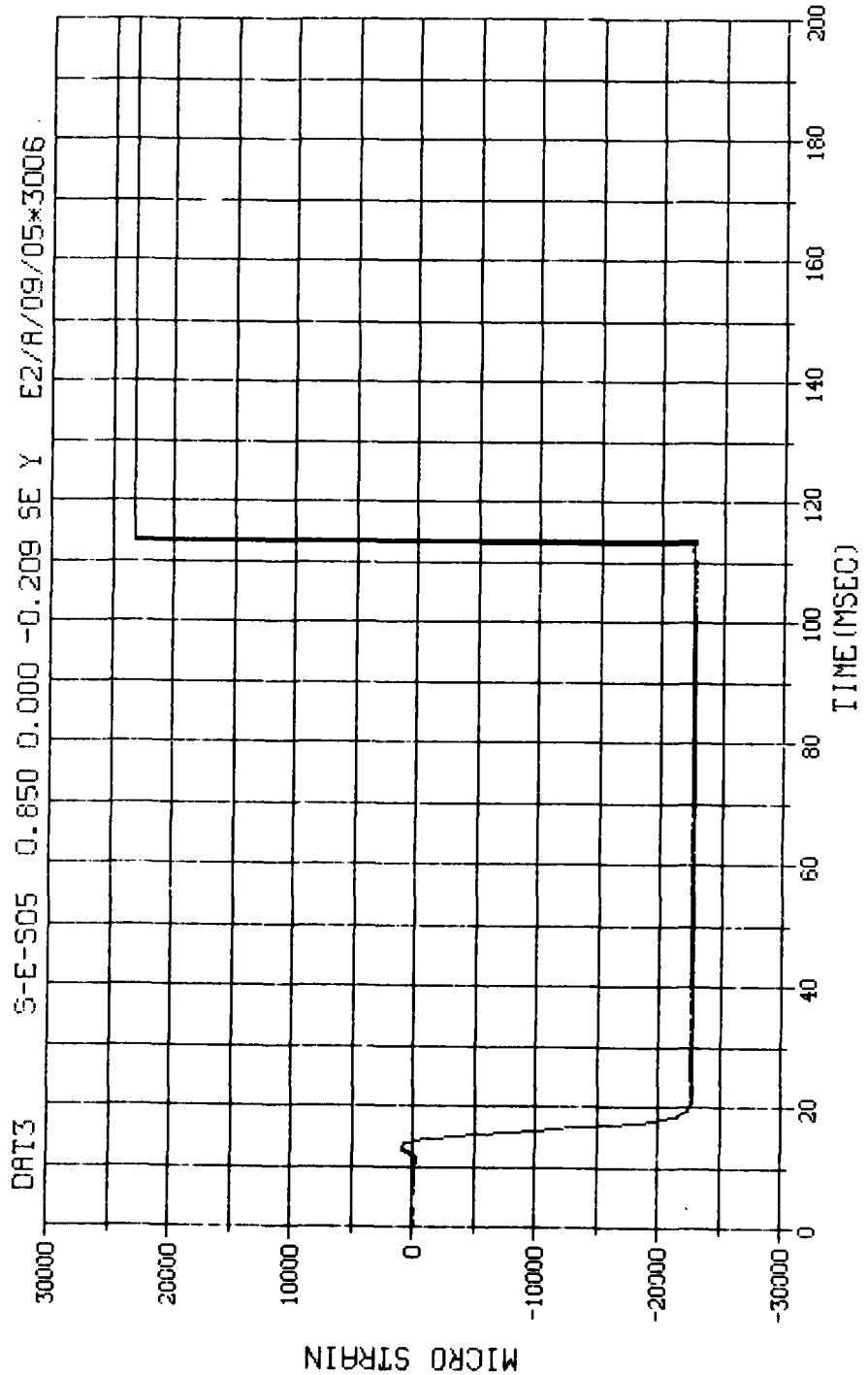
N.N. = 3003	E.U. = 0.000, 10000.000	VSN=66142
TSKIP=7.000	DIGITS=0.000, 872.625	TAPE22
S.R. =25.00 KHZ	4. 4 PM, TUE, 13 SEP 83.	FILE=148 1



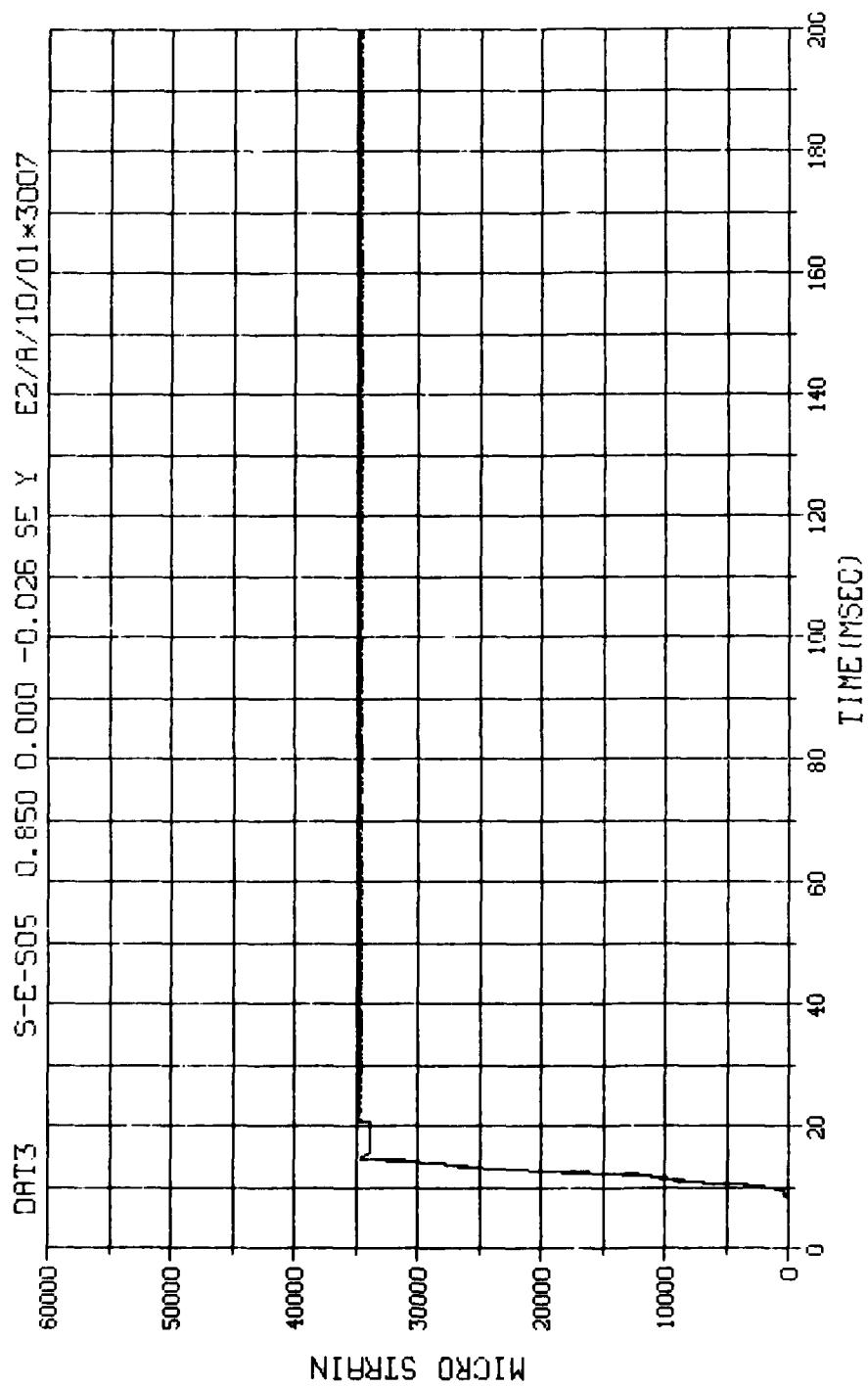
M.N. = 3004	E.U. = 0.000, 10000.000	VSN=66142
SKIP=7.000	DIGITS=0.000, 877.500	TAPE22
S.R. =25.00 KHZ	4. 4 PM, TUE, 13 SEP 83.	FILE=150 1



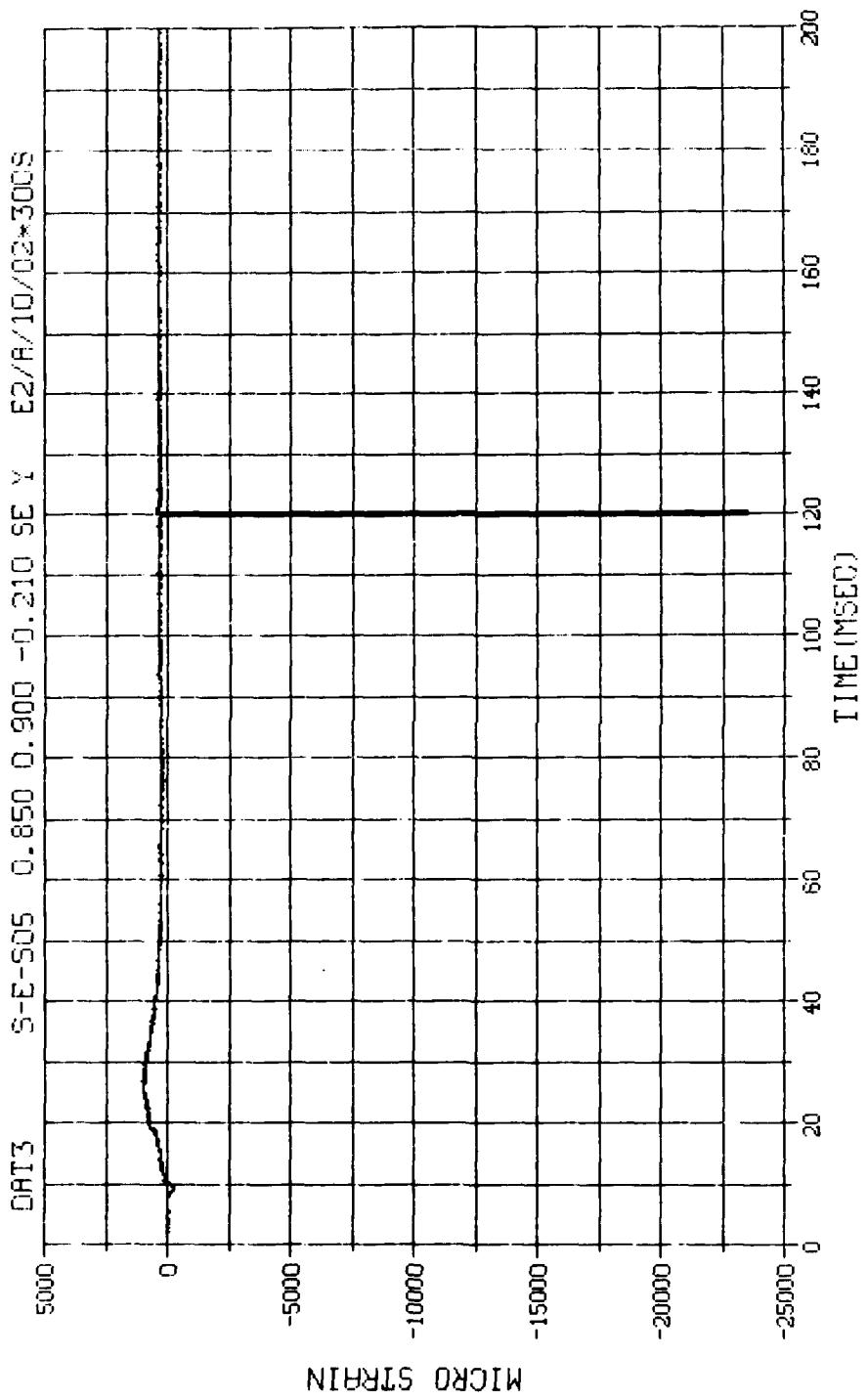
M.N. = 3005	E.U. = 0.000, 4000.000	WSN=66142
SKIP=7.000	DIGITS=0.000, 862.375	TAPE22
S.R. =25.00 KHZ	4. 4 PM, TUE, 13 SEP 83.	FILE=152 1



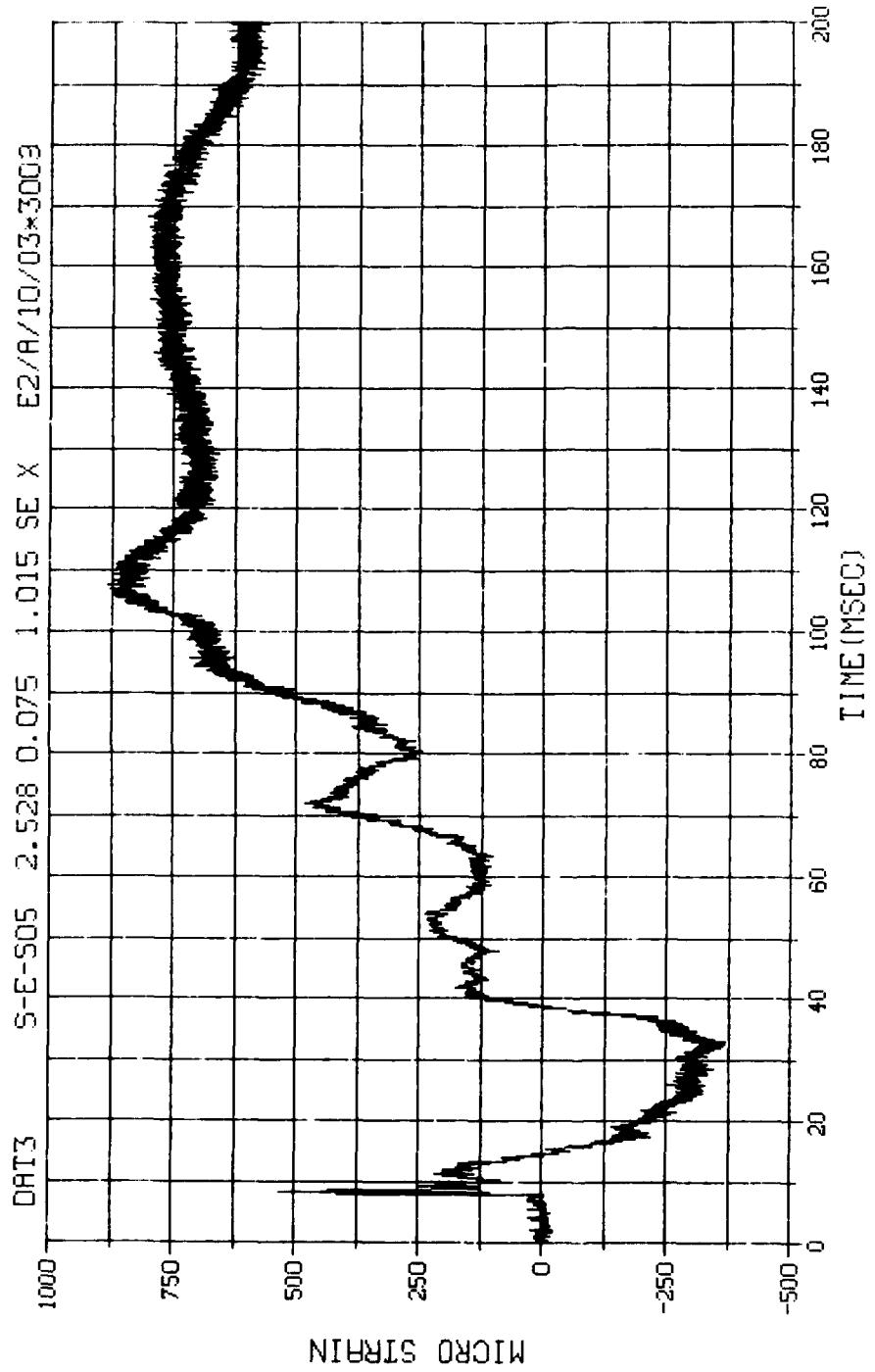
M.N. - 3006	E.U. -0.000,10000.000	VSN-66142
SKIP=7.000	DIGITS=0.000,890.500	TAPE22
S.R. =25.00 KHZ	4. 4 PM, TUE, 13 SEP 85.	FILE=154
		1



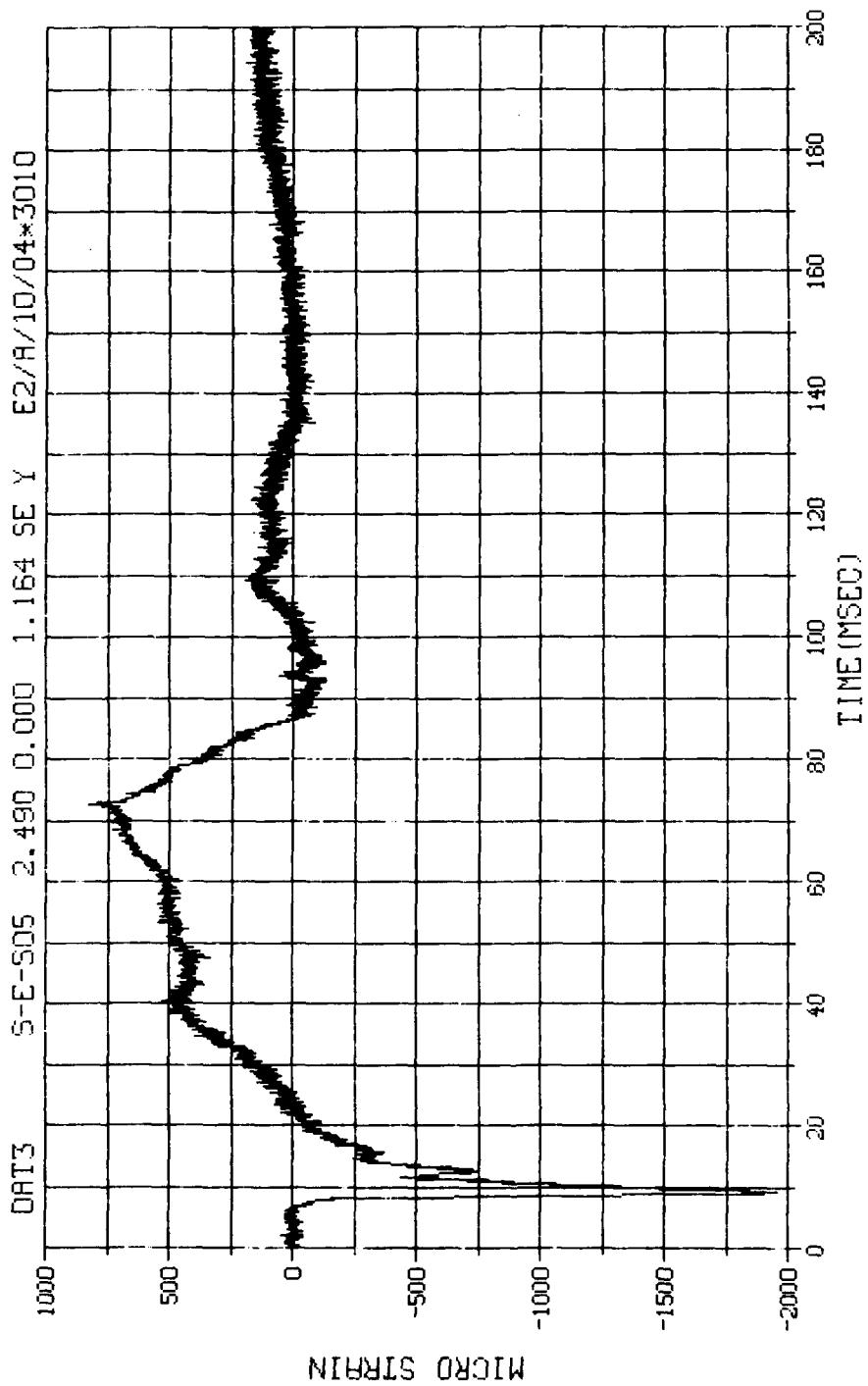
M.N. - 3007	E.U. -0.000, 15000.000	VSN-66142
SKIP=7.000	DIGITS=0.000, 888.250	TAPE22
S.R. =25.00 KHZ	4. 4 PM, TUE, 13 SEP 83.	FILE=156 1



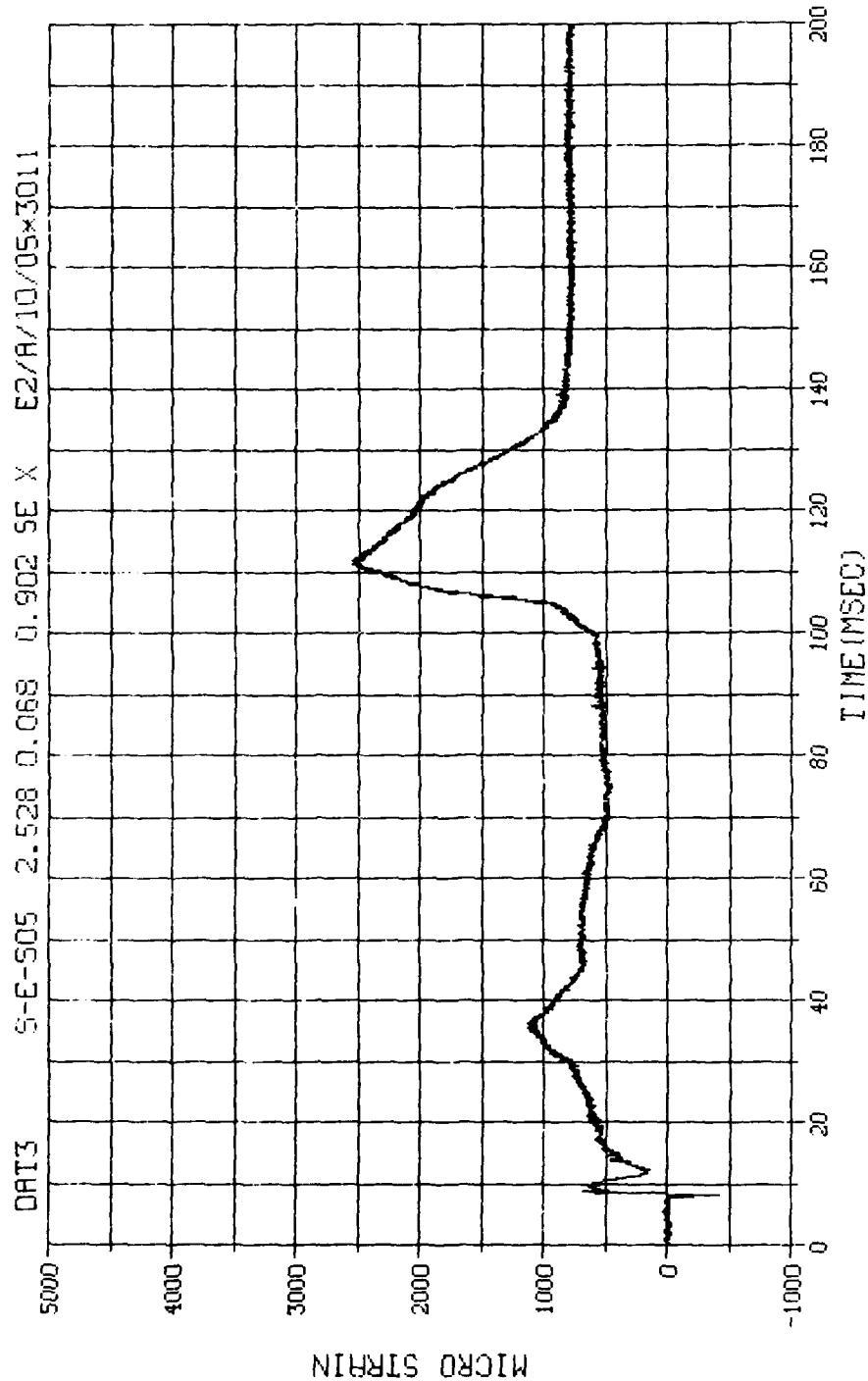
M.N. = 3008	E.U. = 0.000, 10000.000	VSN-66142
T5KIP=7.000	DIGITS=0.000, 874.500	TAPE22
S.R. = 25.00 KHZ	4. 4 PM, TUE, 13 SEP 83,	FILE=158 1



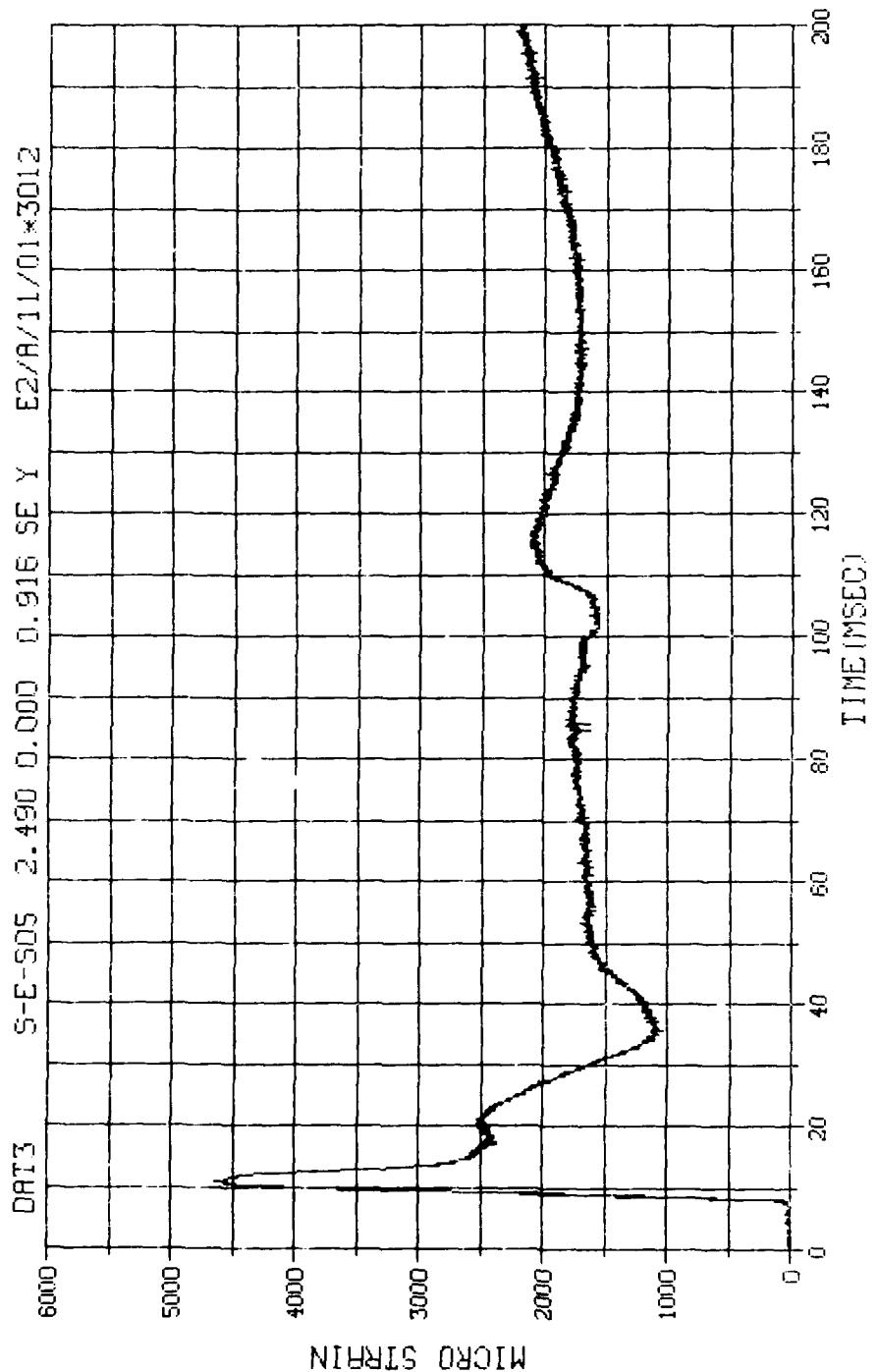
M.N. = 3009	E.U. = 0.000, 4000.000	VSN-66142
SKIP=7.000	DIGITS=0.000, 867.500	TAPE22
S.R. = 25.00 KHZ	4. 4 PM, TUE, 13 SEP 83.	FILE=160_1



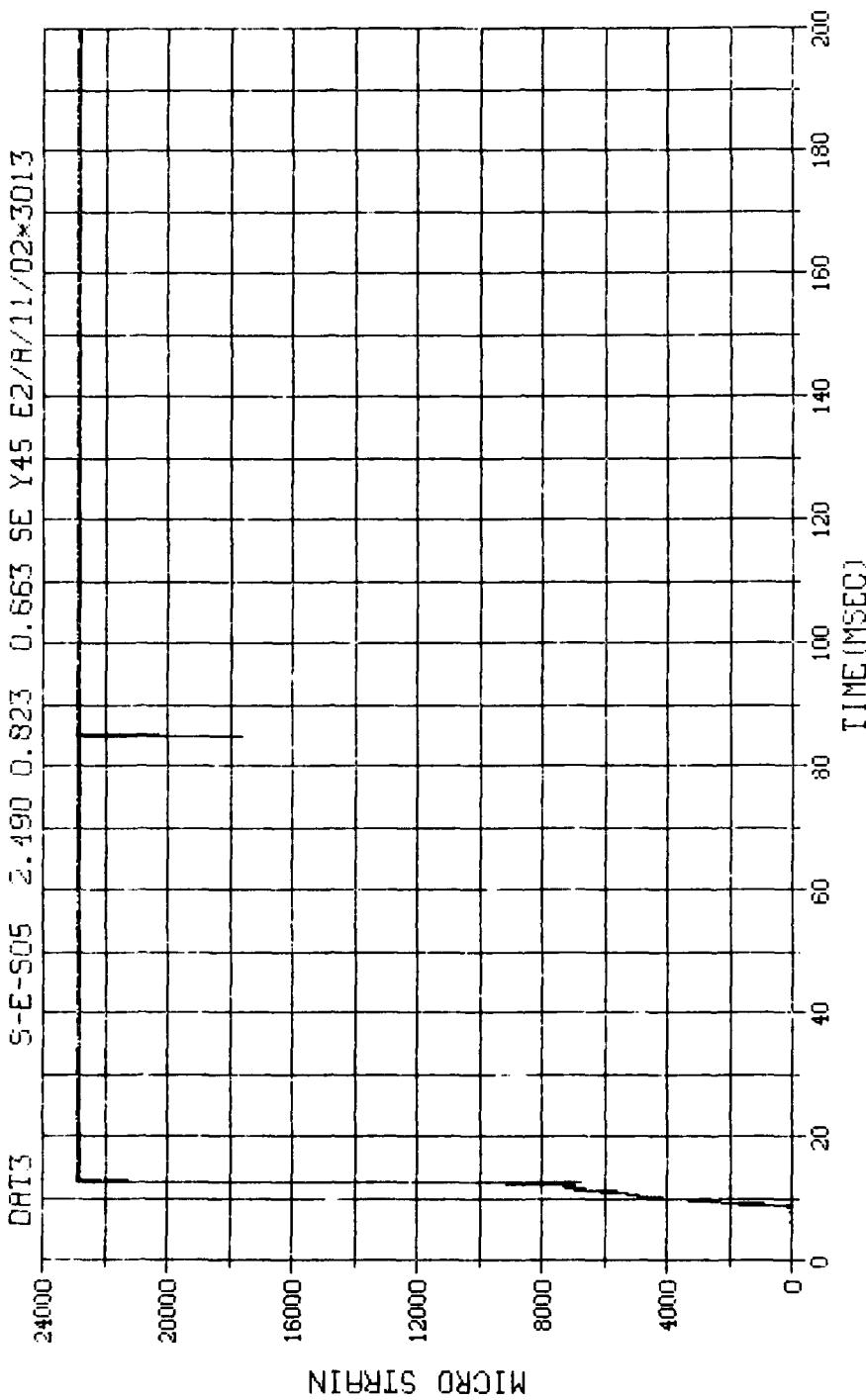
M.N. = 3010	E.U. = 0.000, 7500.000	VSN=66142
SKIP=7.000	DIGITS=0.000, 864.625	TAPE22
S.R. = 25.00 KHZ	4. 4 PM, TUE, 13 SEP 83.	FILE=162 1



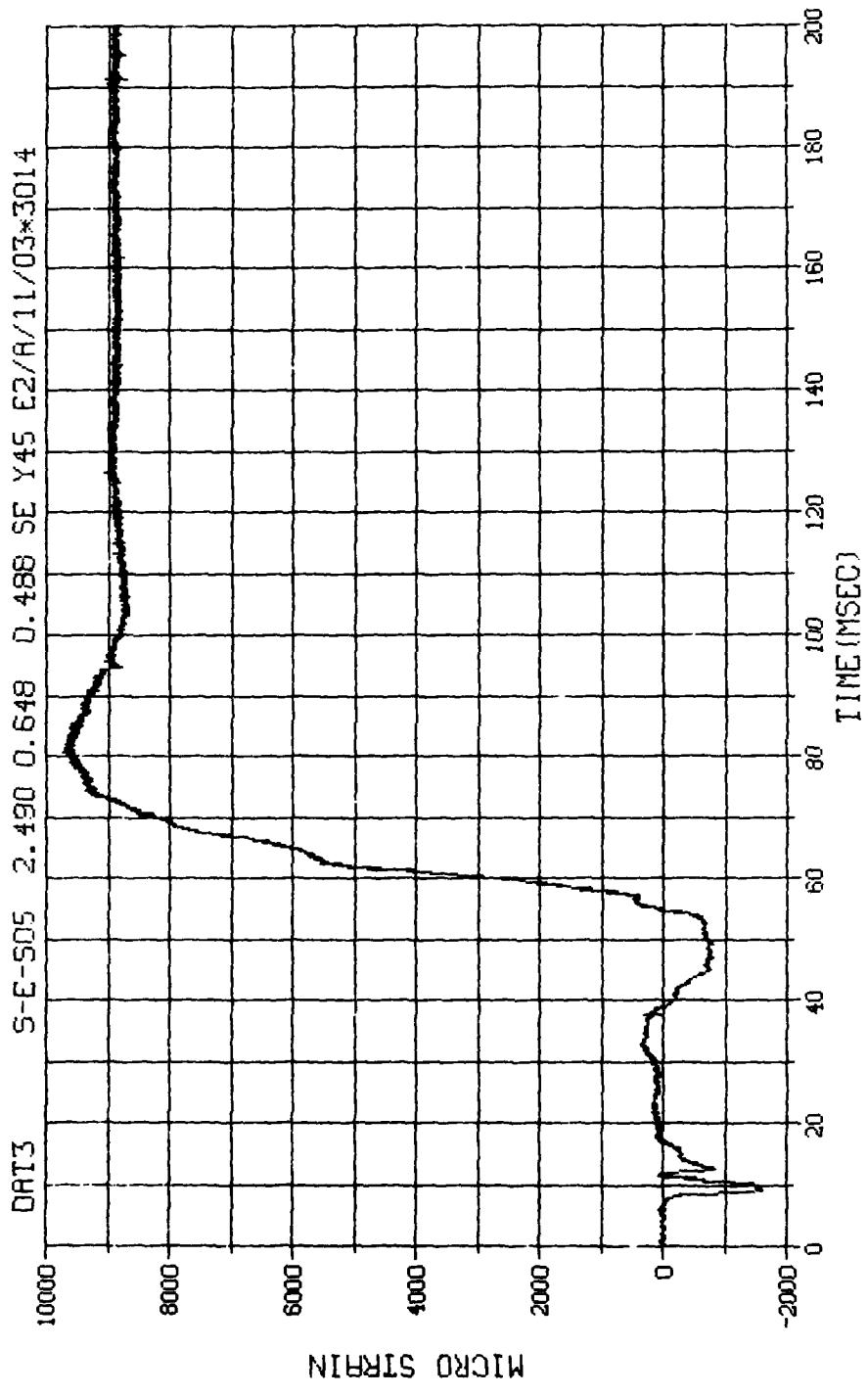
M.N. - 3011 E.U. -0.000, 4000.000 VSN-66142
SKIP=7.000 DIGITS=0.000, 879.875 TAPE22
S.R. =25.00 KHZ 4. 4 PM, TUE, 13 SEP 83, FILE=164



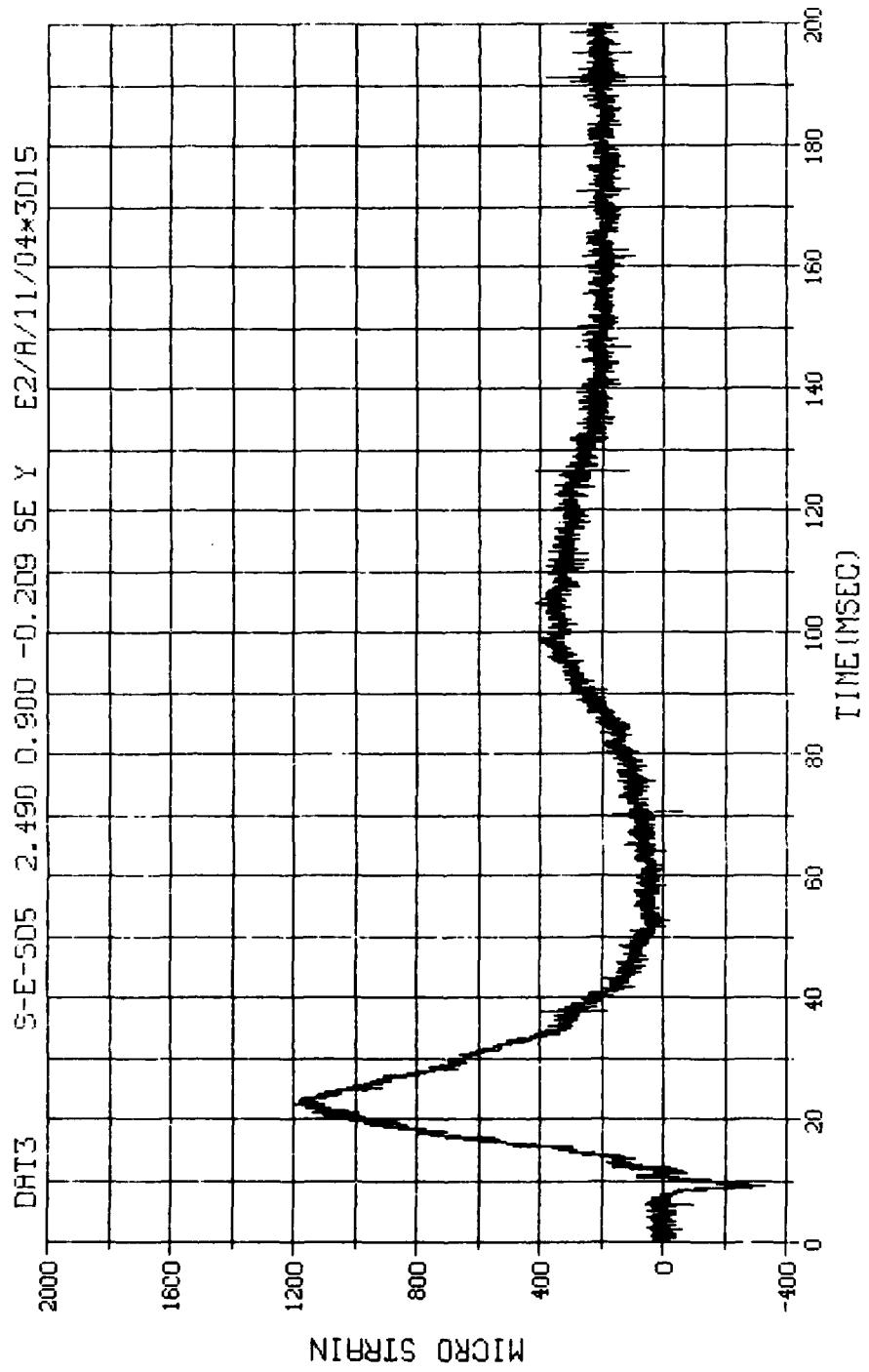
N. N. - 3012	E.U. -0.000, 10000.000	VSN-00142
SKIP=7.000	DIGITS=0.000, 885.750	TAPE22
S.R. =25.00 KHZ	4. 4 PM, TUE, 13 SEP 83.	FILE=156 1



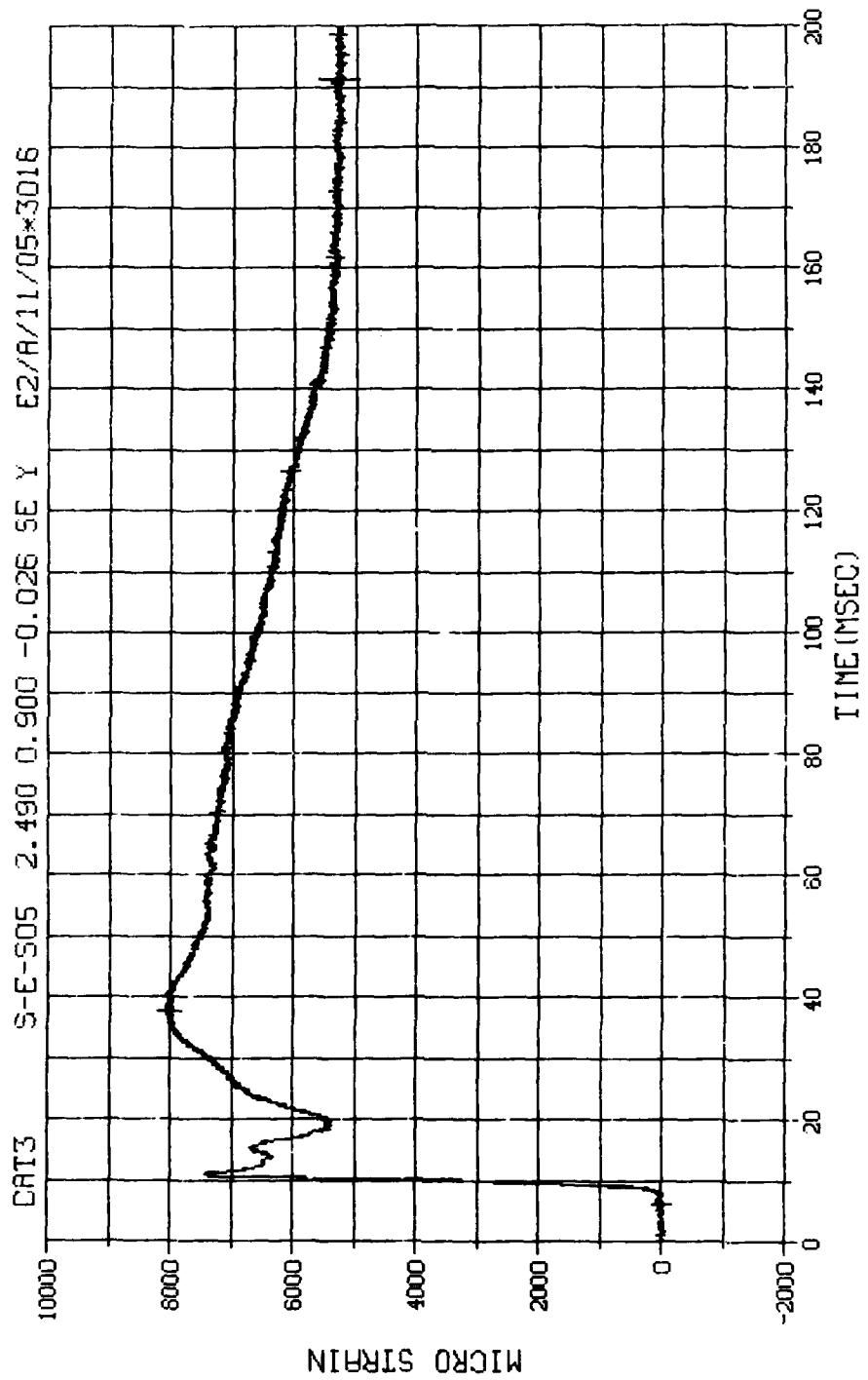
M.N. - 3013	E.U. -0.000, 10000.000	VSN-66142
TSKIP=7.000	DIGITS=0.000, 873.125	THFL22
S.R. =25.00 KHz	4. 4 PM, TUE, 15 SEP 83,	FILE-168.1



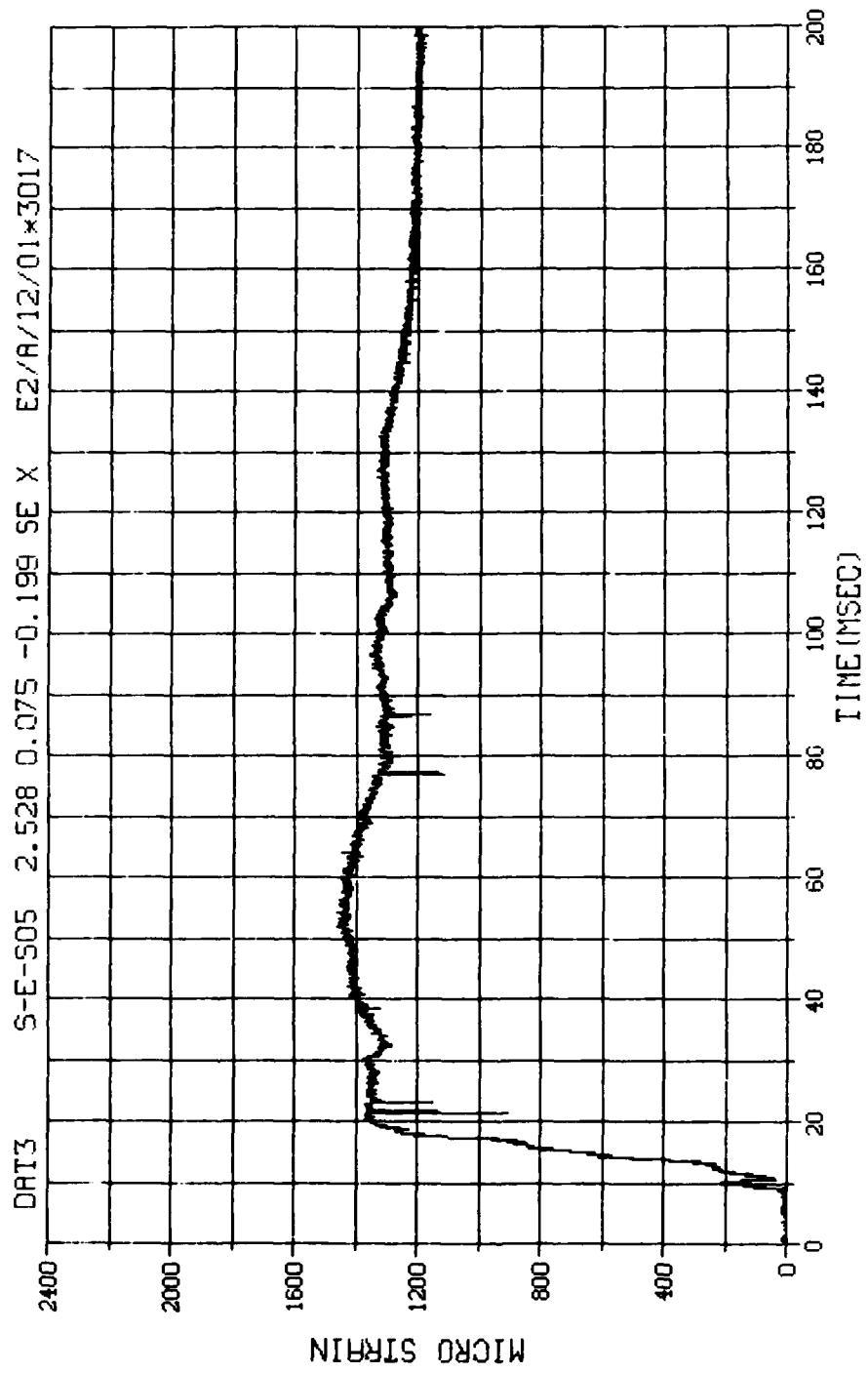
N.N. - 3014	E.U. -0.000, 10000.000	VSN-66142
TSKIP=7.000	DIGITS=0.000, 877.000	TAPE22
S.R. =25.00 KHZ	4. 4 PM, TUE, 13 SEP 83.	FILE=170



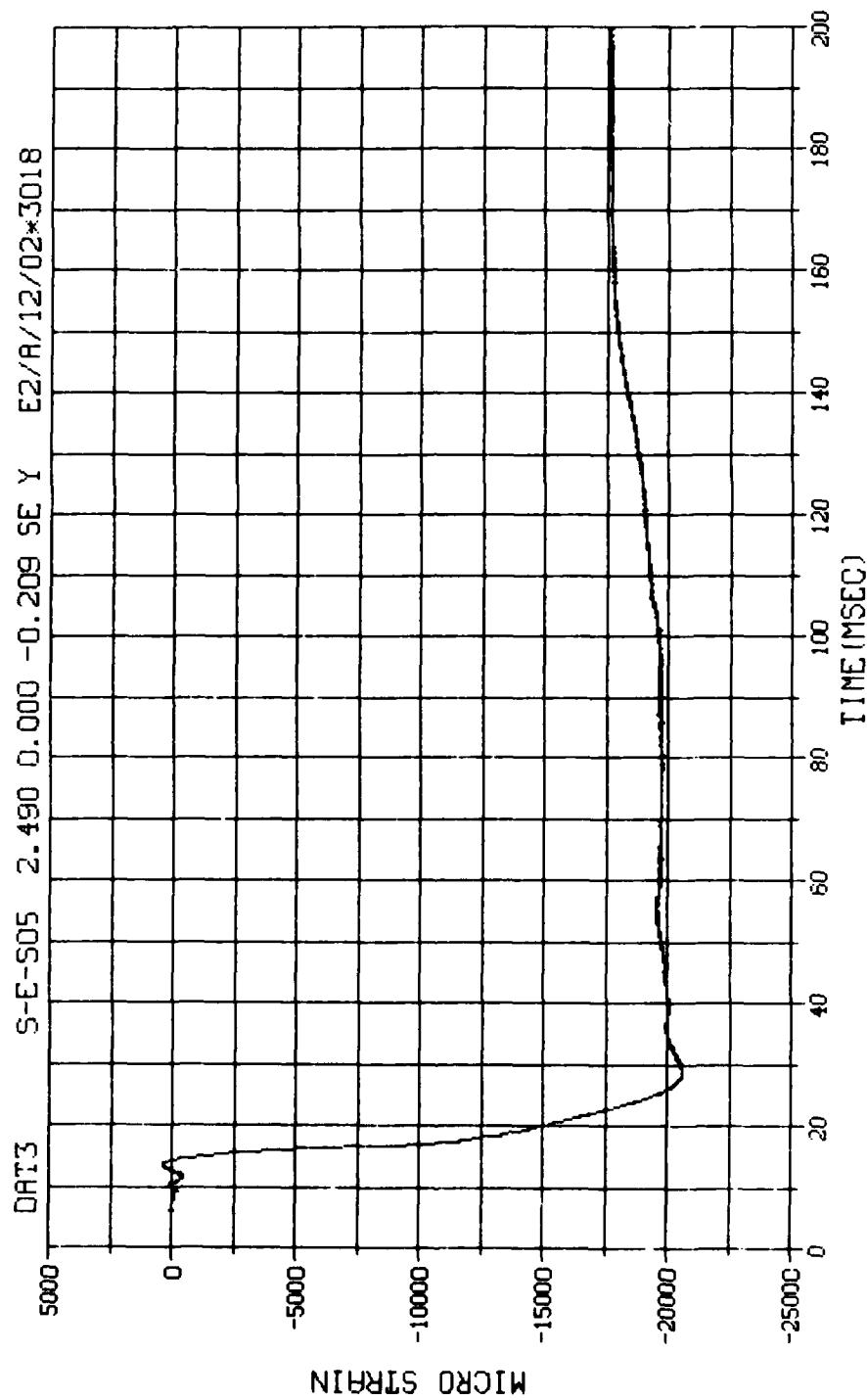
N.N. = 3015 E.U. = 0.000, 10000.000 VSN=00142
TSKIP=7.000 DIGITS=0.000, 900.750 TAPE22
S.R. = 25.00 KHZ 4. 4 PM, TUE, 13 SEP 83. FILE=172



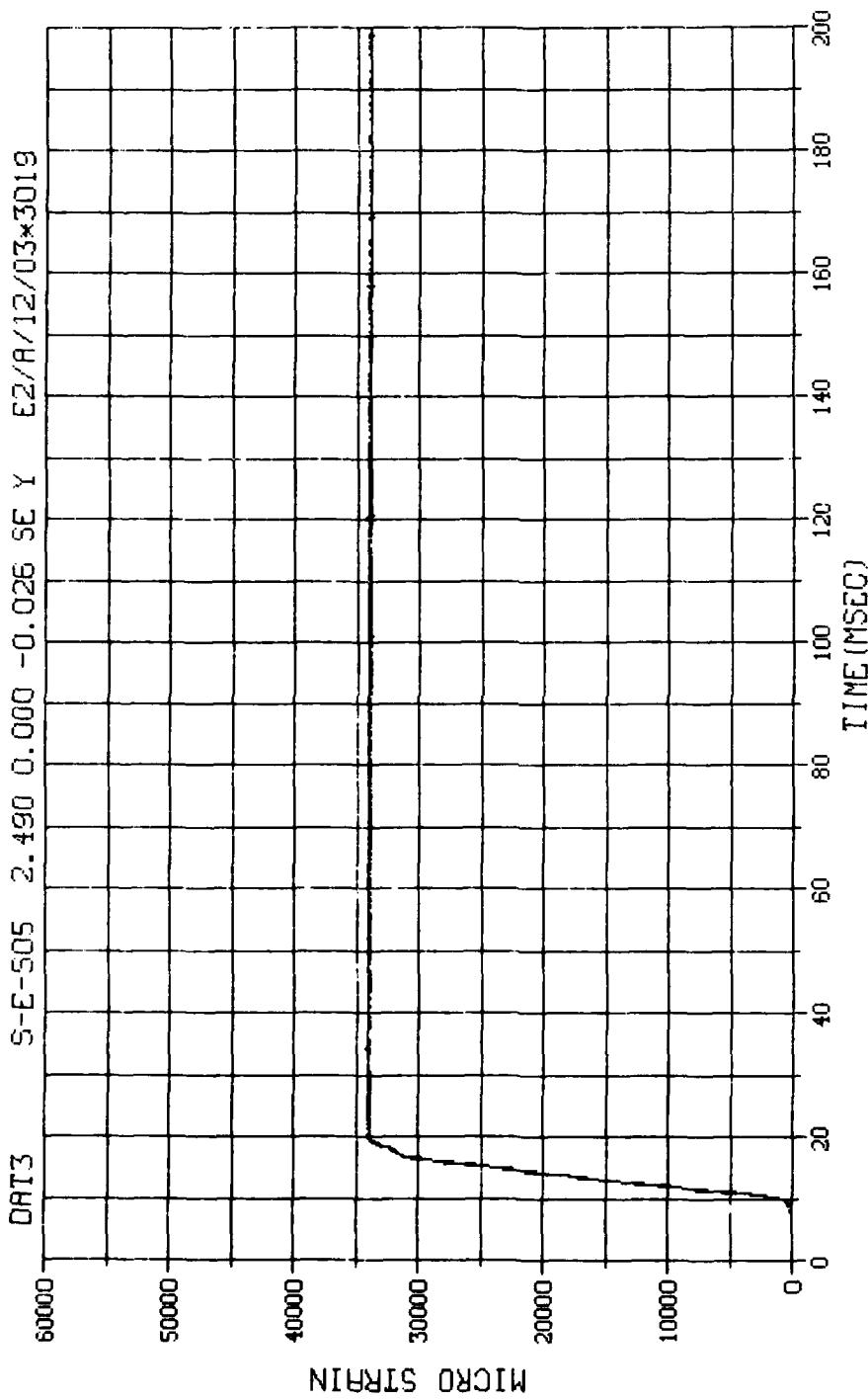
N. N. - 3016 E.U. -0.000, 10000.000 YSN-66142
TSKIP=7.000 DIGITS=0.000, 895.750 TAPE22
S.R. =25.00 KHZ 4. 4 PM, TUE, 13 SEP 83. FILE=174 1



N.N. = 3017	E.U. = -0.000, 4000.000	VSN=66142
SKIP=7.000	DIGITS=0.000, 878.875	TAPE22
S.R. =25.00 KHZ	4. 4 PM, TUE, 13 SEP 83,	FILE=176 1



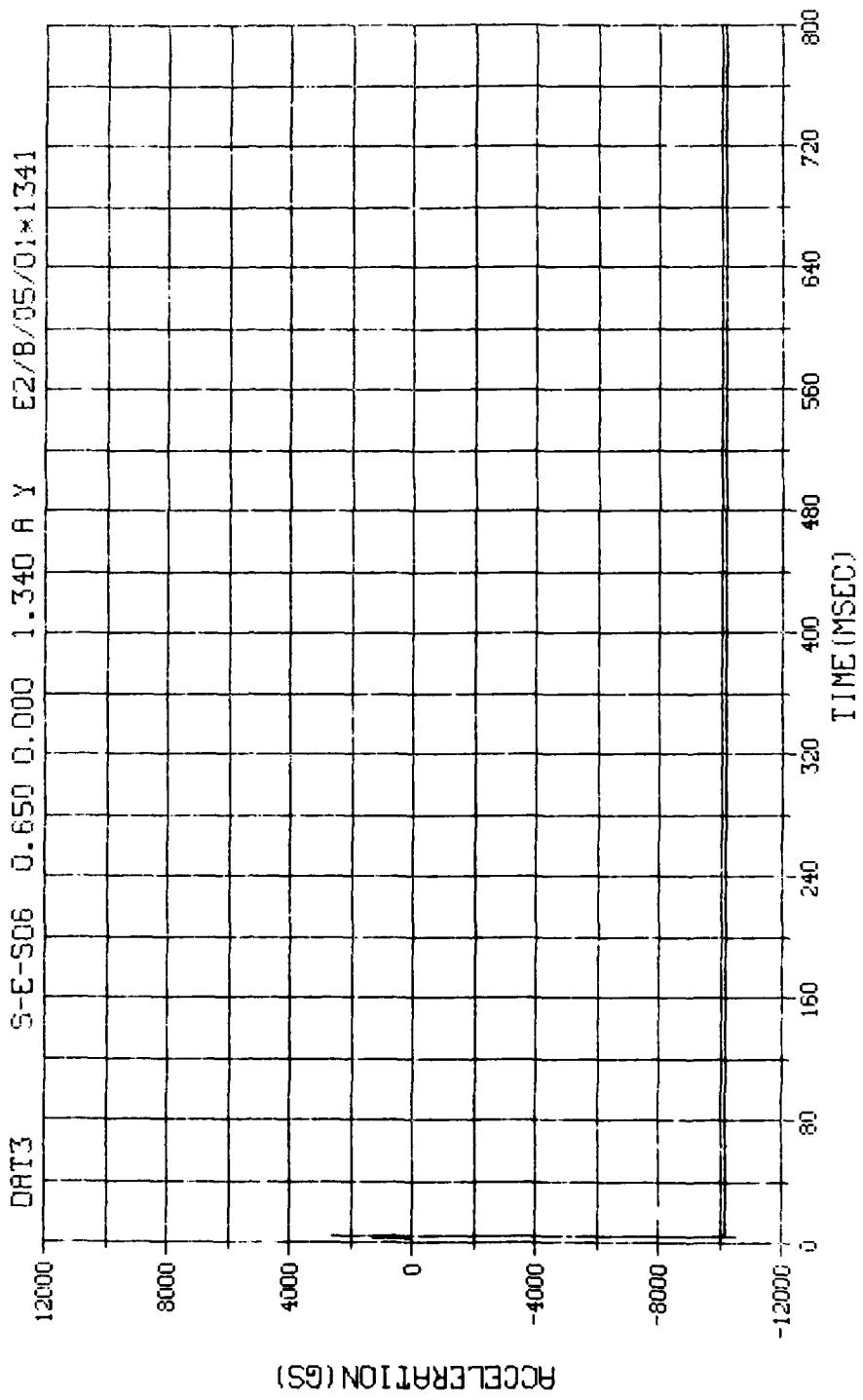
M.N. = 3018	E.U. = 0.000, 10000, 000	VSN-66142
SKIP=7.000	DIGITS=0.000, 872.750	TAPE22
S.R. = 25.00 KHZ	4. 4 PM, TUE, 13 SEP 83.	FILE=178 1



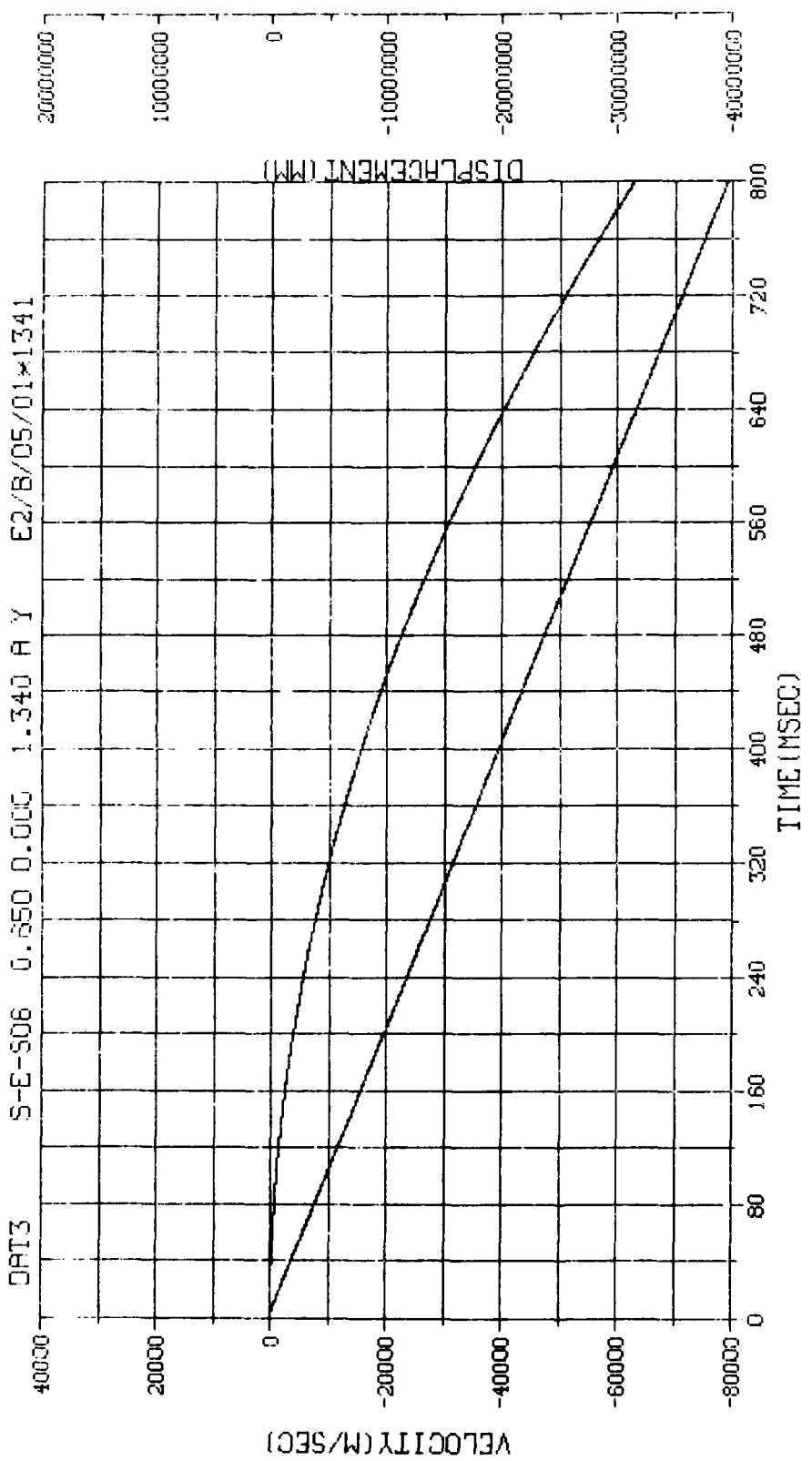
N. N. = 3019	E. U. = 0. 000, 15000. 000	VSN=66142
TSKIP=7. 000	DIGITS=0. 000, 882. 000	TAPE22
S. R. =25. 00 KHZ	4. 4 PM, TUE, 13 SEP 83,	FILE=180 1

APPENDIX H

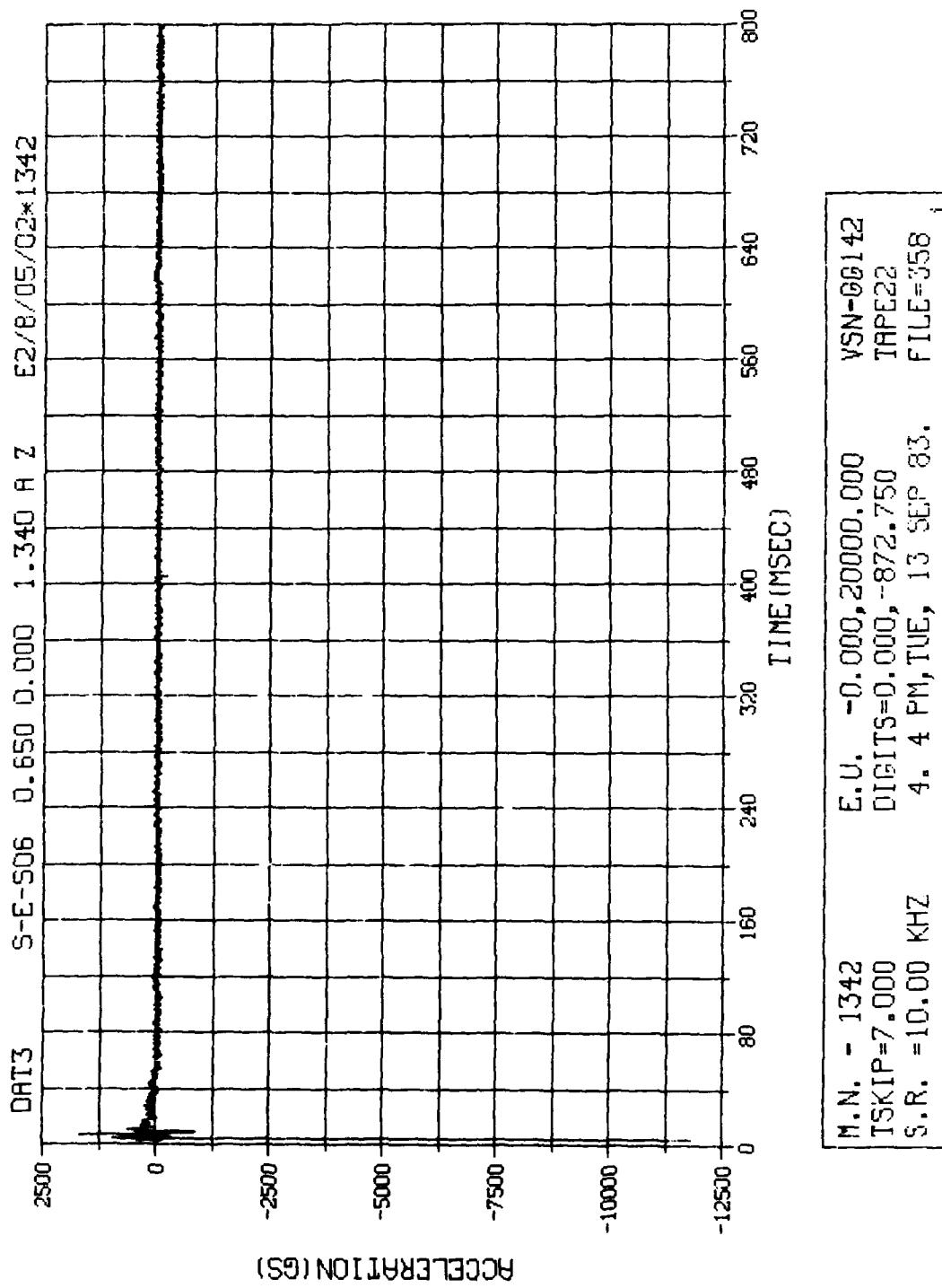
NEAR-FIELD AND STRUCTURAL DATA ARCH A-6

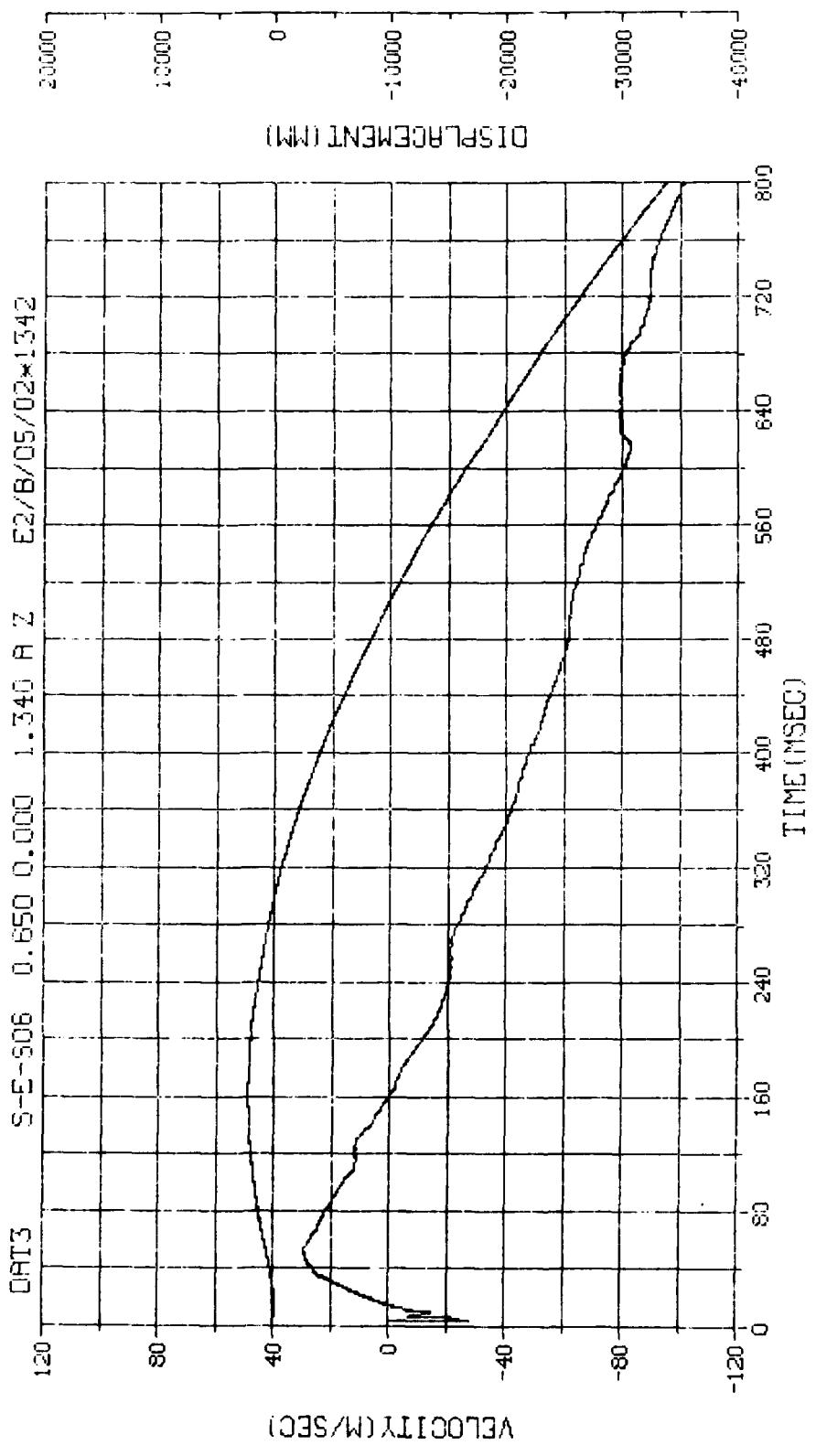


M. N. = 1341	E. U. = 0.000, 4500.000	VSN=66142
TSKIP=7.000	DIGITS=0.000, -890.375	TAPE22
S. R. = 10.00 KHZ	8,47 AM, WED, 14 SEP 83,	FILE=356 1

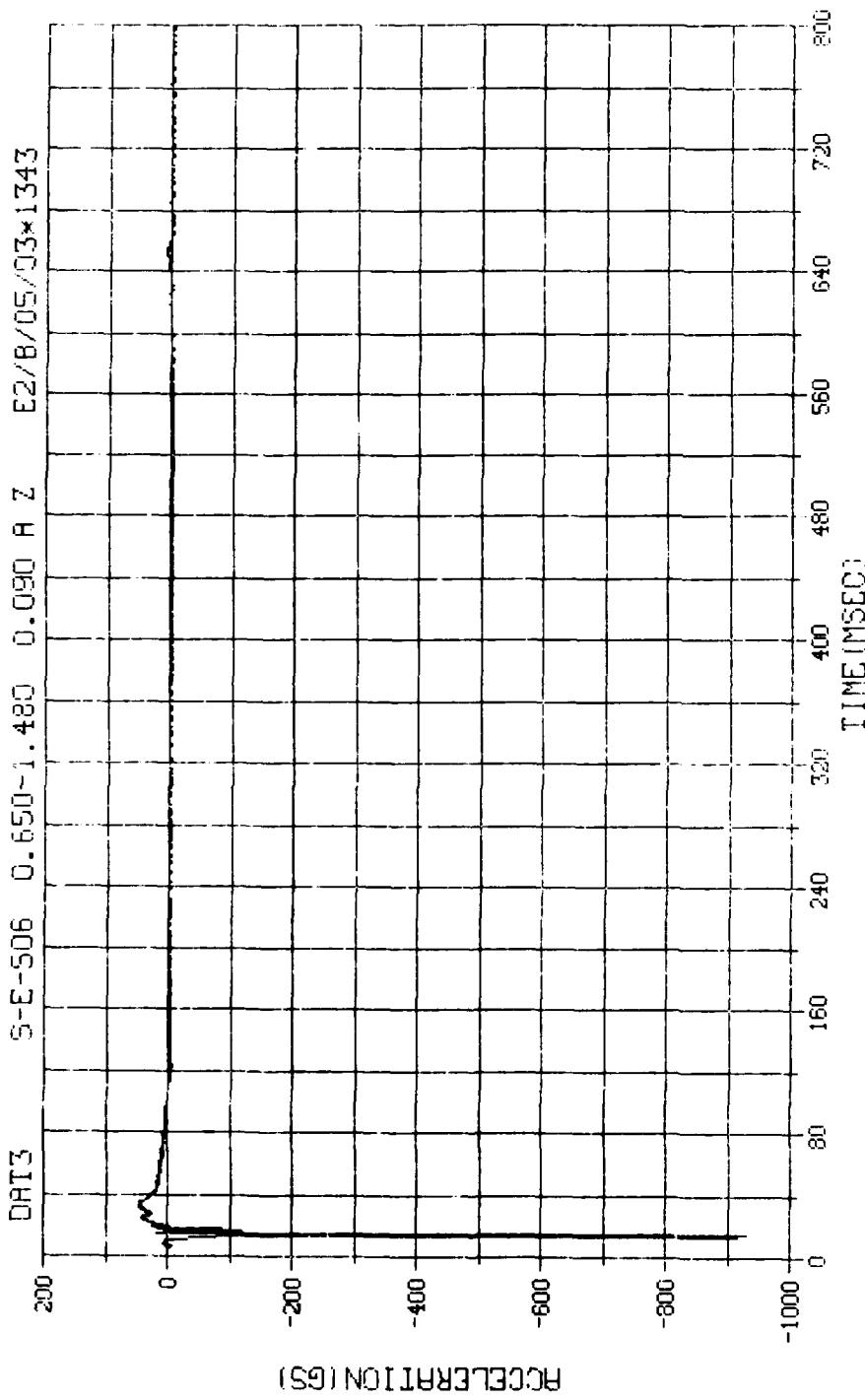


M.N. - 1341	E.U. -0.000, 4500.000	VSN-66142
TSKIP=7.000	DIGITS=0.000, -890.375	THPE22
S.R. = 10.00 KHZ	8.4V AM,NET, 1& SLP 83.	File# 356 2

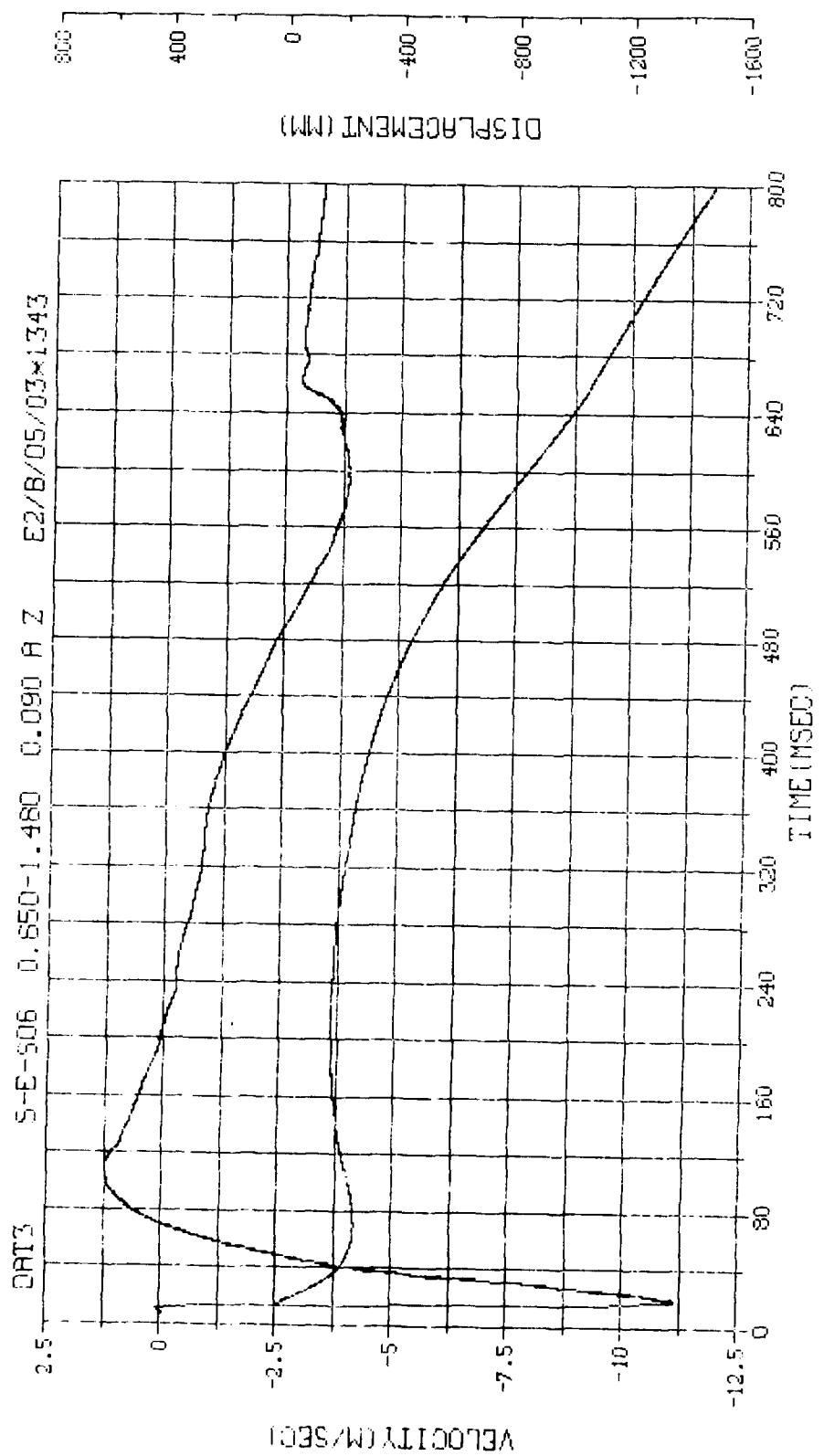




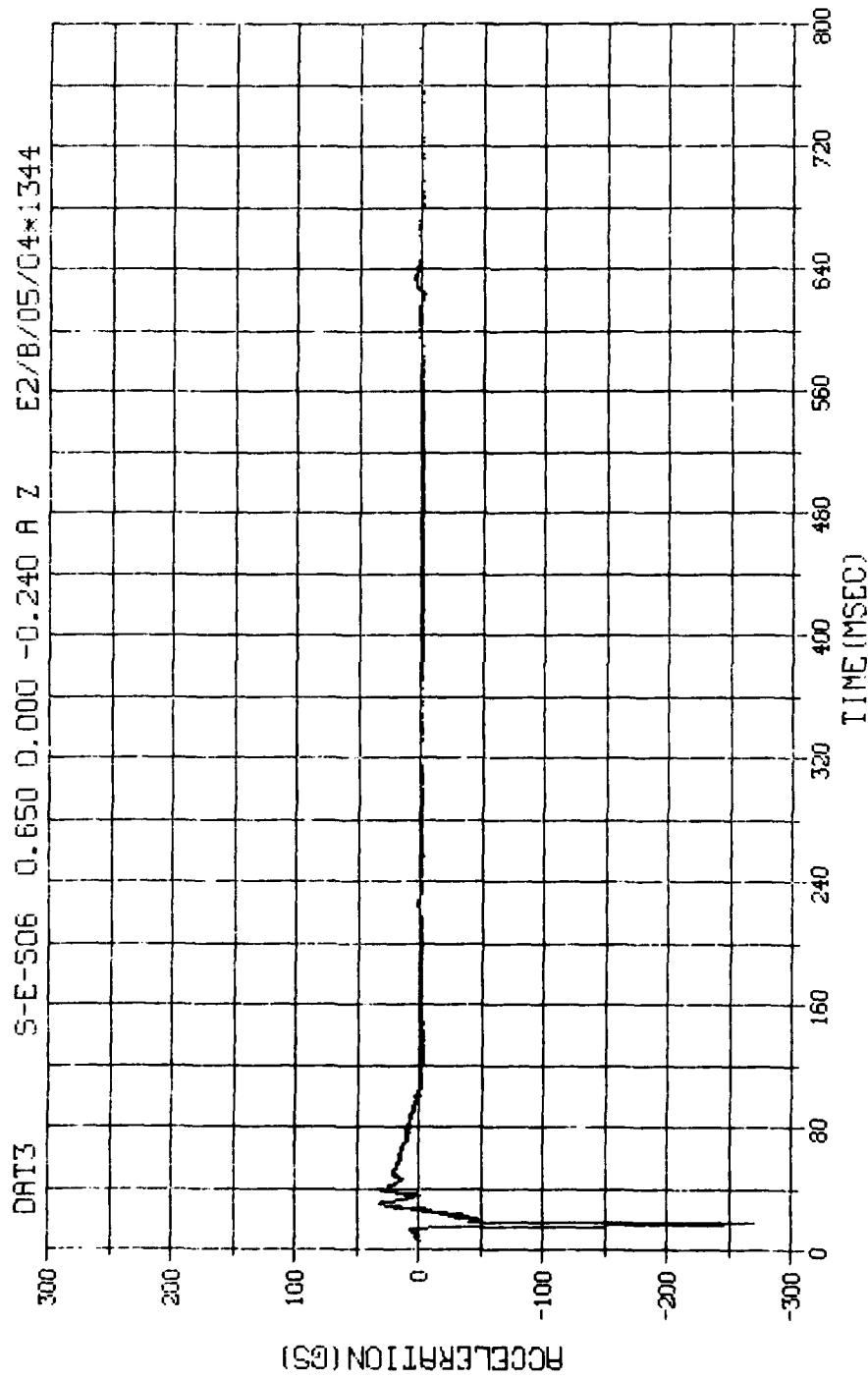
M.N. = 1342	E.U. = 0.000, 20000.000	VSN-06142
TSKIP=7.000	DIGITS=0.000, -872.750	TAPE22
S.R. = 10.00 KHZ	4. 4 PH, TUE, 13 SEP 83.	FILE=358 2]



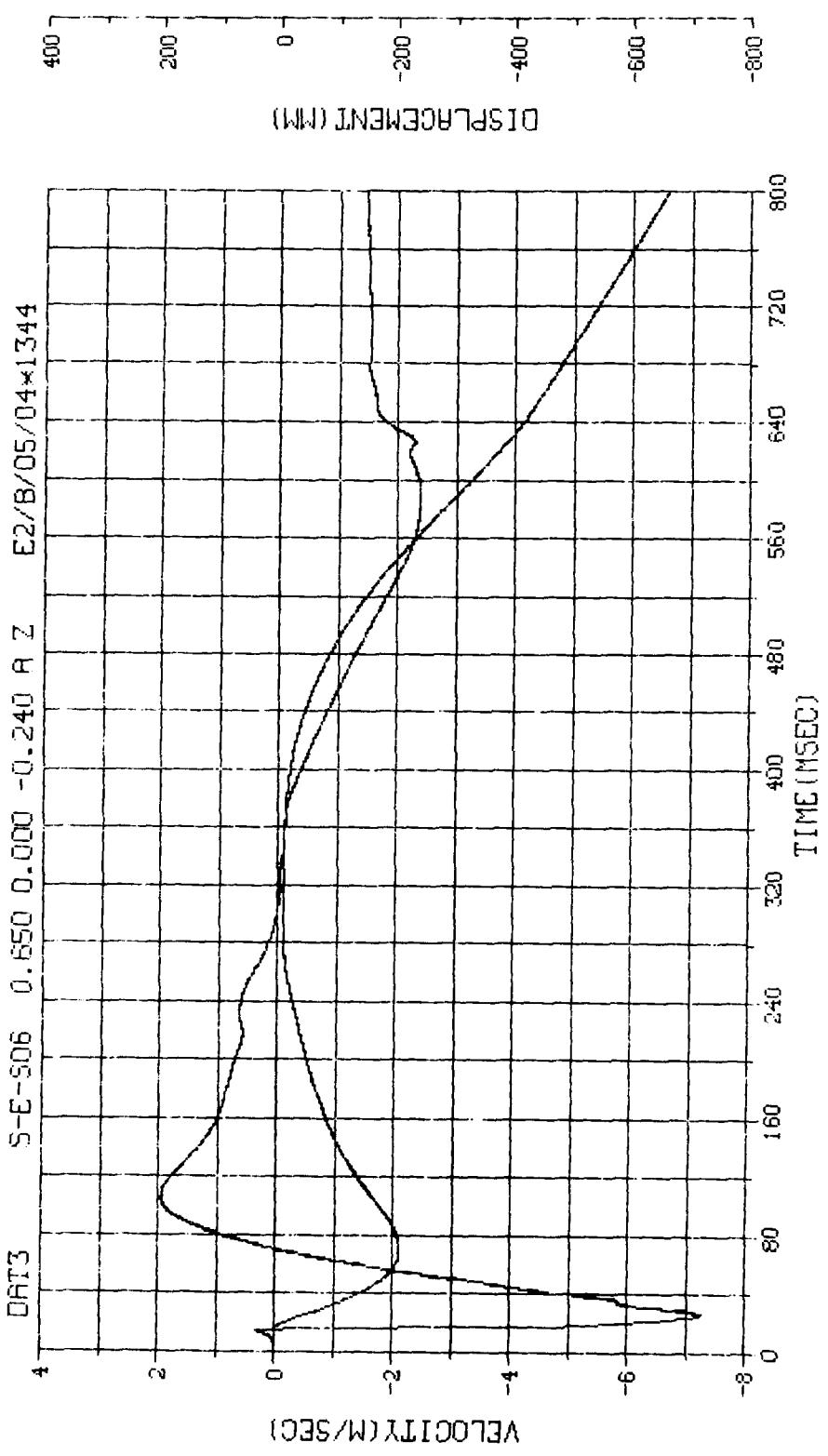
M.N. = 1343 E.U. = 0.000, 450.000 VSN-66142
TSKTP=7.000 DIGITS=0.000, -880.125 TAPE22
S.R. = 10.00 KHZ G.47 H1, HED, 14 SEP 83, FILE=350

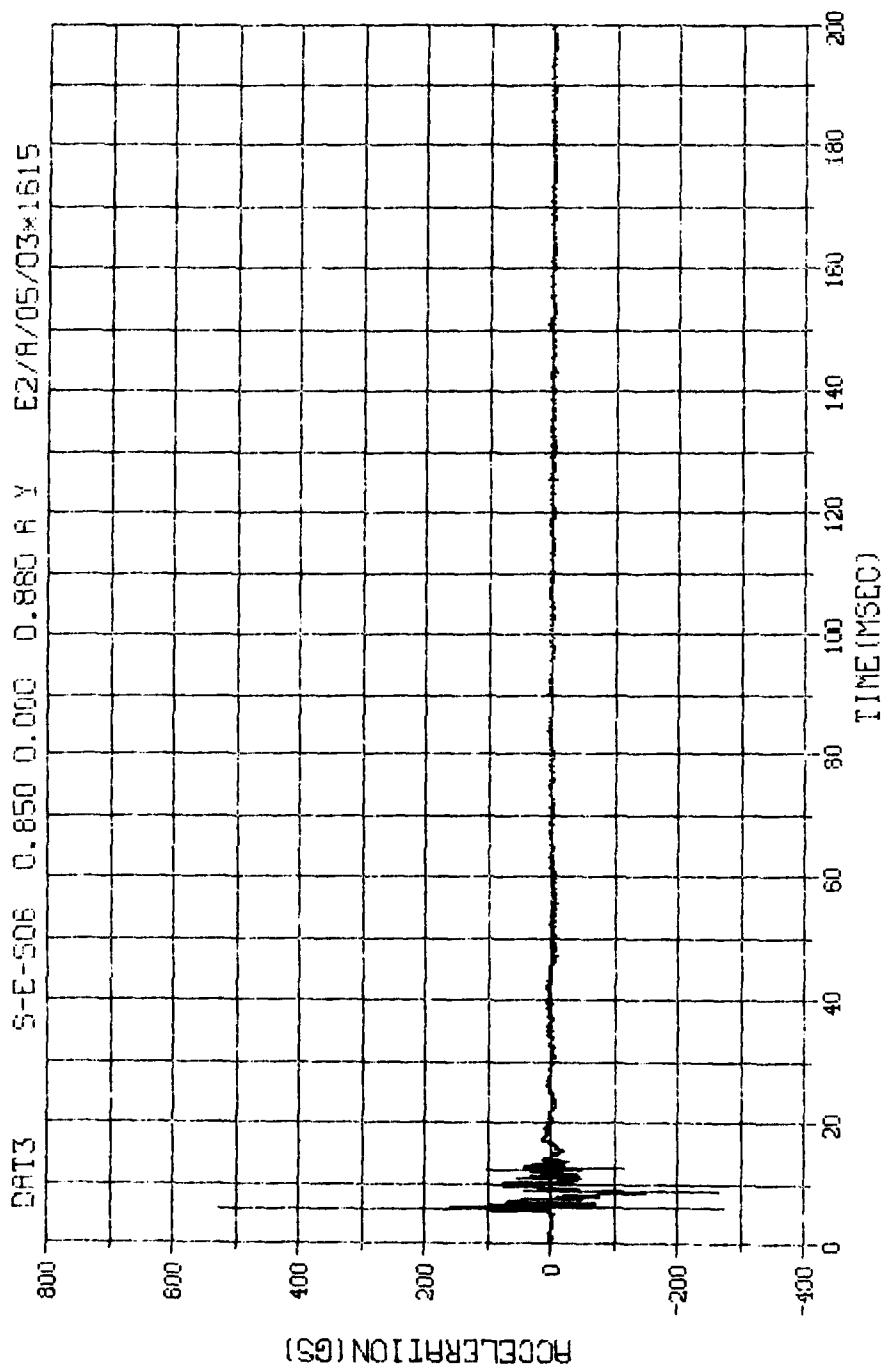


M.N. = 1343	E.U. = 0.000, 450.000	VSN=66142
T5KIP=7.000	DIGITS=0.000, -880, 125	TYPE22
S.R. = 10.00 KHZ	0.47, 611, MED, 14 SEP 85,	FILE=360

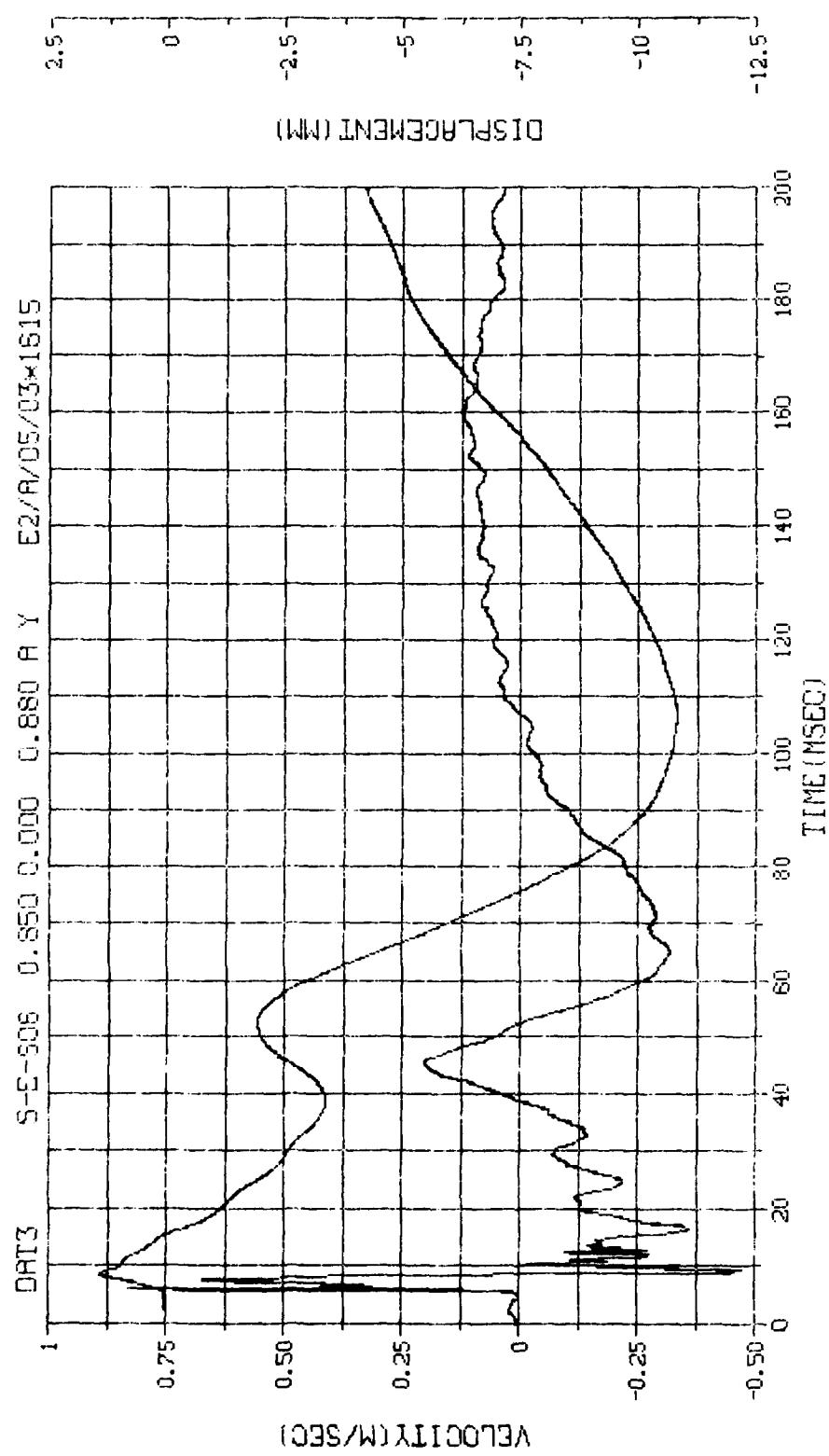


M.N. = 1344	E.U. = -0.000, 200.000	VSN=60142
SKIP=7.000	DIGITS=0,300,-873,125	TAPE22
S.R. =10.00 KHZ	8.47 AM, WED, 14 SEP 83,	FILE=362 1

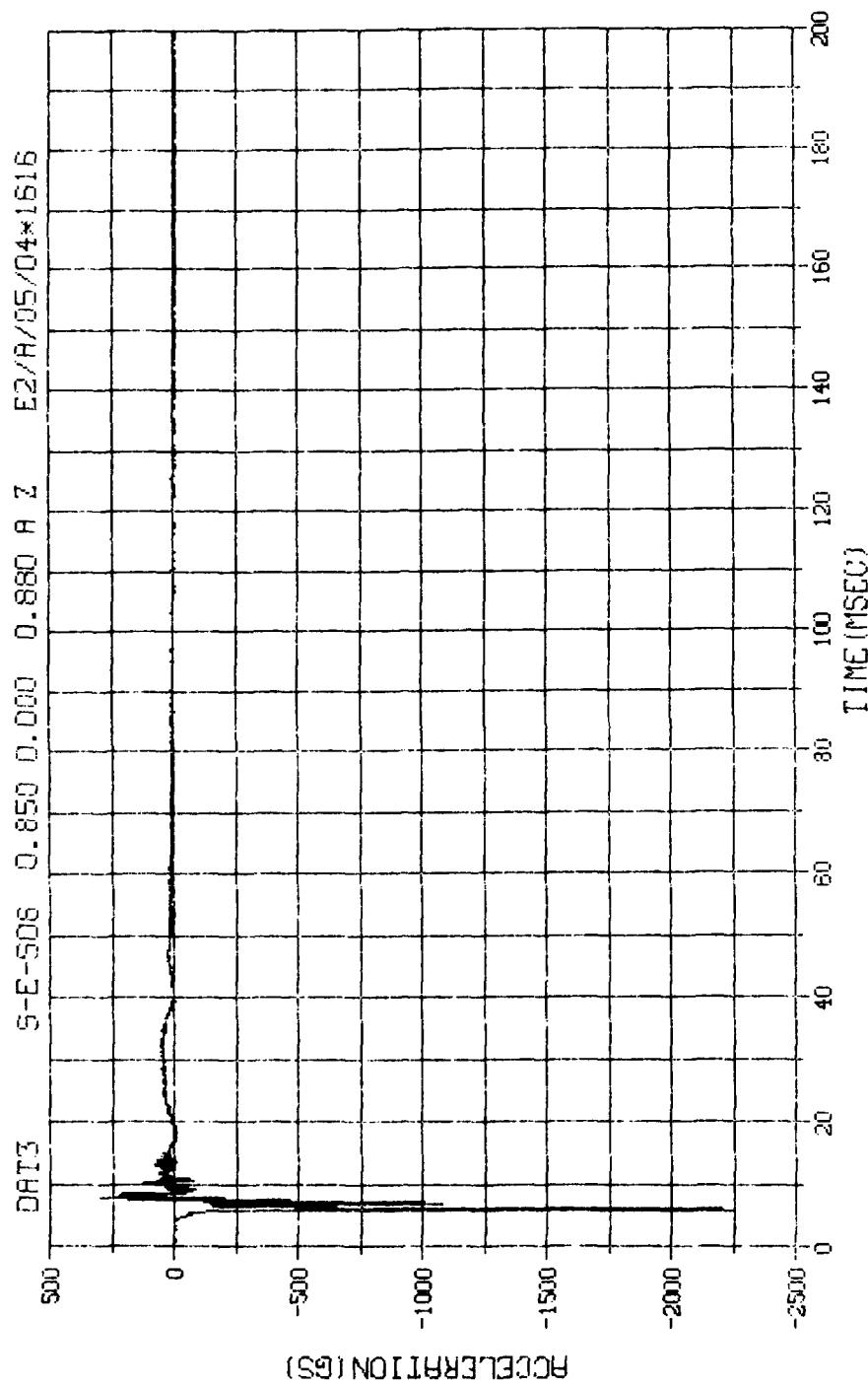




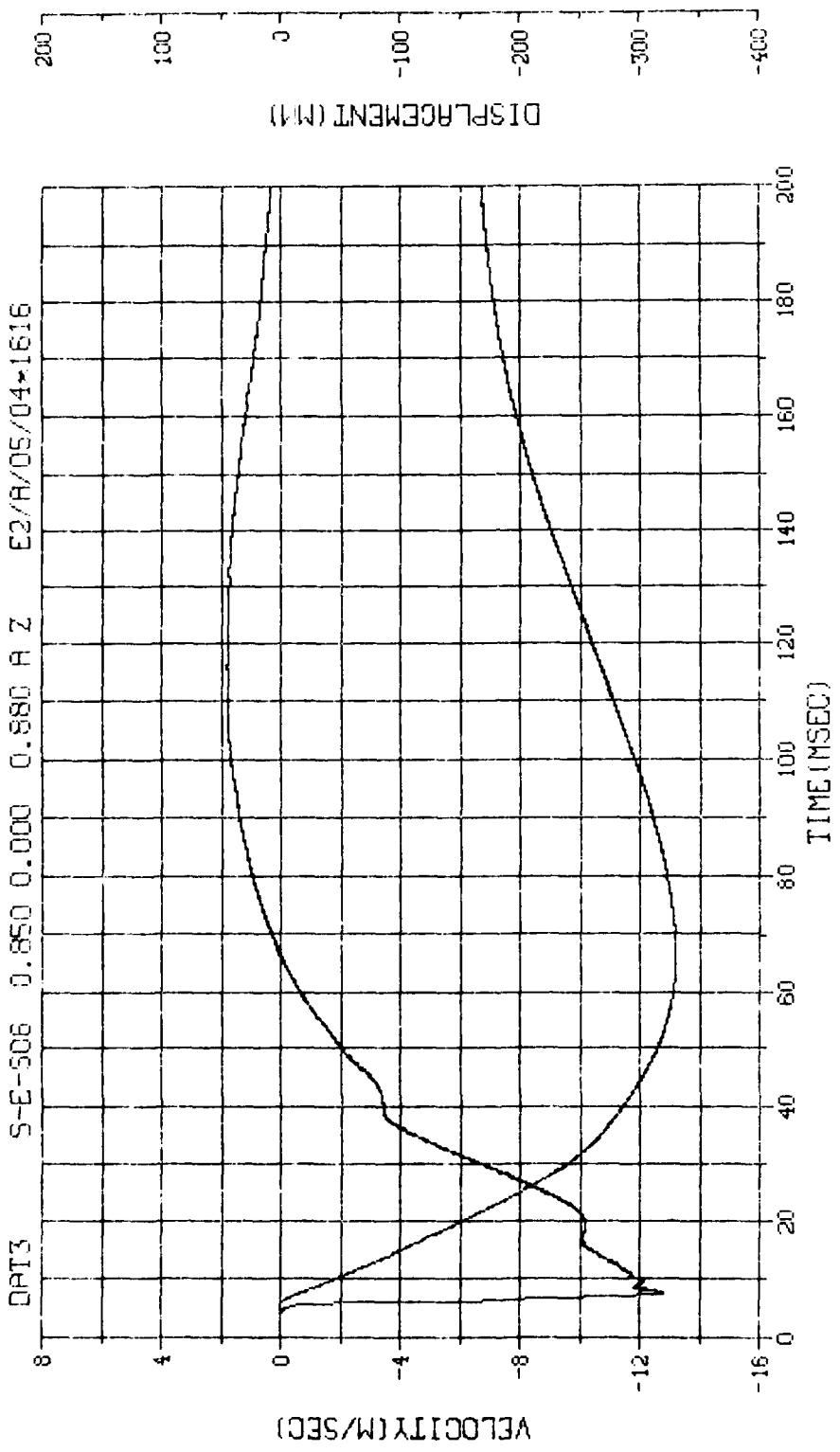
M. N. -91615	E.U. -0.000,1000.000	VSN-FB76
ISKIP=7.000	DIGITS=0.000,886.375	TAPE22
S.R. =25.00 kHz	29.0 NM3 12:17:16	FILE=0
1		



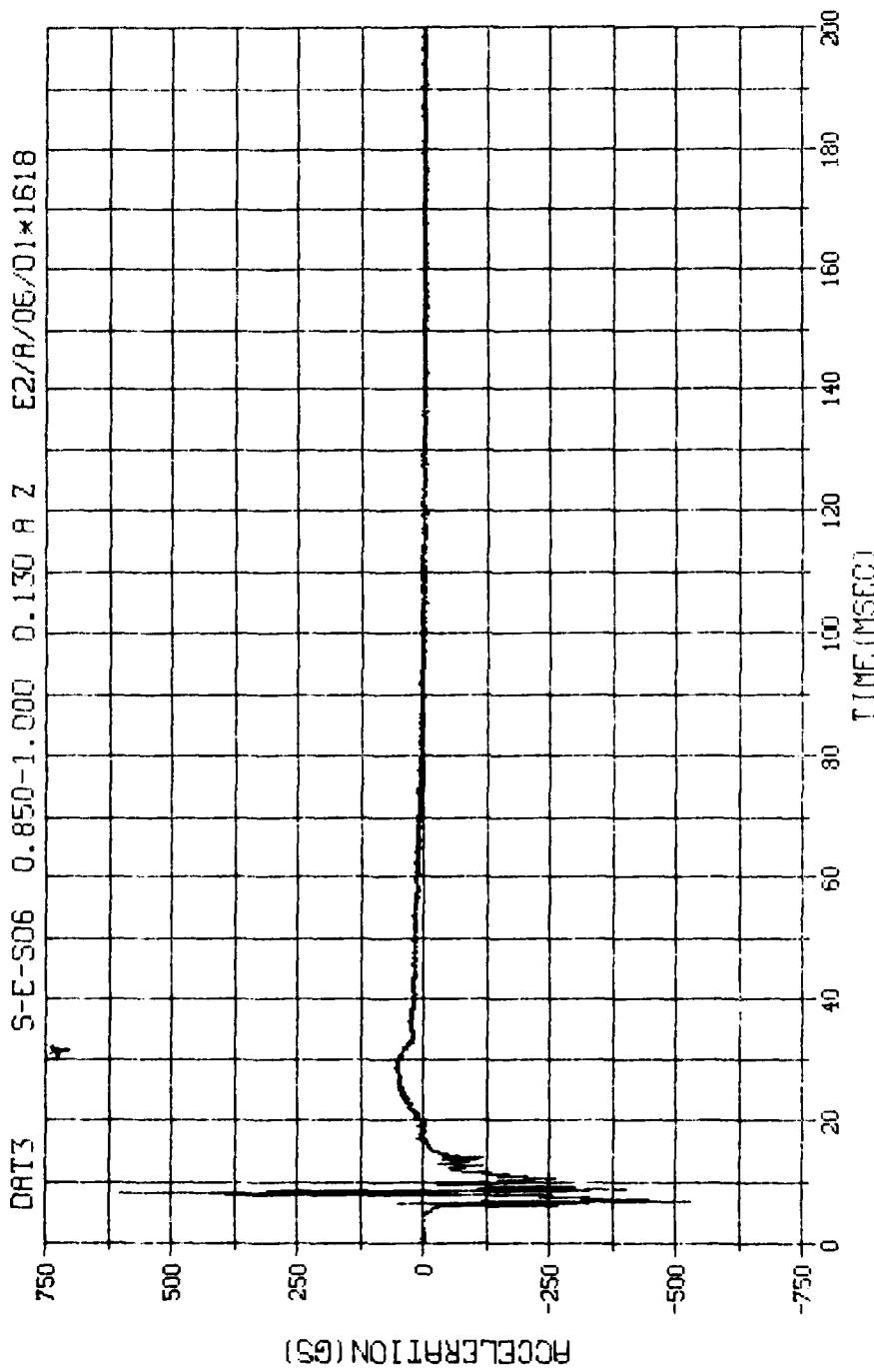
M.N. -91615	Z.U. -0.000, 1000.000	VSN-FB76
TSKIP=7.000	DIGITS=0.000, 886.375	TAPE22
S.R. =25.00 KHZ	280.000 NSEC	FILE=0
	12:17:16	2



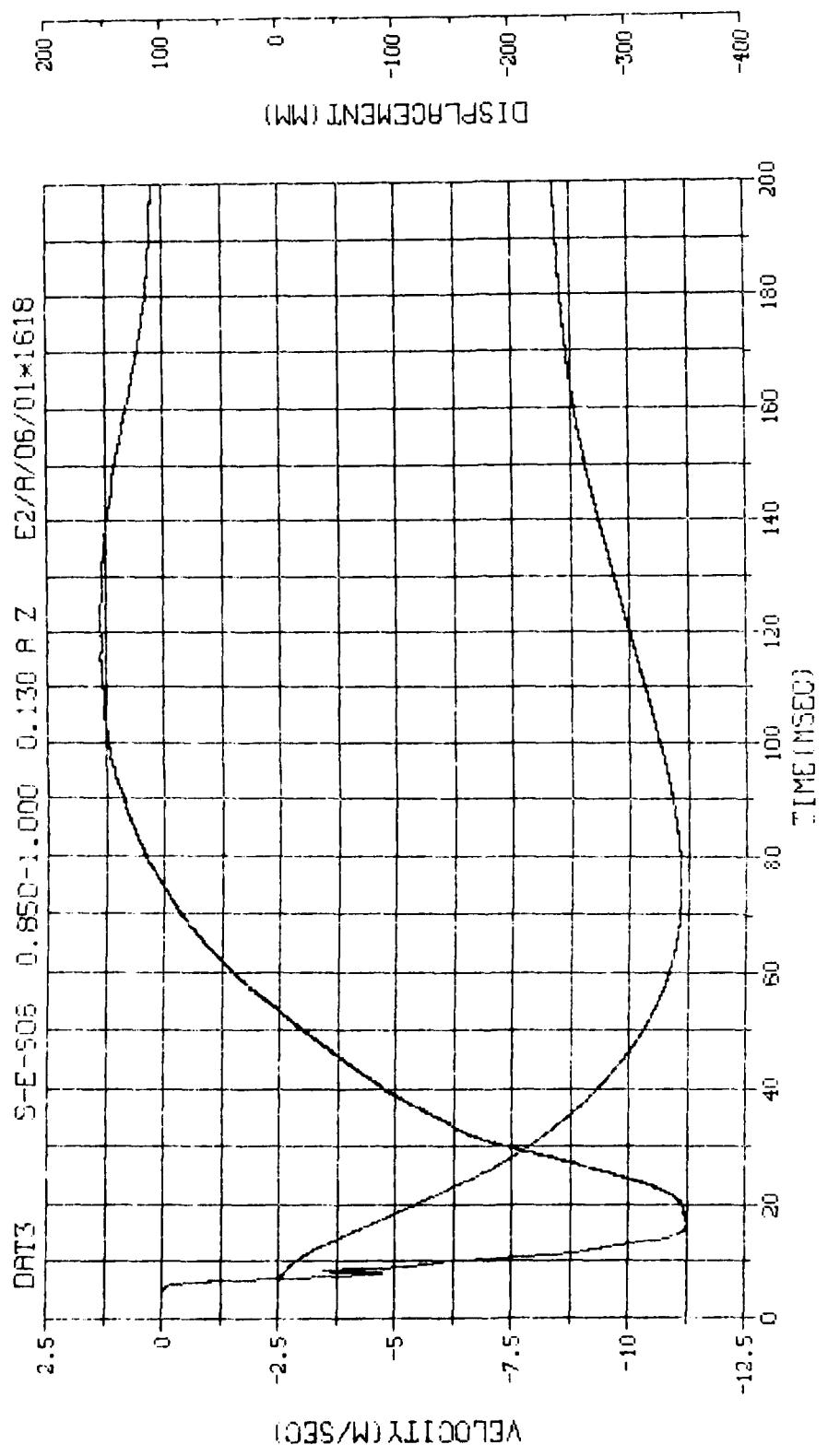
N.N. -91616	E.U. -0.000,1000.000	VSN-FB76
SKIP=7,000	DIGIT5=0,000,873.875	TAPE22
S.R. =25.00 KHZ	28JUN83 12:17:16	FILE=0
1)		



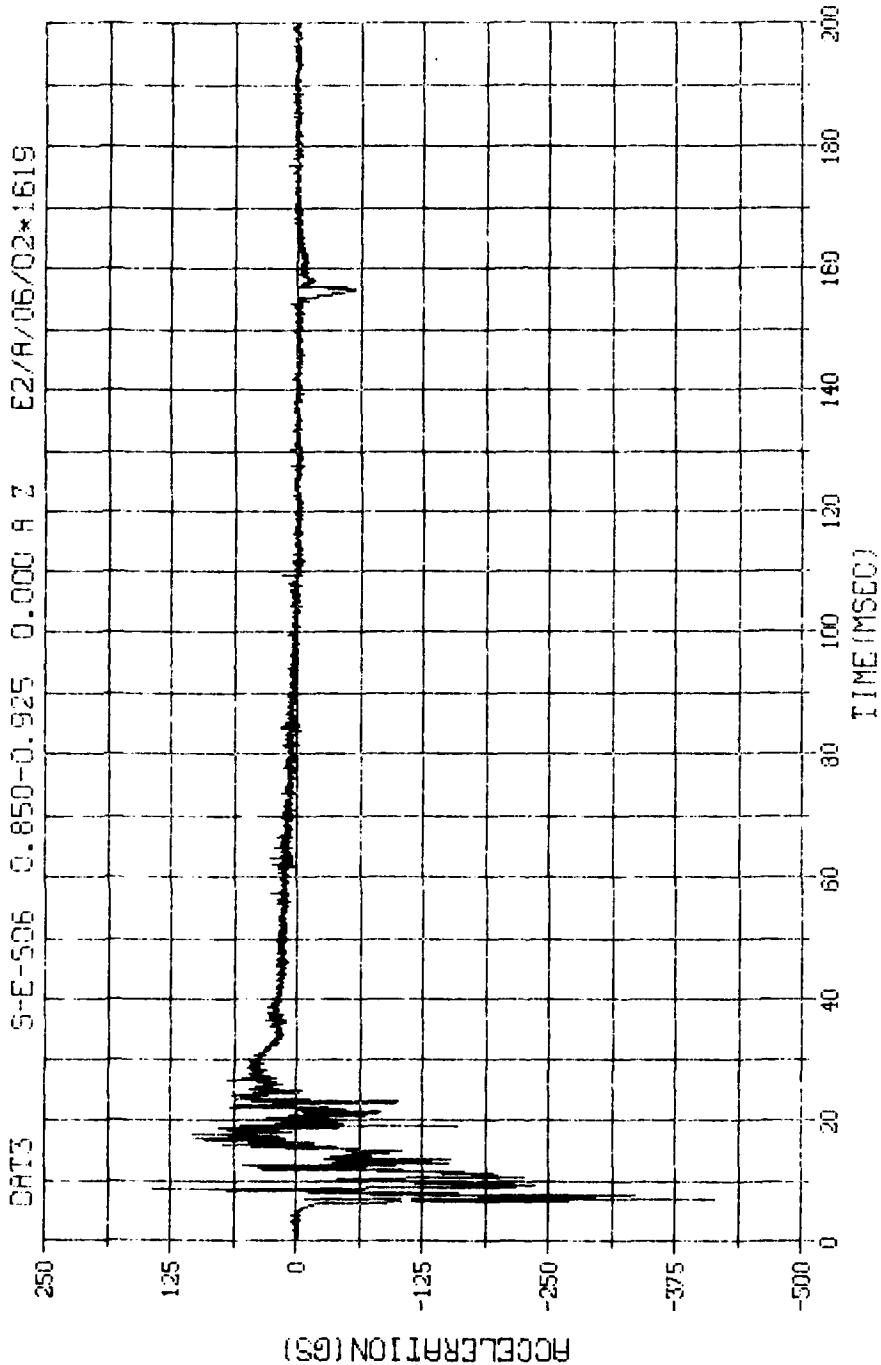
M. N.	-91616	E.U.	-0.000, 1000.000	VSN-FB76
SKIP	7.000	DIGITS	0.000, 873.875	TYPE22
S. R.	=25.00 KHZ		29JUN83 12:17:16	FILE=D
				2



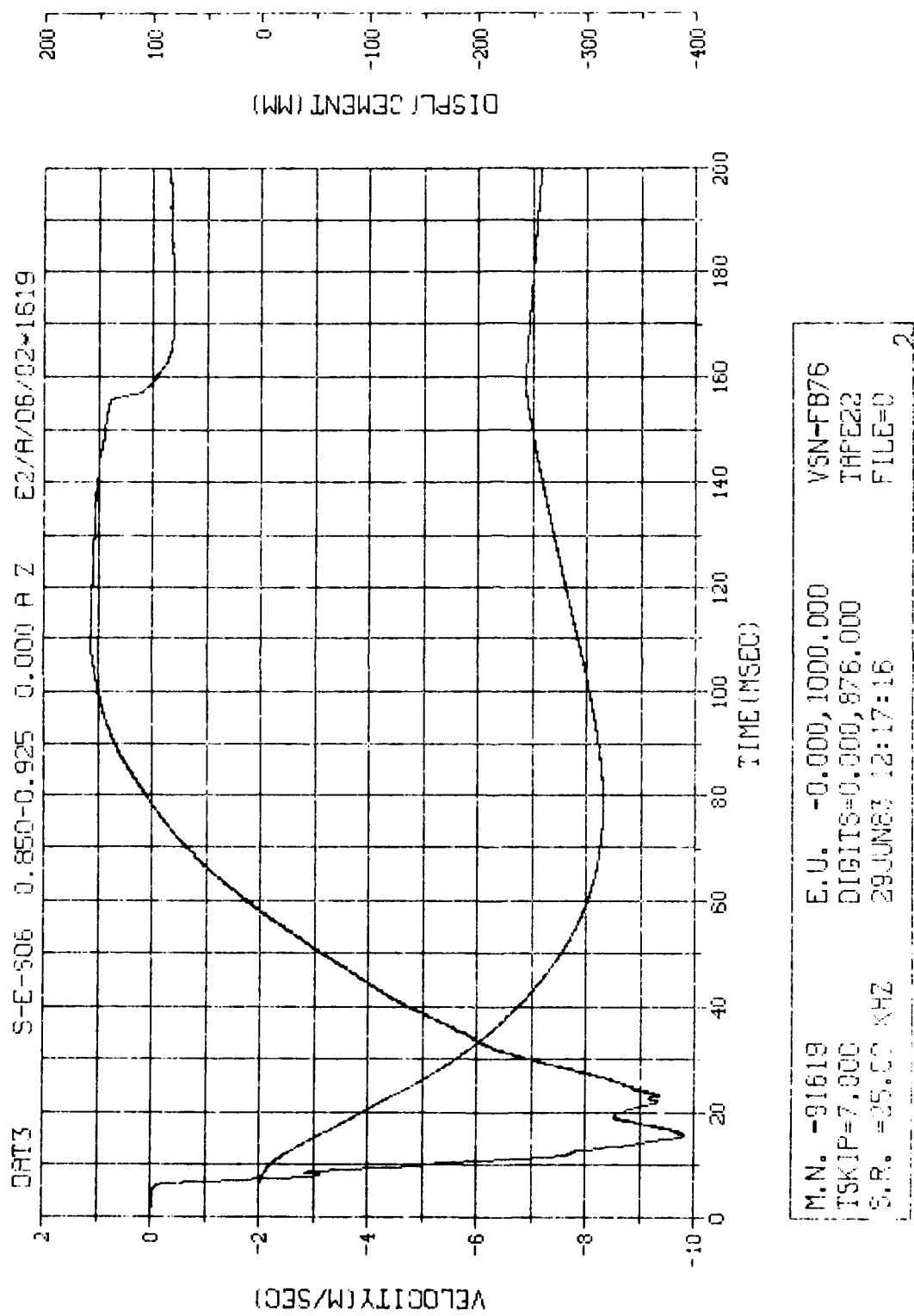
N.N. -91618	E.U. -0.000,1000.000	VSN-FB76
15KIP=7.000	DIGITS=0.000,891.000	TAPE22
S.R. =25.00 KHZ	29 JUN 83 12:17:16	FILE=0 1



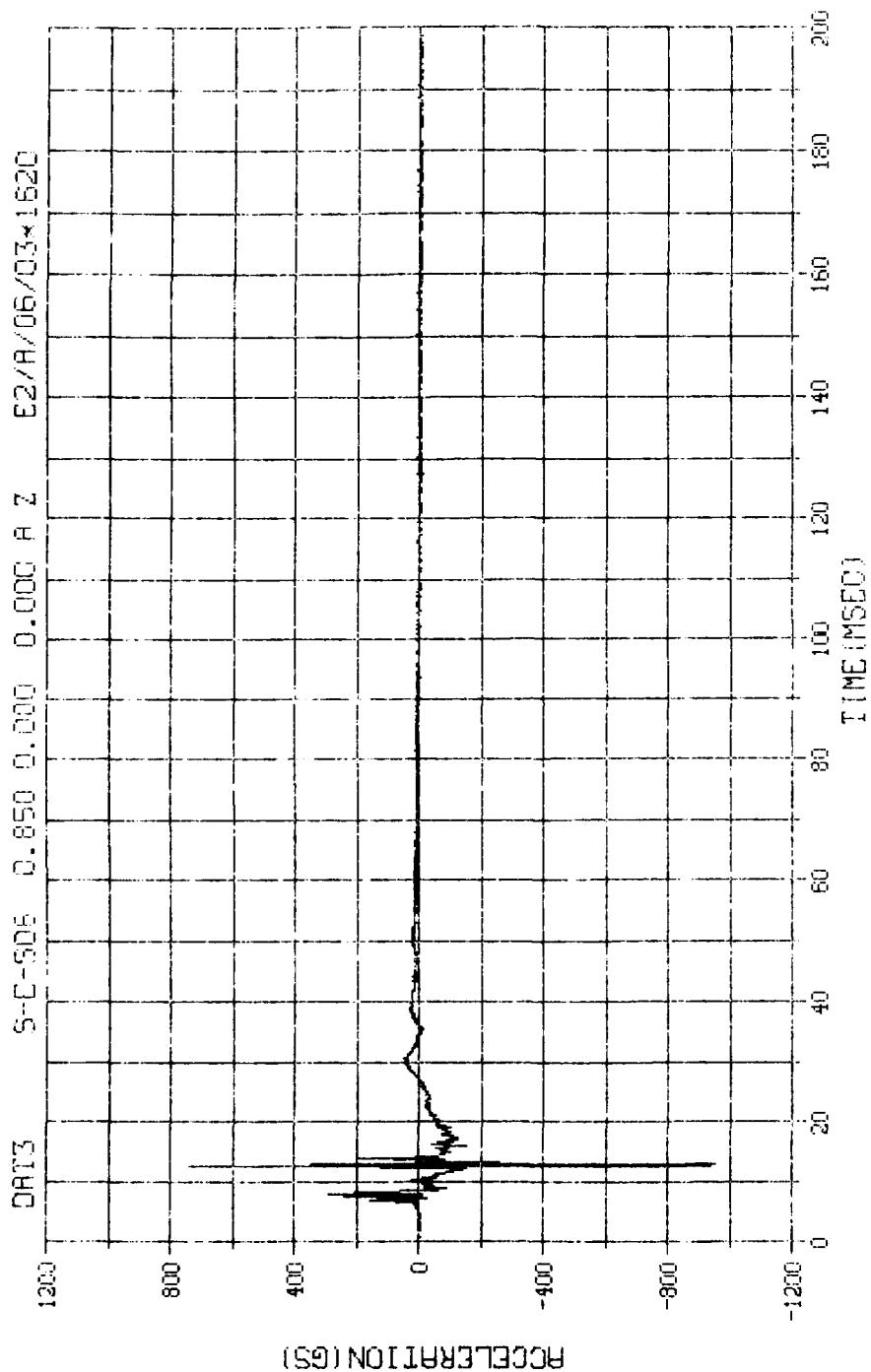
M.N.	-91618
TSKIP	=7.000
S.R.	=25.00 KHz
TYPE22	
FILE=0	2
WSN-FB76	
E.U.	-0.000,1000,000
DIGITS	=0,000,99,000
284MHz	,23:17:16



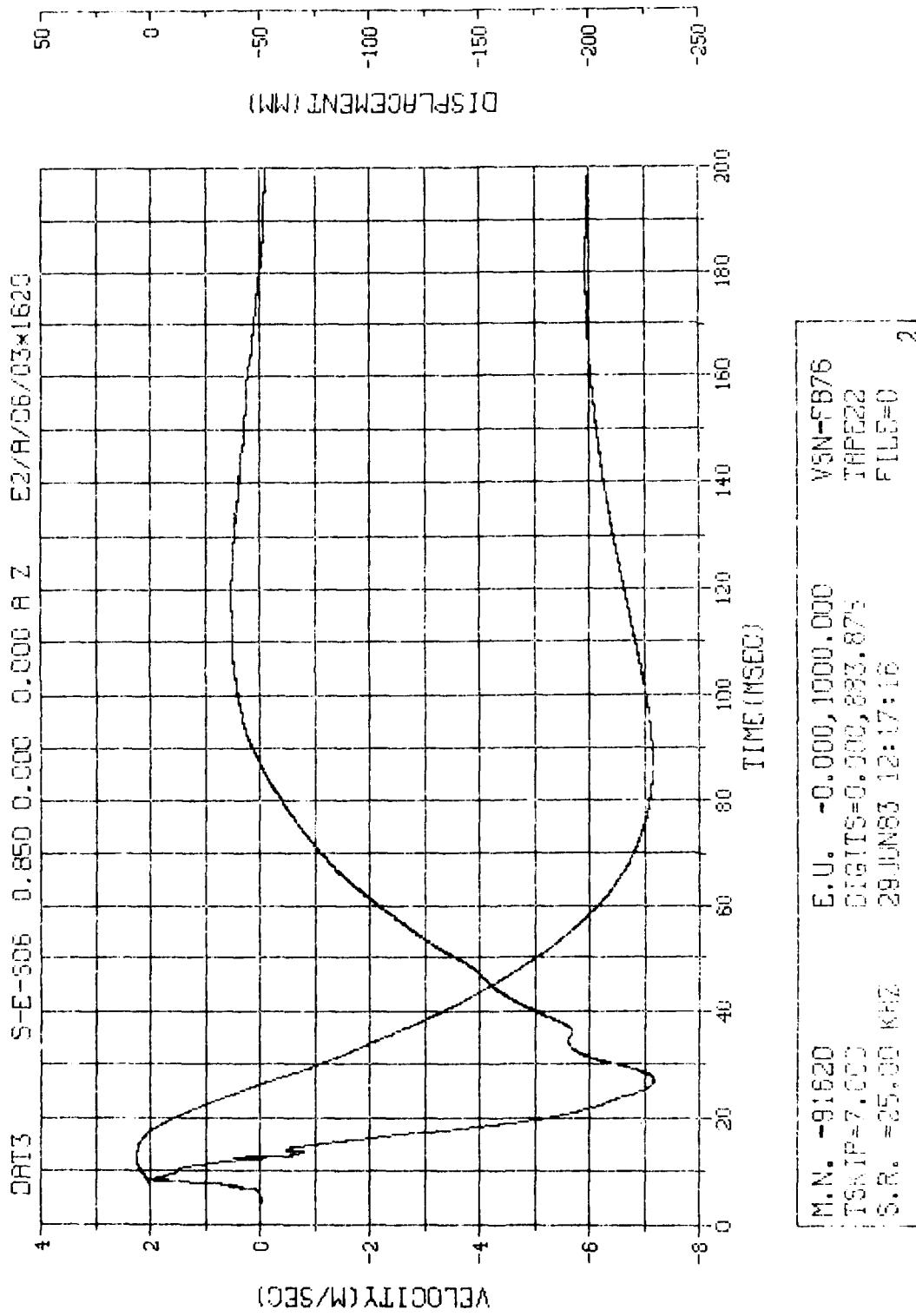
M.N.	-91619	E.U.	-0.000, 1000.000	VSN-FB76
SKIP	=7.000	DISITS	=0, 300, 876.000	TAPE22
S.R.	=25.00	KHZ	29 JUN 83 12:17:16	FILE=J 1

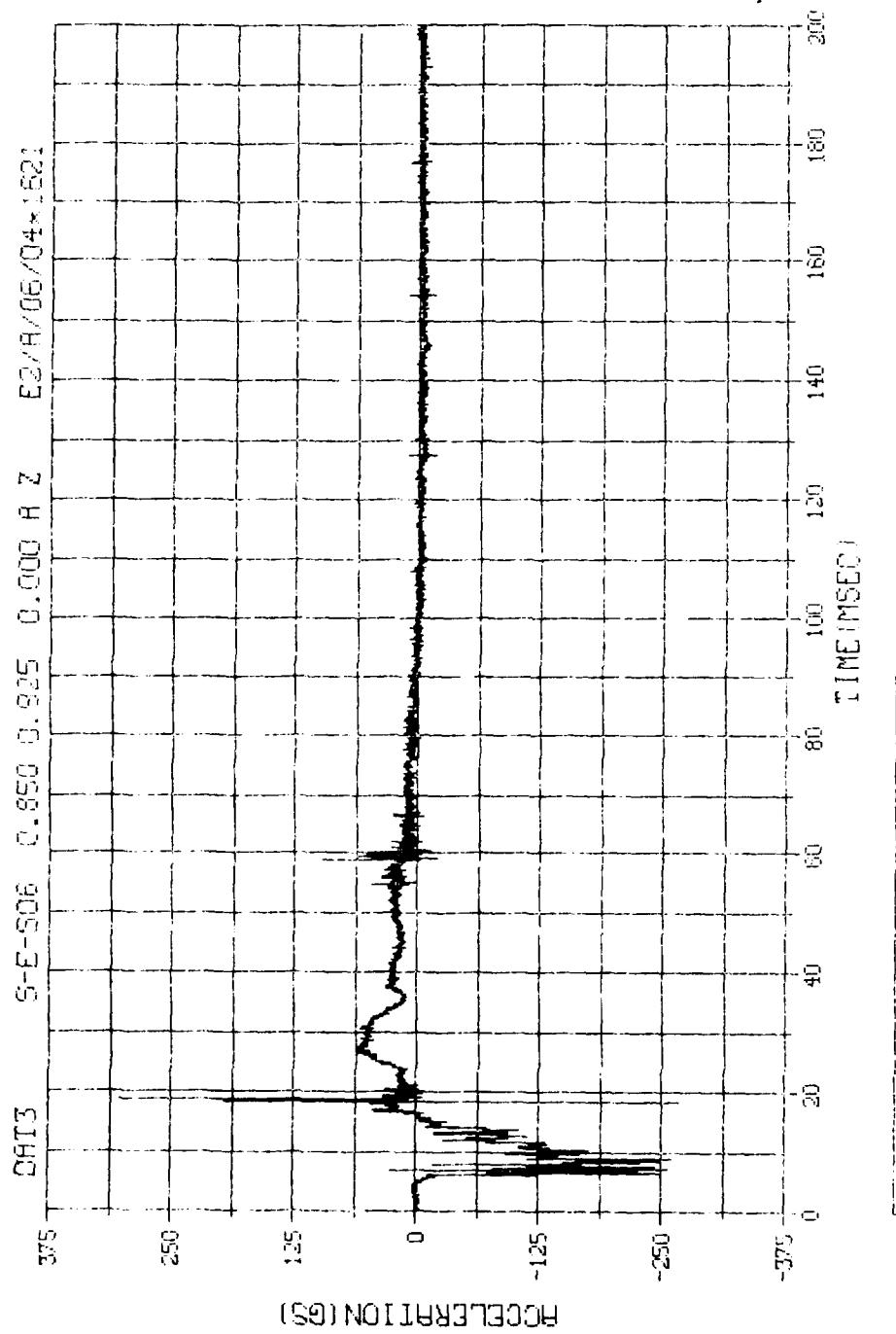


M.N. -91619	E.U. -0.000,1000.000	VSN-FB76
TSKIP=7,000	DIGITS=0,000,876.000	THF22
S.R. =25.52 KHz	29JUN87 12:17:15	FILE=0
2		

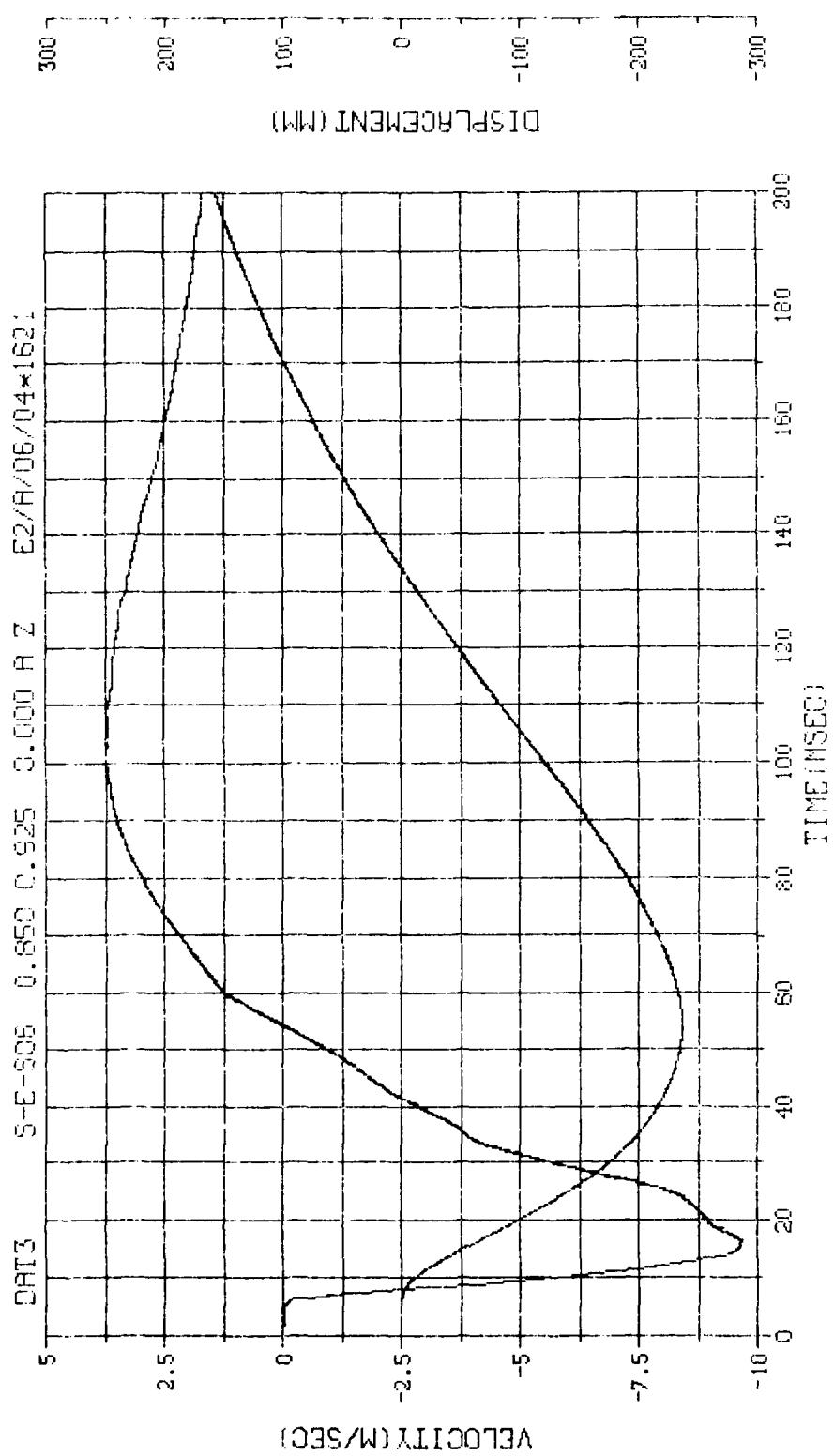


R.N. -91620	E.U. -9,000,1000,000	WSN-FB76
TSKIP=7.000	DIGITS=3,300,983,875	TAPE22
S.R. =25.00 kHz	29 JUNE 13 12:17:16	FILE=0
		1

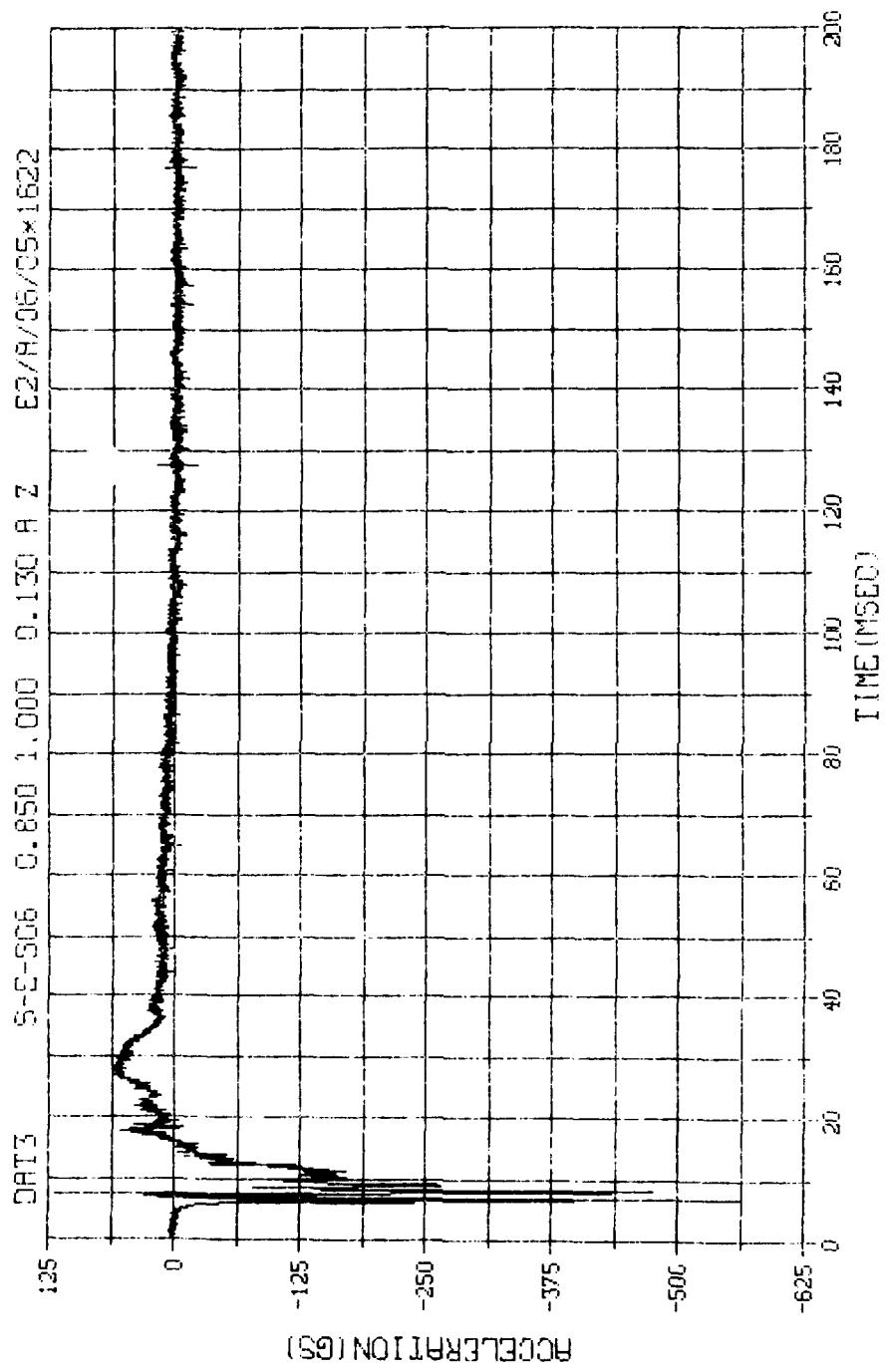




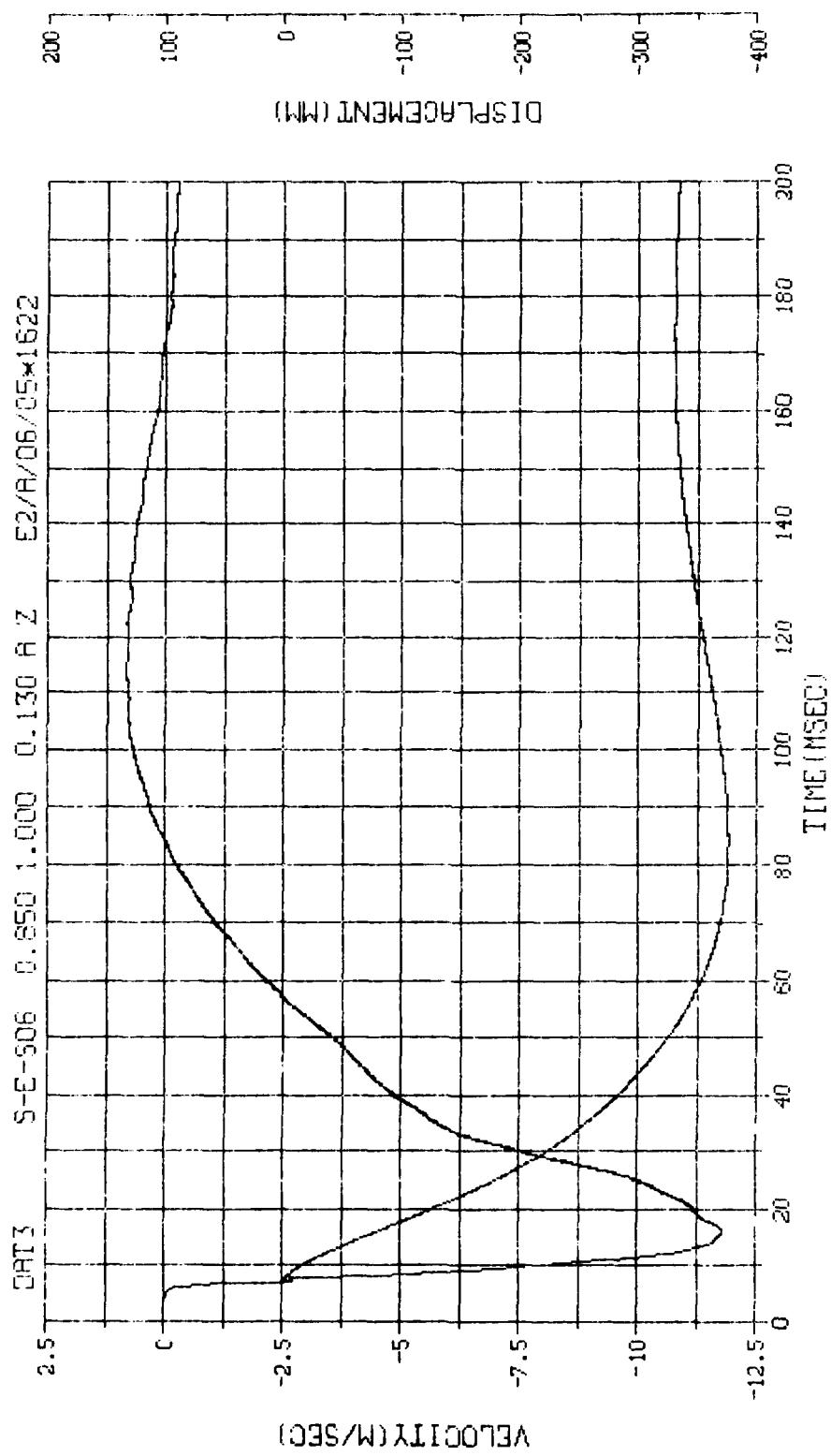
414



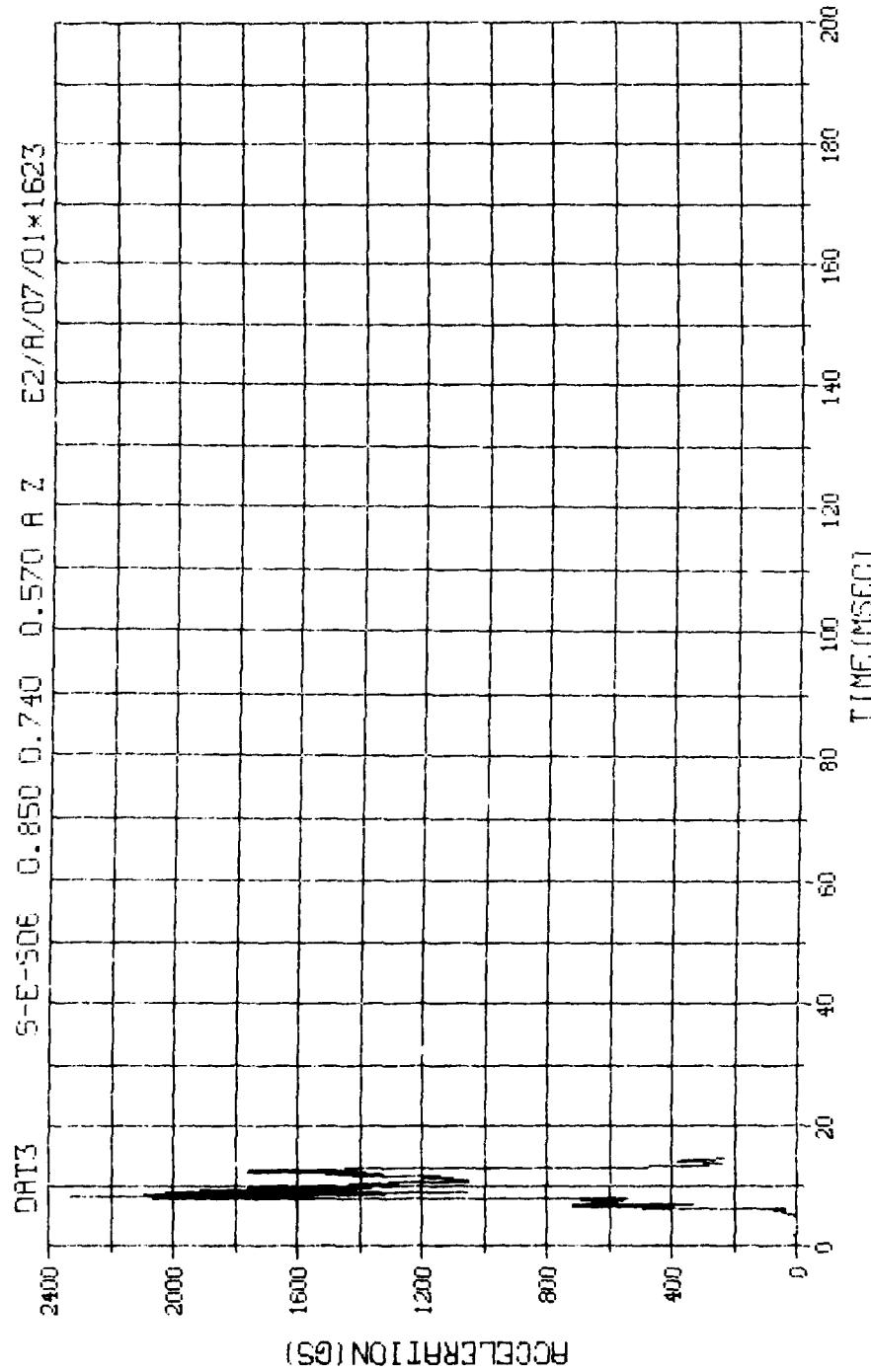
M.N. = -91621	E.I. = 0.000, 1000.000	VSN-FB76
TSKIP=7,000	BINITS=9.000, 37.4, 265	THSE22
S.R. = 25.30 kHz	28 JUN 87 12:17:16	TRUE=0
		2



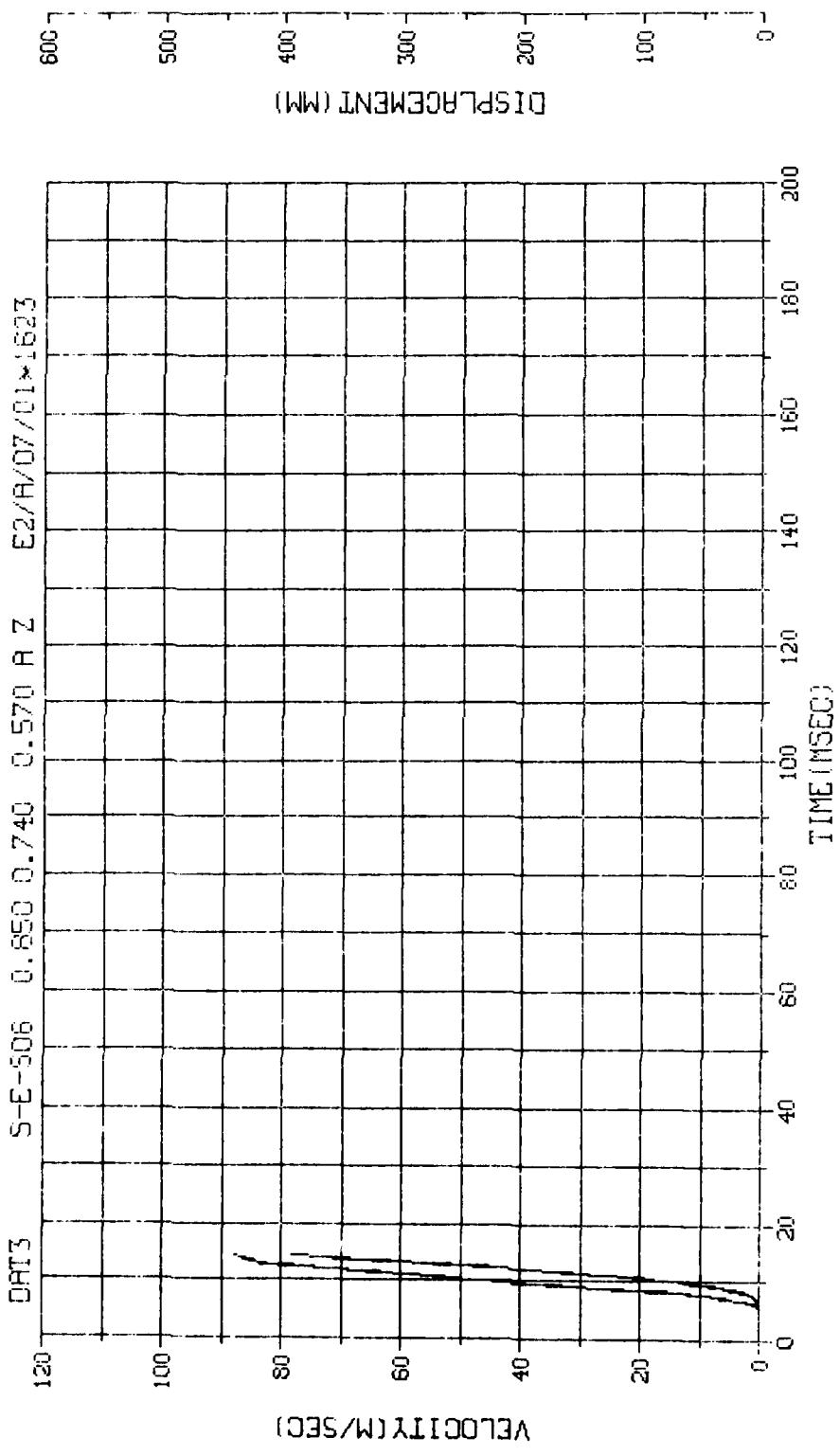
M.N. -91622	E.U. -0.000,1000.000	VSN-FB76
T5K, P=7.000	STARTS=0.000,901.000	TRPE22
S.R. = 25, 36 kHz	28.0083 12:17:16	FILE=0
		1



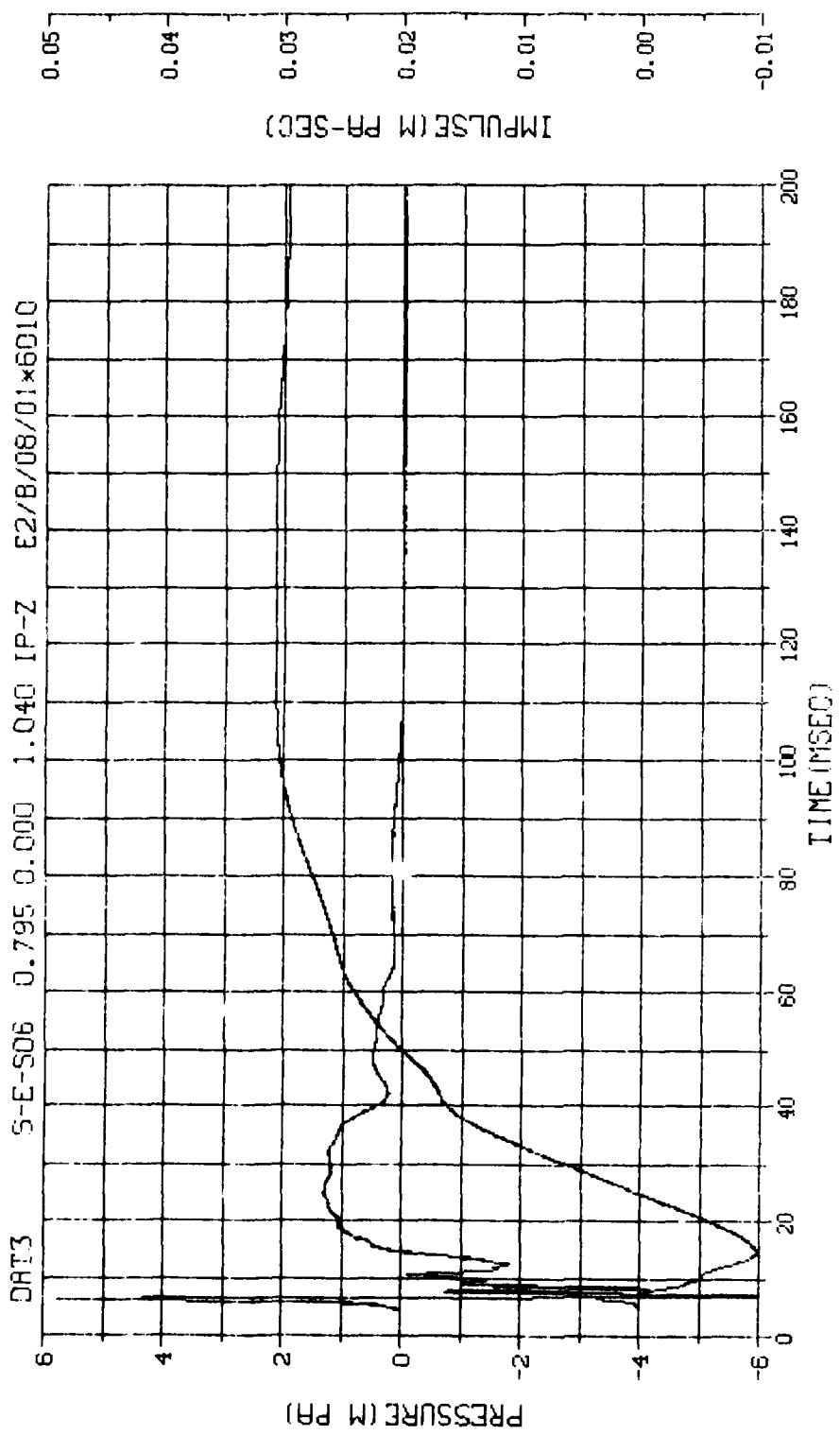
M.N. = 91622	E.U. = 0.000, 1000.000	VSN-FB76
TSKIP=7.000	DIGITS=0.000, 901.000	TRP22
S.R. = 25.00 KHZ	29-JUN-93 12:17:16	FILE=0
		2



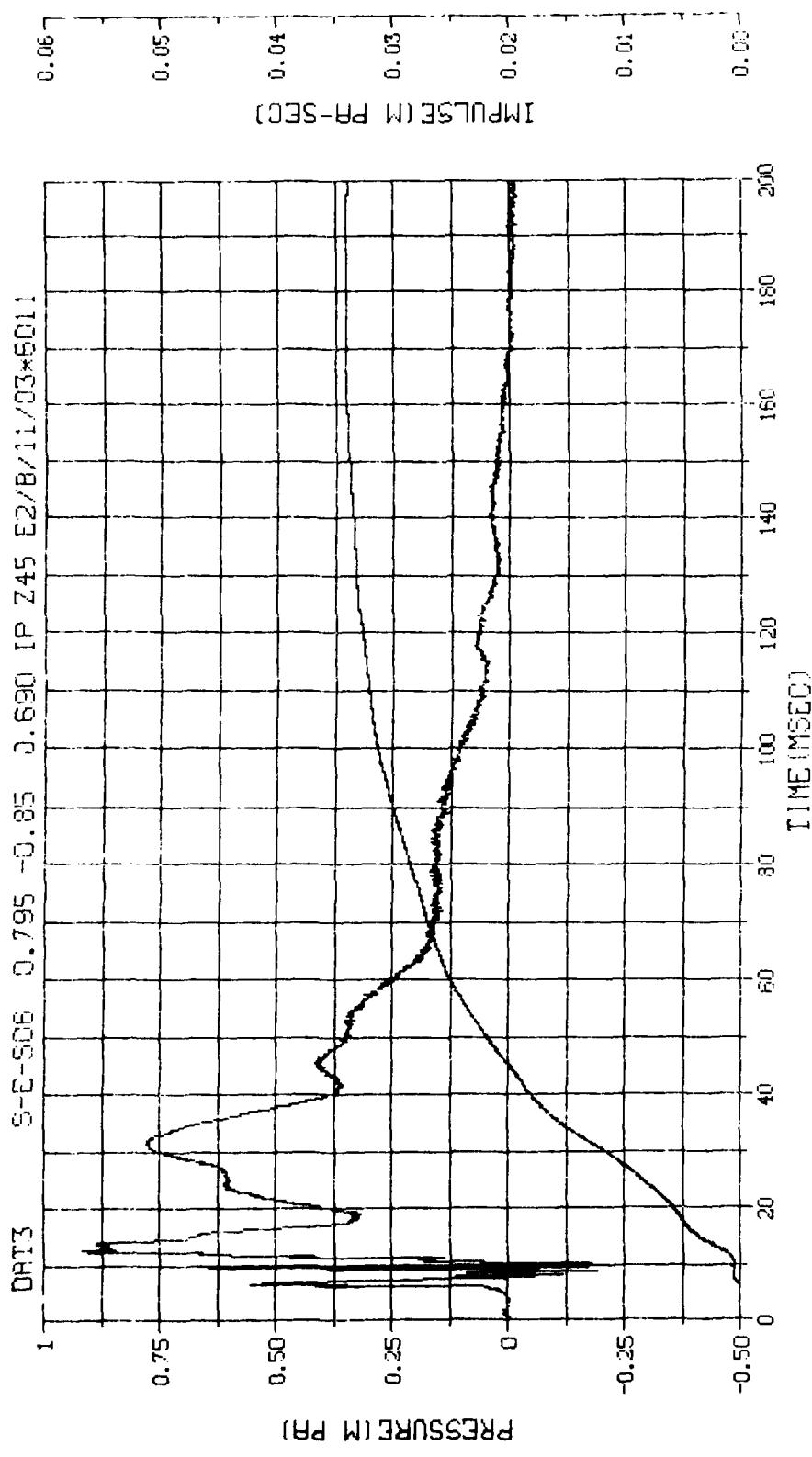
M. N. -71623	E.U. -0.000,1000.000	VSN-FB75
TSKIP=7.000	DIGITS=0.000,891.875	TAPE22
S.R. =25.00 kHz	29 JUN 85 12:17:16	FILE=0



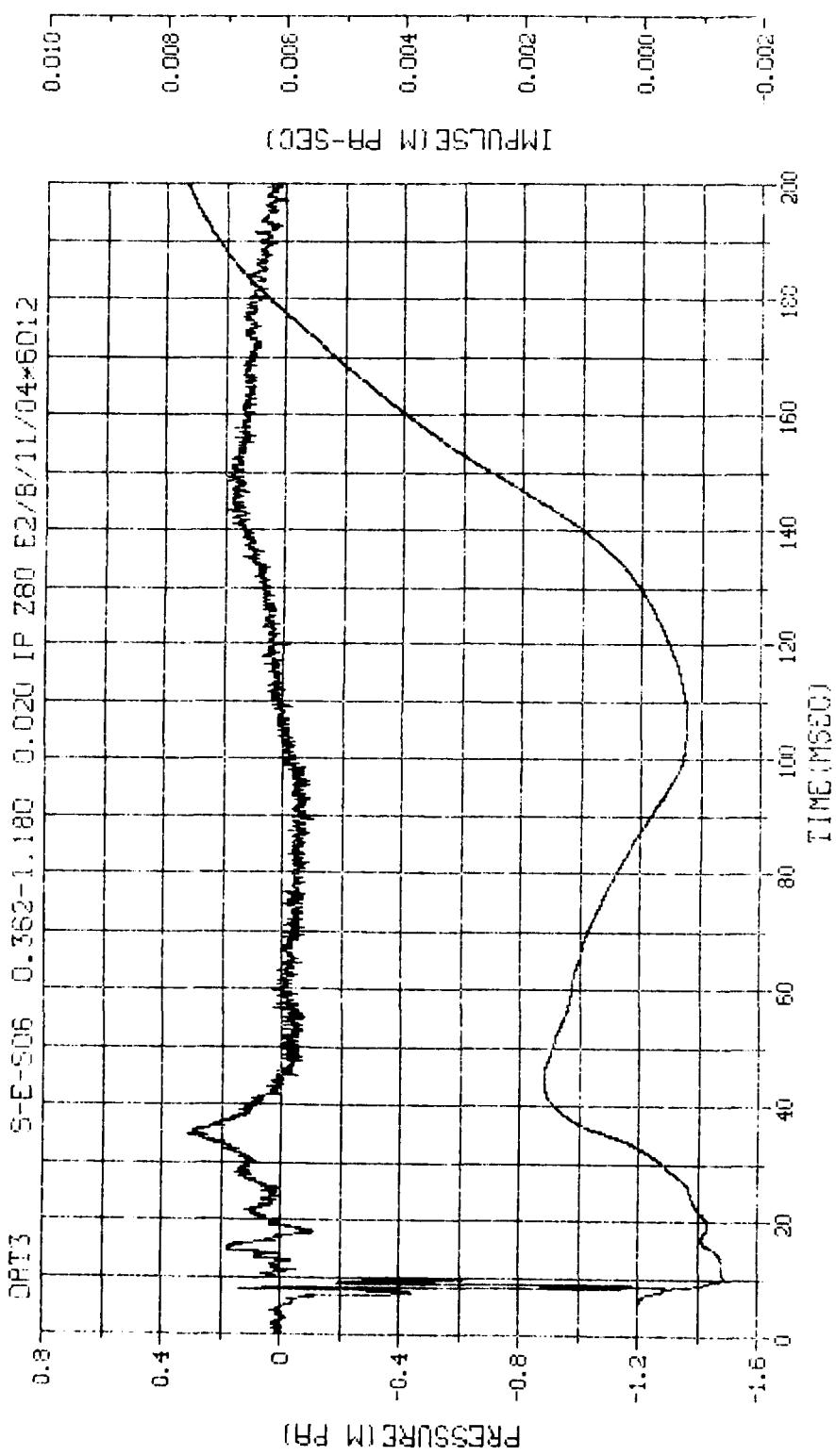
M.N. -71623	E.U. -0.000, 1000.000
SKIP=7,050	DIGITS=0,000,891,875
S.R. =25.00 kHz	29.0585 12:17:16
	VSN-F676
	TAPE22
	FILE=0



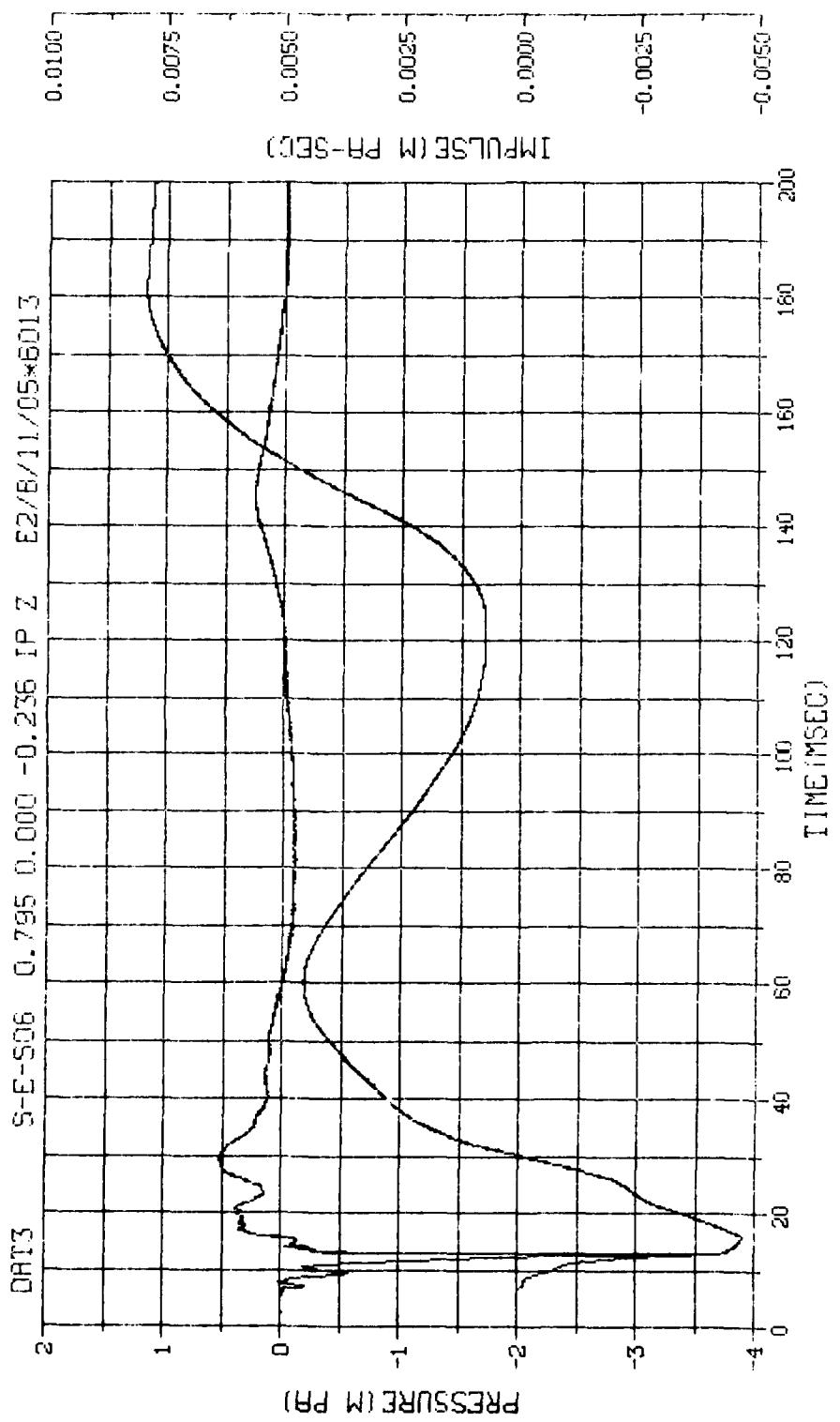
M.N. -96010	E.U. -0.000, 2.500	VSN-FB76
SKIP=7.000	DIGITS=0.000, -870.000	TRPE22
S.S. =10.00 KHZ	29 JUN 83 12:17:16	FILE=0



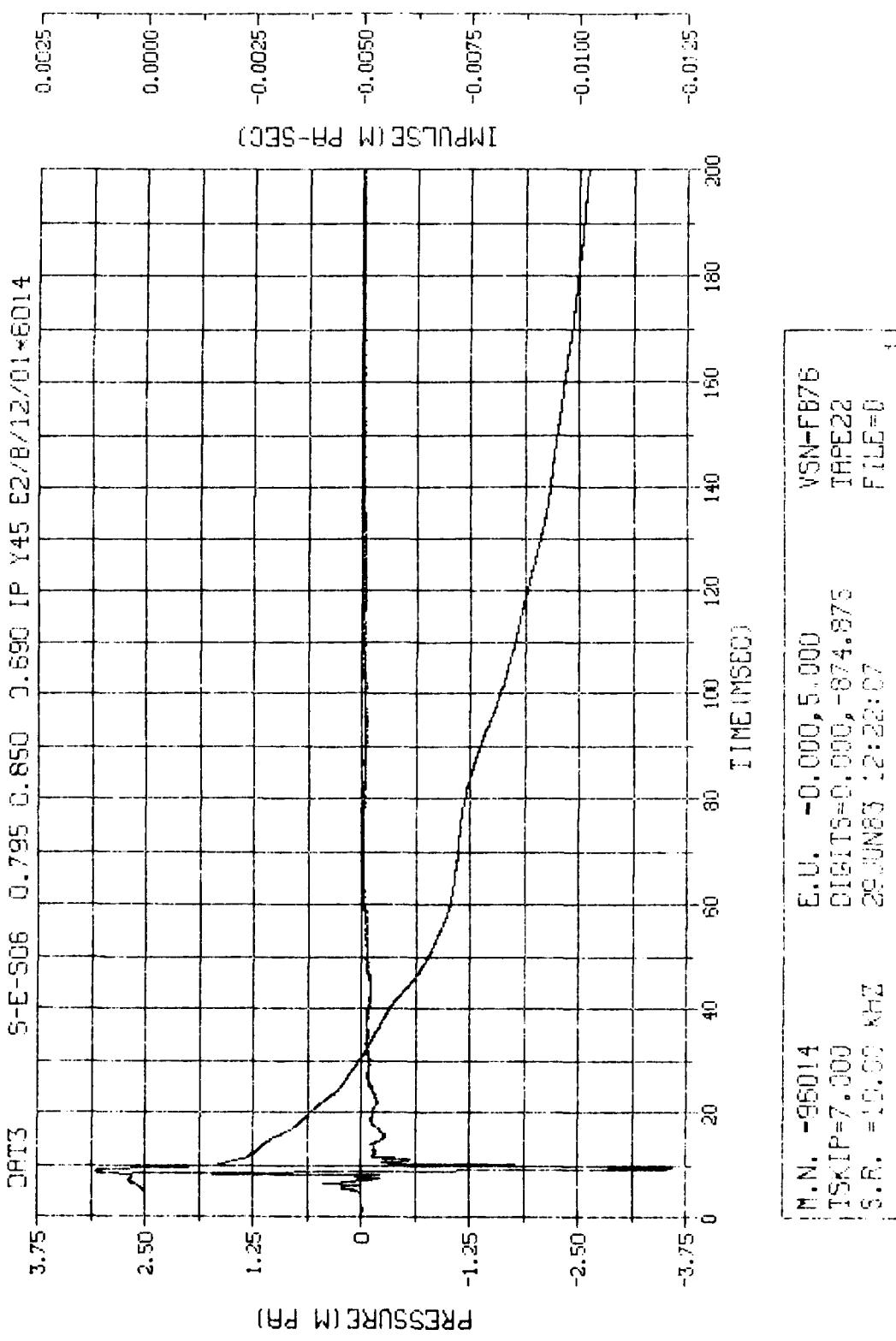
N.N. -96011	E.U. -0.000, 2.500	VSN-FB75
ISKIP=7.000	DIGITS=0.000, -860.625	TAPE22
S.R. =10.00 KHZ	29 JUNE 3 12:17:16	FILE=0
		1

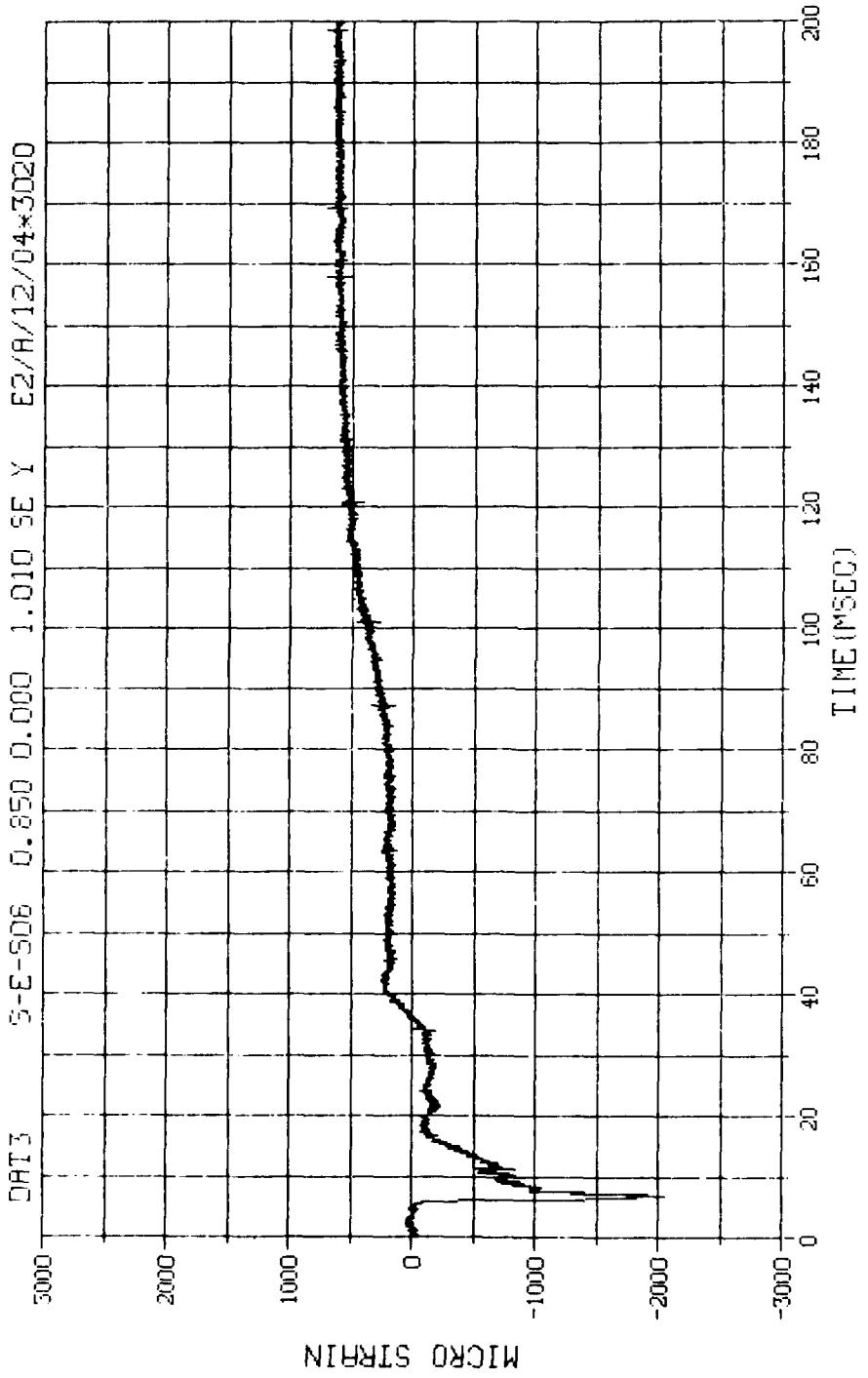


M.N. = 6012	E.U. = 0.000, 10.000	VSN-FB76
TSKIP=7.000	DIGITS=0.300, -853.000	TRFE22
S.S. = 10.00 KHz	29 JUN 83 12:17:15	FLUE=0
		[1]

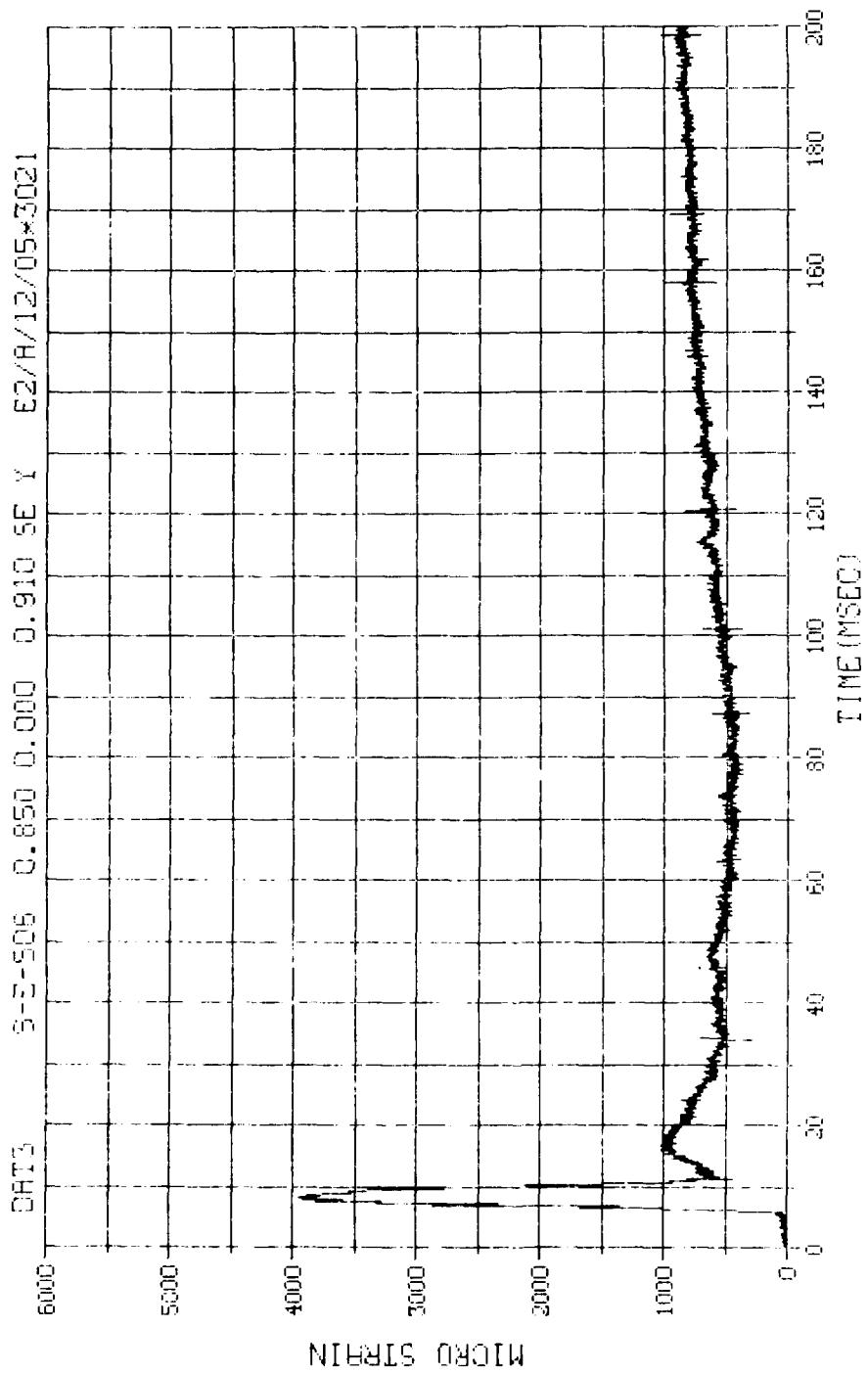


N.N. = 6013	E.U. = 0.000, 2.500	VSN-F876
SKIP=7.000	DIGITS=0.000, -885.250	TAPE22
S.R. = 10.00 KHZ	29 JUN 83 12:17:16	FILE=0
		1]

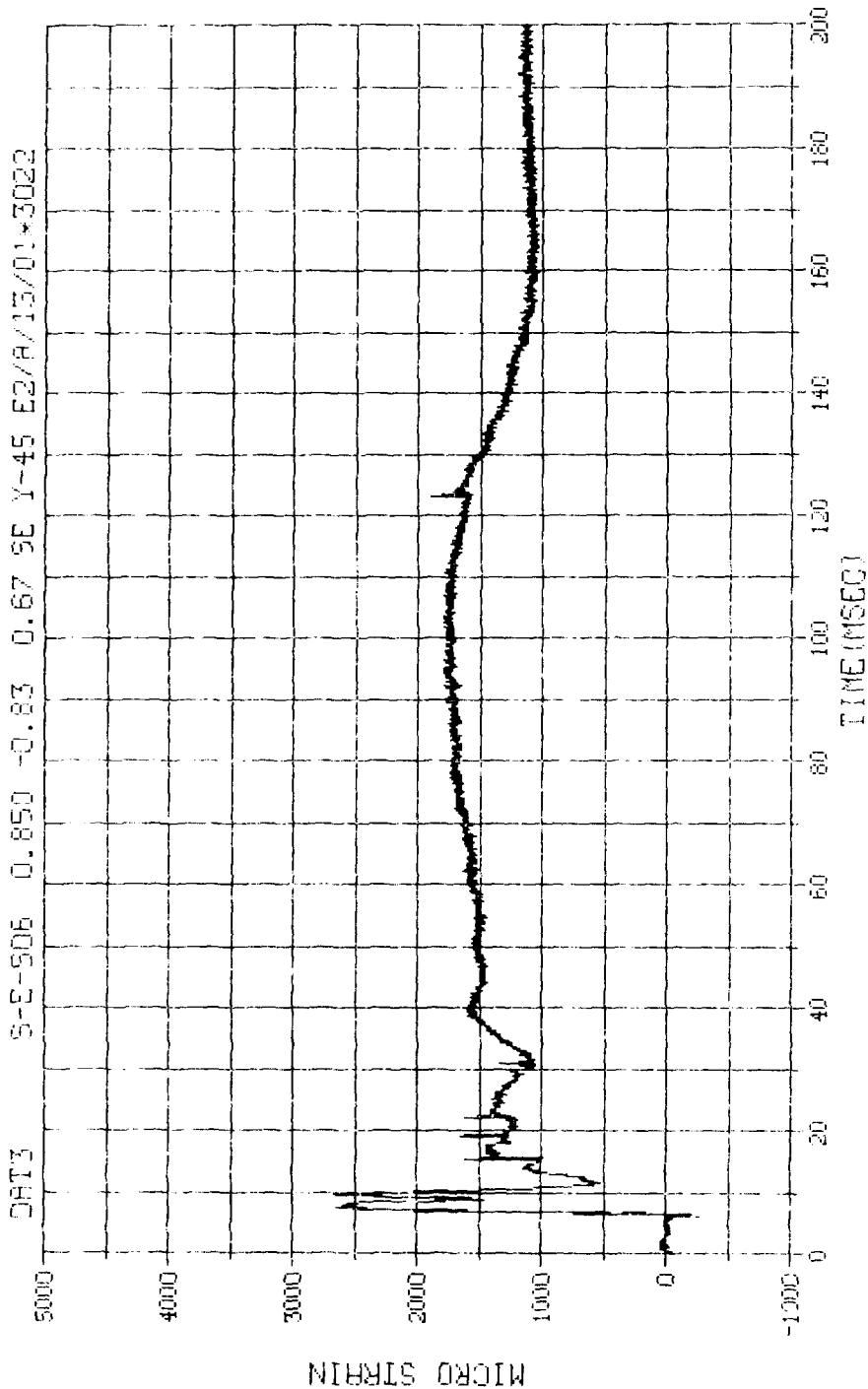




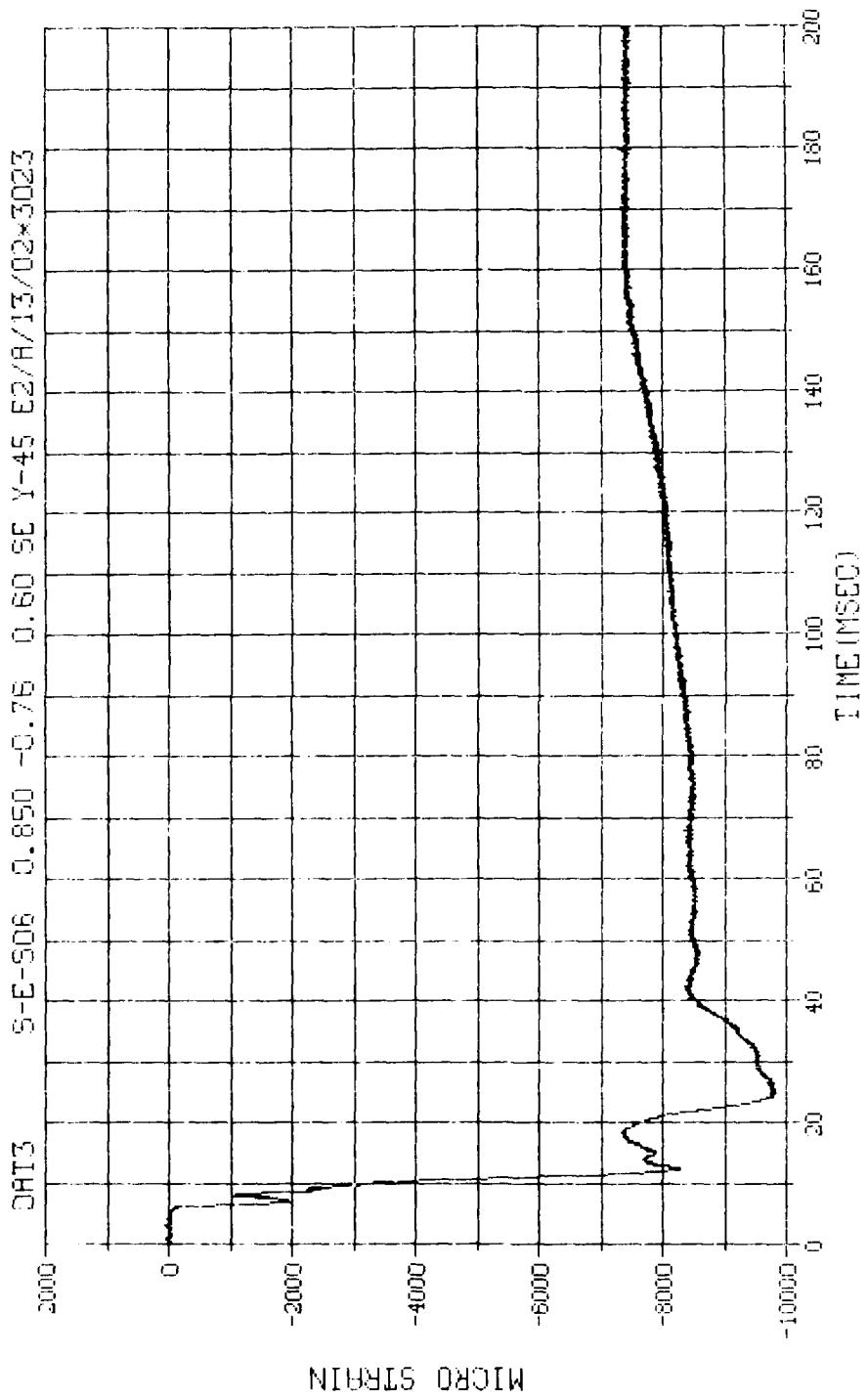
M.N. - 3020	E.U. -0.000, 7500.000	VSN-60142
TSKIP=7.000	DIGITS=0.000, 867.000	TAPE22
S.R. =25.00 KHZ	4. 4 PM, TUE, 13 SEP 83.	FILE=182 1



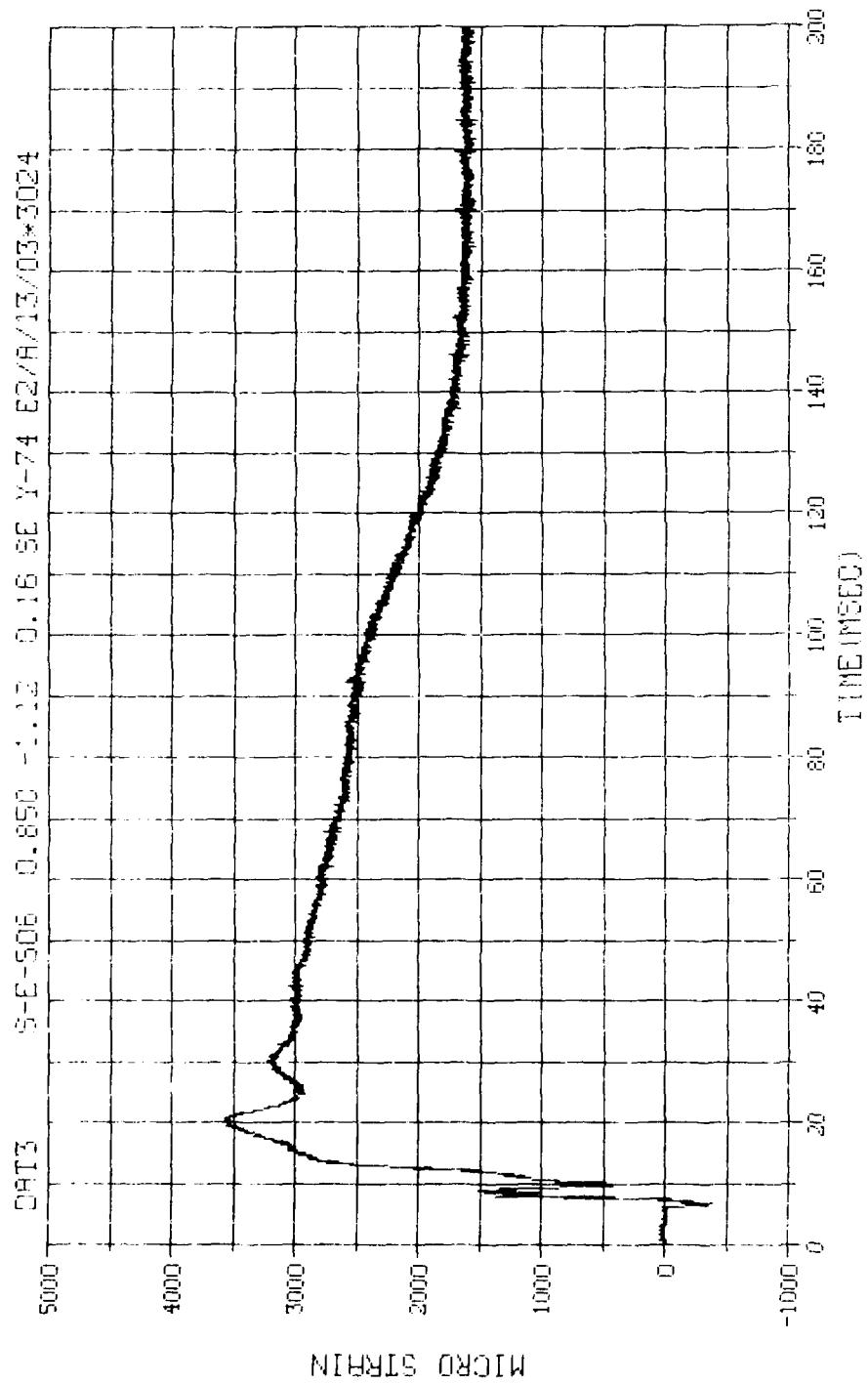
N. N. = 3021	E.U. = 0.000, 10000.000	VSN=60142
T5Y 1P=7.000	DIGITS=0.000, 895.000	TAPE22
S.R. = 25.00 kHz	4. 4 PM, TUE, 13 SEP 97,	FILE=184_1



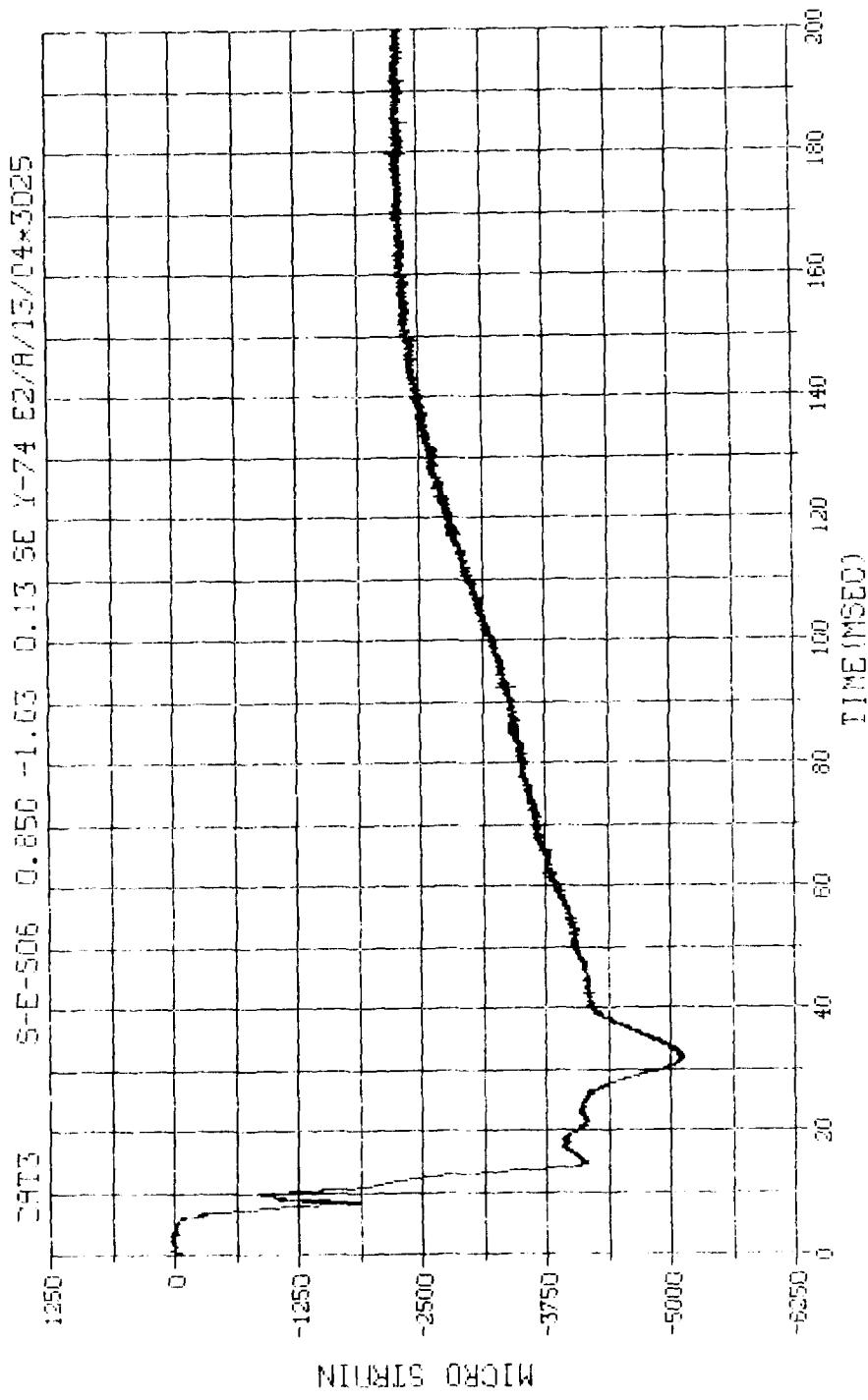
N. N. = 3022	E.U. = 0.000, 10000.000	VSN-00142
SKIP=7.000	DIGIT5=0,000,001,250	TAPE22
S.R. =25.00 KHZ	4. 4 PM, TUE, 13 SEP 83.	FILE=186



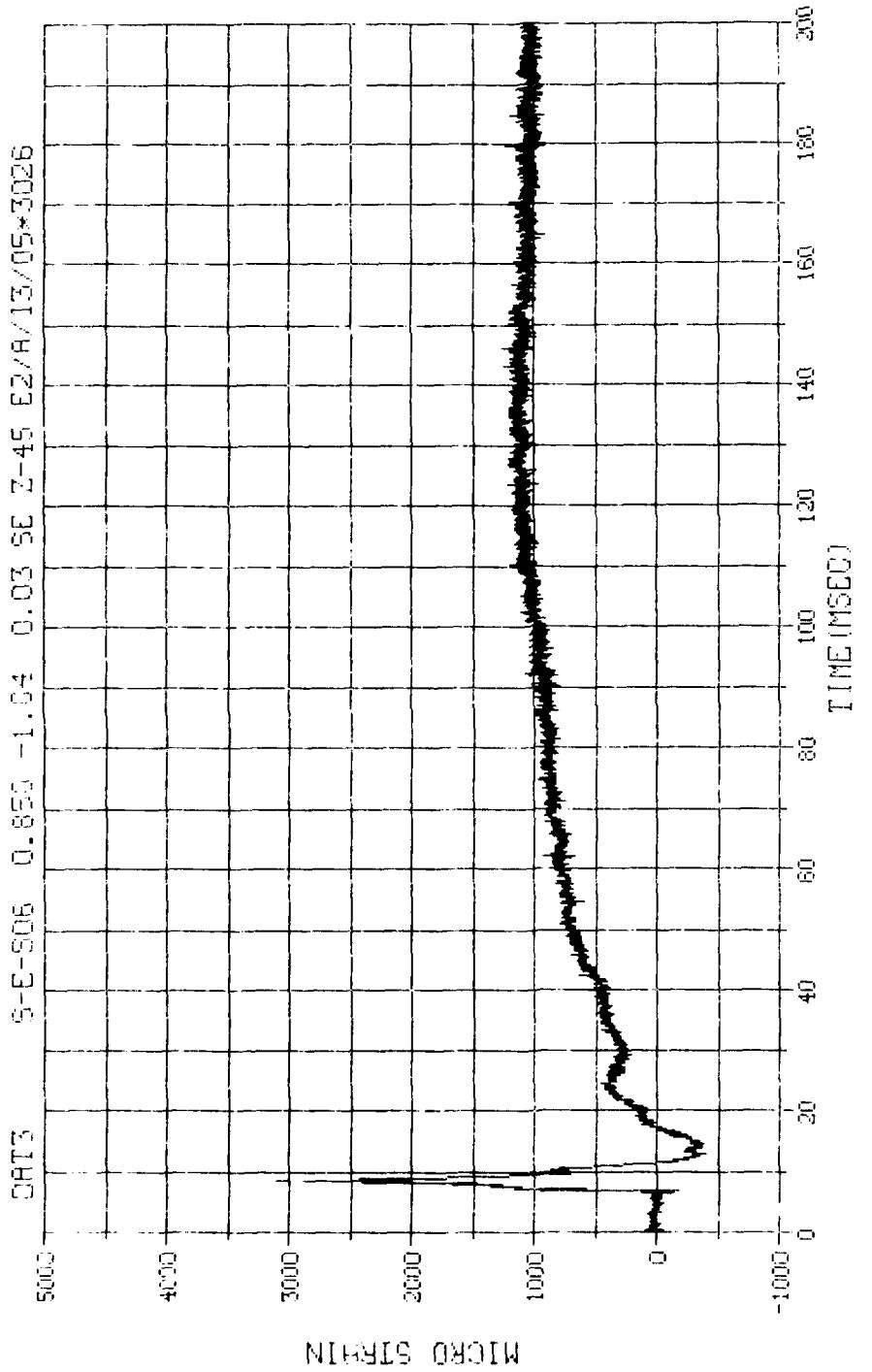
N.N. - 3023	E.U. -0.000,10000.000	VSN-66142
TSKIP=7.000	DIGITS=0.000,873.875	TAPE22
S.R. =25.00 KHZ	4. 4 PM, TUE, 13 SEP 83,	FILE=188 1



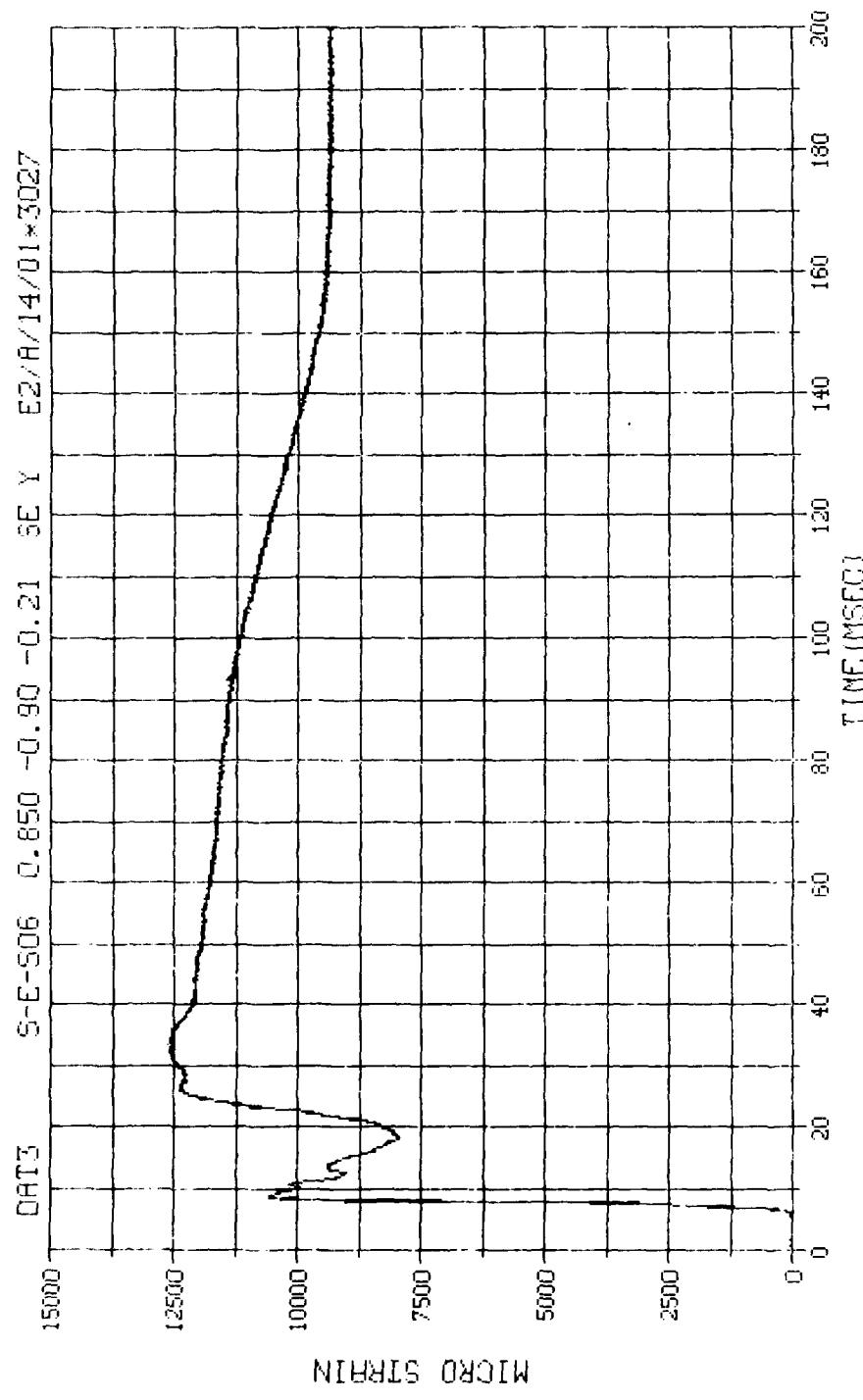
H.N. = 3024	E.U. = 0.000, 7500.000	VSN=66142
T5KIP=7.000	DIGIT5=0.000, 873, 625	TRFE22
S.R. = 25.00 kHz	4, 4 PM, TUE, 13 SEP 93	FILE=190_1



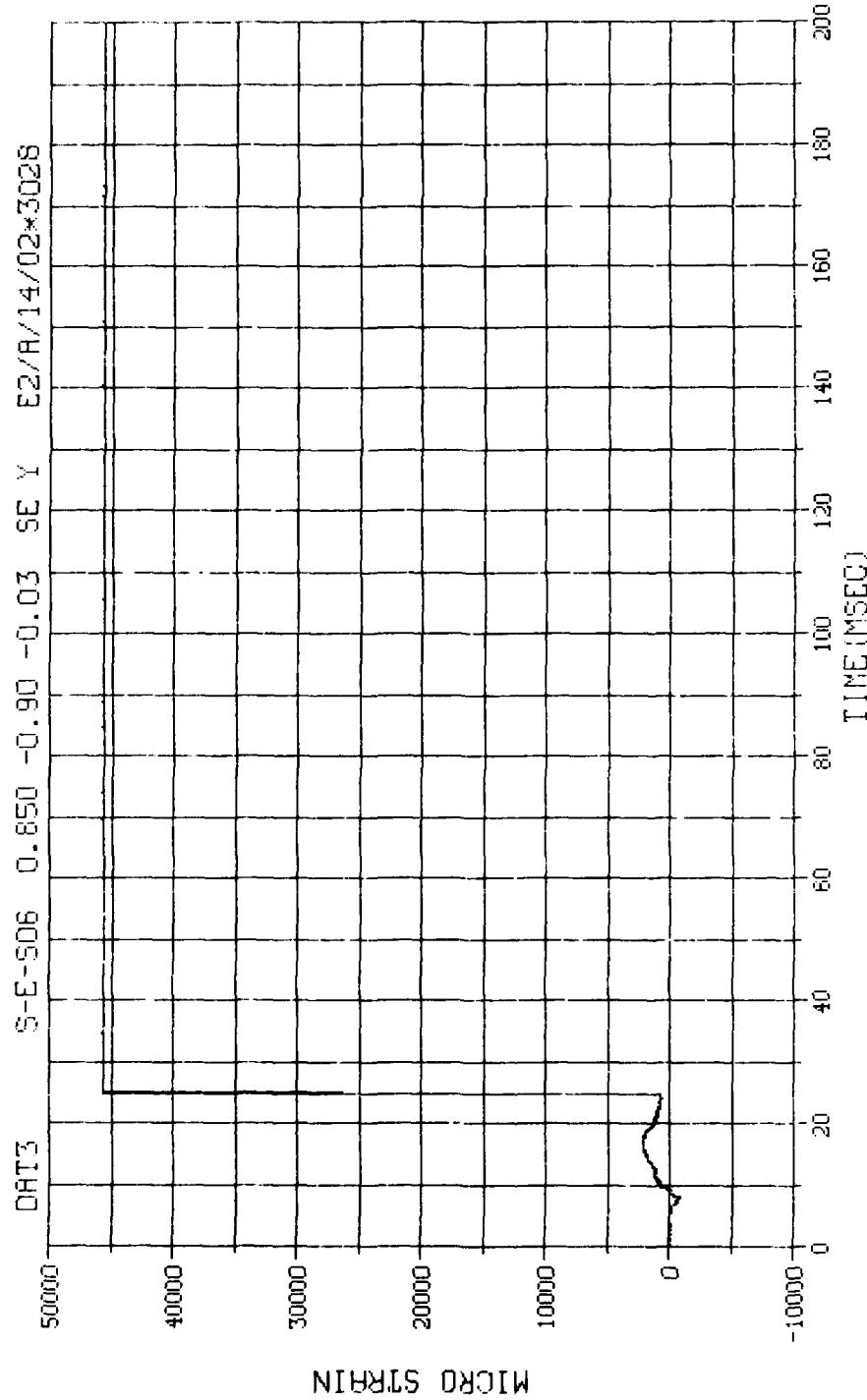
Y.M. = 3025	E.U. = 0.000, 7500.000	VSN-66142
75.1PF=7.000	DIGITS=0.000, 864.500	TAPE22
5.9. = 25.00 KHZ	4.4 PM, TUE, 13 SEP 83,	FILE=192 1



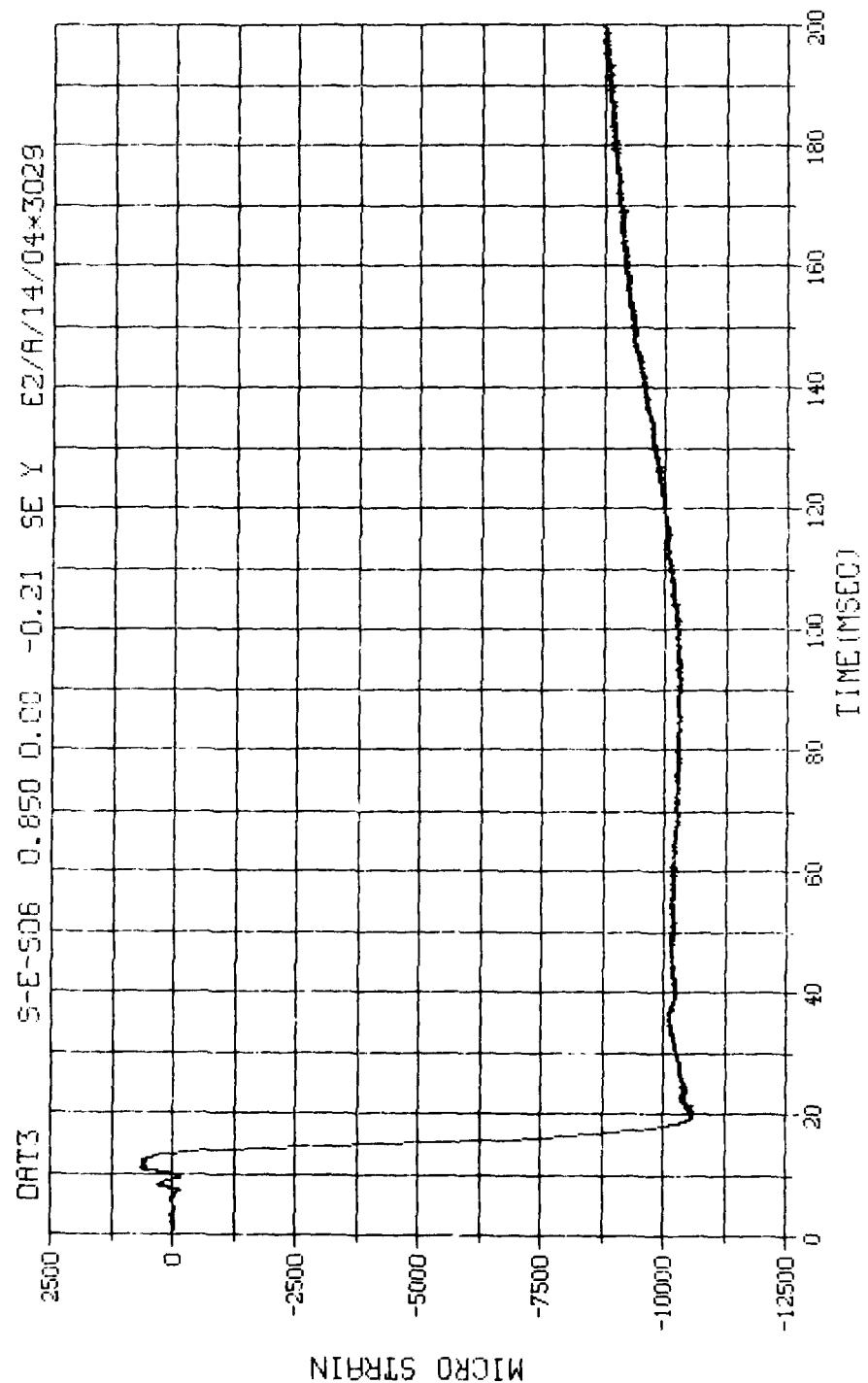
M.N. = 3026	E.U. = 0,000,10000,000	VSN=66142
SKIP=7.000	DIGITS=0,000,893,125	TAPE22
S.R. =25.00 KHZ	4. 4 PH, TUE, 13 SEP 83,	FILE=194



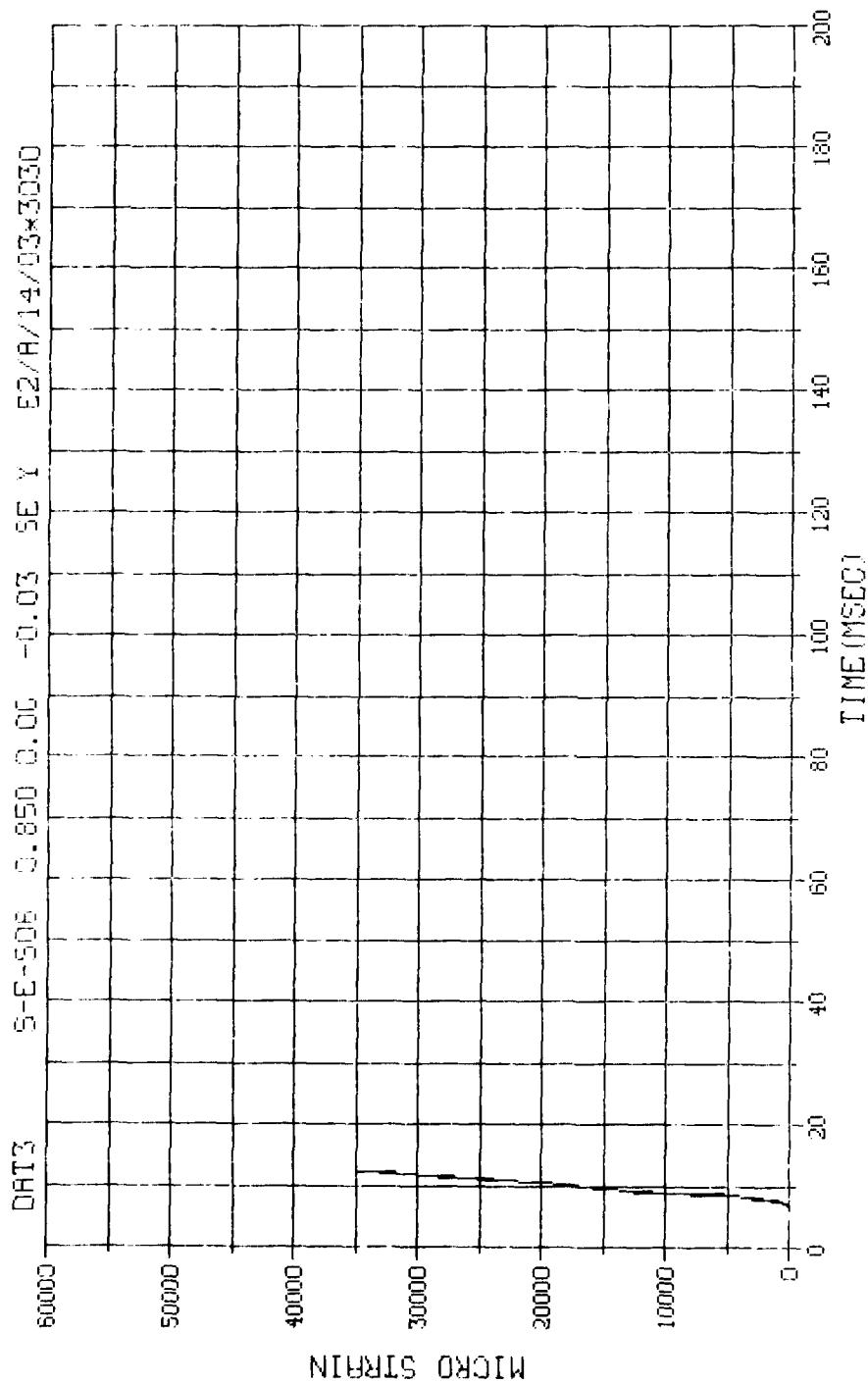
M.N. = 3027	E.U. = 0.000, 10000.000	VSN=00142
TSK1FP=7.000	DIGIT5=0.000, 885.000	TAPE22
S.R. = 25.00 KHZ	4. 4 PM, TUE, 13 SEP 83.	FILE=196



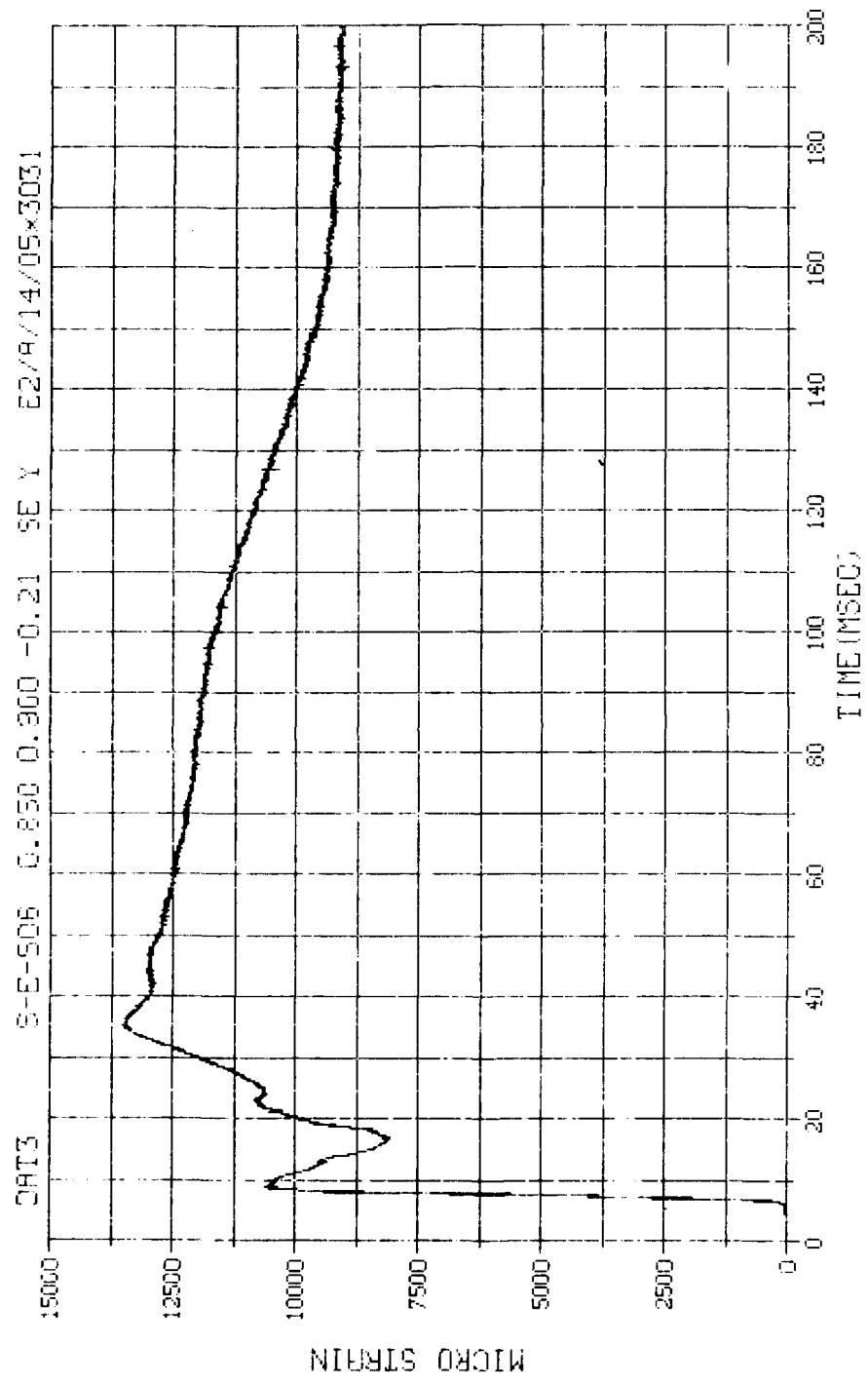
M.N. = 3028	E.U. = 0.000, 19900.000	VSN=06142
TSKIP=7.000	DIGITS=0.000, 875.250	TAPE22
S.R. =25.00 KHZ	4. 4 PM, TUE, 13 SEP 83.	FILE=198



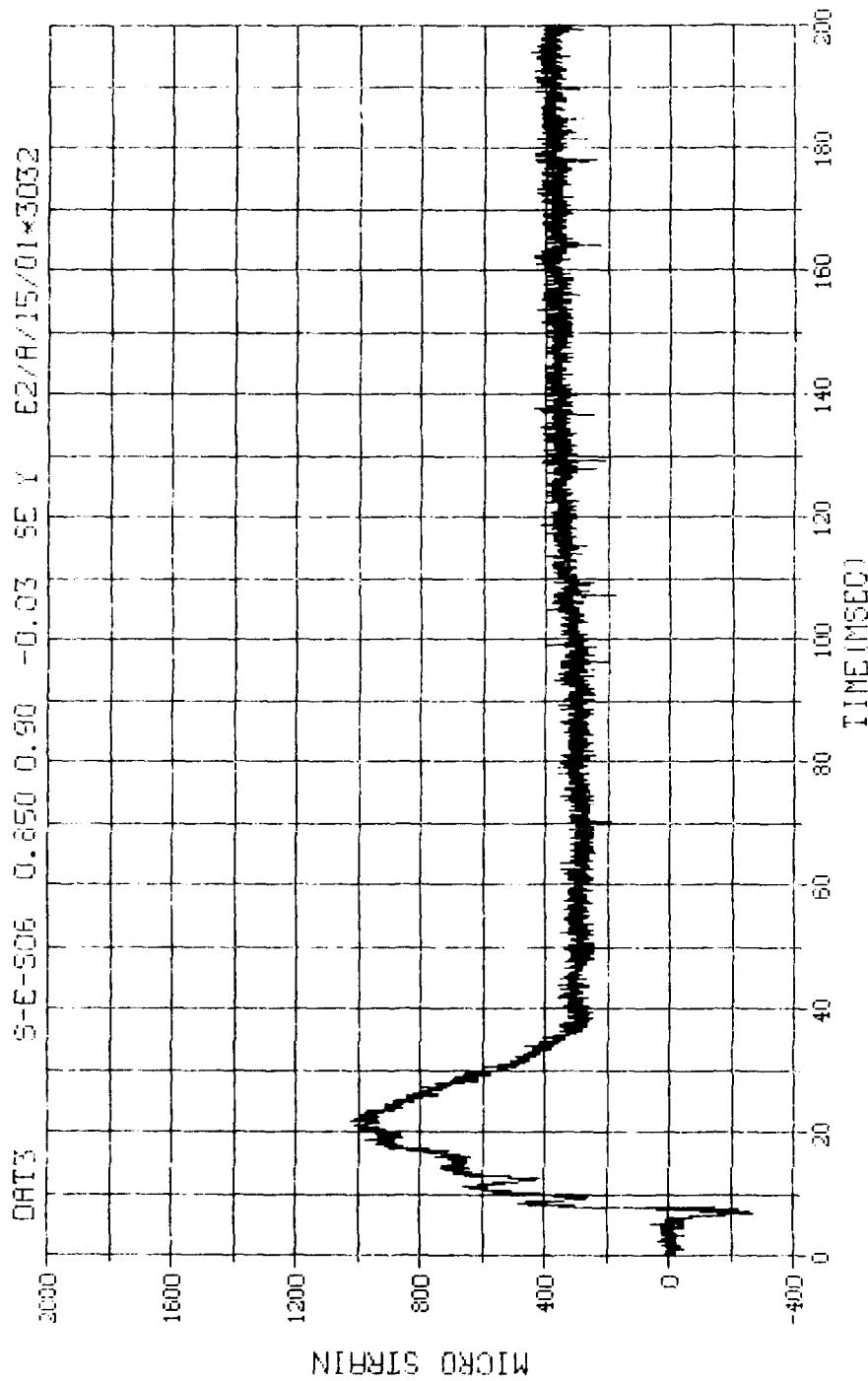
M.N. = 3029	E.U. = 0.000, 10000.000	VSN=66142
SKIP=7.000	DIGITS=D.000, 869.577	TAPE22
S.R. = 25.00 KHZ	4. 4 PM, TUE, 13 SEP 83,	FILE=202 1



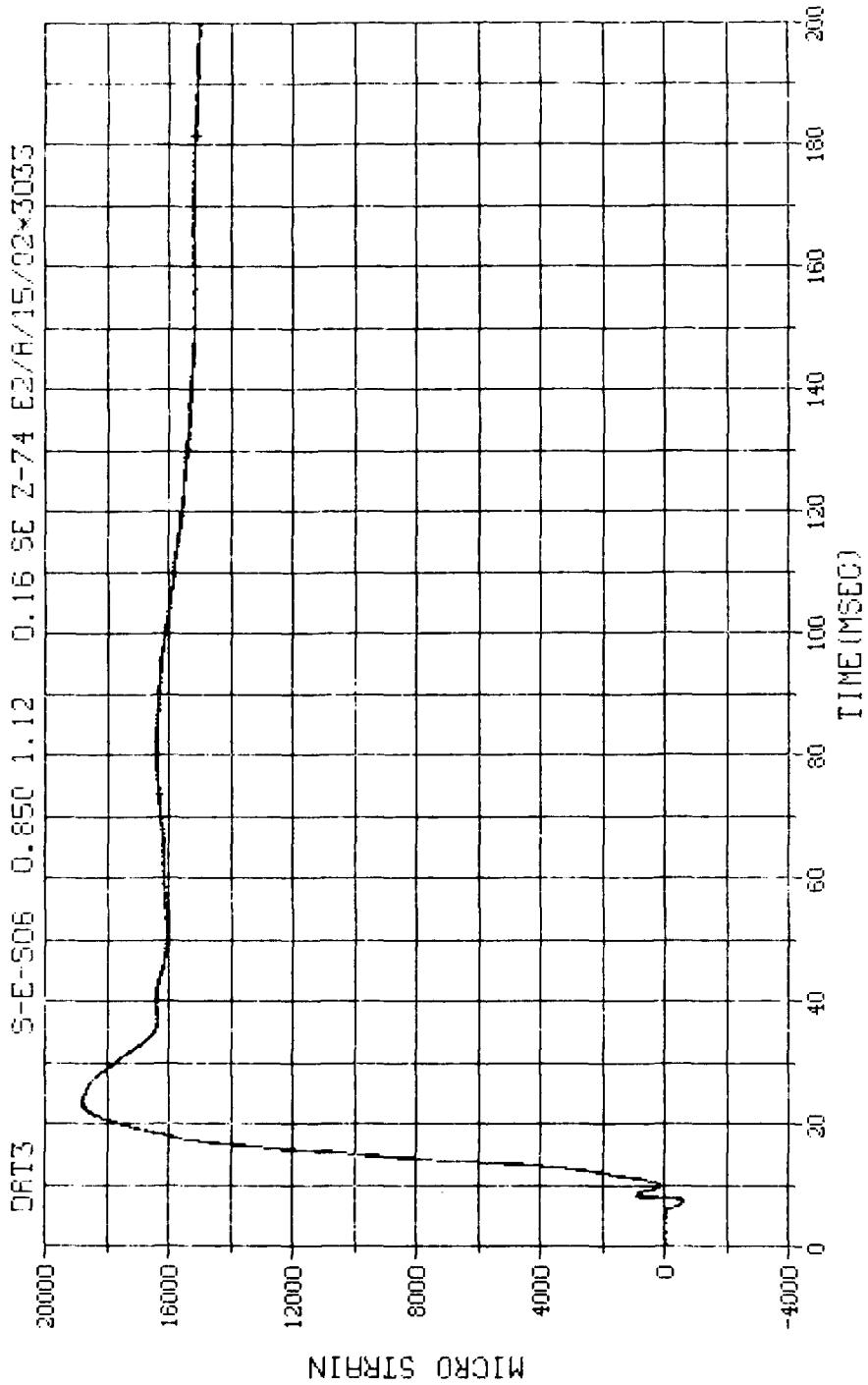
M.N. = 3030	E.U. = 0.000, 15000.000	VSN=66142
SKIP=7,000	DIGITS=0,000, 877,125	TAPE22
S.R. = 25.00 KHz	4. 4 PM, TUE, 13 SEP 93.	FILE=200 1



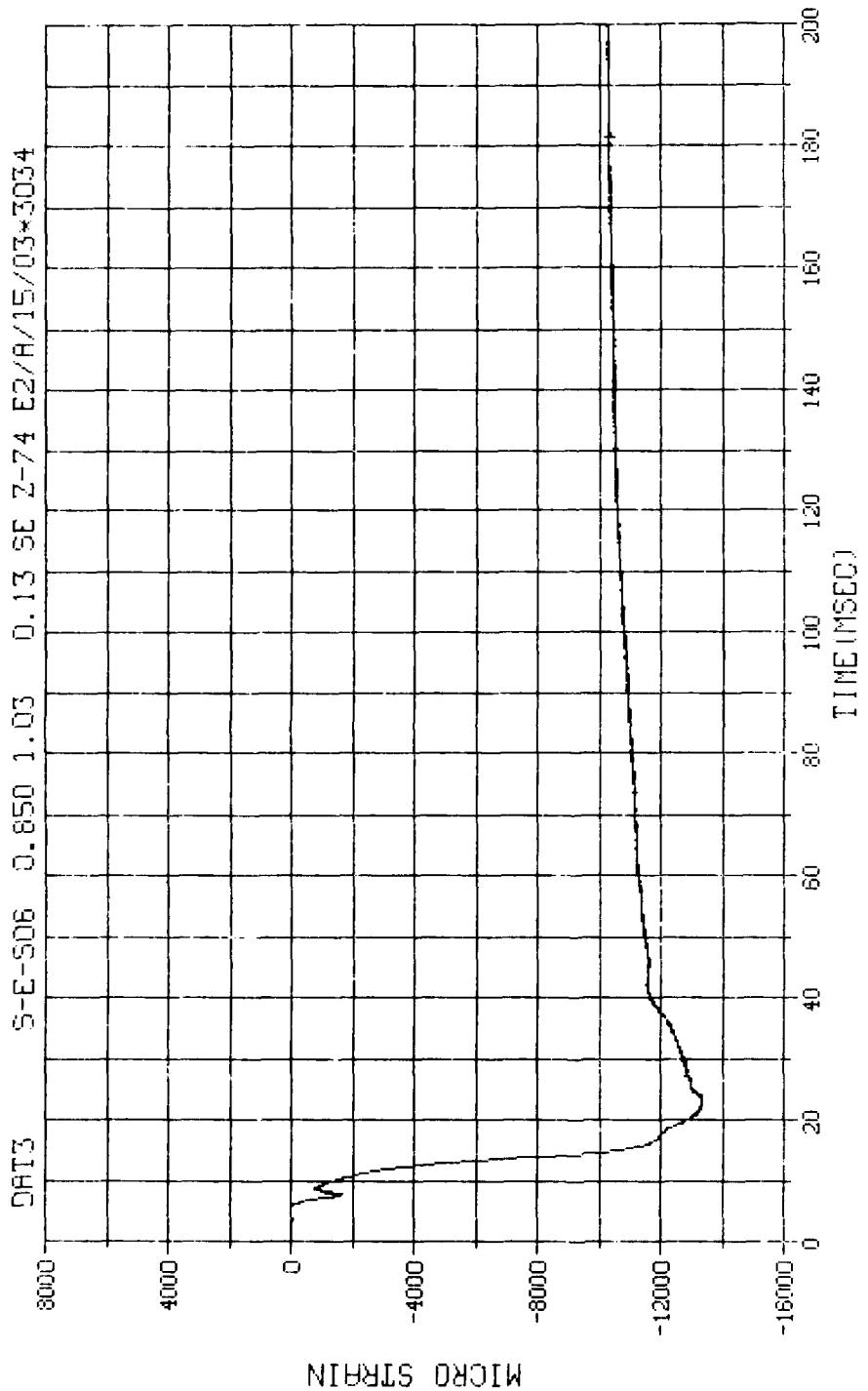
M.N. = 3031	E.U. = 0.000, 10000.000	VSN=00142
SKIP=7.000	DIGITS=0.000, 896.375	TRPE22
S.R. = 25.00 KHZ	4. 4 PM, TUE, 13 SEP 93.	FILE=204_1



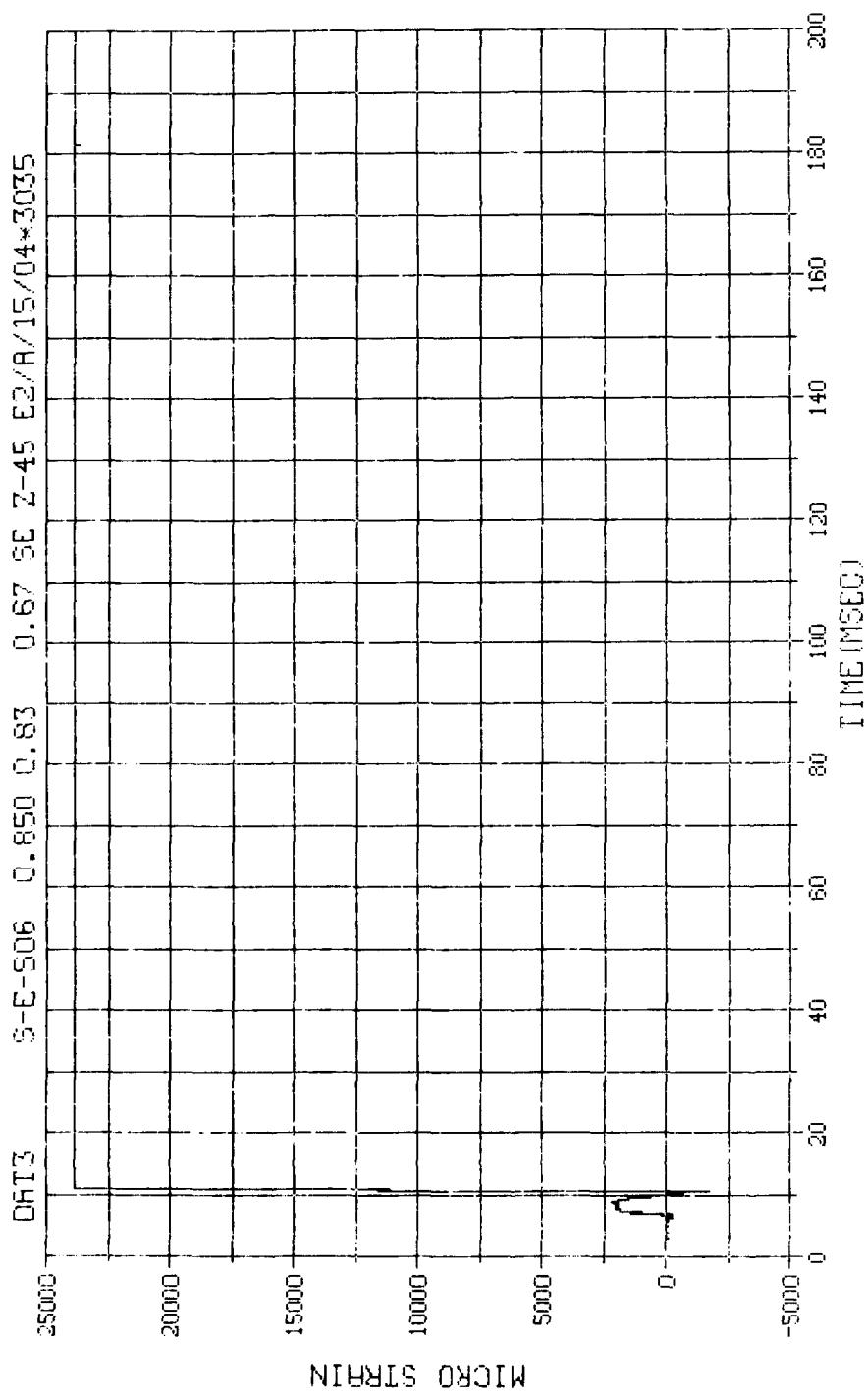
M.N. - 3032 E.U. -0.000, 10000.000 VSN-66142
TSKTP=7.000 DIGITS=0.000, 889.900 TAPE22
S.R. =25.00 KHZ 4. 4 PM, TUE, 13 SEP 83. FILE=206_1



M.N. = 3033	E.U. = 0.000, 7500.000	VSN-06142
SKIP=7.000	DIGITS=0.000, 679.125	THPE22
S.R. = 25.00 KHZ	4. 4 PM, TUE, 15 SEP 83.	FLUJ-208 1

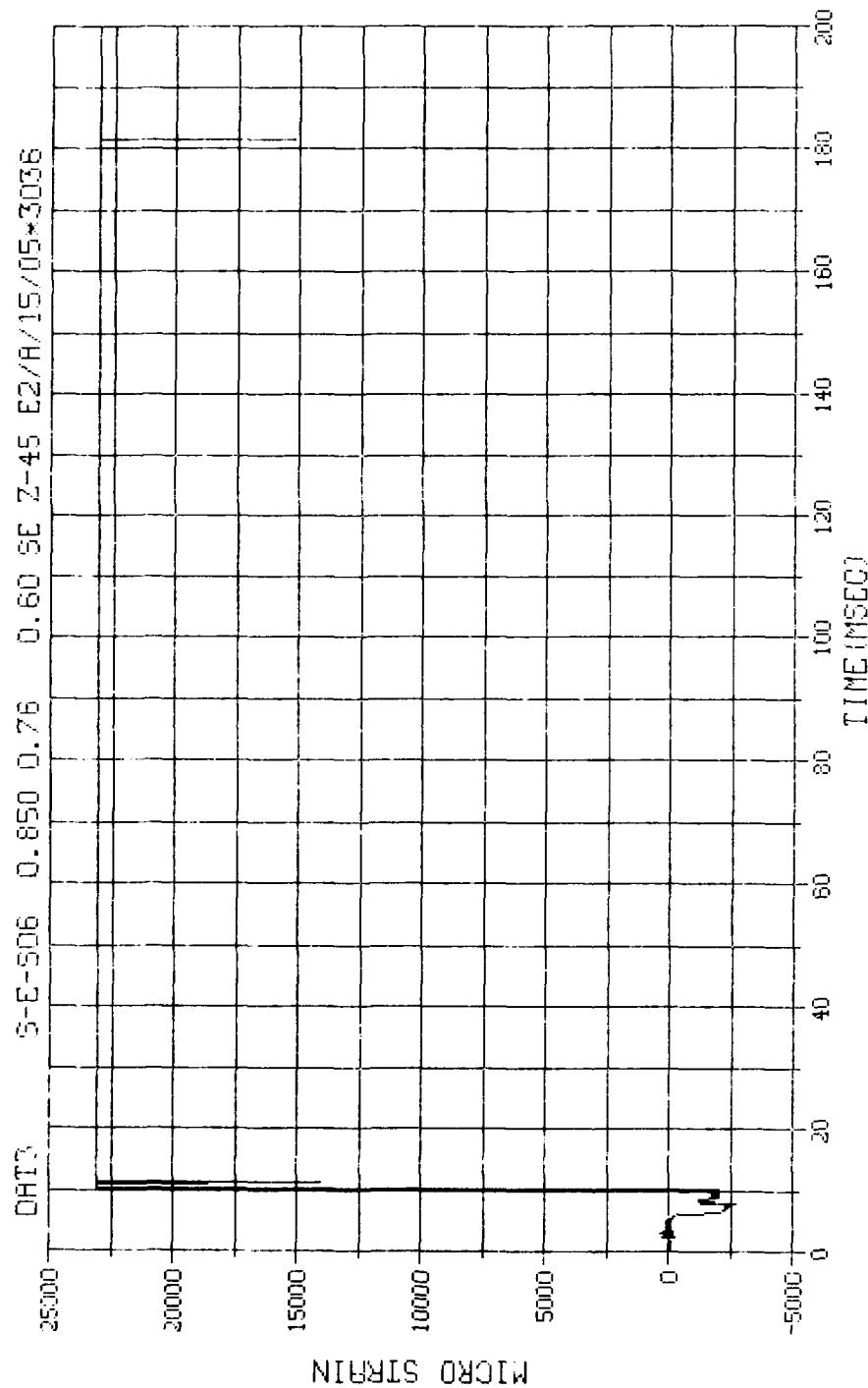


M.N. - 3034 E.U. -0.000,7500.000 VSN-66142
SKIP=7.000 DIGITS=0.000,879.375 TAPE22
S.R. =25.00 KHZ 4. 4 PM, TUE, 13 SEP 83, FILE=210



M.N.	• 3035	E.U.	-0.000, 10000.000
TSKTP	=7.000	DIGIT3	=0.000, 668.375
S.R.	=25.00 KHZ	4, 4 FM	13.551, 97,
			FLG=212, 11

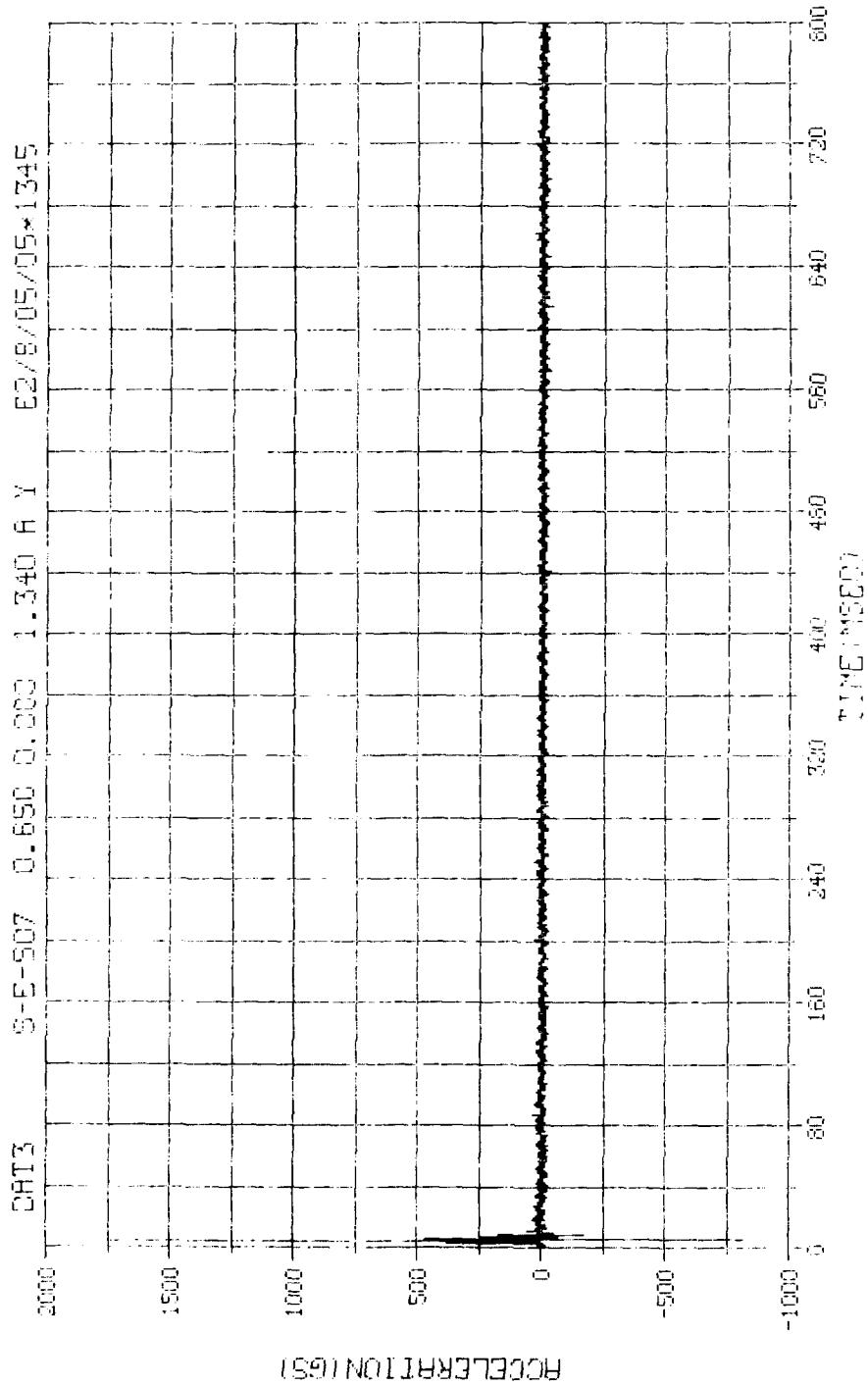
VSN-G6142
TAPE22



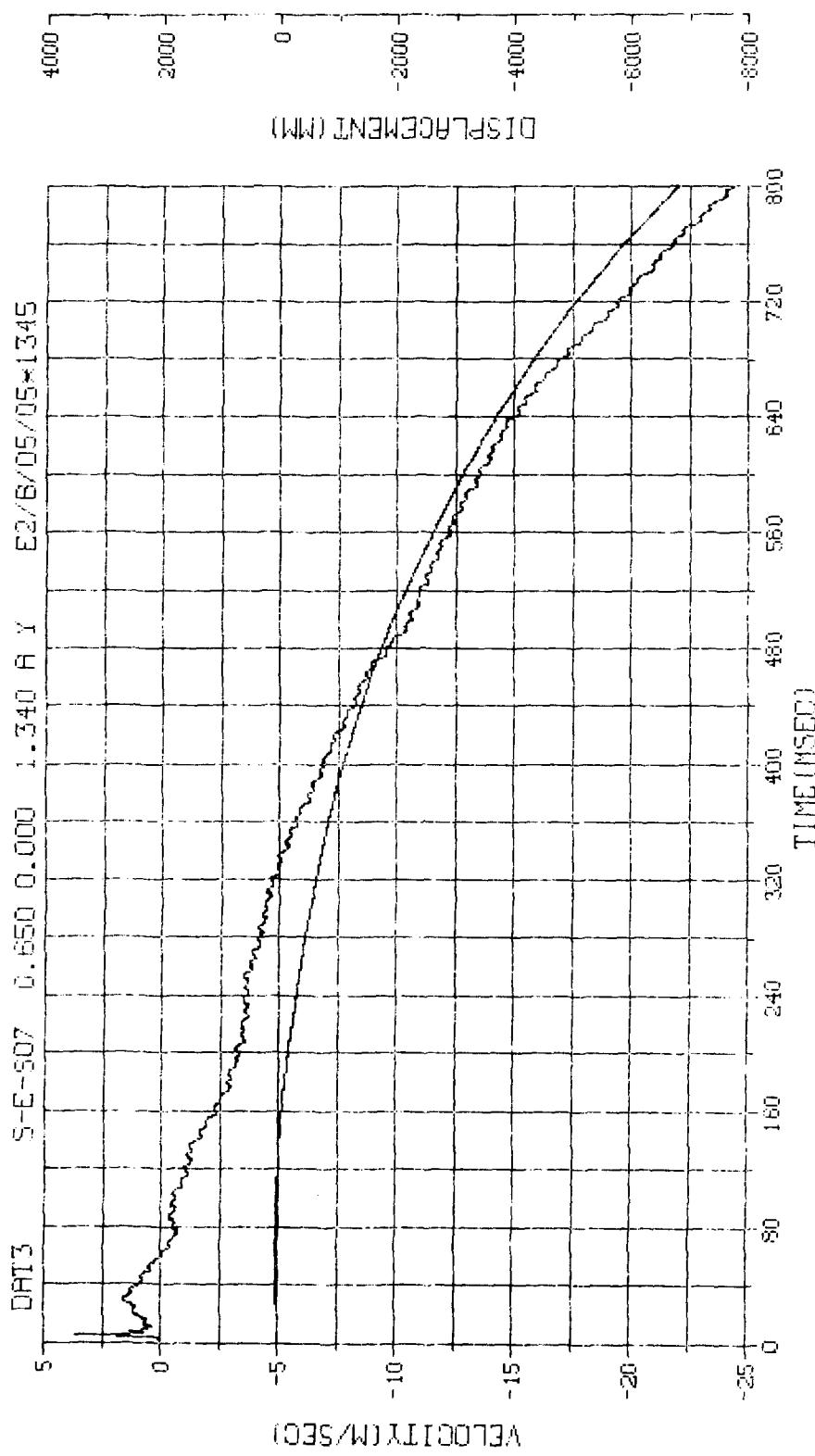
M.N. - 3036	E.U. --0.090, 10000.000	VSN-66142
SKIP=7.000	DIGIT5=0.000, 894.625	TAPE22
S.R. =25.00 KHZ	4. 4 FM, TUE, 13 SEP 83.	FILE=214 1

APPENDIX I

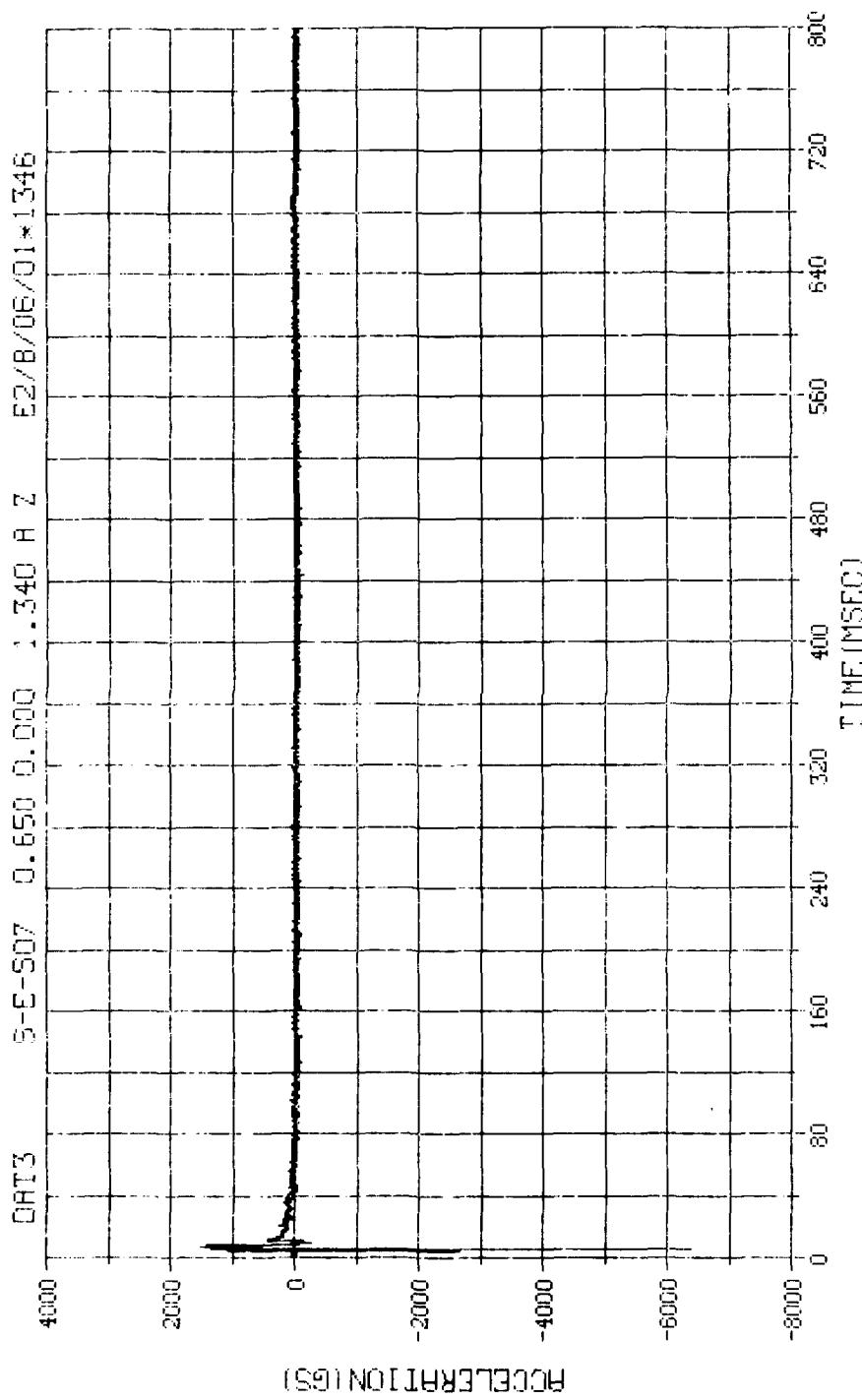
NEAR-FIELD AND STRUCTURAL DATA ARCH A-7



M.N. = 1345	E.D. = 2.300.000	VSN-66142
Tekip=7.000	RIGHTS=7.000.000	TYPE22
S.R. = 10.00 kHz	S.47 R.457.14 SEP 83.	F1/F=354

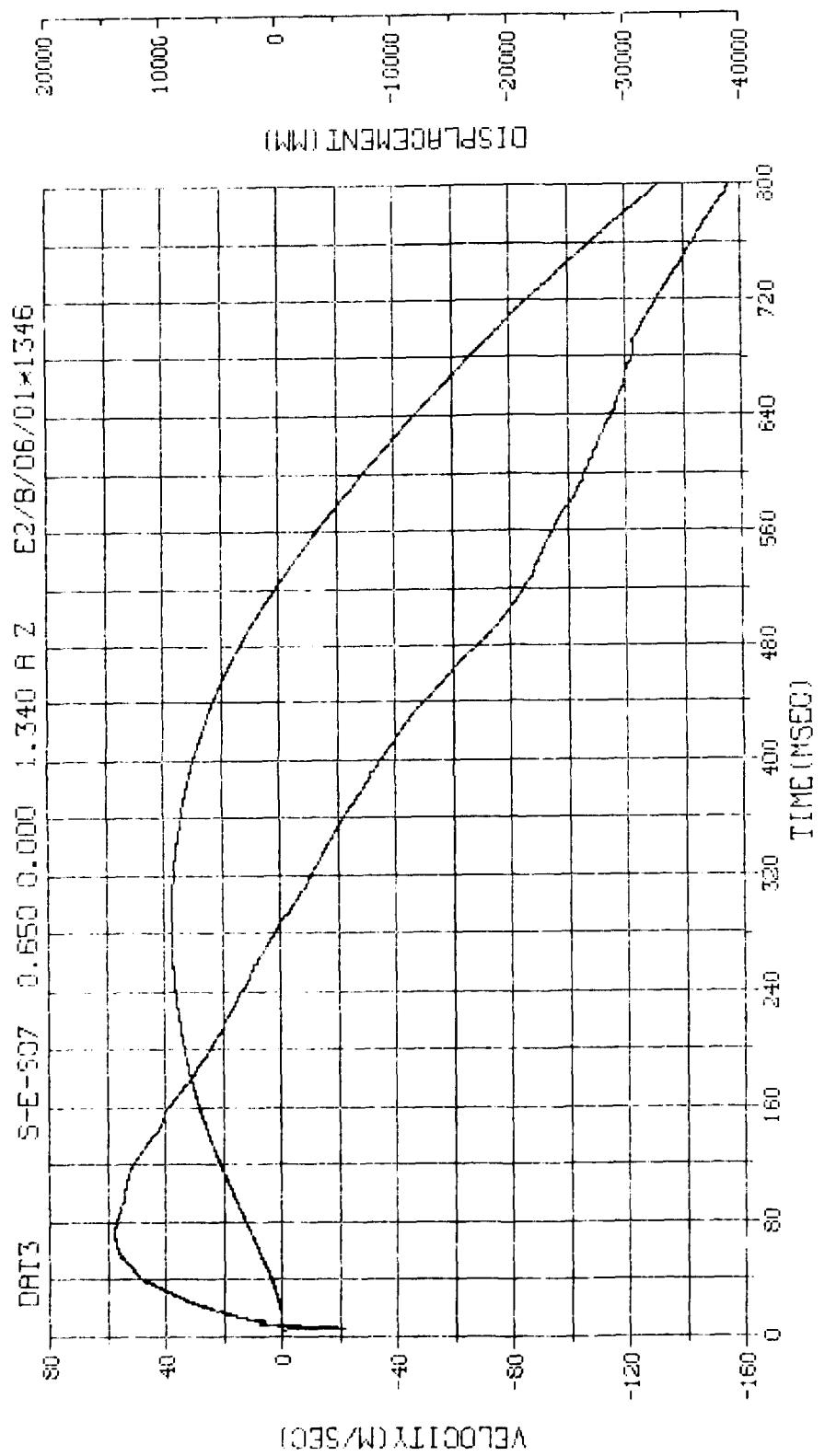


M.N. = 1345	E.U. = 0.000, 4500.000	VSN=66142
TSKIP=7.000	DEBITS=0.000, -7000.000	THPE32
S.R. = 10.000	E, 47 MM, 453, 14 SFP 83,	FILE=364
	-----	-----

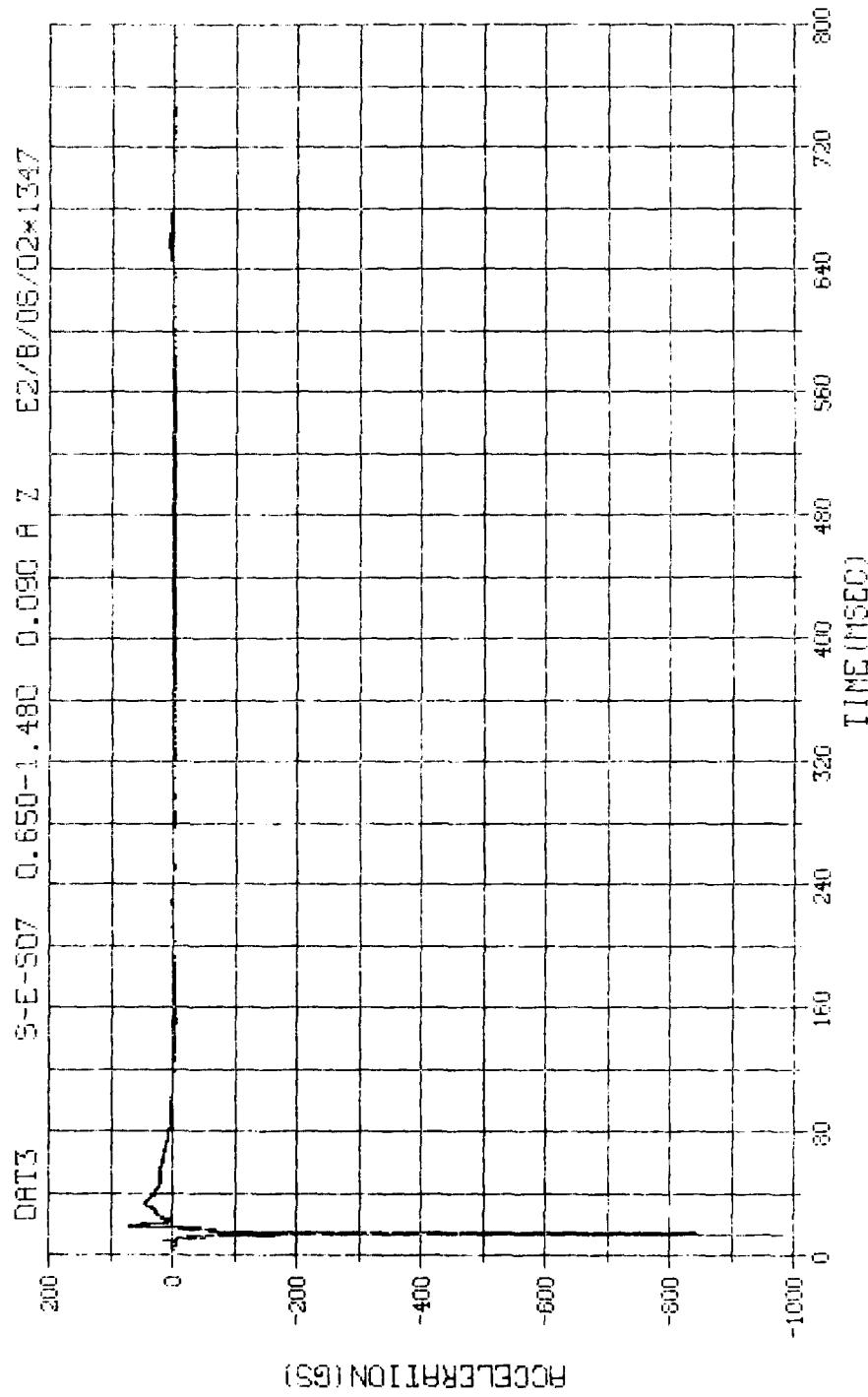


446

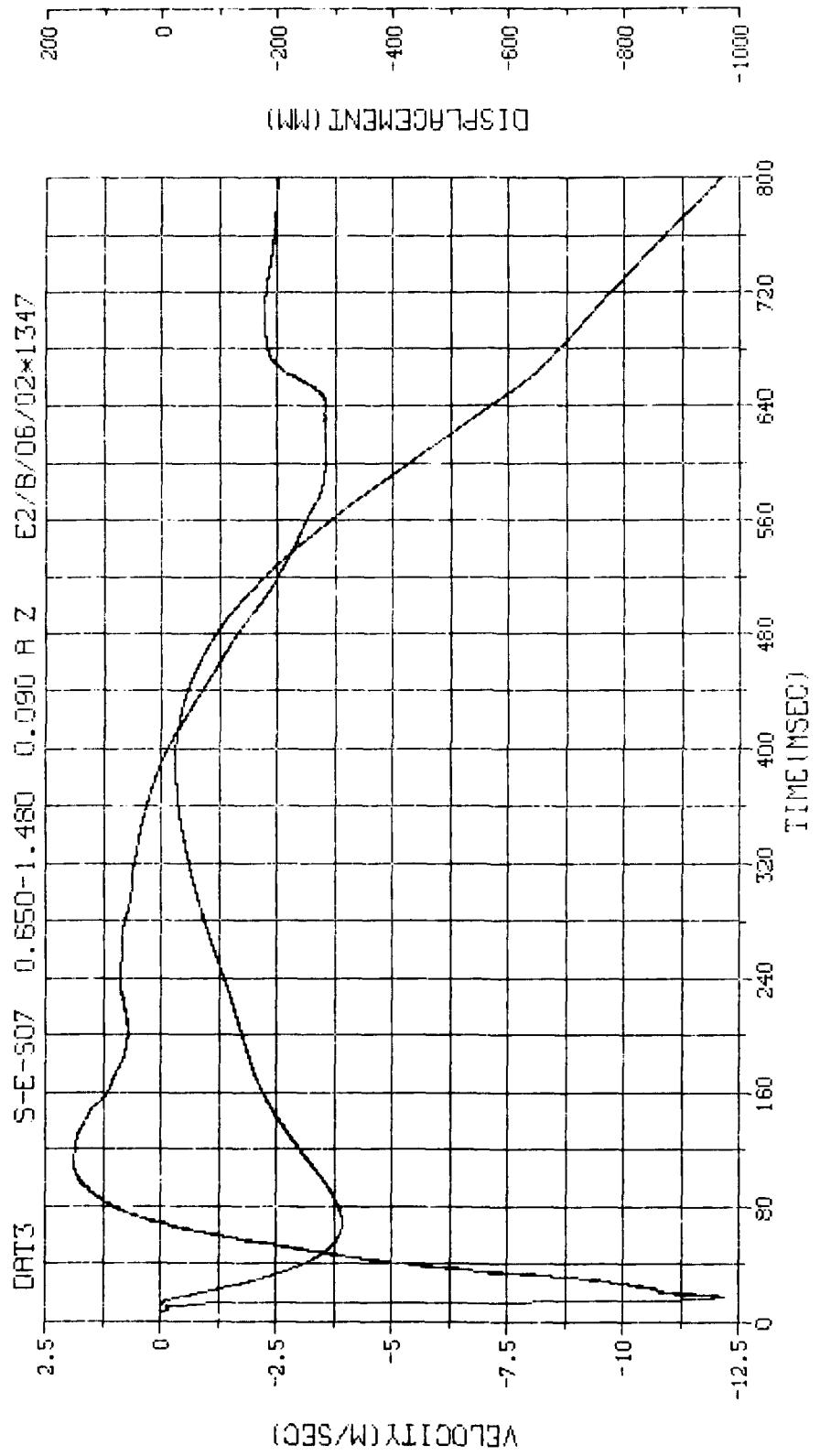
M. N. = 1346	E. U. = 0, 000, 20000, 000	VSN=66142
TSKIP=7.000	DIGITS=0, 000, -892.375	TAPE22
S. R. = 10.00 KHZ	4. 4 PH. TUE, 13 SEP 83,	FILE=366
		1]



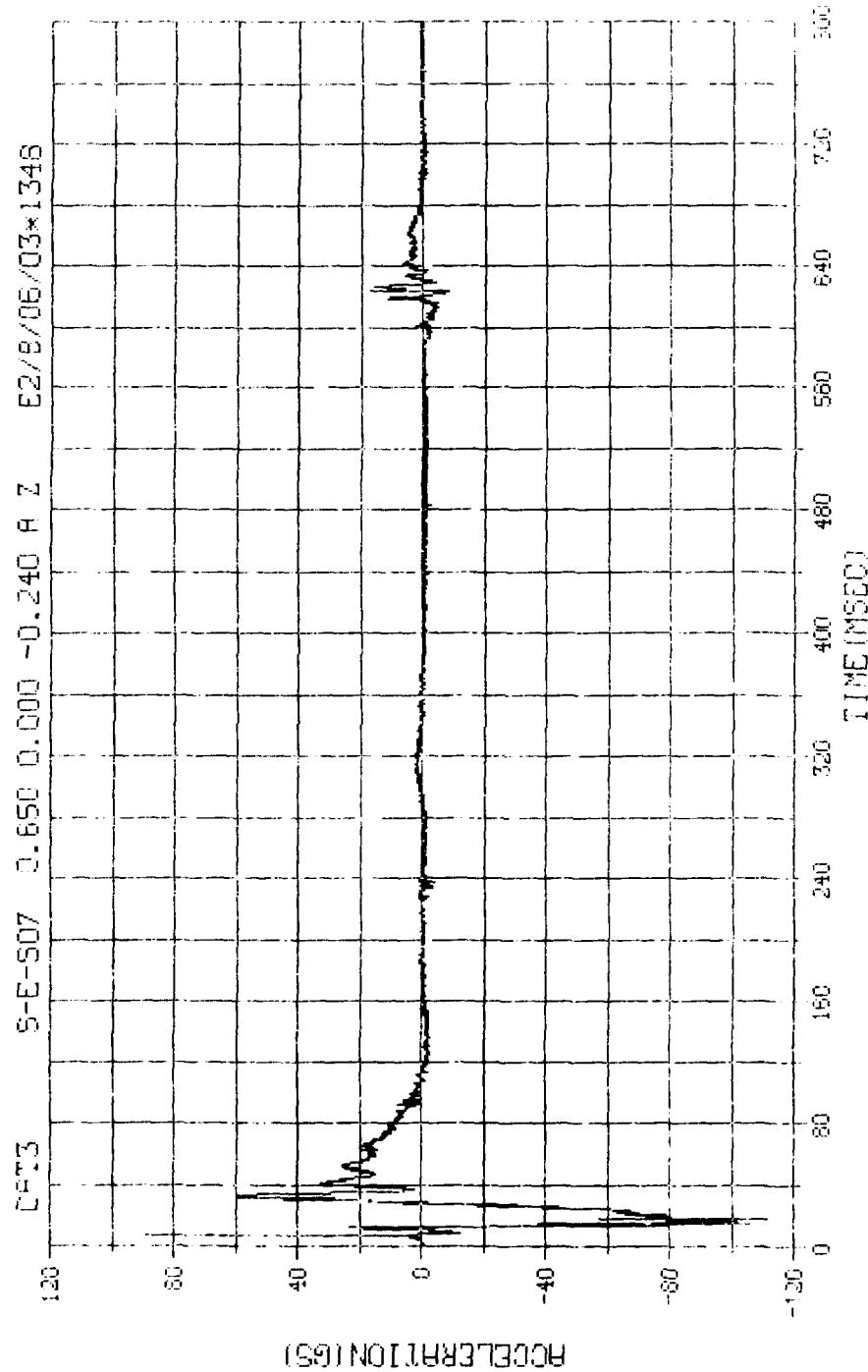
M. N. = 1345	E. U. = 0.000, 20000.000	VIN-66142
SKIP=7.000	DIGITS=0.000, -892.375	TAPE22
S.R. = 10.00 KHZ	4. 4 PM, TUE, 13 SEP 83.	FILE=366 2



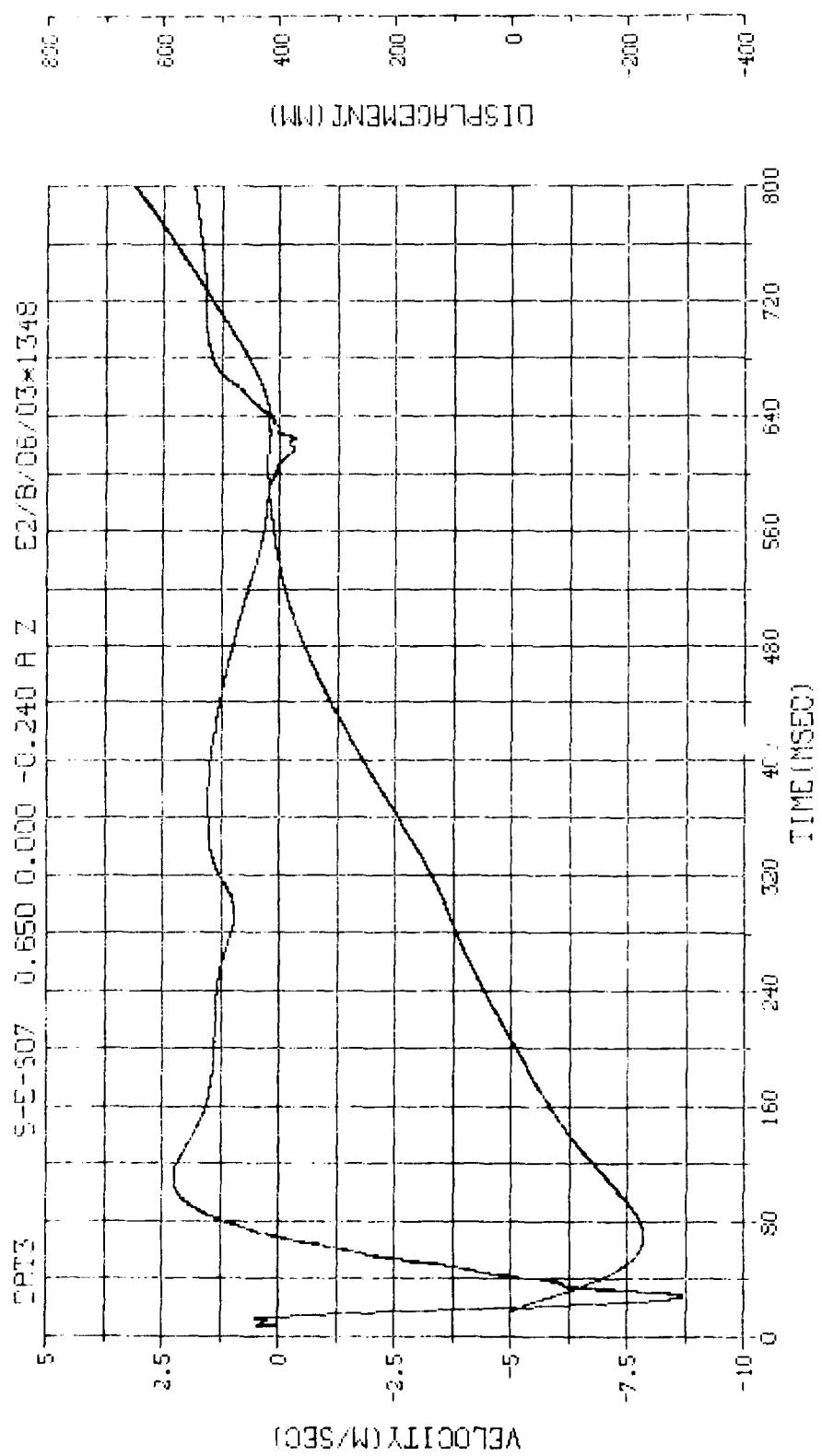
M.N. = 1347	E.U. = 0.000, 450.000	W.SN-06142
TSPLP=7.0719	GIGITS=0.000,-878.250	TRPES2
S.R. = 10.000 1416	G.47 H.P. 900.14 35.50.	POL5=358



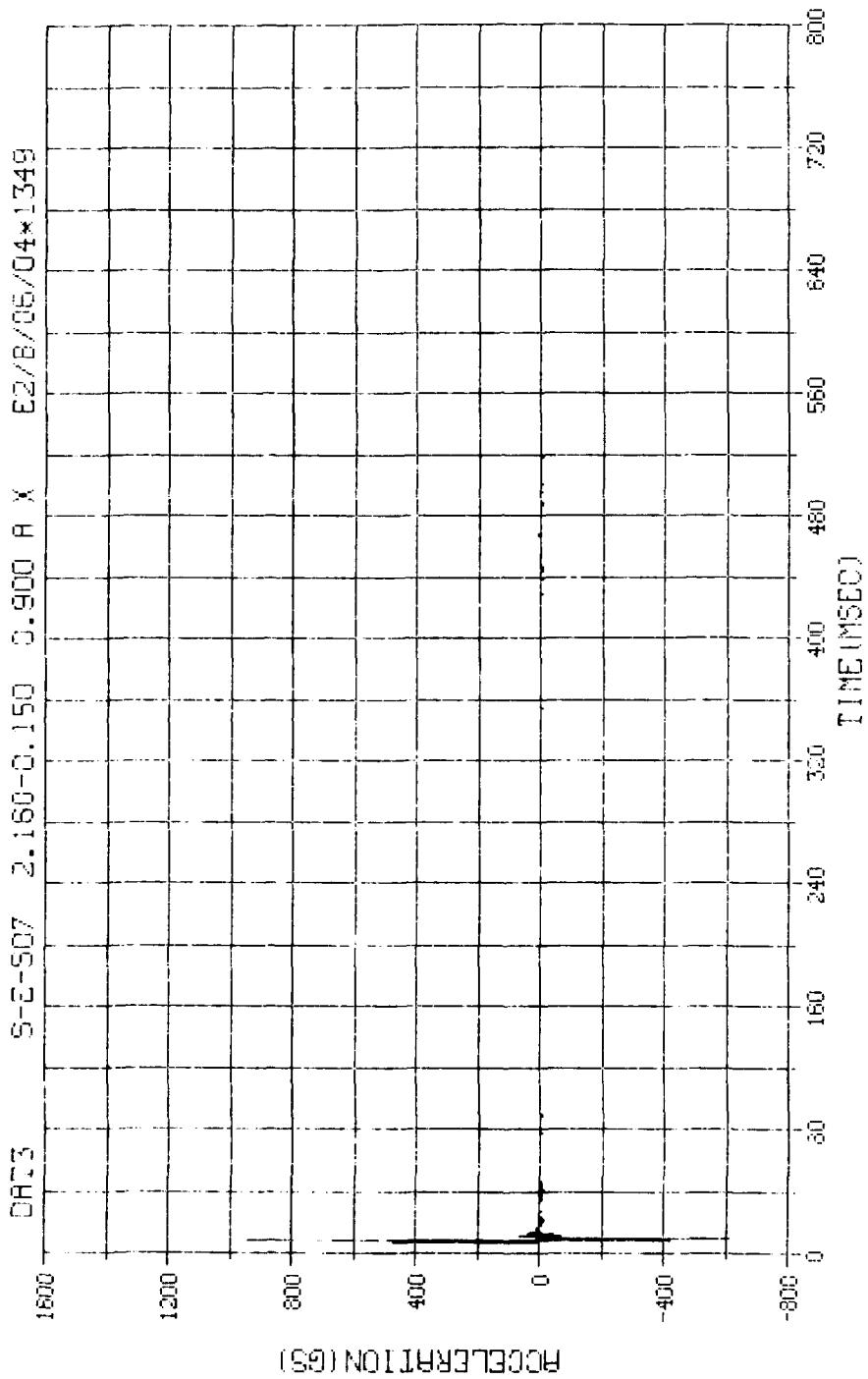
M.N. = 1347	E.U. = 0.000, 450.000	VSN-66142
TSKIP=7.000	DIGITS=0.000, -878.750	TRFE22
S.R. =10.00 KHZ	8.47 AM, WED, 14 SEP 83.	FILE=368_2



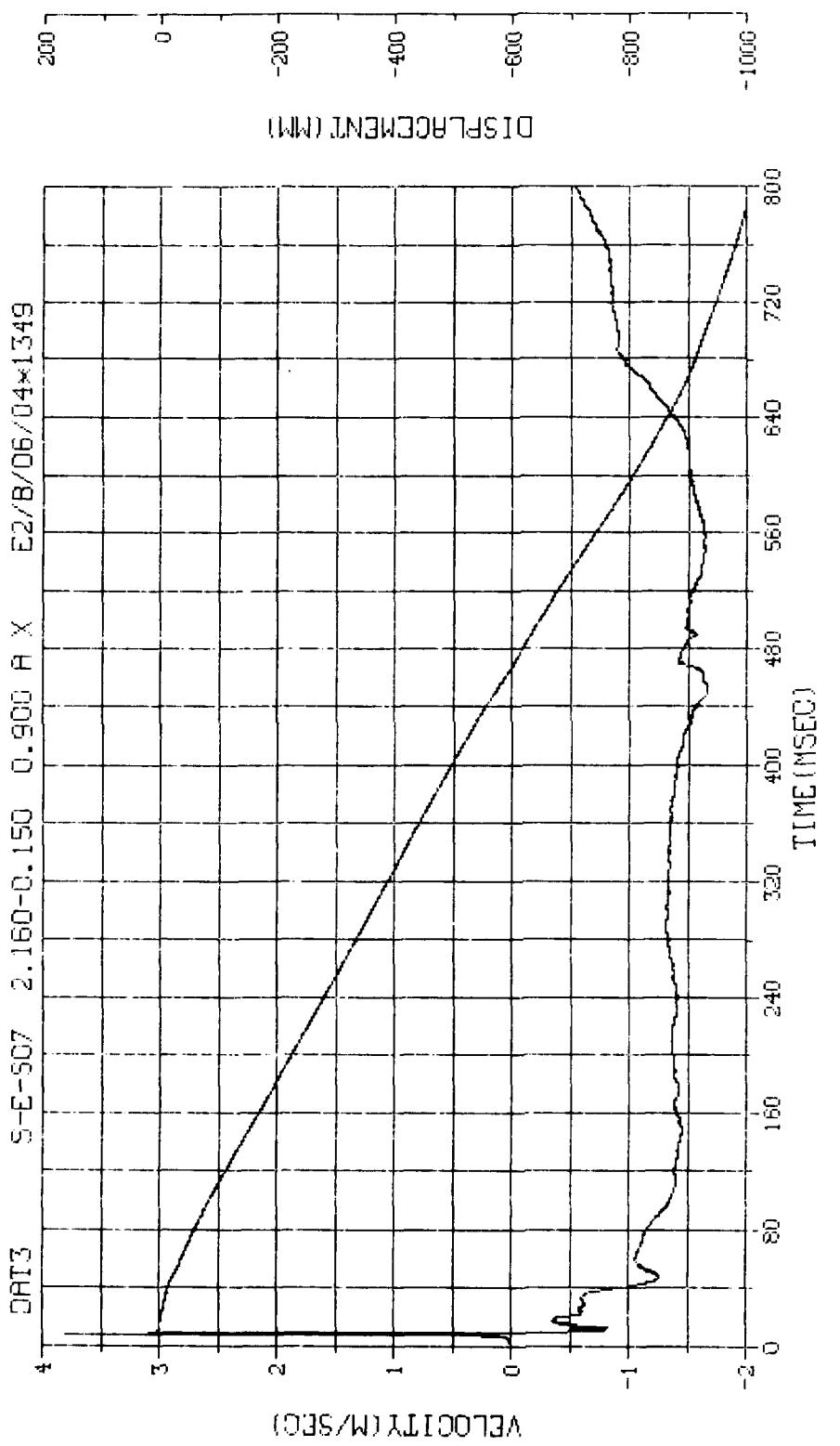
W. N. = 1348	E.U. = 0.000, 200.000	VSN-66142
TSRP=7.000	DIGITS=0.000, -884.125	TAPE22
S.R. = 10.00 KHZ	8.47 AN, WEO, 14 SEP 83,	FILE=370



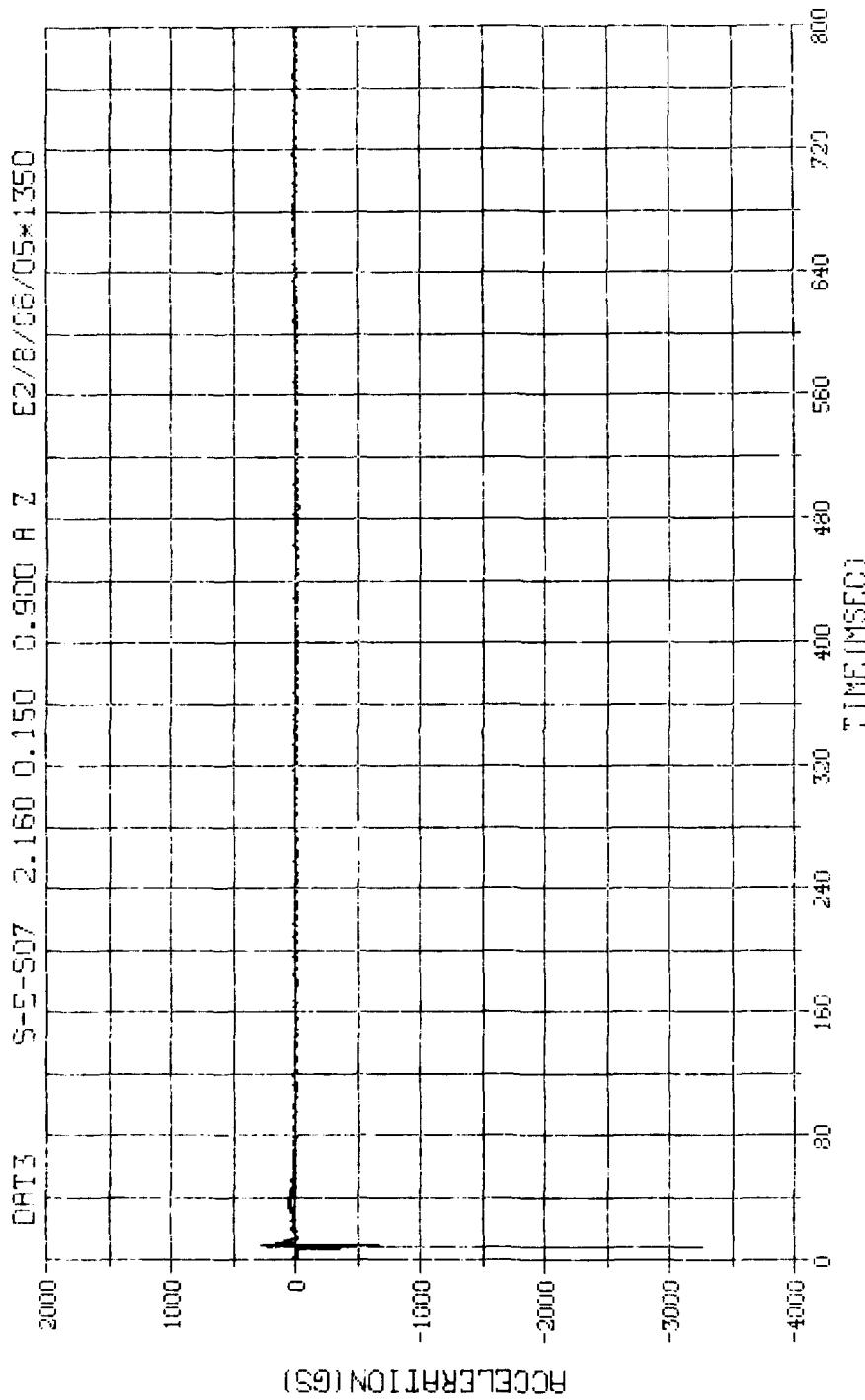
M. N. = 1348	E. G. = 0.000, 200.000	VSN=60142
TSKIP=7,000	SIGITS=0.000, -884.125	TRPE22
S. R. = 10.00 KHZ	6.47 RM, WED, 14 SEP 83.	FILE=370_2



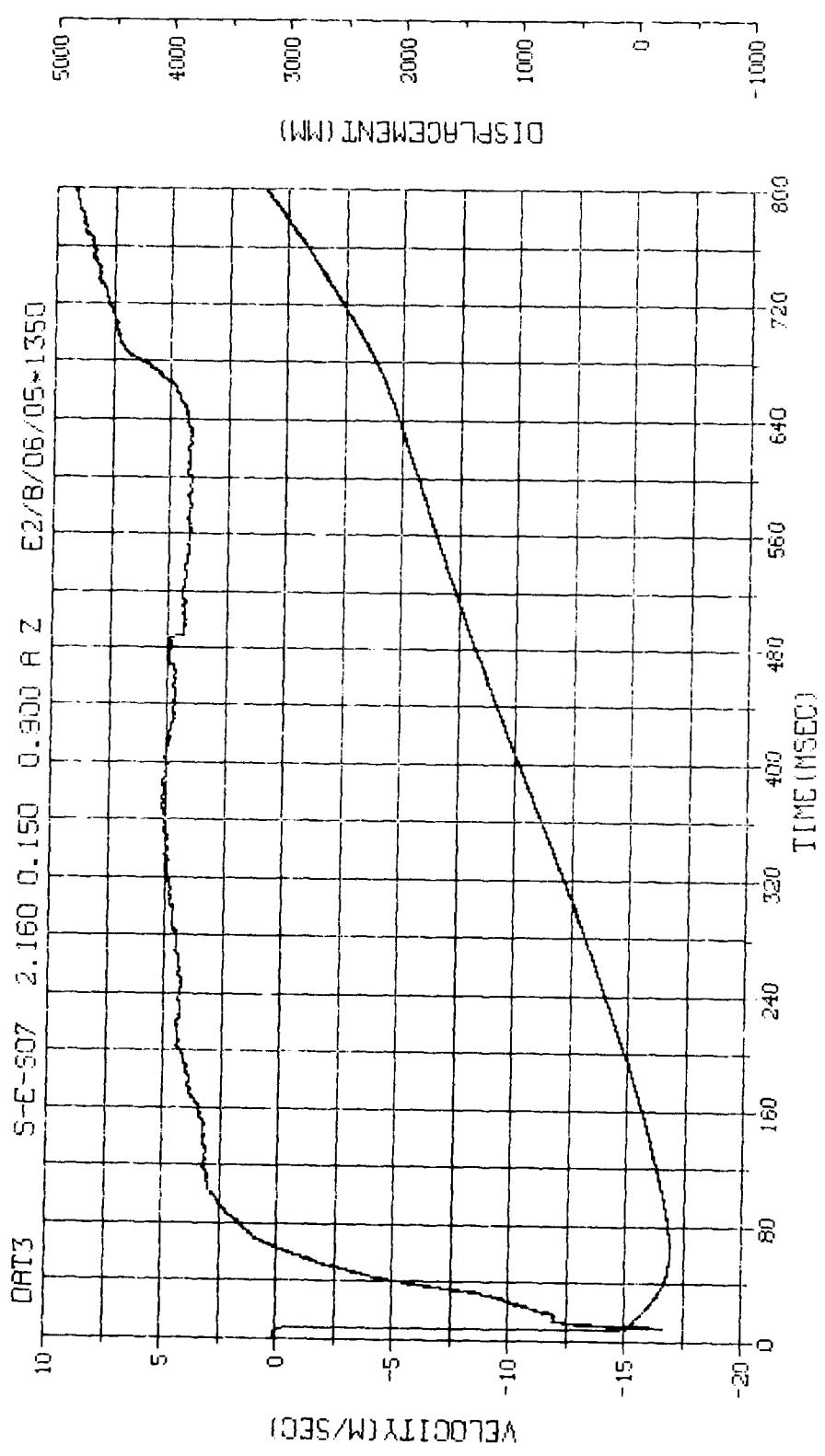
M.N. = 1349	E.U. = 0.300, 400.000	VSN-66142
SKIP=7.000	DIGITS=0.300, 868.750	TAPE22
S.R. = 10.00 KHZ	4. 4 PM, TUE, 13 SEP 83.	FILE=372



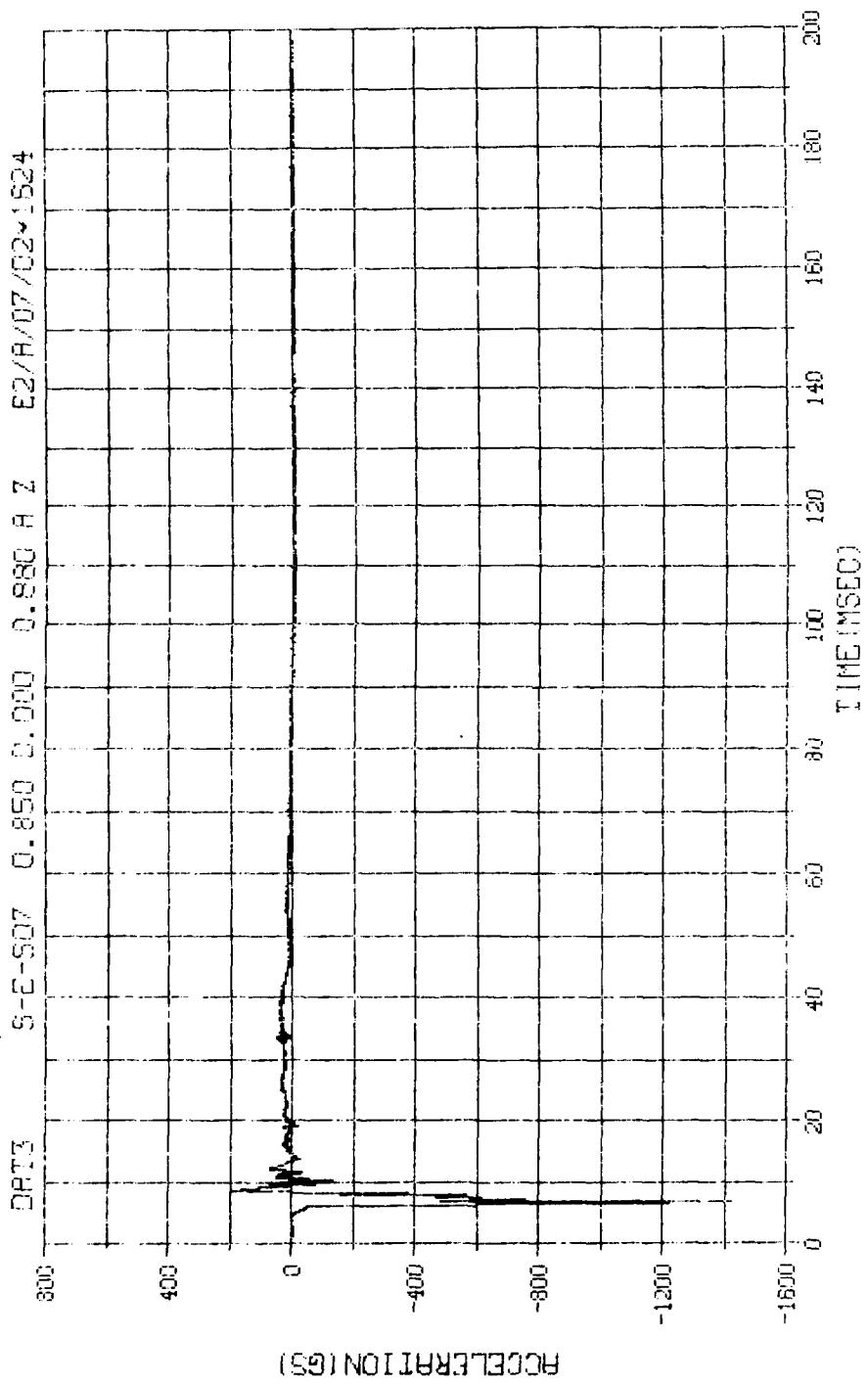
M.N. = 1349	E.U. = 0.000, 400.000	VSN=GG142
SKIP=7.000	DIGITS=0.000, 868.750	TAPE22
S.R. =10.00 KHZ	4. 4 PM, TUE, 13 SEP 83.	FILE=372 2



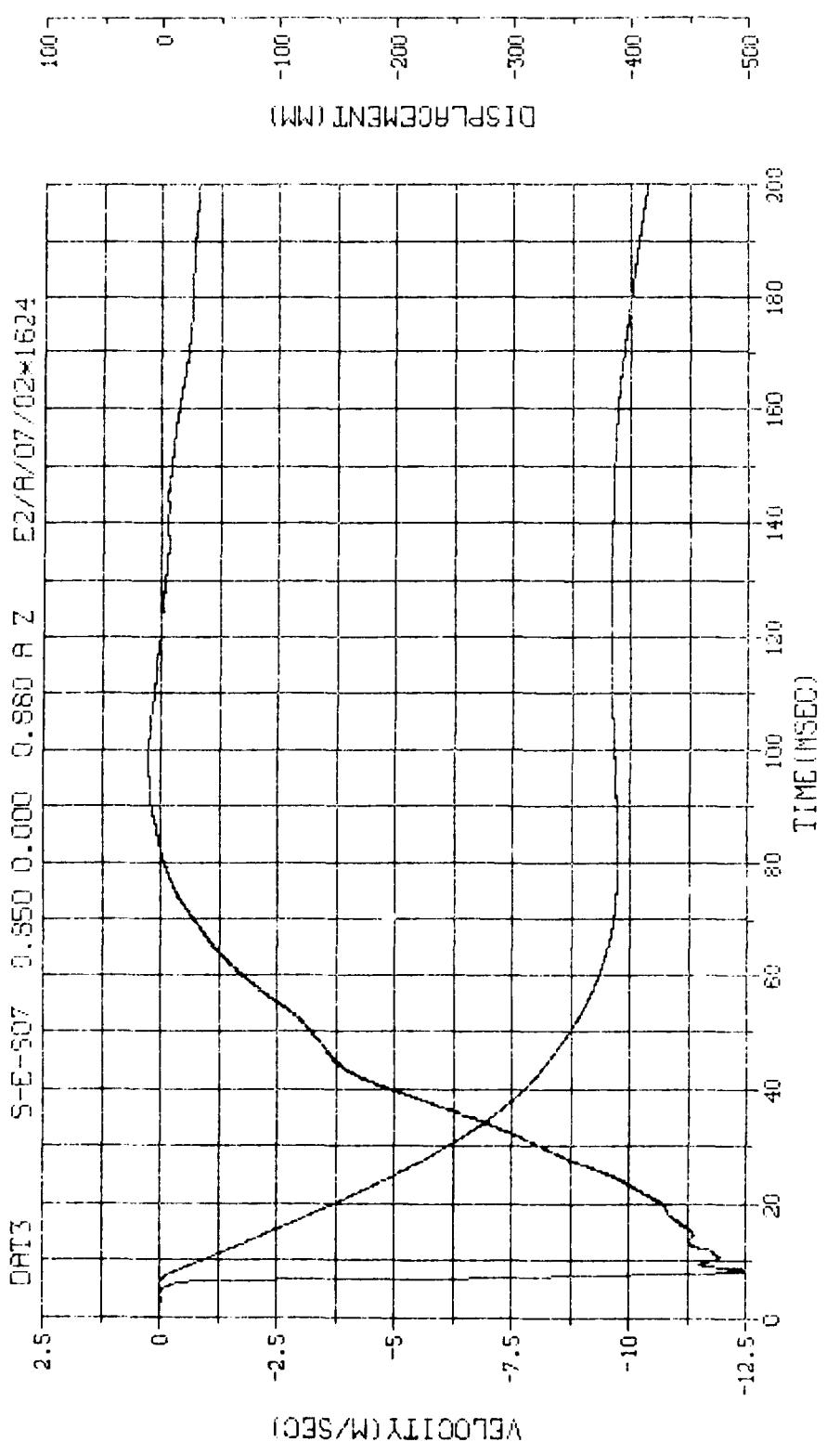
1. N. = 1350	E.U. = 0.000, 2400.000	VSN-66142
15KIP=7.000	DIGITS=0.000, 899.500	TAPE22
5.R. = 10.00 KHZ	4. 4 PM, TUC, 13 SEP 83.	FILE=374_1



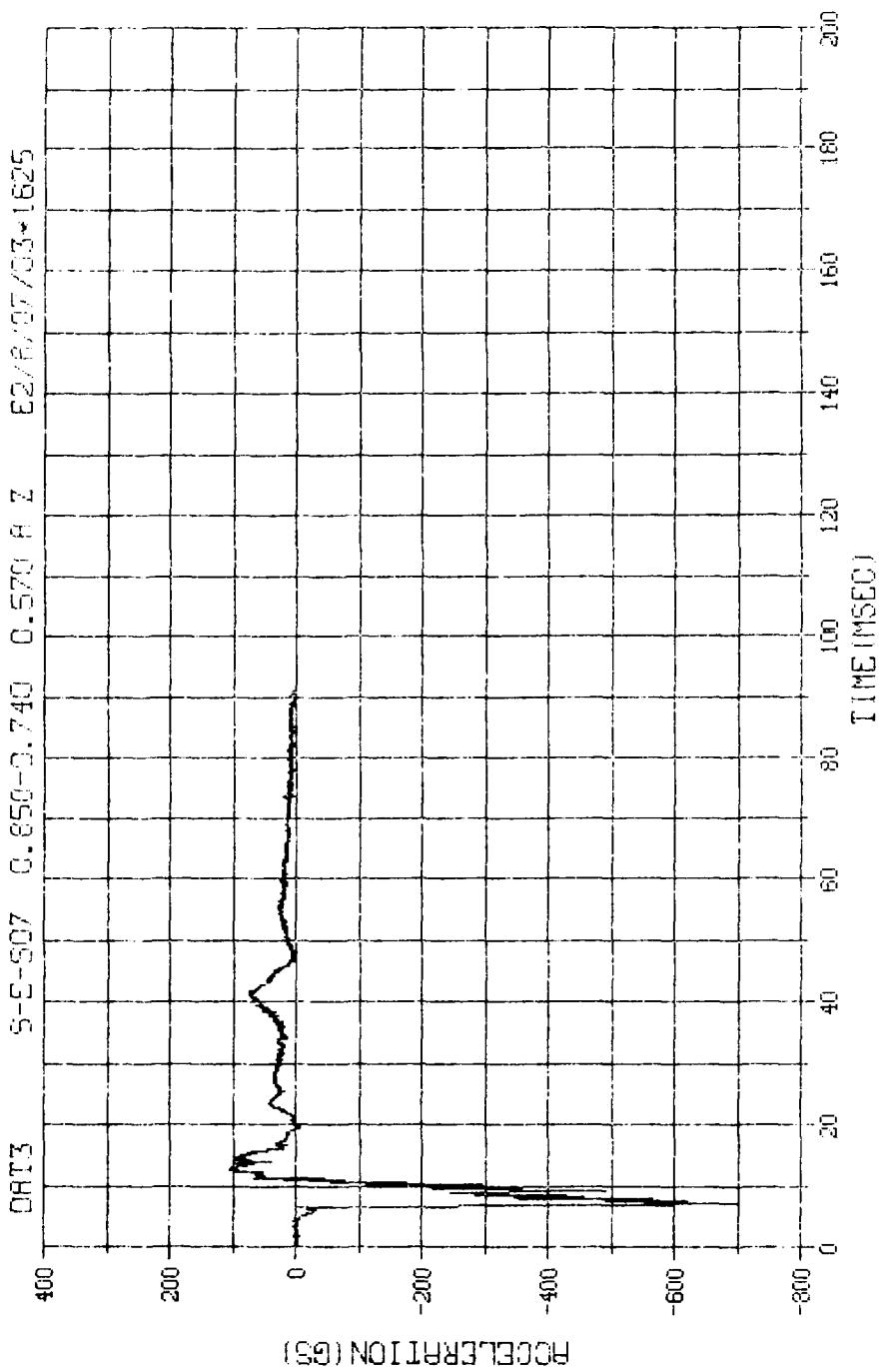
M.N. = 1350	E.U. = 0.000, 2400.000	VSN=66142
TSKIP=7,000	DIGITS=0.000, 899.500	TAPE22
S.R. =13.00 KHZ	4. 4 PM, TUE, 13 SEP 83.	FILE=374_2.

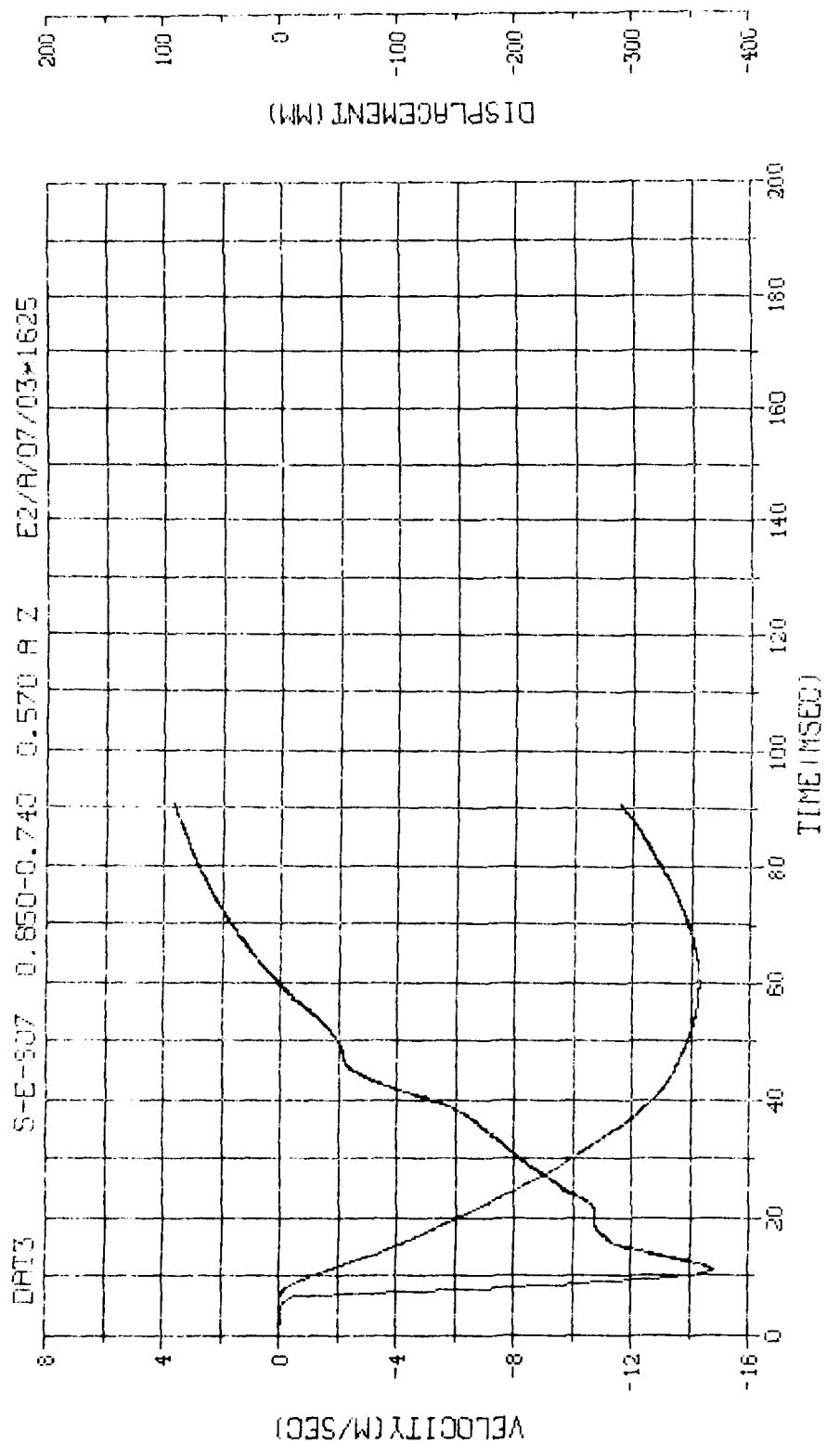


N.W. -91624	E.U. -0.000,1000.000	VSN-FB76
TSVTP=7,000	DIGITS=6,000,880,125	
S.R. = 25,00 KHz	ESUMS=13,7,6	
	TYPE23	
	STL3=0	
	1	



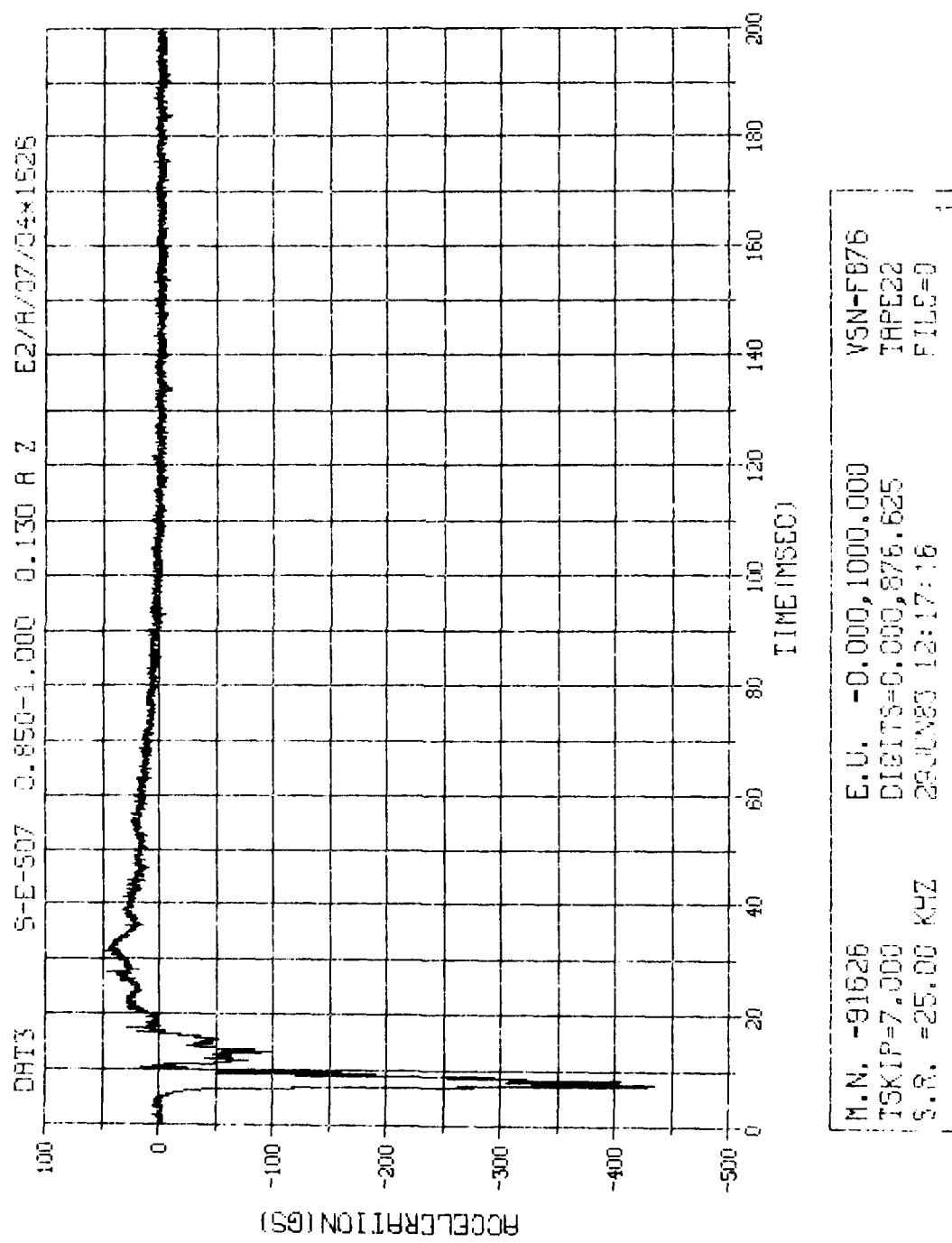
N.N. -91624	E.I. -0.000,1000,000	V5N-FB76
TSKIP=7.000	SDITS=0.000,880,125	TRPE22
S.R. =25.00 KHZ	280ANS3 12:17:16	F1,LG=0
		2

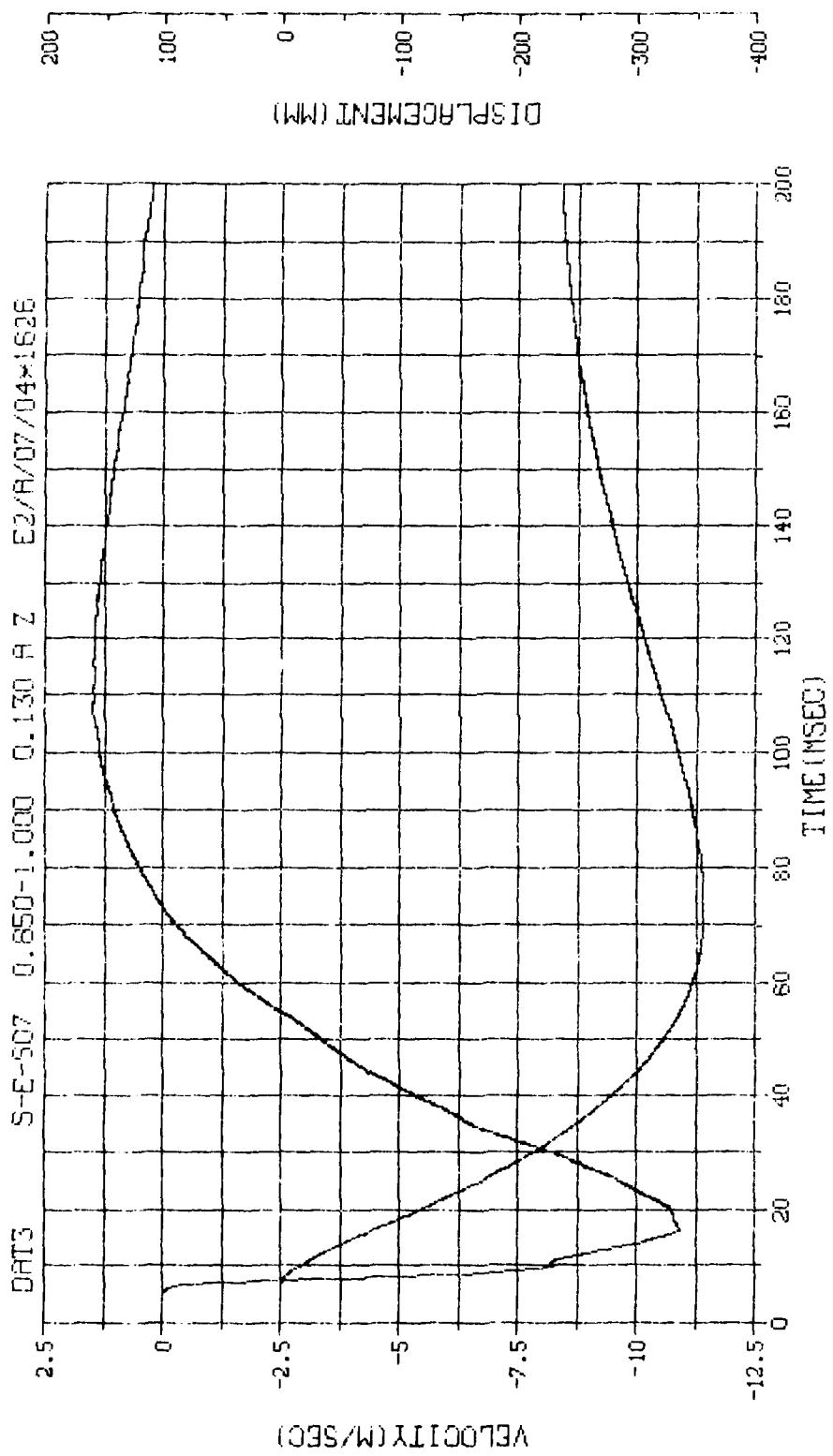




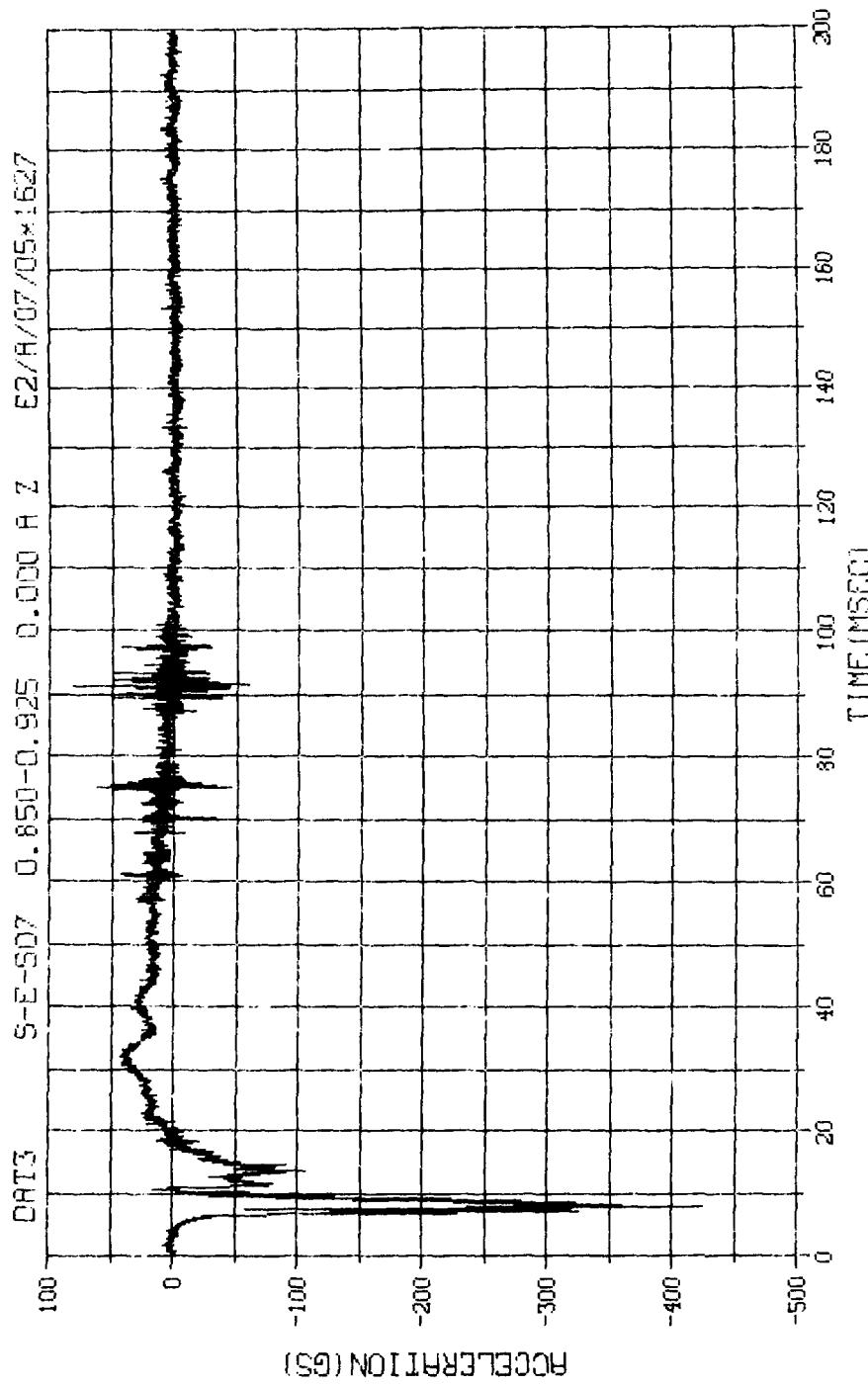
M.N. -71625	E.U. -0.000,1000.000
TSKIP=7.000	DIGITS=0.000,000.125
S.R. =25.00 KHZ	TRIG22
	PLUG=0
	2

29 JUN 83 12:17:16

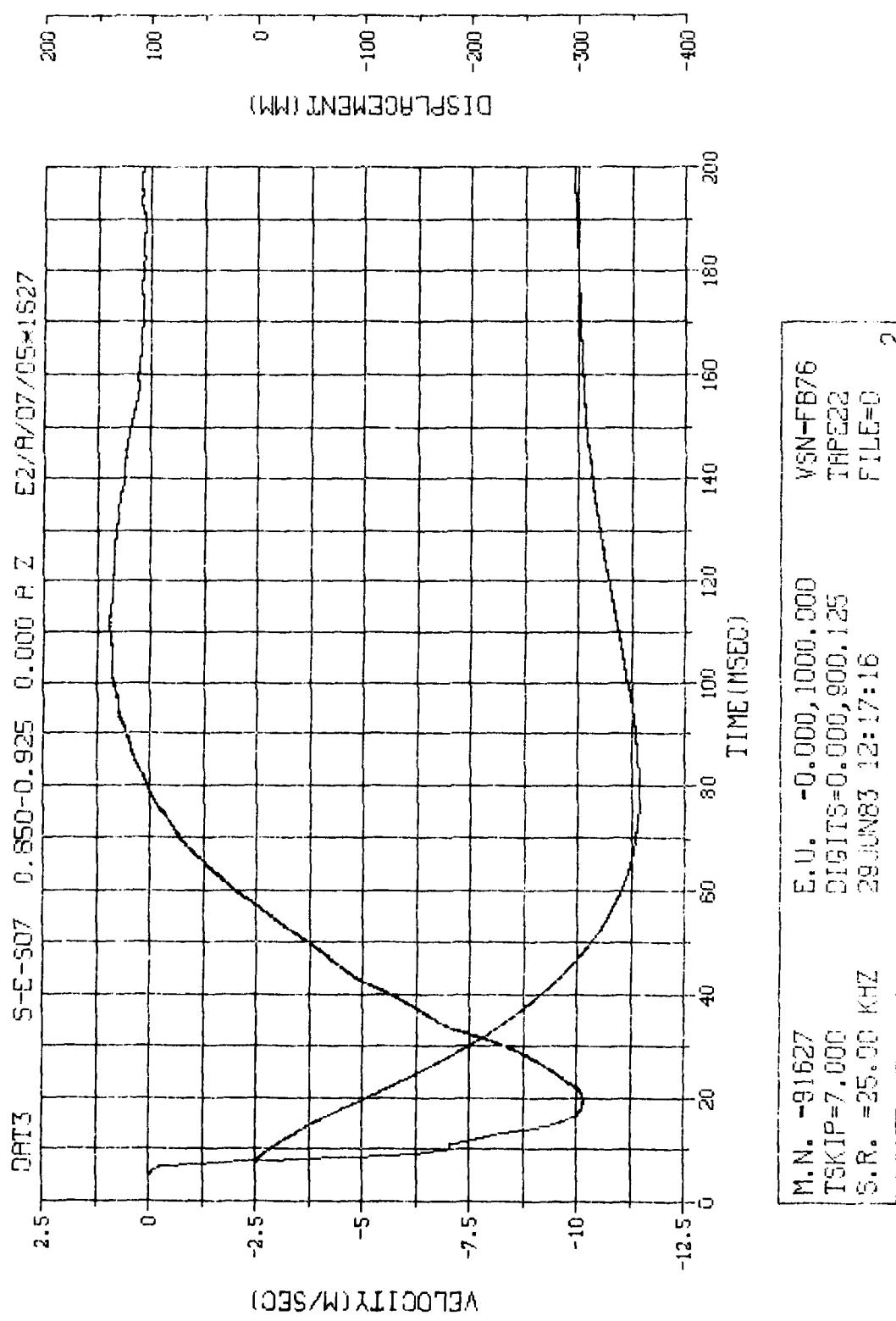


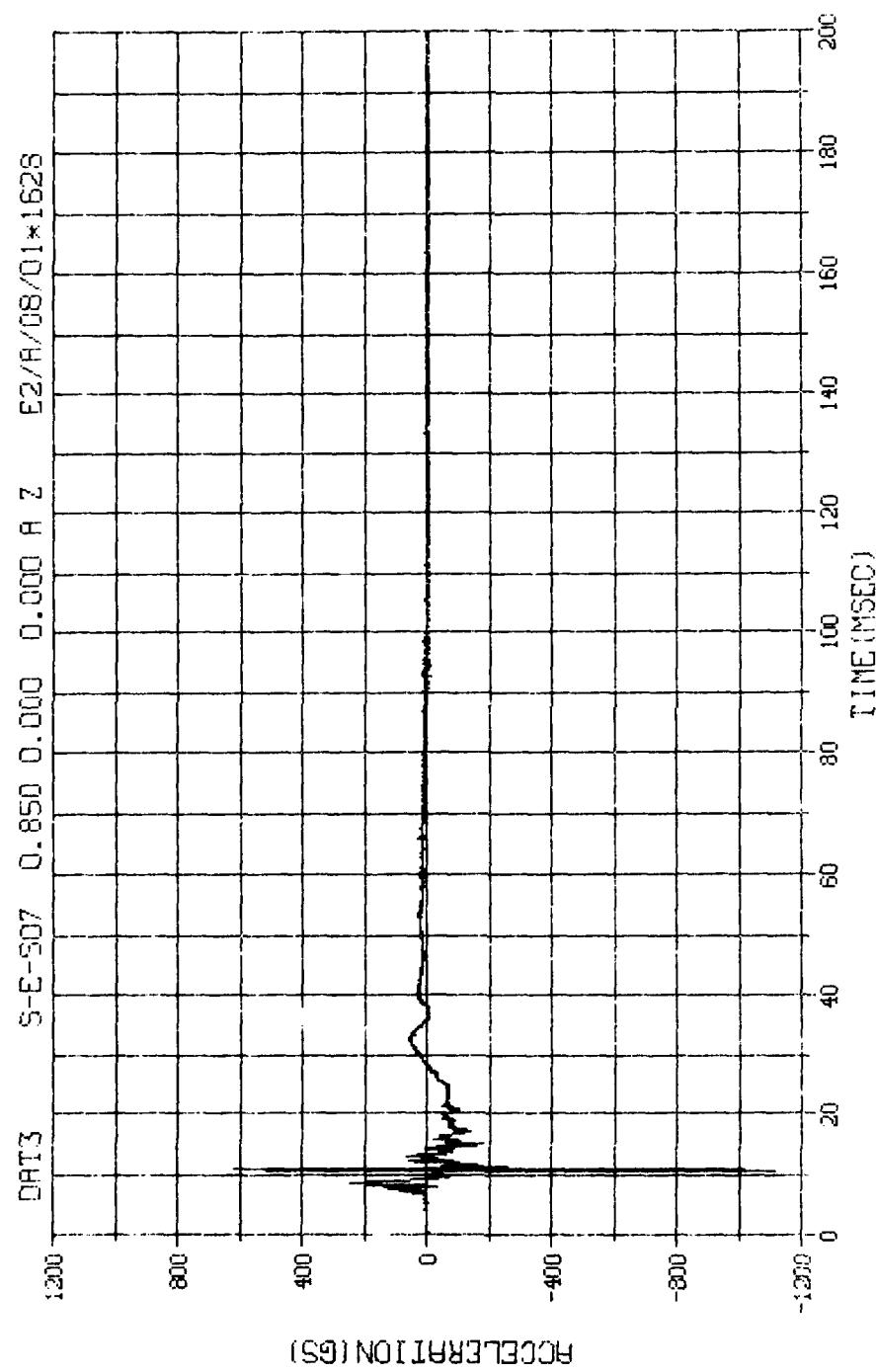


M.N. -S1626	E.U. -0.000,1000.000	VSN-FB76
TSKIP=7.000	DIGITS=0.000,876.625	TAPE22
S.R. =25.00 KHZ	25JUN83 12:17:16	FILE=D 2

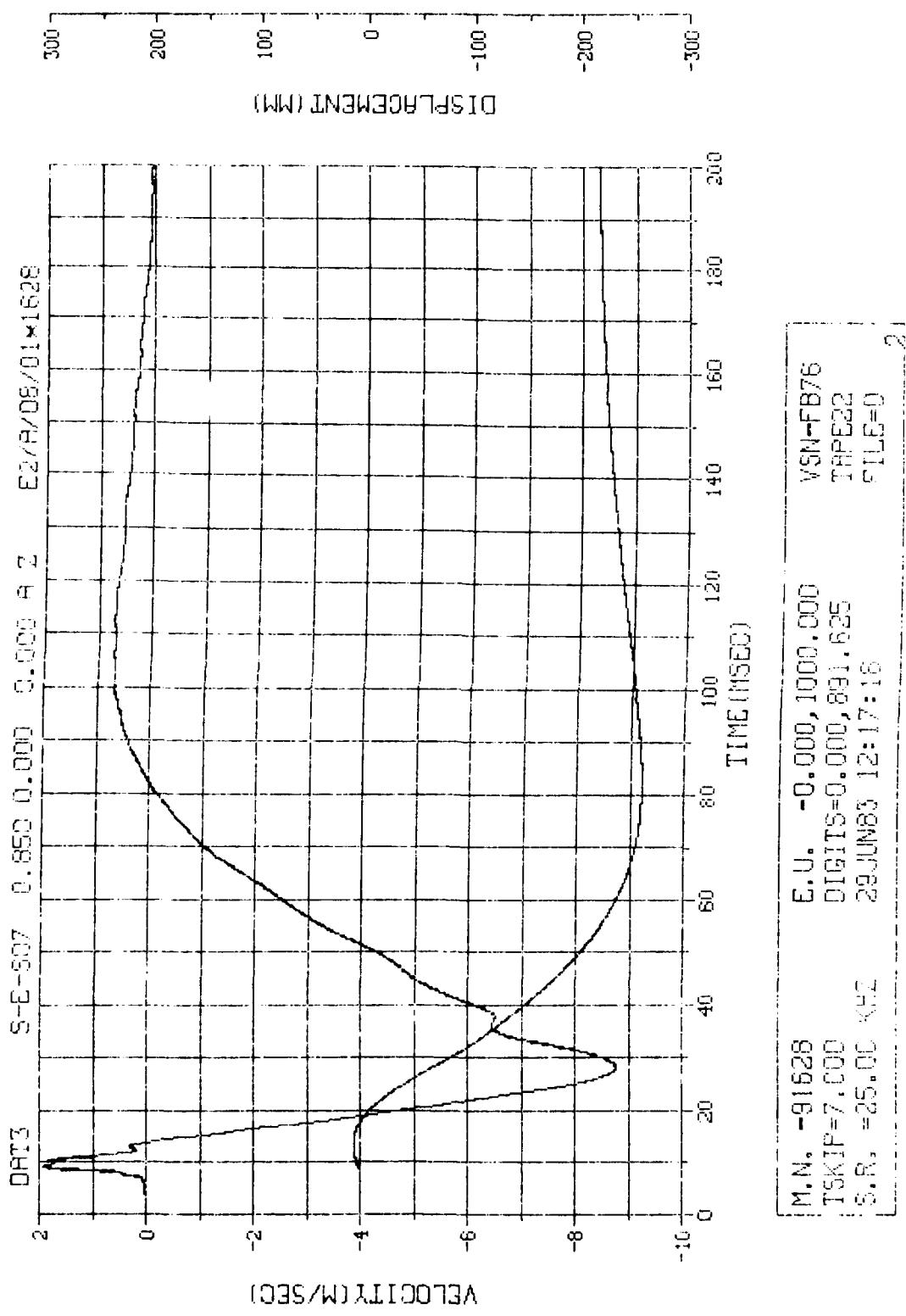


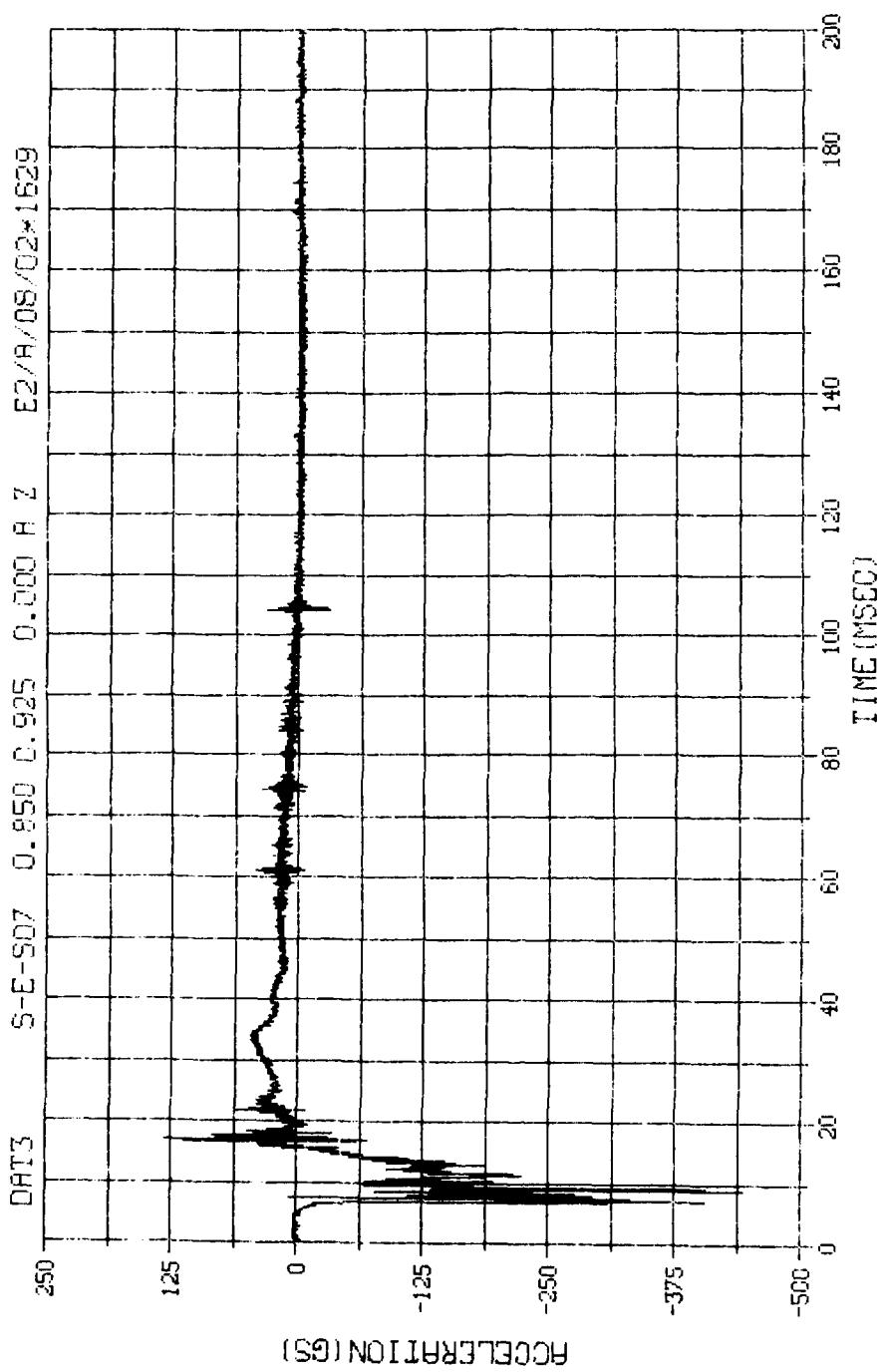
N.N. -91627	E.U. -0.000,1000.000	VSN-F875
TSKIP=7.000	DIGITS=3.000,500,125	TAPE23
S.R. =25.00 kHz	29-JUN-83 12:17:16	FILE=0



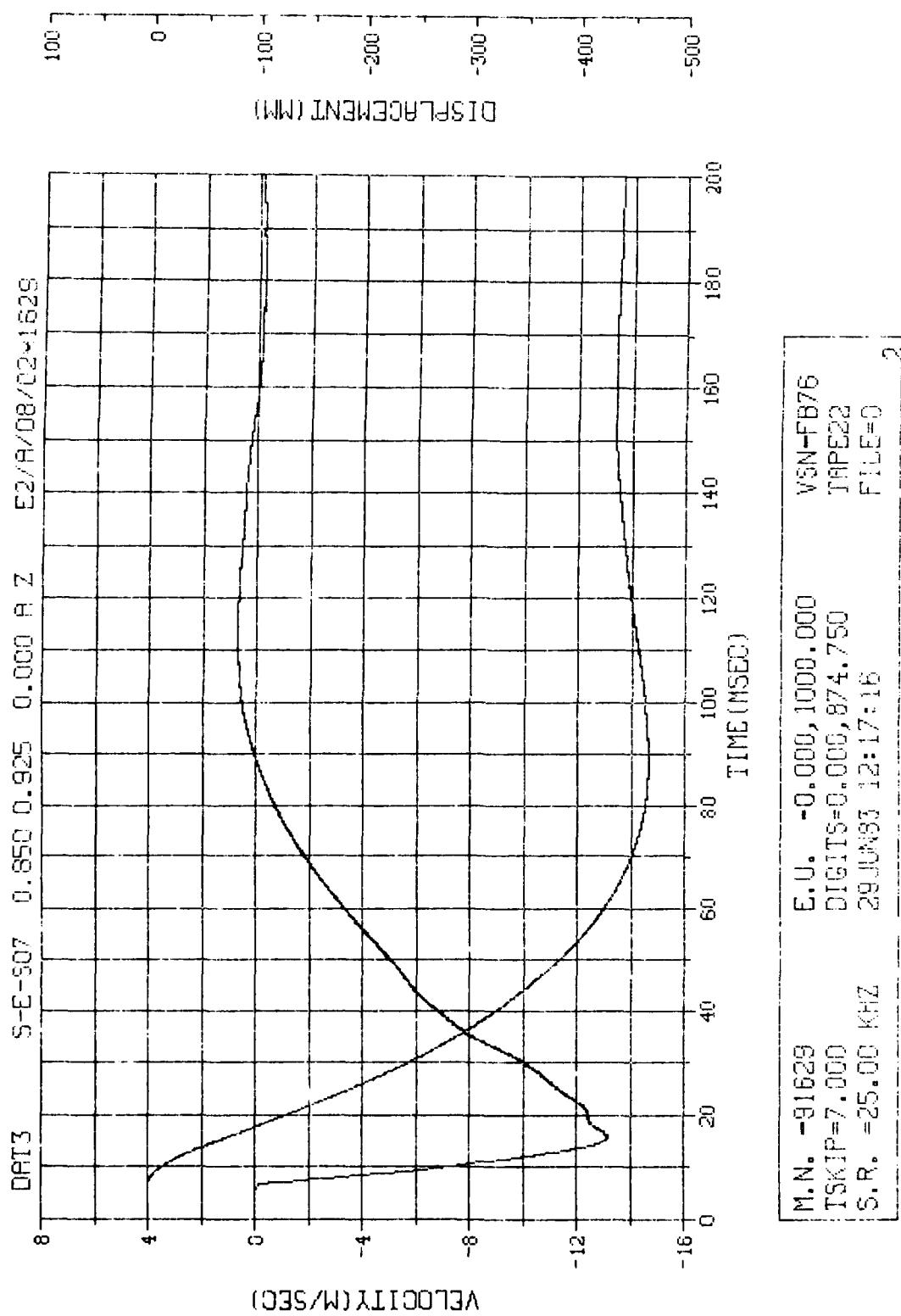


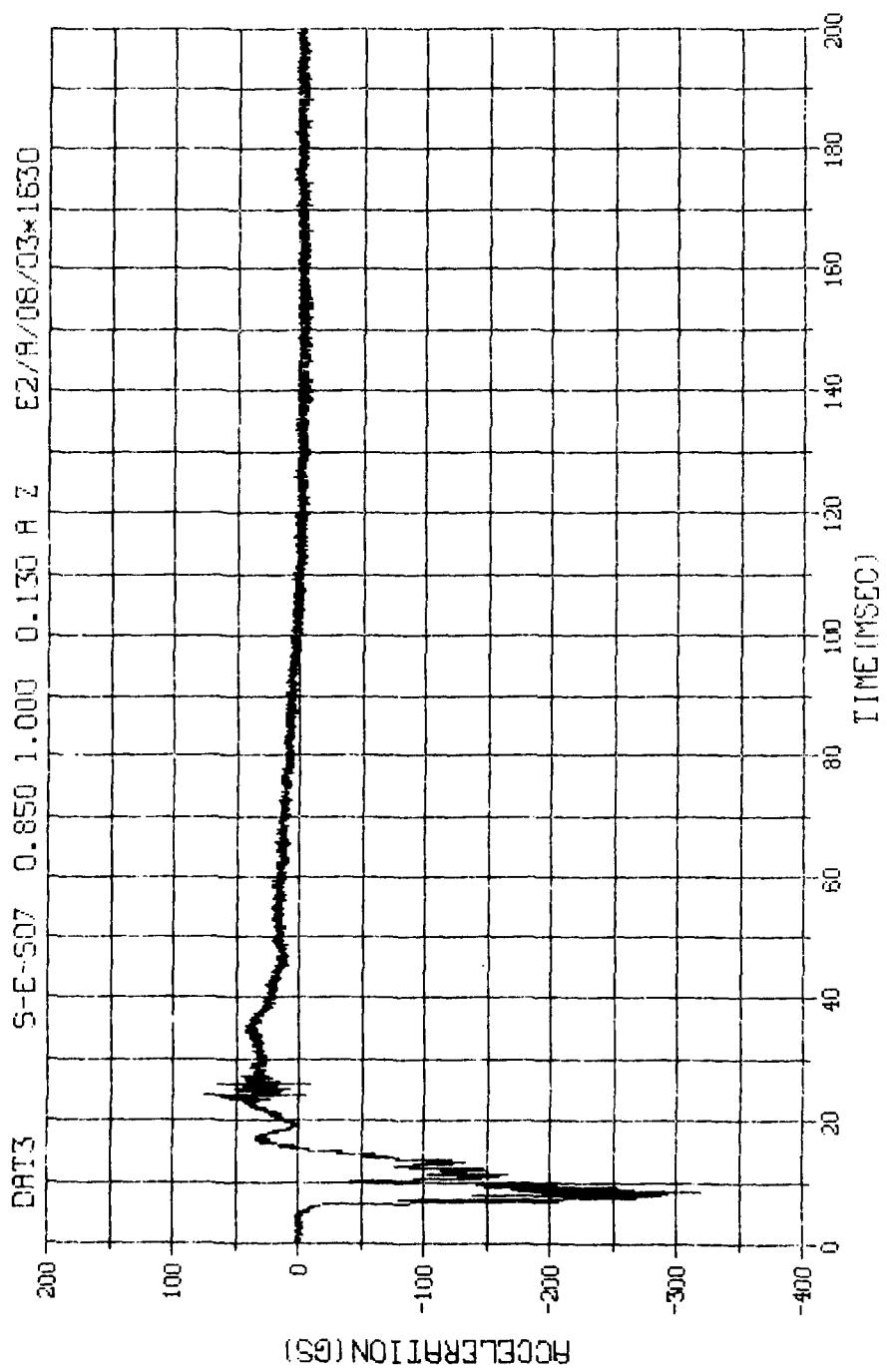
M.N. -91628	E.U. -0,000,1000,000	VSN-F876
SKIP=7,000	DIGITS=0,000,891,625	TAPE22
S.R. =25,00 KHZ	26-JUN-83 ; 2:17:15	FILE=0
1		



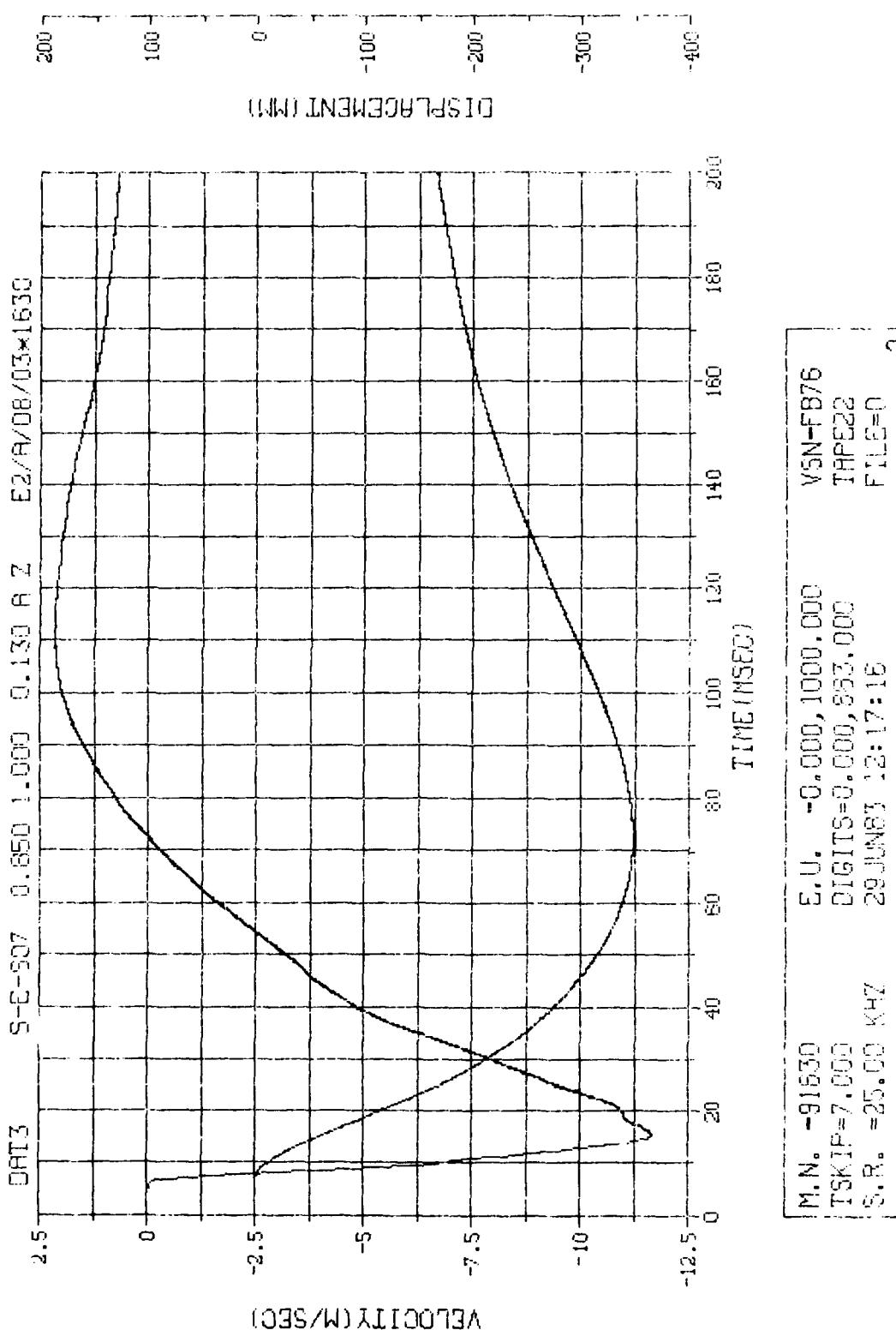


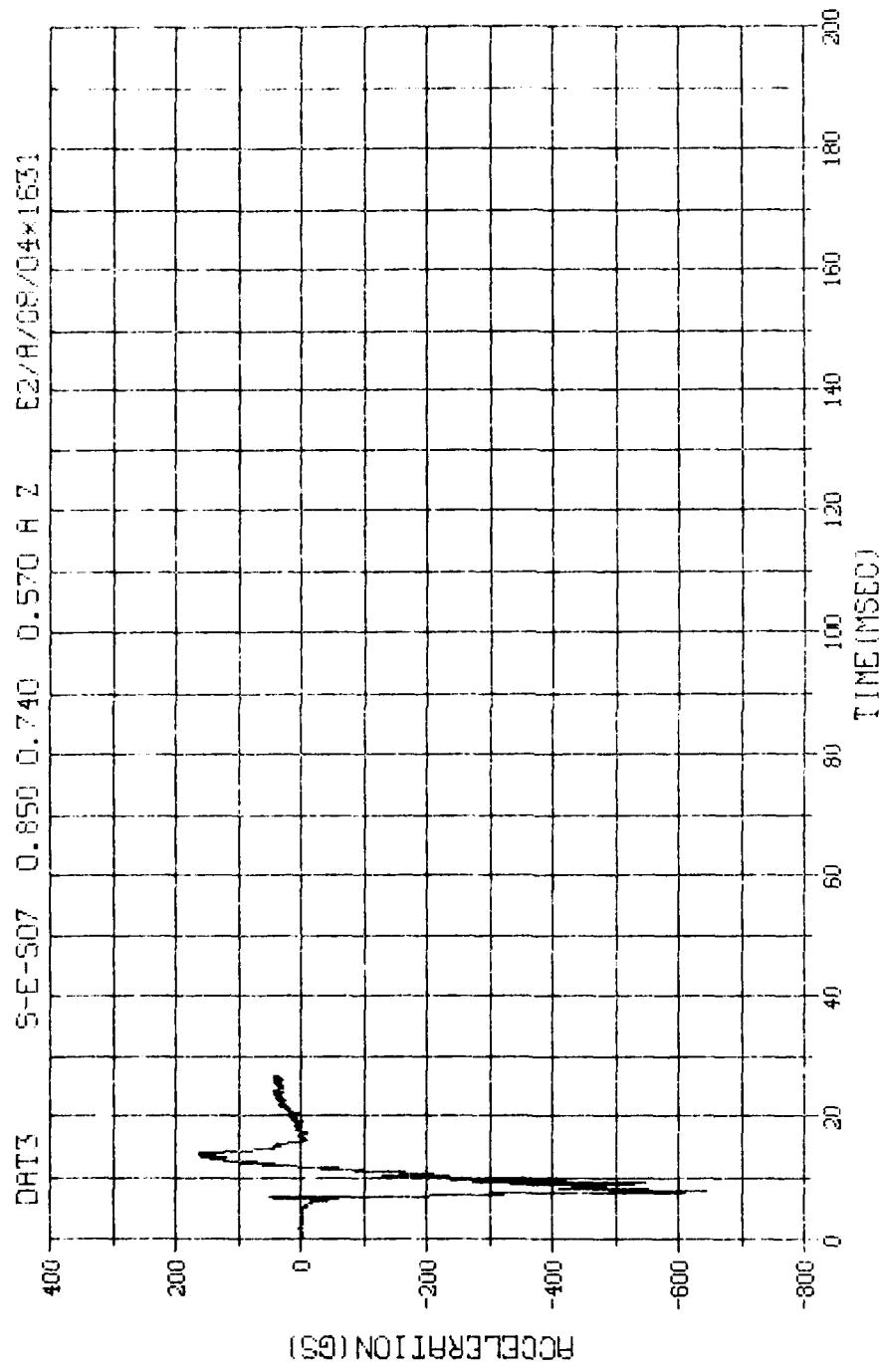
R.N.	-91629	E.U.	-0.000, 1000.000
TSKIP	=7.000	DIGITS	=0.000, 874.750
S.R.	125.00 KHZ	TAPE22	
		FILE=0	1



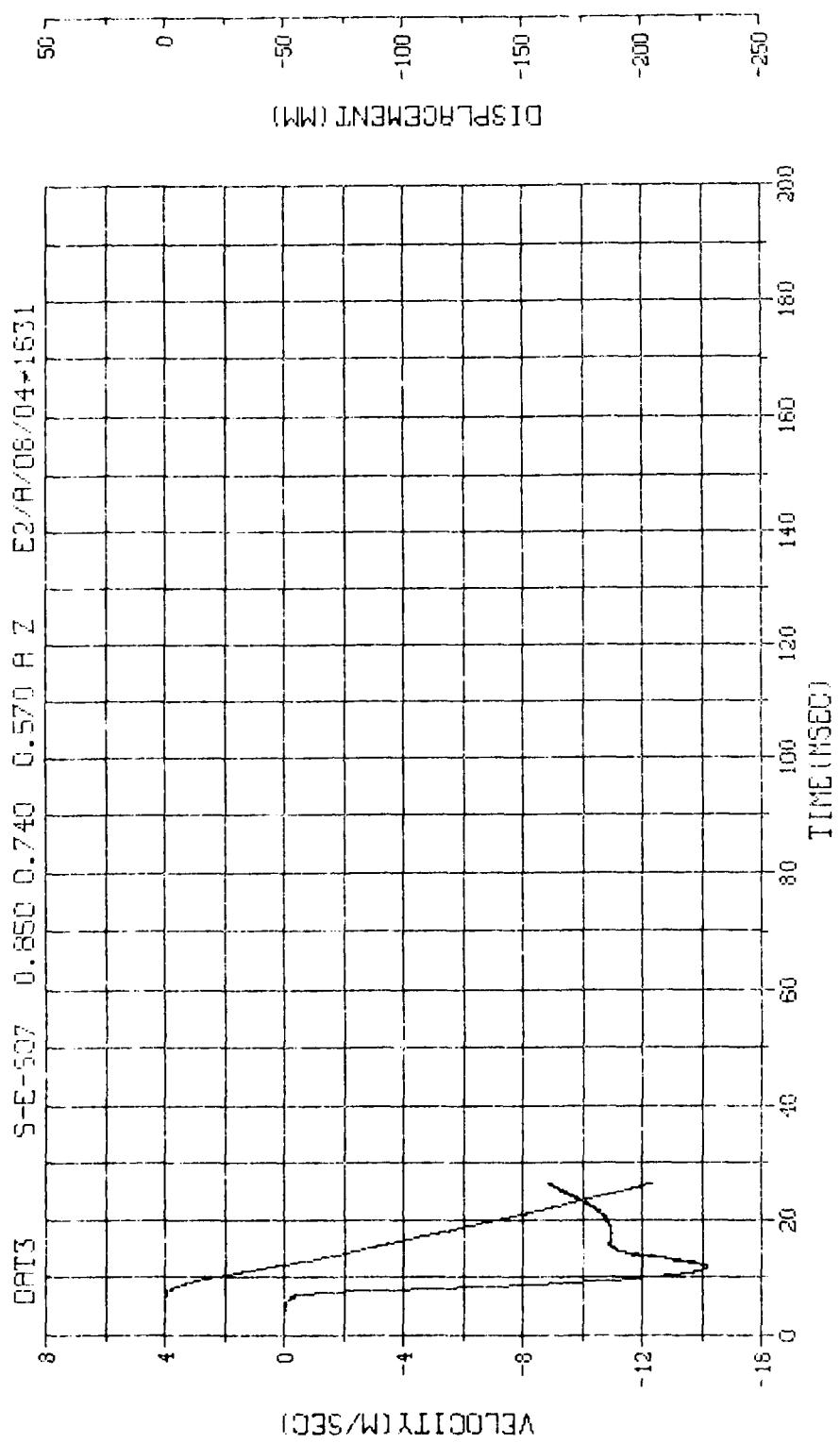


M.N. -91630	E.U. -0.000,1000.000	VSN-FB75
TSKIP=7.000	DIGITS=0.000,883.000	TRPES22
S.R. =25.00 KHZ	29 JUN 83 12:17:16	FILF=0

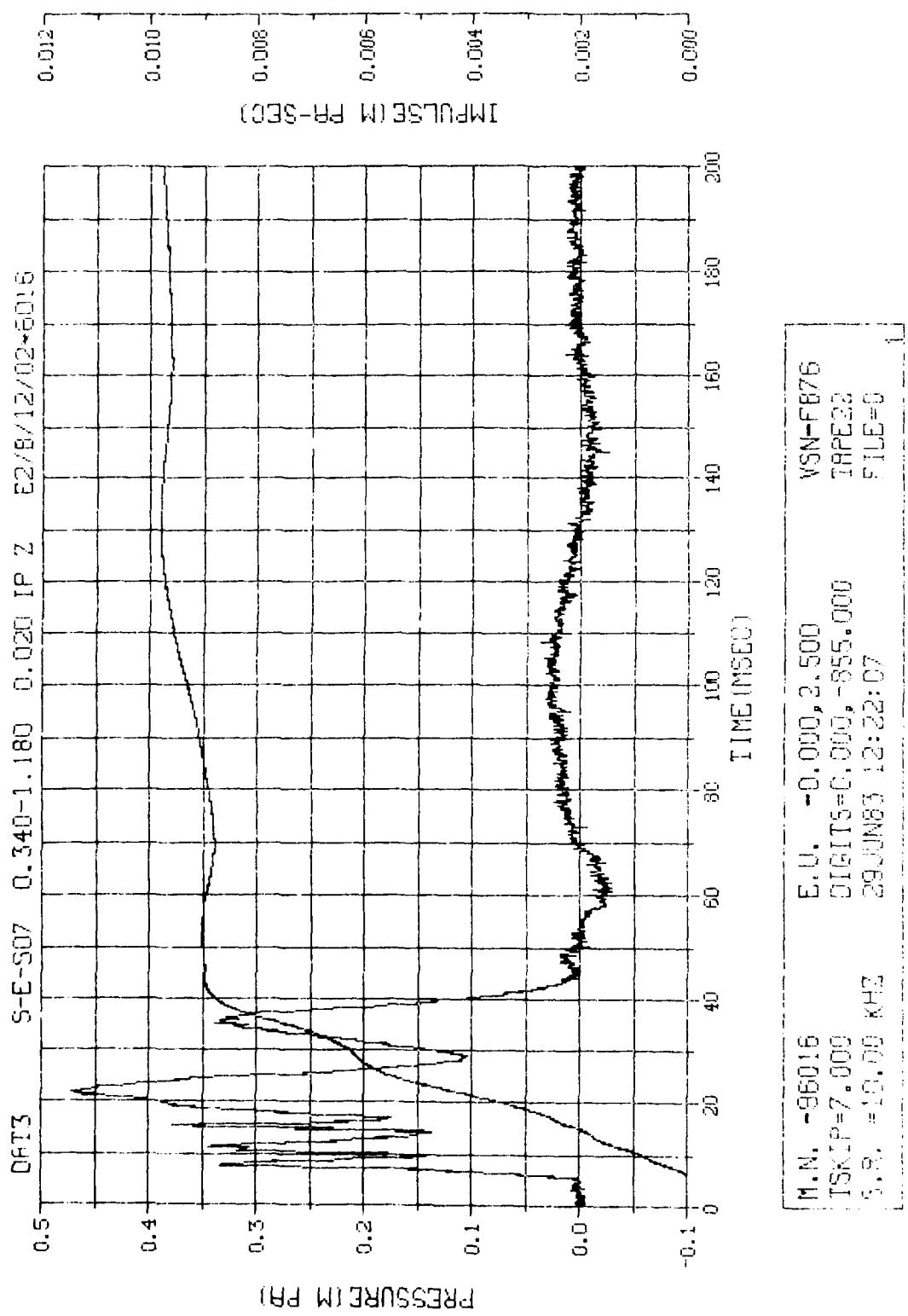




H.N. -71631	E.U. -0.000,1000.000	VSN-FB76
TSKIP=7.000	DISLT5=0.000,875.250	TRPC22
S.R. =25.00 KHZ	29.JUN.63 12:17:16	FILE=0
		1



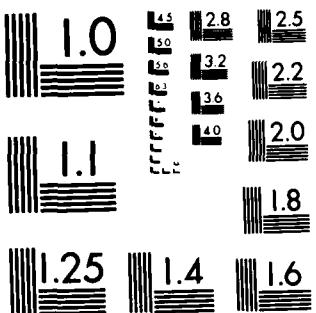
M.N. -71631	E.U. "0.000, 1000.000	WSN-FB76
TSKIP=7.000	DIGITS=0.000, 876, 250	TYPE22
S.R. =25.00 KHZ	28-JAN-83 12:17:16	FILE=0
		2



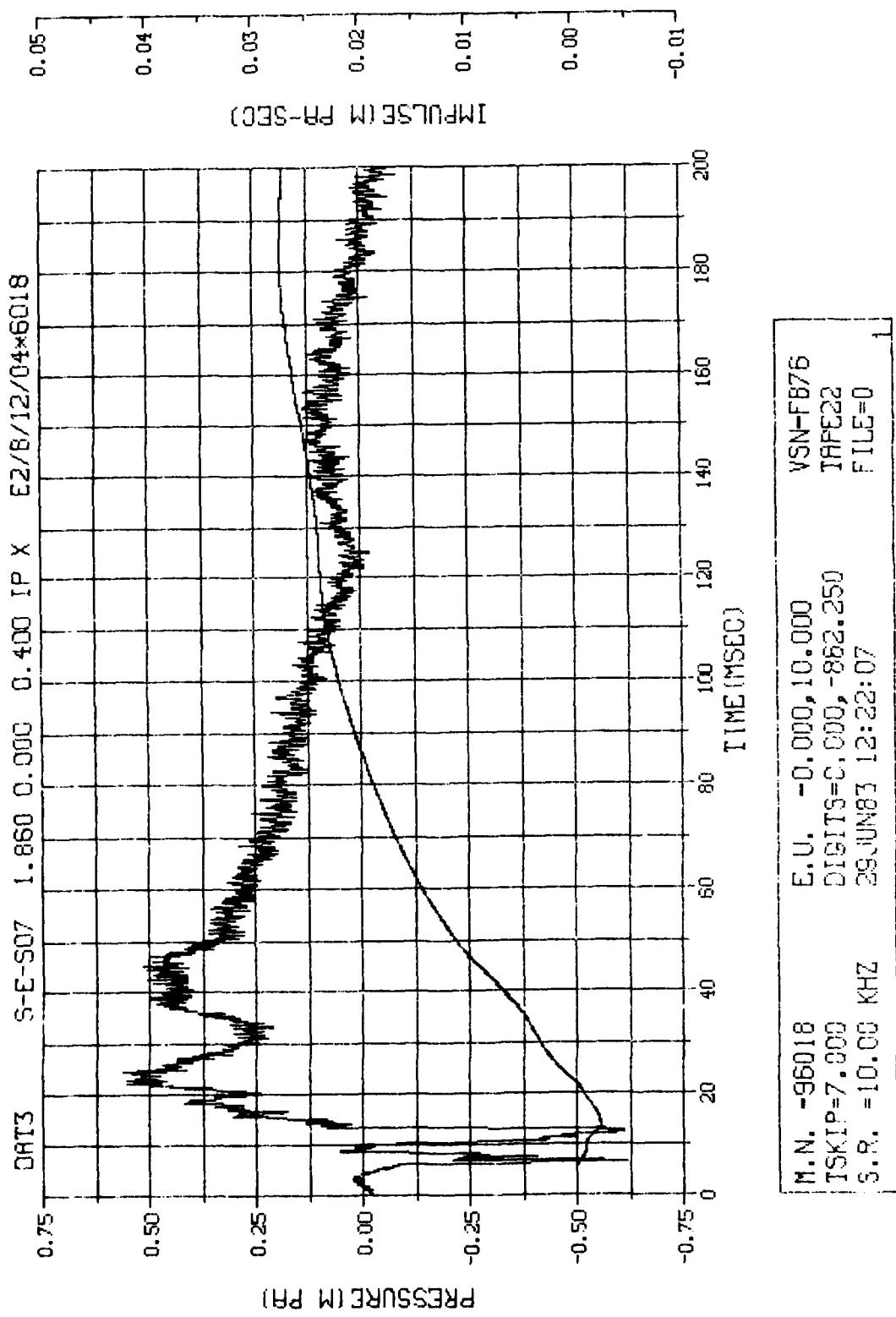
AD-A171 212 KACHINA TEST SERIES: DYNAMIC ARCH TEST THREE (DAT-3) 6/6
ANALYSIS REPORT (U) AIR FORCE WEAPONS LAB KIRTLAND AFB
NM J L SMITH ET AL. MAR 86 AFWL-TR-85-63 F/G 19/4 NL

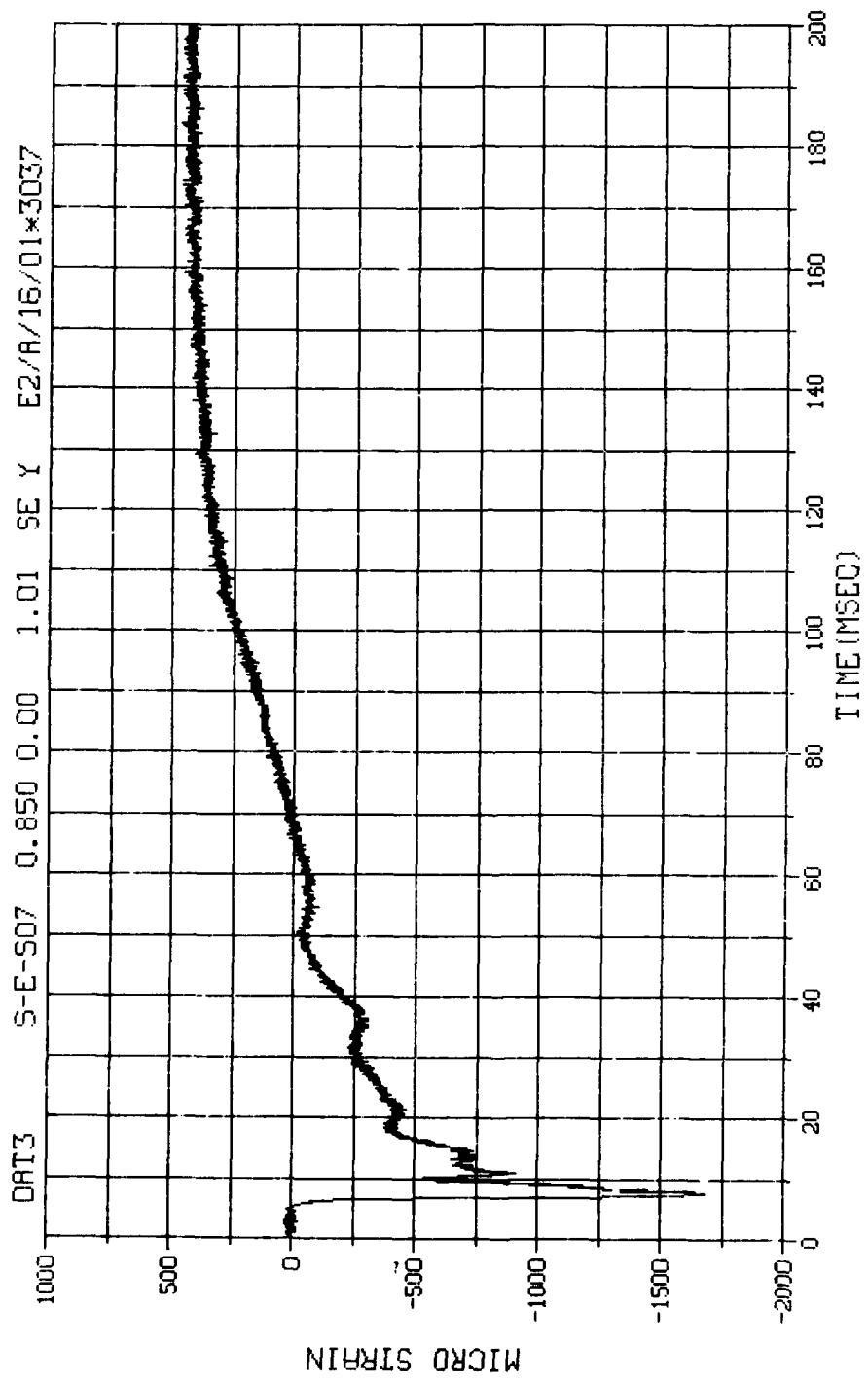
UNCLASSIFIED

END
DATE
PAGED
9 86

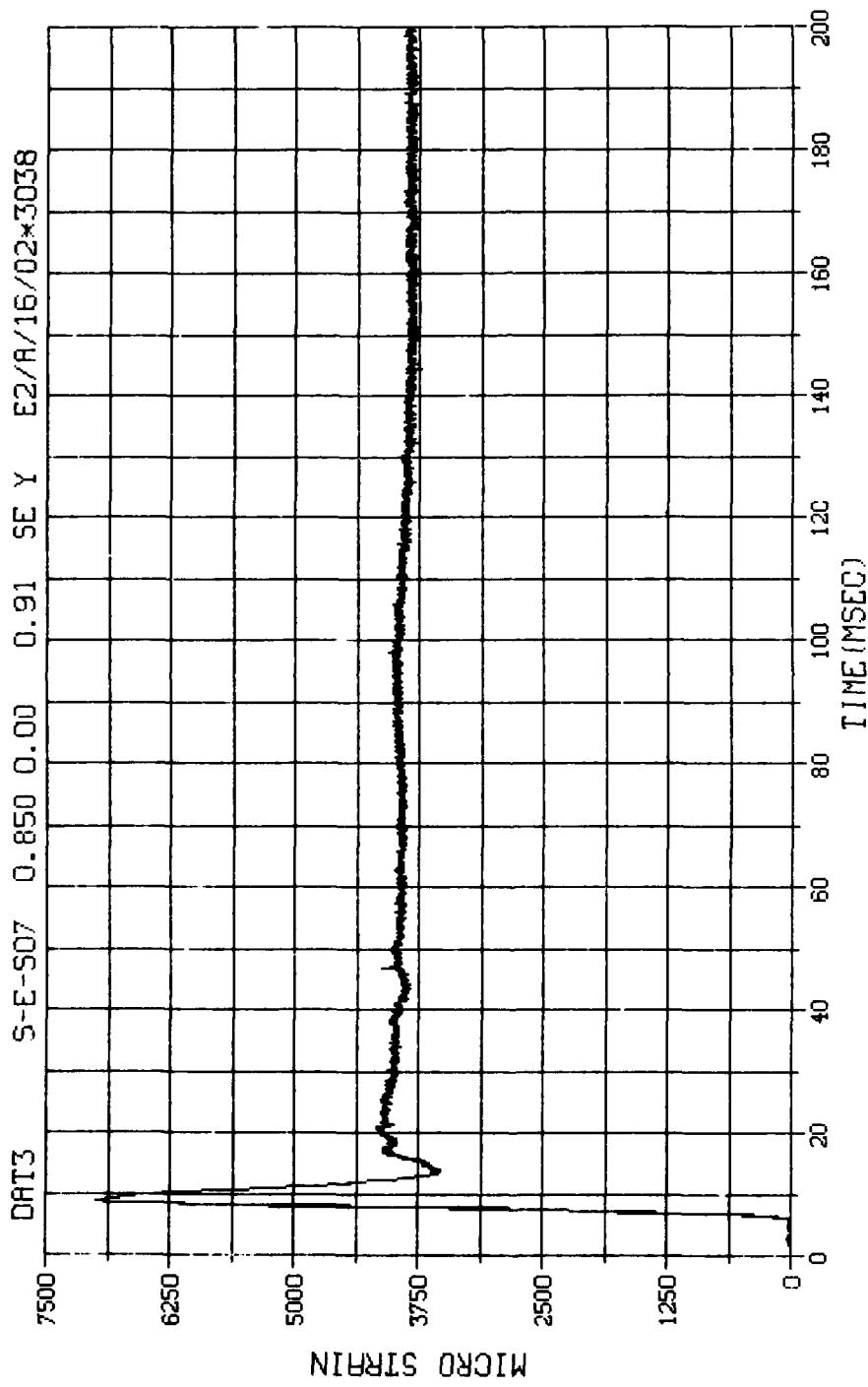


MICROCOPY RESOLUTION TEST CHART
NATIONAL BUREAU OF STANDARDS-1963-A

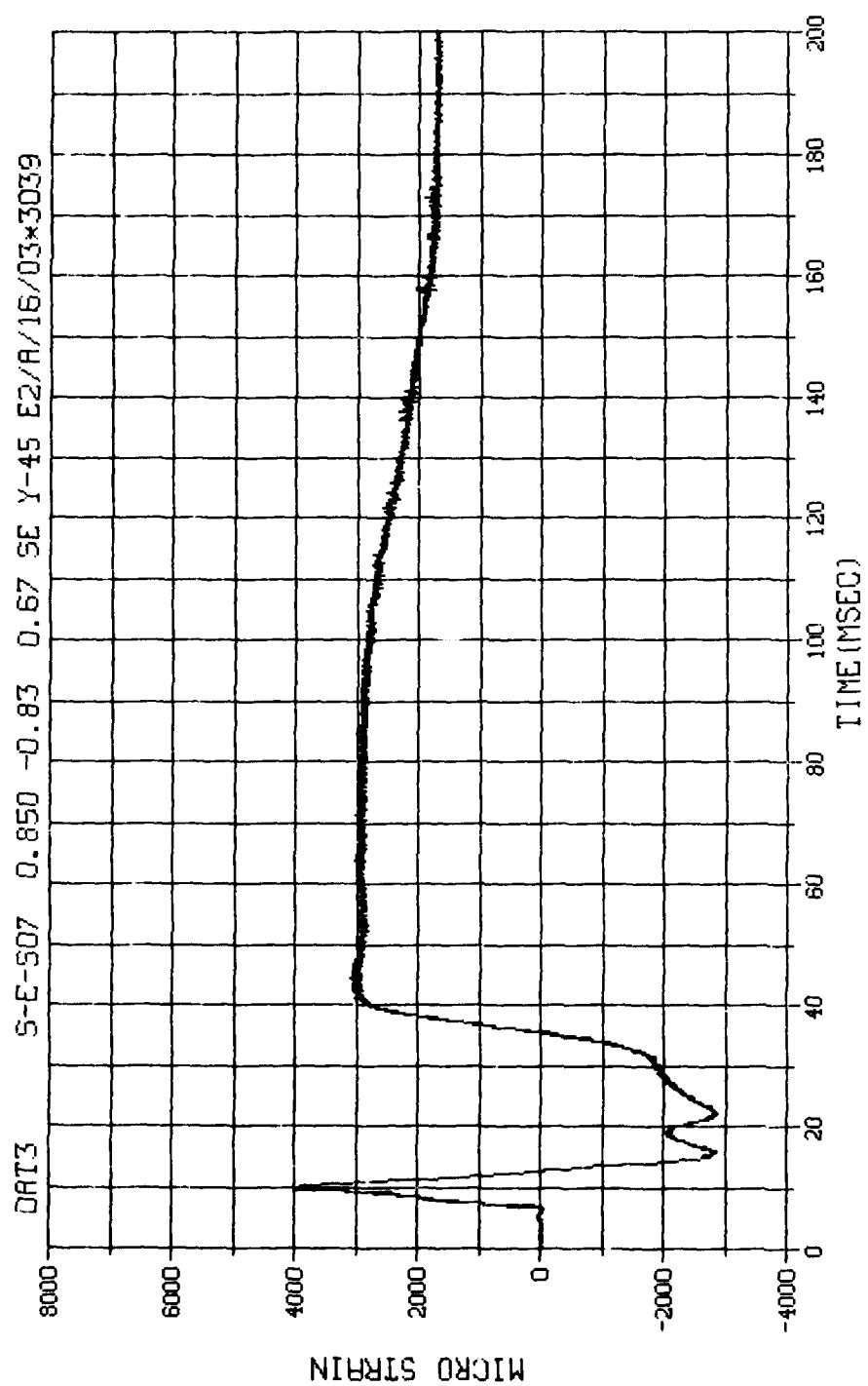




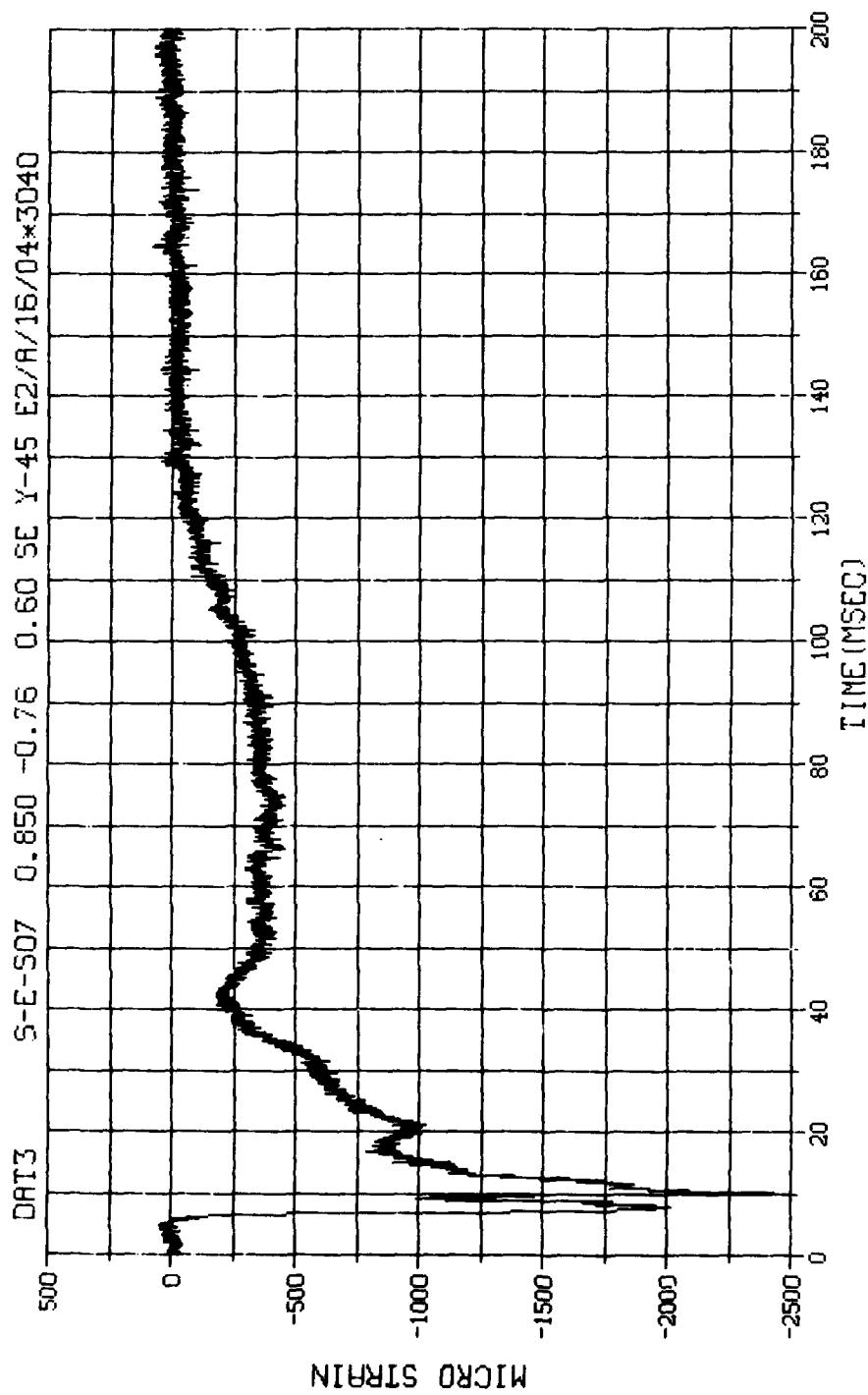
M.N. = 3037	E.U. = 0.000, 7500.000	VSN=60142
TSKIF=7.000	DIGITS=0.000, 887.000	TAPE22
S.R. =25.00 KHZ	4. 4 PM, TUE, 13 SEP 83.	FILE=216_1



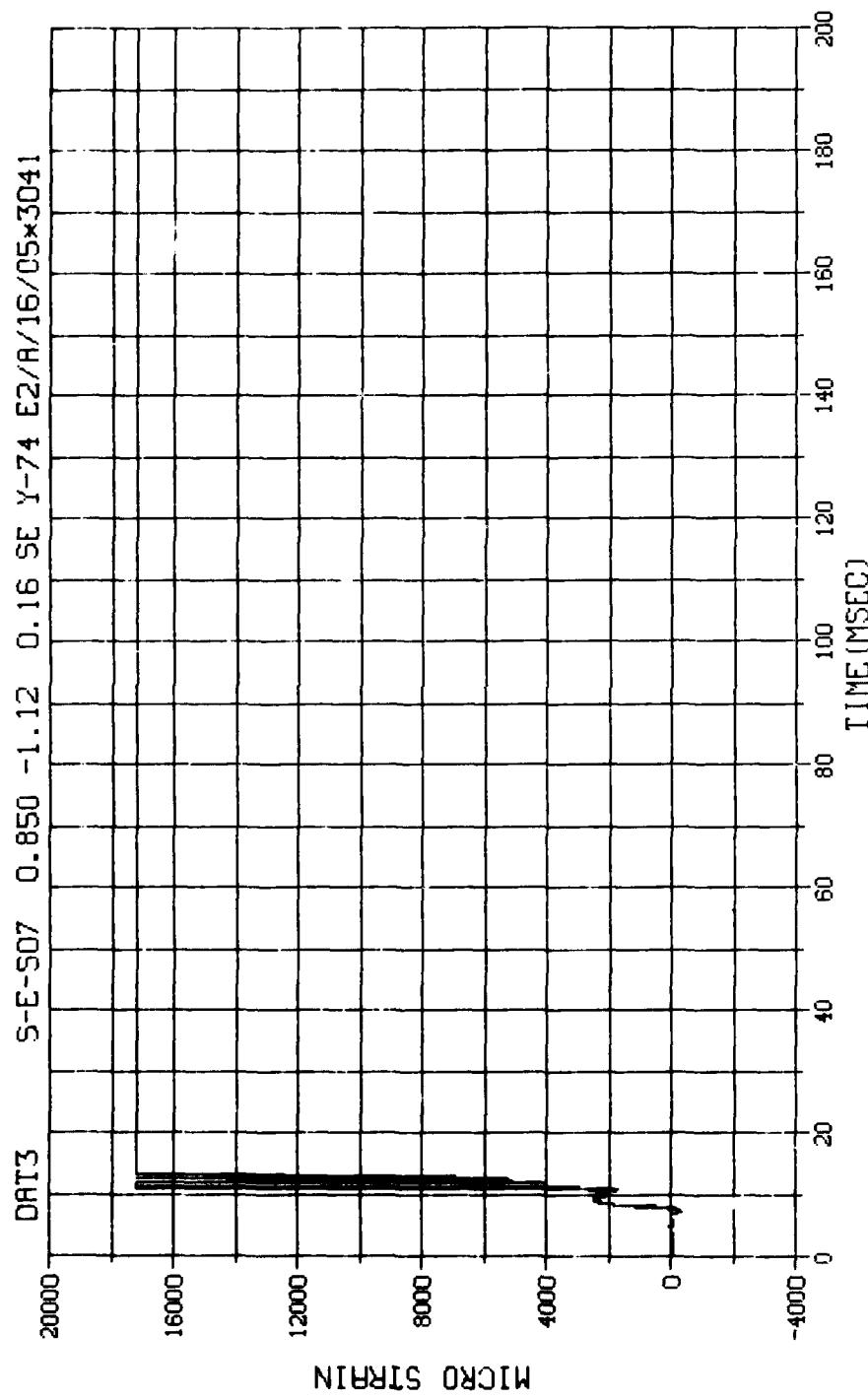
M.N. - 3038	E.U. -0.000,10000.000	VSN-00142
TSKIP=7.000	DIGITS=0.000,869.375	TAPE22
S.R. =25.00 KHZ	4. 4 PM, TUE, 13 SEP 83.	FILE=218



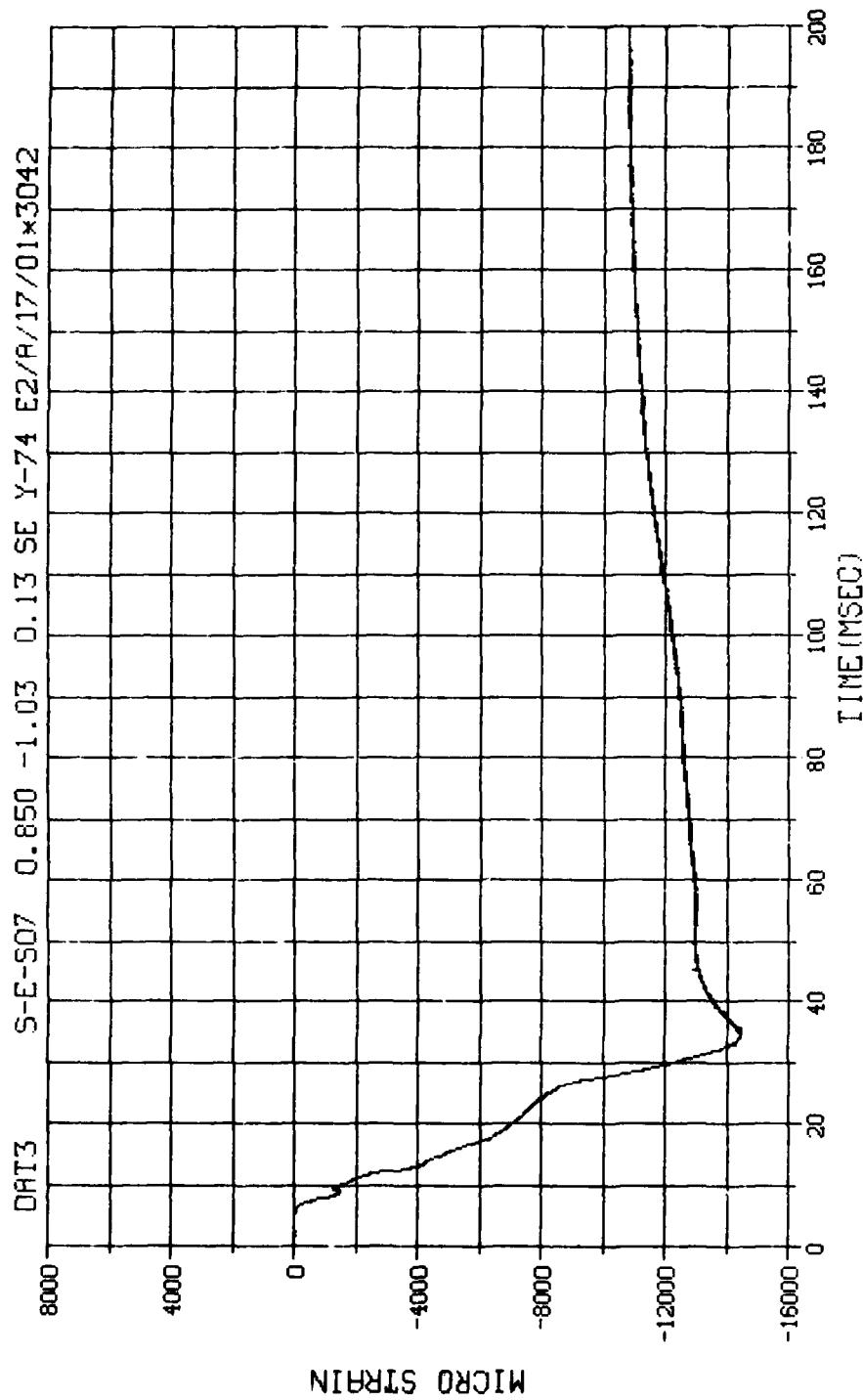
M.N. - 3039	E.U. -0.000,10000.000	VSN-GG142
TSKIP=7.000	DIGITS=0.000,881.500	TAPE22
S.R. =25.00 KHZ	4. 4 PM, TUE, 13 SEP 83.	FILE=220 1



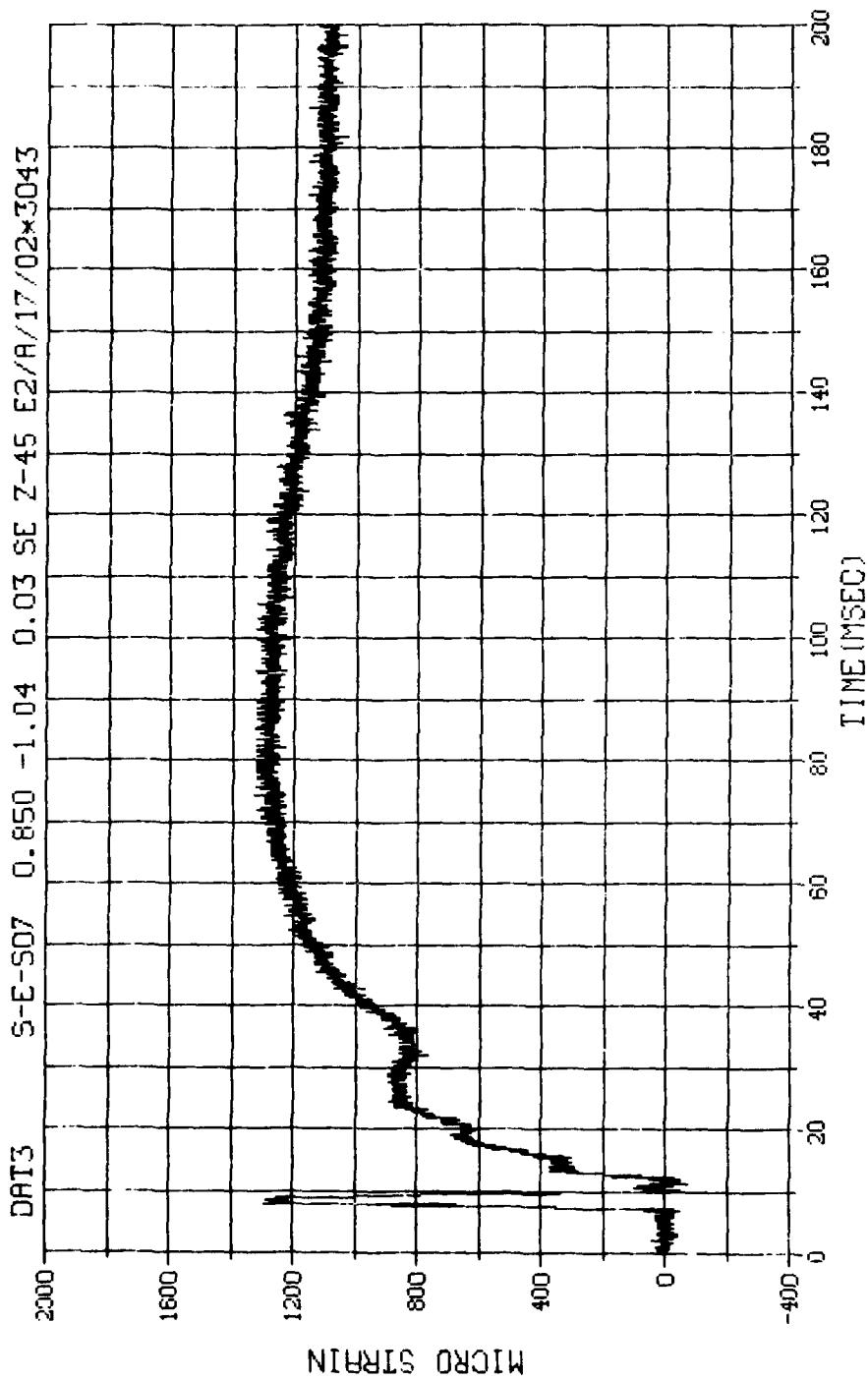
N.N. = 3040	E.U. = 0.000, 10000.000	VSN=06142
TSKIP=7.000	DIGITS=0.000, 871.375	TAPE22
S.R. =25.00 KHZ	4. 4 PM, TUE, 13 SEP 83.	FILE=222 1



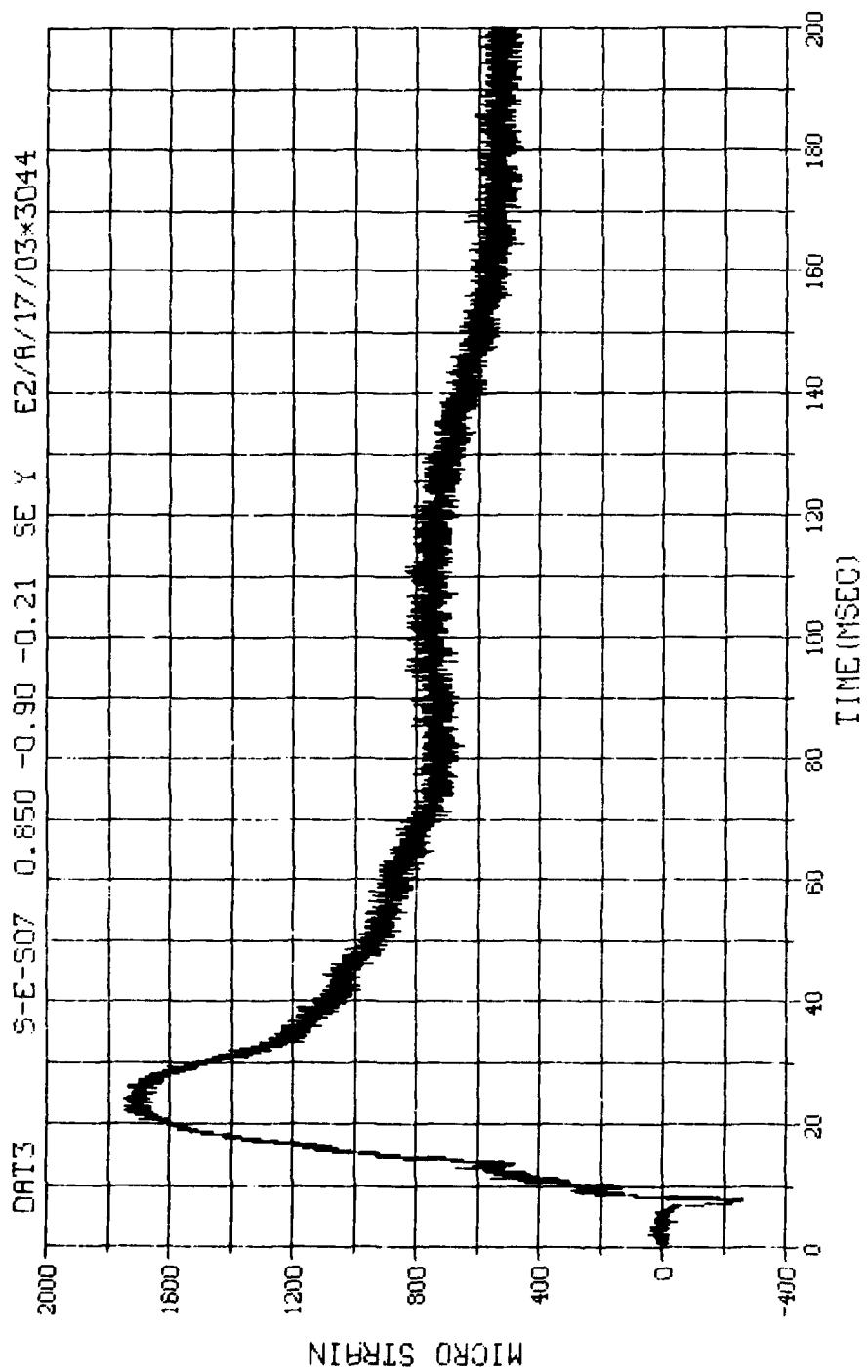
N.N. = 3041	E.U. = 0.000, 7500.000	VSN=06142
TSKIP=7.000	DIGITS=0.000, 901.000	TAPE22
S.R. =25.00 KHZ	4. 4 PM, TUE, 13 SEP 83.	FILE=224 1



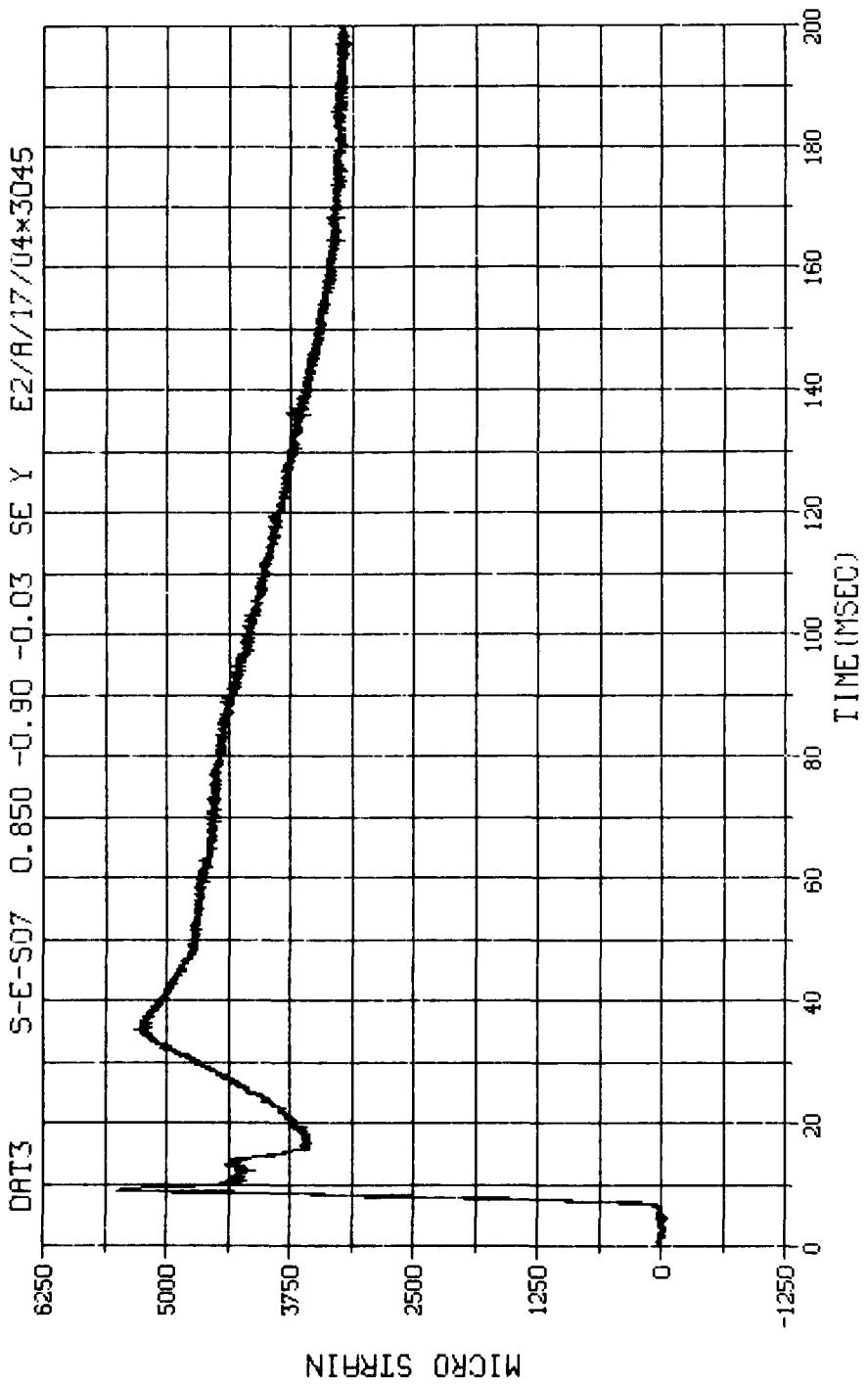
N.N. = 3042	E.U. = 0.000, 7500.000	VSN=60142
SKIP=7.000	DIGIT3=0.000, 881.250	TAPE22
S.R. =25.00 KHZ	4. 4 PM, TUE, 13 SEP 83.	FILE=226 1



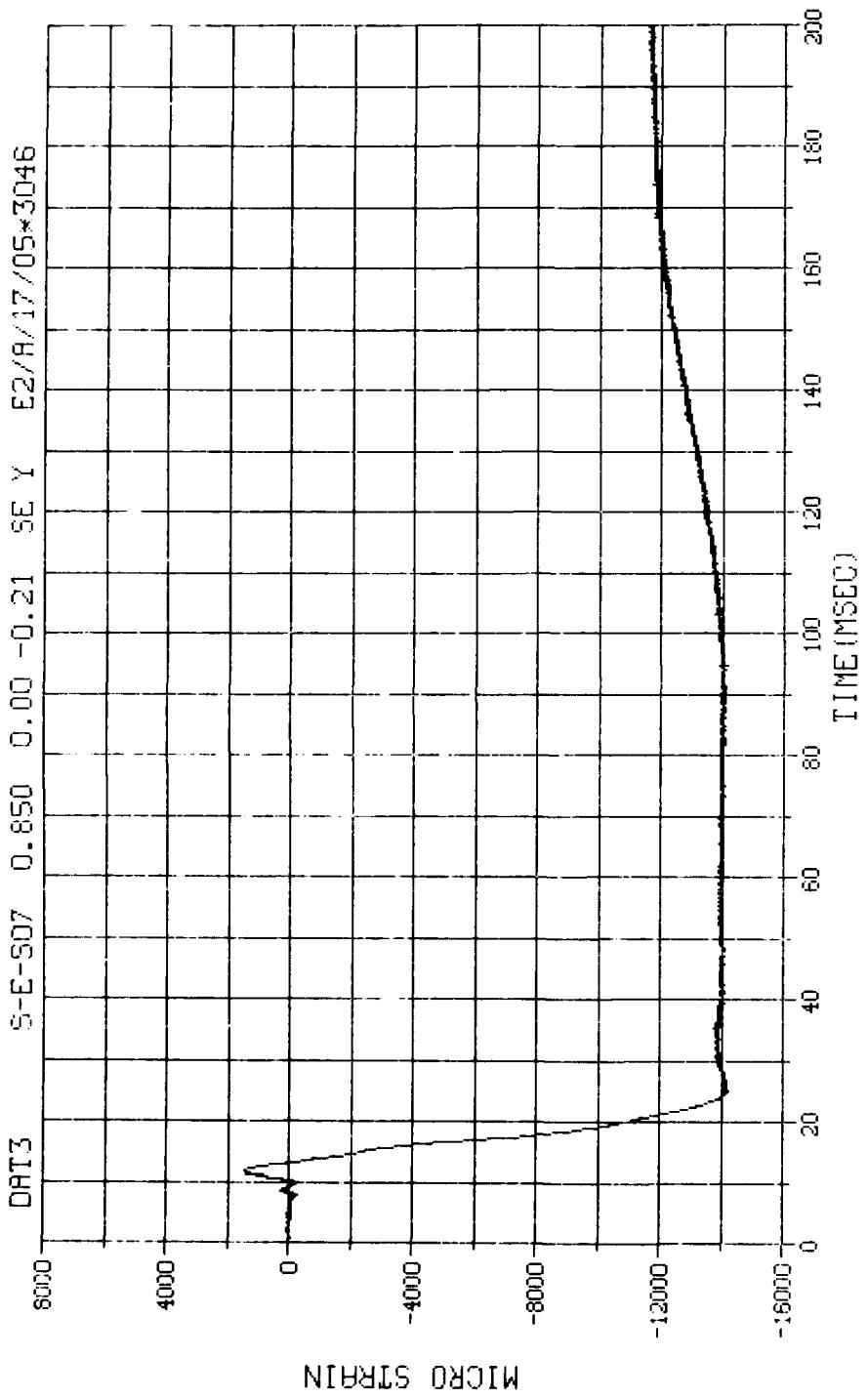
N.N. = 3043	E.U. = 0.000, 10000.000	VSN=66142
SKIP=7.000	DIGITS=0.000, 869.875	TAPE22
S.R. =25.00 KHZ	4. 4 PM, TUE, 13 SEP 83.	FILE=228 1



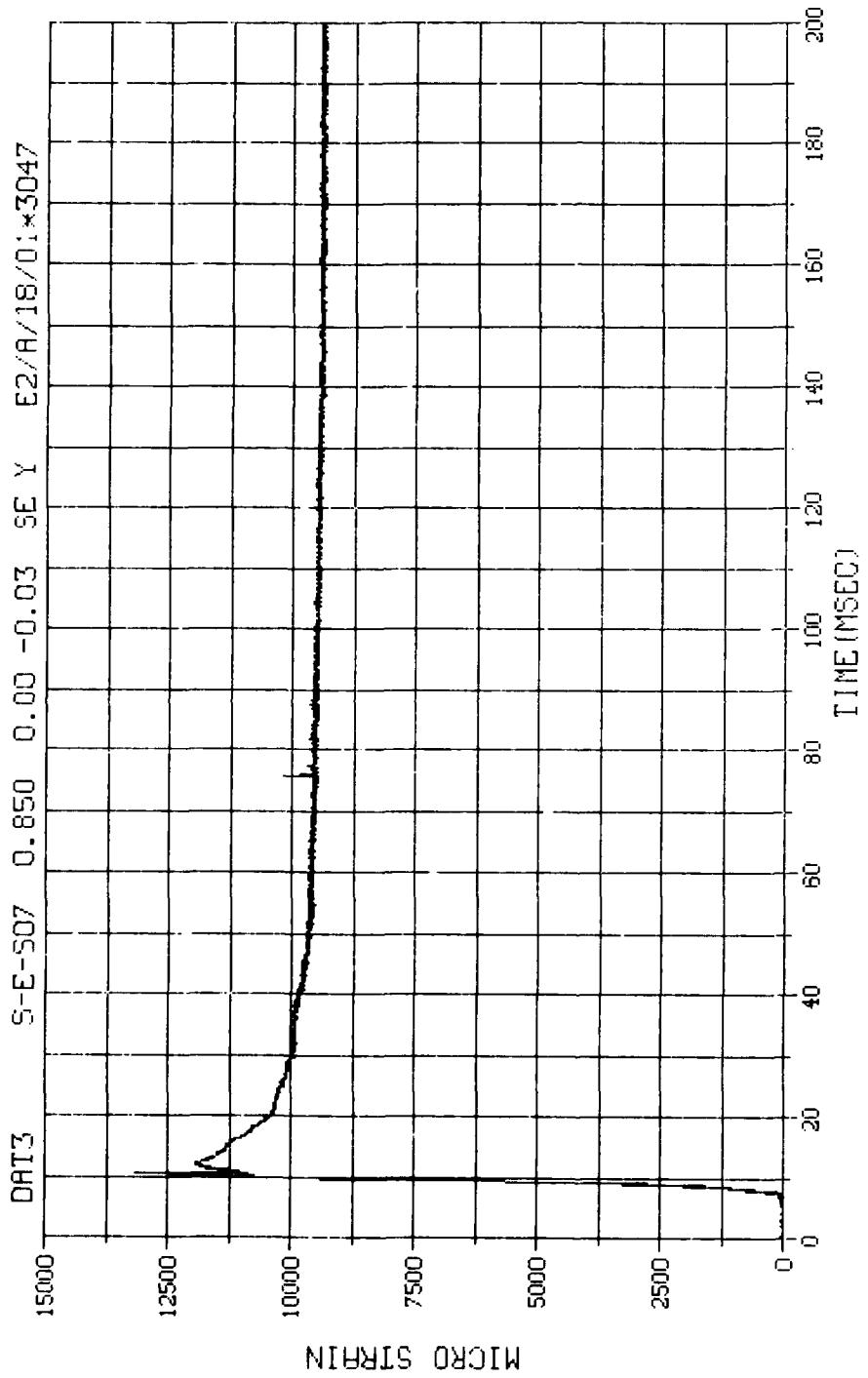
N.N. = 3044	E.U. = 0.000, 10000.000	VSN=66142
TSKIP=7.000	DIGITS=0.000, 882.500	TAPE22
S.R. = 25.00 KHZ	4. 4 PM, TUE, 13 SEP 83,	FILE=23D 1



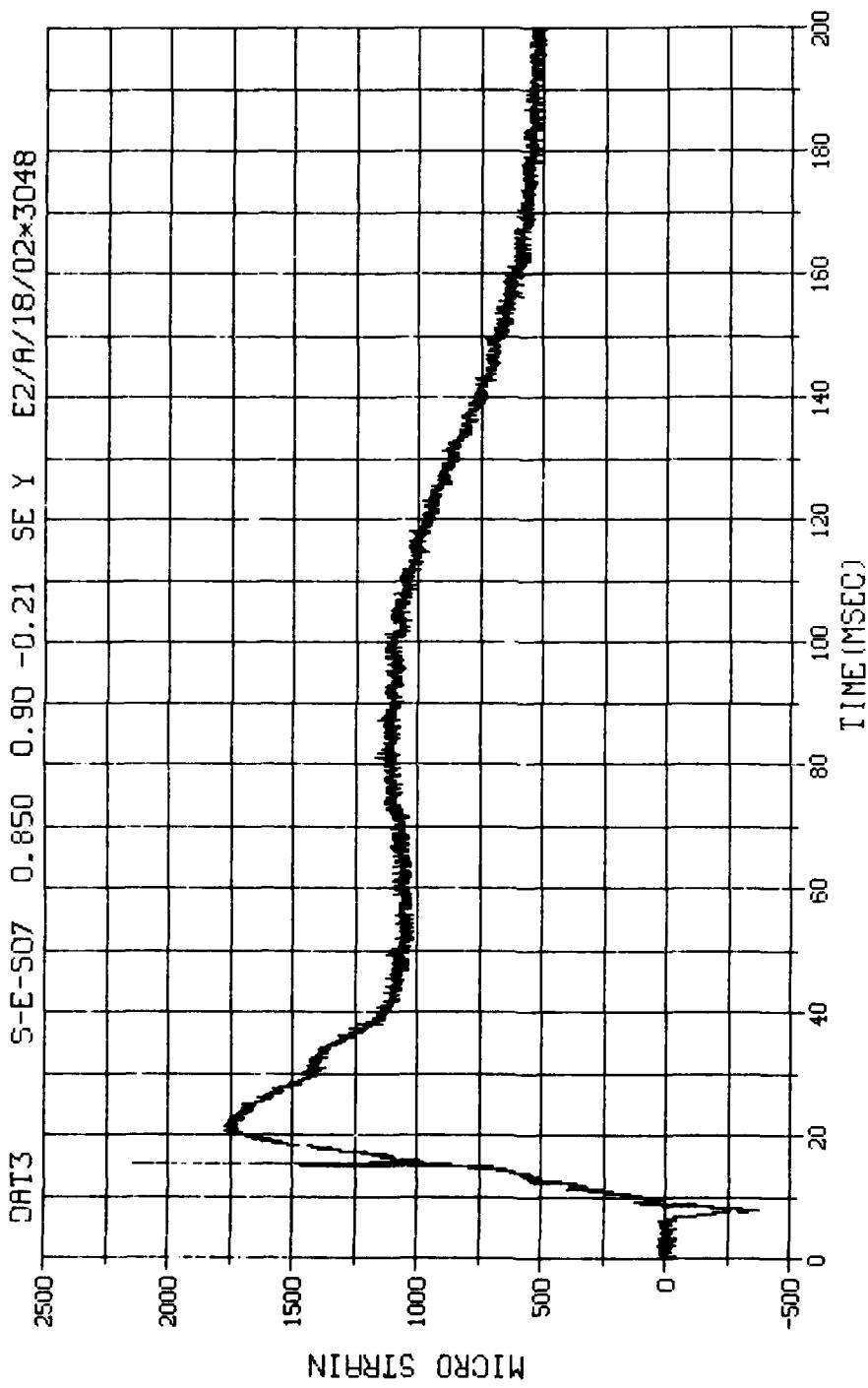
N.N. = 3045	E.U. =0.000,10000.000	VSN=66142
SKIP=7.000	DIGITS=0.000,868.875	TAPE22
S.R. =25.00 KHZ	4. 4 PM, TUE, 13 SEP 83.	FILE=232 1



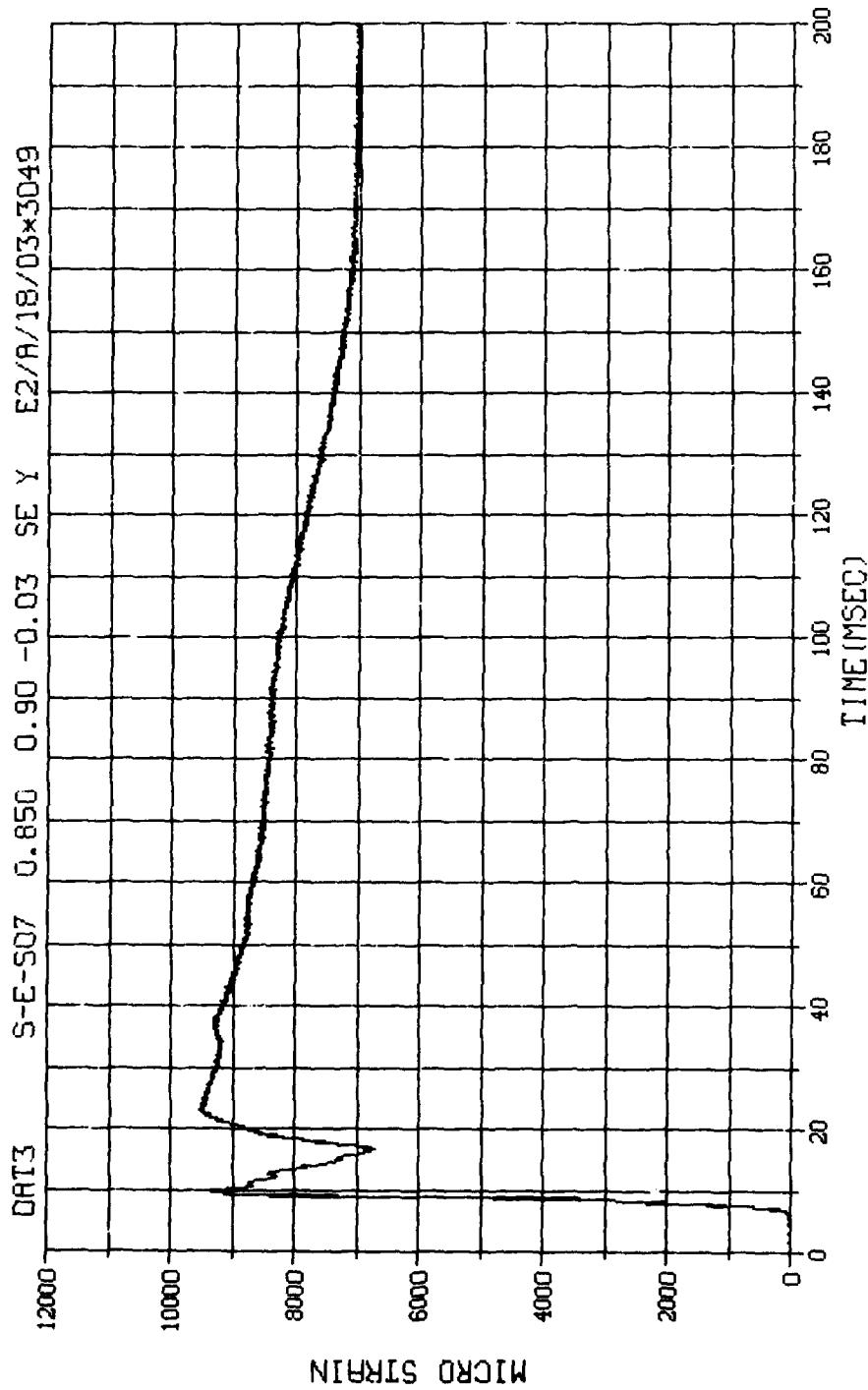
N.N. = 3046	E.U. = 0.000,10000.000	VSN=00142
SKIP=7.000	DIGITS=0.000,894.750	TAPE22
S.R. =25.00 KHZ	4. 4 PM, TUE, 13 SEP 83,	FILE=234 1



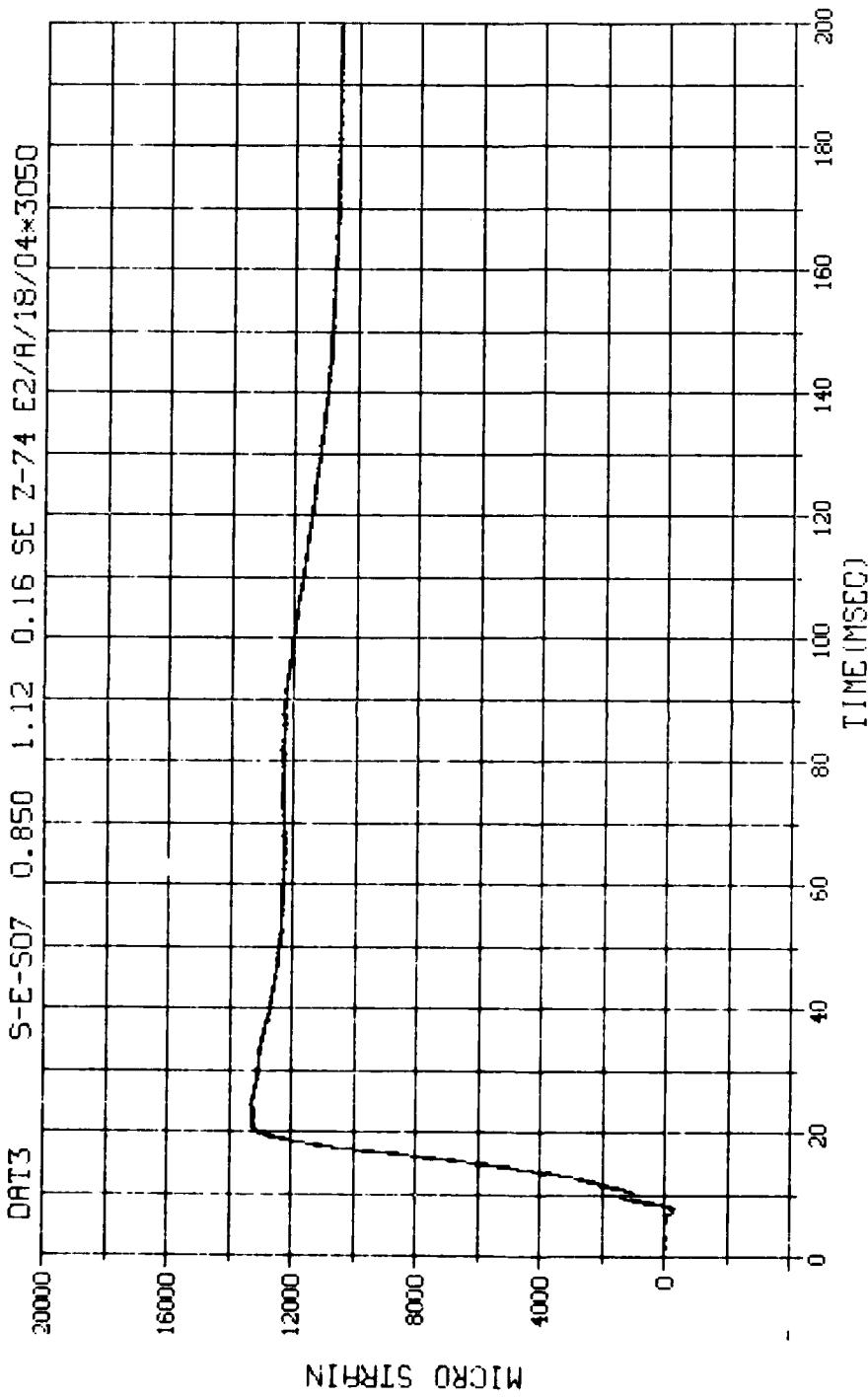
M.N. = 3047	E.U. = 0.000, 15000.000	VSN-06142
TSKIP=7.000	DIGITS=0.000, 891.875	TAPE22
S.R. =25.00 KHZ	4. 4 PM, TUE, 13 SEP 83.	FILE=236



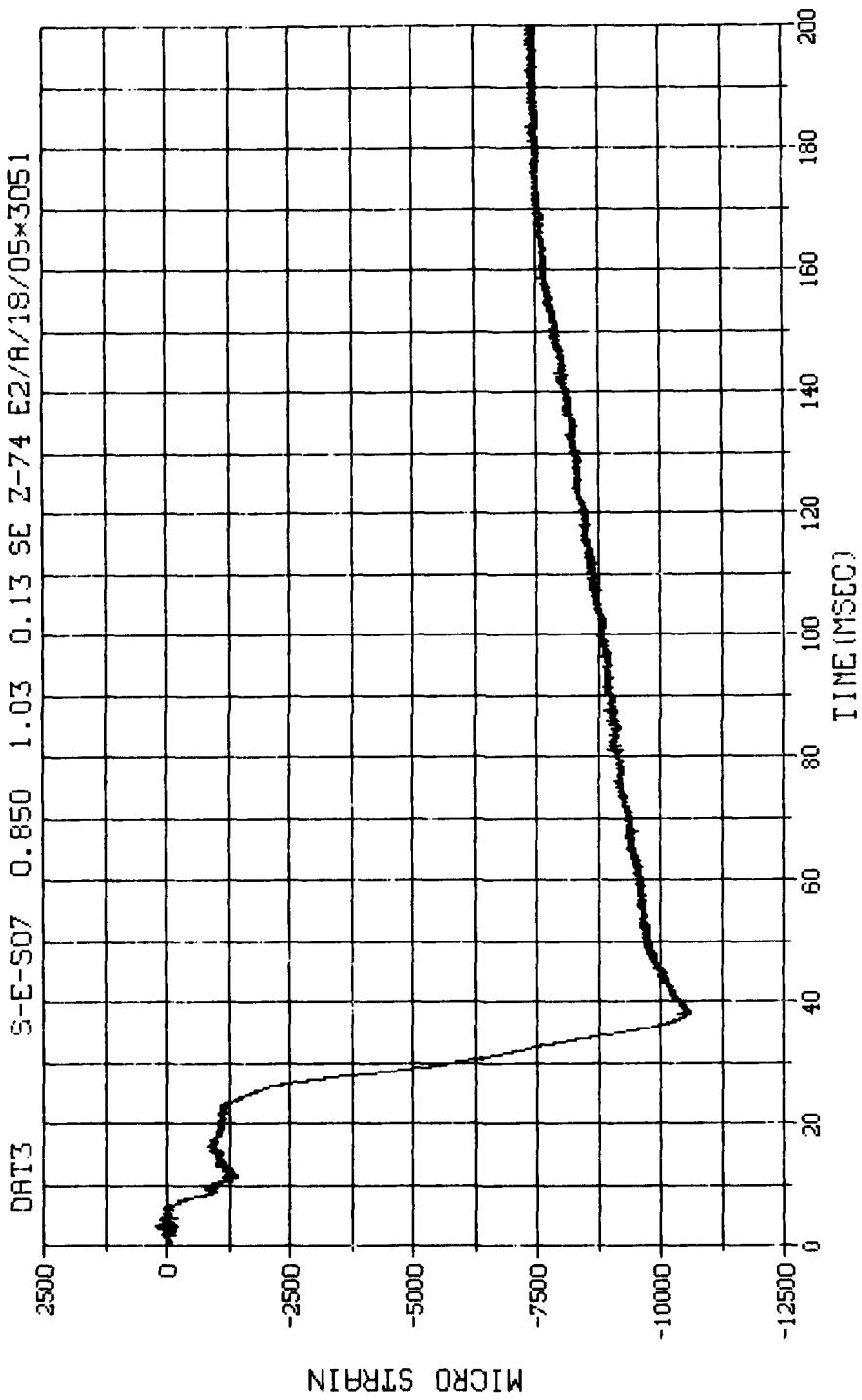
N.N. = 3048	E.U. = 0.000, 10000.000	VSN=GG142
TSKIP=7.000	DIGITS=0.000, 870.750	TAPE22
S.R. =25.00 KHZ	4. 4 PM, TUE, 13 SEP 83.	FILE=238 1



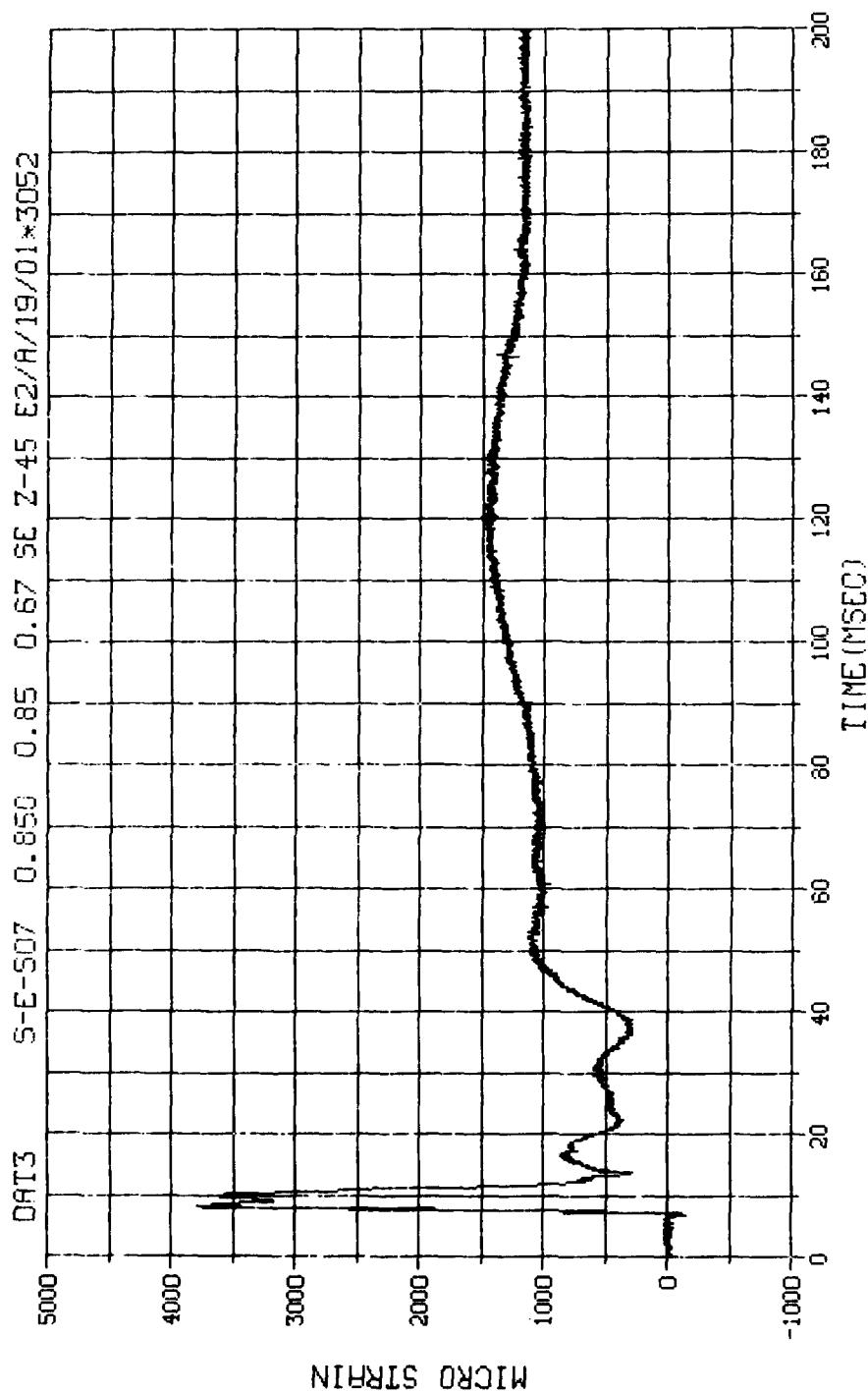
M.N. - 3049	E.U. -0.000, 10000.000	VSN-66142
SKIP=7.000	DIGITS=0.000, 878.500	TAPE22
S.R. =25.00 KHZ	4. 4 PM, TUE, 13 SEP 83.	FILE=240 1



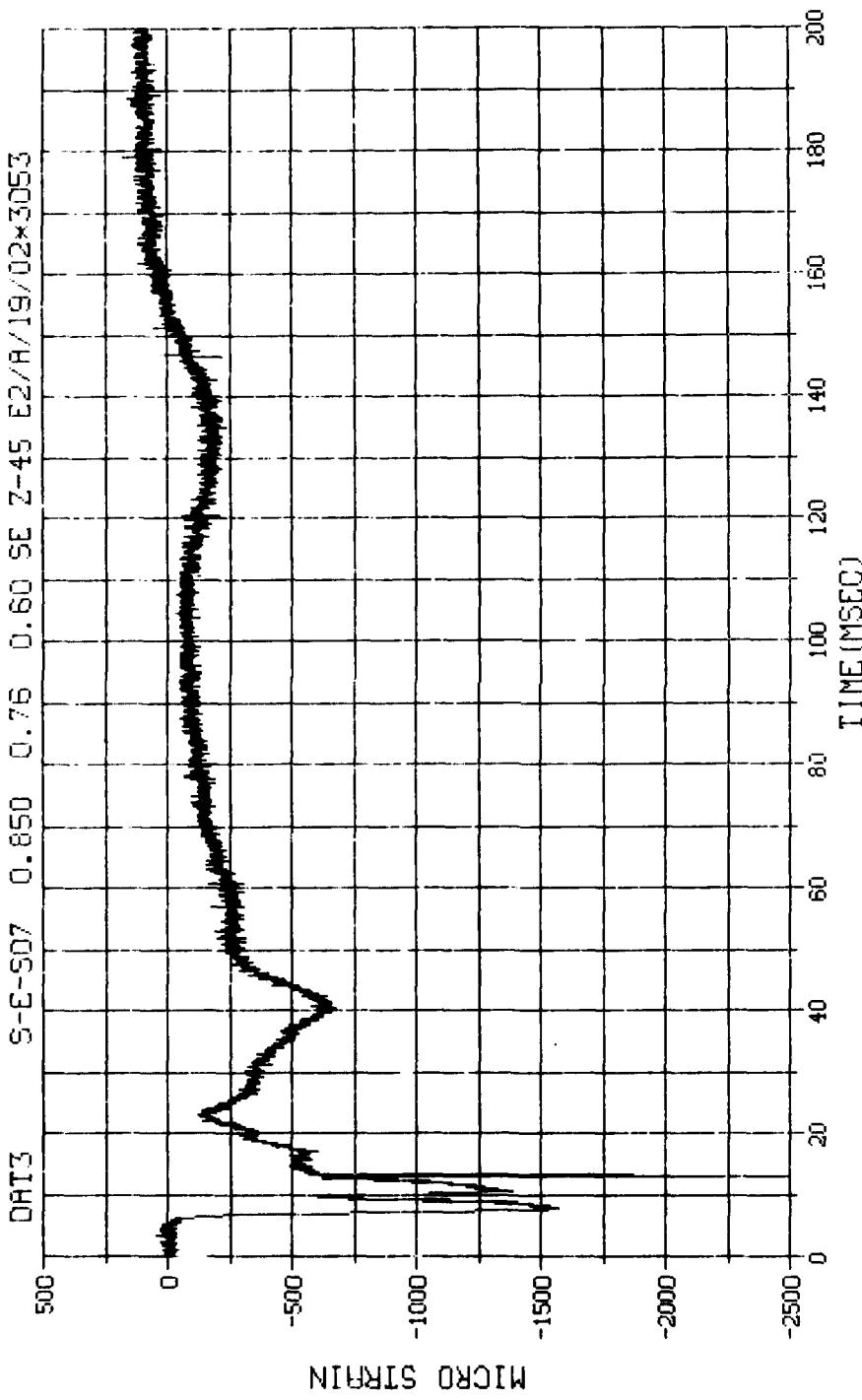
N.N. = 3050	E.U. = 0.000, 7500.000	VSN=66142
TSKIP=7.000	DIGITS=0.000, 865.125	TAPE22
S.R. = 25.00 KHZ	4. 4 PM, TUE, 13 SEP 83.	FILE=242_1



N.N. = 3051	E.U. = 0.000, 14960.000	VSN-66142
SKIP=7.000	DIGITS=0.000, 896.375	TAPE22
S.R. = 25.00 KHZ	4. 4 PM, TUE, 13 SEP 83,	FILE=244 1



M.N. - 3052 E.U. -0.000,10000.000 VSN-66142
TSKIP=7.000 DIGITS=3.000,895.625 TAPE22
S.R. =25.00 KHZ 4. 4 PM, TUE, 13 SEP 83. FILE=246 1



N.N. - 3053 E.U. -0.000,10000.000 VSN-00142
TSKIP=7.000 DIGITS=0.000,870.125 TAPE22
S.R. =25.00 KHZ 4. 4 PM, TUE, 13 SEP 83. FILE=248

